Charge-Transfer Complexes for Amine Synthesis

Keishi Kohara

Department of Chemistry

Queens' College, University of Cambridge

This thesis is submitted for the degree of Doctor of Philosophy

August 2020

Declaration

This thesis is the result of my own work and includes nothing which is the outcome of work done in collaboration except as declared in the Preface and specified in the text. It is not substantially the same as any that I have submitted, or, is being concurrently submitted for a degree or diploma or other qualification at the University of Cambridge or any other University or similar institution except as declared in the Preface and specified in the text. I further state that no substantial part of my thesis has already been submitted, or, is being concurrently submitted for any such degree, diploma or other qualification at the University of Cambridge or any other University or similar institution except as declared in the Preface and specified in the text. It does not exceed the prescribed word limit for the relevant Degree Committee.

Abstract: Charge-Transfer Complexes for Amine Synthesis - Keishi Kohara

A method to generate α-amino radicals, via a photoinduced charge-transfer complex, is reported. A multicomponent radical fragmentation-cyclization reaction was developed, combining secondary amines, cyclopropyl carboxaldehydes and alkenes, to generate cyclopentyl methylamines. To initiate the fragmentation step, single-electron reduction of alkyliminium ions to α-amino radicals was achieved, using an aromatic thiol and visible light irradiation.

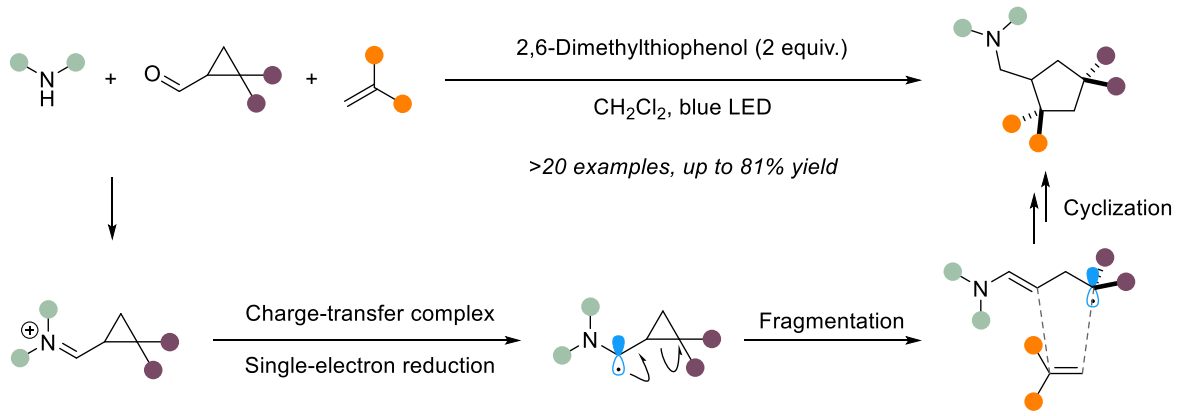

Mechanistic and computational studies supported the formation of a transient, ion-pair charge-transfer complex between iminium and thiolate ions. DFT calculations indicated that irradiation of the complex with visible light could promote intra-complex electron transfer from the thiolate HOMO to the iminium LUMO.

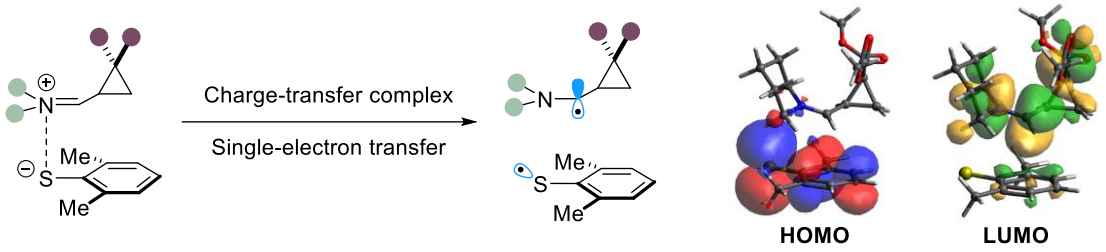

This method of α-amino radical formation was extended to acyclic aldehydes, by development of a radical reductive amination, using thiol as the single-electron reductant and hydrogen atom source. Subsequently, the chemoselective reductive amination of secondary amines over primary amines was attempted. Preliminary studies on a di-amine drug indicated that the radical reductive amination had high selectivity for primary aminothiazoles over secondary amines, contrasting with existing polar reductive amination techniques.

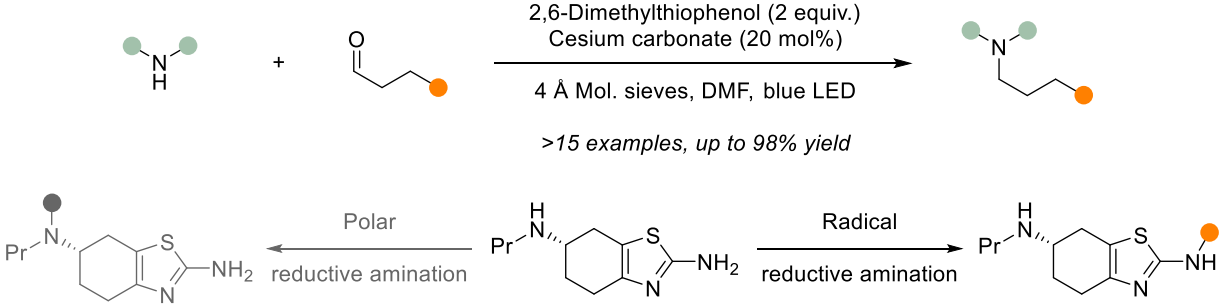

Acknowledgements

I would like to thank Professor Matthew Gaunt for the opportunity to conduct research towards a PhD and study a range of interesting chemical questions. Thank you for your supervision and feedback, as well as your efforts to create a laboratory environment that enables us to focus on research. I am also grateful to Dr Jon Pillow for his support and advice, and Cambridge Display Technology for the PhD studentship. Thank you to Nic, Naomi and Carlos for all their work maintaining the lab, Duncan, Andrew and Peter in the NMR service, and other departmental staff.

I have been fortunate to work with extremely talented and determined colleagues in the group. Thank you to Manuel and Ala, for proof-reading my thesis, and for their sincere interest in helping and sharing knowledge with others. Thank you to Antonio for proof-reading and our work together on the reductive amination. Thanks also to Philipp and Amir for their collaborative studies.

I am grateful to John for his sage advice and putting up with me - the countless discussions with you have helped shape this thesis. Thanks to Patrick W for his advice and friendship in and outside the lab, which have been invaluable. Thanks to the other members of my year, particularly Nils for the Golden Houses/droning/advice, and Connie for her friendship and emergency food trips. Thanks to Will, Henry, Patrick D, Dom and the banjo, Scarlett, and all other members of the group.

Outside the lab, Bee - your friendship has been a constant throughout the PhD, for which I feel extremely fortunate. Thanks to Mao for the last 10 years, and other friends at home. Jenny - as well as enduring my lockdown rants about mechanism, thank you for the love and joy that you have brought me. Finally, thank you to my family for their constant support, and everything they have done to enable life here.

Abbreviations

Å	Ångstrom
Ac	Acetyl
AIBN	2,2'-Azobisisobutyronitrile
aq.	Aqueous
Ar	Aryl
atm	Atmosphere
BET	Back electron transfer
Bn	Benzyl
Bu	Butyl
Boc	*tert*-Butyloxycarbonyl
br	Broad (spectral)
Bu	Butyl
Bz	Benzoyl
° C	Degrees Celsius
CBz	Benzyloxycarbonyl
CIF	Crystallographic information file
COSY	Correlation spectroscopy
CT	Charge transfer
cal	Calorie
cat	Catecholato
δ	Chemical shift in parts per million, downfield from tetramethylsilane
DABCO	1,4-Diazobicyclo[2.2.2]octane
DCE	1,2-Dichloroethane
DEAD	Diethyl azodicarboxylate
DEPT	Distortionless enhancement by polarization transfer
DFT	Density functional theory
DG	Directing group
DIBALH	Diisobutylaluminium hydride
DIPEA	*N*,*N*-diisopropylethylamine
DMA	Dimethylacetamide
DMF	*N*,*N*-dimethylformamide
DMSO	Dimethyl sulfoxide
DMTP	2,6-Dimethylthiophenol
dr	Diastereomeric ratio
$E_{1/2}$	Half-wave potential

EDA	Electron donor acceptor
EDG	Electron donating group
equiv.	Equivalents
er	Enantiomeric ratio
ESI	Electrospray ionization
Et	Ethyl
EWG	Electron withdrawing group
FG	Functional group
FID	Flame ionization detector; Free induction decay
FT	Fourier transform
g	Gram
GCMS	Gas chromatography mass spectrometry
h	Hour
HEH	Hantzsch ester
HFIP	Hexafluoroisopropanol
HMBC	Heteronuclear multiple bond correlation
HMQC	Heteronuclear multiple quantum correlation
HOMO	Highest occupied molecular orbital
HPLC	High performance liquid chromatography
HRMS	High resolution mass spectrometry
Hz	Hertz
IP	Ionization potential
J	Joule
J	Coupling constant
K	Kelvin
k	Rate constant
L	Liter
LDA	Lithium diisopropylamide
LCMS	Liquid chromatography mass spectrometry
LUMO	Lowest unoccupied molecular orbital
M	Molar
m	*Meta*
M^+	Parent molecular ion
Me	Methyl
MeOEt-HEH	Bis(2-methoxyethyl) Hantzsch ester
Mes	2,4,6-Trimethykphenyl (mesityl)

min	Minute
Mol	Mole
mp	Melting point
MS	Molecular sieves
Ms	Methylsulfonyl (mesyl)
Mw	Molecular weight
m/z	Mass to charge ratio
NMP	*N*-Methylpyrrolidone
NMR	Nuclear magnetic resonance
NOESY	Nuclear Overhauser effect spectroscopy
o	*Ortho*
p	*Para*
PE	40/60-Petroleum ether
Ph	Phenyl
pin	Pinacolato
Piv	Pivalate
ppm	Parts per million
Pr	Propyl
Quant.	Quantitative
R	Undefined group
Redox	Reduction-oxidation
RSM	Recovered starting material
rt	Room temperature
s	Second; singlet (spectral)
SCX	Strong cation exchange
SET	Single electron transfer
SOMO	Single occupied molecular orbital
TBS	*tert*-Butyldimethylsily
TD-DFT	Time dependent density functional theory
TEMPO	(2,2,6,6-Tetramethylpiperidin-1-yl)oxyl
TFA	Trifluoroacetic acid
THF	Tetrahydrofuran
TIPS	Triisopropylsilyl
TLC	Thin layer chromatography
TMS	Trimethylsilyl
TOF	Time of flight

TRIP-thiophenol	2,4,6-Triisopropylthiophenol
Ts	*p*-Toluenesulfonyl (tosyl)
TS	Transition state
UV	Ultraviolet
V	Volt
vis	Visible
v/v	Volume per unit volume
w/w	Weight per unit weight

Table of Contents

Declaration **3**

Abstract **5**

Acknowledgements **6**

Abbreviations **7**

Table of Contents **11**

1. Introduction **15**

1.1. Visible Light Photochemistry **15**

1.2. Charge-Transfer Complexes **19**

1.2.1. Early Synthetic Studies 20

1.2.2. Contact Ion Pairing 22

1.3. Photoredox Catalysis **25**

1.4. Recent Advances in Photoinduced Reactions **28**

1.4.1. Charge-Transfer Complexes in Synthesis 28

1.4.2. Exogenous Charge-Transfer Partners 35

1.4.3. Direct Substrate Excitation 39

1.5. Summary **42**

2. Generation of α-Amino Radicals via a Charge-Transfer Complex **43**

2.1. Strategies for Aliphatic Amine Synthesis **43**

2.1.1. Methods to Generate α-Amino Radicals 44

2.2. Project Aims **50**

2.3. Photoredox Catalyzed Fragmentation-Cyclization **52**

2.3.1. Introduction 52

2.3.2. Reaction Discovery 55

2.3.3. Reaction Optimization 58

2.4. Charge-Transfer Complex α-Amino Radical Formation **65**

2.4.1. Reaction Discovery 65

2.4.2. Control Studies 67

2.4.3. Alternative Mechanistic Hypotheses 72
2.4.4. Computational Studies 78
2.4.5. Mechanistic Discussion 86
2.4.6. Reaction Scope 89
2.5. Summary 95
3. Radical Reductive Amination 96
3.1. Introduction 96
3.1.1. Hydrogenative and Hydridic Methods 96
3.1.2. Radical Methods 97
3.2. Project Aims 100
3.3. Charge-Transfer Complex Reductive Amination 101
3.3.1. Reaction Discovery 101
3.3.2. Reaction Scope 104
3.3.3. Mechanistic Discussion 106
3.3.4. Chemoselective Reductive Amination 108
3.4. Summary 115
4. Conclusion and Outlook 116
5. Experimental Procedures 119
5.1. General Procedures 121
5.2. Characterization 122
5.2.1. Charge-Transfer Cyclization 122
5.2.2. Radical Reductive Amination 141
6. References 149
Appendices 166
A.1. ^{1}H and ^{13}C NMR Spectra 166
A.1.1. Charge-Transfer Cyclization 166
A.1.2. Radical Reductive Amination 204
A.2. Computational Data 217
A.2.1. Geometry Optimization 217

A.2.2. Time-Dependent DFT 223

A.3. UV-Vis Absorption Spectra 227

A.4. X-Ray Crystallographic Data 231

1. Introduction

1.1. Visible Light Photochemistry

A goal of modern organic synthesis is to achieve useful bond formations, with minimal handling of raw materials and production of waste. These processes should utilize mild activation methods that limit energy use, with limited undesired side-reactivity. Synthetic photochemistry is an advancing method that aims to address these goals. In its purest form, photochemistry requires simply the input of photons, and can be used to conduct multiple bond connections, generating high molecular complexity in a single step.[1–4]

At its core, synthetic photochemistry involves the promotion of a molecule to its excited state, to initiate radical chemistry. The promotion of a molecule to its excited state is useful for the generation, or release, of strain in the molecule. This has enabled the assembly of molecular structures, which may not be achievable by thermal methods. A prototypical example is the [2+2] photocycloaddition, to generate strained cyclobutanes - a process formally denied under thermal conditions according to Woodward-Hoffmann rules, due to symmetry-based restrictions (Figure 1a).[5]

The ability to handle open-shell radical species enables new reactivity pathways, which can be distinct and complementary to ionic pathways. For instance, photochemistry has been transformational in enabling the generation and manipulation of high-energy alkyl radicals. In the pharmaceutical industry, this has directly contributed to greater incorporation of sp^3 centers and desirable pharmacophores in drug molecules, thus expanding accessible chemical space (Figure 1b).[6] Initially, the foundations of radical chemistry were established by pioneering studies using stoichiometric redox reagents and UV irradiation, to form radical species. In the last decade, methods have capitalized on the use of visible light and photocatalysts for their generation (Figure 1c). This has allowed the use of exceptionally mild reactions conditions, enabling greater chemoselectivity, thereby limiting unintended by-products and waste.

These factors have greatly encouraged the uptake of photochemistry (particularly photoredox catalysis) within academic and industrial research. For instance, photochemistry is now commonly used in the pharmaceutical industry, in the late-stage modification of drug candidates,[7] or in the kilo-scale production of active pharmaceutical ingredients.[8] Overall, the development of further photochemical techniques continues to be an exciting area of research, with the potential for high uptake and utility in wider society.

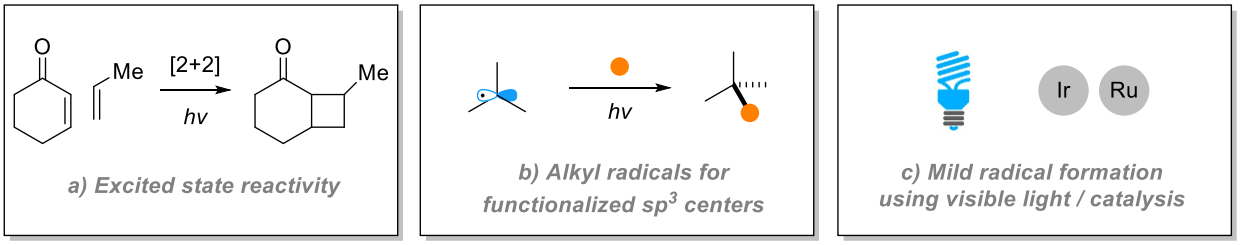

Figure 1: Photochemistry for radical generation, in modern organic synthesis

Two fundamental laws of photochemistry are as follows:[9]

1) Only absorbed light is effective in a photochemical reaction (Grotthuss-Draper)
2) Light absorption is a quantum process, where conventionally, one photon is absorbed by one molecule (Stark-Einstein)

Einstein formalized the photoelectric effect, which showed that electrons were ejected from a metallic surface in an evacuated tube, when irradiated with light. It was observed that light below a certain frequency cannot eject an electron, no matter how intense the light. The photon therefore contains a quantum of electromagnetic energy *E* at a given frequency *v*, expressed by Equation 1:

$$E = h\nu = h\frac{c}{\lambda}$$

Equation 1: Planck-Einstein relation

Photophysical processes can be visualized by a Jablonski diagram, shown in Figure 2. Absorption of a photon leads to an electronic excitation from the S_0 singlet state to an excited singlet state S_n. Radiative processes involve the absorption or emission of photons; upon absorption, the two possible emissive processes are fluorescence from singlet state S_n and phosphorescence from triplet state T_n. Meanwhile, nonradiative processes involve isoenergetic (i.e. horizontal) transitions between two states, such as internal conversion (IC) and intersystem crossing (ISC). They also include nonradiative vertical transitions called vibrational relaxation (VR), where excess vibrational energy is transferred to the surrounding medium through intermolecular collisions. These processes map a molecule's photoexcitation and relaxation process, without effecting significant changes to the electronic and molecular ground state structure.

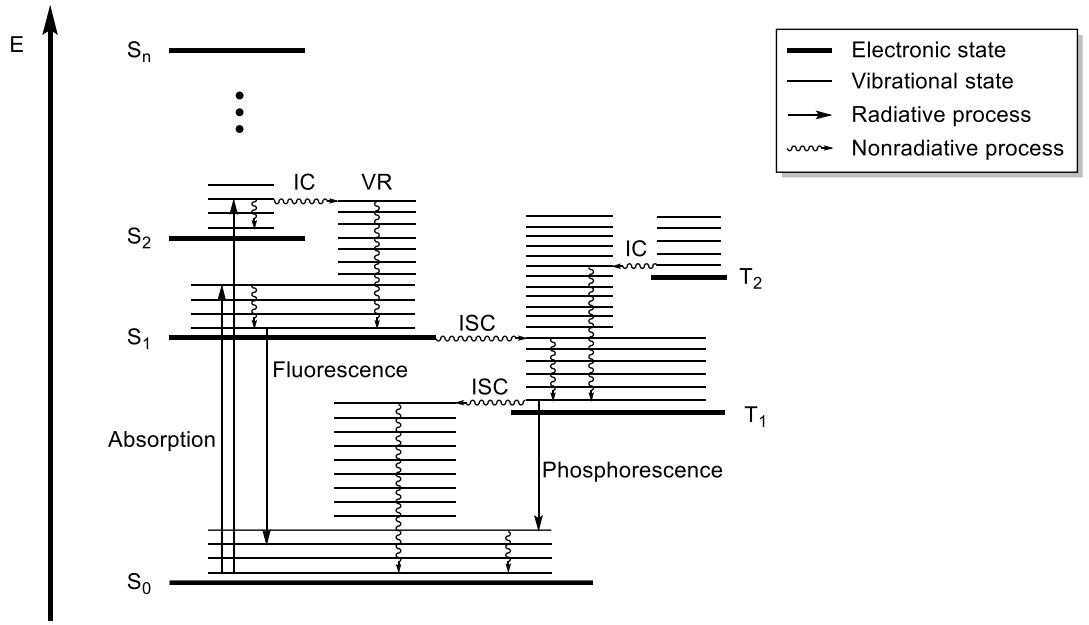

Figure 2: Jablonski diagram of photophysical processes

Quenching of the excited state refers to any process that reduces the radiative quantum yield of the fluorophore. These are bimolecular processes, where a quencher interacts with the excited state molecule, either through energy or electron transfer. In energy transfer, the excess energy of the donor is transferred to the acceptor, by Förster or Dexter transfer mechanisms. Förster energy transfer involves the transfer of energy through nonradiative dipole-dipole coupling, whereas Dexter transfer involves the nonradiative bilateral exchange of electrons. Meanwhile, electron transfer results in a new charge distribution, and can occur by inner and outer sphere mechanisms, depending on the interacting molecules and the degree of orbital overlap. These bimolecular processes can only occur if they are faster than the competing background photophysical processes shown in the Jablonski diagram.

Another way to visualize these processes is through a molecular orbital treatment (Figure 3). When a molecule in its ground state (**F**) is irradiated with light of energy ΔE, an electron can be promoted from the HOMO to the LUMO, forming ^{1}**F*** in the excited singlet state. The excited state can either relax to the ground state or undergo bimolecular energy/electron transfer processes. The excited state ^{1}**F*** has the property of being more oxidizing and reducing compared to the ground state, since it has a relatively lower energy electron hole which can accept an electron, and a relatively higher energy electron which can be donated.

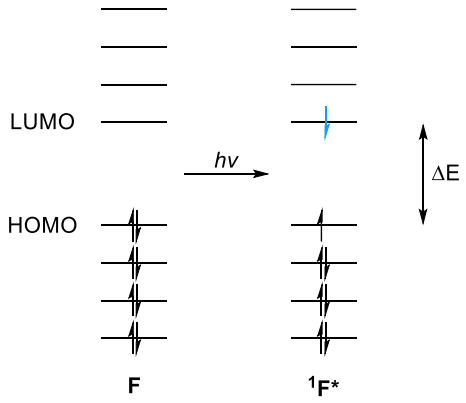

Figure 3: Orbital treatment of photoinduced electron transfer

The size of the HOMO/LUMO energy gap of most organic molecules means that small molecules can typically only absorb light in the ultraviolet range (λ = 200-380 nm). For instance, the π-π* excitation of 1-pentene has a maximum absorption at λ_{max}= 178 nm, observable by UV-vis absorption spectroscopy. Molecules with heteroatoms, non-bonding electrons, or extended conjugation, enable mixing of molecular orbitals, which can lower the HOMO-LUMO gap, shifting the absorption maximum to longer wavelengths (bathochromic shift). For instance, isoprene, which has two double bonds in conjugation, has a red-shifted λ_{max} of 222 nm.

Consequently, early synthetic applications of photochemistry required the use of high energy UV light for the promotion of short wavelength transitions. These used broadband xenon and mercury arc lamps, which emit light between 250 nm to 1000 nm, in combination with optical filters (e.g. Vycor, Pyrex) to limit spectral bands. These lamps could reach temperatures as high as 600 °C, with significant emission of infrared radiation, therefore water cooling and cuvette filters were often utilized. The requirement of dedicated equipment, safety

considerations of high-energy light and the possibility of deleterious side reactions arising from reagent/solvent excitation, presented significant disadvantages of using UV light.

More recently, it has been possible to harness visible light for photochemistry, due to the development of the fields of photoredox catalysis and charge-transfer complexation. These techniques have allowed safer and more convenient sources of light to be used, such as incandescent and compact fluorescent lamps. As well as wavelength of light, intensity is a key consideration since photonic flux decreases exponentially with the depth of the medium (Beer-Lambert law). While CFLs are extremely cheap, their intensities are not as strong and can be diffuse, with multiple emission bands existing, some of which is in the UVA region.[10] As a result, light-emitting diodes (LEDs) have become widespread as powerful sources of visible light. LEDs generally have high intensities and narrow emission windows, which allow specificity in band irradiation (Figure 4).[11] Further advancements have included small-scale reactors that standardize the photoirradiation process,[12] and manufacturing-scale flow photoreactors for synthesis of active pharmaceutical ingredients.[8] The following section will explore the processes of visible light mediated charge-transfer complexation and photoredox chemistry in greater detail.

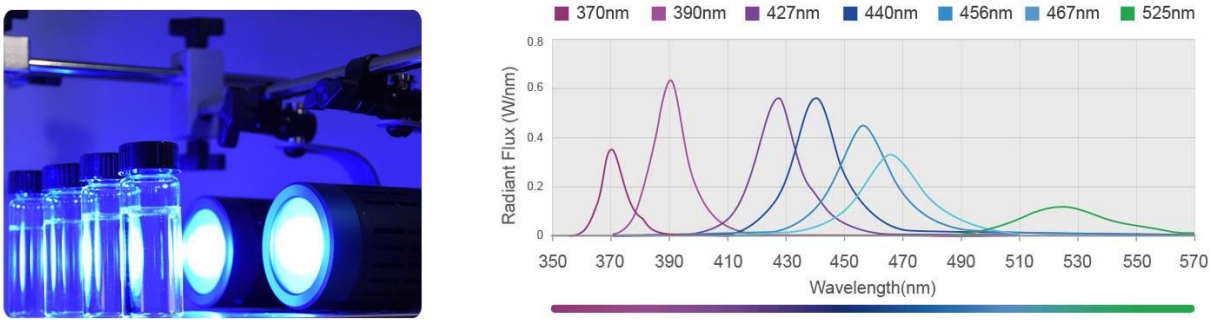

Figure 4: Modern LEDs, with options for defined wavelength emission. Adapted from the Kessil website[13]

1.2. Charge-Transfer Complexes

In the 1940s, Hildebrand and co-workers noted that solutions of iodine changed color dramatically upon addition of aromatic hydrocarbons. They attributed this phenomenon to 'an acid-base interaction, in the electron donor-acceptor sense'.[14,15] Several groups had observed that the mixing of electron-rich and electron-poor molecules, which by themselves do not absorb visible light, led to the formation of new colored species. Mulliken formalized these phenomena in the 1950s, resulting in the foundation of our current understanding of charge-transfer complexes.[16,17] Donor and acceptor molecules can undergo weak and reversible association in the ground state, forming an electron-donor-acceptor (EDA), or charge-transfer (CT) complex. The mixing of molecular orbitals results in a new HOMO and LUMO of the molecular complex, where the HOMO/LUMO energy gap is typically smaller than the gap of the original molecules. Upon irradiation with visible light, an electronic transition can occur from the HOMO to the LUMO.

A prototypical example is the interaction of tetracyanoethylene (TCNE) and acenaphthylene (ACN). In the UV-vis absorption spectrum of TCNE, the absorption diminishes at λ_{tail} = 470 nm, while the absorption of ACN diminishes at λ_{tail} = 500 nm (Figure 5).[18] However, an equimolar mixture of the two shows the appearance of a new, broad, charge-transfer band that extends to λ_{tail} = 700 nm. This represents the absorption of the CT complex formed by TCNE and ACN, and the resulting photoinduced electron transfer occurring from the ACN HOMO to the TCNE LUMO.

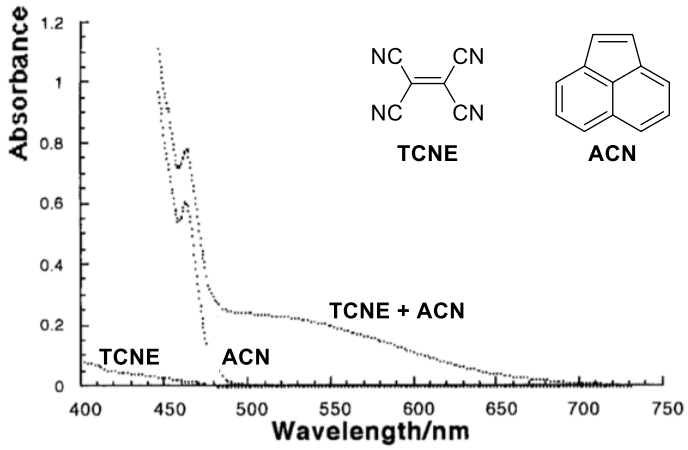

Figure 5: Appearance of charge-transfer band upon mixing donor and acceptor molecules. Adapted from Haga et al.[18]

As shown in **Path I** of Figure 6, donor **D** can associate with acceptor **A** to form a CT complex.[19,20] Irradiation of the complex with light induces excitation and single-electron transfer from **D** to **A**, generating a solvent-cage enclosed radical cation and radical anion. Back-electron transfer (BET) is an extremely rapid process (up to k in the order of 10^{11} s^{-1}) that can reverse the electron transfer, generating the original donor and acceptor molecules.[21,22] For example in the case of ACN and TCNE, single-electron transfer (SET) continuously leads to a back-and-forth process with BET, since there is no productive forward path from the radical species. When a fragmentation or mesolysis process exists from the radical species, at a comparative rate to BET, the cycle

of ET/BET can be escaped. For instance, the radical anion **A** could fragment by mesolysis, to generate radical **A** and $\mathbf{X}^{-}$.

An alternative route to SET (**Path II**) starts with direct irradiation of the HOMO-LUMO transition of **D**, generating photoexcited **D***. Associative interactions with molecule **A** can lead to the formation of exciplex **(D*)A**, which can undergo SET, generating the radical cation/anion pair. Again, BET is a deleterious process which competes with productive radical reactivity.

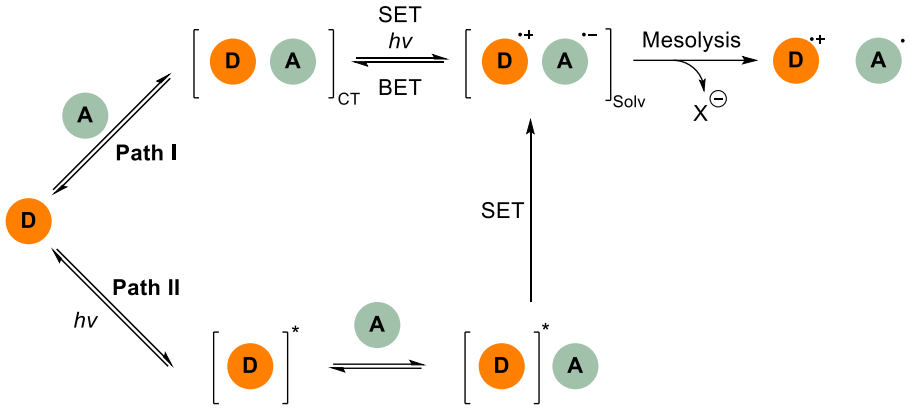

Figure 6: Single electron transfer by charge-transfer complex, and by local band irradiation

There are three main experimental probes that can be used to support the formation of a charge-transfer complex. Firstly, a bathochromic shift in the spectroscopic absorption band, upon mixing donor and acceptor molecules is a strong indicator of potential CT complexation. The method of continuous variation (Job plot) can be used, to measure the change in light absorbance depending on the molar fraction of donor, thereby determining the stoichiometry of the binding complex. Secondly, isolation of an X-ray crystal structure of the complex can be informative, as it shows the orientation of the donor/acceptor molecules in the solid state, which can potentially indicate the orbitals contributing to intracomplex interactions in the solution state. Finally, selective laser-induced optical excitation of the HOMO-LUMO transition can be achieved with time-resolved spectroscopy.[20]

1.2.1. Early Synthetic Studies

The spectroscopic phenomena of charge-transfer complexes were evident from the 1950s; however, applications towards synthesis developed significantly in the 1970s. Following a previous procedure involving UV irradiation,[31] Cantacuzène reported that enamine **1** reacted with perfluoroalkyl iodide to generate the perfluoroalkylated aldehyde **8**, without use of an external initiator or UV irradiation (Scheme 1).[23,24] The CT complexation of amines and perfluoroalkyl iodides was known at the time,[25] and it was envisaged that complexation between the enamine and $C_6F_{13}I$ could lead to CT complex **2**, resulting in SET from the nitrogen lone pair to the perfluoroalkyl iodide σ^*_{C-I} orbital. The most likely mechanism involved a chain propagation pathway, where radical anion **3** expels iodide to form the C_6F_{13} radical **4**, which carries out radical addition to

another molecule of enamine **1**. The resulting α-amino radical **5** abstracts a halide from $C_6F_{13}I$, to regenerate the perfluoroalkyl radical. Finally, elimination of iodide from **6**, followed by hydrolysis, generates aldehyde **8**. Shortly after this work, further related CT complex transformations were reported, including complexation between enamines/*p*-nitrobenzyl chlorides (Russell)[26] and tertiary amines/*p*-nitrobenzyl chlorides (Kornblum).[27]

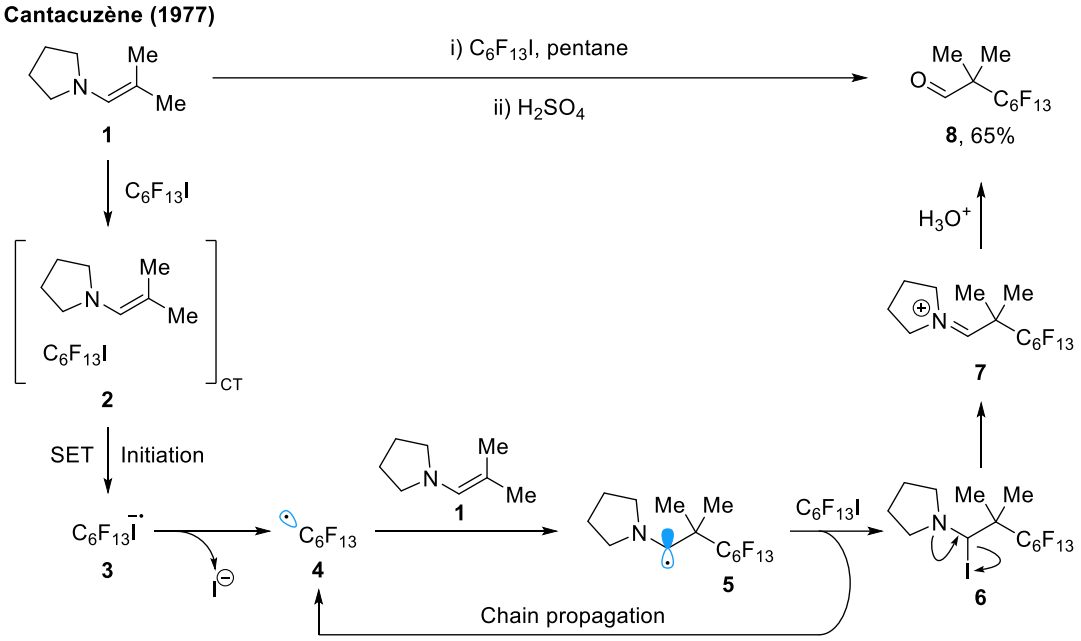

Scheme 1: Early synthetic example of visible light mediated charge-transfer complexes

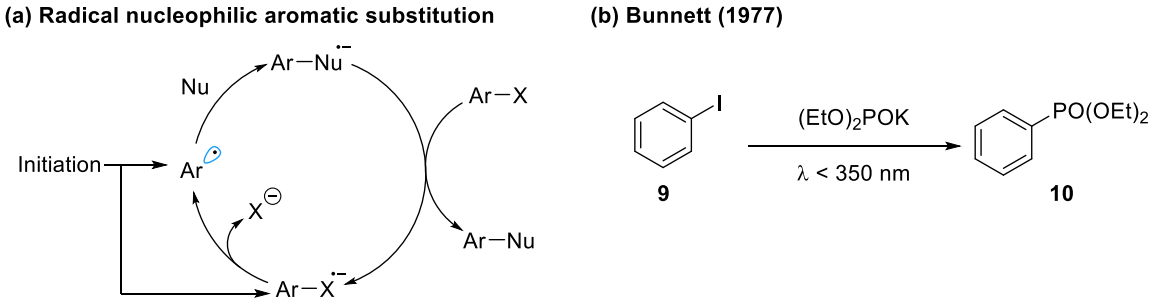

Scheme 2: Charge-transfer complexes as initiators in radical nucleophilic aromatic substitution

The association of aromatic molecules in CT complexes are often favorable, particularly when they are functionalized with electron-donating/withdrawing substituents. This can be attributed to secondary orbital interactions which promote complexation, and stabilization of the resulting radical species, through conjugation into the aromatic ring. Radical nucleophilic substitution reactions ($S_{RN}1$) typically involve an initiation step to generate an aryl radical or Ar–X radical anion, which undergoes mesolysis to form the aryl radical (Scheme 2a).[28] Nucleophilic attack results in Ar–Nu radical anion, which propagates the radical chain reaction, through SET with another equivalent of Ar–X. One possible mechanism for the initiation step is

thought to be through a CT complex between the aryl halide and nucleophile. Bunnett reported in 1977 that the reaction between iodobenzene **9** and phosphite ions proceeded through such a mechanism (Scheme 2b),[29,30] later supported by light filter and UV-vis absorption experiments.[31]

Studies conducted by Kochi in the late 1970s investigated the reaction of tetraalkyl tin **11** and tetracyanoethylene **12** (Scheme 3).[32,33] This study was significant, as it showed that both light or heat could excite the charge-transfer complex, and Kochi was able to study these mechanisms independently. The reaction proceeded at 22 °C in the dark, and at −35 °C only when visible light irradiation was applied. Their studies showed that CT complex **13** was a likely common intermediate for both processes, leading to radical ion pair **14**, which then fragmented to the tin cation and a methyl radical. Triad **15** then undergoes recombination to form the alkene addition product **16**. These studies also supported that the CT complex could be a critical precursor in reactions, as opposed to an inactive resting state. Further examples of CT complexes that are activated by thermal rather than photochemical initiation have been reviewed elsewhere.[34–36]

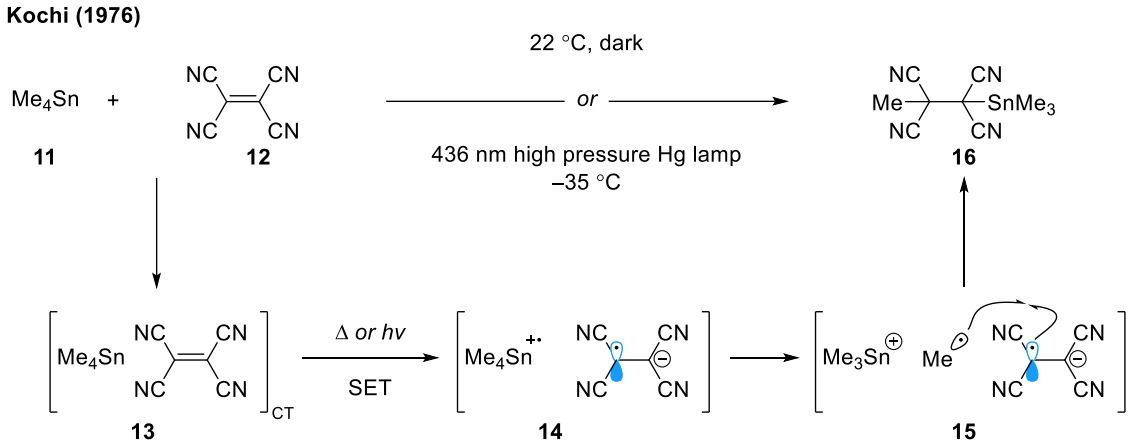

Scheme 3: Photoinduced and thermal activation of charge-transfer complex

These early, seminal examples were crucial in formalizing the types of donors and acceptors that could form CT complexes, as well as understanding their thermodynamic, kinetic and spectroscopic properties.[37,38] Nonetheless, these measurements often required specialist equipment, which limited their use, and exploration into the application of CT complexes for synthesis only developed substantially from 2010.

1.2.2. Contact Ion Pairing

Up to now, the discussion has focused on instances where neutral donor and acceptor molecules associate, resulting in CT complexation, and the generation of a radical ion pair (Figure 7a). Kochi, among others, have closely studied cases where electrically charged partners form a contact ion pair (CIP) CT complex.[39–42] Irradiation of the CIP complex results in electron transfer, which generates an uncharged geminate radical pair (Figure 7b).

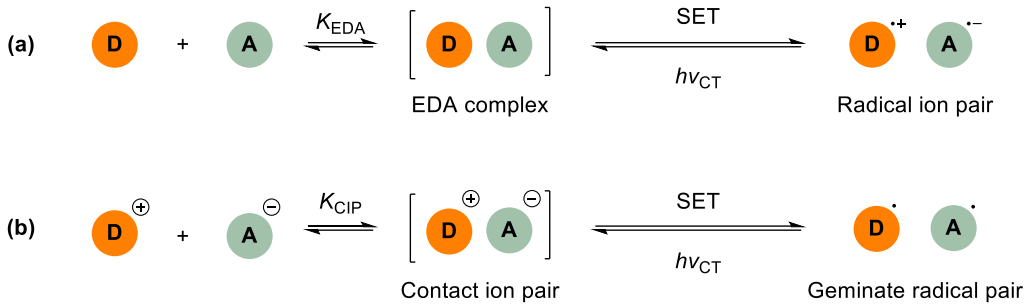

Figure 7: Radical formation, from neutral and charged starting materials

An early example of CIP CT complexes can be attributed to Kosower, who studied the CT absorption bands of pyridinium iodides.[43–46] Kochi formally investigated the CT bands of metallocenium and pyridinium salts of carbonylmetalates, such as $[Tl]^+[Co(CO)_4]^-$ and $[Py]^+[V(CO)_6]^-$.[47,48] When colorless aqueous solutions of pyridinium chloride **17** and $[Na]^+[Co(CO)_4]^-$ **18** were mixed together, burgundy colored crystals formed immediately, which was attributed to the formation of CT complex **19** (Scheme 4).[49] Further X-ray crystallographic evidence identifying the possible orbitals involved have also been reported.[49,50]

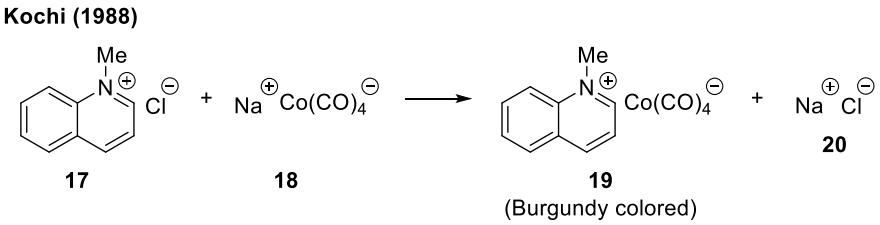

Scheme 4: Mixing of colorless salt solutions leads to colored precipitate

Regarding synthetic applications of CIP CT complexes, the combination of pyridinium salt **21** and organoborate **22** was found to form a bright yellow precipitate, which upon light irradiation, gave the methylated product **26** in 75% yield (Scheme 5).[51] Irradiation of the CIP **23** generates radical pair **24**, then scission of the B–Me bond forms BH_3 and a methyl radical (**25**). Radical-radical recombination of pyridine and methyl radicals was proposed to give the methylated product **26**.

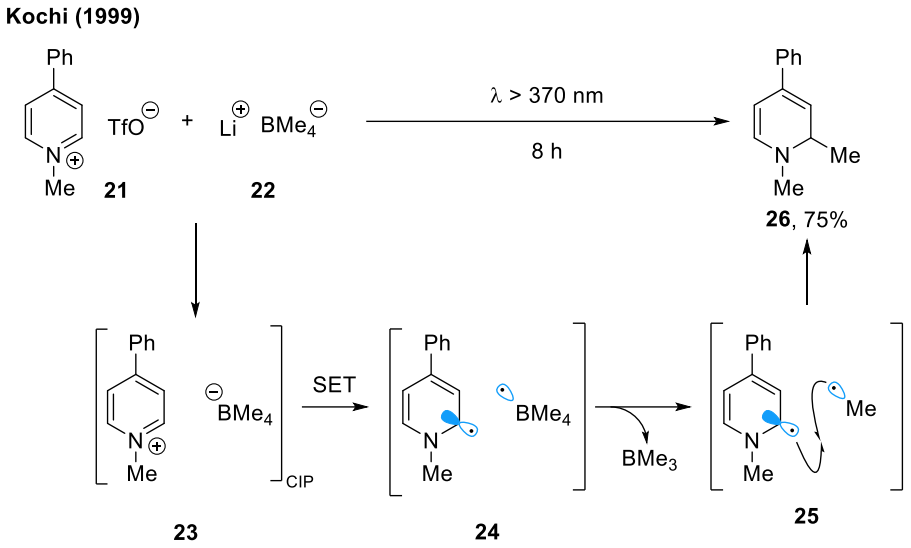

Scheme 5: Photoinduced methylation via contact ion pair charge-transfer complex

A further study by Kochi found the formation of colored charge-transfer salts between methylviologen **27** and carboxylate anion **28**.[52,53] Irradiation of the CT complex **29** led to electron transfer, followed by radical decarboxylation, then oxidation under the reaction conditions, led to the quantitative formation of diarylketone **32**. Methyl viologen acceptors are commonly used acceptors in CIP CT complexes, particular in the development of electrochromic materials, forming complexes with donors including halides,[54,55] carboxylates,[56] and benzenethiolates.[57,58] The potential application of contact ion pairing in charge-transfer complexes has been largely overlooked in organic synthesis, and recent examples will be discussed in Chapter 2.

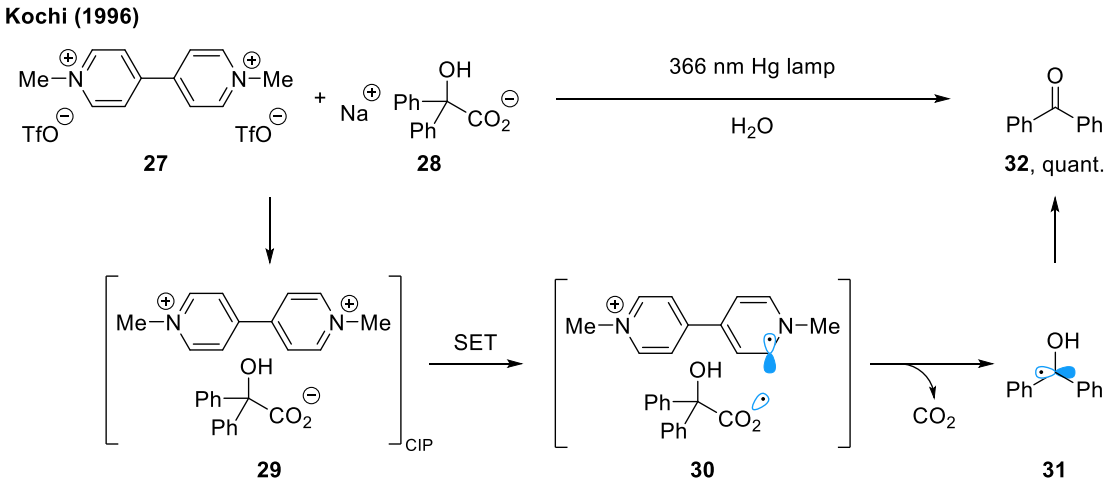

Scheme 6: Methylviologen salts as effective charged acceptors

1.3. Photoredox Catalysis

An alternative method to convert visible light into chemical energy is to use photoredox catalysis. This uses catalytic amounts of polypyridyl metal complexes such as $Ru(bpy)_3^2$, or organic dyes such as Eosin Y (Figure 8), which are able to absorb visible light. This is due to appropriately sized energy level gaps between occupied and unoccupied orbitals. After excitation of the photocatalyst, it can undergo electron transfer with organic substrates, to generate radicals from substrates which cannot absorb visible light. In addition to electron transfer, polypyridyl metal complexes[59,60] and other compounds such as thioxanthones[61] have been used as energy transfer catalysts, for example in photocycloaddition reactions. Overall, photoredox catalysis has been significant in enabling radical reactivity of a diverse set of molecules, under mild reaction conditions.

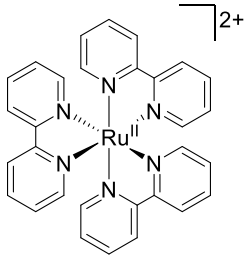

$[Ru(bpy)_3]^{2+}$
33

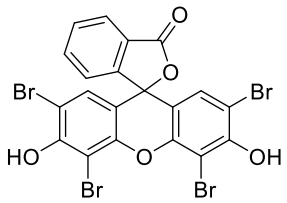

Eosin Y
34

Figure 8: Examples of photoredox catalysts

The use of photoredox catalysis in organic reactions was pioneered by groups of Kellogg,[62] Deronzier[63] and Okada[64] from as early as 1978, however there has been a significant resurgence since 2008 in their application to modern synthesis.[65,66] There are three main considerations when choosing a photocatalyst:[67]

i. Ground state and excited state redox potentials that are matched to substrate redox potentials
ii. Effective absorption of light to give a sufficiently long-lived excited state, which allows intermolecular electron transfer to be kinetically favorable
iii. Stability of the catalyst under the reaction conditions

The catalyst $Ru(bpy)_3^{2+}$ exhibits two absorption peaks at λ = 290 nm (ligand π to π^* transition) and 450 nm (metal t_{2g} to ligand π^* charge-transfer, MLCT). Absorption of visible light (λ > 380 nm) populates the MLCT band, promoting an electron from the metal centered t_{2g} orbitals to the bipyridyl ligand π^* orbital, resulting in an oxidized Ru^{III} metal center and reduced ligand center. The singlet state resulting from MLCT undergoes rapid ISC to the more stable triplet MLCT state (**35**, Figure 9). Direct relaxation of the excited triplet state back to the ground state (phosphorescence) is slow because this process is spin forbidden, therefore the triplet state has a substantially long lifetime of 1.1 µs. This allows useful electron transfer pathways to occur, prior to catalyst decay. As before, the excited state has the property of being a stronger oxidant and reductant, than the ground state species.

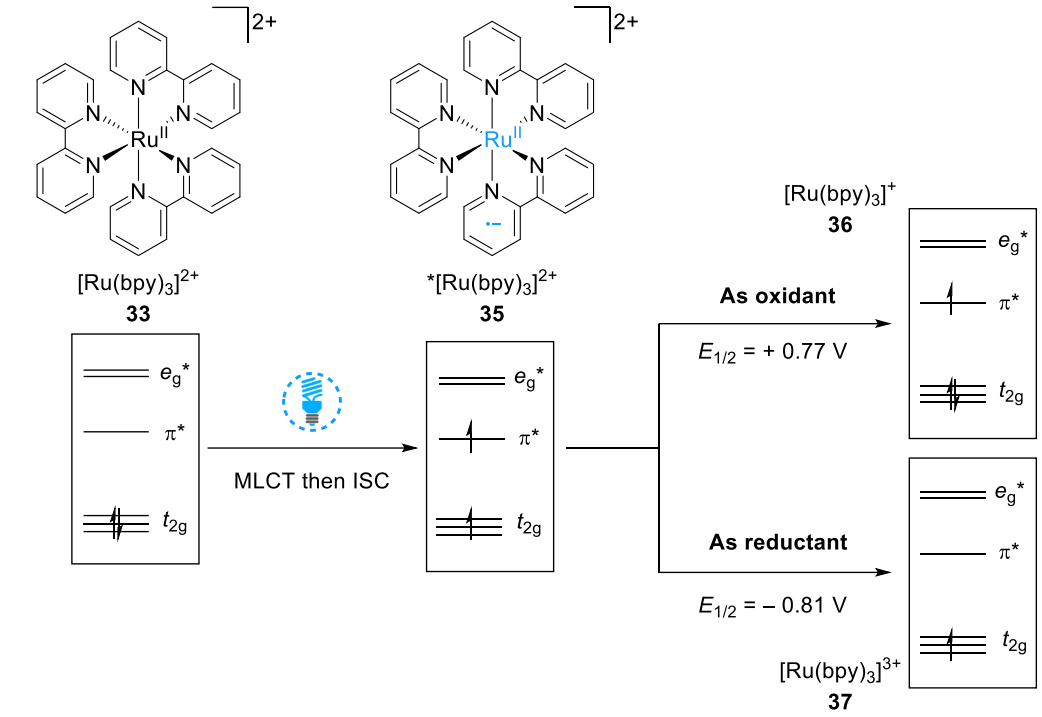

Figure 9: Simplified molecular orbital picture of $Ru(bpy)_3^{2+}$ electronic processes

In the case where the catalyst undergoes reduction (reductive quenching cycle), the acceptance of an electron from donor **D** results in $[Ru(bpy)_3]^+$, which is now moderately reducing (Figure 10). Reduction of acceptor **A** regenerates the ground state $[Ru(bpy)_3]^{2+}$, completing the catalytic cycle. The ability to carry out both reduction and oxidation in this way offers flexibility in designing synthetic pathways. If a stoichiometric quantity of exogenous reductant is used for catalyst turnover, a net reductive process, with respect to the target substrate, can be achieved.

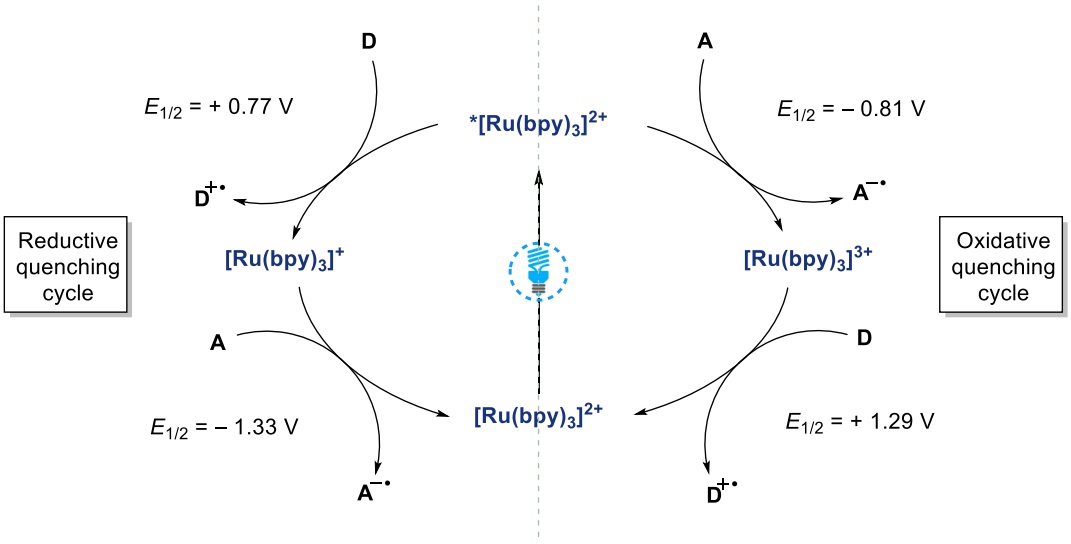

Figure 10: Photoredox cycles of $Ru(bpy)_3^{2+}$

The two generally accepted mechanisms for electron transfer are inner sphere and outer sphere transfer. These are sometimes known as bonded and non-bonded electron transfer in the context of organic molecules. In

Marcus theory, the extent of interaction between the donor and acceptor is determined by the overlap of electronic wave functions. Electron transfer by charge-transfer complexes are inner-sphere process, where the distance between donor and acceptor is expected to be $r = 3.0 – 3.3$ Å. Conversely, photoredox catalysis occurs via outer sphere electron transfer, where the electronic wave functions do not overlap significantly, and the interatomic distance is $r = 5.0 – 6.0$ Å.

Although the main body of this thesis begins with an investigation into photoredox-catalyzed reactions, the focus turns to the development of a photoredox catalyst-free methodology. Recent examples of photoredox catalyzed reactions have been reviewed elsewhere,[68–70] and examples relevant to this thesis are described at the start of Chapter 2.

1.4. Recent Advances in Photoinduced Reactions

1.4.1. Charge-Transfer Complexes in Synthesis

Over the last decade, there have been significant advances in transformations involving visible light promoted charge-transfer complexes.[71–73] This has occurred alongside the development of photoredox catalysis; in fact CT complex reactions were often initially discovered, when photoredox catalyzed reactions were found not to require the photocatalyst. The MacMillan group reported in 2011 the photocatalytic trifluoromethylation of enolsilanes **38** to give **40** (Scheme 7a).[74] The photoredox catalyst $[Ru(bpy)_3]^{2+}$ was used to reduce CF_3I to the CF_3 radical, and oxidize the substrate later in the catalytic cycle. To their surprise, they found that electron-rich silylketene acetals derived from esters and amides, such as **41**, could undergo trifluoromethylation without using a photocatalyst (Scheme 7b). The authors presumed a photoinduced charge-transfer between the silylketene acetal and CF_3I was occurring, citing the works of Mariano[75] and Fukuzumi,[76] who had previously studied the CT electron transfer of silyl ketene acetals using UV light. It may be that the CFL used by MacMillan contains UV light, or the use of CF_3I as a CT acceptor causes a redshift in the absorption to the visible region, however further experimental evidence was not presented here.

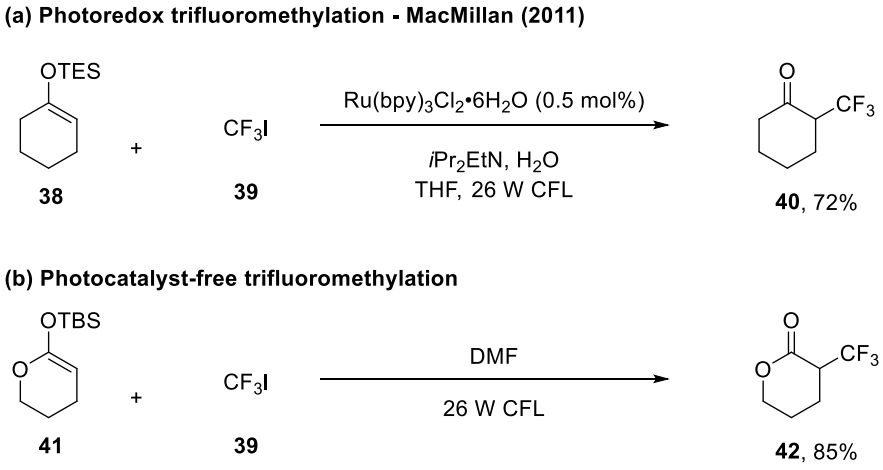

Scheme 7: Photoinduced trifluoromethylation with and without photocatalyst

In 2013, Chatani reported the iridium catalyzed arylation of arenes and heteroarenes using diaryliodonium salts (Scheme 8).[77] The reaction was initially developed with a photocatalyst, generating arylated products, such as pyrrole derivative **45** in 88% yield (Scheme 8a). The excited photocatalyst was thought to reduce the iodonium salt, generating the aryl radical, which could conduct radical addition with arenes. It was found that with *N*-methyl pyrrole as the substrate, the reaction could be conducted without a photocatalyst, albeit with a lower yield of 54% (Scheme 8b). It was proposed that CT complexation between the pyrrole and iodonium salt could form complex **46**, that undergoes electron-transfer.[78] This was corroborated by UV-vis spectroscopic analysis, which showed a new red-shifted band to λ_{tail} = 400 nm, upon mixing of the reactants. Mesolysis of the iodonium salt generates a phenyl radical, which was proposed to recombine with the pyrrole radical cation (**47**).

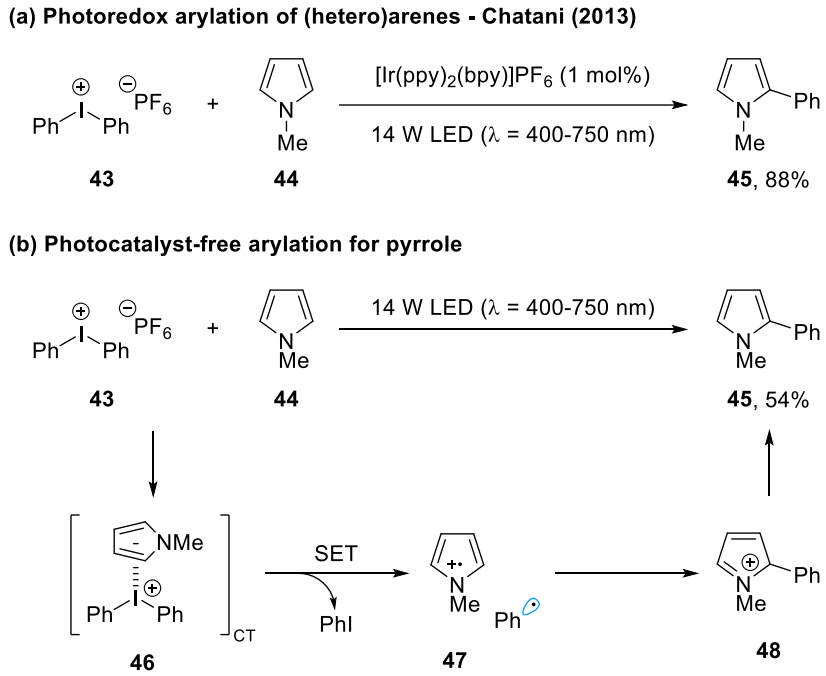

Scheme 8: Photoinduced arylation of *N*-methyl pyrrole via a charge-transfer complex

Melchiorre demonstrated, in their seminal 2013 study, the merger between organocatalysis and charge-transfer complexes.[79] Inspired by historical studies conducted into enamines and di-nitro arenes, as CT donor and acceptor moieties respectively, the group successfully performed the enantioselective α-alkylation of aldehydes to form the product **52** in excellent yield and enantiomeric excess (Scheme 9a).[80,81] Initially, the group proposed a closed cycle mechanism, whereby catalytically generated chiral enamine was proposed to form CT complex **53** with benzyl bromide **50**, resulting in radical ion pair **54**. It was thought that in-cage mesolysis of the benzyl bromide could form radical pair **55**, which undergoes recombination to generate iminium **56**, followed by hydrolysis to form **52**.

Upon further mechanistic study, it was found that a radical chain process was the more likely mechanism (Scheme 9b). Although the initiation required the same CT complex, radical ion pair **54** was thought to undergo cage escape and mesolysis, generating benzyl radical **58**. Radical addition occurs with another equivalent of enamine **59**, then chain propagation occurs with benzyl bromide **50**, to form iminium **56** (also known as a Kornblum-Russell $S_{RN}1$-type alkylation).[82,83] Hydrolysis of the iminium would then give alkylated aldehyde **52**. The same group also demonstrated later that indoles could also act as CT donors with electron deficient benzyl bromide acceptors.[84]

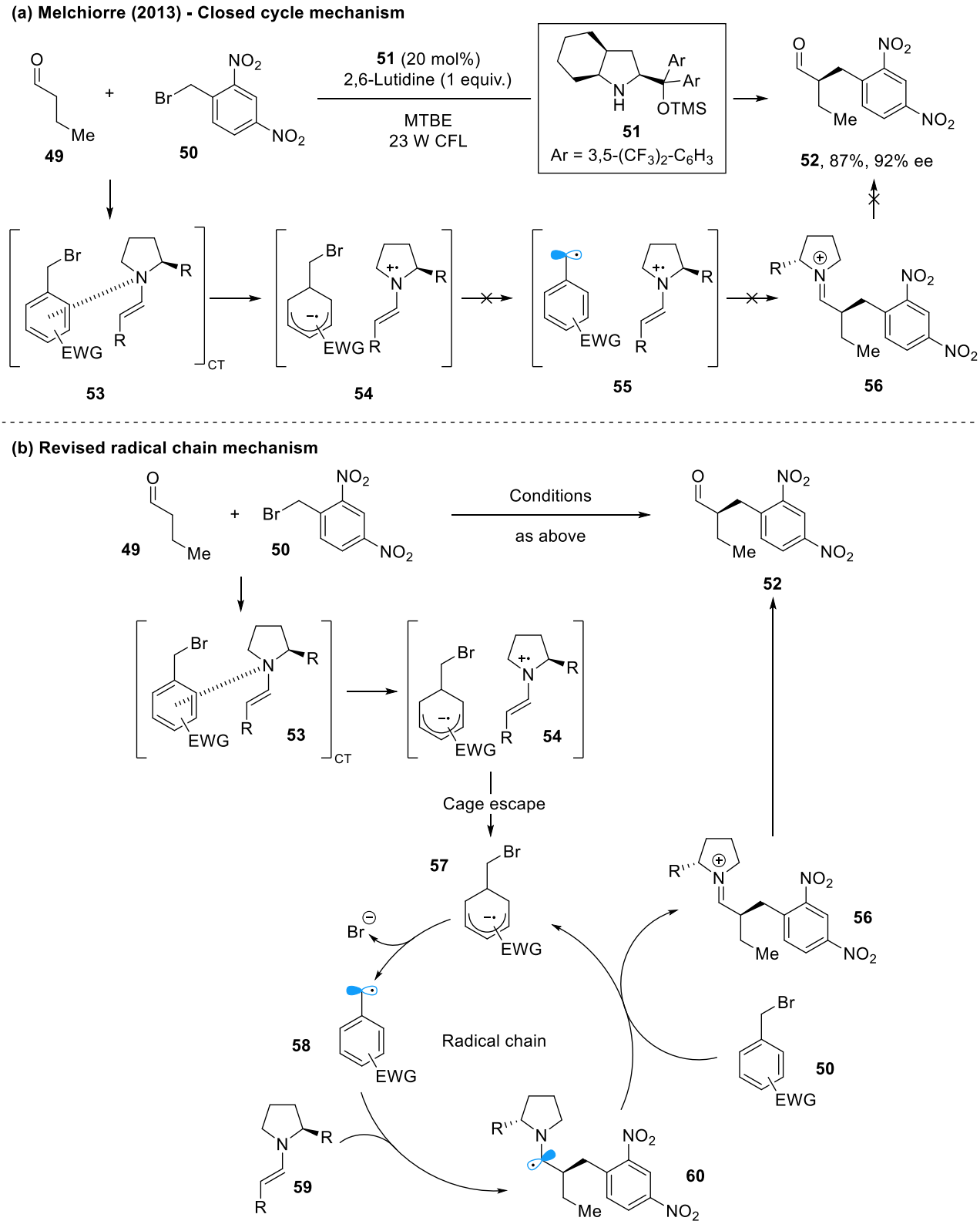

Scheme 9: Enantioselective alkylation operating via a radical chain mechanism

These studies exemplify that in many cases, electron transfer via a charge-transfer complex often acts as an initiation step in a radical chain mechanism. The distinction between the two mechanisms can be an important consideration in photochemistry and photoredox catalysis and can be useful in determining how a reaction is

optimized, or in designing enantioselective processes. Principally, quantum yield measurements provide a way of identifying radical chain reactions.[85] Quantum yield (Φ) is the ratio of moles of product formed, over einsteins of light absorbed. A reaction operating with a closed cycle, without chain propagation, can exhibit a maximum Φ of 1. This is a maximum value, since any non-productive photochemical processes (e.g. phosphorescence, back electron transfer) can decrease the quantum yield. Consequently, a quantum yield less than 1 does not unambiguously indicate a closed loop system. Radical chain processes can potentially form multiple equivalents of product from every photon; therefore, a quantum yield greater than 1 is a strong indicator of a chain process.

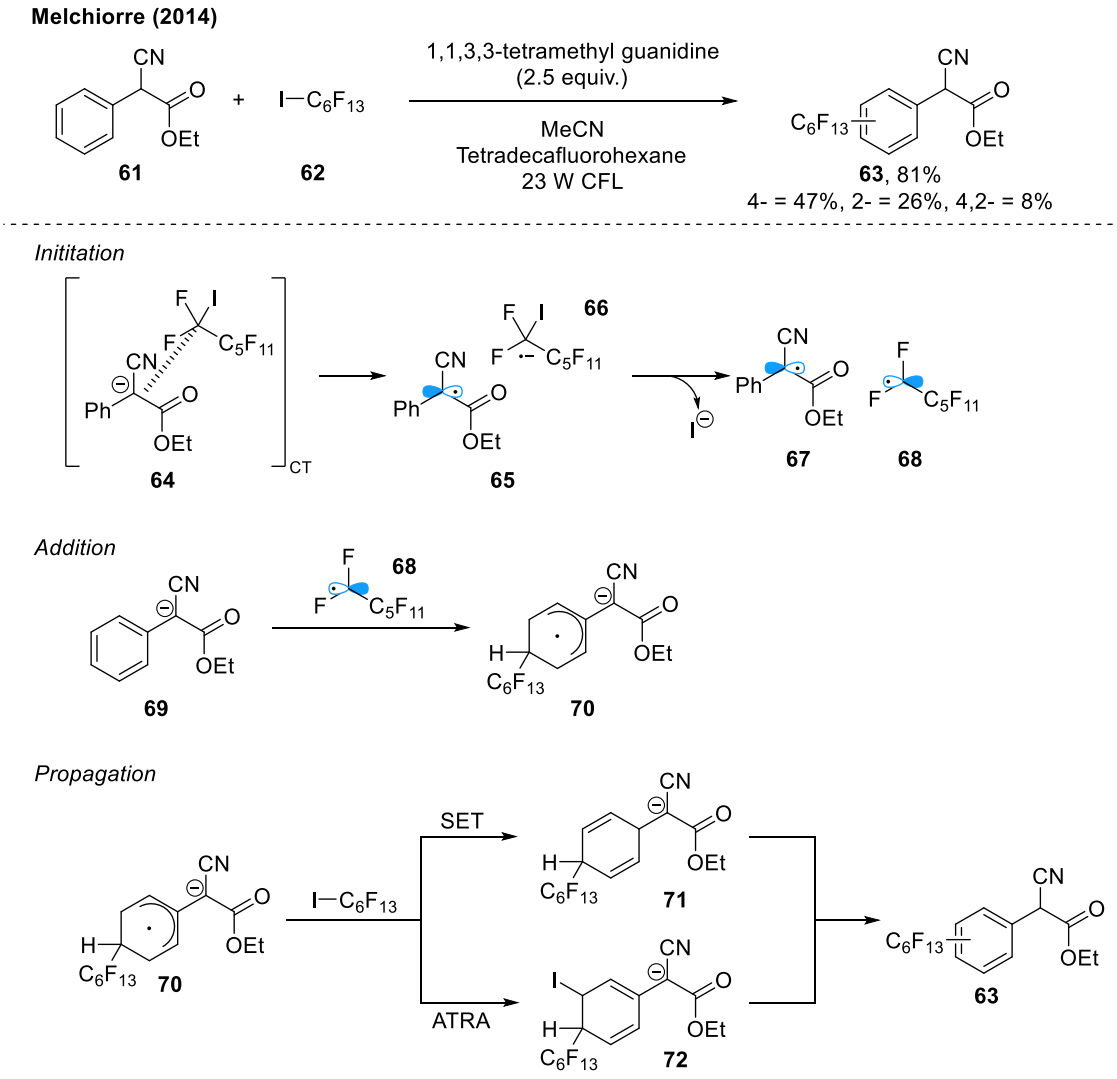

Scheme 10: Chain reaction for the perfluoroalkylation of aromatic rings

In 2014, Melchiorre used base to convert an electrophilic α-cyano ester **61** into an electron-rich enolate, which could act as a CT donor with perfluoroalkyl halide **62** (Scheme 10).[86,87] Instead of the expected α-trifluoromethylated product from radical recombination, surprisingly, the trifluoromethyl group was found to react with the aromatic ring, resulting in 4-, 2- and 4,2-substituted products (**63**, total yield = 81%). Upon radical initiation by CT complex **64**, fragmentation leads to radical pair **65**, **66** . An observed Φ > 1 and

mechanistic experiments showed that homolytic aromatic substitution occurs via radical addition to the aromatic ring. Chain propagation then occurs, either via single electron transfer with $C_6F_{13}I$ or atom transfer radical addition. Following this work, similar CT complexes between phenolate/perfluoroalkyl iodides,[88] hydrazones/perfluoroalkyl iodides,[89] and oxindolates/aromatic iodides have been reported.[90] An enantioselective variant has also been developed, using chiral quaternary ammonium salts as phase transfer catalysts.[91]

The potential for CT complexation to functionalize biologically relevant macromolecules was shown by Ragains in 2016, who initially discovered a photoredox catalyzed *O*-glycosylation reaction starting from thioglycoside **74** (Scheme 11).[92] The reaction was found to proceed without the photocatalyst, and DFT calculations found that a CT complex **75** between the electron-rich methoxystyrene and electron-poor Umemoto's reagent, was the likely source of radical formation. A putative mechanistic pathway started with SET via a CT complex, followed by in-cage radical recombination between the trifluoromethyl radical and the substrate benzylic radical. Intramolecular attack of the sulfur atom to the pendant carbocation would result in the formation of thioacetal **76**. The cyclic disulfide could also eliminate to form oxonium **77**. Both **76** and **77** were considered possible intermediates towards the *O*-glycosylated product **78**.

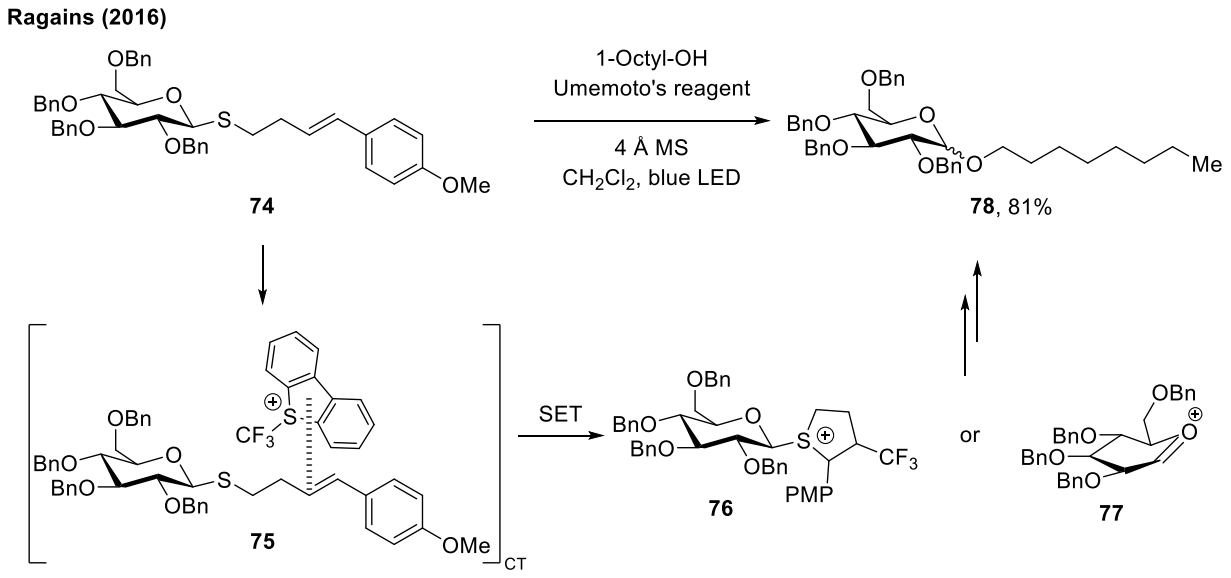

Scheme 11: Photoinduced glycosylation in biologically relevant systems

Miyake showed in 2017 that thiolate donors could form CT complexes with aryl bromide acceptors (**81**), generating an aryl bromide radical anion and thiyl radical (Scheme 12).[93] Upon mesolysis, radical recombination (**82**) was proposed to afford the C–S cross-coupling product **83**. Later, the same group showed that phenolates could engage in CT complexation with ethynylbenziodoxol(on)es to form iodovinyl phenyl ethers.[94]

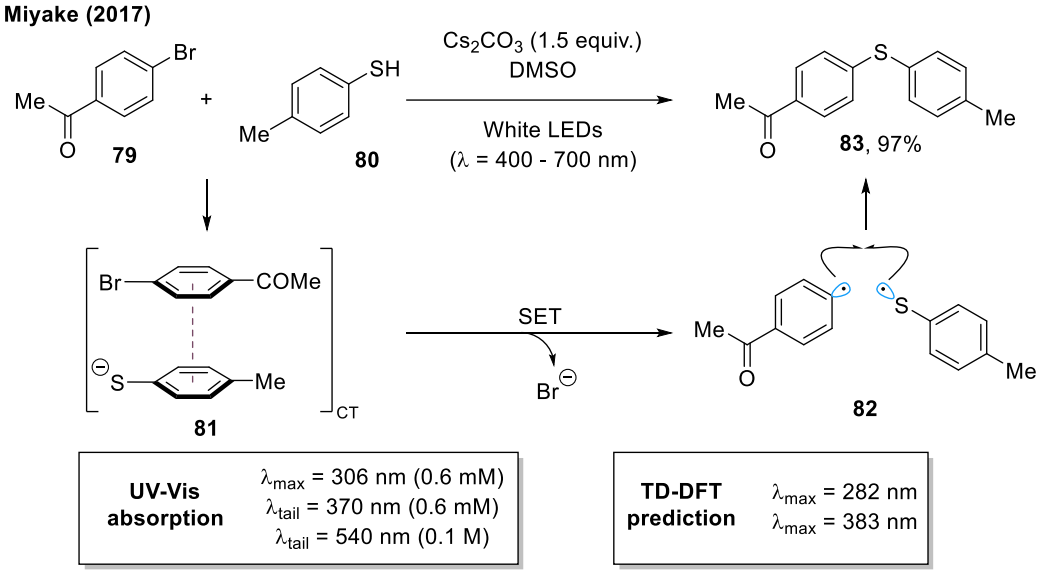

Scheme 12: Charge-transfer between aromatic bromides and thiolates

König has reported the mild C–H arylation of anilines utilizing CT complexation between aniline and bromothiophenes,[95] while Sundén has used the coordination of *N,N*-dimethylanilines and maleimides, to generate α-amino radicals.[96] Wang has also described the association of deprotonated aromatic sulfinic acid and isocyanobiphenyls.[97] Intramolecular CT complexation has also been achieved, for instance by Melchiorre, who designed a catalyst that could deliver an electron-rich carbazole in close proximity to a conjugated iminium,[98] and by Unsworth who achieved an intramolecular charge-transfer between an indole and a tethered ynone.[99]

Gilmour demonstrated in 2019 that phenyl ketoacids could complex to α,β-unsaturated iminium ions, generating radical pair **88** (Scheme 13).[100] Radical decarboxylation of the carboxyl radical moiety gave the acyl radical, which could then recombine with the previously generated benzyl radical (**89**), resulting in enamine **90**. Hydrolysis of the enamine then afforded aldehyde product **91**. Diphenyl conjugated secondary aldimines, such as **92**, have also been shown by Yu to be suitable CT acceptors, when associated with phenyl ketoacids (Scheme 14).[101] Yu demonstrated that aromatic ketoacids were most compatible, since non-aromatic ketoacids produced acyl radicals, but also alkyl radicals, through decarbonylation of the acyl radical. This led to complex and uncontrollable product distributions.

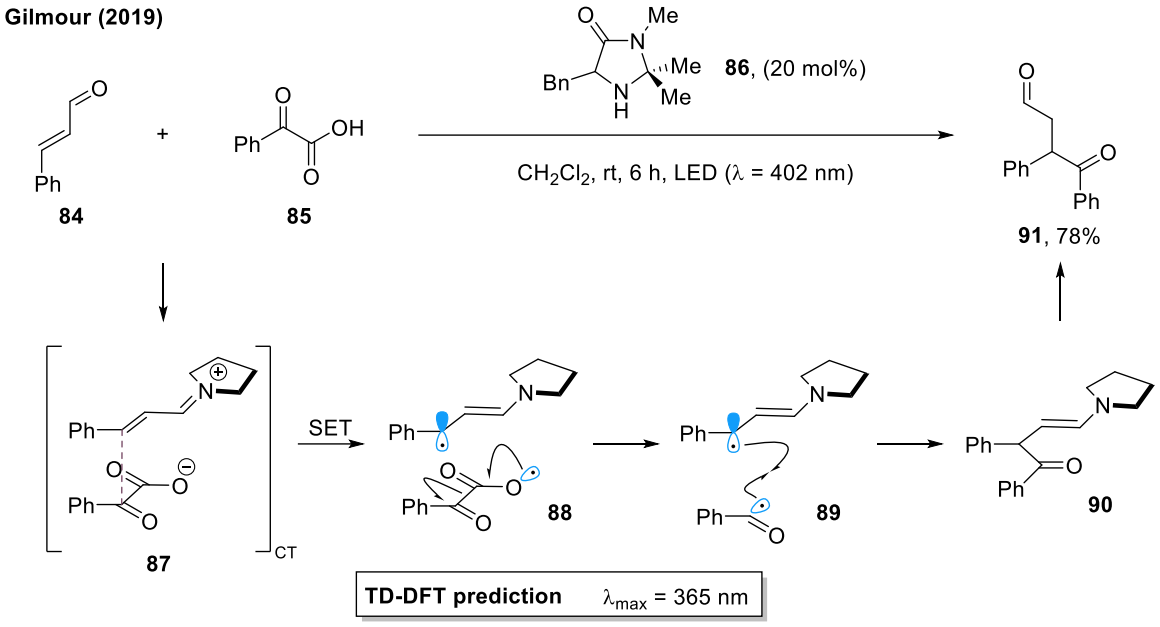

Scheme 13: Phenyl ketoacids as donors in charge-transfer complexes

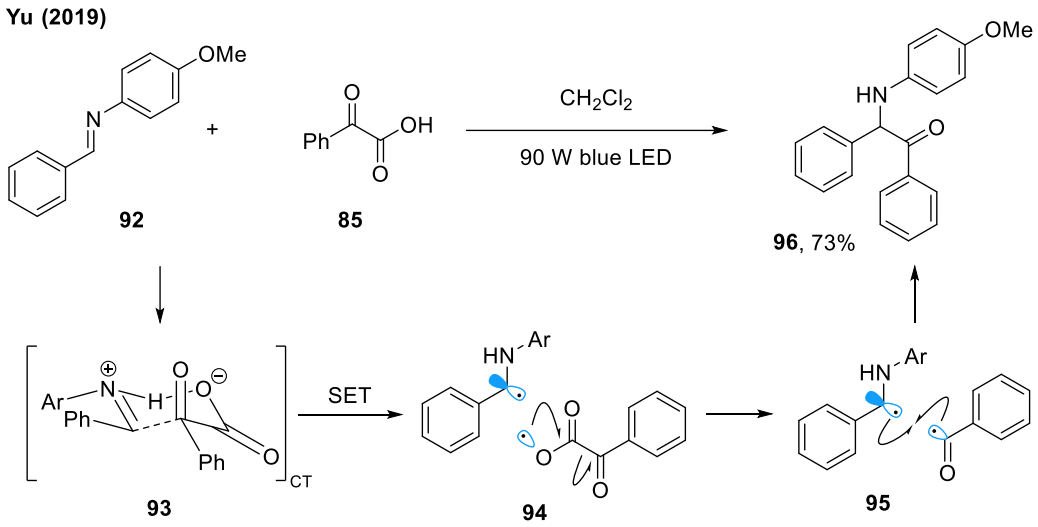

Scheme 14: Charge-transfer complex between aldimines and phenyl ketoacids

Finally, Chen has developed the radical addition of radical species (derived from trifluoroborates, boronic acids and dihydropyridines) to aromatic ketoacids (Scheme 15).[102] Boronic acid **97** could undergo radical addition to **98**, generating tertiary alcohol product **99** in 71% yield. The proposed mechanism envisaged that a CT complex **102** forms between boronic acid **100** and ketoacid **101**, generating alkyl radical **103** and initiating the reaction. Radical addition to activated boronic acid **104** leads to intermediate **105**, which undergoes homolytic cleavage to generate alkyl radical **103**, propagating the reaction. Boronic acid exchange followed by hydrolysis led to the product **109**.

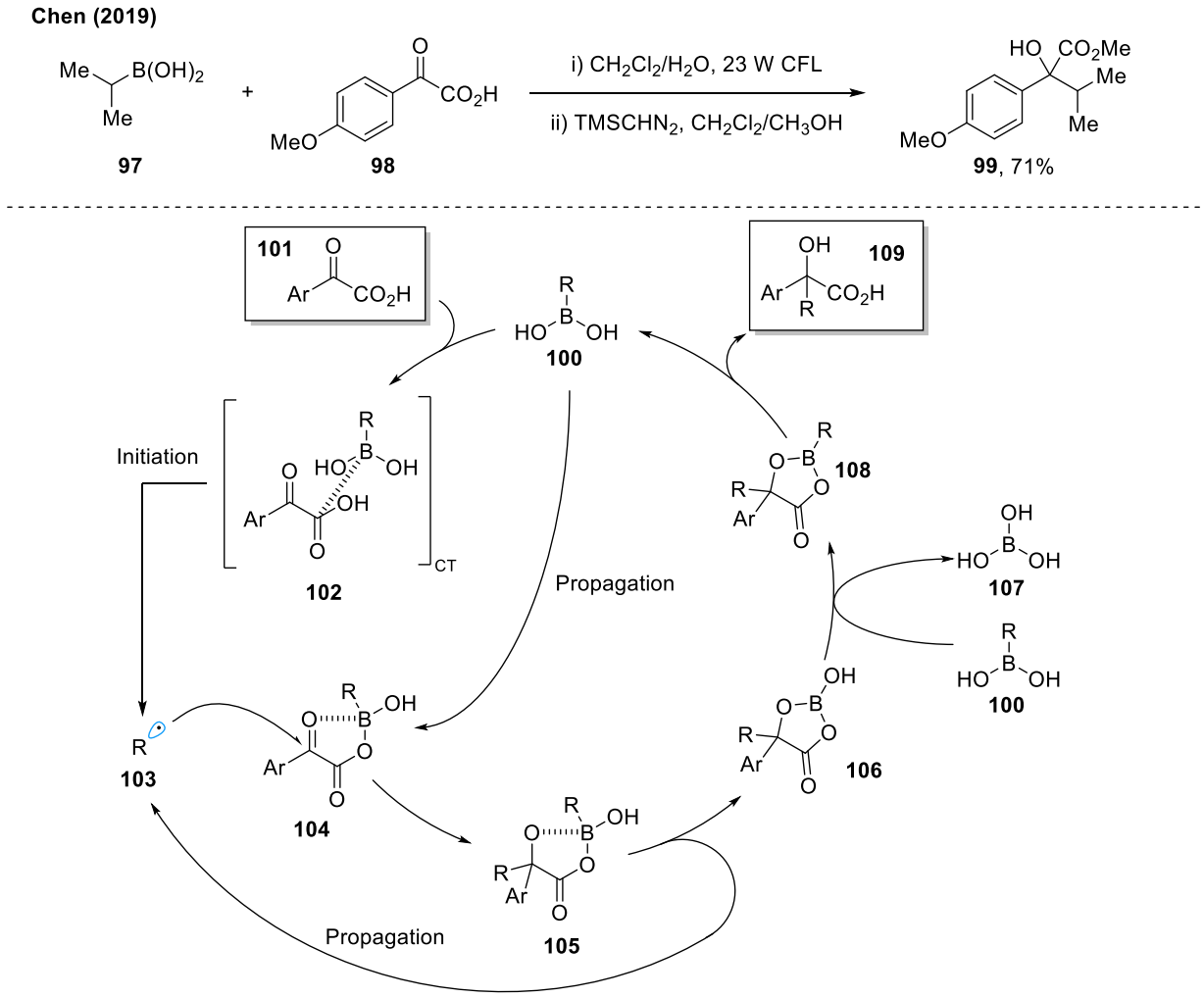

Scheme 15: Radical addition to activated aromatic ketoacids

1.4.2. Exogenous Charge-Transfer Partners

The preceding examples have focused on cases where the interacting components in the charge-transfer complex are ultimately incorporated into the product. This can sometimes restrict the range of compatible substrates, since it may be necessary for donor or acceptor components to be polarized, forcing certain functional groups to be present. One emerging method to overcome this is to use an exogenous CT component or CT auxiliary, which are geared towards CT complexation, but are subsequently not incorporated into the final product. For example, Jørgensen first showed in 2013 that tristrimethylsilylsilane (TTMSS) could reduce bromoacetophenone **110** to acetophenone **111**, without incorporating the TTMSS radical into the final product.[103] A radical cyclization was also conducted to generate **113** in 62% yield, and the role of TTMSS as a CT donor was further substantiated by Paixão in 2015.[104]

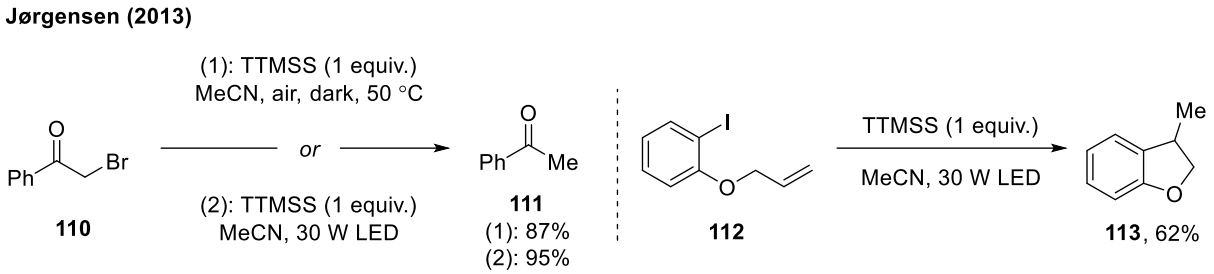

Scheme 16: Photoinduced radical reduction and cyclization using exogenous donors

Inspired by the use of 2,4-dinitrosubstituted aryl rings as CT complex acceptors, the Leonori group connected their oxime substrate to a dinitro-aryl CT auxiliary (**114**), that could associate with an exogenous triethylamine donor to form CT complex **115** (Scheme 17).[105] Electron transfer, followed by radical fragmentation of the aryl moiety successfully gave the *N*-centered radical **117**, which could cyclize onto the pendant alkene. The product **120** was proposed to occur via alkyl radical **118** attacking the NO_2 group of the phenoxide **119**, followed by N–O homolysis, then hydrogen atom transfer. Wu has also reported sulfinic acids to be compatible donors using this auxiliary strategy.[106]

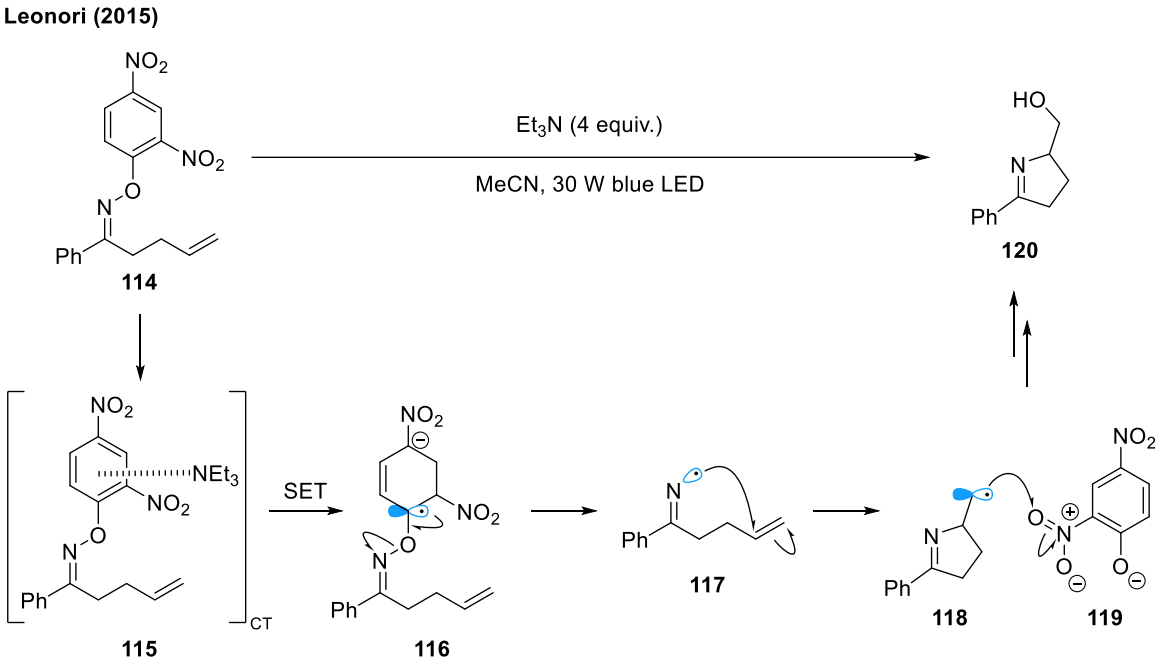

Scheme 17: Charge-transfer complexation between an auxiliary acceptor and exogenous donor

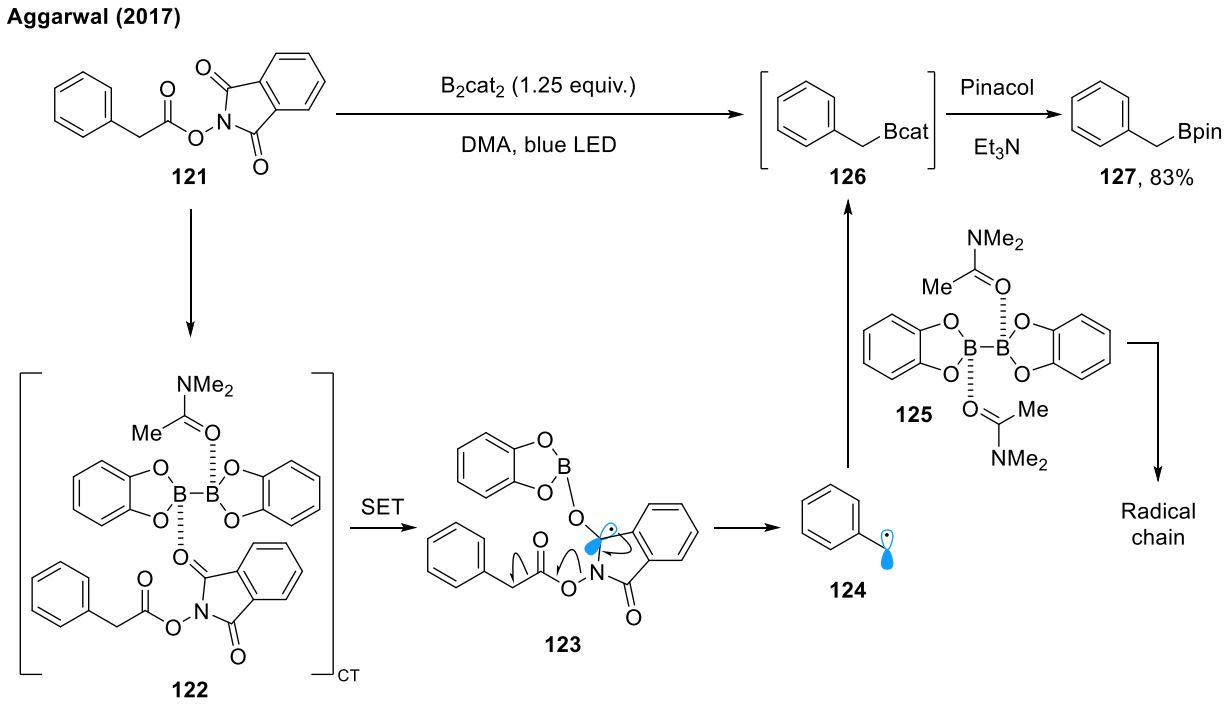

Scheme 18: Putative ternary complex enables electron transfer in borylation reaction

Since 2017, Aggarwal has studied the use of charge-transfer active auxiliaries to enable the reactivity of commonly found functional groups. They first reported the photoinduced decarboxylative borylation of carboxylic acids, starting with *N*-hydroxyphthalimide ester derivative **121** (Scheme 18).[107] It was found that the reaction had a strong dependence on the presence of DMA, and based on UV-vis absorption studies, a ternary CT complex involving *N*-hydroxyphthalimide, B_2cat_2 and DMA was proposed (**122**). Radical decarboxylation of **123** gave alkyl radical **124**, which reacted with DMA-ligated B_2cat_2 **125** to form boronic ester **126**, which was isolated as the pinacol boronic ester **127**. This indicated a radical chain process, with the CT complex SET acting as an initiation step. Glorius published a similar method in the same year using a putative pyridine-diboronate ester donor, complexing with redox-active esters acceptors.[108]

Meanwhile, Chen has conducted the CT complexation of *N*-alkoxyphthalimides and Hantzsch ester, to form radicals from alcohol derivatives.[109] Aggarwal later reported an alternative auxiliary for the deoxygenative borylation of alcohols,[110] and the use of *N*-alkylpyridinium salts for the deaminative borylation of amines.[111] Regarding the donor component, Hantzsch ester[112] and thioester[113] donors have also been used for deaminative transformations.

Furthermore, Fu disclosed in 2019 the activation of *N*-hydroxyphthalimide ester derivative **129** using a combination of catalytic triphenylphosphine and sodium iodide (Scheme 19).[114] Based on control and UV-vis absorption studies, a speculative CT complex involving these three components was proposed (**130**). Upon electron transfer and radical decarboxylation, a Minisci reaction could be carried out, to form **134** in 96% yield. As well as *N*-hydroxyphthalimides, *N*-alkylpyridinium salts and Togni's reagent could also be used to generate radicals via similar CT complexes, showcasing the potential to replace traditional photocatalysts in several

different scenarios. Bach also recently reported the activation of tetrachlorophthalimide esters using a catalytic quinuclidine donor, which could act as a CT reductant and a ground-state oxidant in the reaction.[115]

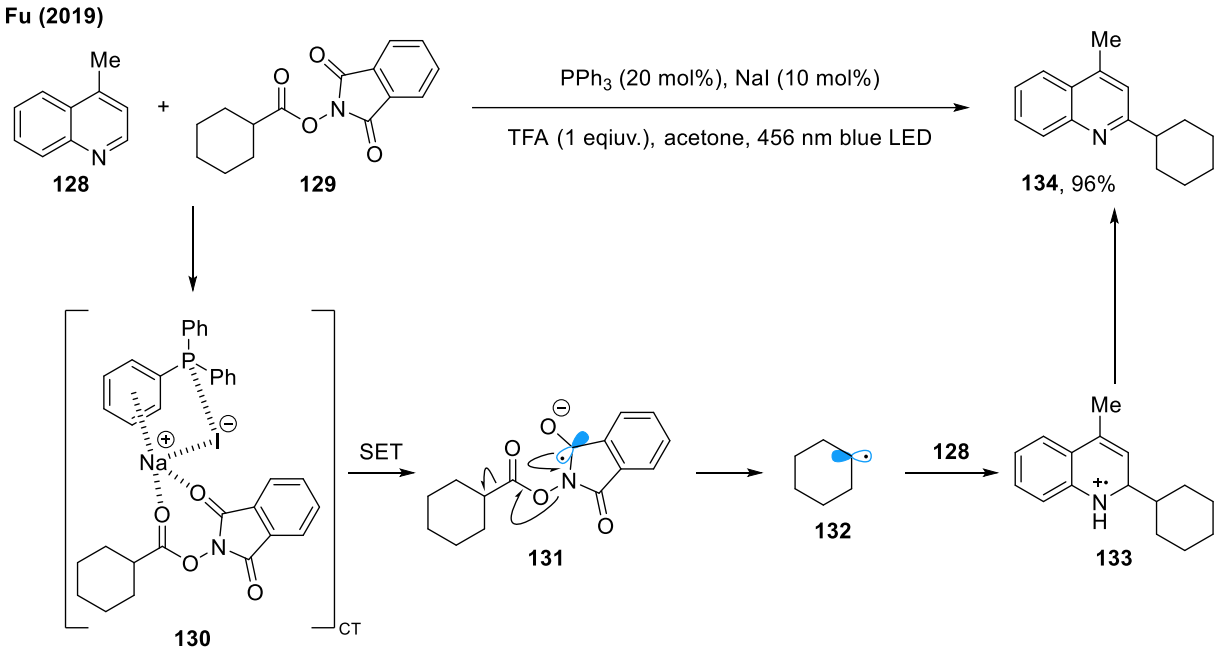

Scheme 19: 'Catalytic' reaction activation via a putative charge transfer complex

Finally, the utility of CT complexes has been extended to biocatalysis to achieve stereoselective radical processes. In their first report in 2016, Hyster demonstrated the enantioselective dehalogenation of α-bromo lactones using a photobiocatalytic system with nicotinamide-dependent ketoreductases (KREDs) (Scheme 20).[116] In their mechanistic proposal, the NAD(P)H cofactor is bound to the enzyme active site (green oval in scheme) and inclusion of α-bromo lactone **135** into the active site forms putative complex **136**. Based on absorbance measurements, the enzyme was proposed to be essential in enabling a CT complex to form between the two components. Electron transfer generates radical ion pair **137**, which undergoes mesolysis to form radical pair **138**. Hydrogen atom transfer then occurs in the chiral environment, providing the enantioenriched product **140**. The deactivated cofactor can then be regenerated using isopropyl alcohol and enzymatic processes. Following these findings, the Hyster laboratory also reported the enantioselective hydroalkylation of alkenes using a similar strategy with flavoenzymes.[117] These examples highlight the potential to selectively enable charge-transfer complexation within an enzyme pocket.

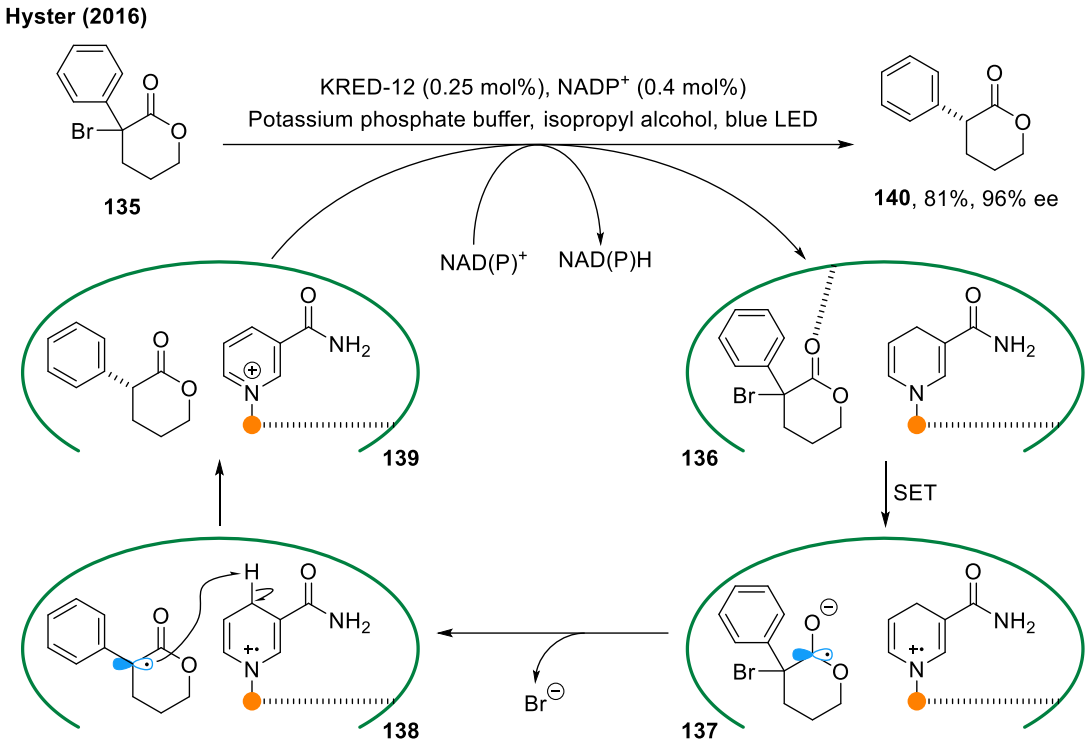

Scheme 20: Enzyme mediated charge-transfer complexation

1.4.3. Direct Substrate Excitation

The use of visible light to directly photoexcite organic molecules is relatively difficult since most molecules typically only absorb light in the UV region. One method for the direct irradiation of molecules has been to append visible light absorbing chromophores to the substrate. Pioneering work by Barton in 1962 established *S*-acyl xanthates as photoactive species, which could be irradiated with visible light (Scheme 21).[118,119] These compounds have an absorption band at around 400 nm, resulting in a distinctive yellow color. Light from a tungsten lamp was used to effect photoexcitation of *S*-acyl xanthate **141** to **142**, followed by fragmentation of the relatively weak C–S bond, to generate acyl radical **144**. This radical underwent further decarbonylation to give alkyl radical **145**, which then recombined with the initial xanthate radical **143** to form xanthates. Finally, alkaline hydrolysis led to formation of thiol **147** in 97% yield. Although the related alkyl xanthates cannot absorb visible light, the addition of catalytic *S*-acyl xanthate could initiate a radical chain process that could enable radical reactivity for alkyl xanthates.[120] A wide variety of transformations, initiated by the visible light irradiation of xanthates, have since been reported.[121]

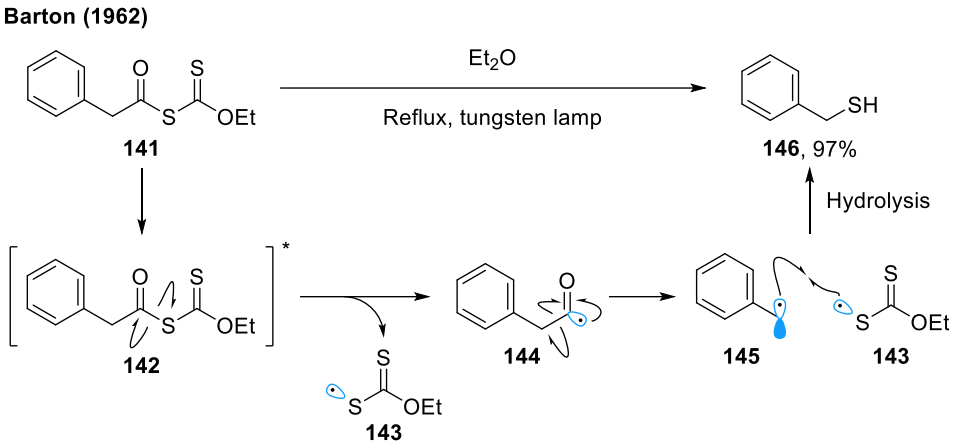

Scheme 21: Direct visible light photoexcitation of *S*-acylxanthates

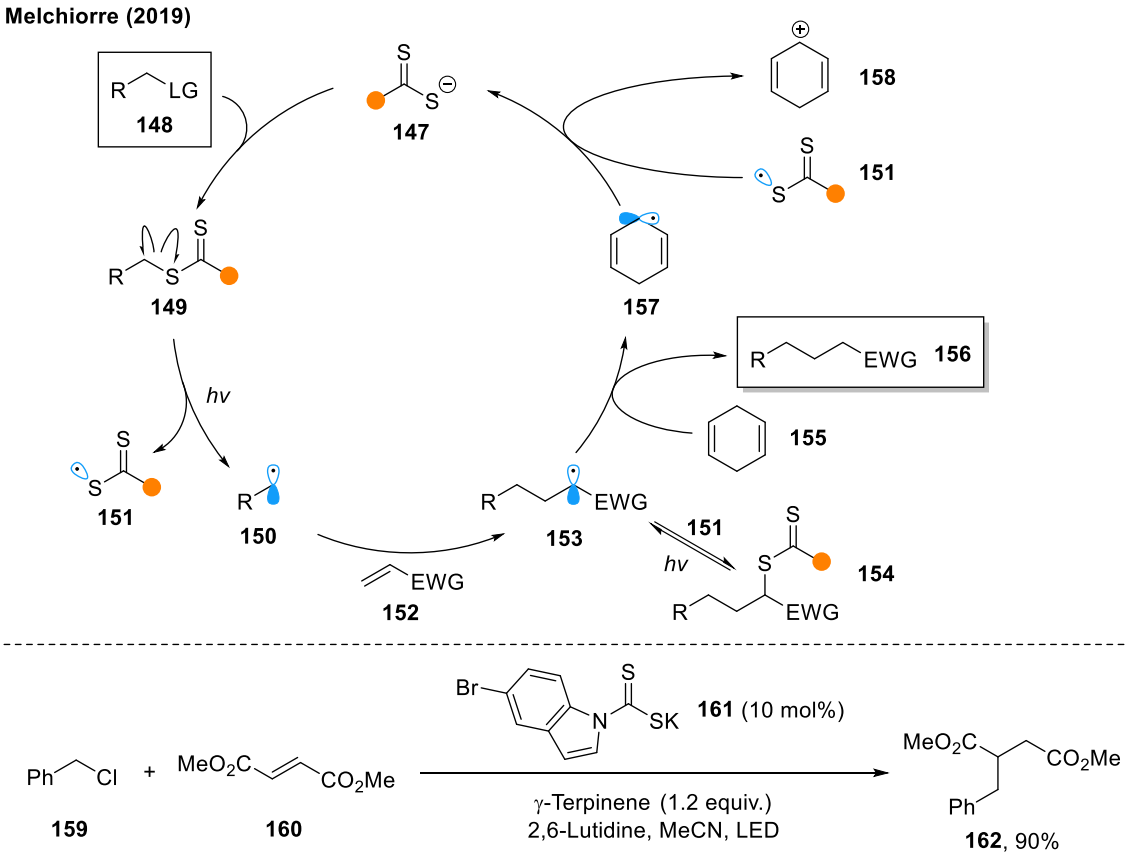

Scheme 22: Catalytic generation of photoactive dithiocarbamates

These methods greatly expanded the availability of radical species using visible light, however they still relied on stoichiometric quantities of pre-functionalized xanthates. They also often resulted in the inclusion of xanthate in the final product. Melchiorre recently investigated a strategy involving the catalytic generation of photoactive dithiocarbamate substrates from alkyl electrophiles (Scheme 22).[122] In their proposed mechanistic cycle, the dithiocarbamate catalyst **147** performs nucleophilic substitution on the alkyl halide substrate **148**, generating photoactive dithiocarbamate **149**. Upon visible light irradiation, the C–S bond is cleaved and alkyl

radical **150** undergoes radical addition with an electrophilic radical acceptor **152**, generating radical **153**. Although this radical can be trapped by dithiocarbamate radical **151** to form **154**, the C–S bond of **154** can also be photochemically cleaved. Eventually, hydrogen atom transfer between **153** and cyclohexadiene **155** affords product **156**. This strategy was used to functionalize benzyl chloride **159** to **162** in 90% yield and was compatible with a wide range of electrophilic precursors.

Finally, it is important to differentiate whether a photochemical process is occurring due to charge-transfer complexation, or direct band irradiation. This was encountered by Melchiorre, following their work on the charge-transfer α-alkylation of aldehydes. In their original work, it was concluded that enamine **49** and electron-deficient aromatic species **50** form CT complex **53** (Scheme 23a).[80] Subsequently, a study was conducted on the reactivity of enamine **49** and diethyl bromomalonate **164** (Scheme 23b).[123] In this case, no charge-transfer band was observed upon mixing the reaction components. The authors concluded that in the absence of suitable CT properties on acceptor **164**, enamine **49** could absorb visible light directly.[124] Upon photoexcitation to **167**, collision with ground-state **164** could induce electron transfer, generating radical ion pair **168**. The Melchiorre group have demonstrated further examples of direct photoexcitation with visible light, including the formation of radicals using phenols[125] and conjugated iminium ions.[126]

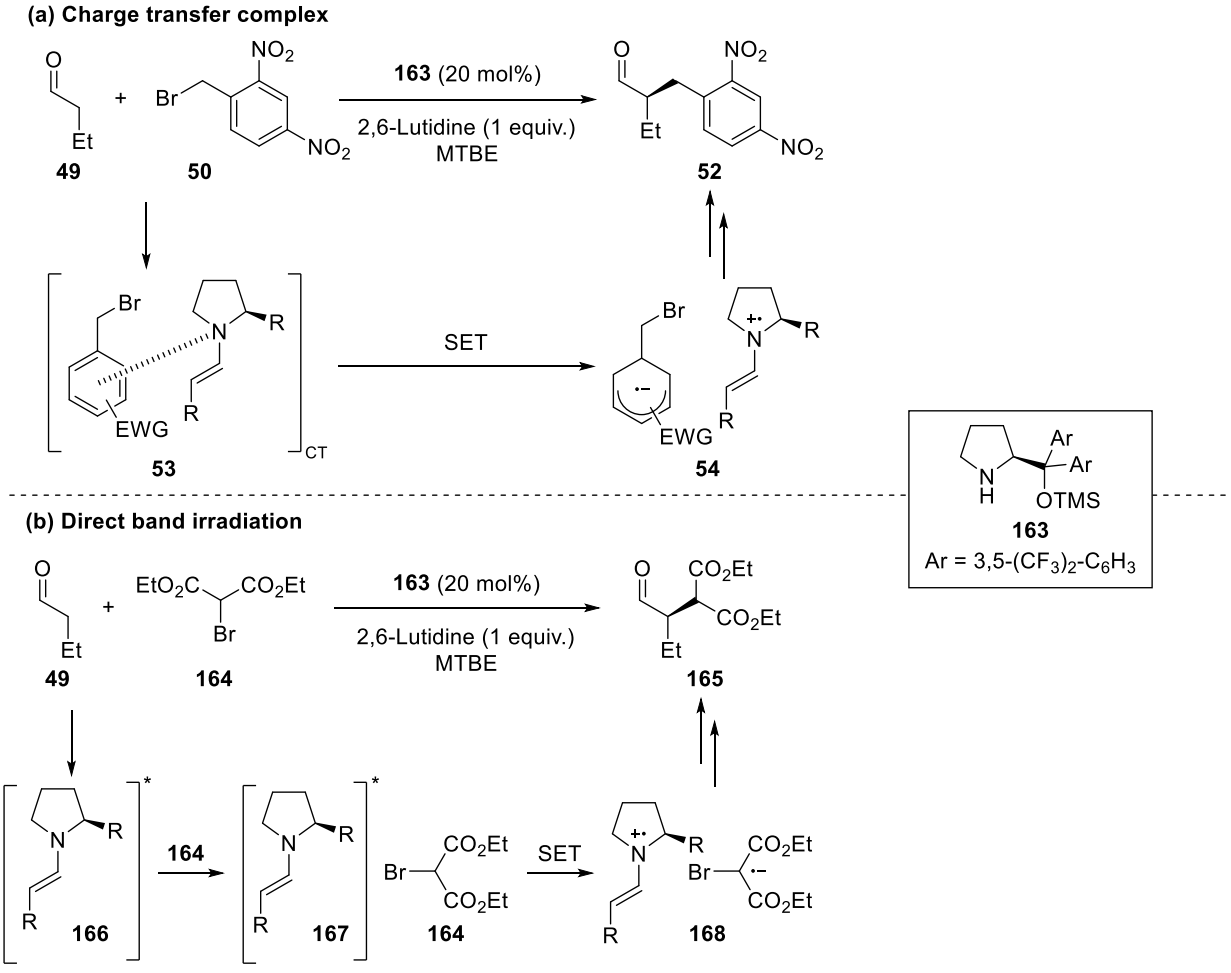

Scheme 23: Enamine can undergo charge-transfer complexation and direct photoexcitation with visible light

1.5. Summary

Over the last decade, the photochemistry of charge-transfer complexes has enabled new opportunities in synthetic radical chemistry. Starting with the association of electronically polarized substrates, more general platforms are being developed, which allow radical generation under very mild conditions, and increase the potential for chemoselective and stereoselective transformations. The use of catalytic and exogenous charge-transfer reactants has been enabling in opening a wider range of organic substrates to undergo photoinduced activation.

Catalyst-free processes via charge-transfer complexes can be complementary to photoredox catalysis, for instance, when advanced intermediates have several oxidizable/reducible functionalities, which the photocatalyst may target indiscriminately. Large-scale syntheses may prefer to employ catalyst-free conditions, since photocatalysts are often based on complexes of expensive precious metals such as iridium. Charge-transfer strategies may offer opportunities for the mild derivatization of biological targets (e.g. bioconjugation), by avoiding the use of traditional metal photocatalysts. The following chapters will describe our investigations into novel photoinduced methods, which are proposed to occur via (exogenous) charge-transfer complex processes.

2. Generation of α-Amino Radicals via a Charge-Transfer Complex

2.1. Strategies for Aliphatic Amine Synthesis

Aliphatic amines are defined as molecules where only hydrogen or alkyl substituents are connected to the nitrogen atom.[127] They range from primary amines (two hydrogens and one alkyl group), with increasing order upon alkyl substitution, up to quaternary ammoniums (four alkyl groups). The amine group has hydrogen bond donor and acceptor properties, making them critically important for the interaction between drugs and biological targets of interest such as proteins and enzymes. At the same time, amines can modulate basicity, lipophilicity, and solubility, to ensure favorable uptake by the body. Consequently, the aliphatic amine functionality is present in over 40% of small molecule drugs, with other applications in detergents, emulsifiers, fine chemicals and crop protection.[128]

Aliphatic amine synthesis can be broadly split into three methods (Figure 11). The first method involves synthesis of the aliphatic amine scaffold, which uses lower order amine feedstocks to synthesize higher order amines via C–N bond formation. Archetypal methods here include C–N alkylation,[129,130] hydroamination[131–135] and reductive amination.[136–138] Other methods include carbene N–H insertion,[139] transition metal catalyzed allylic amination[140–142], and functionalization (e.g. acylation/cyanation/azidation), followed by reduction to the amine.[143–145] The second method involves post-functionalization strategies, which take an existing amine backbone, and uses the amine functionality to direct reactivity onto the carbon chain. This includes transition metal-catalyzed cyclometallation followed by functionalization,[146–148] radical generation on the carbon chain,[149] or carbenoid insertion.[150] The final method of amine synthesis could be considered a combination of the two, increasing the order of alkylation whilst introducing further functionalization. Examples include the Mannich[151], Strecker[152] or Petasis[153] reactions among others,[154] which are thought to involve condensation of a secondary amine with a carbonyl species to form an iminium ion, which then undergoes addition, to generate a tertiary amine.

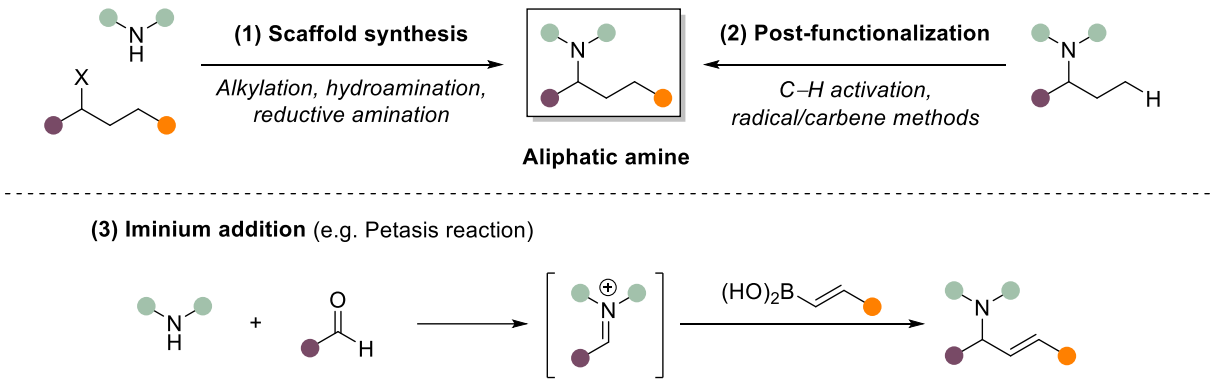

Figure 11: Strategies for aliphatic amine synthesis

More recently, the generation of α-amino radicals has become an effective alternative for the multicomponent construction of aliphatic amines.[155] Starting with a primary, secondary or tertiary amine, many methods to

generate these radicals have been developed, opening up previously inaccessible reactivity pathways. Formation of α-amino radicals has been approached in three broad ways (Figure 12). Hydrogen atom abstraction of the α-hydrogen of a tertiary amine **169** can form α-amino radical **170**, enabling C–H functionalization of a previously unreactive α-nitrogen center. Another method of generation is via oxidation of amine **169**, followed by deprotonation. Finally, the α-amino radical can be generated via single-electron reduction of an iminium ion **171**, originating from condensation between a secondary amine and an aldehyde.

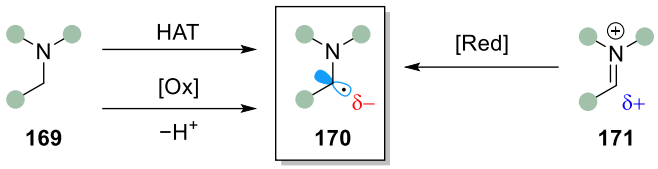

Figure 12: General methods of generating an α-amino radical

The generated α-amino radical is relatively nucleophilic in character, thus showing good reactivity with electrophilic species. This nucleophilicity is attributed to the delocalization of the α-amino radical with the adjacent nitrogen lone pair.[156] This predicts that two of the electrons will be in a bonding orbital, with the third in an energetically close antibonding orbital (three-electron bond). These MO interactions are also the basis of why α-amino radicals are relatively stabilized, with stabilization increasing with greater degree of *N*-alkylation. The nucleophilic character therefore offers complementary reactivity to the precursor iminium ion, which is electrophilic in nature.

2.1.1. Methods to Generate α-Amino Radicals

Over several decades there has been a wealth of reported methods for α-amino radical formation, and advancements in the field have been widely reviewed.[155,157–161] In summary, one could categorize the field into three general methods of generation:

i. Homolytic cleavage of α-amino C–X bond
ii. Single-electron oxidation of amine
iii. Single-electron reduction on imine

Homolytic cleavage of α-amino C–X bond

The earliest example of α-amino radical formation could be attributed to Urry in 1952,[162] who used peroxide and heat to abstract a hydrogen atom from the α-position in piperidine. One pitfall of this method is that multiple C–H bonds adjacent to the nitrogen will have similar bond enthalpies, resulting in a mixture of radicals being potentially formed. Therefore, regioselectivity must be controlled by substrate design (e.g. using symmetrical amines) or by blocking the other undesired α-positions. For instance, MacMillan utilized a symmetrical *N*-Boc protected pyrrolidine **172**, in conjunction with photoredox catalysis and a quinuclidine additive, to abstract the α-hydrogen atom of **174** (Scheme 24).[163] This generated radical intermediate **176**,

which could participate in a nickel catalytic cycle, by reaction with in situ generated complex **177**. Upon formation of **178**, reductive elimination was proposed to form the arylated amide product **179**.

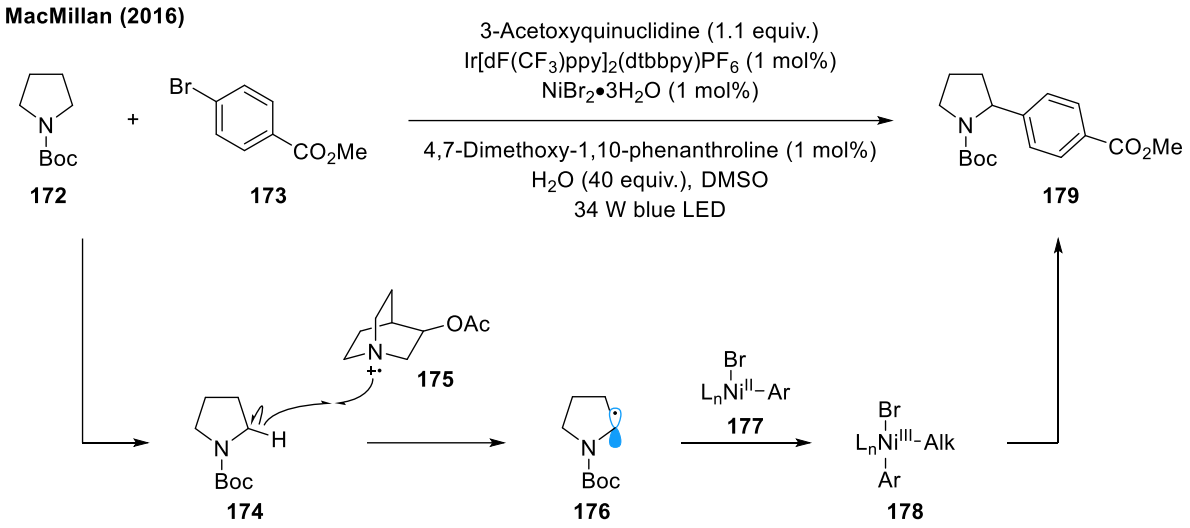

Scheme 24: Hydrogen atom abstraction to generate α-amido radical

Another method of controlling regioselectivity is to pre-functionalize the starting materials. Homolytic methods using α-heteroatom amides as precursors to α-amido radicals, using tributyltin hydride, was first developed by Bachi in 1981.[164–167] This was inspired by prior studies on the reduction of selenides[168] and sulfides[169] with tributyltin hydride, via a homolytic cleavage mechanism. This method of radical formation was extended by Padwa in 1983 for the generation of α-amino radicals from thioaminals (Scheme 25).[170] Heating of AIBN and Bu_3SnH generated tributyl tin radicals, which could induce homolytic cleavage of the C–S bond, favored by the strength of the generated Sn–S bond. α-Amino radical **181** was envisaged to cyclize onto the pendant alkene, generating pyrrolidine **183**. However, only the direct reduction product **182** was observed, resulting from hydrogen atom transfer with tributyl tin hydride. Later reported methods have continued to use tributyl tin hydride or tris(trimethylsilyl)silane, AIBN and stirring at 80 °C to form radicals via homolytic cleavage.[171,172]

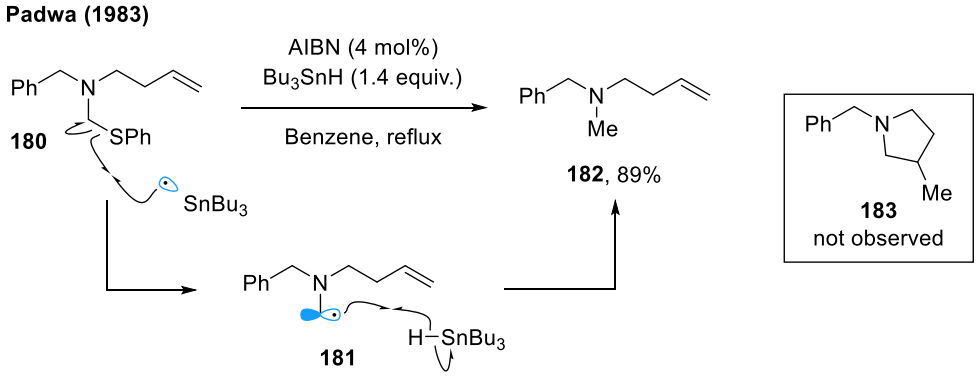

Scheme 25: Homolytic cleave of heteroatomic bonds for α-amino radical formation

Single-electron oxidation

Another method to generate an α-amino radical from the existing amine scaffold is to carry out one-electron oxidation of amine **184**, to give aminium radical cation **185** (Scheme 26). This greatly acidifies the neighboring α-hydrogen atom, and ensuing deprotonation gives α-amino radical **186**.[173] The oxidative process has been achieved in a number of way, for instance with one-electron oxidants,[174] and through electrochemistry[175] and photochemistry by UV irradiation.[157]

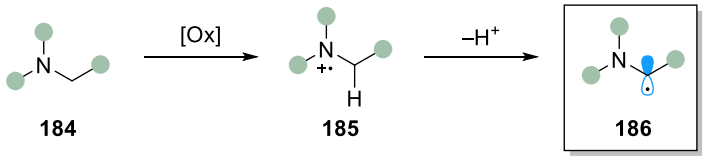

Scheme 26: Oxidative method of α-amino radical formation

A potential pitfall of this method is that the regioselectivity of the deprotonation step must be controlled. One solution was studied by Mariano, Davidson among others, through the use pre-functionalized amine substrates, which have α-fragmentation patterns that are surrogates of α-deprotonation (Scheme 27). Initially, oxidation of the amine substrate (**187**, **188**, **189**) generates the corresponding aminium radical cation (**190**, **191**, **192**). Then, α-desilylation,[176] α-decarboxylation[177] and other fragmentation processes[178] can occur, to generate α-amino radical **194** with regioselective control.

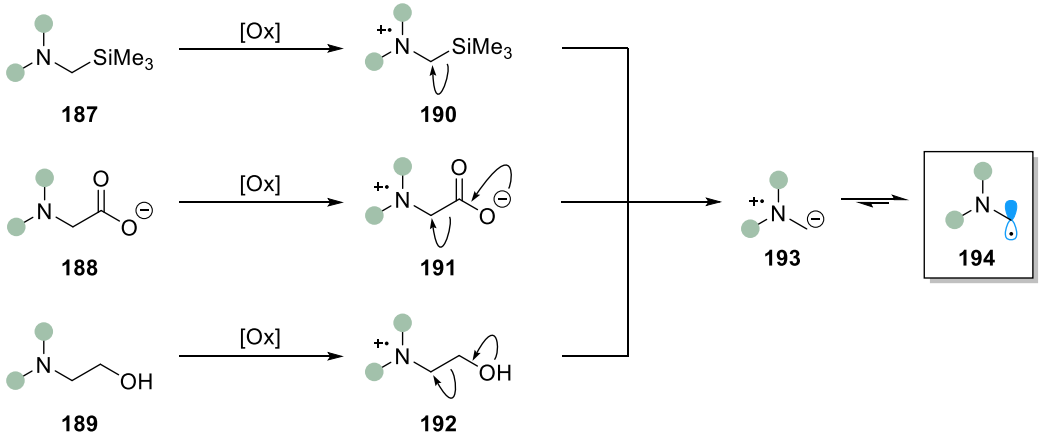

Scheme 27: Regioselective methods of α-amino radical formation

Recently, visible light mediated photocatalysis has greatly facilitated the formation and manipulation of radical species. The oxidative method of generating α-amino radicals described above, was first translated to photocatalysis by Stephenson in 2010. The group used an iridium photocatalyst to oxidize the amine to the aminium radical cation, followed by deprotonation to α-amino radical **196** (Scheme 28).[179] **196** is relatively reducing, and is prone to further oxidation to iminium ion **197**, which reacts with the nitronate anion to give **198**. In this case, it was thought that adventitious oxygen or nitromethane acted as the terminal oxidant to regenerate the photocatalyst. Many reports using this methodology have been disclosed, highlighting the wide breadth of possible photocatalytic transformations.[180–183]

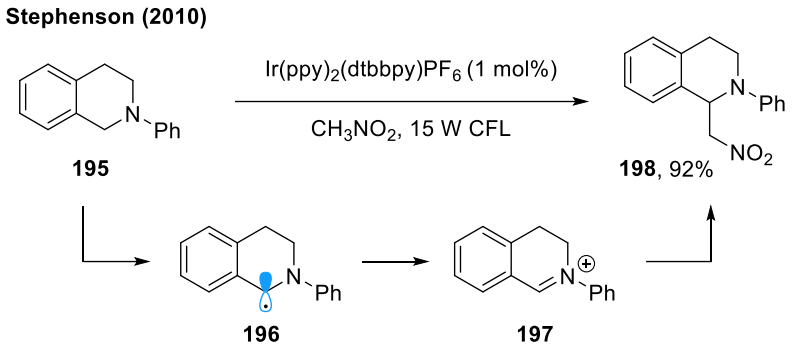

Scheme 28: Photocatalytic oxidation to generate α-amino radicals

Furthermore, photocatalytic variants of regioselective α-amino and α-amido radical formation have been reported. Using similar precursors to those shown in Scheme 27, photocatalysis has been used for substrate oxidation, followed by desilylation or decarboxylation processes.[184]

Single-electron reduction

Reductive methods typically involve the single-electron reduction of iminium and imine substrates to generate the α-amino radical. (Scheme 29). Beginning in 1983, Kunai reported the electrochemical reduction of isolable tetra-substituted iminium salt **199**, utilizing the generated α-amino radicals in Giese reactions.[185] Martin showed that strong stoichiometric reductants such as SmI_2 could also be employed to reduce similar substituted iminium ions (**200**).[186] Later, it was shown by Enholm and Nishimura that aldimines (**202**) could be reduced to the corresponding radical.[187,188] Finally, instead of using isolable tetra-substituted iminium salts, Aurrecoechea showed that alkyliminiums could be reduced by using α-aminobenzotriazoles (**204**) as in situ precursors of iminium ions, thus preventing undesired reduction of the aldehyde starting material by SmI_2.[189]

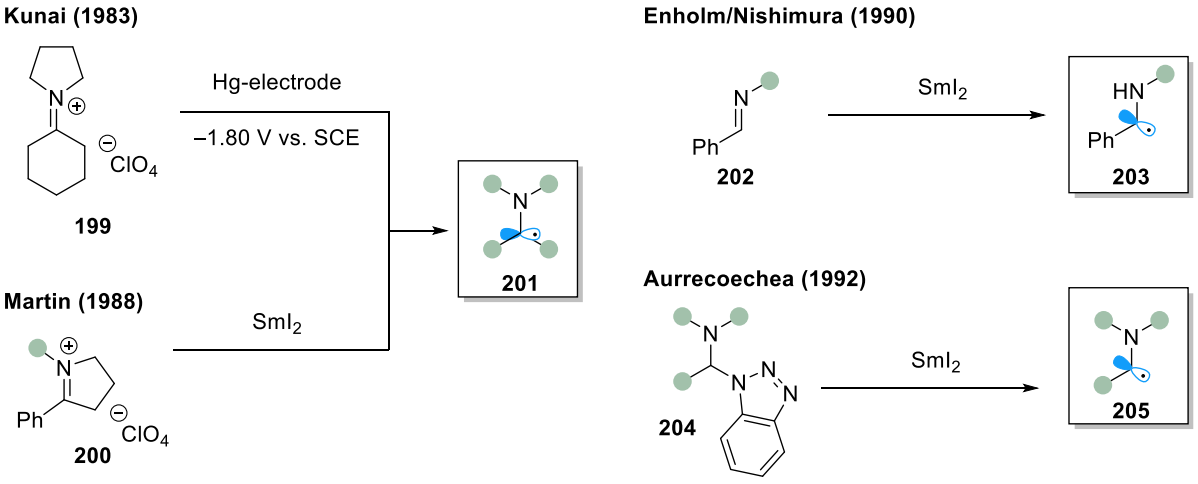

Scheme 29: Reductive methods of α-amino radical formation

The photochemical single-electron reduction of iminium ion salts was studied during the 1970s and 80s, particularly by Mariano.[190,191] The iminium ion possesses one photochemical transition, between the C=N π-π* orbitals, which occurs in the UV region. For instance, alkyl-substituted (**206**), *C*-phenyl conjugated (**207**),

and hydroxy-vinyl (**208**) substituted iminium salts have absorptions at λ_{max} = 222 nm, 275 nm and 317 nm respectively (Scheme 30a). The presence of the iminium positive charge significantly lowers the HOMO and LUMO energies, in comparison to ethene. The relatively low lying LUMO of iminium salts thus facilitates the process of single-electron reduction to give the α-amino radical. UV irradiation from a medium-pressure mercury lamp could excite conjugated iminiums, which could be quenched by electron-rich donors, such as olefins, arenes and alcohols.[192] A report by Mariano showed that irradiation of iminium salt **209**, led to exciplex-mediated electron transfer with **212**, generating radical pair **213** and **214**. Radical-radical recombination and quenching with methanol gave **215** in 81% yield (Scheme 30b).[193]

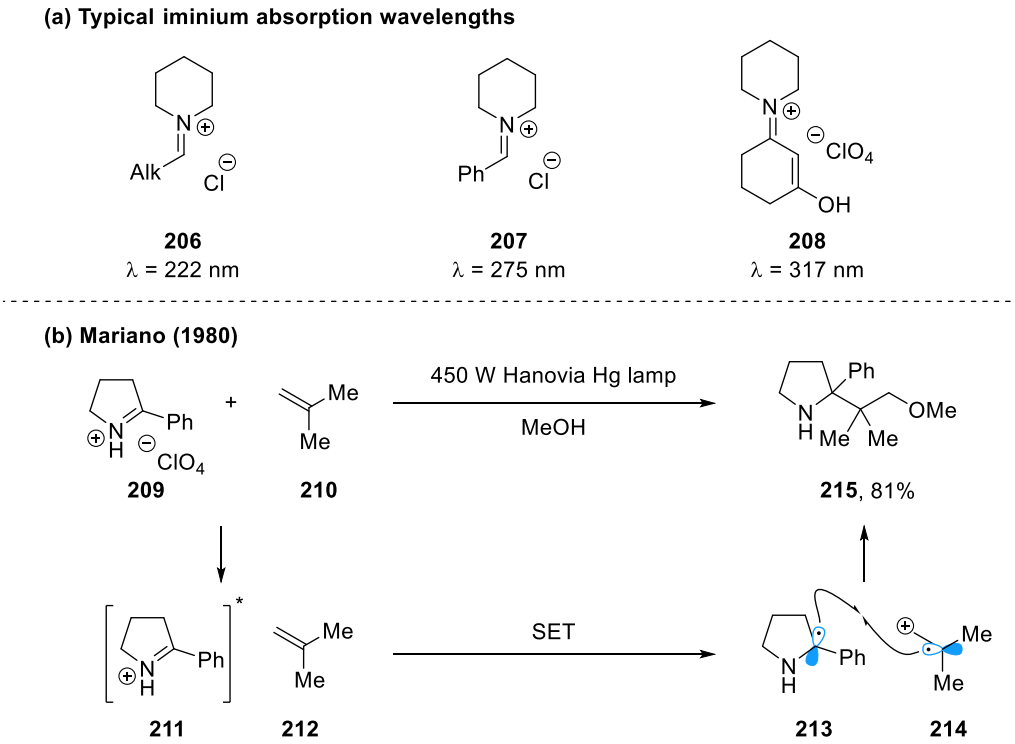

Scheme 30: Using UV irradiation for the reduction of iminium ions

The reduction of aromatic aldimines (**216**) using photoredox catalysis was first reported in 2014 by MacMillan (Scheme 31),[194] among other groups.[195–199] The process was not extended beyond aromatic aldimines until 2018 where Wenger utilized in situ generated aliphatic aldimines and ketimine intermediates (**218)**, in a radical reductive amination reaction.[200] Later that year, Gaunt reported the single electron reduction of aliphatic iminium ions derived from secondary amines and aldehydes, extending the reactivity of the generated α-amino radicals to Giese additions.[201]

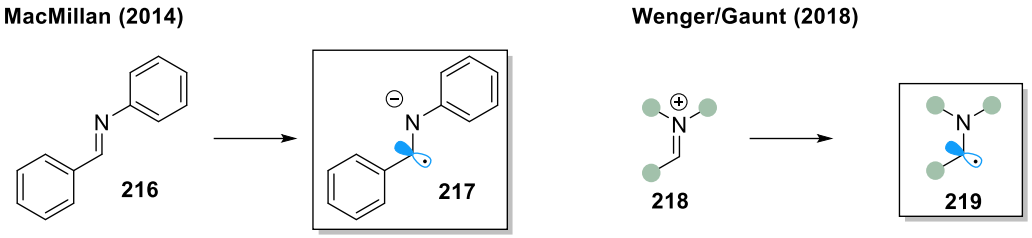

Scheme 31: Photocatalytic reduction to generate α-amino radicals

Finally, charge-transfer complexation has been used for the reduction of iminium ions. Melchiorre[98] and Gilmour[100] have reported recently the charge-transfer reduction of α,β-unsaturated iminium ions to highly stabilized radicals, described earlier in Chapter 1. In these cases, the radical was found to react exclusively at the β-amino position, instead of the α-amino position. Charge-transfer mediated α-amino radical formation was reported by Yu in 2019, who described the complexation between preformed aromatic aldimines (**92**) and α-keto acids (**85**), via a putative cyclic transition state **93**, to generate benzylic α-amino radical **220** (Scheme 32).[202]

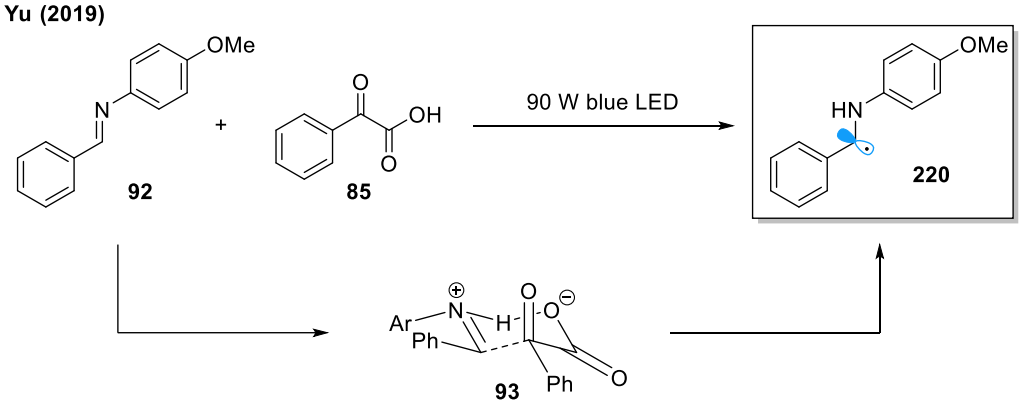

Scheme 32: Generation of α-amino radical by a charge-transfer complex

The resurgence of visible light mediated photoredox catalysis and charge-transfer chemistry has greatly facilitated the mild generation and manipulation of radical intermediates. By avoiding the use of typically harsher, stoichiometric oxidants and reductants, these fields of photochemistry have provided significant advantages in widening the scope of possible transformations for α-amino radicals. Charge-transfer manifolds have the potential to exhibit high selectivity due to the bespoke interactions between donor and acceptor molecules. Hence, the development of further methods of charge-transfer activation, would be a natural progression in the field of α-amino radical generation.

2.2. Project Aims

In 2018, the Gaunt group demonstrated the single-electron reduction of alkyliminium ions, generated by the condensation of secondary amines and aldehydes (Scheme 33).[201] The photoredox catalyst $Ir(ppy)_3$ and Hantzsch ester were used, to generate the reductive conditions necessary for the single-electron reduction of alkyliminiums. The generated α-amino radicals were intercepted by electron-poor and highly stabilizing alkene acceptors, such as butyl acrylate, to form tertiary amines in a concise fashion.

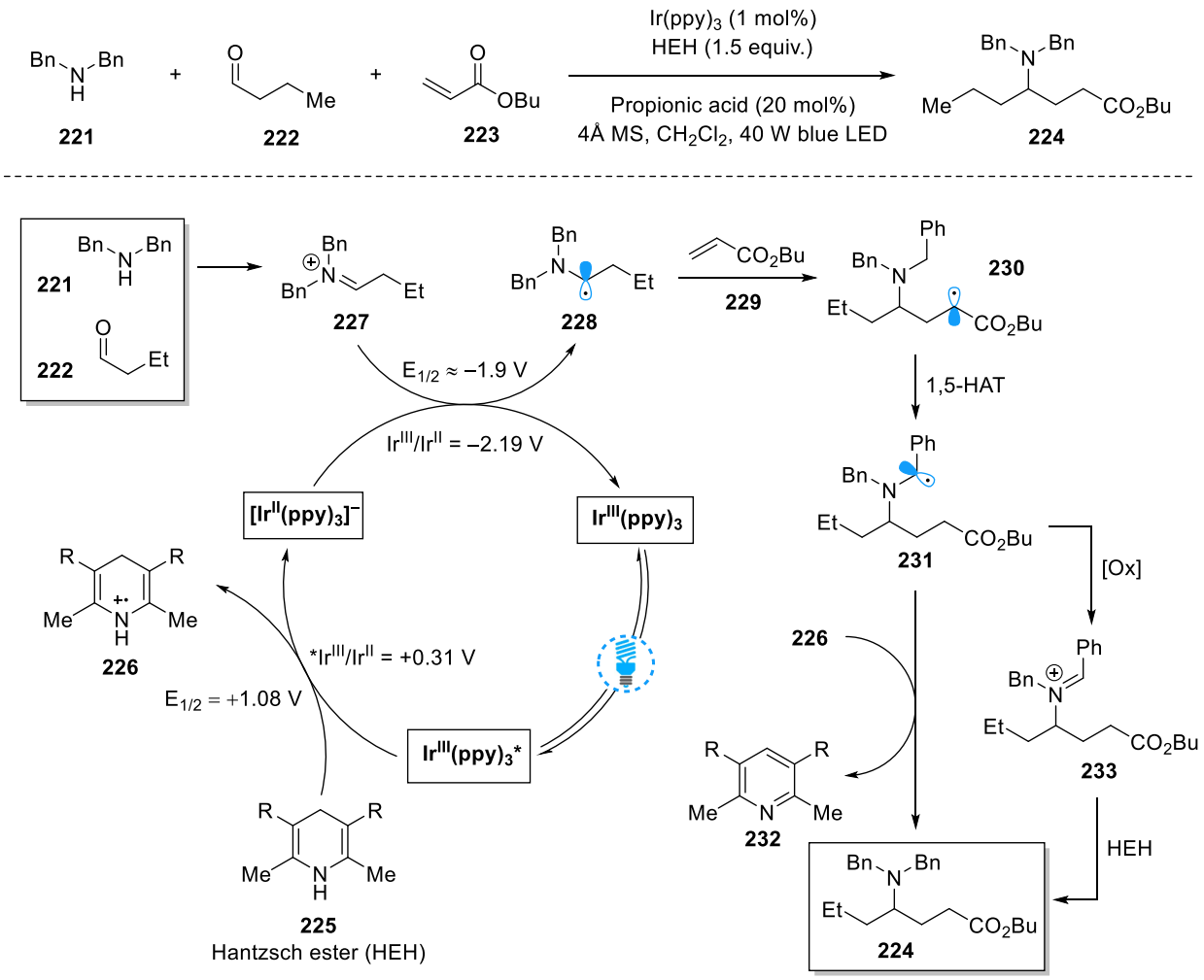

Scheme 33: Multicomponent synthesis of tertiary alkylamine using photocatalysis. R = CO_2Et

In their mechanistic proposal, the reaction begins with visible light excitation of $Ir^{III}(ppy)_3$ to the photoexcited $Ir^{III}(ppy)_3$*, which is quenched by Hantzsch ester **225**, resulting in the Hantzsch ester radical cation (**226**) and $[Ir^{II}ppy_3]^-$.[203] The highly reducing Ir^{II} species carries out reduction of in situ generated alkyliminium **227**, to α-amino radical **228** (Ir^{III}/Ir^{II}, $E_{½}^{red}$ = −2.19 V vs. SCE in MeCN, cf. $E_{½}^{red}$ = −1.4 V to −2.0 V vs. SCE in MeCN for iminium ions).[204] Radical addition of **228** into electrophilic butyl acrylate, results in stabilized radical **230**, which undergoes 1,5-hydrogen atom transfer (HAT) to give benzylic radical **231**. Reaction termination was proposed to occur via HAT with the Hantzsch ester radical cation **226** (or Hantzsch ester), to give tertiary

amine **224**. Alternatively, oxidation of **231** to the benzylidene iminium ion **233**, via a separate photoredox catalytic cycle, then polar reduction with Hantzsch ester could also give the desired product.

Based on the observed tertiary amine products, it was clear that the α-amino radical was the key intermediate in the reaction, however the unequivocal validation of this species, was not conclusively determined.[205] Consequently, in our project design plan, we chose to investigate the nature of the α-amino radical species further, primarily by means of a cyclopropyl radical clock. Investigation of the α,α-cyclopropyl amino radical, and its subsequent fragmentation, would lead to two goals (Scheme 34):

i. It was envisaged that β-C–C bond scission of the cyclopropyl ring would produce an acyclic radical species, that could be intercepted by olefins, to generate cyclic scaffolds.

ii. The radical clock could be used as a probe, to discover novel methods of α-amino radical generation.

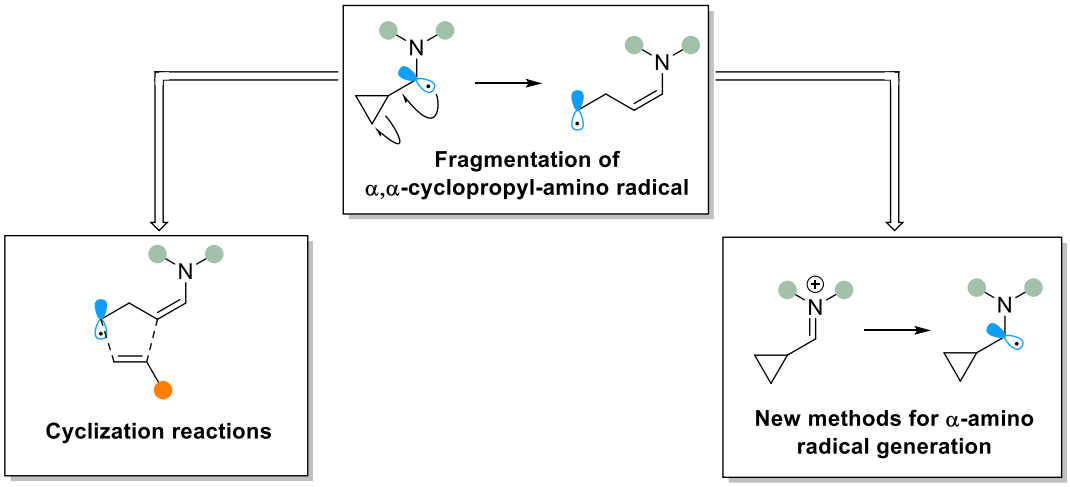

Scheme 34: Overarching project aims, using the fragmentation of α,α-cyclopropyl-amino radicals

2.3. Photoredox Catalyzed Fragmentation-Cyclization

2.3.1. Introduction

Cyclic scaffolds are important structural elements, which have been incorporated into contemporary drugs to modulate electronic distribution, three dimensionality and scaffold rigidity.[206,207] To develop a new cyclization reaction, we envisaged the condensation of secondary amine **234** with cyclopropyl carboxaldehyde **235**, forming alkyliminium **237** (Scheme 35). In the presence of reducing photocatalytic conditions, as reported previously in our laboratory, single-electron reduction could form α-amino radical **238**, initiating β-C–C bond scission and forming acyclic radical **239**. In a tandem process, the radical could be intercepted by acceptor **236** to give **240**, then undergo intramolecular cyclization with the pendant enamine, to form α-amino radical **241**. Finally, reduction via hydrogen atom transfer would generate cyclopentyl methylamine **242**.

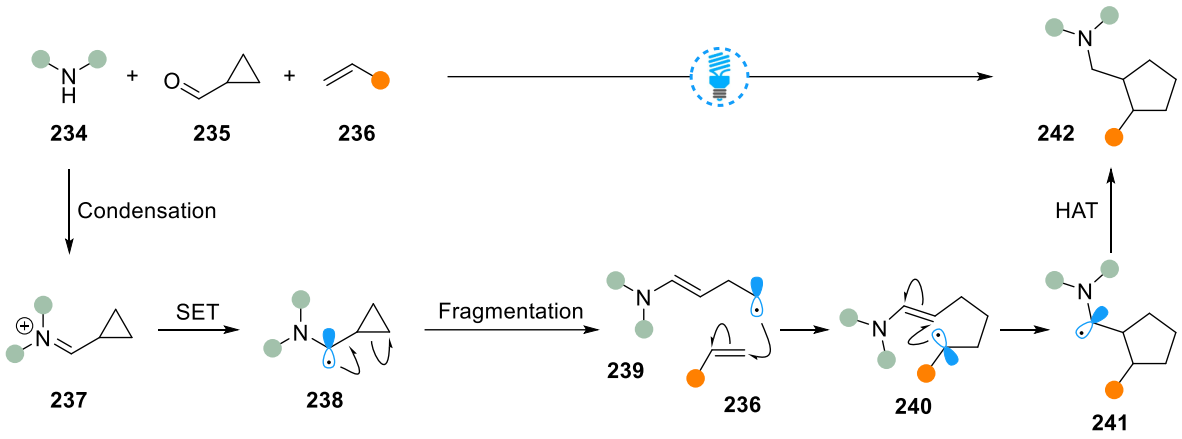

Scheme 35: Initial reaction design plan

Despite the prevalence of literature methods to manipulate α-amino radicals, the generation of α,α-cyclopropyl amino radicals has been overlooked. In contrast, the radical fragmentation and reactivity of α,α-cyclopropyl-ketyl radicals has been widely studied. One of the earliest reports was by Motherwell, who demonstrated the single-electron reduction of α-cyclopropyl ketone **243** with SmI_2 (Scheme 36).[208] Upon fragmentation of the ketyl radical **244**, intermediate **245** was generated, which cyclized onto the pendant alkyne chain to form spirocyclic **246**, in 57% yield. The α-cyclopropyl ring is common in radical fragmentation reactions, due to the relatively large ring strain of 28 $kcalmol^{-1}$ (due to angle and torsional strain). This allows β-C–C bond scission to be kinetically favorable, compared to radical termination.[209] Using stoichiometric radical initiation methods such as AIBN and SmI_2, a wide range of cyclopentane ring forming reactions have been developed to date.[210–213]

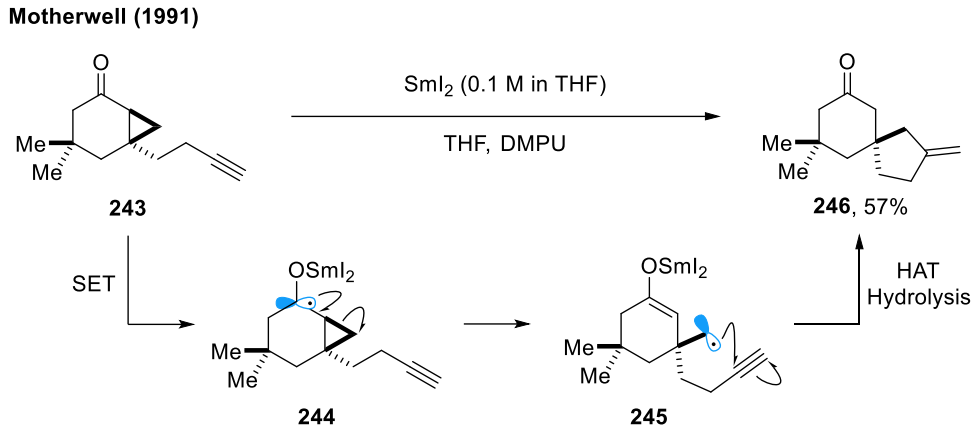

Scheme 36: Early example of radical-initiated tandem fragmentation-cyclization reactions

The resurgence of photoredox catalysis has led to a few related radical fragmentation cyclization transformations.[214] Most notably, Yoon reported an intramolecular,[215] and subsequently elegant intermolecular enantioselective process, which utilizes the fragmentation of a cyclopropyl radical ketyl species (Scheme 38).[216] They utilized a gadolinium Lewis acid with chiral ligand **249**, which facilitated photocatalyst-mediated single-electron reduction of **247** to **250**, through coordination of the ligand to the ketone moiety. Fragmentation provided intermediate **251**, followed by radical addition to styrene, and cyclization to eventually give cyclopentyl ketone **254**, in high yield and enantioselectivity.

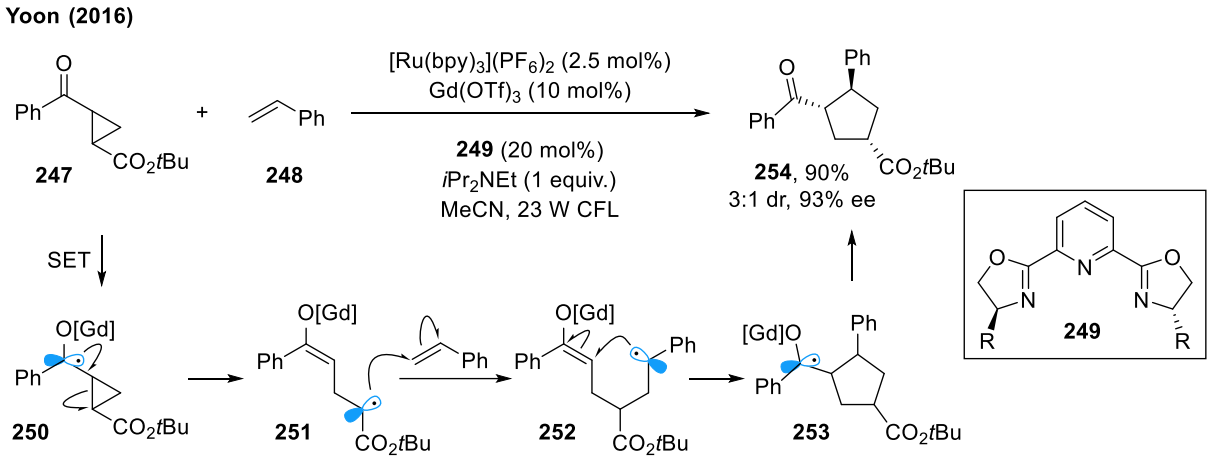

Scheme 37: Photoredox catalyzed asymmetric radical fragmentation-cyclization

Finally, another class of 'photocycloaddition' was established by Zheng in 2012 (Scheme 38).[215] Their process oxidized a tertiary amine **255** to its radical cation **256**, to initiate cyclopropyl fragmentation to **257**. Radical addition to styrene generated **258**, followed by intramolecular cyclization, to give the fused 5,5-product **259**.

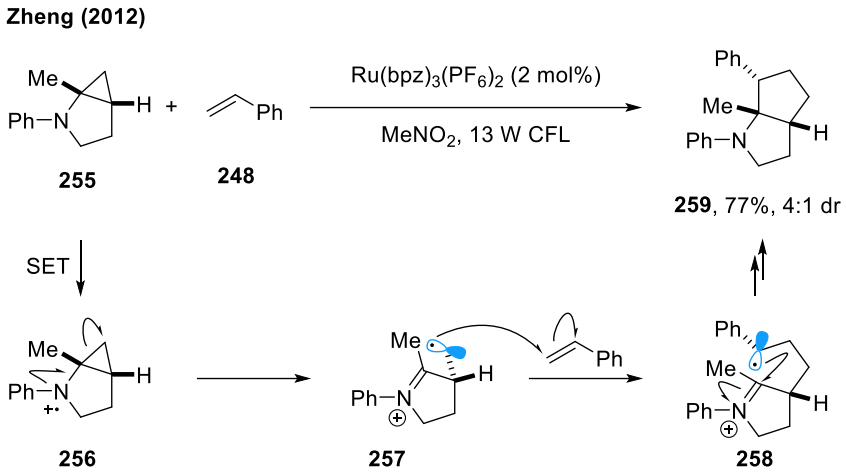

Scheme 38: Radical fragmentation-cyclization reaction starting from the aminium radical cation

Regarding the fragmentation of α,α-cyclopropyl amino radicals, two related examples have been reported – the first by Py, who described the single electron reduction of α-cyclopropyl nitrones using SmI_2 (Scheme 39).[217] Using the diphenyl substituted starting material **260**, the α-nitrone radical **261** underwent β-C–C bond scission, followed by HAT, then tautomerisation to form the acyclic nitrone **263** in 35% yield.

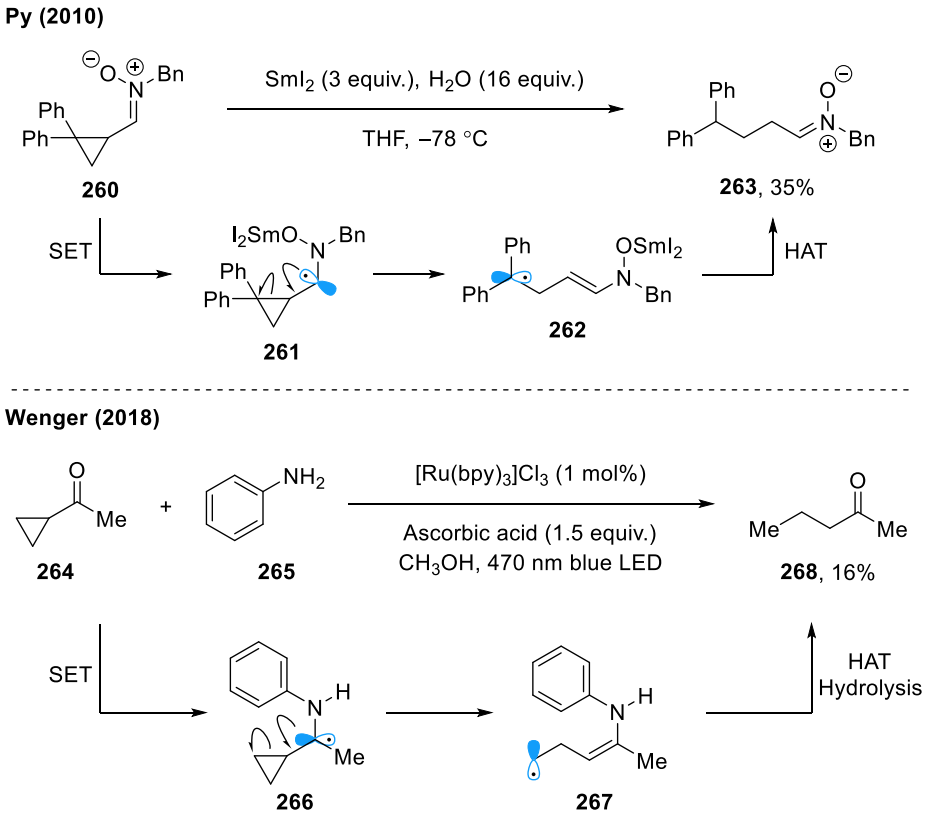

Scheme 39: Examples related to generating α,α-cyclopropyl-amino radicals

The second example, reported by Wenger in 2018, was part of their mechanistic experiments in their report on a photoredox catalyzed reductive amination.[218] Single electron reduction of the in situ generated iminium ion generated α-amino radical **266**, and in the absence of HAT additive 3-mercaptopropionic acid, the radical

species was found to undergo ring fragmentation to **267**. Subsequently, HAT and hydrolysis led to the isolation of acyclic ketone **268** in 16% yield.

In summary, while photocatalytic 'cycloadditions' have so far mostly focused on aromatic cyclopropyl ketones as precursors, there have been limited reports related to the fragmentation of α,α-cyclopropyl-amino radicals. One could hypothesize that compared to enyl radicals, it has been relatively difficult to control the reactivity of enamyl radical resulting from β-C–C bond scission. This could be due to competitive or uncontrollable hydrolysis of the enamine moiety during the reaction.

2.3.2. Reaction Discovery

Using piperidine and dibenzylamine as test amine substrates, radical acceptors **248, 271-279**, of varying electronic properties, were investigated (Scheme 40). Styrenyl acceptors **248** and **271** were found to be completely unreactive, while acceptors **272-275** gave complex mixtures, with some indications of desired product. Vinyl sulfone and acrylate acceptors **276-278** underwent conjugate addition with piperidine; however, with the more sterically hindered dibenzylamine, the desired cyclopentane product could be detected by GC-MS, as a complex mixture of products.

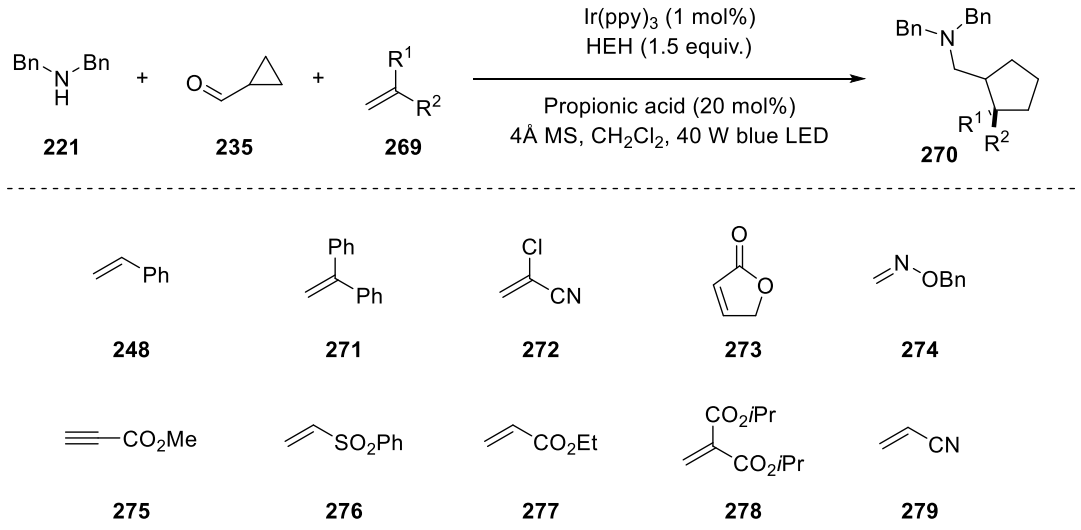

Scheme 40: Initial design plan and alkenes tested

Using acrylonitrile **279**, it was possible to isolate cyclopropyl product **280** in 15% yield, and the cyclopentyl product **281** in 42% yield, as a mixture of 4 diastereomers (Scheme 41a). Firstly, it was determined whether cyclopropane **280** was an intermediate prior to cyclopentane formation, or part of a separate reaction pathway. Cyclopropane **280** was re-subjected to the reaction conditions, which showed complete recovery of the starting material (Scheme 41b). This indicated that the cyclopropane was likely not an intermediate in the desired product pathway.

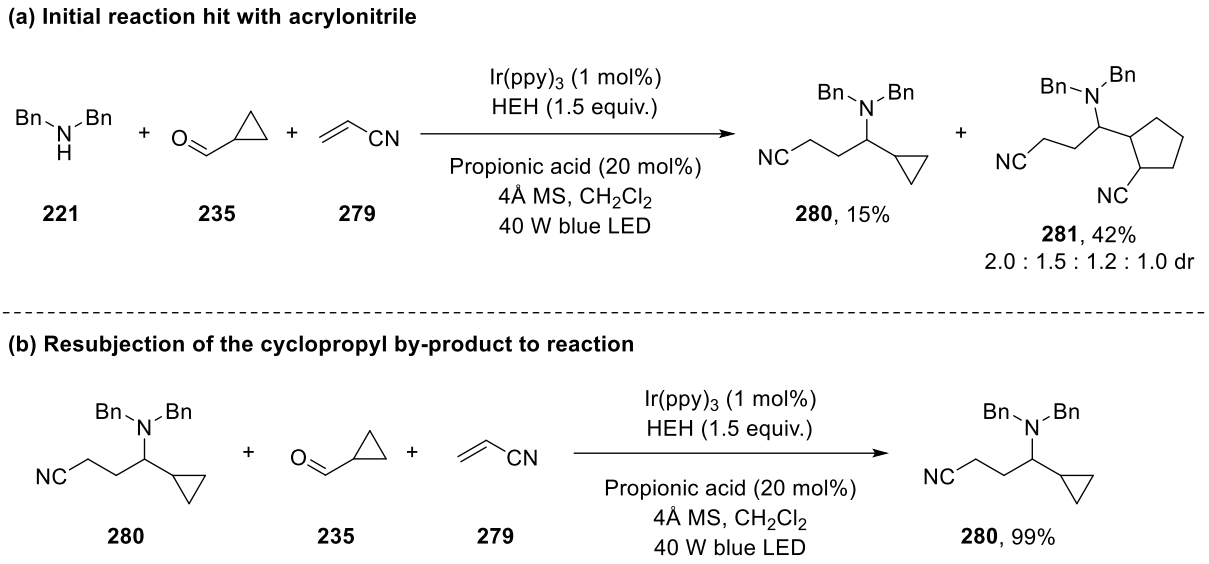

Scheme 41: Initial signs of successful photocycloaddition

Based on previous reports from our laboratory, our working hypothesis for a catalytic cycle is shown in Scheme 42. The excited photocatalyst is reduced by Hantzsch ester to generate the Ir^{II} catalyst, which reduces cyclopropyl iminium **282**, generating α-amino radical **283**. This radical can undergo radical addition to acrylonitrile, then HAT with Hantzsch ester (or its radical cation **226**), to generate undesired cyclopropane **280**. On the other hand, radical fragmentation of the cyclopropane **283** can generate intermediate **285**, which is trapped by acrylonitrile and undergoes cyclization to give α-amino radical **287**. It was intended that radical intermediate **287** would be quenched by Hantzsch ester here. However, the nucleophilic α-amino radical was found to undergo further radical addition to acrylonitrile, generating **288**, and ultimately **281** upon HAT.

The discovery of this reaction was significant in validating the presence of the α-amino radical intermediate and providing a lead for a novel cyclization reaction. Two primary issues were identified – firstly, radical addition of the cyclopropyl α-amino radical to acrylonitrile, was an undesired outcome of the reaction. Secondly, the incorporation of an additional equivalent of acrylonitrile resulted in an uncontrollable level of functionalization. To minimize the undesired pathways, the rate for cyclopropyl ring opening must be faster than the rate of α-amino radical addition to acrylonitrile, which in turn, must be slower than the rate of HAT for the α-amino radical.

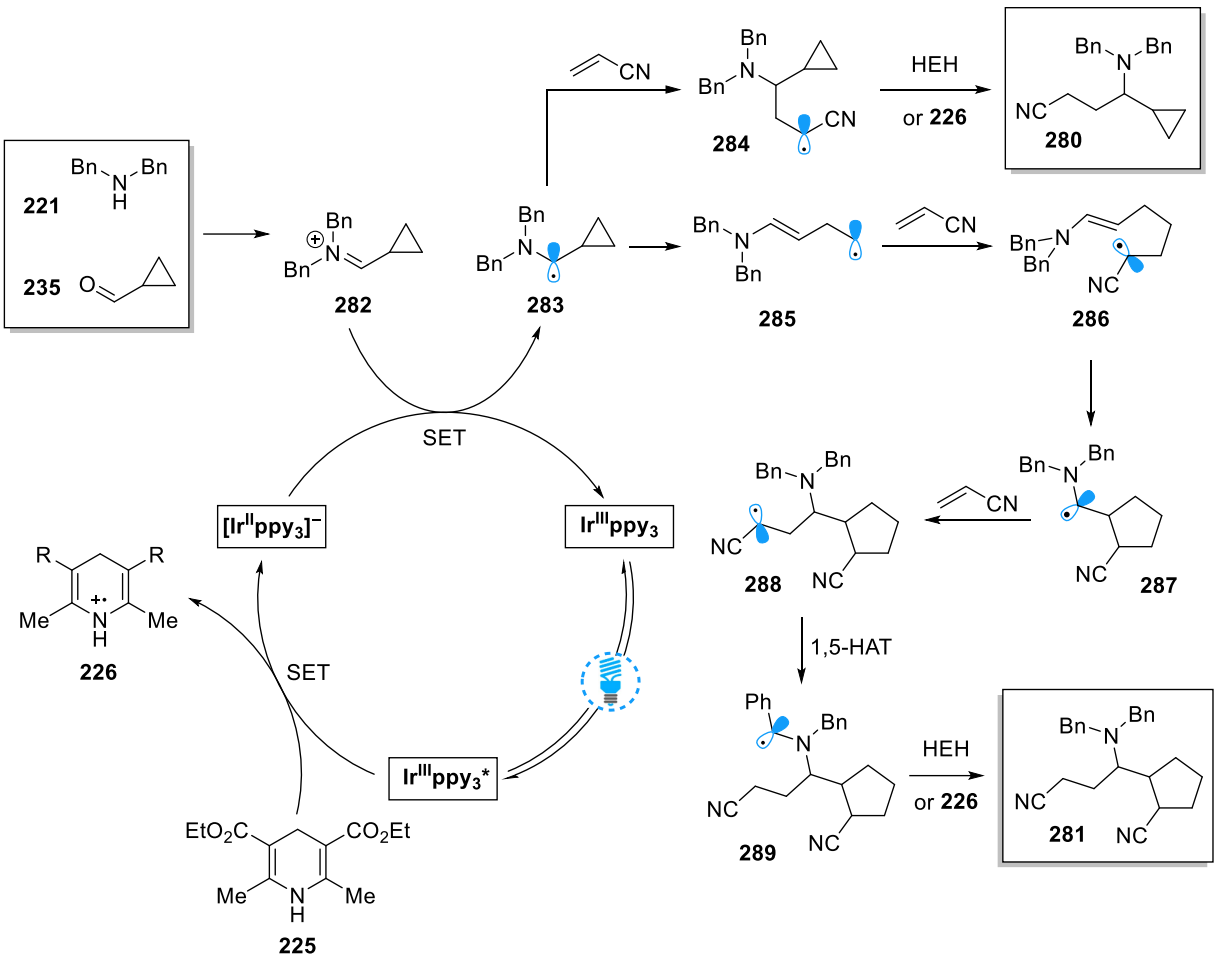

Scheme 42: Proposed catalytic cycle, affording cyclopropyl and cyclopentyl products

In addressing the first issue, it has been established that the rate of radical-initiated β-C–C bond scission can be accelerated by stabilization of the resulting radical species.[219] As summarized by Newcomb, the rate of radical fragmentation (**290** to **291**) can be increased by an order of magnitude, upon substitution of H with a CH_3 group, and by three orders, upon substitution with a CO_2CH_3 group (Table 1).

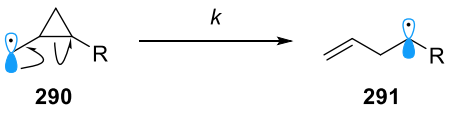

R	k (s^{-1})
H	7×10^{7}
CH_3	1×10^{8}
CO_2CH_3	7×10^{10}
Ph	1.5×10^{11}

Table 1: Rate of radical fragmentation, depending on cyclopropane substitution

It was envisaged that substitution of the cyclopropyl ring would similarly increase the rate of ring-opening, potentially beyond the rate of direct radical addition to acrylonitrile. Synthesis of the dimethyl substituted cyclopropane carboxaldehyde **294** was achieved in two steps starting from 3-methyl-2-buten-1-ol **292**. Subjecting **294** to the reaction conditions afforded cyclopentane **295** in an improved 56% yield, with no cyclopropane by-product detected (Scheme 43a). While successful in preventing direct radical addition, over-alkylation remained an issue.

It was anticipated that by changing the electronic substitution of the cyclopropyl ring, the radical resulting from fragmentation would have a different electronic character. This could allow radical reactivity with electron-rich alkenes, which in turn, would slow down the rate of alkene addition, by the nucleophilic α-amino radical.[220] Cyclopropyl carboxaldehyde **298** bearing a geminal di-ester motif was synthesized, and upon screening the reactant with a range of electronically distinct acceptors, it was found that methylenecyclopentane **300** gave the spirocyclic product **301** in 29% yield (Scheme 43b). The uncyclized product **302**, resulting from radical fragmentation and HAT, was also isolated in 22% yield. No evidence of double addition product was observed, even when dibenzylamine was used as the amine substrate (where the second radical addition of alkene could be promoted by ensuing 1,5-HAT, forming a stabilized benzyl radical).

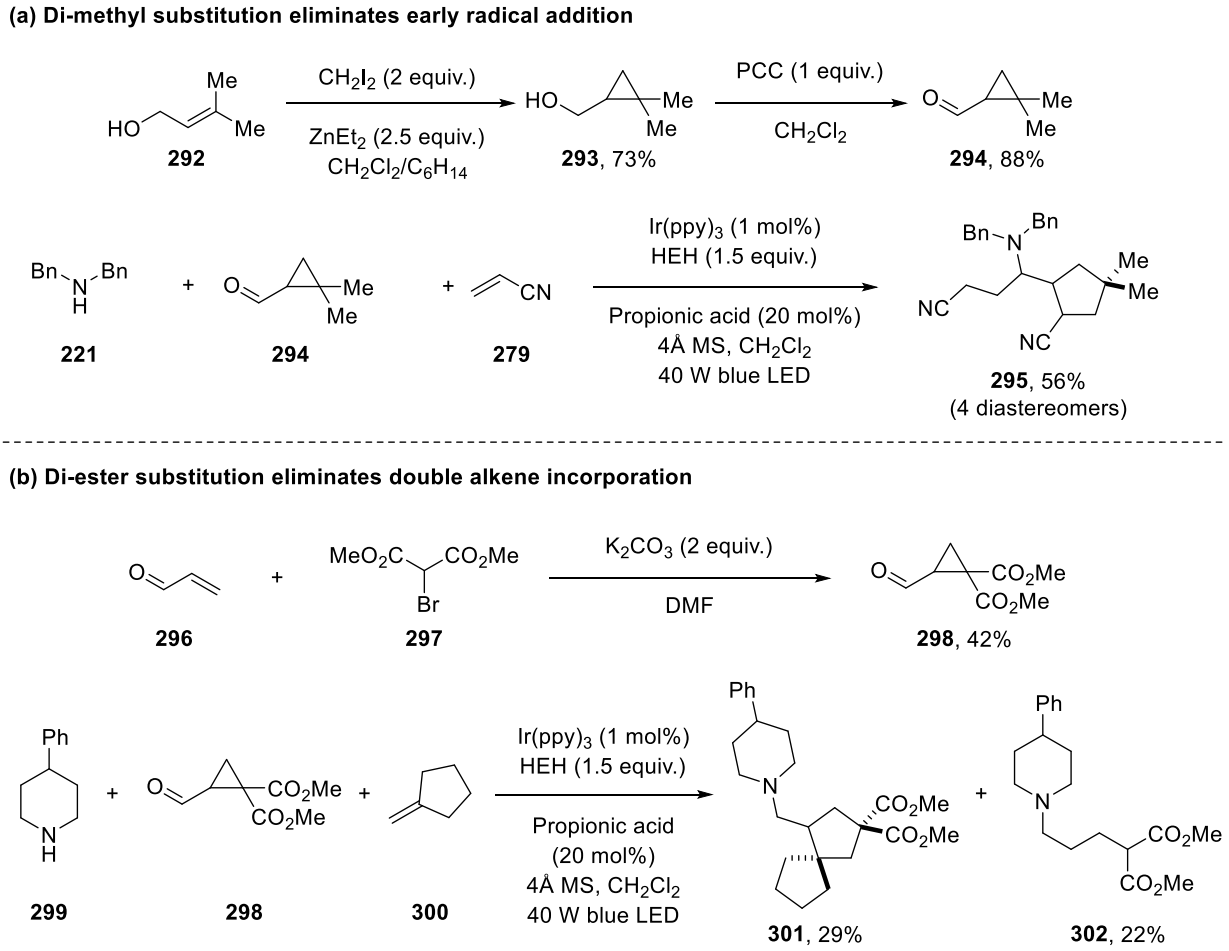

Scheme 43: Substitution of cyclopropane ring eliminates undesired pathways

2.3.3. Reaction Optimization

To further optimize the reaction conditions, polarity matching of hydrogen atom transfer was first considered. This is where the rates and selectivity of hydrogen atom abstraction can be rationalized by polarity effects in the transition state – the 'electrophilic' or 'nucleophilic' characters of the radical and the hydrogen atom donor.[221,222]

In the desired product-forming **Path I** shown in Scheme 44a, radical **303** undergoes reversible radical addition of styrene, then reversible radical addition to the enamine, to form α-amino radical **305**. The α-amino radical must undergo HAT at a sufficiently fast rate to form the product **308**. Considering the nucleophilic nature of the α-amino radical and nucleophilicity of the Hantzsch ester hydrogen atoms, there exists a potential polarity mismatch, reducing the rate of HAT. At the same time, if we consider the unproductive **Path II**, there exists a polarity-matched HAT between electron-deficient radical **303** and electron-rich HEH, resulting in undesired by-product **311**. Hence, we proposed that the addition of a catalytic quantity of an electrophilic hydrogen atom source, such as 2,4,6-triisopropylthiophenol (TRIP-thiophenol, **306**), could sequester α-amino radical **305**, driving the equilibrium towards product formation. The thiol could then be regenerated by a polarity matched HAT between thiyl radical **307** and **309**, generating thiol **306** and Hantzsch pyridine **310**. Upon addition of 20 mol% TRIP-thiophenol to the reaction, an increase in yield of **301** from 29% to 49% was observed (Scheme 44b).

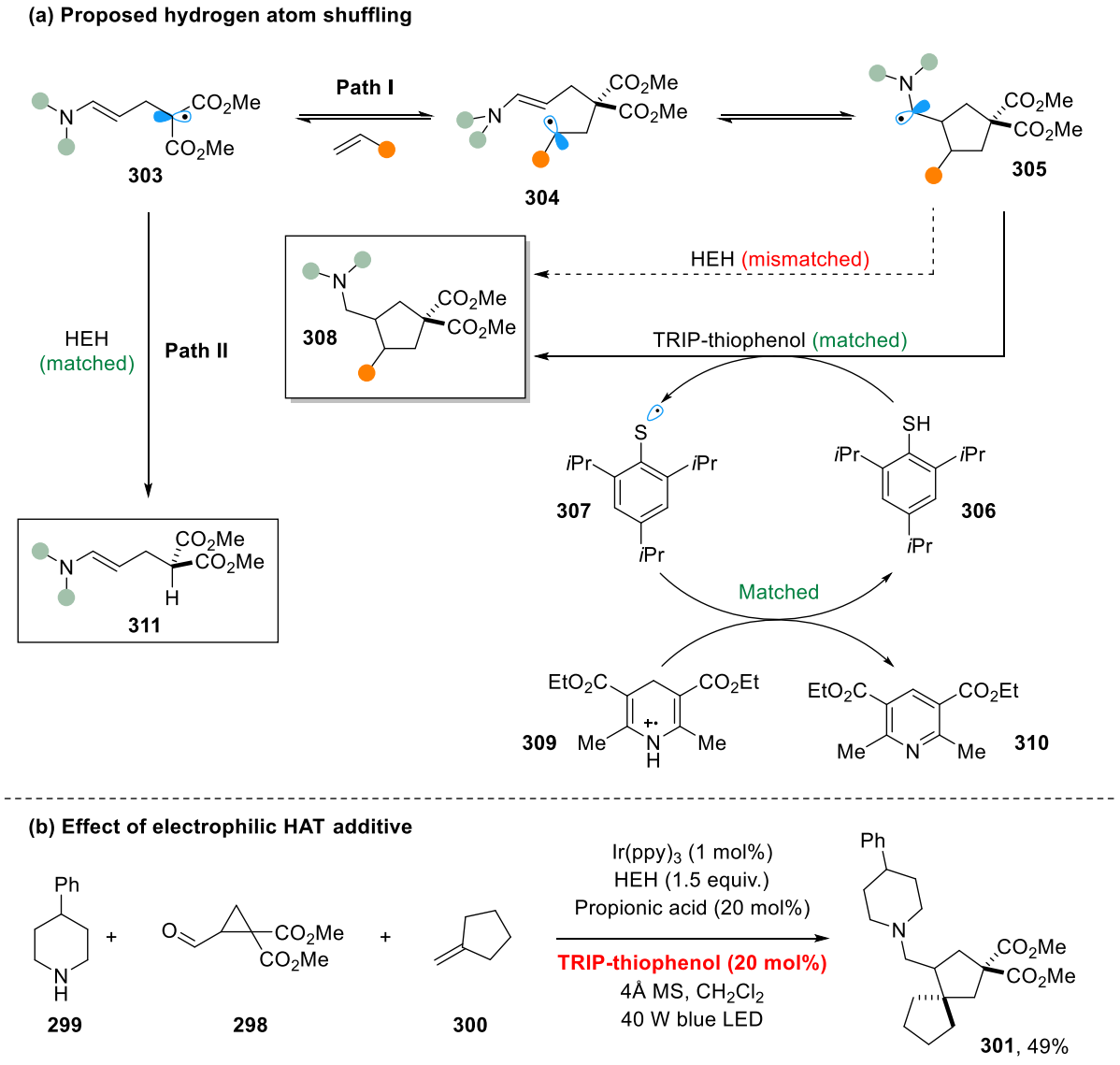

Scheme 44: Improved reaction yield using polarity-matched hydrogen atom transfer

With our procedure improved, we could generate useful quantities of product, which was used to confirm the connectivity of the product and the stereochemistry of the major diastereomer. Using dimethylamine and 4-bromostyrene, combined with the more polar bis(2-methoxyethyl) Hantzsch ester (MeOEt-HEH, **314**) to aid in purification, it was possible to isolate 68% of a single diastereomer of **315** (Scheme 45). This was converted to its perchlorate salt **317** using perchloric acid. Upon crystallization and single crystal X-ray diffraction, the cyclopentyl connectivity was confirmed (**318**), with the major diastereomer being the *cis* isomer, matching our putative NMR assignment by NOESY. The preference for *cis* is in line with other reported works on 1-hexenyl radical cyclization, with bulky substitution at C1 and geminal substitution at C3. The transition state in such cases has been shown to favor a *cis*-chair orientation (**316** – putative transition state).[223]

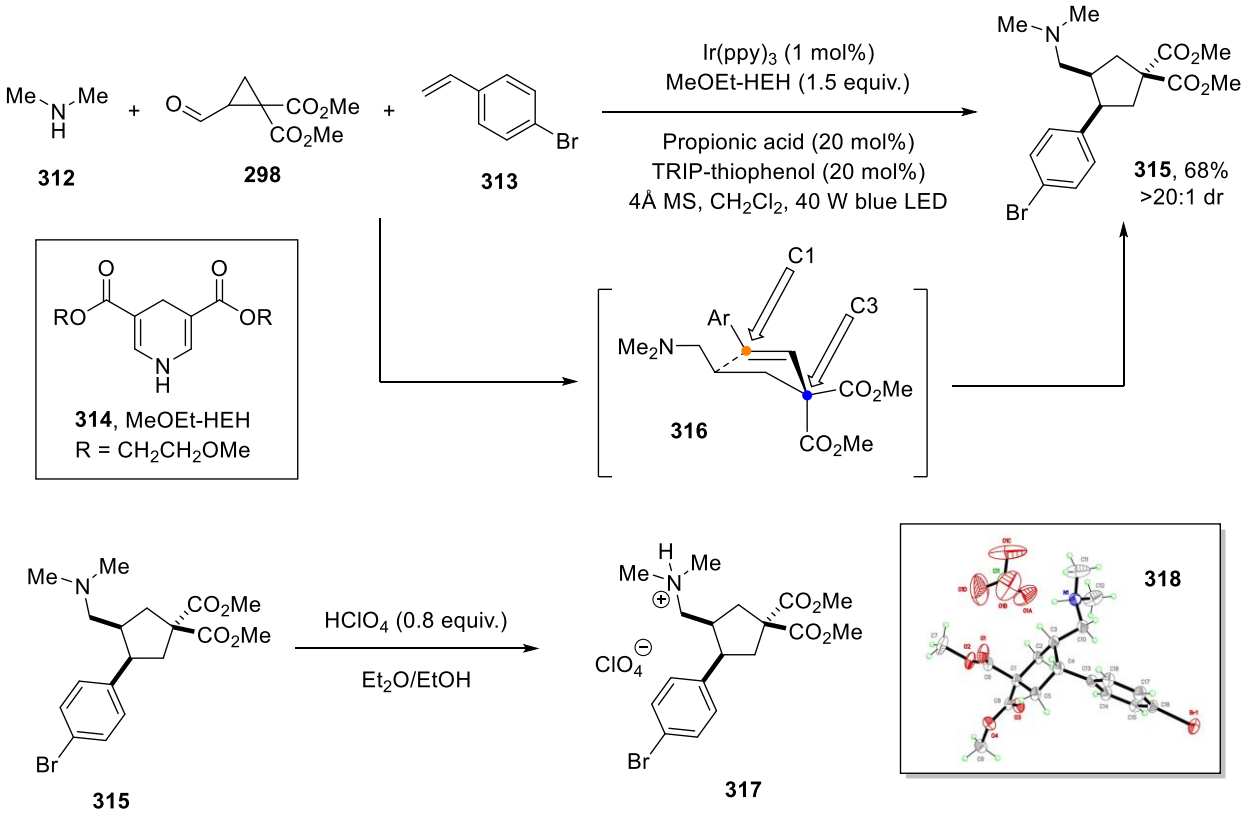

Scheme 45: Confirmation of product structure via crystallization and X-ray diffraction

Next, a model system combining 4-phenylpiperidine **299**, carboxaldehyde **298** and styrene **248** was devised, to determine the optimal reaction conditions (Table 2). A selected summary of the results is described here. The reaction was moderately successful in a wide range of solvents, with CH_2Cl_2 continuing to be the optimal solvent (Table 2). More polar solvents were not effective, for example in promoting formation of the charged iminium intermediate. Photocatalysts of varying reduction potentials were investigated, which did not show a clear trend based on their reduction potentials (Table 3). $Ir(ppy)_3$ continued to be used as the photocatalyst, based on its efficacy and availability.[224] Intriguingly, it was also found that the reaction gave 36% yield without photocatalyst. Though we did not investigate further at this point, we considered the possibility of Hantzsch

ester acting as the photocatalyst,[225] or as an electron-rich species, in the context of charge-transfer complexes, as reported by Chen and others.[226,227]

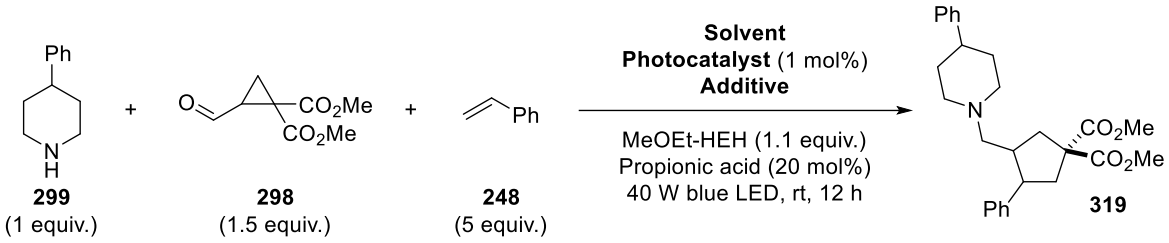

Entry	Solvent	Yield (%)	dr
1	DMSO	7	5:1
2	MeCN	24	2:1
3	EtOAc	34	7:1
4	DMF	38	7:1
5	DCE	56	6:1
6	CH_2Cl_2	63	7:1

Table 2: Screening of solvents. Additive = TRIP-thiophenol (20 mol%). GC-MS assay yield using dodecane as internal standard

Entry	Photocatalyst	Yield (%)	dr
1	-	36	2:1
2	$Ir[dF(CF_3)ppy]_2(dtbpy)PF_6$	40	2:1
3	$Ir(dtbbpy)(ppy_2)PF_6$	46	6:1
4	**320**	53	5:1
5	**321**	55	3:1
6	**322**	59	4:1
7	$Ir(ppy)_3$	63	7:1

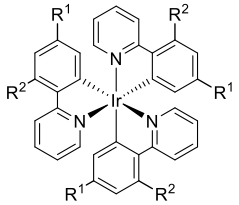

320: $R^1 = CF_3$, $R^2 = H$
321: $R^1 = F$, $R^2 = F$
322: $R^1 = F$, $R^2 = H$

Table 3: Screening of catalysts. Additive = TRIP-thiophenol (20 mol%). GC-MS assay yield using dodecane as internal standard

Entry	HAT additive	Equiv.	Yield (%)	dr
1	-	-	0	-
2	1,4-Cyclohexadiene	1.0	0	-
3	2-Phenylmalonitrile	0.2	4	1:1
4	Phenylsulfinic acid	0.2	29	1:1
5	Triphenylsilanethiol	0.5	44	9:1
6	4-Mercaptobenzoic acid	0.5	46	9:1
7	4-Methoxythiophenol	0.5	52	9:1
8	Thiophenol	0.5	57	9:1
9	Triisopropylsilanethiol	0.5	61	9:1
10	TRIP-thiophenol	0.5	67	10:1
11	2,6-Dimethylthiophenol	0.5	77	9:1
12	Tetradecanethiol	2.0	80	9:1
13	Triisopropylsilanethiol	2.0	85	9:1

Table 4: Screening of hydrogen atom transfer additives. GC-MS assay yield using dodecane as internal standard

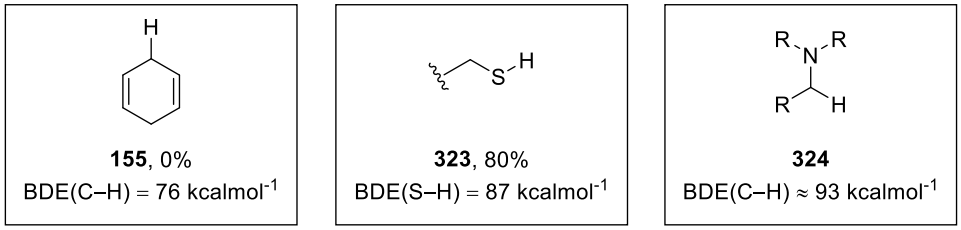

Figure 13: Bond dissociation energies of key reacting species.[228–230] GC-MS assay yield using dodecane as internal standard

Given the significant effect of TRIP-thiophenol on reaction yield, we looked to investigate changes in the electronic and steric character of HAT additives. Additives were tested at different equivalencies, with more equivalents being attempted when no yield was observed. It was found that 0% yield was observed with 1,4-cyclohexadiene (**155**, BDE = 76 kcalmol^{-1}), while tetradecanethiol gave 80% yield (**323**, BDE = 87 kcalmol^{-1}) (Figure 13). Given that the generated α-amino C–H bond has a BDE of ~93 kcalmol^{-1} (**324**), HAT of the α-amino radical is thermodynamically favored, regardless of HAT additive. This suggested that polarity matching was a key factor in determining successful product formation. The final optimal conditions utilized 2 equivalents of triisopropylsilanethiol (TIPS-SH),[231] giving a yield of 85% and 9:1 dr (Entry 13). Using these conditions, charting the reaction progress showed that the reaction was complete in 3 hours, where 44% of product formed within 5 minutes (Figure 14).

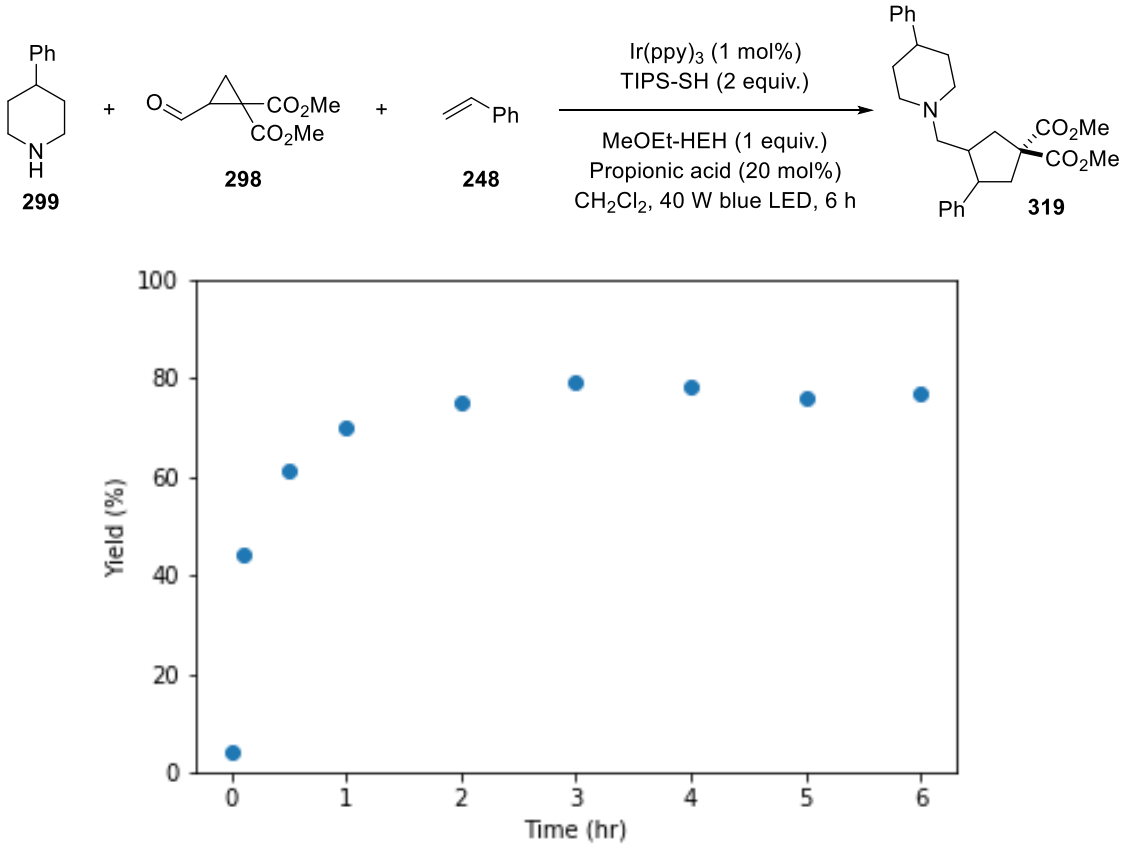

Figure 14: Recording reaction progress over time, using optimal photoredox reaction conditions

Prior to further reaction optimization, it was briefly questioned whether the Hantzsch ester was required for the photocatalytic reduction step, or the hydrogen atom transfer step. We considered whether iminium reduction could be achieved without Hantzsch ester, either by generating Ir^{II} elsewhere in the catalytic cycle (as shown in Scheme 46a), or excited Ir^{III} could reduce the iminium ion. By omitting Hantzsch ester and molecular sieves, it was proposed that upon radical fragmentation and cyclization with an alkene, the highly reducing α-amino radical **329** could be oxidized via the catalytic cycle to generate iminium **330**. This species could then be hydrolyzed to generate cyclopentyl aldehyde **331**. A first attempt of this reaction was successful, generating **331** in 18% yield (Scheme 46b). This reaction was not pursued further, due to the similarity of the reaction products to Yoon's cyclopentyl ketone synthesis.[216] However, given that the amine is not incorporated into the final product, there remains the possibility for an enantioselective cyclopentyl carboxaldehyde synthesis to be developed using secondary amine organocatalytic manifolds.[232]

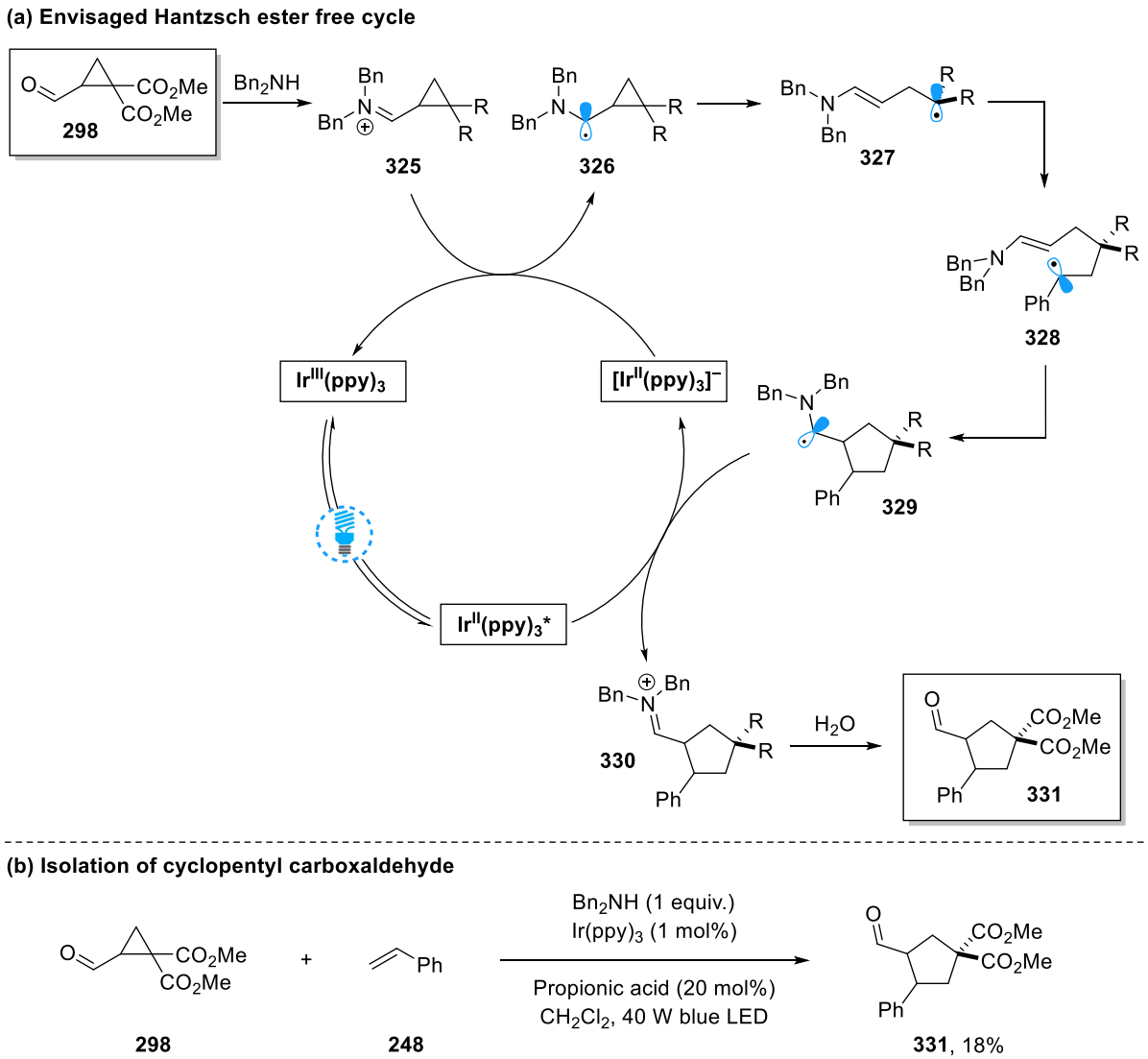

Scheme 46: Net redox neutral photocatalytic cyclopentyl aldehyde synthesis. R = CO_2Me

In summary, the photocatalytic conditions developed in this section effectively demonstrated the feasibility of α-amino radical formation, radical fragmentation, addition, and cyclization, to generate highly functionalized

cyclopentane products. At this point, the mechanistic rationale and atomic inefficiency of utilizing two hydrogen atom donors – thiol and Hantzsch ester – in the reaction was questioned. The following sections describe our efforts to understand and streamline the components necessary for the fragmentation-cyclization reaction.

2.4. Charge-Transfer Complex α-Amino Radical Formation

2.4.1. Reaction Discovery

Previously, the development of a photocatalytic fragmentation cyclization reaction was detailed, utilizing triisopropylsilanethiol (TIPS-SH) to carry out polarity-matched HAT on the α-amino radical intermediate. The thiol was subsequently regenerated in a hydrogen atom cycle with Hantzsch ester. Instead of using hydrogen atom regeneration, the potential to use a stoichiometric quantity of thiol as the sole hydrogen atom donor was considered (Scheme 47). The thiyl radical **333** generated from HAT in **Path I** could simply dimerize to form disulfide by-product **334**, thus negating the need for regeneration with Hantzsch ester. This would also have the benefit of removing the possibility of polarity-matched HAT occurring between electron-deficient radical **303** and Hantzsch ester (**Path II**), therefore reducing the quantity of by-product **311**.

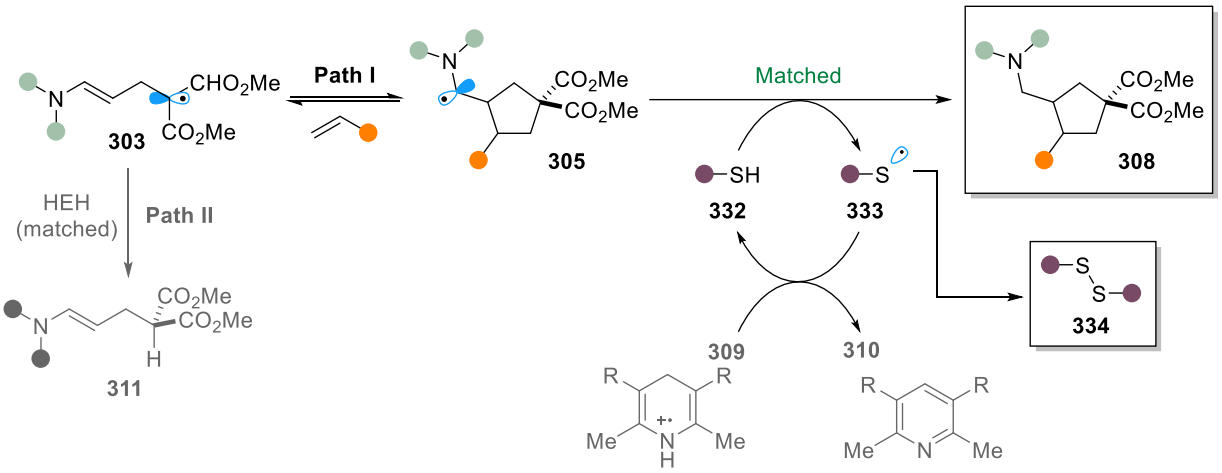

Scheme 47: Use of stoichiometric thiol and removal of Hantzsch ester. R = CO_2Et

When the reaction was attempted using 2 equivalents of TIPS-SH and no Hantzsch ester, desired product **319** was obtained in 18% yield (Scheme 48a). Furthermore, it was found that the reaction with 2,6-dimethylthiophenol (DMTP) resulted in 77% yield of **319**. Hantzsch ester could, therefore, be removed from the reaction. In the earlier screening of photocatalysts, the use of Hantzsch ester, TRIP-thiophenol and no photocatalyst, gave 36% yield of the desired product. Now, attempting the cyclization reaction with 2 equivalents of TIPS-SH, whilst omitting Hantzsch ester and photocatalyst, a yield of 0% was observed (Scheme 48b). However, using 2 equivalents of DMTP, without Hantzsch ester and photocatalyst, the desired product was observed in 75% yield. The products were fully characterized and compared against compounds verified by single crystal X-ray diffraction. In this way, it was possible to translate the radical cyclization reaction, into a process that was free of photocatalyst and Hantzsch ester.

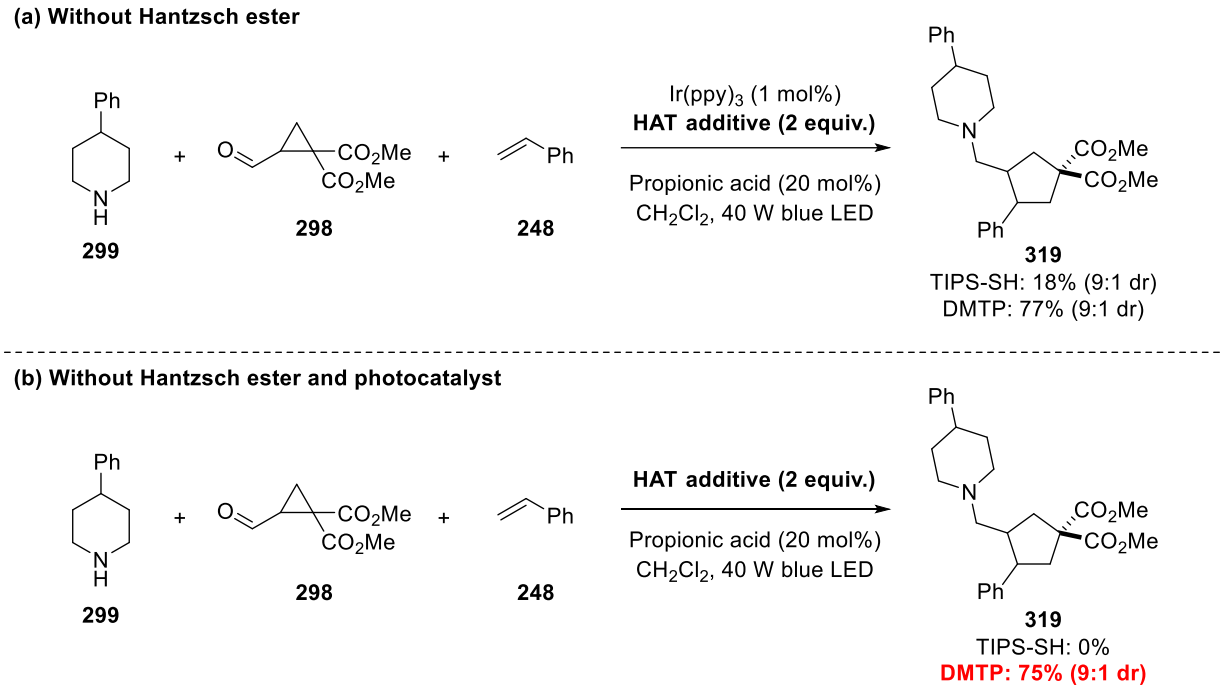

Scheme 48: Towards a photocatalyst-free method of α-amino radical generation

Following these discoveries, a short optimization study was carried out. Using 1.5 equivalents of styrene and DMTP, the reaction was found to be just as effective without propionic acid (Table 5, Entry 1, 2). Although acid was previously required to catalyze iminium formation, we presumed that the thiol (*p*Ka = 6.6 in H_2O, 10.3 in DMSO) could serve a similar function, when present in stoichiometric amounts. Increasing the reaction time had no effect by itself (Entry 3), however by increasing the time and equivalents of styrene and DMTP to 3, the yield was increased to 98% (Entry 4). We found that it was possible to reduce the equivalents of styrene and DMTP to 2, without a reduction in yield (Entry 5). Lowering the quantity of styrene and thiol further had a depreciative effect on yield (Entry 6-9). Following the reaction over time indicated a slower rate of reaction, compared to the earlier photocatalytic variant, with 24 hours being required for maximum conversion (Figure 15). Regardless, lower equivalents of styrene could be used (2 equivalents) compared to photocatalytic conditions (5 equivalents), since no Hantzsch ester was present, which previously favored undesired by-product formation (**Path II**, Scheme 47).

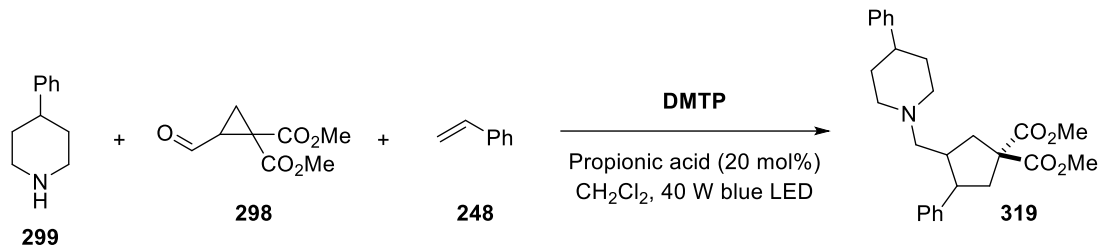

Entry	Styrene (equiv.)	DMTP (equiv.)	Propionic acid (mol %)	Time (h)	Yield (%)	dr
1	1.5	1.5	20	12	70	10:1
2	1.5	1.5	-	12	75	10:1
3	1.5	1.5	-	22	74	10:1
4	3	3	-	22	98	10:1
5	2	2	-	24	99	10:1
6	2	1	-	24	72	10:1
7	1	1	-	24	60	10:1
8	2	0.5	-	24	27	10:1
9	1	0.5	-	24	19	10:1

Table 5: Optimization of photoinduced radical cyclization and reaction time study. Time study with 3 equivalents of DMTP

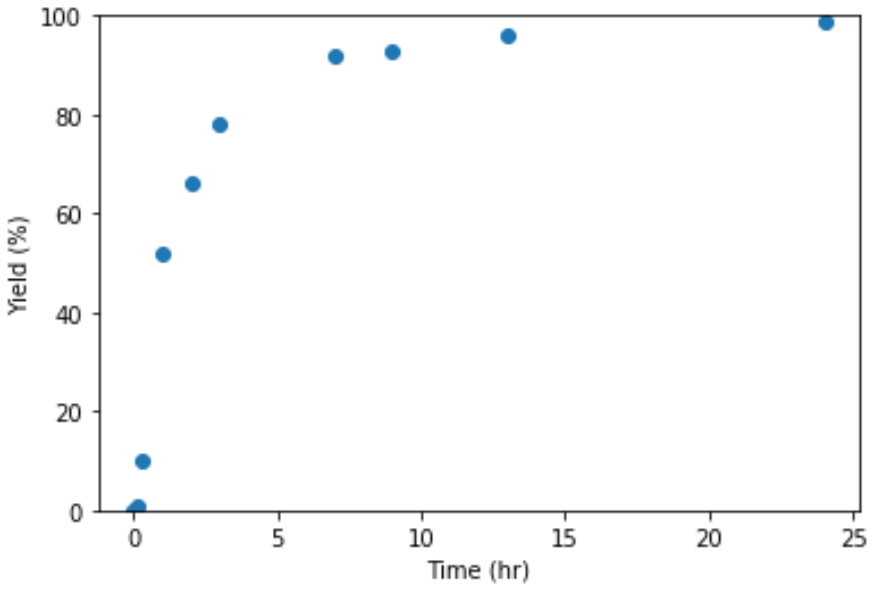

Figure 15: Reaction progress over time for photocatalyst-free conditions. Conditions as above, using styrene (3 equiv.) and DMTP (3 equiv.)

2.4.2. Control Studies

With optimal reaction conditions in hand, the origin of radical formation was investigated through control and mechanistic studies. First, varying the light source showed a clear dependence on light (Table 6), with the reaction performing best with the Kessil A160WE Tuna Blue 40 W blue LED (Entry 1).[13] Strips of weaker intensity Ledxon 467 nm LED strips could also be used to good effect (Entry 2),[233] while a standard 30 W

white CFL gave a lower yield of 76% (Entry 3). The reaction was set up in darkened conditions (complete exclusion of light was not possible in standard lab conditions) and the reaction vial covered with black tape. The vessel was placed on a stirrer plate in front of a Kessil lamp, to mimic any incidental heating, without irradiating with light. This gave a significantly reduced yield of 11% (Entry 4). Vials prepared in the dark and placed in a 40 °C oil bath, and at ambient temperature, both gave yields of 6% (Entry 5, 6).

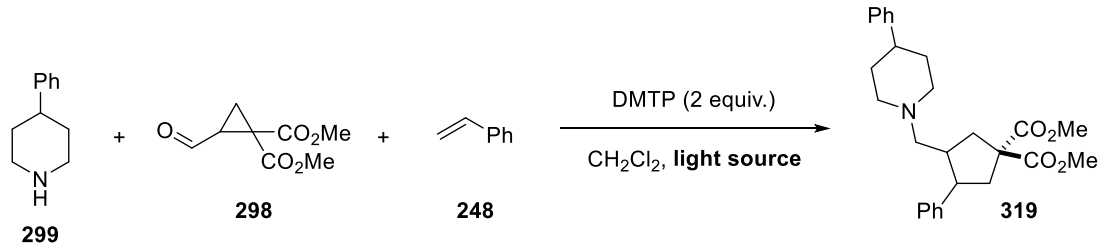

Entry	Light source	Yield (%)
1	Kessil 40 W blue LED	99
2	Ledxon 14.4 W 467 nm blue LED strip	90
3	30 W white lamp	76
4	Black tape, Kessil 40 W blue LED	11
5	Black tape, 40 °C oil bath, dark	6
6	Black tape, dark	6

Table 6: Effect of light source on photoinduced cyclization

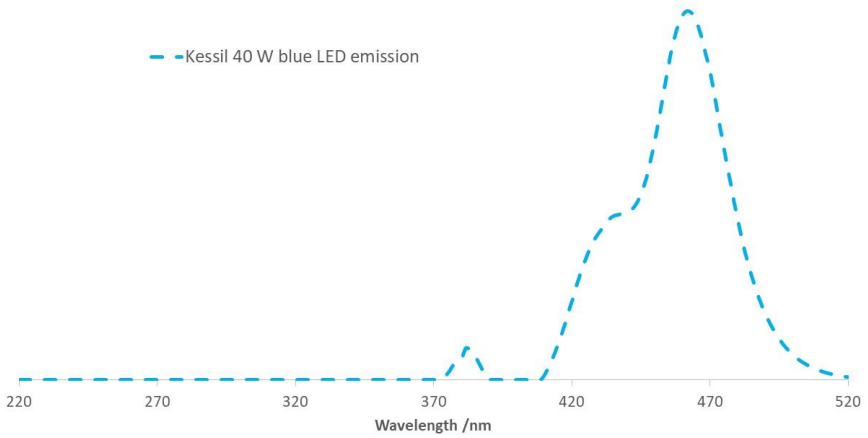

Figure 16: Kessil lamp emission spectrum[13]

The Kessil lamps used in the laboratory are an earlier model which do not have the capability to select a precisely tuned wavelength. The reported emission spectrum of the lamp shows the strongest lamp intensity at λ = 460 nm, with a shoulder at λ = 430 nm, and a small peak at λ = 380 nm (Figure 16).[13] The wavelength of light that enables a photochemical reaction is a crucial determinant of the type of mechanism in action, and a

way to investigate this is to use light filters which block off regions of transmitted light. Longpass light filters at 420 nm and 455 nm were obtained from Edmund Optics (SCHOTT GG-420/GG-455),[234] which block off light below 420 nm and 455 nm, and transmits light above these wavelengths (Figure 17).

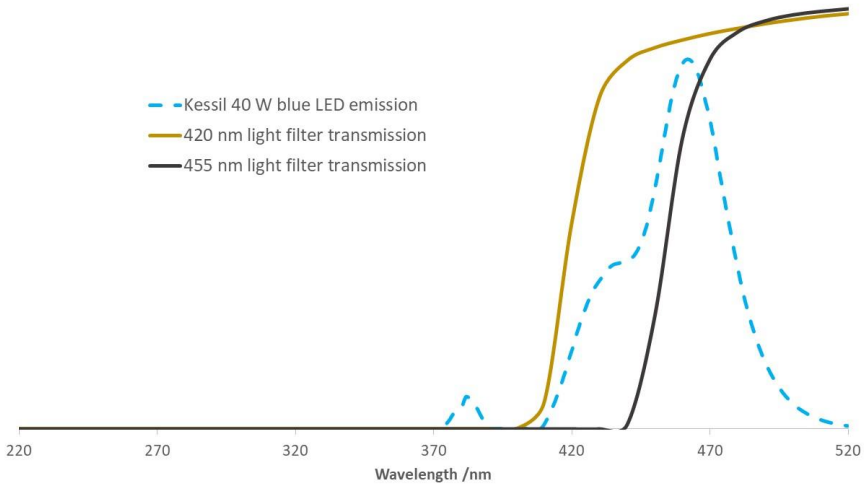

Figure 17: Effect of longpass filters on light transmission

Use of the 420 nm light filter gave a slightly reduced yield of 83%, indicating that light with wavelength around, or above 420 nm was critical for radical formation (Table 7, Entry 3). Furthermore, 57% yield was observed, using the 455 nm filter (Entry 4). This indicated that the reaction could still be promoted by light deep in the visible region ($\lambda > 450$ nm), where organic molecules typically cannot absorb. Furthermore, use of the Ledxon LED strips (reported emission peak of 467 nm, tolerance of ±3 nm), gave 90% yield, further indicating that long wavelength visible light was capable of reaction activation (Entry 2).

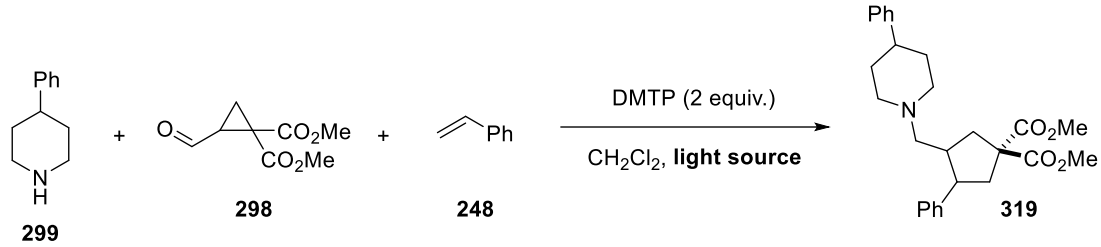

Entry	Conditions	Yield (%)
1	40 W blue Kessil lamp	99
2	Ledxon 467 nm LED	90
3	Kessil lamp + 420 nm filter	83
4	Kessil lamp + 455 nm filter	57

Table 7: Investigating the effect of longpass light filters

Until now, reaction have been conducted using degassed CH_2Cl_2, prepared by freeze-pump-thaw cycles; a standard procedure for photochemical reactions, to prevent radical quenching by oxygen. Preparing the reaction under air and using dry, but non-degassed CH_2Cl_2, gave a moderate yield of 67%, indicating a radical

reaction was likely, with some tolerance of oxygen (Table 8, Entry 2). Adding 1 and 2 equivalents of the radical quencher TEMPO to the reaction gave 35% and 0% yield respectively, indicating that a radical process was being inhibited by TEMPO (Entry 3, 4). Unfortunately, the identity of TEMPO adducts could not be observed by ^{1}H NMR or LC-MS.

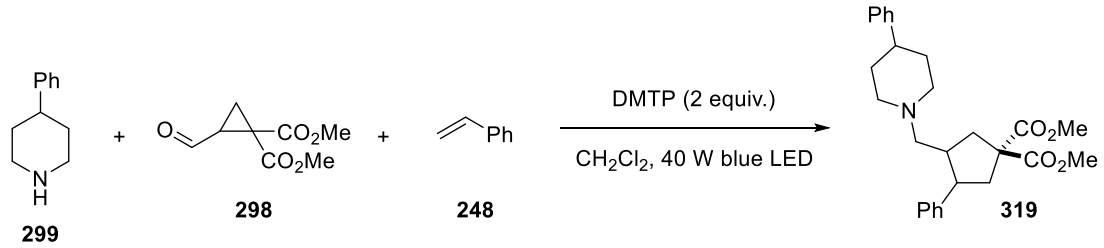

Entry	Conditions	Yield (%)
1	No variation	99
2	Non-degassed CH_2Cl_2, under air	67
3	TEMPO (1 equiv.)	35
4	TEMPO (2 equiv.)	0

Table 8: Investigating inhibitors of radical reactions

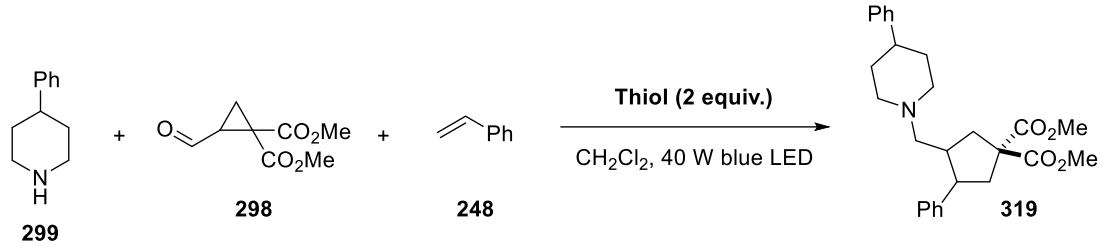

Entry	Thiol	BDE (kcalmol^{-1})	Yield (%)
1	2,6-Dimethylthiophenol	-	99
2	2,4,6-Trimethylthiophenol	-	64
3	Thiophenol	79.1 (E)	34
4	3,5-Dimethylthiophenol	-	31
5	4-Methylthiophenol	78.3 (E)	19
6	Triisopropylthiophenol	-	18
7	4-Methoxythiophenol	76.9 (E)	14
8	4-Nitrothiophenol	81.4 (E)	0
9	Dodecanethiol	88.7 (E)	0
10	Triisopropylsilanethiol	88.2 (T)	0
11	Methyl thioglycolate	87.1 (T)	0
12	2,2,2-Trifluoroethanethiol	-	0
13	*L*-cysteine	87.7 (T)	0
14	*N*-Acetyl-*L*-cysteine	-	0

Table 9: Effect of thiol on photoinduced cyclization. BDEs have been reported where available (E = Experimental, T = Theoretical)[235–239]

Next, a screening of thiols was conducted, investigating a range of aromatic and aliphatic thiols (Table 9). Intriguingly, this showed that that only aromatic thiols led to product formation (Entry 1-7). This could be

attributed to the lower BDE of the aromatic thiol S–H bond (~78 kcalmol^{-1}), due to π-cloud stabilization of the thiyl radical. However, BDE was not useful in distinguishing the efficacy of different aromatic thiols - some thiols with relatively low BDEs such as 4-methylthiophenol and 4-methoxythiophenol (Entry 5, 7) gave poorer yields, compared to thiophenol (Entry 3).

Having varied the light source and additives, the reaction components were investigated in turn (Scheme 49). Irradiating the aldehyde **298**, in the presence of DMTP, showed complete recovery of the starting material, indicating that ring opening of the aldehyde cannot occur (Scheme 49a). Irradiating the amine, aldehyde and thiol, led to the disappearance of diagnostic cyclopropyl signals upon ^{1}H analysis of the crude reaction mixture (Scheme 49b). Subjecting the crude mixture to aqueous HCl revealed acyclic aldehyde **338**, obtained in assay yield of 90% and isolated in 65% yield. This indicated that the amine is required for ring opening, and in the absence of an alkene acceptor, radical intermediate **336** can undergo HAT to form enamine **337**, and aldehyde **338** upon hydrolysis.

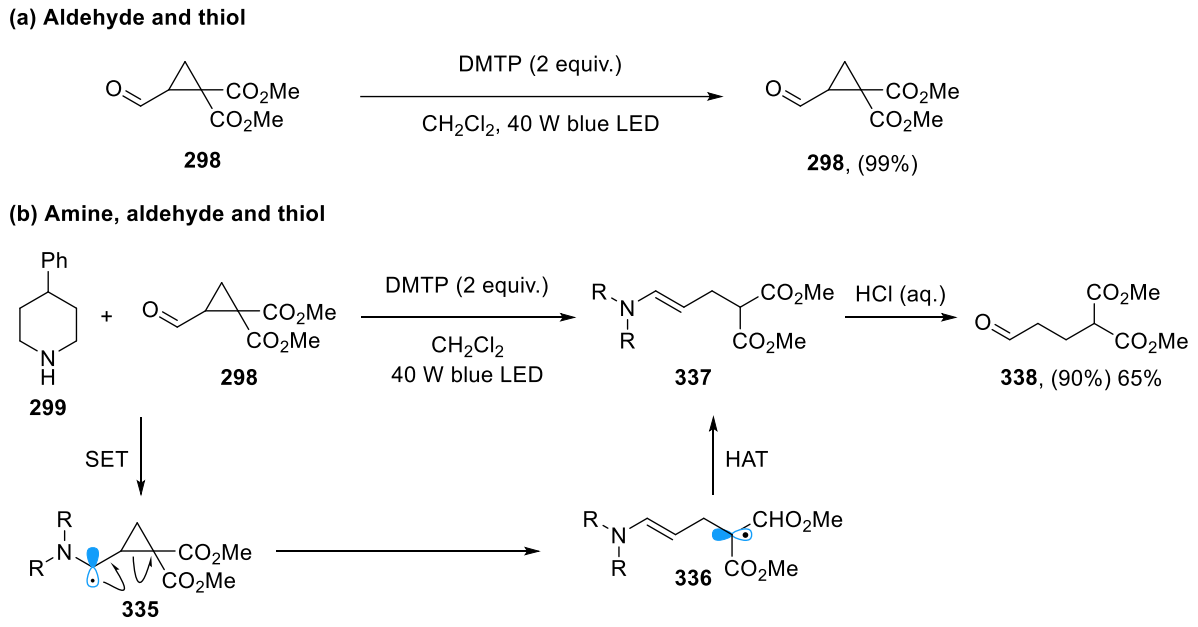

Scheme 49: Control studies investigating reaction components. Brackets denote ^{1}H NMR yield using TCE as internal standard

Next, sequentially combined reaction mixtures were analyzed by ^{1}H/^{13}C NMR, which showed that a mixture of amine and thiol in deuterated CH_2Cl_2 led to no change, compared to the starting materials (Scheme 50a). This was also the case when aldehyde and thiol were combined (Scheme 50b). Meanwhile, mixing amine and aldehyde led to the formation of hemiaminal **341** (Scheme 50c). Finally, mixing all 3 components showed complete and rapid (<5 mins) conversion to thioaminal **342** (Scheme 50d).

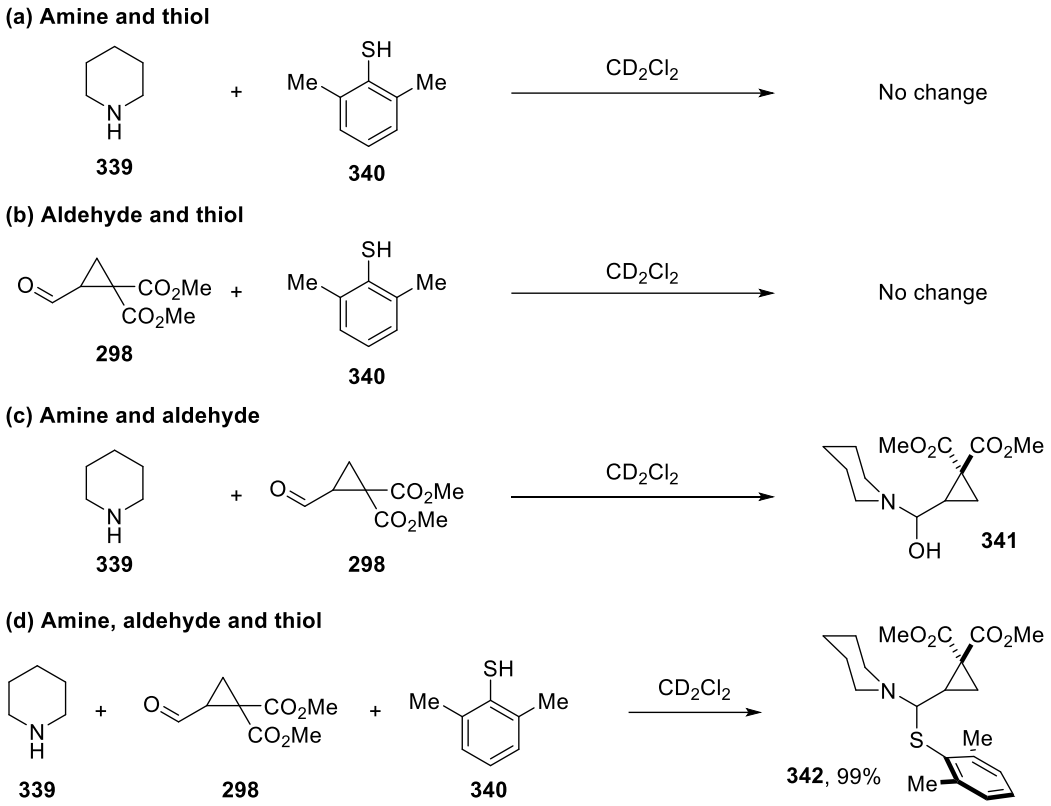

Scheme 50: NMR analysis of reaction mixtures. ^{1}H NMR yield determined by comparison with TCE internal standard

Given the full conversion of the reaction components to thioaminal **342**, it was hypothesized whether the thioaminal could absorb visible light, generating excited state **343** (Scheme 51). From the excited state, C–S bond cleavage could potentially occur, generating α-amino radical **344**.

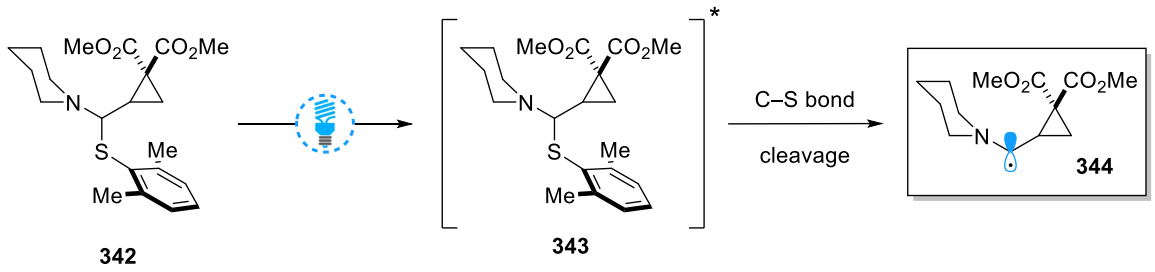

Scheme 51: Possibility of thioaminal excitation, leading to C–S bond cleavage

2.4.3. Alternative Mechanistic Hypotheses

Photoinduced Thioaminal Excitation

To determine the visible light absorbing species, UV-vis absorption measurements for each reaction component were conducted. The absorptions of: i) thiol (**340**), ii) thiol & amine (**340, 339**), iii) thiol, amine & aldehyde (i.e. thioaminal **342**) were measured between concentrations c = 0.33 mM to 33 mM. At the lowest

concentration, c = 0.33 mM, a peak was observed at λ_{max} = 237 nm for all three instances, indicating that the thiol aromatic ring was responsible for this absorption (Figure 18).

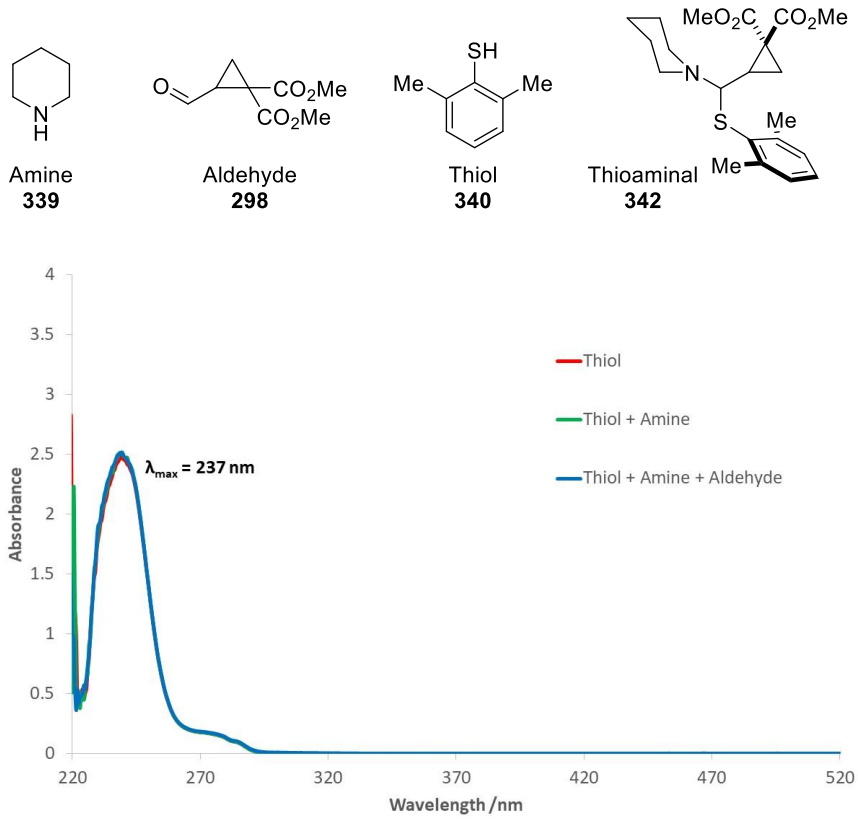

Figure 18: Absorption of mixtures in CH_2Cl_2 (c = 0.33 mM)

At higher concentrations, a small peak at λ_{max} = 255 nm was visible for the aldehyde in isolation (Figure 19), however this was dwarfed by the thiol absorption, upon addition of thiol. At c = 33 mM, the thiol absorption is sufficiently high to saturate the machine detector, and the peak diminishes at approximately λ_{tail} = 385 nm.

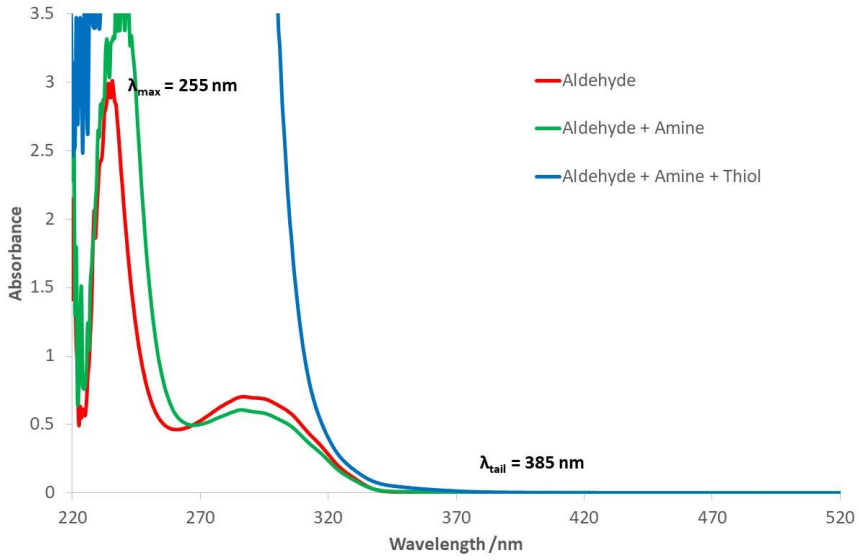

Figure 19: Absorption of mixtures in CH_2Cl_2 (c = 33 mM)

When the thioaminal absorption was compared with the Kessil lamp emission, there was no overlap between the two spectra (Figure 20). This was further accentuated when the 455 nm longpass light filer is considered. Therefore, it was concluded that the thioaminal cannot absorb light to initiate the reaction. This was not surprising, given that the molecule has no extended chromophores, and similar molecules have previously required UV light from a mercury lamp to initiate photoinduced bond cleavage.[240]

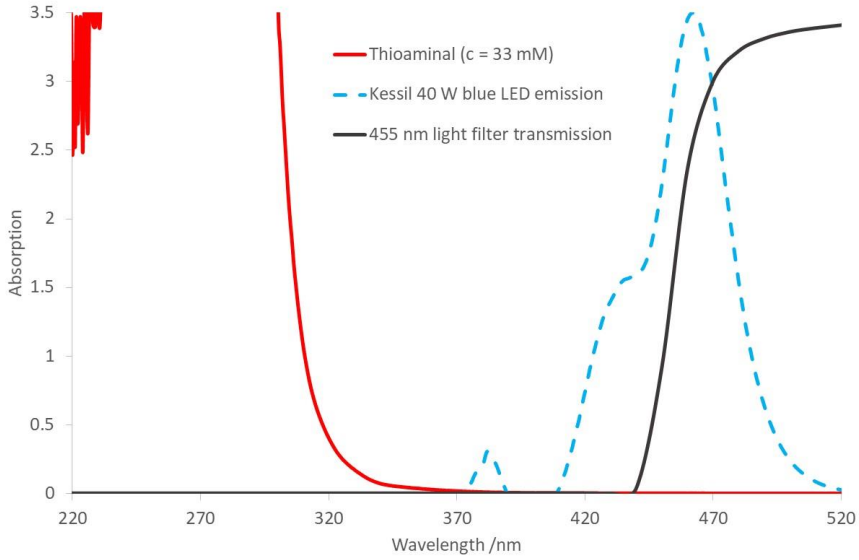

Figure 20: Comparison of thioaminal absorption and lamp emission spectra

Disulfide Energy Transfer

It has previously been reported that the photoexcitation of diaryl disulfides require UV light (λ_{max} = 250 nm). Although unlikely, it is possible that an alternative mechanism involves excitation of the DMTP disulfide by-product **345** (Scheme 52).[230] The disulfide could be present in trace quantities in commercial DMTP, or could be generated from DMTP, either due to oxidation by adventitious oxygen, or light irradiation. One possible pathway could involve photoinduced excitation of disulfide to **346**, which could undergo energy transfer with thioaminal **342**, generating excited state thioaminal **343**. This species could then undergo C–S bond cleavage, generating α-amino radical **344**.

Recording the ^{1}H NMR spectrum of commercial DMTP showed no DMTP disulfide **345** was present. Furthermore, irradiation of DMTP, followed by ^{1}H NMR analysis, showed 91% recovery of DMTP and 0% disulfide (Scheme 53). Finally, conducting UV-vis absorption analysis of DMTP disulfide at high concentration (c = 33 mM) showed that the absorption band diminished at λ_{tail} = 440 nm (Figure 21).[241,242] Therefore, the absorption profile of the disulfide was not compatible with the reaction being operational with a 455 nm longpass filter. Given the above evidence, the disulfide energy transfer mechanism was deemed unlikely.

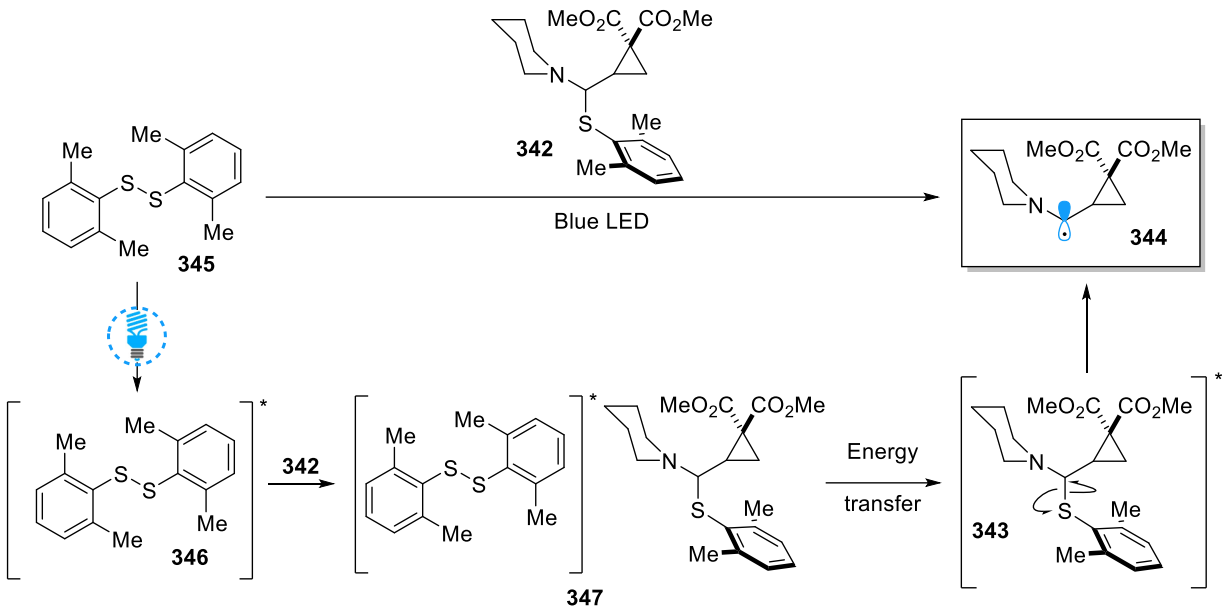

Scheme 52: Possible mechanism involving energy transfer, mediated by excited diaryl disulfide

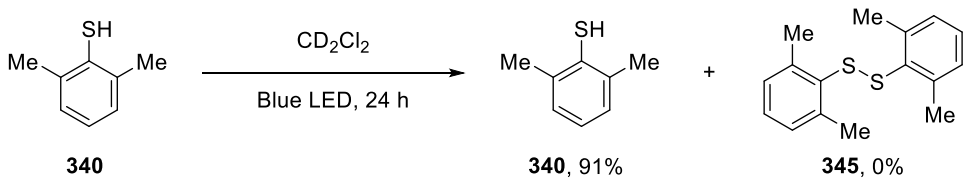

Scheme 53: No disulfide generation under reaction conditions

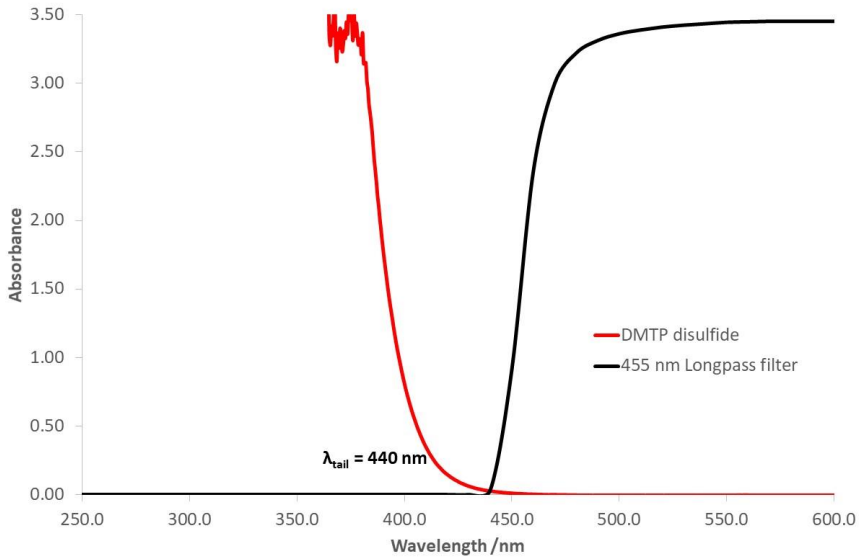

Figure 21: Absorption of DMTP disulfide **345** (CH_2Cl_2, c = 33 mM)

Thiyl Radical Homolytic Substitution

It is also possible that oxidation of thiolate, in the presence of adventitious oxygen, could generate thiyl radical **348** (Scheme 54). It may then be possible for the thiyl radical to carry out bimolecular homolytic substitution (S_H2) at the thioaminal **342**, leading to **344**. S_H2 reactions at C–S bonds are known between tributyl tin radicals and activated C–S bonds (e.g. thioaminals),[243] however these reactions require high temperatures and are made favorable by the formation of a strong Sn–S bond (BDE = 112 kcalmol^{-1}).[244] Thiyl radicals are also known to react with disulfides, forming transient tri-atomic species, that fragment into crossed mixture of disulfide and thiyl radicals.[245] In this case, generation of radicals was achieved by pulses of high energy electrons from a Van de Graaff generator.[246]

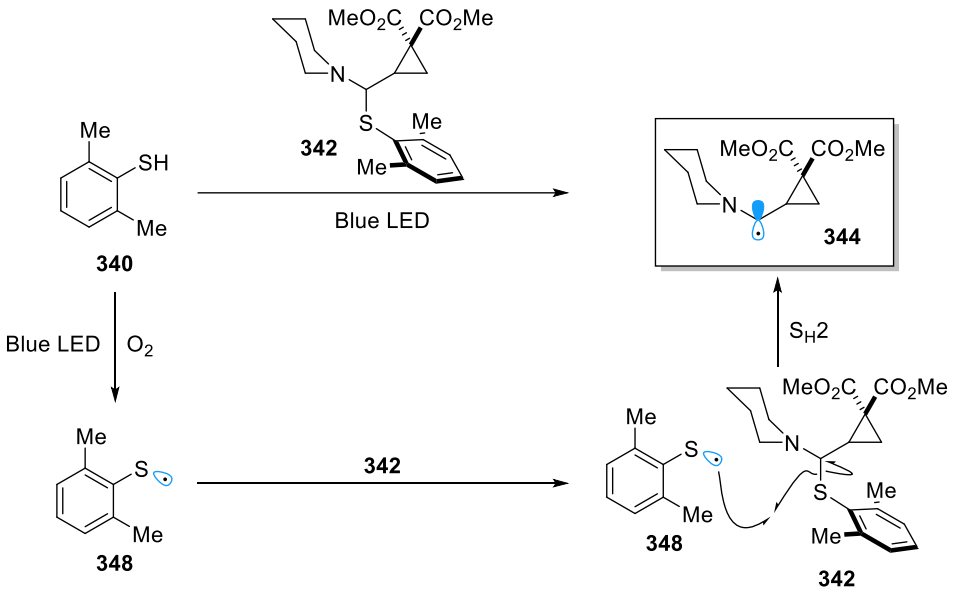

Scheme 54: Possible mechanism involving homolytic substitution at sulfur

On the other hand, S_H2 by a thiyl radical to form a relatively weak diaryl disulfide bond (BDE ≈ 50 kcalmol^{-1}), at the expense of a relatively strong C–S bond (BDE ≈ 65 kcalmol^{-1}) has not been reported. Steric hindrance due to the *ortho* dimethyl groups of DMTP would further disfavor the S_H2 mechanism. If a S_H2 mechanism were operational, irradiation of the thiol with light should generate significant quantities of disulfide, via thiyl radical formation. Furthermore, alkyl thiols should be more suitable for the reaction, since the dialkyl S–S bond resulting from S_H2 is ~15 kcalmol^{-1} stronger, compared to aryl thiols (BDE ≈ 65 kcalmol$^{=1}$ for dialkyl disulfides, BDE ≈ 50 kcal mol^{-1} for diaryl disulfides).[230]

Earlier, it was shown that irradiating DMTP with blue LEDs did not generate DMTP disulfide **345**. Therefore, it is unlikely that thiyl radicals can form spontaneously under light irradiation. Secondly, it was noted that a control reaction using DMTP previously generated acyclic aldehyde **338** in 90% yield, with 0% remaining starting material **298** (Scheme 55a). The ring-opening reaction was attempted using benzyl mercaptan, which gave 0% yield of the desired acyclic product **338**, and 76% yield of the starting material **298** (Scheme 55b). It was also observed that both DMTP and benzyl mercaptan formed their respective thioaminal species (**350** and

351) upon mixing. Therefore, the lack of thiyl radical formation under LED irradiation, and the lack of reactivity with alkyl thiols, suggested that S_H2 of the thioaminal by thiyl radicals was an unlikely mechanistic process.

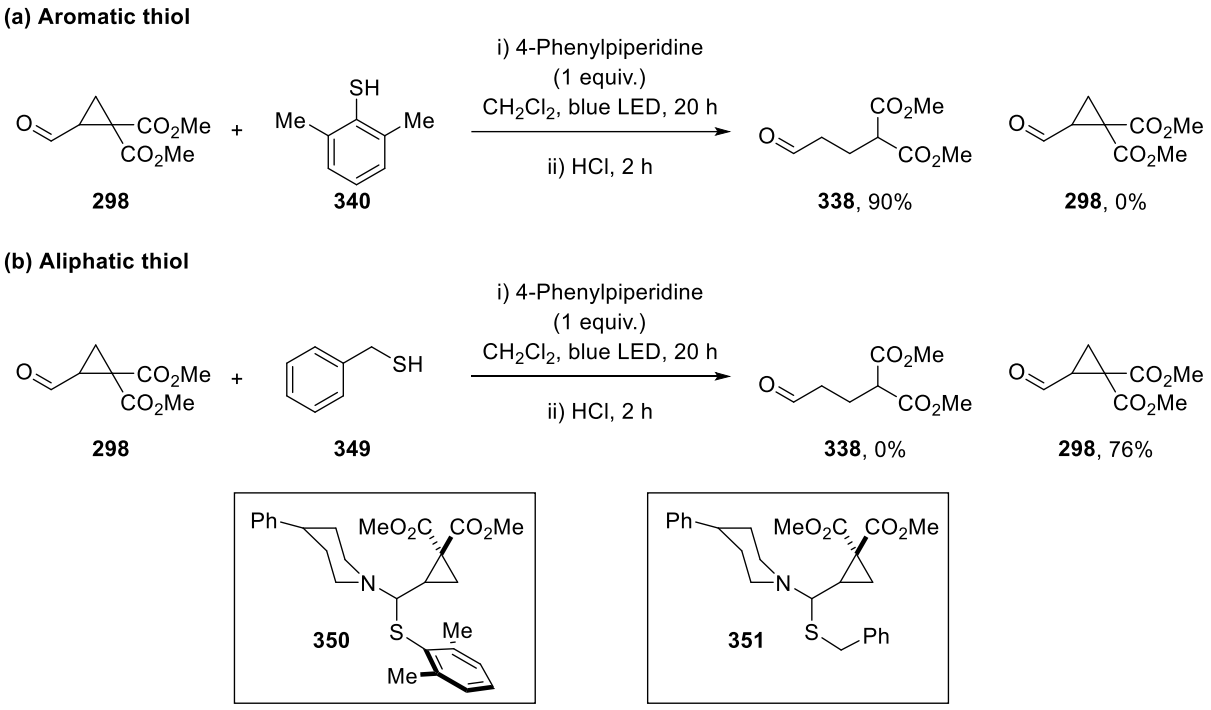

Scheme 55: α-Amino radical mediated ring-opening, using aromatic and aliphatic thiols

Photoinduced Thiol Excitation

A final mechanistic hypothesis involves direct excitation of the thiolate anion, followed by exciplex formation with ground state iminium and SET. To probe this, the UV-vis absorption of the sodium salt of DMTP was recorded (Figure 22). This showed that between the concentrations c = 0.33 mM and 33 mM, λ_{tail} reached 380 nm, which again was not compatible with longpass filter data.[240]

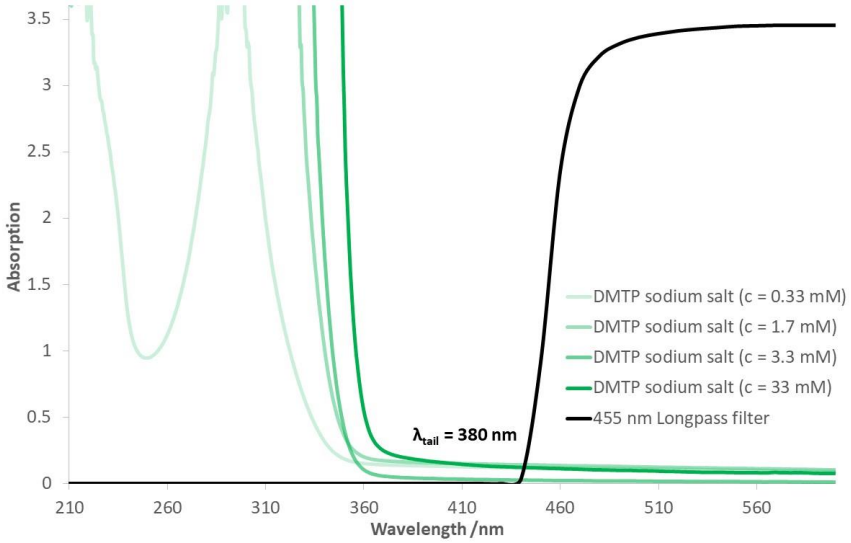

Figure 22: Absorption of sodium salt of 2,6-dimethylthiophenol (MeCN, c = 0.33 – 33 mM)

2.4.4. Computational Studies

After consideration of the above mechanisms, it was proposed that a charge-transfer (CT) complex could be the origin of radical formation. It was envisaged that thioaminal **342** could dissociate into its constituent iminium and thiolate ions (Scheme 56). Then, the electron-rich thiolate could act as a donor to the electron-rich iminium, forming a CT complex **352**. Visible light irradiation at an appropriate wavelength could induce excitation to **353**, which could lead to SET. This would reduce the iminium ion, whilst oxidizing the thiolate ion, thus generating an α-amino radical and a thiyl radical (**354**).

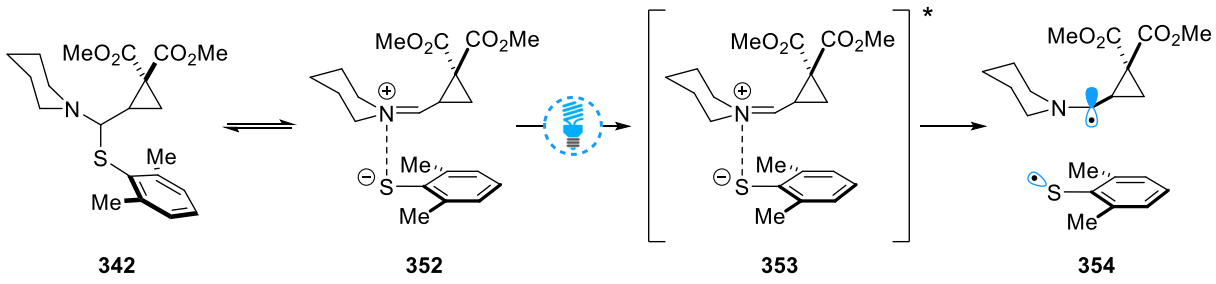

Scheme 56: Hypothesis for radical formation, by charge-transfer complex

A DFT study was conducted to investigate the feasibility of the proposed iminium-thiolate CT complex.[247] While standard DFT can predict ground-state properties, development of time-dependent DFT (TD-DFT) was extended in 1984, through derivation of a Hohenberg-Kohn-like theorem for the time-dependent Schrödinger equation.[248] The resulting techniques in TD-DFT allowed predictions of the interaction of electromagnetic fields with matter, and consequently the calculation of photo-absorption spectra.[249–251]

TD-DFT can give information on the electronic configurations that span the excited state wavefunction. This includes: i) transition energy, ii) oscillator strength and iii) molecular orbital composition of the transitions.

The transition energy gives the λ_{max}, where absorption of a photon could promote excitation. The oscillator strength denotes the intensity of transition between two states, which determines transition rates for absorption, and is correlated to the experimental molar absorption coefficient. The excited state wavefunction is not a single excited configuration, rather, it is represented as a linear combination of coefficients of the orbitals involved. The MO composition indicates the most important electronic configurations involved in the transition, as expressed by the largest coefficients.

DFT calculations were performed with the Gaussian 16 package (Revision A.03),[252] and geometry optimizations were performed with the B3LYP functional[253] and Pople 6-311+G(d,p) basis set.[254] Single-point energies were further evaluated using the 6-311+G(2d,p) basis set. Optimizations were performed in CH_2Cl_2 solvent using the conductor-like polarizable conductor model (CPCM)[255,256] of solvation, to account for charged species. London dispersion interaction correction was accounted for using the D3 version of Grimme's dispersion with Becke-Johnson damping.[257] With TD-DFT calculations, the CAM-B3LYP[258] and ωB97X-D[259] range-separated hybrid functionals were used to account for long and short range interactions – both gave similar outcomes.

To begin, the structure of thioaminal **342** was subjected to geometry optimization, and TD-DFT (CAM-B3LYP functional) was used to calculate its UV-vis absorption profile (Figure 23). We calculated 3 excited configurations (denoted by the three vertical green lines in Figure 23), with an overwhelmingly high oscillator strength transition at λ_{max} = 239 nm, as shown by the relative heights of the green lines. This transition was from the HOMO to the LUMO of the molecule, and visualization of the orbitals showed that these MOs were the thioaminal π and π* orbitals, respectively. This matched the measured absorption of λ_{max} = 237 nm (Figure 18).

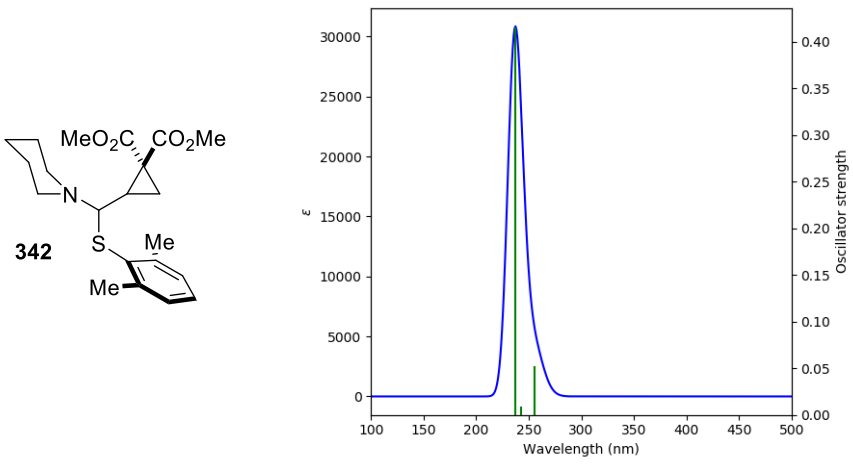

Figure 23: TD-DFT calculated absorption spectrum for thioaminal. Green line denotes oscillator strength. GaussSum used for visualization[260]

Next, geometry optimization was conducted on the putative iminium-thiolate complex, which successfully converged to a local energy minimum (Figure 24). Frequency analysis for the optimized structure gave exclusively positive frequencies, indicated a minimum energy point. The converged structure had a $r_{(N–S)}$

interatomic distance of 3.63 Å, which is comparable to the sum of the van der Waals radii of N and S atoms (3.55 Å).[261] The adjacent C(sp^2) atoms had an interatomic distance of $r_{(c-c)}$ 3.13 Å, and while not a perfect comparison, can be compared to the van der Waals distances for aromatic molecules of 3.40 Å. Interatomic distances, of the order of $r_{(D-A)}$ = 3.1 ± 0.3 Å, have been reported to be indicative of the presence of charge-transfer intermolecular forces.[73,262] Subjecting other orientations of the thiolate, relative to the iminium, to geometry optimization led exclusively to the thioaminal species. Additionally, increasing the interatomic distance between the N/S atoms, or the distance between adjacent C(sp^2) atoms, led to thioaminal convergence. Finally, replacement of the iminium, with an imine derived from a primary amine (or its protonated variant) and running the geometry optimization also resulted in convergence to the thioaminal. These findings indicated that electrostatic attraction, due to the formal positive charge of the iminium ion, was necessary for the complex to achieve a local energy minimum. Energetically favorable interactions due to the neighboring C(sp^2)/C(sp^2) atoms were also relevant in the formation of a local energy minimum.

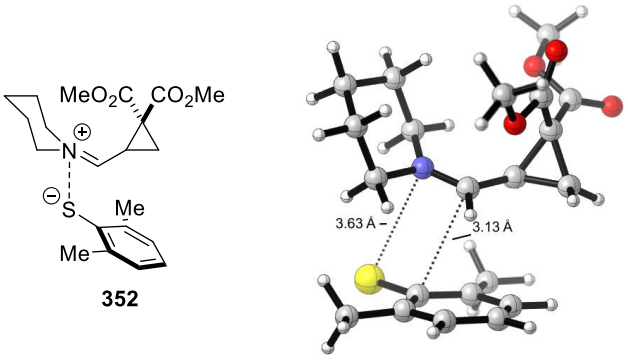

Figure 24: Local energy minimum found for iminium-thiolate complex. CYLview used for visualization[263]

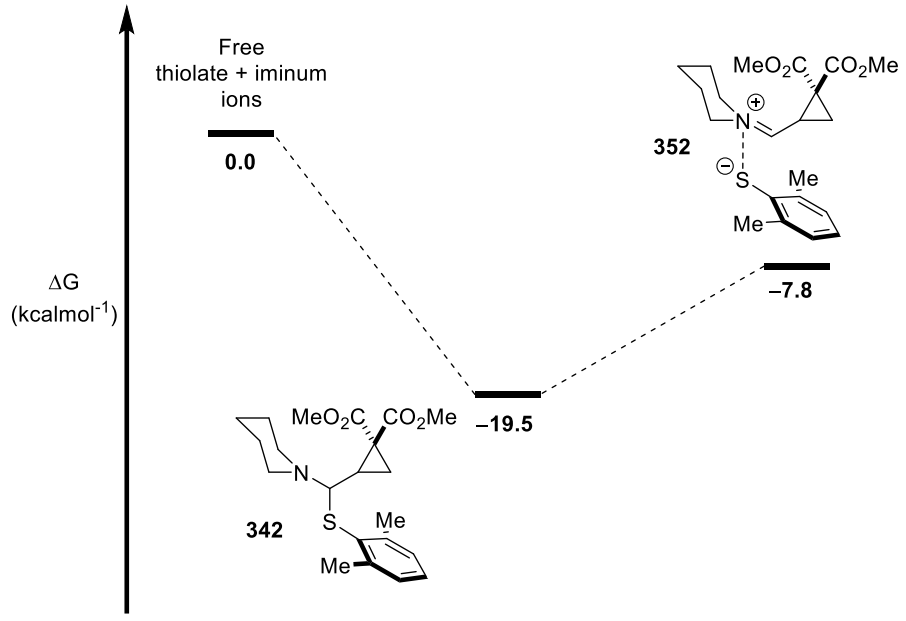

Figure 25: Calculated Gibbs free energy map for possible intermediates

Plotting the relative Gibbs free energies of the free iminium & thiolate ions, thioaminal **342** and iminium-thiolate CT complex **352**, showed that the global energy minimum was the thioaminal at −19.5 kcalmol^{-1} (relative to the free ions) (Figure 25). The CT complex was situated at −7.8 kcalmol^{-1}, indicating that intermolecular forces were present between the iminium and thiolate, which provide energetic stabilization, relative to the free ions. The −11.7 kcalmol^{-1} energy difference between the CT complex and the thioaminal highlights the potential transiency of the complex, with a predicted equilibrium constant of K_{eq} = 3.8x10^{8} at 298 K.

(a) Calculated excitations for complex

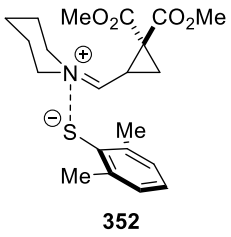

352

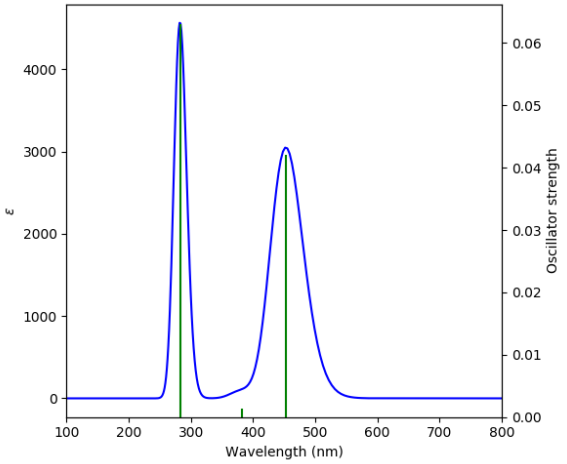

Electronic configuration	Wavelength (nm)	Oscillator strength (f)	Initial MO identity	Final MO identity	Contribution to transition
1	283	0.063	HOMO-2	LUMO	80%
			HOMO	LUMO+5	2%
			HOMO	LUMO+7	12%
2	382	0.001	HOMO-1	LUMO	97%
3	453	0.042	HOMO	LUMO	98%

(b) Visualization of HOMO and LUMO

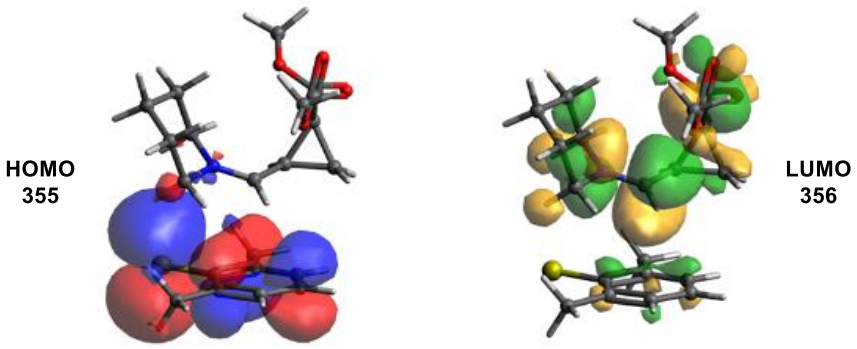

Figure 26: Predicted electronic transitions for iminium-thiolate complex. Visualization with Avogadro[264]

Upon running TD-DFT calculations on complex **352**, electronic transitions were calculated at λ_{max} = 283 nm, 382 nm and 453 nm with oscillator strength f = 0.063, 0.001, 0.042 respectively (Figure 26a). The new transition in the visible region at λ = 453 nm was relatively intense (f = 0.042) and comprised solely of a

transition between the HOMO and the LUMO of the complex (98% contribution). Visualization of the orbitals showed that the HOMO was comprised of the thiolate S lone pair electrons/π bonding orbitals (**355**), and the LUMO was comprised of the $\pi^*_{(C=N)}$ antibonding orbital (**356**) (Figure 26b). This indicated that irradiation at λ = 453 nm promotes an intracomplex electron transfer, from the thiolate to the iminium. In other words, photoexcitation reduces the iminium to the α-amino radical and oxidizes the thiolate to the thiyl radical. This was strongly supportive of our hypothesis of a charge-transfer complex mechanism.

Comparison of the calculated absorption (λ_{max} = 453 nm), with the Kessil lamp emission and 455 nm longpass filter, indicated that the filter partially blocks, but does not completely inhibit the calculated absorption (Figure 27). This could explain why the use of 420 nm and 455 nm light filters still allowed product formation to occur in 83% and 57% yield, respectively.

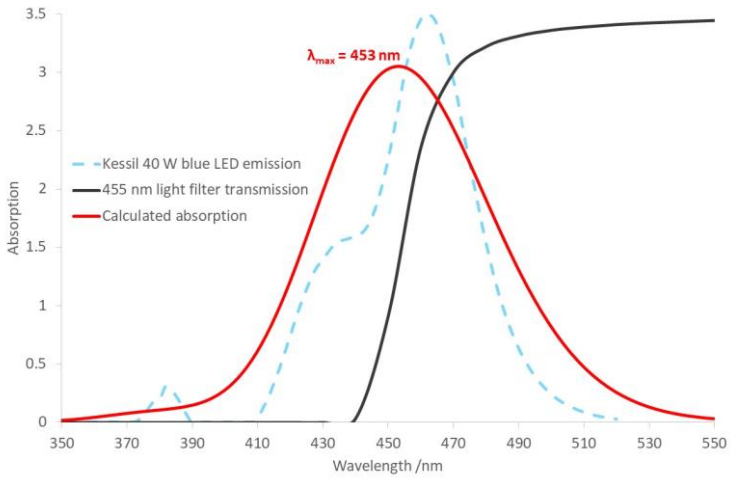

Figure 27: Comparison of filtered lamp emission and calculated absorption

Conducting TD-DFT calculations on 4-methoxythiophenol, instead of DMTP, gave similar results that were indicative of a CT complex (see Appendices). However, when the CT complex involving 4-nitrothiophenol was studied (**357**), the corresponding transitions were markedly different (Figure 28a). Of the three transitions, the dominant transition was transition 3 at λ = 410 nm, a HOMO to LUMO transition. Visualizing these orbitals showed that the HOMO was made up of the thiolate π-orbitals (**358**), however the LUMO was now based on the thiolate π*-orbitals (**359**) (Figure 28b). This is likely due to the nitro group lowering the energy of the thiolate MOs. These findings were in agreement with the previously observed yield of 0%, when 4-nitrothiophenol was used as the reductant (Table 9). It is also possible that the nitro group withdraws electron density and lowers the reducing ability of the thiolate, thus making it thermodynamically incapable of reducing the iminium ion.

(a) Calculated excitations for complex

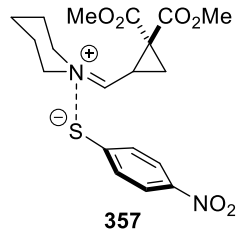

357

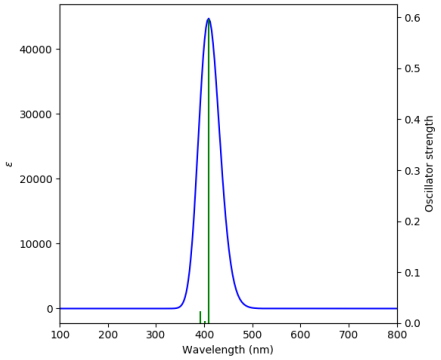

Electronic configuration	Wavelength (nm)	Oscillator strength (f)	Initial MO identity	Final MO identity	Contribution to transition
1	392	0.023	HOMO	LUMO+1	98%
2	401	0.005	HOMO-1	LUMO	87%
			HOMO-1	LUMO+1	2%
			HOMO-1	LUMO+9	5%
3	410	0.597	HOMO	LUMO	95%

(b) Visualization of HOMO and LUMO

HOMO
358

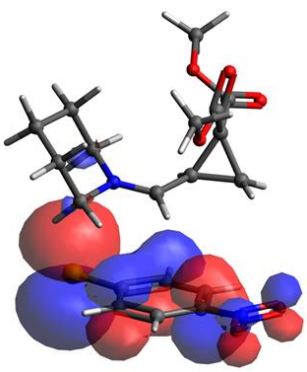

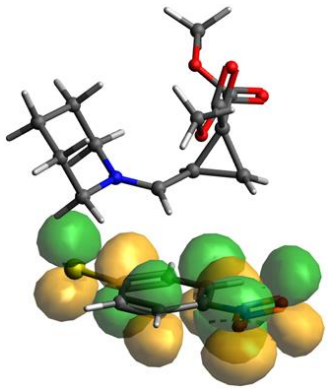

LUMO
359

Figure 28: Predicted transitions for 4-nitrothiophenol complex

Concurrently, the model reaction for the synthesis of **319** was conducted, using different solvents as the reaction medium (Table 10). This showed that the reaction had a dependence on solvent polarity, where solvents with low dielectric constants gave excellent yields (Entry 1-4), while more polar solvents gave lower yield (Entry 6-8).

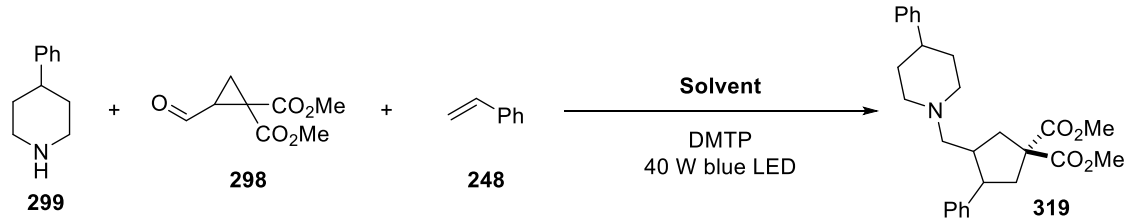

Entry	Solvent	ε	Yield (%)
1	CH_2Cl_2	8.9	99
2	EtOAc	6.1	99
3	THF	7.5	99
4	Benzene	2.3	99
5	MeCN	36.6	85
6	H_2O	80.1	12
7	DMF	38.3	8
8	DMSO	47.2	0

Table 10: Effect of solvent on photoinduced cyclization. ε = Dielectric constant[244]

The intermolecular forces in CT complexes are known to be less robust and directional than other weak forces such as hydrogen bonding, therefore they are generally highly sensitive to reaction conditions, such as solvent.[71,265] Both polar and non-polar solvents have been reported to be effective for CT complex-mediated reactions. Most reports utilizing CT complexes describe the complexation of two uncharged species (**361**), where upon electron transfer, two charged species are generated (**362**) (Scheme 57).[84] In such cases, it has been reported that polar solvents are effective in stabilizing the charged products of electron transfer (**362**) and preventing detrimental back electron transfer.

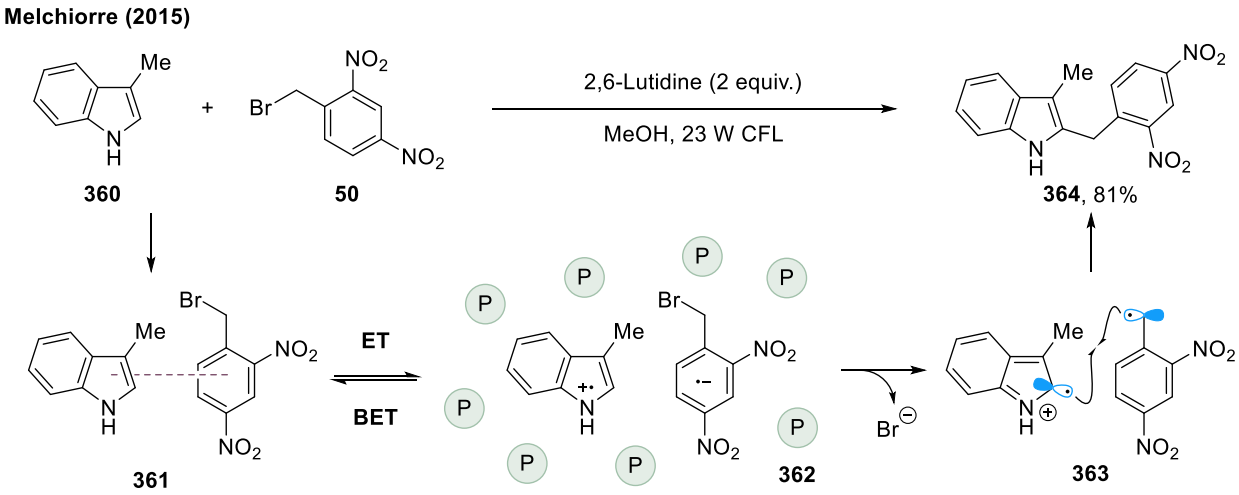

Scheme 57: Polar solvent could help stabilize charged intermediate after electron transfer. P: Polar solvent molecule

Whilst speculative, it is possible that since SET from the CT complex **352** results in uncharged radical species **354**, non-polar solvents could be beneficial in favoring electron transfer, and disfavoring back electron transfer (Scheme 58).

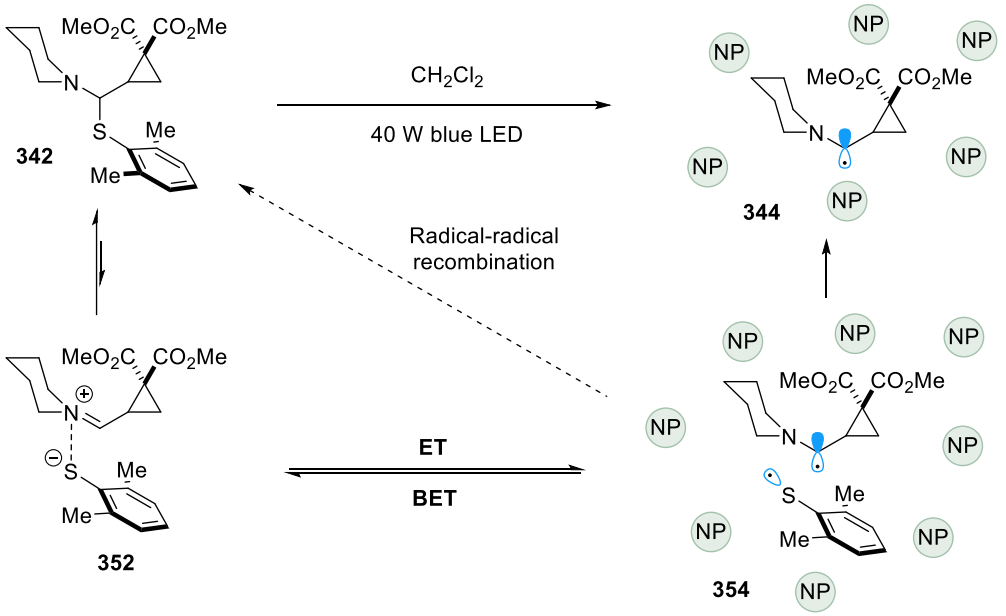

Scheme 58: Putative effect of solvent on charge-transfer α-amino radical formation. NP: Non-polar solvent molecule

Separately, the model reaction below was conducted in the presence of a 1,3-dinitrobenzene additive (Scheme 59). This additive can be used as an efficient CT acceptor, that disrupts other CT complexes from forming. The reaction gave 0% yield, which could be attributed to the formation of a competitive, strongly bound CT complex between the DMTP thiolate and 1,3-dinitrobenzene.

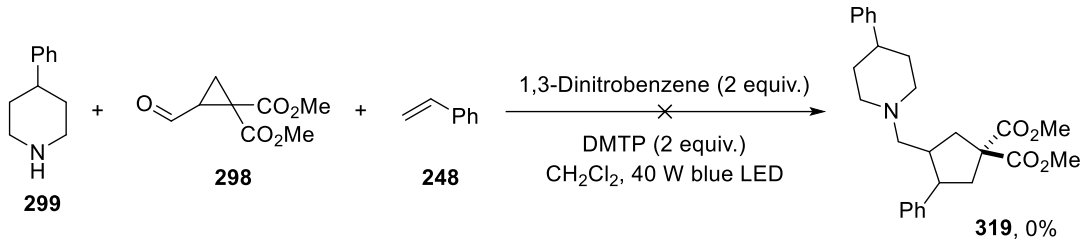

Scheme 59: Charge-transfer acceptor additive hinders reaction

Finally, we looked to test the significance of ion-pairing between the positively charged iminium and negatively charged thiolate, in the CT complex. Using a primary amine **365** in the model cyclization reaction, the desired product **366** was not observed (Scheme 60a). The reaction was also attempted with 0-1 equivalents of trifluoroacetic acid, which could have encouraged iminium formation and CT complexation. Furthermore, the ring-opening reaction of **298**, in the absence of an alkene acceptor, was investigated with primary amines (Scheme 60b). Running the reaction with and without addition of TFA, the starting material **298** was observed in 80% yield, indicating that primary amines could not promote α-amino radical formation.

The potential CT complexes of the imine and protonated iminium were also studied with the aforementioned computational methodology. Using a primary amine, successful convergence to a local energy minimum was not possible for the corresponding CT complexes; instead, the experiments converged to the thioaminal species. Both empirical and *in silico* evidence suggested that primary amines could not be used to generate α-amino radicals, supporting our hypothesis that ion-pairing may play a part in enabling the CT complex.

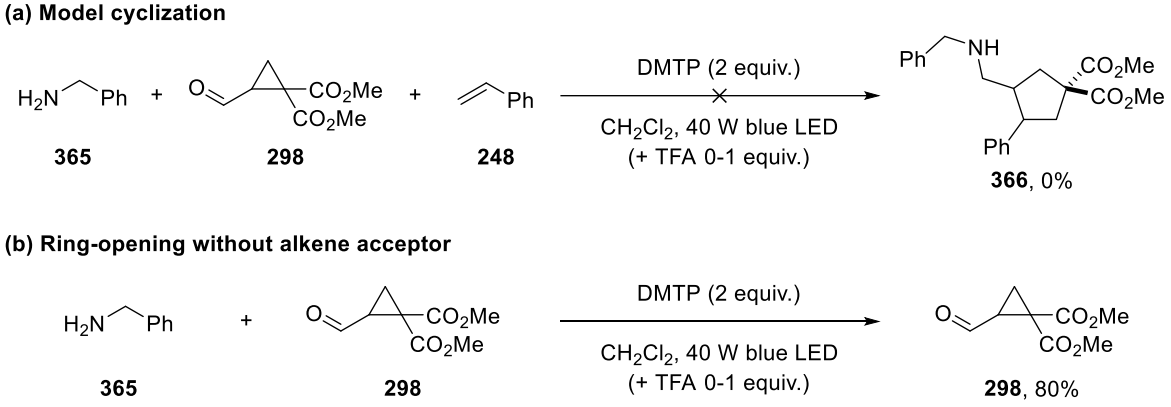

Scheme 60: Attempted reactions with primary amines. ^{1}H NMR yield using TCE as internal standard

2.4.5. Mechanistic Discussion

The literature precedence for thiolate and iminium ions engaging in CT complexation was considered. Regarding the thiolate component, Miyake has reported the complexation of thiolate ions with aryl bromides, generating putative CT complex **81** (Section 1.4.1. Scheme 12).[93] UV-vis absorption measurements indicated formation of a potential CT band, where the band absorption tailed off at λ_{tail} = 540 nm at high concentration (0.1 M). Furthermore, TD-DFT calculations predicted CT transitions at λ = 282 nm (high intensity) and λ = 383 nm (very low intensity). Both these absorptions contained local and charge-transfer band characteristics, which the authors cited as further evidence for a CT complex. Liao has also reported the CT complexation of thiolate ions.[266] Therefore, it was found that thiolate ions could feasibly act as an electron donor in CT complexes.

In these instances of thiolate donors acting as CT donors, the thiol component is incorporated into the final product. An emerging process in modern charge-transfer chemistry is the use of exogenous donors/acceptors, or redox auxiliaries, which prevent incorporation of the CT component in the final structure. In our reaction manifold, it was possible to use the thiol as a putative CT donor, without incorporation of the thiol in the final product. It is possible that there may be further instance where aromatic thiols can be utilized as photoinduced reagents, which effect single-electron reduction on organic substrates, without further reaction of the thiyl radical.

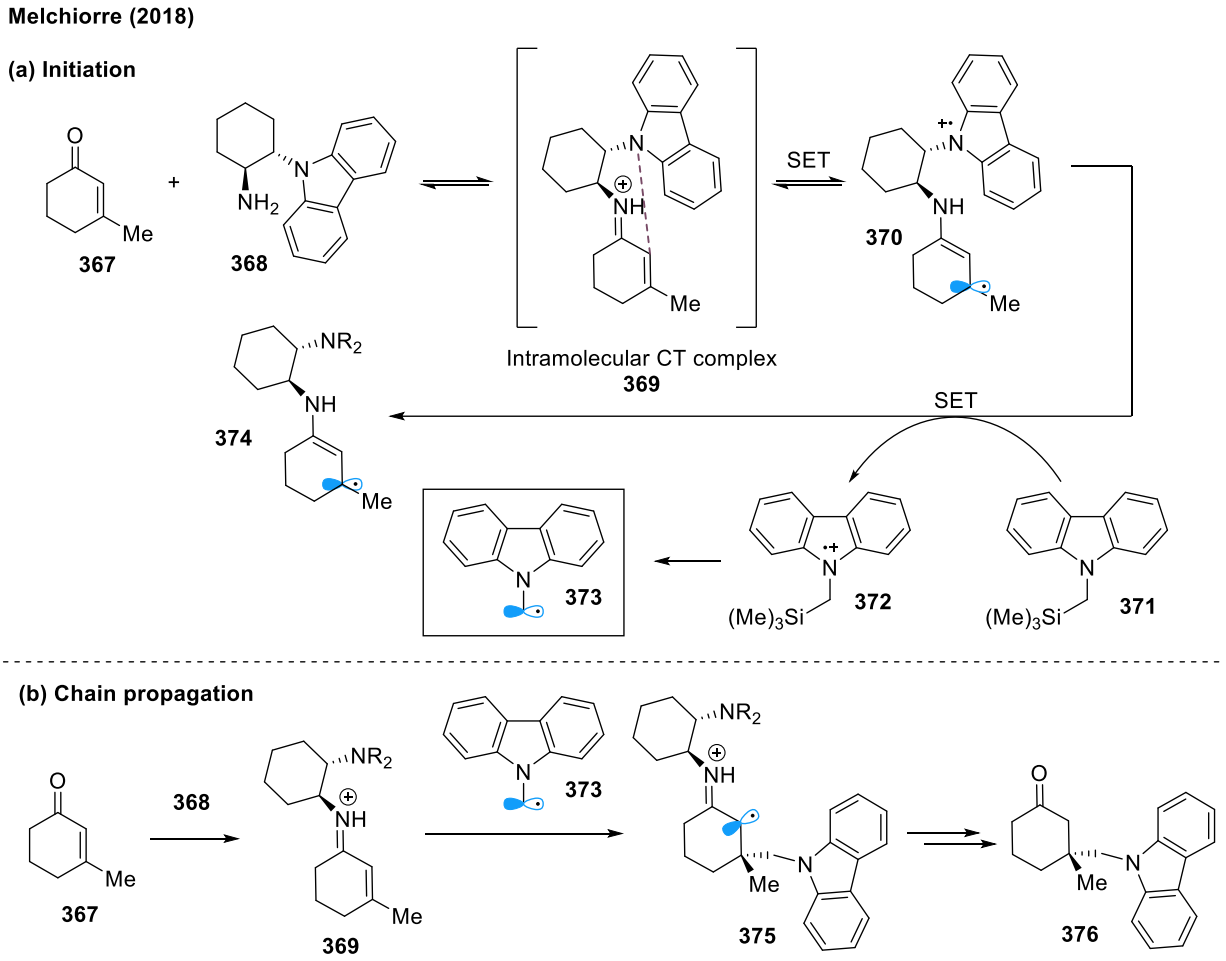

Scheme 61: Melchiorre's enantioselective radical conjugate addition, initiated by a charge-transfer interaction

Next, the iminium ion as a CT acceptor was considered. Melchiorre reported in their enantioselective radical conjugate addition reaction, that an intramolecular CT complex was involved in the initiation step (Scheme 61).[98] Cyclic enone **367** condensed with primary amine **368**, functionalized with a carbazole. Protonation of the resulting imine with acid led to putative formation of intramolecular CT complex **369**, involving coordination between the carbazole donor and the α,β-unsaturated iminium. Upon SET, radical intermediate **370** was thought to be generated. **370** was then reduced by alkyl silane **371**, generating aminium radical cation **372**, which fragmented to α-amino radical **373**. This radical intermediate then conducted radical addition to another molecule of α,β-unsaturated iminium **369**, generating **375**. Finally, SET with further alkyl thiol, then hydrolysis, could afford the final ketone product **376**. In support of the CT complex, the authors observed a small peak in the UV-vis absorption spectrum, upon mixing the reaction components (λ_{max} = 400 nm, λ_{tail} = 470 nm, c = 1.0 mM).

Gilmour has also reported the complexation of α,β-unsaturated iminium ions, with phenyl α-ketocarboxylates (Section 1.4.1. Scheme 13). Condensation of organocatalyst **86** and cinnamaldehyde **84** produced an α,β-unsaturated iminium ion, which was proposed to form CT complex **87**. Electron transfer was proposed to generate an enamine radical species, and a carboxyl radical species (**88**). Decarboxylation to **89**, followed by

radical-radical recombination, was proposed for the formation of enamine **90**. Upon hydrolysis, the product **91** was generated. TD-DFT calculations were invoked to propose a CT absorption at λ_{max} = 365 nm. Their mechanistic hypothesis was supported by a UV-vis absorption study, which showed a slight bathochromic shift, upon mixing the reaction components (λ_{tail} = 420 nm, c = 5.0 mM) (Figure 29). This would imply that at equilibrium, the phenyl conjugated α,β-unsaturated iminium ions, and the corresponding CT complex, form in sufficiently high concentration to be detected by the UV-vis absorption spectrometer.

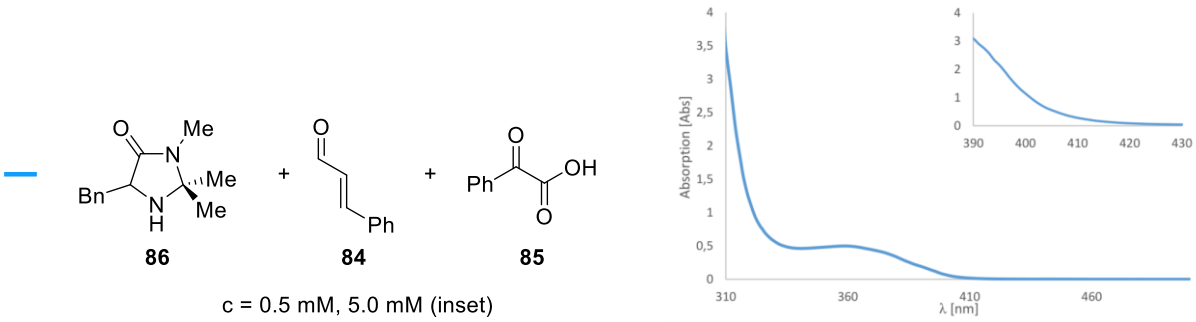

Figure 29: UV-vis absorption for complexation between α,β-unsaturated iminiums and ketoacetate

The works of Melchiorre and Gilmour both involved participation of a phenyl-conjugated α,β-unsaturated iminium ion, which presumably could form in sufficiently high concentration at equilibrium to participate in CT complexation. SET also resulted in generation of a radical , stabilized by aromatic and allylic conjugation, which reacted exclusively at the γ-amino position. On the other hand, Yu has reported the single electron reduction of conjugated aldimine **92**, through putative complexation with phenyl ketoacid **85**, to form CT complex **93** (Section 1.4.1. Scheme 14).[202] Upon light irradiation, formation of α-amino radical **94** was proposed. Upon mixing the 3 reaction components, UV-vis absorption measurements showed a bathochromic shift in the absorption band to λ_{tail} = 470 nm (Figure 30). Although the measurement concentration was not reported, the authors determined that the complex had putative 1:1 stoichiometry, through a Job plot. In this case, the protonated iminium is likely present in high concentration, allowing CT complexation to also occur to an observable extent.

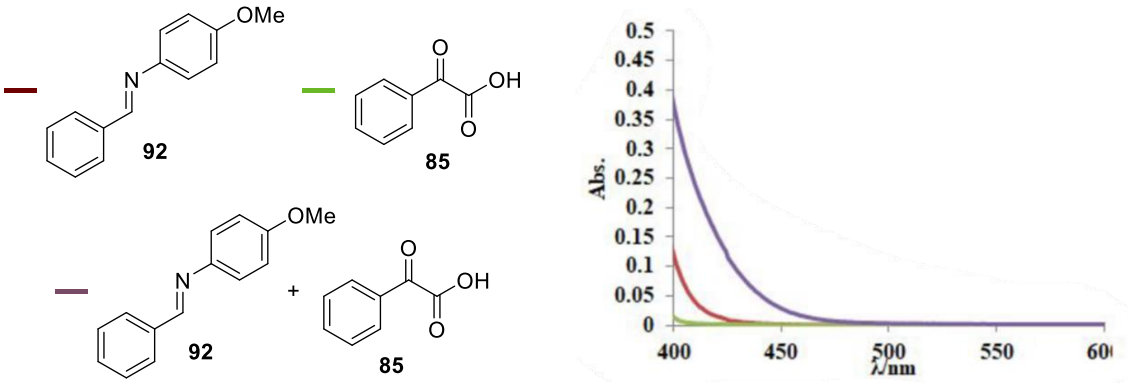

Figure 30: UV-vis absorption measurements for complexation between aldimines and ketoacetate

During earlier UV-vis absorption measurements of reactant mixtures, it was noted that the presiding thioaminal species did not absorb light beyond λ_{tail} = 385 nm, even at high concentration (c = 33 mM). Calculating the Gibbs free energies of the thioaminal and the putative CT complex, indicated that the thioaminal was relatively more stable ($\Delta G = -11.7$ kcalmol^{-1}) (Scheme 62). This suggested that at equilibrium, the concentration of iminium species, and the corresponding CT complex, would be significantly lower than observed by Yu and Gilmour, who utilized highly conjugated iminium species. The low concentration of alkyliminium ions present at equilibrium, could explain why changes in the absorption band were not observable, during UV-vis absorption studies.

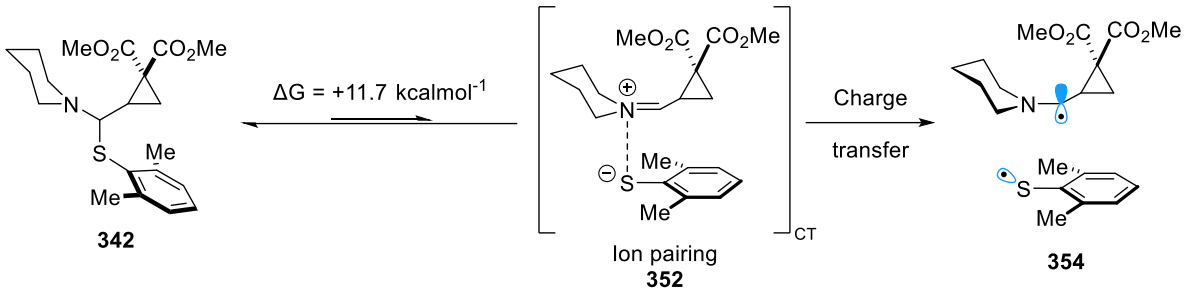

Scheme 62: Potential effect of ion pairing in enabling transient charge-transfer complexation

To our knowledge, there have previously been no reports of the single electron reduction of unconjugated iminium species, by a CT complex. In this context, it is possible that contact ion pairing between the iminium and thiolate ions provides a stabilizing electrostatic force, which enables complexation of the transient iminium species (**352**). Following early reports on contact ion pairing within CT complexes, which were described in the introduction, the application of contact ion pairing to organic synthesis has been underdeveloped. The reports by Gilmour and Yu represent recent examples of contact ion pairing within CT complexes. The putative iminium-thiolate ion pair complex described here may play a role in enabling transient CT complexation to occur.

2.4.6. Reaction Scope

Having concluded the optimization and mechanistic studies, the functional group tolerance of the activation mode was studied. Starting with the secondary amine fragment, cyclic amine substrates commonly used as building blocks in medicinal chemistry excelled in the reaction (Scheme 63) – tolerating 4-cyanopiperidine (80% yield, **379**), morpholine (84%, **380**), protected piperazine (77%, **381**), ketals (78%, **382**), free alcohols (72%, **383**) and thiazolidine (72%, **384**). Acyclic amines were successful in the reaction, with *N*-benzylmethylamine giving 81% yield (**385**), *N*,*N*-dibenzylamine giving 55% yield (**386**), and *N*-methylaniline giving 77% yield (**387**). Secondary amine drugs were subjected to the reaction, which showed that desloratadine gave **388** in an acceptable yield of 62%, as a 1:1 mixture of diastereomers. The presence of diastereomers was attributed to the reduced conformational mobility of the diaryl[*a*,*d*]cycloheptane ring. This

is because in its minimum energy conformation, the substituents of the bis-olefin are not in the same plane, leading to helical chirality.[267,268] Meanwhile, the reaction of fluoxetine afforded **389** in 72% yield and 1:1 dr.

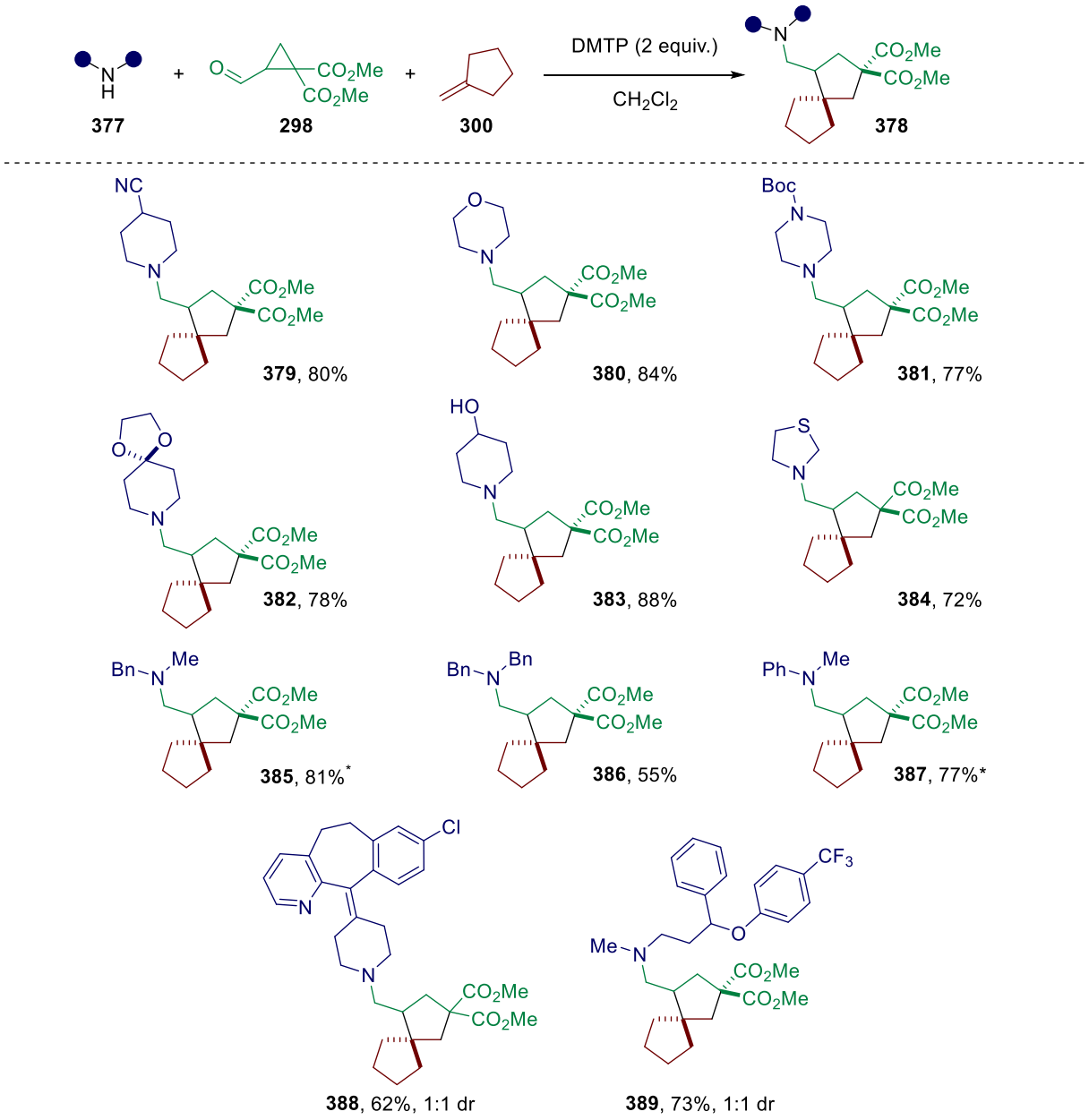

Scheme 63: Amine scope for charge-transfer radical cyclization. *3 equivalents of alkene

Some amine substrates were found to give poor or no reactivity, such as pyrrolidine **390** and azepane **391** which gave poor yields respectively (47%, 24%) (Scheme 64). Using *L*-proline methyl ester hydrochloride **392** as the amine, only trace amounts of the desired product was generated. Indoline **393** did generate the corresponding product in 89% yield; however, the result was an inseparable mixture with the oxidatively aromatized indole by-product (1.0 : 0.6 ratio). Reactions using indole **394** and tetramethyl piperidine **395** did not produce the desired products, reflecting the reduced nucleophilicity at nitrogen, due to conjugation and steric encumberment. With sterically hindered amines like diisopropylamine and tetramethylpiperidine, pre-

heating of the reaction vessel to 80 °C was conducted, before and/or during light irradiation; however, no product was observed.

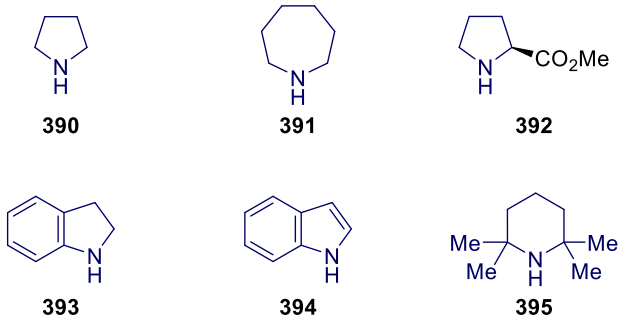

Scheme 64: Amines which performed poorly or gave poor selectivity

The alkene scope was found to accommodate a variety of different functionalities (Scheme 65). The use of simple olefin partners, such as methylenecyclopentane, is typically rare in radical addition reactions[269] and is not known for radical cyclization reactions to make cyclopentanes.[210,213,214,216] This is because there is no potential for polarity matching between the incoming radical and the alkene acceptor. Furthermore, simple olefin partners do not offer as much stabilization upon radical addition, compared to electron-withdrawing or aromatic stabilizing groups.

Exocyclic alkenes were found to be effective in the reaction, generating spirocyclic products **379**, **399** and **400** in 80%, 79% and 76% yield. For a number of these reactions, the highest yield could be obtained by using a slightly higher equivalence of alkene acceptor (up to 5 equivalents). Reaction with an exocyclic alkene, containing a protected piperazine, gave 78% yield of **401**. Incorporation of acyclic alkene 2-ethyl-1-butene gave 66% yield of **402**. Notably, the unactivated terminal alkene 1-hexene also gave **403**, in 59% yield and a dr of 9:1. Styrenyl acceptors were found to work well; reactions using styrene, 4-bromostyrene and 4-methoxystryene generated products **404**, **405** and **406** in 80%, 68% and 59% yield respectively, all proceeding with 9:1 dr. The electron-poor acceptor 4-vinylpyridine gave **407** in 60% yield and 9:1 dr, while butyl acrylate gave **408** in 43% yield and 1:1 dr. Finally, the electron-rich acceptor 2,3-dihydrofuran was found to give the corresponding 5,5-fused product **409** in 59% yield and >20:1 dr, confirmed by X-ray diffraction of a single crystal **410**.

Reaction with cyclohexene **411** gave no product, showing the difficulty of radical addition to 1,2-substituted alkene sites (Scheme 66).[270] It was also found that alkynes such as phenylacetylene **412** could not be incorporated. The use of 4-nitrostyrene **413** gave no product, potentially due to charge-transfer complexation between the electron-deficient alkene and electron-rich thiol, and/or competing thiol-ene reactivity between thiyl radicals and 4-nitrostyrene.

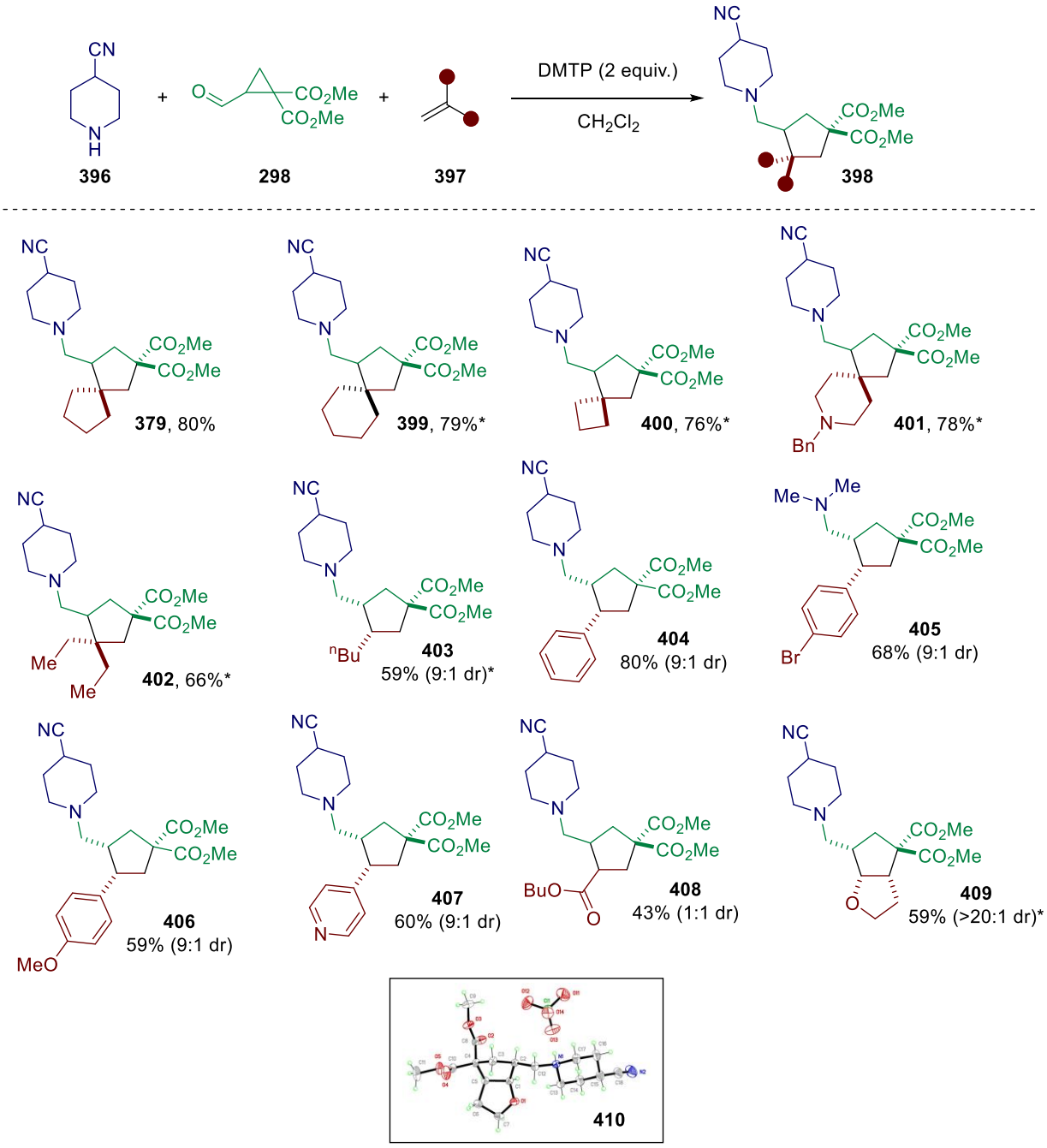

Scheme 65: Alkene scope for charge-transfer radical cyclization. *5 equivalents of alkene

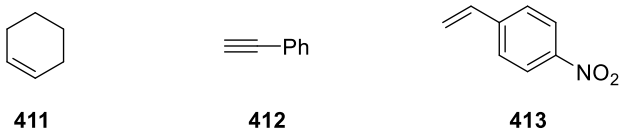

Scheme 66: Poorly performing alkenes

Regarding the cyclopropyl carboxaldehyde component, the reaction with mono-ester substituted **416** was attempted. Using **416**, *N*-methyl benzylamine and styrene, it was possible to observe the product in 54% yield

with some diastereoselectivity, however, it was not possible to cleanly isolate the products. Conducting the reaction with simple cyclopropane carboxaldehyde gave the direct reductive amination product **417** in 82% yield (as determined by ^{1}H NMR) and 64% yield after isolation. In cases where there is no cyclopropyl substitution, the rate of HAT between the nucleophilic α-amino radical and stoichiometric thiol likely outcompetes the rate of cyclopropyl ring fragmentation. It is also possible that radical fragmentation of the unsubstituted cyclopropyl ring is reversible.

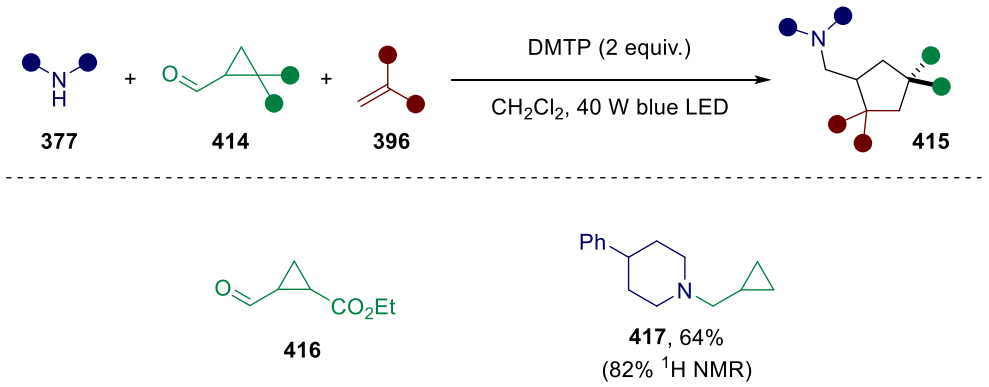

Scheme 67: Aldehyde scope for charge-transfer cyclization. Brackets denote ^{1}H NMR yield using TCE and internal standard

It was proposed that the high concentration of thiol present in the reaction was preventing formation of the desired di-substituted cyclopentane product. To lower the concentration of thiol to catalytic quantities, an alternative radical formation method was required. Previously, it was shown that photocatalytic conditions and an acrylonitrile acceptor, could be used to generate di-substituted cyclopentane **281** (Scheme 68a). Our studies suggested that by using styrene, double incorporation of the alkene could be avoided. Furthermore, by using a catalytic quantity of hindered thiol, premature HAT before cyclopropyl ring fragmentation could be disfavored. Using styrene and TRIP-thiophenol, the di-substituted cyclopentane **418** was successfully obtained in 77% yield and 3:1 dr (Scheme 68b).

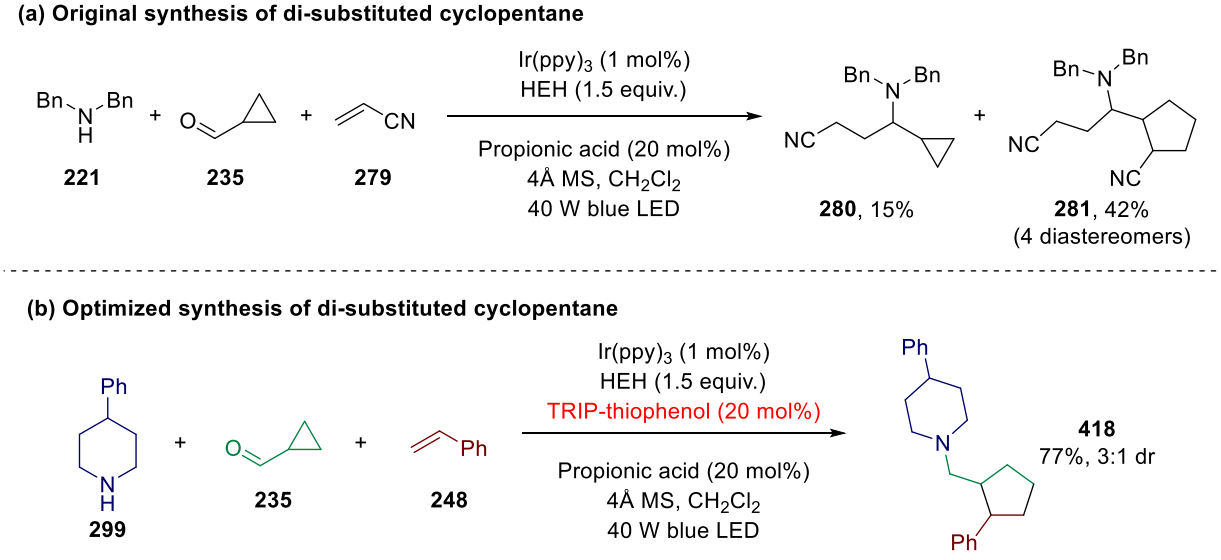

Scheme 68: Photoredox catalyzed synthesis of di-substituted cyclopentanes

In summary, the novel method of α-amino radical generation was tolerant of a wide range of functional groups, including with late-stage drug fragments. A key issue is the underlying dependence on successful condensation between the secondary amine and the carbonyl, which currently prevents reactivity of sterically hindered amines with aldehydes, and with ketones in general.

2.5. Summary

This chapter has described the development of a method for α-amino radical generation. This was initiated by exploratory investigations into the activity of α,α-cyclopropyl-amino radicals, generated via photoredox catalysis. The resulting radical could be intercepted using alkene partners, generating cyclopentyl methylamines (**319**) in a multicomponent fashion (Scheme 69a). More significantly, the cyclopropyl ring became a key probe, with which α-amino radical formation could be detected, leading to a photocatalyst-free method of forming α-amino radicals. This was used to achieve the multicomponent synthesis of cyclopentyl methylamines (**379**, Scheme 69b). Mechanistic experiments showed that radical formation could occur with visible-light irradiation above λ = 455 nm. Computational experiments rationalized the most likely mechanism to be the formation of a visible-light promoted, charge-transfer complex, between iminium and thiolate ions (Scheme 69c).

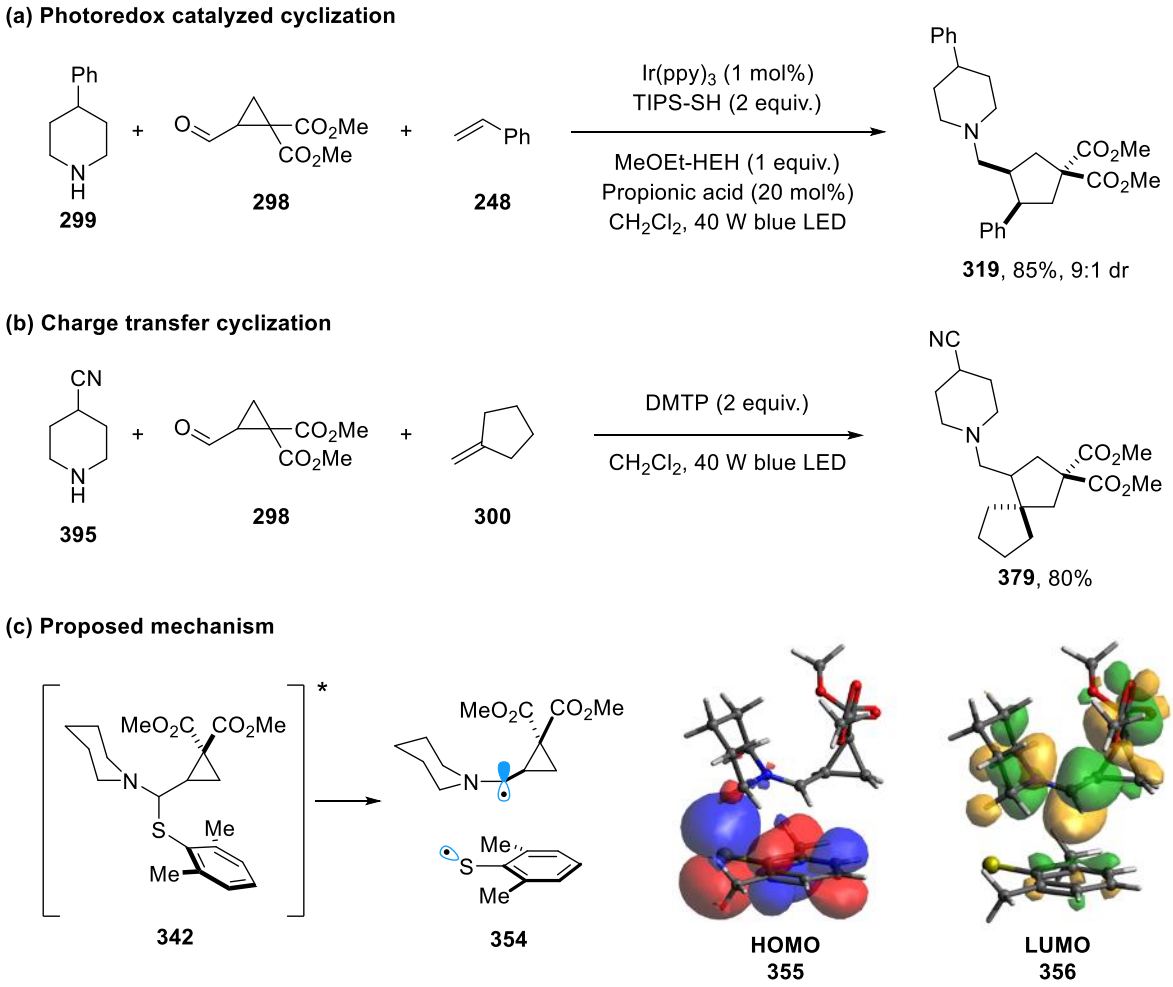

Scheme 69: Development of a fragmentation-cyclization reaction, via charge-transfer complex α-amino radical formation

3. Radical Reductive Amination

3.1. Introduction

3.1.1. Hydrogenative and Hydridic Methods

Reductive amination is one of the foremost methods for C–N bond formation, suitable for accessing all classes (primary, secondary, tertiary) of amine.[271] In this chapter, the method of 'direct' reductive amination will be discussed. This is where the amine, carbonyl and reductant are mixed, leading to the generation of an imine/iminium intermediate in situ, which is reduced to give the amine product. Reductive amination has grown to be highly used in research and medicinal chemistry, reported as being the sixth most used reaction by major pharmaceutical companies.[272] A wide variety of substrates can be employed, including aliphatic aldehydes and ketones, aromatic aldehydes and ketones, which can be combined with amines, from ammonia to aromatic amines. Some limitations are present, owing to steric hindrance on the amine or ketone components, weakly electrophilic carbonyl groups, or poorly nucleophilic amines, which lead to sluggish reactivity. In these cases, additives such as molecular sieves or Lewis acids can be used to increase the rate of reactivity.

In the case of direct reductive amination, the choice of reductant is crucial to the efficiency of the reaction since the reductant must reduce the imine selectively, over the initial carbonyl compound. The first class of reduction is catalytic hydrogenation using a metal catalyst and H_2, which is an atom economical method often utilized in large scale reactions.[273,274] However, this relies on the corresponding carbonyl reduction being slow, and the reaction can be hampered by low yields, selectivity and tolerance to functional groups such as nitro, cyano and sulfide compounds.

The second method utilizes hydride reducing agents – the first reports of reduction with Schiff bases appeared in the late 1950s;[275] however, Schellenberg first reported in 1963 the use of sodium borohydride ($NaBH_4$) as a reducing agent.[276] The next advance came in 1971 by Borch and Durst, who reported the more selective sodium cyanoborohydride ($NaBH_3CN$) as a reducing agent.[277] The utility of this reagent stemmed from the different selectivity it exhibits at different pH, its stability under acidic media (pH ≈ 3) and good solubility in standard organic solvents. Importantly, the reductive amination could be carried out under neutral/weakly acidic conditions, promoting imine/iminium formation, and limiting reduction of the carbonyl compound. While highly convenient and high yielding, some limitations remained, such as the requirement of a large excess of amine, and the production of toxic cyanide containing by-products. Subsequently, a host of modified procedures have been developed, using Lewis acid additives,[278] resins,[279] metals,[280] metal hydrides[281] and electrochemical methods.[282]

A further advancement came in the development of sodium triacetoxyborohydride (STAB-H), which was initially conceived in the large-scale synthesis of a drug candidate. STAB-H is now widely used as a convenient reductant, whose use does not require preformation of the imine, and eliminates toxic cyanide

contaminants.[283,284] The steric and electron-withdrawing effects of the three acetoxy groups stabilize the boron-hydrogen bond, making it a mild reductant, which reduces reduction of the carbonyl precursor.

3.1.2. Radical Methods

Recently, visible-light mediated photoredox catalysis has provided a platform to enable new synthetic methodologies via single-electron transfer. This has led to the emergence of a third, mechanistically distinct method of achieving reductive amination.[285] The first report came from Wenger in 2018, who used the photocatalyst $[Ru(bpy)_3]^{2+}$, to reduce the iminium species generated from the condensation of primary amine **265** and ketone **419**, forming α-amino radical **421** (Scheme 70).[286] The key reductive Ru^{I} state was generated from initial reductive quenching with ascorbate. However, it was found that ascorbate was a poor hydrogen atom donor for the HAT step, due to a polarity mismatch between the nucleophilic α-amino alkyl radical and the electron-rich ascorbate. Therefore, the addition of mercaptopropionic acid **422** was required, which led to polarity-matched HAT between the thiol and α-amino radical, to form product **426**. A matched HAT between the thiyl radical and ascorbate regenerated the thiol **422**. The authors noted that a potential advantage over thermal conditions, could be the ability to append a photoactive group with spatial control, by irradiating certain parts of a cellulose support with light.

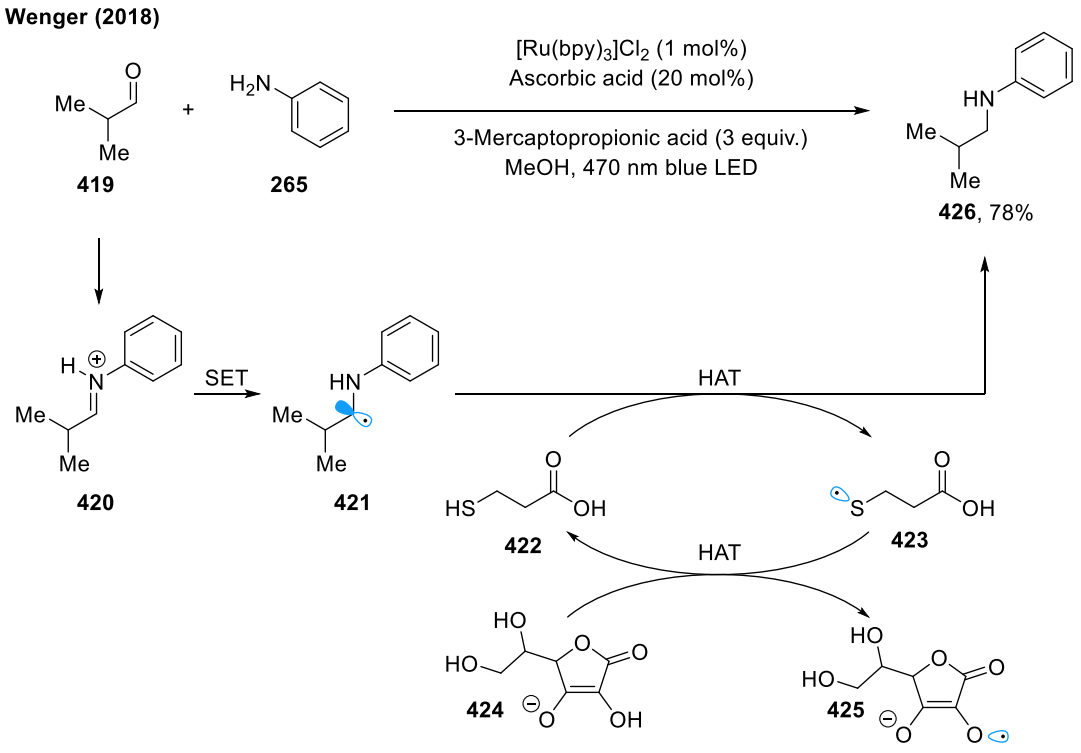

Scheme 70: Radical reductive amination, by photocatalytic α-amino radical generation

Molander subsequently reported the reductive amination of benzaldehydes and secondary amines with a photocatalyst, via generation of α-amino radical **430** (Scheme 71). Here it was proposed that aminal **428** undergoes oxidation to **429**, followed by a putative deprotonation fragmentation process, generating the α-

amino radical. The radical was then proposed to undergo reduction to the benzyl-stabilized anion **431**, followed by protonation. In cases where this reduction was thermodynamically unfavorable (e.g. with *p*-anisaldehyde), a thiol additive was added, to conduct HAT on α-amino radical **430**. Another method by Polyzos[287] and Walsh[288] conducted the reductive amination of diarylimines with triethylamine as the hydrogen atom source. Peng has also used quantum dots as photocatalysts, to conduct reductive amination with anilines and benzaldehydes.[289] Finally, Gilmore reported the photoredox reductive amination of alkyl ketones using ammonia gas, to generate the corresponding primary amines.[290]

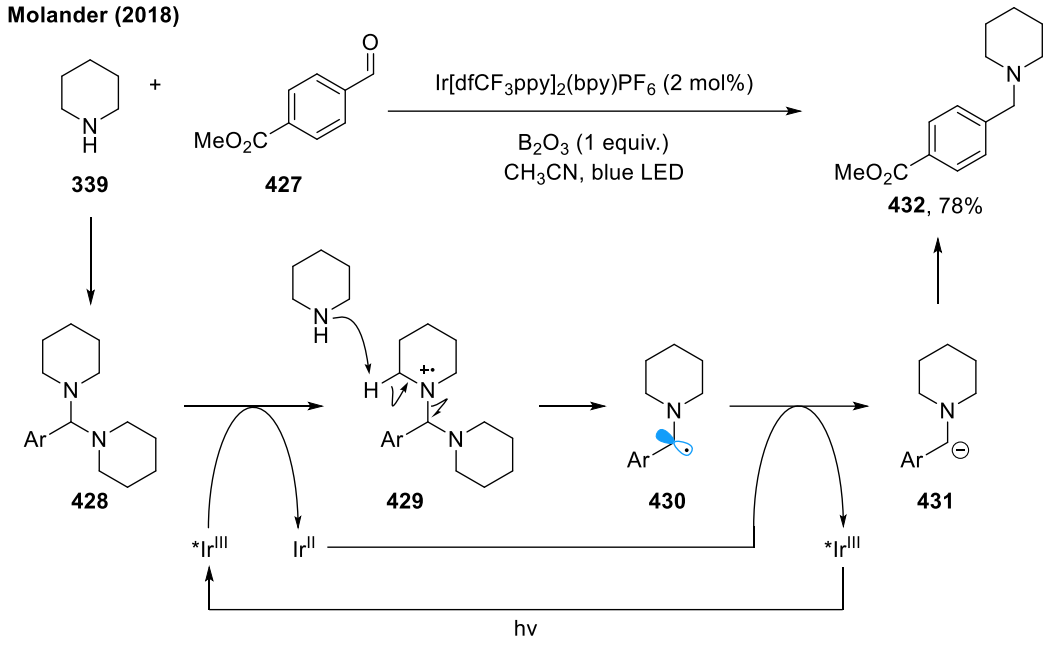

Scheme 71: Reductive amination via single electron oxidation of aminal

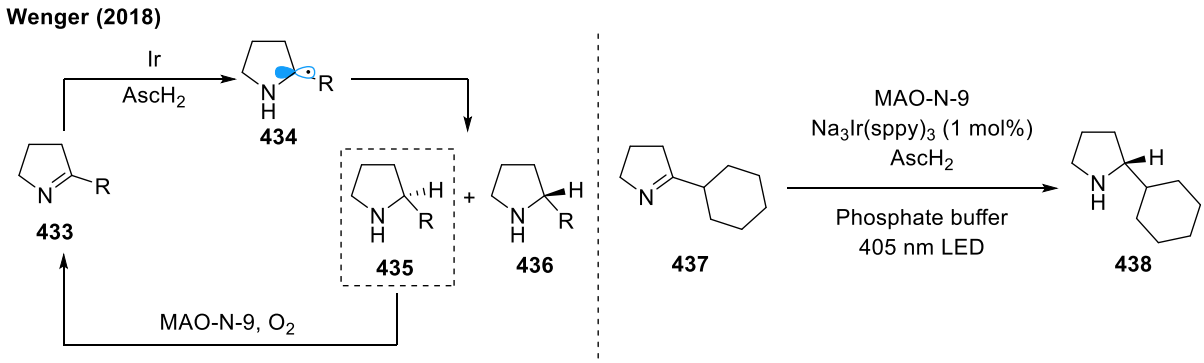

Scheme 72: Enantioselective radical reductive amination with enzymatic catalysis

In terms of enantioselective reactions, Wenger reported in 2018 a strategy where a preformed cyclic imine **433** could be reduced, under acidic photocatalytic conditions, to the α-amino radical **434** (Scheme 72).[291] Hydrogen atom transfer with ascorbic acid initially gave the racemic mixture of amines **435** and **436** with no steric discrimination. Monoamine oxidase (MAO-N-9) was effective in catalyzing the oxidation of the *(S)*-

enantiomer of the amine (**435**), back to the starting material (**433**). This repeated enzymatic recycling process ultimately led to accumulation of the *(R)*-amine (**436**), which was obtained in excellent yield and enantioselectivity, albeit over a limited range of substrates.

3.2. Project Aims

The previous chapter discussed the development of a novel photoinduced method to generate α-amino radicals, using aromatic thiols as a putative charge-transfer donor, to reduce iminium ions. Whilst attempting the radical cyclization reactions, in certain cases, it was observed that the reductive amination product was obtained. For instance, when an amine **221** was reacted with cyclopropyl carboxaldehyde **235**, the reductive amination product **439** was obtained in 64% yield (Scheme 73). However, it was found that when acyclic butyraldehyde **222** was used, only 8% of the product **440** was observed. Therefore, the development of a photoinduced reductive amination, which could be extended to a wider class of aldehyde substrates, was investigated.

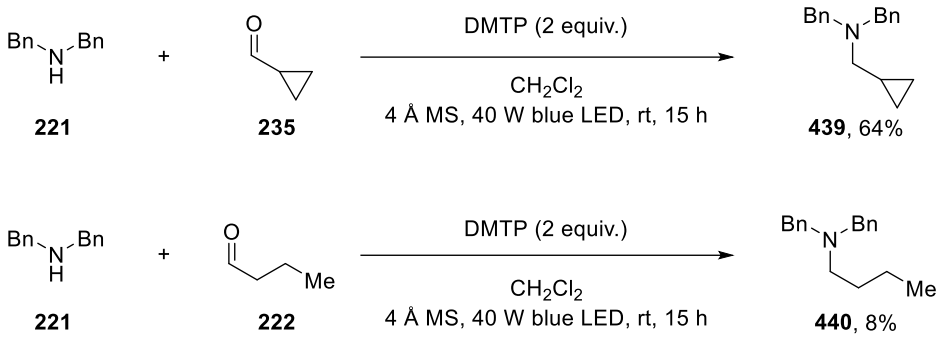

Scheme 73: Preliminary results for photoinduced radical reductive amination

3.3. Charge-Transfer Complex Reductive Amination

3.3.1. Reaction Discovery

Based on the observation that cyclopropyl carboxaldehyde **235** generated the desired product, while butyraldehyde did not, it was hypothesized that the presence of a labile α-hydrogen was detrimental to the reaction (Scheme 74). It was proposed that the α-hydrogen could facilitate formation of an enamine species, which could act as an unfavorable resting state for the reaction. Attempting the reaction with benzaldehyde **441** showed successful reactivity, with isolation of tertiary amine **442** in 78% yield.

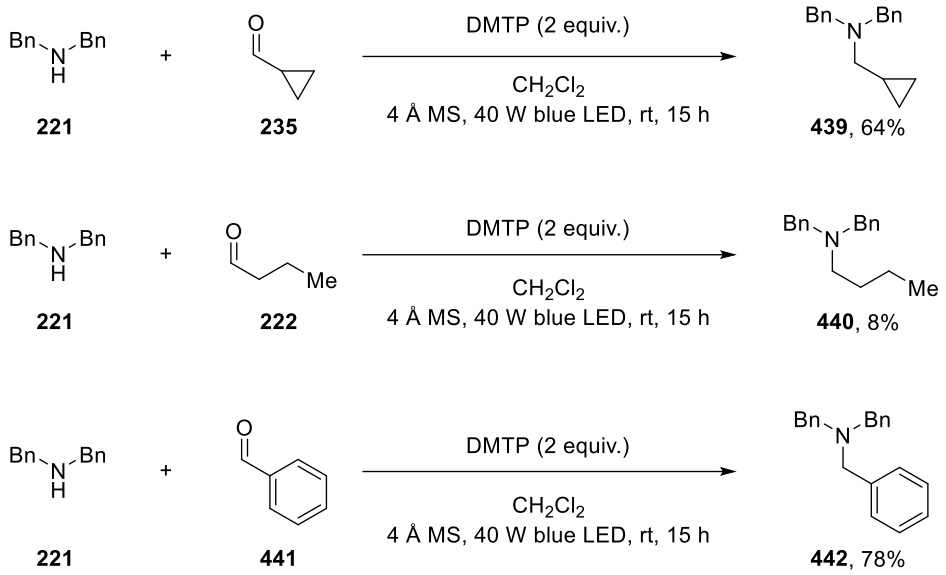

Scheme 74: Significance of α-carbonyl hydrogen in radical reductive amination

To develop reaction conditions for the radical reductive amination, a screening study of the reaction conditions was conducted, in conjunction with Philipp Pflüger (Table 11). Upon investigating solvents, it was found that DMSO and DMF were marginally better at promoting the reaction, giving 14% and 12% yield respectively (Solvent Screen, Entry 8, 9). Using DMF as the solvent, a screening of various Lewis/Brønsted acid and base additives found that cesium carbonate was effective, giving an assay yield of 77% (Additive Screen, Entry 6). A further screening of different bases found that most bases with a pK_{aH} of greater than 8 were effective, with potassium *tert*-butoxide giving 89% yield (Base Screen, Entry 5). Concurrently, an equivalence screen using cesium carbonate showed that 0.5 equivalents of this base could also be used (Base Equivalence Screen, Entry 3), with additional base (over 1 equivalents) leading to lower yield (Entry 4). The putative purpose of the base is described later in the Mechanistic Discussion. A study of reaction concentration found that 0.1 M was the optimal concentration (Concentration Screen, Entry 2).

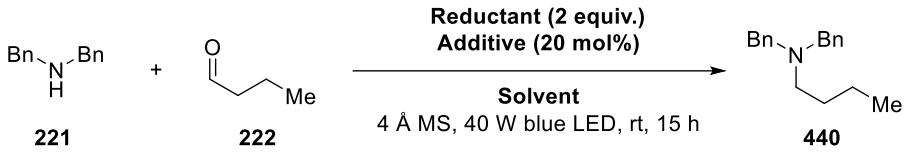

Entry	Solvent Screen*	Yield (%)
1	H_2O	3
2	THF	4
3	EtOAc	4
4	MeOH	5
5	MeCN	5
6	CH_2Cl_2	8
7	DMA	8
8	DMF	12
9	DMSO	14

With DMTP (2 equiv.)

Entry	Additive Screen*	Yield (%)
1	Trifluoroacetic acid	4
2	1,1′-Binaphthyl-2,2′-diyl hydrogenphosphate	5
3	$AlCl_3$	5
4	-	8
5	$B(C_6F_5)_3$	12
6	Cs_2CO_3	77

With DMTP (2 equiv.), DMF

Entry	Base Screen*	$p K_{aH}$	Yield (%)
1	K_2HPO_4	7	13
2	Cs_2CO_3	10	77
3	DABCO	9	81
4	Lithium bis(trimethylsilyl)amide	26	86
5	KO*t*Bu	17	89

With DMTP (2 equiv.), DMF

Entry	Equivalence of Base Screen*	Yield (%)
1	0.1	25
2	0.2	89
3	0.5	94
4	1.0	24

With DMTP (2 equiv.), Cs_2CO_3, DMF

Entry	Concentration Screen (M)*	Yield (%)
1	0.05	93
2	0.1	94
3	0.2	85
4	0.5	59

With DMTP (2 equiv.), KOtBu (0.5 equiv.), DMF

Table 11: Initial screening of conditions. GC-MS yield using dodecane as internal standard. *Conducted by Philipp Pflüger.

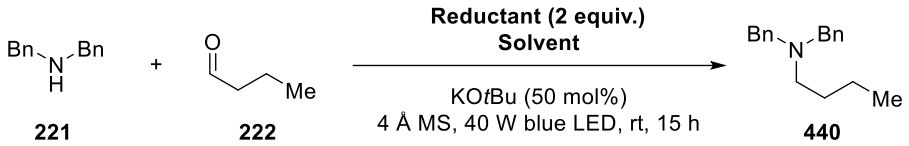

Entry	Solvent Screen*	Yield (%)
1	MeOH	2
2	THF	5
3	CH_2Cl_2	13
4	EtOAc	36
5	DMSO	64
6	MeCN	80
7	DMA	83
8	DMF	94 (88)

With DMTP (2 equiv.), DMF

Entry	Misc. Screen*	Yield (%)
1	Dark	0
2	TEMPO (2 equiv.)	0
3	No molecular sieves	27
4	Air atmosphere	46
5	Heating at 60 °C in dark	46

With DMTP (2 equiv.), DMF

Entry	Reductant Screen*	Yield (%)
1	TIPS-SH	0
2	Cysteine	0
3	Thiobenzoic acid	0
4	3-Mercaptopropionic acid	0
5	2-Naphthalenethiol	48

With DMF

Entry	Aromatic Thiol Screen*	Yield (%)
1	4-Nitrothiophenol	0
2	2,4,6-Trimethylthiophenol	0
3	2,4-Dimethylthiophenol	6
4	4-Methylthiophenol	8
5	Thiophenol	13
6	4-Methoxythiophenol	26
7	2-Methoxythiophenol	66
8	3,5-Dimethylthiophenol	93
9	2,6-Dimethylthiophenol	94

With DMF

Table 12: Further screening of conditions. GC-MS yield using dodecane as internal standard. *Conducted by Philipp Pflüger.

With these basic conditions delineated, the solvent screen was repeated, which found that more polarized solvents were the most effective, with DMF generating an assay yield of 94% (by GC-MS analysis) and an isolated yield of 88% (Table 12, Solvent Screen, Entry 8). A control reaction conducted in darkness gave 0% yield (Misc. Screen, Entry 1), which was also the case when 2 equivalents of TEMPO was included as an additive (Entry 2). Omission of 4 Å molecular sieves led to a fall in yield to 27% (Entry 3), whilst preparation

in air led to a decrease in yield to 46% (Entry 4). Conducting the reaction in darkness with heating to 60 °C led to an assay yield of 46% (Entry 5). This was potentially indicative of a charge-transfer complex, which could be enabled by heat, as well as light.[107] A screening of various hydrogen atom transfer reagents showed that 2,6-dimethylthiophenol (DMTP) remained the optimal reductant (Aromatic Thiol Screen, Entry 9).

3.3.2. Reaction Scope

With optimal reaction conditions in hand, a scope of compatible amines was investigated. Using butyraldehyde, tertiary amine **446** could be isolated in 98% yield (Scheme 75). Aromatic aldehydes could also be used, giving **447** in 93% yield. We were pleased to find that 1 equivalent of 37% aqueous formaldehyde solution could be used to generated methylated product **448** in 93%. This represents a case where other hydride-based reagents, such as sodium triacetoxyborohydride, may fail due to hydrolysis, or may be required in large excess.[283] Using this methylation method, **449** could be generated in 78% yield. Increasing the steric hindrance of the amine further, by using a tetramethyl piperidine substrate, resulted in **450** in 39% yield (61% based on recovered starting material).

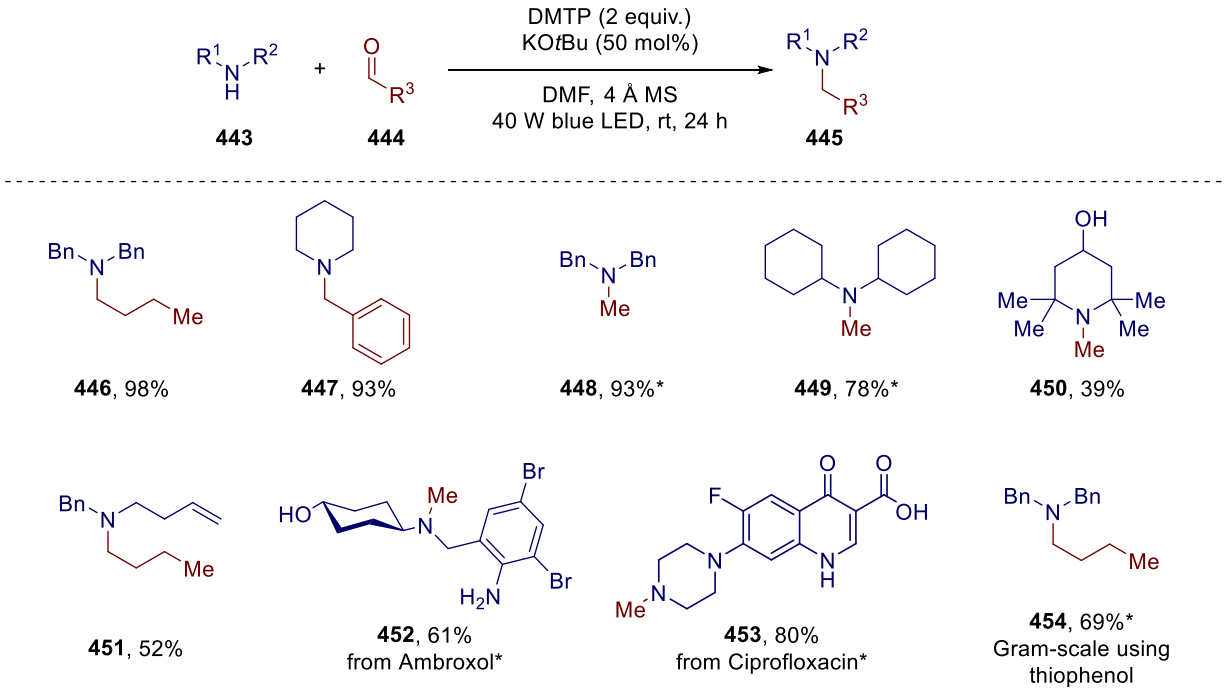

Scheme 75: Scope for photoinduced radical reductive amination. *Conducted by Philipp Pflüger

Reacting an amine substrate with a pendant alkene gave 52% of the uncyclized product **451**, with no indication of the cyclized product, which could arise from 1,5-*trig* cyclization. Conducting the reaction on secondary amine pharmaceuticals, such as Ambroxol, gave **452** in 61% yield, showing selectivity for the secondary alkylamine in the presence of an aniline moiety. **453** was generated in 80% yield from Ciprofloxacin, using aqueous formaldehyde solution. Finally, the reductive amination of butyraldehyde was performed on gram-

scale, using the less expensive thiophenol as the reductant. This produced tertiary amine **454** in 69% yield, demonstrating potential applicability to large-scale industrial settings.

The radical reductive amination of secondary amines with ketones such as **455** was investigated, using acid additives, and pre-heating before/during the reaction, in an attempt to force condensation (Scheme 76). However, the direct reductive amination of ketones was not possible. Using the di-carbonyl substrate **457** could generate the reductive amination product at the aldehyde position in 68% yield, with 0% yield of the ketone-derived product (Scheme 76b). Furthermore, by using pre-formed enamine substrate **459,** it was possible to use the radical reductive amination to generate product **460** in 78% yield (Scheme 76c). Therefore, it was possible to generate the formal ketone reductive amination product when pre-formed enamines were utilized.

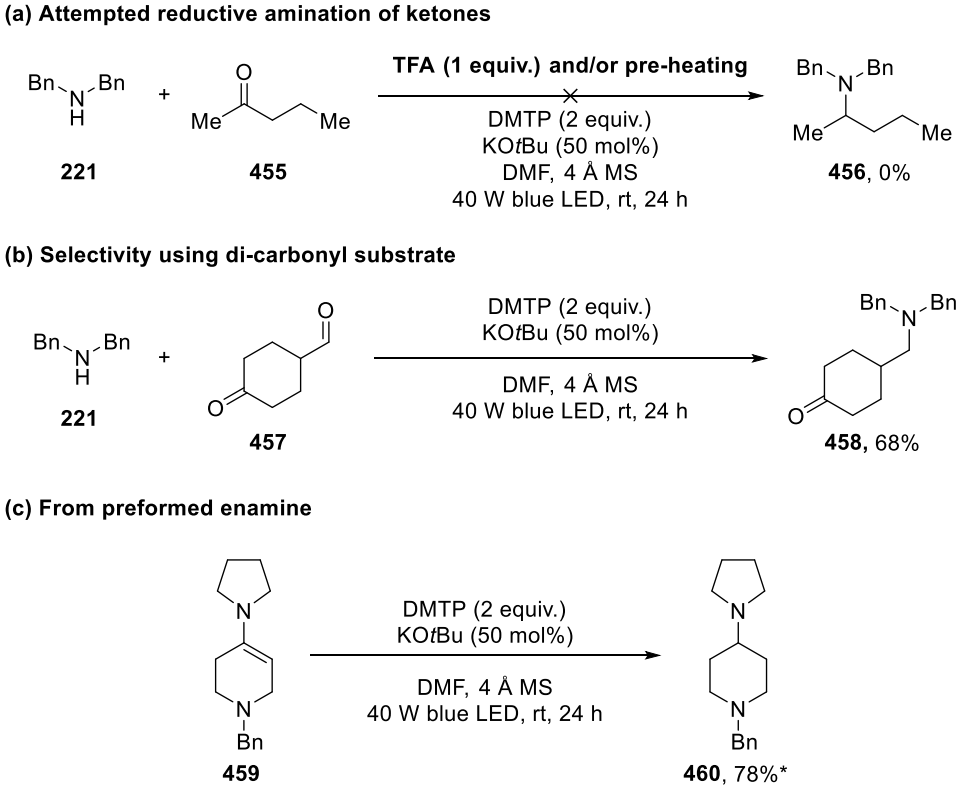

Scheme 76: Investigating radical reductive amination of ketones. *Conducted by Philipp Pflüger

Finally, given the ubiquity of existing reductive amination procedures in the literature, methods to increase the attractiveness of our procedure, were considered. One potential drawback was the use of two equivalents of 2,6-dimethylthiophenol as the reductant - a widely available, however still moderately priced reagent (£62/5g via Sigma-Aldrich).[292] Kavoos Kolahdouzan was investigating the utility of disulfides as precursors to thiyl radicals, reported by Nicewicz[293] and Li.[294] With Antonio Pedrina, it was found that instead of stoichiometric thiol, a catalytic quantity of disulfide reagent **345** could be used (Scheme 77). In combination with super-stoichiometric quantities of 1,4-cyclohexadiene (£21/5g via Sigma-Aldrich),[295] it was possible to generate the tertiary amine **461** in 98% yield. As well as being potentially cheaper overall, the oxidation of 1,4-cyclohexadiene in the reaction forms benzene as the primary by-product, which can be easily removed.

Meanwhile, malodorous thiols can be excluded, in favor of catalytic quantities of crystalline, odor-free disulfide.

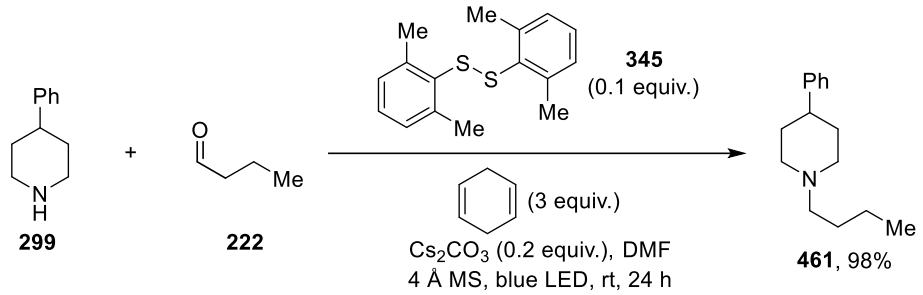

Scheme 77: Use of catalytic disulfide and cyclohexadiene as a terminal reductant

3.3.3. Mechanistic Discussion

The mechanism of the radical reductive amination, including the catalytic disulfide variant, was considered. As before, UV-vis absorption measurements of the mixtures of reactants did not show the appearance of a charge-transfer band, which would be indicative of spontaneous formation of a high concentration of charge-transfer complex. ^{1}H NMR analysis of the reaction mixture containing *N*,*N*-dibenzylamine **221**, butyraldehyde **222** and DMTP, indicated complete formation of enamine species **463** (Scheme 78). In the case when piperidine was utilized, the corresponding thioaminal species could also be observed, indicating that the ratio of enamine to thioaminal could be dependent on the steric bulk of the amine fragment.

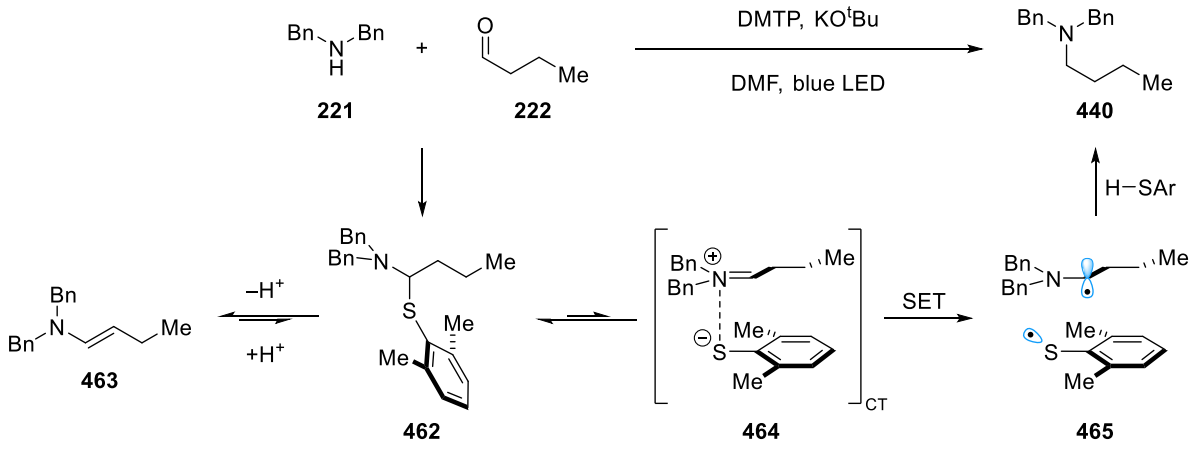

Scheme 78: Proposed mechanism for charge-transfer reductive amination

It was proposed that deprotonation of the iminium intermediate generated by condensation (or by elimination from thioaminal **462**) leads to enamine **463**. The enamine **463** acts as an inactive resting state, which prevents formation of the iminium-thiolate CT complex **464**. Formation of the enamine also results in a relatively higher concentration of protic thiol in the reaction. It is possible that the increased concentration of a proton source could disrupt formation of the ion-pair CT complex **464**. Therefore, it was hypothesized that catalytic base could ensure deprotonation of the thiolate ion, as part of complex **464**, and upon SET, α-amino radical **465** is

formed. This radical then undergoes HAT with thiol to generate the product **440**. Using 1 equivalent or more of base led to a steep reduction in yield, since an equivalent of thiol must remain for HAT to occur. This led to the rationalization that 'buffered' conditions, using 2 equivalents of thiol and 0.2 equivalents base, were optimal for the reaction.

(a) Calculated excitations for complex

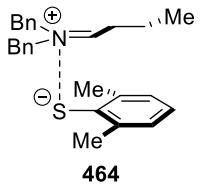

464

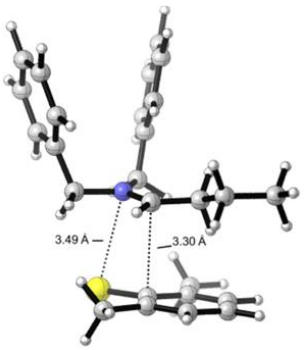

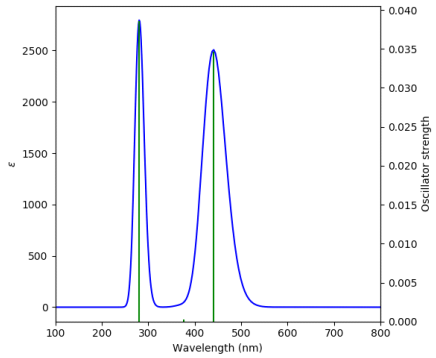

Electronic configuration	Wavelength (nm)	Oscillator strength (f)	Initial MO identity	Final MO identity	Contribution to transition
1	281	0.039	HOMO-2	LUMO+9	5%
			HOMO	LUMO+1	5%
			HOMO	LUMO+6	13%
			HOMO	LUMO+7	12%
			HOMO	LUMO+9	5%
			HOMO	LUMO+10	48%
			HOMO	LUMO+14	2%
2	377	0.000	HOMO-1	LUMO	98%
3	441	0.035	HOMO	LUMO	98%

(b) Visualization of HOMO and LUMO

HOMO 466

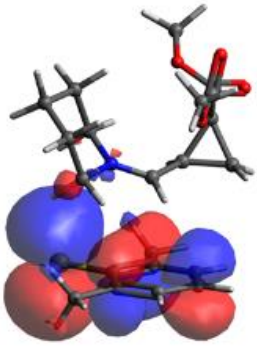

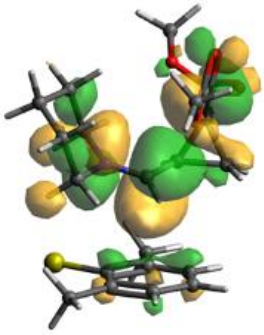

LUMO 467

Figure 31: Predicted electronic transition for iminium thiolate complex in radical reductive amination

A computational analysis using TD-DFT was applied to the aliphatic aldehyde system, as described in the previous chapter. This led to the calculation of a local minimum energy complex **464**, with inter-atomic distances of 3.49 Å and 3.30 Å between the N/S atoms and adjacent C(sp^2) atoms respectively (Figure 31a). Calculation of the electronic transitions of this complex showed transitions with high oscillator strengths (probability) at λ = 281 and 441 nm. At λ = 441 nm, 98% of the transition could be attributed to an electronic transition between the HOMO to the LUMO orbital. Visualization of these orbitals showed that the HOMO

was largely made up of the thiolate π-orbitals (**466**) and the LUMO was largely made up of the iminium π*-orbitals (**467**) (Figure 31b). Like before, this indicated that irradiation at λ = 441 nm could promote an intermolecular transition from the thiolate to the iminium, generating thiyl and α-amino radicals.

Regarding the mechanism for the radical reductive amination using catalytic disulfide, the catalytic cycle below is proposed (Scheme 79). Disulfide **345** is proposed to undergo homolytic cleavage upon LED irradiation, to generate thiyl radical **348**, reported by Nicewicz[293] and Li.[294] The thiyl radical **348** can undergo polarity-matched HAT with the nucleophilic hydrogen atom donor 1,4-cyclohexadiene **155**, generating **157**. The thiol is then able to participate in formation of thioaminal **462**, and the CT complex **464**. Upon light irradiation, this generates α-amino radical **468** and thiyl radical **348**, whereby the thiyl radical can re-enter the catalytic cycle. Meanwhile, the α-amino radical undergoes HAT with further available thiol, generating product **440** and an equivalent of thiyl radical, which can re-enter the catalytic cycle.

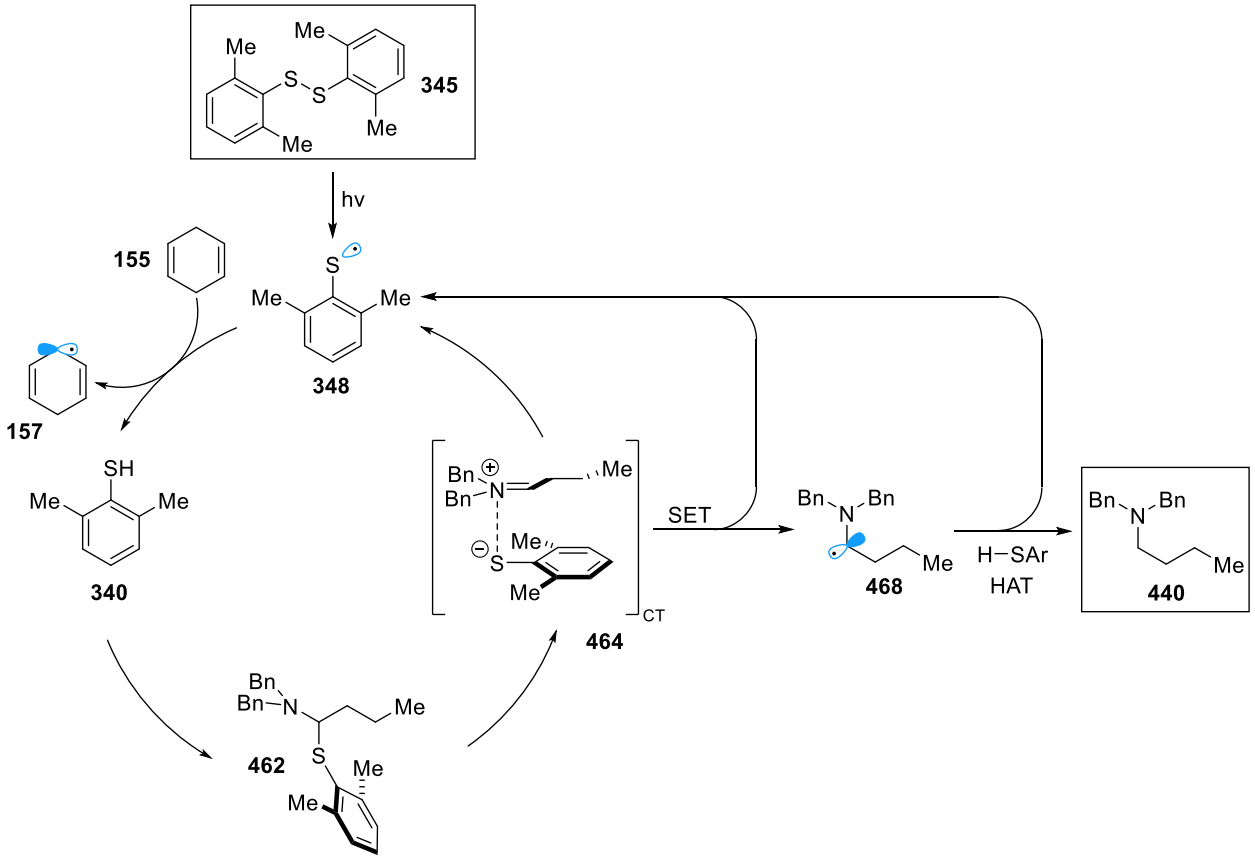

Scheme 79: Proposed catalytic cycle for reductive amination, with disulfide initiator

3.3.4. Chemoselective Reductive Amination

When using sodium acetoxyborohydride to perform the reductive amination of aldehydes with primary amines, formation of the dialkylated amine can be a problematic side reaction. A study of a broad range of primary amines and aldehydes by Abdel-Magid et al. showed that this was usually not the case, and could often be

suppressed by addition of excess primary amine.[283] However in certain cases, a considerable amount of di-alkylation was observed, for instance when cinnamaldehyde, hydrocinnamaldehyde and some straight chain aldehydes were used.

Given the competing reactivity of primary and secondary amines with aldehydes, reductive aminations are rarely utilized in situations where two amine groups are present. This is due to the difficulty in controlling selectivity, and in separating complex mixtures of typically polar, mixed products. Instead, di-amines are constructed with orthogonally protected nitrogen atoms, and various protecting group manipulations are used to independently modify each group. This strategy is often used for simple building blocks, which have widely available protected variants. However, for more complex fragments or late-stage intermediates, several time or material-intensive synthetic steps may be required, to functionalize di-amines selectively.

Few comprehensive studies on the selective reductive amination of secondary amines over primary amines have been conducted. Previous cases have been limited to isolated examples involving the synthesis of fragment analogues for structure-activity relationships, where di-amine substrates are utilized, however yields are often not reported.[296–299] In one case a secondary amine selective Petasis bioconjugation has been reported, where the *N*-terminal proline was selectively functionalized in the presence of free lysine residues.[300]

In this work, it was hypothesized that the formation of the putative charge-transfer complex could be favored by a cationic iminium ion, originating from condensation between a secondary amine and an aldehyde. Therefore, it may be possible to achieve the selective functionalization of secondary amines, in the presence of primary amines. This was guided by earlier studies, which investigated the ring-opening reaction of **298** (Scheme 80). Secondary amines such as **299** led to successful ring-opening, via α-amino radical formation, generating **338** in 90% yield. Meanwhile primary amines, with and without acid additives, led to recovery of the starting material **298** in 80% yield.

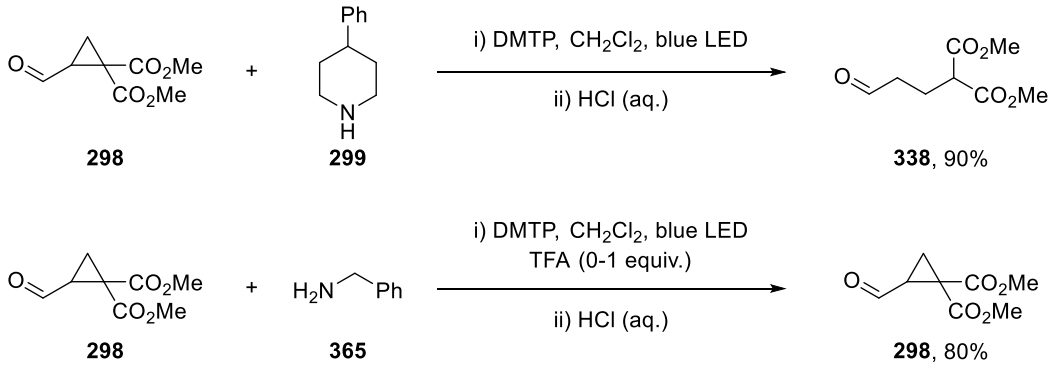

Scheme 80: Ring-opening reaction using secondary and primary amines. ^{1}H NMR yield using TCE as internal standard

For the radical reductive amination, various changes in reaction conditions were required. The solvent was changed to DMF, and the addition of catalytic base (cesium carbonate or potassium *tert*-butoxide) and molecular sieves was necessary. Therefore, further investigations were conducted into the proposed selectivity for the radical reductive amination. Conducting the radical reductive amination with benzylamine **365** led to

isolation of 28% of impure mono-alkylated product **469** (Scheme 81a). Other products, such as the di-alkylated product **470** and enamine **471** were observed, as an intractable mixture. Using di-amine substrate **472**, Phillip Pflüger found it was initially possible to isolate tertiary amine product **473** in 60% yield. This resulted from radical reductive amination at the secondary amine, followed by Boc protection of the primary amine (Scheme 81b). However, assay yields could not be determined by spectroscopic methods, and it was later observed that these results were irreproducible. A maximum consistent yield of 35% was later observed for **473**. The regiochemistry of the product was confirmed by X-ray diffraction of a single crystal **474**. Reaction with the di-amine substrate **475**, which contains a less hindered primary amine, gave a consistent yield of 43% for **476**, after benzoyl protection.

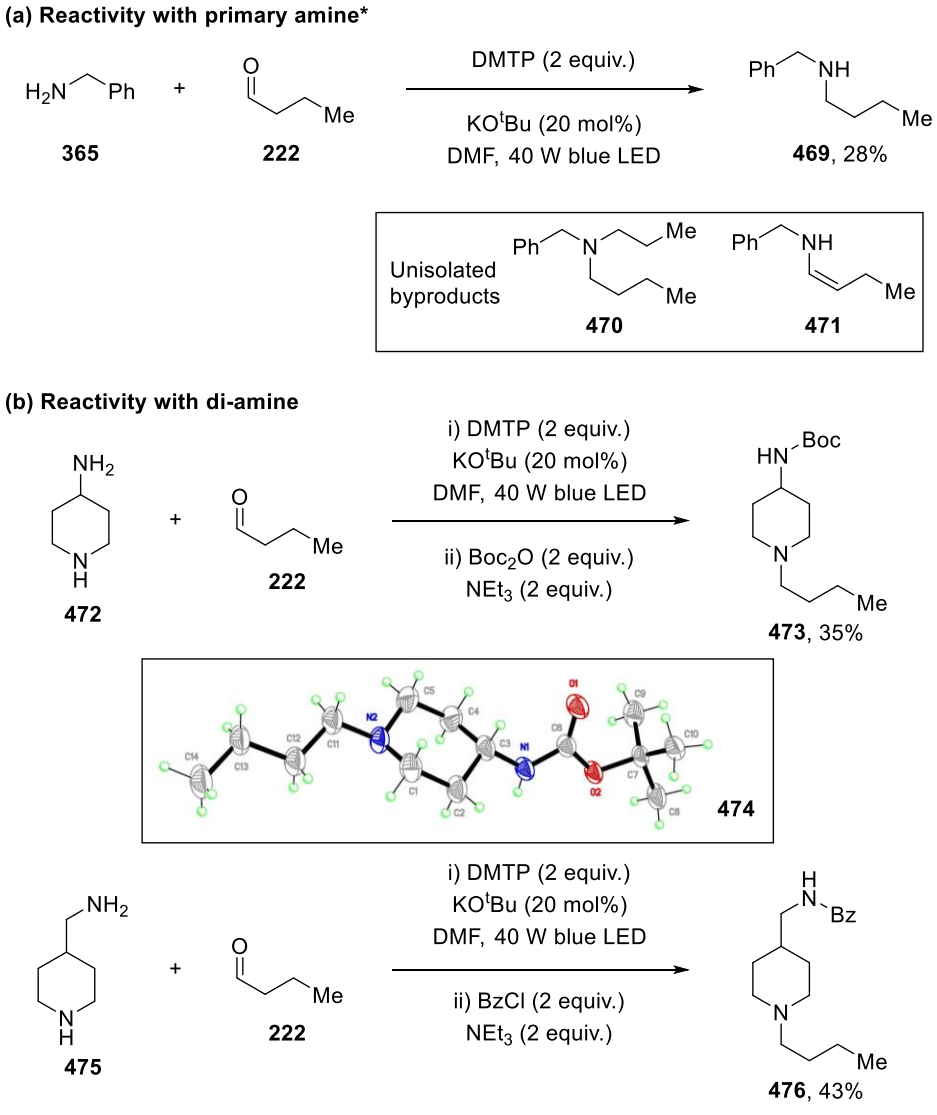

Scheme 81: Reactivity of primary amine in radical reductive amination. *Conducted by Philipp Pflüger

It was proposed that acyclic di-amines, such as **477**, could be suitable precursors for the reaction (Scheme 82). However, it was found that intramolecular formation of aminal **479** was favored. This led to formation of **480** in 34% yield upon benzoyl protection, and 34% yield of the protected starting material **481**.

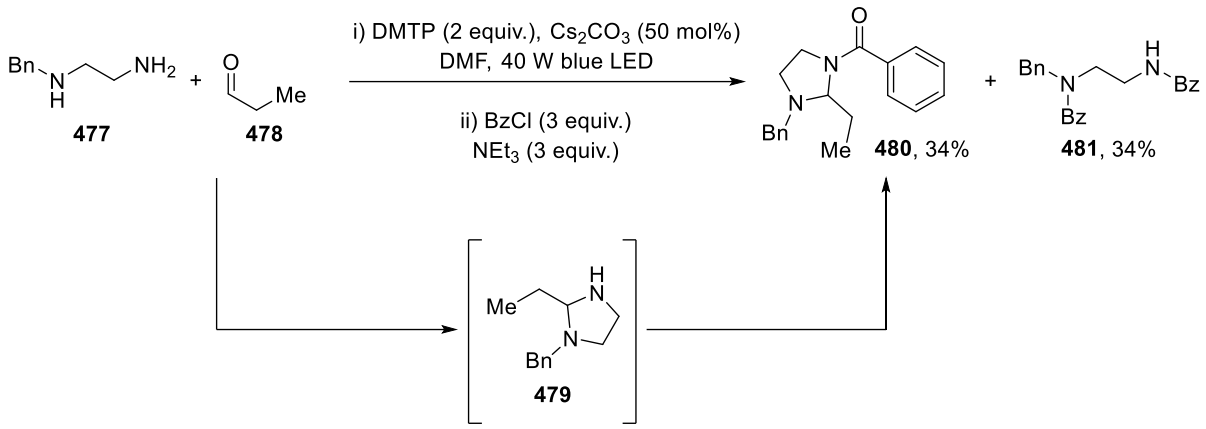

Scheme 82: Acyclic di-amines led to competitive aminal formation

Returning to the piperidyl substrates, it was necessary to accurately determine the products of the reaction and the overall mass balance. It was not possible to analyze or isolate the various unprotected amine products, arising directly from the radical reductive amination (**482-486, 472**). This was due to overlapping product peaks by analytical methods (^{1}H NMR, GC-MS), as well as some products having identical masses (Figure 32a). Therefore, by protecting the amines with a benzoyl group, identification and isolation of the amine products was possible (**487-492**, Figure 32b).

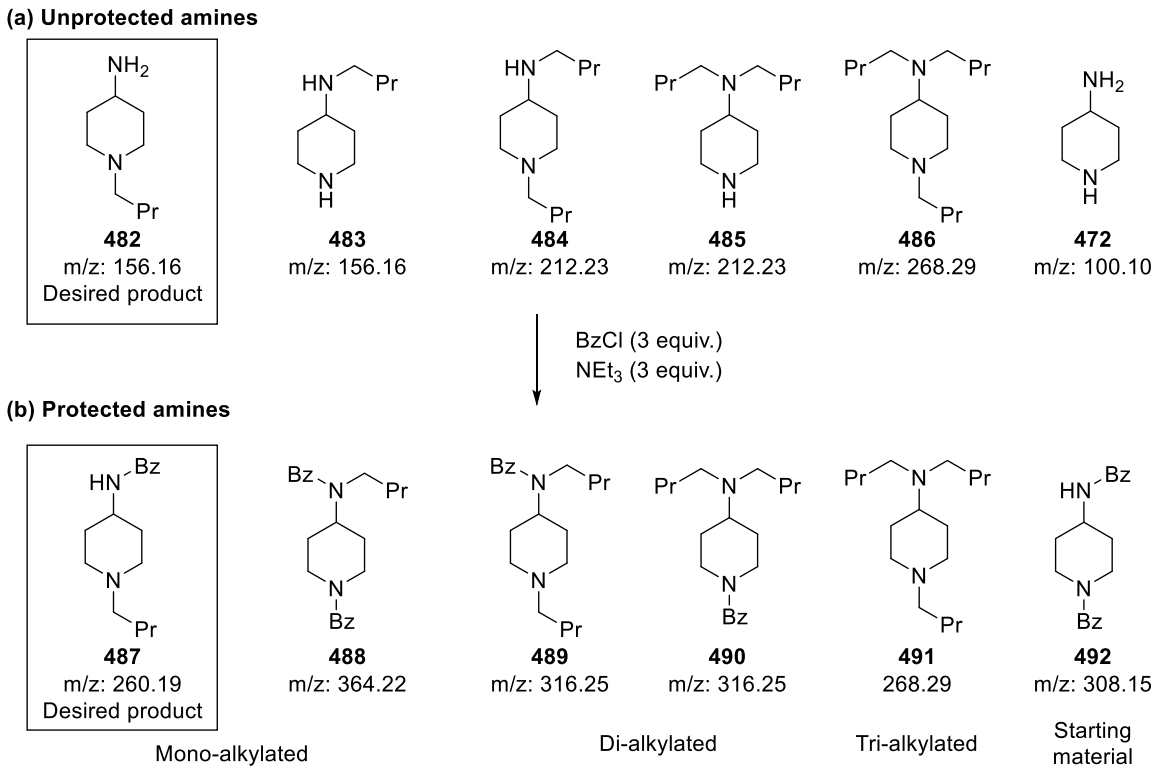

Figure 32: Structures and m/z data for alkylated di-amine products

Using 4-aminopiperidine **472**, 1 equivalent of hydrocinnamaldehyde **493**, and benzoyl chloride as the protecting reagent, running the radical reductive amination led to isolation of the desired mono-alkylated product **494** in 45% yield (Scheme 83). The protected starting material **495**, undesired mono-alkylated **496**

and di-alkylated **497** were obtained in 26% yield, as a co-eluting mixture of products. The other di-alkylated product **498** was also isolated in 13% yield. This gave a total isolated mass balance of 84%.

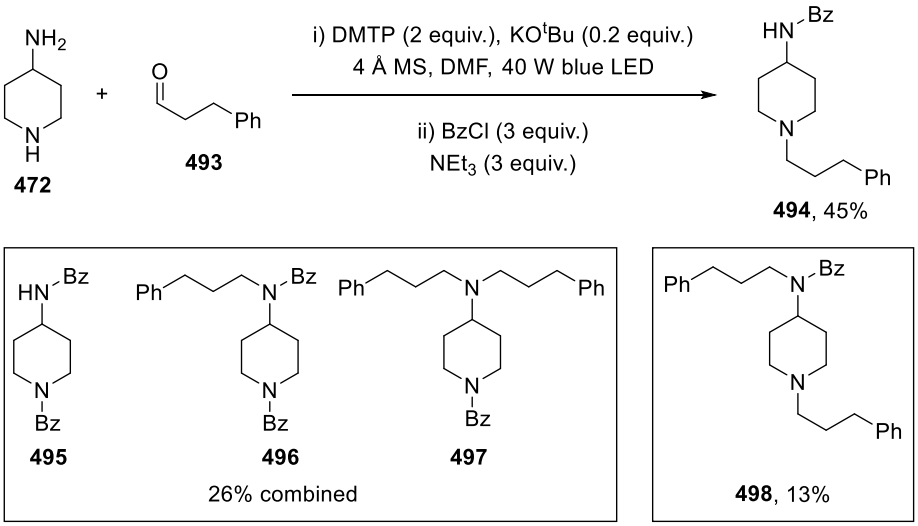

Scheme 83: Full isolation of reductive amination using 4-aminopiperidine

Having identified that total mass balance could be reasonably accounted for, the optimal method for reaction assay was determined. Despite benzoyl protection, the product peaks could not be differentiated by ^{1}H NMR, and product peaks overlapped when ^{19}F NMR was attempted (using a trifluoroacetyl protecting group). GC-MS analysis led to similarly broad and overlapping product peaks. LC-MS analysis with authentically prepared product calibration curves was initially promising, due to good peak separation. However, when compared to isolated yields, analysis by LC-MS was deemed inconsistent.

Consequently, HPLC analysis was employed to assay the reaction mixture. The 4-(aminomethyl)piperidine substrate **475** was chosen, since this presented a greater challenge in differentiating between a secondary amine and a less hindered primary amine (Scheme 84). Authentic product samples were prepared for the possible products: Desired mono-alkylated product **476**, protected starting material **499**, di-alkylated by-product **500** and mono-alkylated by-product **501**. Using catalytic disulfide and stoichiometric 1,4-cyclohexadiene, analysis of the crude mixture by HPLC gave an assay yield of 43% for the desired product **476**. This was corroborated by an isolated yield of 43%, by flash column chromatography. Furthermore, the protected starting material **499** was observed in 22% yield (by HPLC analysis), with an isolated yield of 17%.

Whilst initially promising, the peaks for the other potential by-products (**500**, **501**) could not be located within the HPLC trace of the crude mixture. Instead, two new peaks were identified, and these products were isolated using semi-preparative HPLC. These unknown compounds were related to known by-products **500** and **501**, however, each had m−2 m/z values, compared to their expected masses. Given these mass profiles, it was likely that these products were the result of over-alkylation, followed by undesired oxidation of the product to enamine species **502** and **503**.

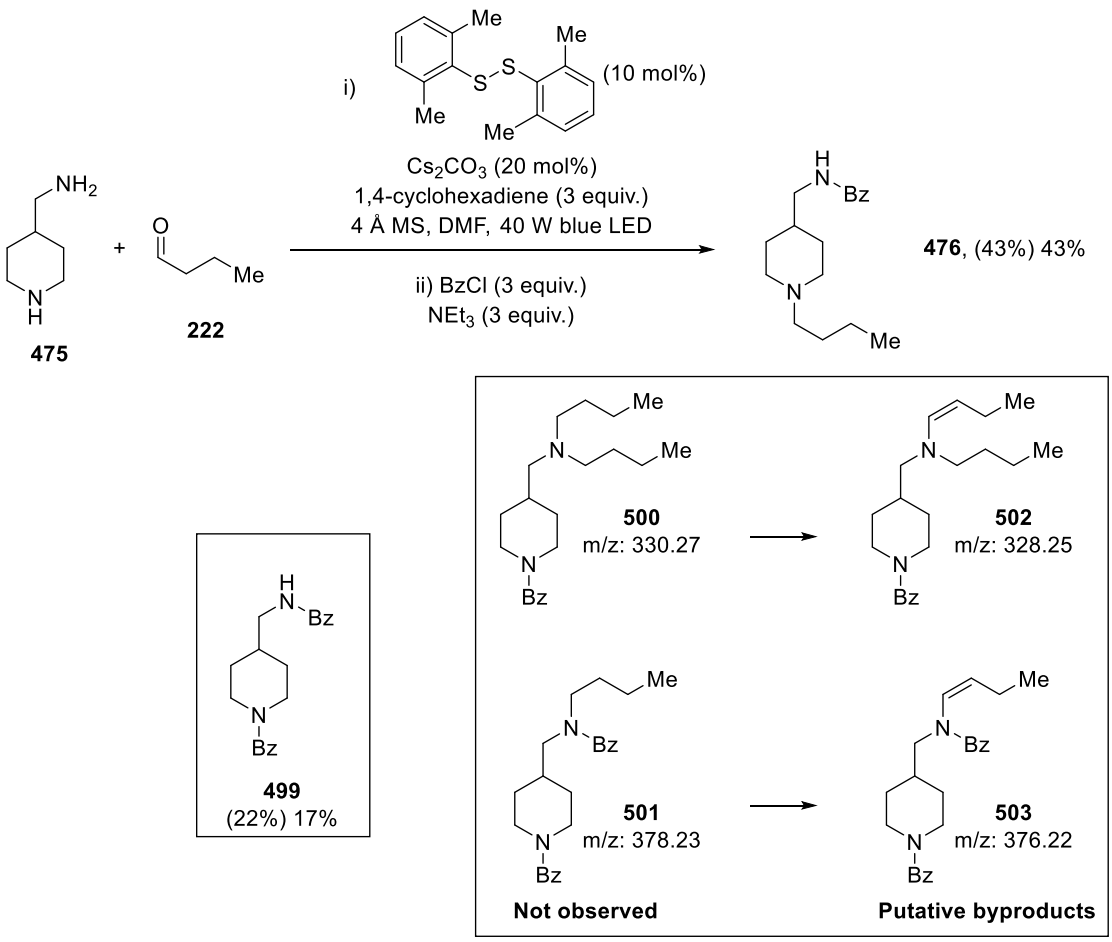

Scheme 84: HPLC analysis and isolation of product arising from radical reductive amination of di-amine. Brackets denote assay yield by HPLC analysis, against *N*,*N*-dibenzylaniline internal standard

To conclude, it was possible to validate that moderate selectivity could be achieved for the model substrate 4-aminopiperidine, which contains a piperidyl secondary amine and a primary amine. The desired secondary amine alkylated product could be obtained in 45% yield; however, the exact distribution of the remaining mass balance could not be determined. Using 4-(aminomethyl)piperidine, which contains a less hindered primary amine, it was possible to obtain the desired product in 43% yield. However, alkylation at the primary amine continued to be observed, and analysis of the reaction mixture was hampered by the probable formation of enamine byproducts.

Finally, while investigating the reaction scope for the radical reductive amination, a curious divergence in selectivity was observed when using the drug pramipexole **504** (Scheme 85). Pramipexole is a di-amine, containing a secondary amine and an aminothiazole derived primary amine. When the radical reductive amination was conducted using 1 equivalent of butyraldehyde, reactivity was observed at the primary amine, generating **505** in 83% yield (Scheme 85a). The regioselectivity was subsequently confirmed by X-ray diffraction of a single crystal **506**. Using propionaldehyde, similar reactivity was observed at the primary amine, forming **507** in 95% yield (Scheme 85b). In contrast, hydridic reductive amination with sodium acetoxyborohydride was selective for the secondary amine, forming **508** in 67% yield (Scheme 85c). ^{1}H and

^{13}C NMR were used to differentiate between these products, aided by the symmetry inherent to the tertiary amine in **508**.

Regarding the origin of selectivity, it is possible that the relatively bulky cyclohexyl substitution of the secondary amine moiety disfavors radical reductive amination. The steric bulk could disfavor thioaminal formation, or formation of the CT complex. At the same time, it is possible that secondary orbital interactions or conjugation, provided by the aminothiazole moiety, enable the radical reductive amination to occur at the primary amine. Further study into the reactivity of aminothiazoles, and related aminoheterocycles, would be of interest to further generalize this mode of selectivity.

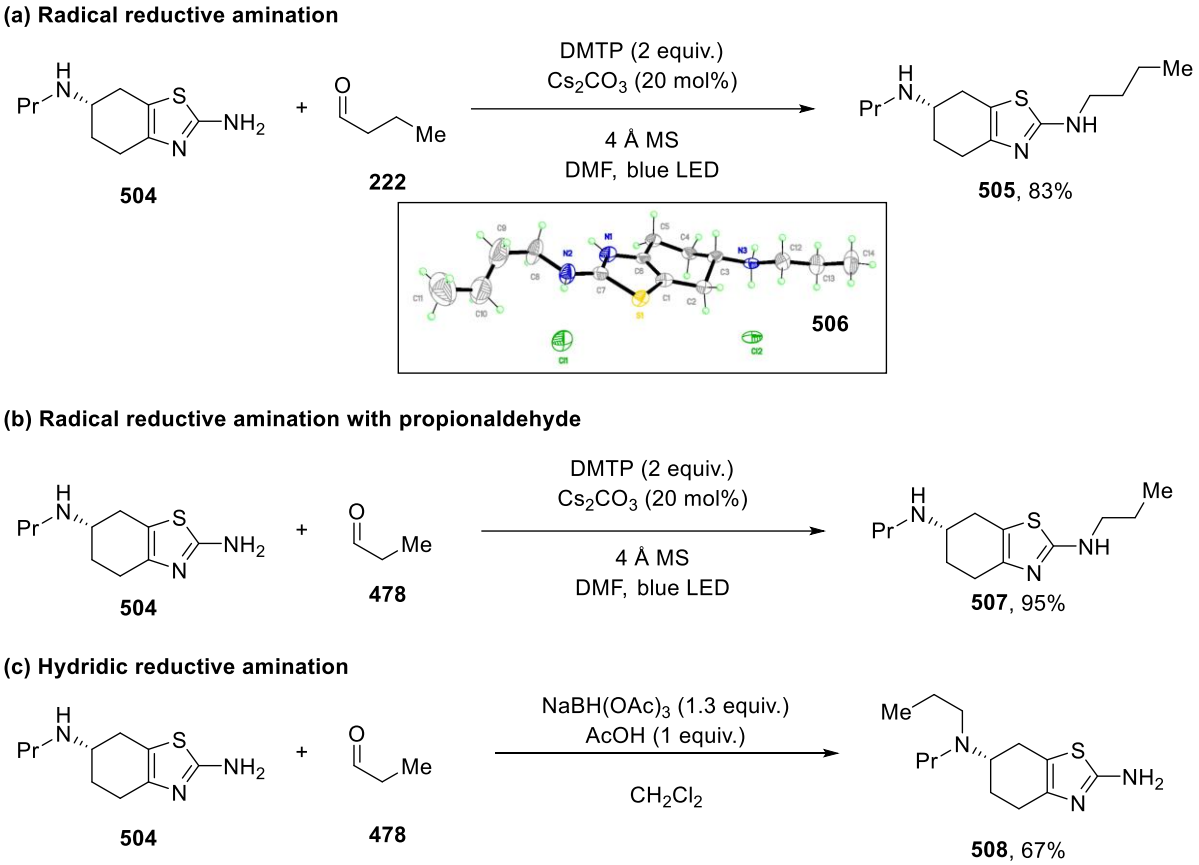

Scheme 85: Divergent regioselectivity using the drug pramipexole

3.4. Summary

Starting from a relatively specialized method to generate α,α-cyclopropyl-amino radicals from iminium ions, it was possible to generalize this method of α-amino radical formation to a wider class of acyclic aldehydes. A radical reductive amination of secondary amines was developed, which is metal-free and comparatively atom economical, when compared to existing techniques (Scheme 86a). A method using catalytic disulfide and 1,4-cyclohexadiene as the terminal reductant was also developed (Scheme 86b). Attempts were made to discover a general methodology, for the selective functionalization of secondary over primary amines. However, this was hampered by complex product distributions and undesired side-reactivity. Finally, promising regioselectivity for primary aminothiazoles over secondary amines was discovered using the radical reductive amination (Scheme 86c). This contrasted with existing hydridic methods of reductive amination, which was found to give the opposite selectivity.

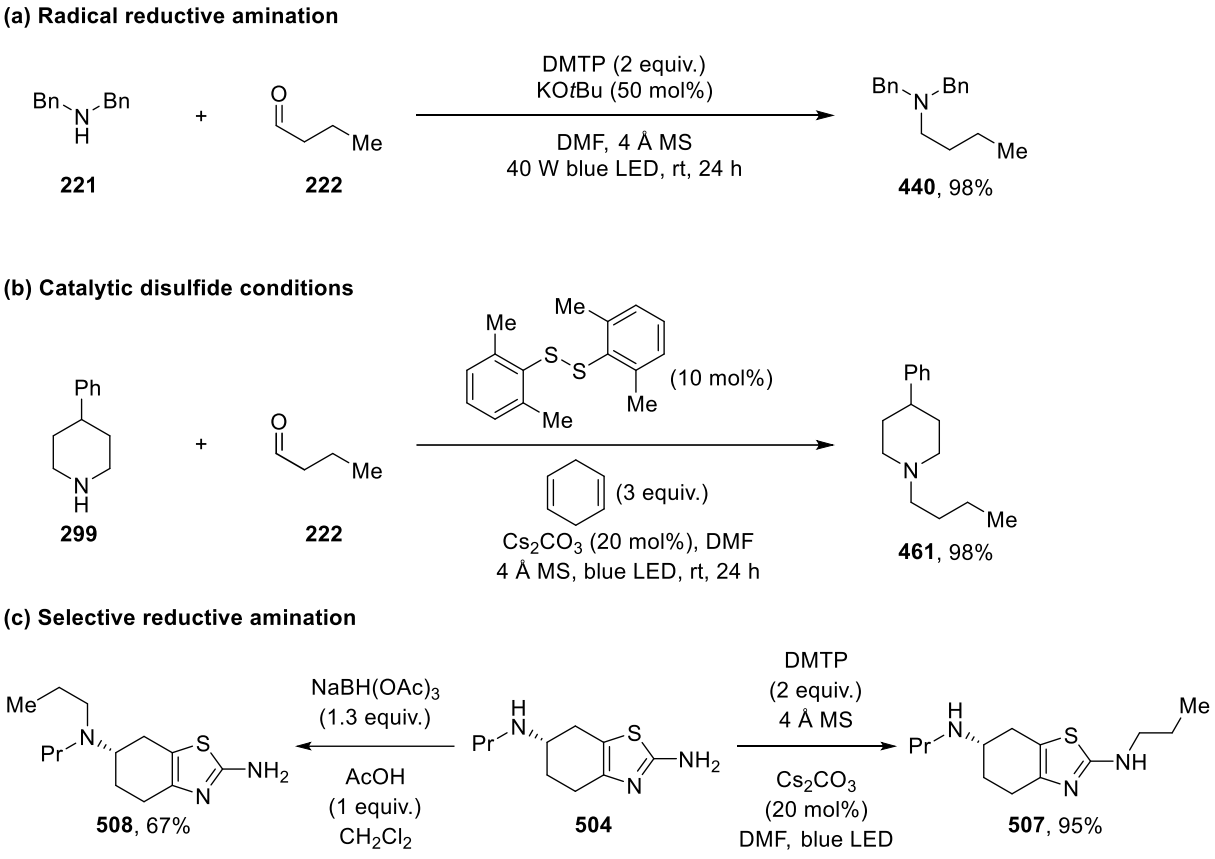

Scheme 86: Summary of radical reductive amination

4. Conclusion and Outlook

In this thesis, the development of α-amino radical formation, via a proposed charge-transfer complex, has been described. Using this radical generation method, a tandem fragmentation-cyclization reaction was realized, resulting in the multicomponent synthesis of cyclopentyl methylamines (Scheme 87a). Regarding next steps, one anticipates that there will be continued interest in the facile generation of cyclic, sp^3-rich scaffolds, in the context of medicinal chemistry. A further avenue of research could involve an expanded toolkit of cyclic methylamine syntheses. This could involve the use of epoxides or aziridines, as strain-release precursors, for the generation of tetrahydrofuran or pyrrolidine products (Scheme 87b).

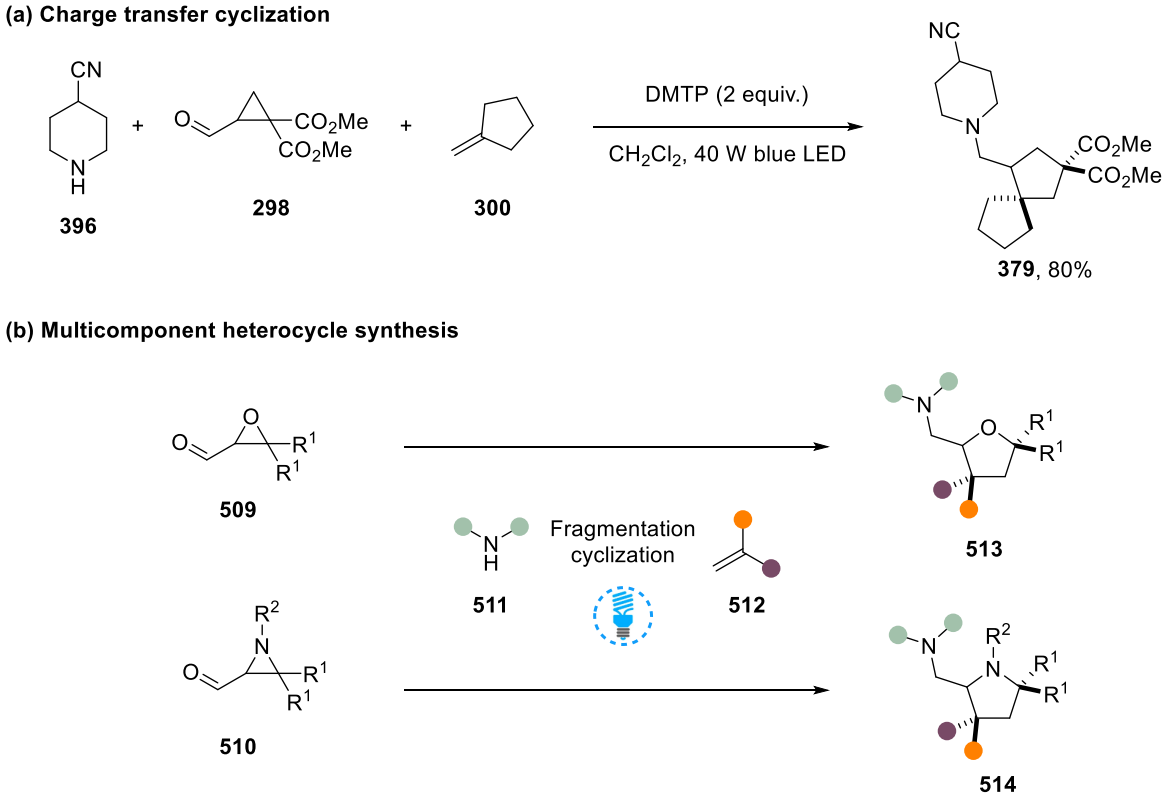

Scheme 87: Proposed multicomponent synthesis of heterocycles

There has been significant research dedicated to the generation of α-amino radicals - starting with pioneering stoichiometric studies, to more recent methods using visible light mediated photoredox catalysis. Consequently, new platforms for α-amino radical generation will be required to demonstrate synthetic utility, beyond currently existing techniques.

Following studies into the multicomponent cyclization reaction, a radical reductive amination procedure was developed, using a related method of α-amino radical formation. This allowed the union on secondary amines and acyclic aldehydes, to form tertiary amines in high yield (Scheme 88a). Research in the short term could focus on the divergence in selectivity observed, when aminothiazoles were utilized. A wider investigation into the reactivity of heterocyclic primary amines may reveal a further class of compatible amines for this

methodology (Scheme 88b). Given the prevalence of aminoheterocycles as medicinal building blocks, the selective reaction of these species could offer streamlined routes towards drug synthesis.

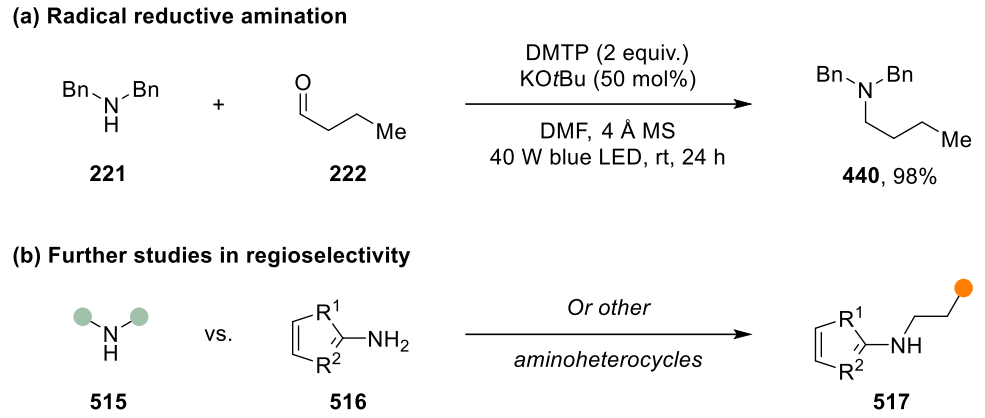

Scheme 88: Proposed studies into reductive amination of heterocyclic primary amines

In terms of a longer-term outlook for the radical reductive amination, in industrial settings, continuous flow hydrogenation with H_2 gas is generally favored over hydric methods, due to better atom economy.[301] By using a flow photoreactor and 1,4-cyclohexadiene as the terminal reductant, it may be possible to develop the radical reductive amination into a metal-free process, suitable for large scale reactions (Scheme 89a).

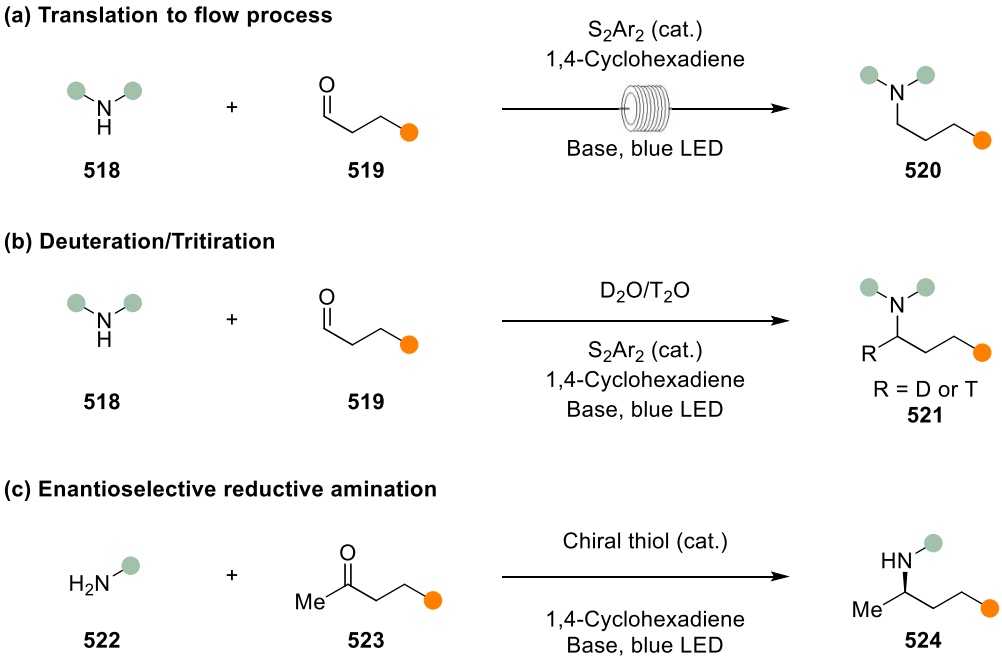

Scheme 89: Future direction for radical reductive amination

Secondly, strong polarity matching between the α-amino radical and thiol may allow other functionality to be incorporated at the α-nitrogen position. For instance, if the radical reductive amination could tolerate small quantities of water, the addition of D_2O or T_2O would generate deuterated or tritiated thiol, which would allow facile access to α-deuterated or α-tritiated tertiary amines using this methodology (Scheme 89b).[302] Thirdly, the ability to use catalytic disulfide/thiol as the reactive hydrogen atom source also opens up opportunities to

achieve enantioselective reductive amination (Scheme 89c), a process which currently relies on the use of transaminase chemistry.[303,304] It may be possible to exploit optically active thiol catalysts, based on binaphthyl, cholesterol, or glucopyranose architectures, to achieve an enantioselective hydrogen atom transfer process.[305,306] Bifunctional catalysts, for instance thiophenylalanine in a peptide-like structure, could also be an interesting avenue to study.

More generally, there have been increasing interest in the use of charge transfer complexes where one, or even none, of the components are incorporated into the final product. The continued development of this field may even offer the promise to replace expensive photocatalysts with cheap, commercial organic small molecules, in the future.[307] In this thesis, it has been possible to exploit visible light and aromatic thiols to generate radical species, whilst avoiding incorporation of the thiyl radical into the final product. This has also allowed the thiol species to be used in catalytic quantities. In the future, it is possible that similar exogenous or transient charge transfer complexes could be used, in conjunction with visible light, to enable radical chemistry with further functional groups.

5. Experimental Procedures

All reactions were conducted under an inert N_2 atmosphere with oven-dried glassware fitted with a magnetic stirrer bar, unless otherwise stated. Anhydrous dichloromethane was obtained from solvent stills (distilled from CaH_2). Dichloromethane used in the light-promoted reaction was dried using 4 Å molecular sieves (beads), degassed (freeze-pump-thaw) and stored in a Schlenk flask under N_2. Comparable results were obtained using commercial anhydrous dichloromethane (Sigma-Aldrich, Sure/Seal). Other solvents employed in light-promoted reaction were used as supplied (Sigma-Aldrich, Sure/Seal). Anhydrous solvents were obtained from solvent stills (diethyl ether was distilled from sodium triphenylmethane ketyl; tetrahydrofuran from lithium aluminum hydride; acetonitrile, dichloromethane, hexane, and toluene from calcium hydride). All commercial reagents were used as supplied unless otherwise stated. Clear glass vials (4 mL) with PTFE/silicon septum lined screw caps were used as the standard reaction vessel (VWR, 548-0521). Irradiation of the reaction mixture was conducted using a 40 W Kessil A160WE LED (Tuna blue) aquarium light (max frequency, max intensity). Organic solutions were concentrated by rotary evaporation below 40 °C. All reactions were monitored by TLC, GCMS, LCMS and/or ^{1}H NMR spectra taken from reaction samples, GC yields determined by reference to dodecane, and NMR yields determined by ^{1}H NMR with reference to 1,1,2,2-tetrachloroethane.

Analytical thin-layer chromatography was performed using Merck Kieselgel 60 F254 0.20 mm precoated glass-backed silica gel plates. Visualization of the chromatogram was performed by UV absorbance (λ_{max} = 254 nm) and/or by staining with aqueous potassium permanganate. Flash column chromatography was performed using silica gel (Merck Geduran Si 60 [40-63 μm]) with the appropriate solvent system.

Proton nuclear magnetic resonance (^{1}H NMR) spectra were recorded on a Bruker DPX 400 (400 MHz)or Avance 500 (500 MHz) spectrometer. Chemical shifts (δ) are recorded in parts per million (ppm) and are quoted to the nearest 0.01 ppm relative to the residual solvent protons ($CDCl_3$ = 7.26 ppm, DMSO-d_6 = 2.50, CD_3OD = 3.31, CD_2Cl_2 = 5.32).[308] Coupling constants (*J*) are quoted in Hertz (Hz), and data reported as follows: Chemical shift (number of protons, multiplicity, coupling constant, assignment). Coupling constants were reported to the nearest 0.1 Hz and multiplicity reported according to the following: s = singlet, d = doublet, t = triplet, q = quartet, sep = septet m = multiplet, br = broad, with associated combinations e.g. dd = doublet of doublets.

Carbon nuclear magnetic resonance (^{13}C NMR) spectra were recorded on a Bruker DPX 400 (101 MHz) or Avance 500 (125 MHz) spectrometer. Chemical shifts (δ) are recorded in parts per million (ppm) and are quoted to the nearest 0.1 ppm relative to the residual solvent protons ($CDCl_3$ = 77.2 ppm, DMSO-d_6 = 29.8, CD_3OD = 49.0, CD_2Cl_2 = 53.8).[308] DEPT 135 and 2-dimensional experiments (COSY, HMBC, HSQC and NOESY) were used to support assignments.

Infrared spectra (FT-IR) were recorded using a Perkin-Elmer Paragon 1000 Fourier transform spectrometer equipped with ATR and analyzed as thin films, with absorption maxima (ν_{max}) quoted in wavenumbers (cm^{-1}). High resolution mass spectrometry was carried out at the National Mass Spectrometry Facility (NMSF) at Swansea University using an LTQ Orbitrap XL spectrometer, or at the Department of Chemistry, University of Cambridge. UV-Vis analysis was conducted on a Shimadzu UV-1800 spectrophotometer. X-ray crystallography was performed on a Nonius Kappa CCD at the Department of Chemistry, University of Cambridge.

5.1. General Procedures

GP A: Charge-transfer fragmentation cyclization

To a 4 mL clear glass screw cap vial was added the solid reagents and a stirrer bar (10 mm, cylindrical). The vial was sealed with a PTFE/Silicone-lined septa cap, a needle was inserted through the septa and the vial was evacuated/backfilled with N_2. Anhydrous degassed CH_2Cl_2 was added, followed by the liquid reagents using a microsyringe, in the order amine, aldehyde, acceptor, thiol. The N_2 needle was removed, and the vial was sealed with parafilm and placed on an upturned crystallization dish on a stirrer plate. A 40 W Kessil A160WE Tuna Blue lamp was placed 3 cm from the face of the vial with a desk-top fan positioned above for cooling. The stirrer plate was set to 1000 rpm and the vial was irradiated for the specified time with the lamp set to max frequency and max intensity. Upon completion, the reaction was analyzed, the solvent was removed *in vacuo* and the crude residue was purified by flash column chromatography to give the desired product.

GP B: Radical reductive amination

To a 4 mL clear glass screw cap vial was added the solid reagents (4 Å molecular sieves and base) and a stirrer bar (10 mm, cylindrical). The vial was sealed with a PTFE/Silicone-lined septa cap, a needle was inserted through the septa and the vial was evacuated/backfilled with N_2. Anhydrous SureSeal DMF was added, followed by the liquid reagents using a microsyringe, in the order amine, thiol, aldehyde. The N_2 needle was removed, and the vial was sealed with parafilm and placed on an upturned crystallization dish on a stirrer plate. A 40 W Kessil A160WE Tuna Blue lamp was placed 3 cm from the face of the vial with a desk-top fan positioned above for cooling. The stirrer plate was set to 1000 rpm and the vial was irradiated for the specified time with the lamp set to max frequency and max intensity. Upon completion, the reaction mixture was filtered over Celite and analyzed. The solvent was removed *in vacuo* and the crude residue was purified by flash column chromatography to give the desired product.

5.2. Characterization

5.2.1. Charge-Transfer Cyclization

2-(3-Cyano-1-(dibenzylamino)propyl)cyclopentane-1-carbonitrile (281)

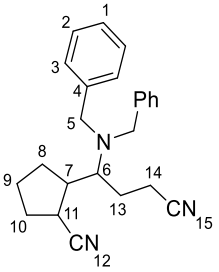

To a 4 mL clear glass screw cap vial was added $Ir(ppy)_3$ (1.6 mg, 0.0025 mmol), Hantzsch ester (95 mg, 0.375 mmol), 4 Å MS (125 mg) and a stirrer bar (10 mm, cylindrical). The vial was sealed with a PTFE/Silicone-lined septa cap, a needle was inserted through the septa and the vial was evacuated/backfilled with N_2. Anhydrous degassed CH_2Cl_2 was added, followed by the liquid reagents using a microsyringe: Dibenzylamine (48 µL, 0.25 mmol), cyclopropanecarboxaldehyde (28 µL, 0.375 mmol), acrylonitrile (33 µL, 0.5 mmol) and propionic acid (4 µL, 0.05 mmol). The N_2 needle was removed, and the vial was sealed with parafilm and placed on an upturned crystallization dish on a stirrer plate. A 40 W Kessil A160WE Tuna Blue lamp was placed 3 cm from the face of the vial with a desk-top fan positioned above for cooling. The stirrer plate was set to 1000 rpm and the vial was irradiated for 5 hours with the lamp set to max frequency and max intensity. Upon completion, the reaction was analyzed, the solvent was removed *in vacuo* and the crude residue was purified by flash column chromatography to give the title product as a colorless oil (37.6 mg, 42%)**.** The diastereomers were separated by normal phase (hexane/isopropyl alcohol) HPLC (7.1 mg, 5.5 mg, 4.2 mg, 3.6 mg. 2.0 : 1.5 : 1.2 : 1.0 dr). By-product **280** was also obtained as a colorless oil (11.4 mg, 15%). **^{1}H NMR** (400 MHz, $CDCl_3$): δ 7.32 (4H, m, H_2), 7.29 (4H, m, H_3), 7.26 (2H, m, H_1), 3.77 (2H, d, J = 13.5 Hz, H_5), 3.64 (2H, d, J = 13.5 Hz, $H_{5'}$), 3.08 (1H, m, H_{11}), 2.89 (1H, td, J = 8.6, 4.2 Hz, H_6), 2.48 (1H, ddd, J = 16.8, 10.5, 5.0 Hz, H_{14}), 2.19 (1H, m, H_7), 2.07 (1H, m, $H_{14'}$), 2.05 (1H, m, H_{10}), 1.95 (1H, m, H_9), 1.88 (1H, m, H_{13}), 1.84 (1H, m, H_{10}), 1.81 (1H, m, H_8), 1.77 (1H, m, $H_{13'}$), 1.73 (1H, m, $C_{9'}$), 1.51 (1H, m, H_8). **^{13}C NMR** (101 MHz, $CDCl_3$): δ 139.2 (C_4), 129.3 (C_3), 128.7 (C_2), 127.6 (C_1), 121.6 (C_{12}), 120.0 (C_{15}), 60.7 (C_6), 54.8 (C_5), 46.1 (C_7), 34.5 (C_{11}), 30.4 (C_{10}), 28.0 (C_8), 26.9 (C_{13}), 22.5 (C_9), 15.5 (C_{14}). **IR** ν_{max} ($CDCl_3$) /cm^{-1}: 2956, 2243, 1717, 1494, 1453, 1270, 1122. **HRMS** (FTMS +p NSI) m/z: $C_{24}H_{27}N_3H$ $[M+H]^+$ requires 358.2278, found 358.2280.

4-Cyclopropyl-4-(dibenzylamino)butanenitrile (280)

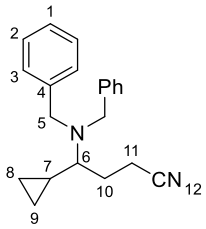

^{1}H NMR (400 MHz, $CDCl_3$): δ 7.32 (8H, d, *J* = 4.4 Hz, H_2 and H_3), 7.24 (2H, m, H_1), 3.82 (2H, d, *J* = 13.6 Hz, H_5), 3.68 (2H, d, *J* = 13.5 Hz, $H_{5'}$), 2.55 (1H, m, H_{11}), 2.22 (1H, m, H_{11}), 1.93 (2H, m, H_6 and H_{10}), 1.79 (1H, m, H_{10}), 0.89 (1H, m, H_7), 0.71 (1H, H_8), 0.46 (1H, m, H_9), 0.45 (1H, m, $H_{8'}$), -0.07 (1H, $H_{9'}$). **^{13}C NMR** (101 MHz, $CDCl_3$): δ 139.9 (C_4), 128.8, 128.5, 127.2 (C_1), 120.4 (C_{12}), 61.5 (C_6), 54.2 (C_5), 28.3 (C_{10}), 14.8 (C_{11}), 10.3 (C_7), 5.1 (C_8), 1.6 (C_9). **HRMS** (FTMS +p NSI) m/z: $C_{21}H_{24}N_2H$ $[M+H]^+$ requires 305.2012, found 305.2013.

(2,2-Dimethylcyclopropyl)methanol (293)

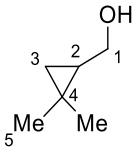

The title compound was prepared using a literature procedure.[309] To a solution of 3-methyl-2-buten-1-ol (1.0 mL, 10 mmol), in CH_2Cl_2 (33 mL) at −40 °C was added 1 M $ZnEt_2$ in hexane (25 mL, 25 mmol) dropwise over 10 minutes. The mixture was stirred for 5 minutes, then CH_2I_2 (1.6 mL, 20 mmol) was added dropwise over 5 minutes with a blast shield in place. The mixture was gradually warmed and stirred over 12 hours. The reaction was quenched with NH_4Cl (aq.) and solids filtered with Celite. From the filtrate, the phases were separated, and the aqueous phase was extracted by CH_2Cl_2 (2x20 mL). The organic phases were dried, filtered, concentrated then purified by flash chromatography (5% MeOH in CH_2Cl_2) to give the title compound as a colorless oil (732 mg, 74%). **^{1}H NMR** (400 MHz, $CDCl_3$): δ 3.75-3.63, 3.58-3.46, 1.27-1.18, 1.12, 1.08, 0.97-0.84, 0.48, 0.13. **^{13}C NMR** (101 MHz, $CDCl_3$): δ 64.3, 27.4, 26.9, 19.9, 18.4, 16.2. Data consistent with literature.[309]

2,2-Dimethylcyclopropane-1-carbaldehyde (294)

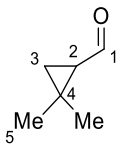

The title compound was prepared using a literature procedure.[309] To an ice-cooled solution of alcohol **293** (836 mg, 8.4 mmol) in CH_2Cl_2 (25 mL) was added pyridinium chlorochromate (1.80 g, 8.4 mmol). The reaction was stirred for 16 hours, then ether (3.5 mL) was added. The mixture was filtered through Celite, washed with

ether (7 mL), then the filtrate was concentrated, keeping the temperature and pressure at 30 °C and 300 mbar. Purification by flash chromatography (CH_2Cl_2) gave the title compound as a colorless oil (719 mg, 88%). **^{1}H NMR** (400 MHz, $CDCl_3$): δ 9.34, 1.71, 1.35, 1.29, 1.20, 1.08. Mass matched by LC-MS. Data consistent with literature.[309]

Dimethyl 2-formylcyclopropane-1,1-dicarboxylate (298)

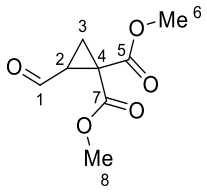

The above compound was prepared using a modified literature procedure.[310,311] To a solution of freshly distilled acrolein (0.80 mL, 12.0 mmol) in DMF (30 mL) was added dimethyl bromomalonate (90%, 1.46 mL, 10.0 mmol) followed by potassium carbonate (2.76 g, 20.0 mmol). The heterogenous mixture was stirred vigorously until the reaction was complete (5 hours). *Note*: When preparing on large scale, separate into smaller batches at the above scale to ensure rapid stirring of mixture. The mixture was cooled to 0 °C and diluted with Et_2O and H_2O. Glacial acetic acid (2.40 mL, 42.0 mmol) was added, neutralizing the mixture to roughly pH = 7. The organic layer was separated, and the aqueous layer was extracted 5 times with Et_2O. The combined organic layers were washing with saturated $NaHCO_3$ solution then brine, dried over $MgSO_4$, filtered and concentrated *in vacuo* at 30 °C. Purification by flash column chromatography (9:1 to 3:7 PE/Et_2O) gave the title product as a colorless oil (861 mg, 42%). **^{1}H NMR** (400 MHz, $CDCl_3$): δ 9.36 (d, *J* = 4.1 Hz, 1H), 3.78 (s, 6H), 2.77 (ddd, *J* = 8.8, 7.0, 4.2 Hz, 2H), 2.09 (dd, *J* = 6.8, 5.0 Hz, 1H), 1.83 (dd, *J* = 8.5, 5.0 Hz, 1H). **^{13}C NMR** (100 MHz, $CDCl_3$) δ 196.4, 168.5, 166.5, 53.5, 53.3, 37.6, 35.0, 19.8. Data consistent with literature.[312]

Bis(2-methoxyethyl) 2,6-dimethyl-1,4-dihydropyridine-3,5-dicarboxylate (314)

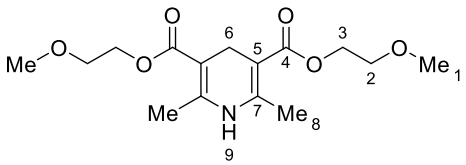

The above compound was prepared using a literature procedure.[313] A 250 mL round bottom flask was equipped with a magnetic stirrer bar, reflux condenser and N_2 inlet. The flask was charged with paraformaldehyde (0.60g, 20 mmol) and NH_4OAc (3.08 g, 40 mmol). The flask was sealed and evacuated/backfilled with N_2 three times, then water (40 mL) and methoxyethyl acetoacetate (11.8 mL, 80 mmol) was added. The mixture was sparged with N_2 for 45 minutes, heated to reflux for 3 hours, then cooled slowly in the dark. Once crystallized, the solid was broken up and recovered by filtration. The solid was washed with a minimum amount of ice-cold water (50 mL) to remove the bright yellow oxidized pyridine by-product. The title compound was obtained as a pale yellow microcrystalline solid (1.33 g, 21%). **^{1}H NMR** (400 MHz, $CDCl_3$): δ 5.17 (s, 1H), 4.25 (t, *J* = 4.9 Hz,

4H), 3.65-3.61 (m, 3H), 3.39 (s, 6H), 3.31 (s, 2H), 2.19 (s, 6H). **HRMS** (FTMS +p NSI) m/z: $C_{15}H_{23}NO_6H$ $[M+H]^+$ requires 314.1598, found 314.1601. Data consistent with literature.[313]

Dimethyl 4-((4-phenylpiperidin-1-yl)methyl)spiro[4.4]nonane-2,2-dicarboxylate (301)

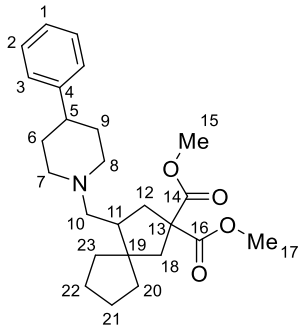

To a 4 mL clear glass screw cap vial was added 4-phenylpiperdine (32.2mg, 0.2 mmol), $Ir(ppy)_3$ (1.4 mg, 0.002 mmol), **314** (94 mg, 0.3 mmol) and a stirrer bar (10 mm, cylindrical). The vial was sealed with a PTFE/Silicone-lined septa cap, a needle was inserted through the septa and the vial was evacuated/backfilled with N_2. Anhydrous degassed CH_2Cl_2 was added, followed by the liquid reagents using a microsyringe: Aldehyde **298** (46.3 µL, 0.3 mmol), methylenecyclopentane (105 µL, 1.0 mmol) and propionic acid (3 µL, 0.04 mmol). The N_2 needle was removed, and the vial was sealed with parafilm and placed on an upturned crystallization dish on a stirrer plate. A 40 W Kessil A160WE Tuna Blue lamp was placed 3 cm from the face of the vial with a desk-top fan positioned above for cooling. The stirrer plate was set to 1000 rpm and the vial was irradiated for 5 hours with the lamp set to max frequency and max intensity. Upon completion, the reaction was analyzed, the solvent was removed *in vacuo* and the crude residue was purified by flash column chromatography (PE/EtOAc 6:4 to 3:7, then 100% CH_2Cl_2 to 9:1 CH_2Cl_2/MeOH), to give the title product as a colorless oil (24.4 mg, 29%). By-product **302** was isolated as a colorless oil (14.7 mg, 22%).

^{1}H NMR (400 MHz, $CDCl_3$) δ 7.33-7.25 (2H, m, H_2), 7.25-7.19 (2H, m, H_3), 7.19-7.15 (1H, m, H_1), 3.72 (3H, s, H_{15}), 3.72 (3H, s, H_{17}), 3.04 (1H, d, *J* = 11.5 Hz, H_7), 2.99 (1H, d, *J* = 2.6 Hz, H_8), 2.61 (1H, dd, *J* = 12.9, 6.1 Hz, H_{12A}), 2.53-2.45 (1H, m, H_5), 2.43 (1H, d, *J* = 13.8 Hz, H_{18A}), 2.40-2.22 (2H, m, H_{10}), 2.17-2.10 (1H, m, H_{11}), 2.13-2.05 (1H, m, H_8), 2.07-2.01 (2H, m, $H_{12B+18B}$), 1.94 (1H, td, *J* = 11.4, 2.8 Hz, H_7), 1.86-1.70 (4H, m, H_{6+9}), 1.71-1.61 (1H, m, H_{20}), 1.63-1.53 (4H, m, H_{21+22}), 1.50-1.44 (1H, m, H_{20}), 1.45-1.37 (1H, m, H_{23A}), 1.32-1.26 (1H, m, H_{23B}). **^{13}C NMR** (101 MHz, $CDCl_3$) δ 173.8 (C_{14}), 173.5 (C_{16}), 146.7 (C_4), 128.5 (C_2), 127.0 (C_3), 126.2 (C_1), 59.6 (C_{10}), 58.0 (C_{13}), 55.8 (C_8), 54.1 (C_7), 53.0 (C_{19}), 52.9 (C_{15}), 52.8 (C_{17}), 47.7 (C_{18}), 43.9 (C_{11}), 42.9 (C_5), 39.9 (C_{12}), 37.9 (C_{20}), 33.8 (C_6), 33.7 (C_9), 31.8 (C_{23}), 24.8 (C_{21}), 24.3 (C_{22}). **HRMS** (FTMS +p NSI) m/z: C25H35NO4H [M+H]+ requires 414.2639, found 414.2632.

Dimethyl 2-(3-(4-phenylpiperidin-1-yl)propyl)malonate (302)

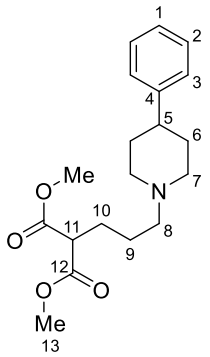

^{1}H NMR (400 MHz, $CDCl_3$) δ 7.33-7.25 (2H, m, H_2), 7.25-7.16 (3H, m, H_{1+3}), 3.74 (6H, s, H_{13}), 3.43 (1H, t, *J* = 7.5 Hz, H_{11}), 3.03 (2H, d, *J* = 11.4 Hz, H_{7A}), 2.49 (1H, tt, *J* = 10.3, 5.1 Hz, H_5), 2.40 (2H, m, H_8), 2.04 (2H, td, *J* = 11.2, 3.7 Hz, H_{7B}), 1.95 (2H, q, *J* = 7.6 Hz, H_{10}), 1.87-1.71 (4H, m, H_6), 1.63-1.50 (2H, m, H_9). **^{13}C NMR** (101 MHz, $CDCl_3$) δ 169.9 (C_{12}), 146.5 (C_4), 128.5 (C_2), 127.0 (C_3), 126.3 (C_1), 58.5 (C_8), 54.5 (C_7), 52.6 (C_{13}), 51.7 (C_{11}), 42.8 (C_5), 33.5 (C_6), 27.1 (C_{10}), 24.9 (C_9). **HRMS** (FTMS +p NSI) m/z: C19H27NO4H [M+H]+ requires 334.2013, found 334.2011.

Dimethyl 3-(4-bromophenyl)-4-((dimethylamino)methyl)cyclopentane-1,1-dicarboxylate (315)

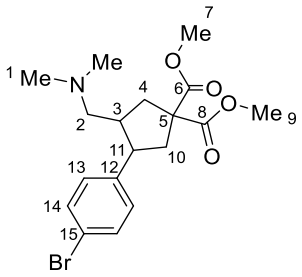

To a 4 mL clear glass screw cap vial was added $Ir(ppy)_3$ (1.4 mg, 0.002 mmol), **314** (69 mg, 0.22 mmol) and a stirrer bar (10 mm, cylindrical). The vial was sealed with a PTFE/Silicone-lined septa cap, a needle was inserted through the septa and the vial was evacuated/backfilled with N_2. Anhydrous degassed CH_2Cl_2 was added, followed by the liquid reagents using a microsyringe: Aldehyde **298** (55.8 mg, 0.3 mmol), 2,4,6-triisopropylthiophenol (9.5 mg, 0.04 mmol), propionic acid (3 µL, 0.04 mmol), 4-bromostyrene (131 µL, 1.0 mmol), dimethylamine solution (40 weight % in H_2O, 25 µL, 0.2 mmol). The N_2 needle was removed, and the vial was sealed with parafilm and placed on an upturned crystallization dish on a stirrer plate. A 40 W Kessil A160WE Tuna Blue lamp was placed 3 cm from the face of the vial with a desk-top fan positioned above for cooling. The stirrer plate was set to 1000 rpm and the vial was irradiated for 5 hours with the lamp set to max frequency and max intensity. Upon completion, the reaction was analyzed, the solvent was removed *in vacuo* and the crude residue was purified by flash column chromatography (100% CH_2Cl_2 to 19:1 CH_2Cl_2/MeOH), to give the title product as a colorless oil (55.0 mg, 68%, >20:1 dr).

^{1}H NMR (400 MHz, $CDCl_3$) δ 7.39 (2H, d, *J* = 8.1 Hz, H_{14}), 7.04 (2H, d, *J* = 8.1 Hz, H_{13}), 3.75 (6H, s, H_{7+9}), 3.36 (1H, m, H_{11}), 2.67 (1H, dd, *J* = 13.8, 7.3 Hz, H_{10A}), 2.60-2.48 (2H, m, $_{H4A+10B}$, 2.48-2.40 (1H, m, H_3), 2.25 (1H, dd, *J* = 13.5, 6.8 Hz, H_{4B}), 2.05 (6H, s, H_1), 1.84 (1H, m, H_{2A}), 1.57 (1H, dd, *J* = 12.1, 4.9 Hz, H_{2B}). **^{13}C NMR** (101 MHz, $CDCl_3$) δ 173.2 (C_6), 172.9 (C_8), 140.1 (C_{12}), 131.3 (C_{14}), 130.1 (C_{13}), 120.2 (C_{15}), 60.4 (C_2), 59.1 (C_5), 53.0 (C_7), 52.9 (C_9), 45.8 (C_{11}), 45.8 (C_1), 40.7 (C_3), 38.2 ($C_{4/10}$), 38.0 ($C_{4/10}$). **HRMS** (FTMS +p NSI) m/z: C18H24BrNO4H [M+H]+ requires 398.0961, found 398.0961.

1-((1*S*,2*R*)-2-(4-bromophenyl)-4,4-bis(methoxycarbonyl)cyclopentyl)-*N*,*N*-dimethylmethanaminium perchlorate (317)

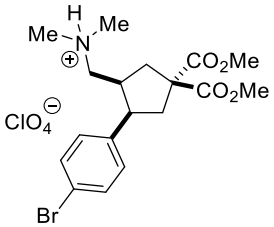

To amine **315** (97.3 mg) dissolved in ether (2 mL) was added perchloric acid (70%, 8.4 µL) dissolved in ethanol (0.1 mL). Gentle heating of the solution followed by recrystallization by slow evaporation gave the above product, which was characterized by single crystal X-ray diffraction.

Dimethyl 3-formyl-4-phenylcyclopentane-1,1-dicarboxylate (331)

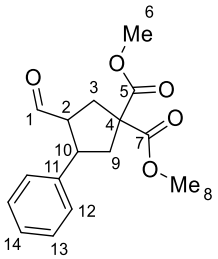

To a 4 mL clear glass screw cap vial was added $Ir(ppy)_3$ (1.6 mg, 0.0025 mmol), Hantzsch ester (95 mg, 0.375 mmol), 4 Å MS (125 mg) and a stirrer bar (10 mm, cylindrical). The vial was sealed with a PTFE/Silicone-lined septa cap, a needle was inserted through the septa and the vial was evacuated/backfilled with N_2. Anhydrous degassed CH_2Cl_2 was added, followed by the liquid reagents using a microsyringe: Dibenzylamine (48 µL, 0.25 mmol), dimethyl 2-formylcyclopropane-1,1-dicarboxylate (47 mg, 0.25 mmol), styrene (57 µL, 0.5 mmol) and propionic acid (4 µL, 0.05 mmol). The N_2 needle was removed, and the vial was sealed with parafilm and placed on an upturned crystallization dish on a stirrer plate. A 40 W Kessil A160WE Tuna Blue lamp was placed 3 cm from the face of the vial with a desk-top fan positioned above for cooling. The stirrer plate was set to 1000 rpm and the vial was irradiated for 5 hours with the lamp set to max frequency and max intensity. Upon completion, the reaction was analyzed, the solvent was removed *in vacuo* and the crude residue was purified by flash column chromatography (19:1 PE/Et_2O to 1:4 PE/Et_2O) to give the title product as a colorless oil (13.0 mg, 18%)**. ^{1}H NMR** (400 MHz, $CDCl_3$): δ 9.62 (1H, d, *J* = 2.0 Hz, H_1), 7.28 (5H, m,

$H_{12+13+14}$), 3.78 (3H, s, H_6), 3.77 (3H, s, H_8), 3.45 (1H, m, H_{10}), 3.07 (1H, app. q, H_2), 2.85 (1H, dd, *J* = 13.6, 7.6 Hz, H_9), 2.65 (2H, d, *J* = 8.8 Hz, H_3), 2.39 (1H, dd, *J* = 13.6, 11.6 Hz, $H_{9'}$). **^{13}C NMR** (101 MHz, $CDCl_3$): δ 201.4 (C_1), 172.2 (C_5), 172.1 (C_7), 141.0 (C_{11}), 129.0 (C_{13}), 127.4 (C_{12}), 127.3 (C_{14}), 59.2 (C_4), 58.2 (C_2), 53.2 (C_6), 53.2 (C_8), 46.2 (C_{10}), 42.6 (C_9), 34.5 (C_3). **IR** (CH_3Cl, cm^{-1}): 2955, 1733, 1434, 1267, 1202, 1168, 1101. **HRMS** (FTMS +p NSI) m/z: $C_{16}H_{18}O_5H$ $[M+H]^+$ requires 291.1227, found 291.1228.

Dimethyl 2-(((2,6-dimethylphenyl)thio)(piperidin-1-yl)methyl)cyclopropane-1,1-dicarboxylate (342)

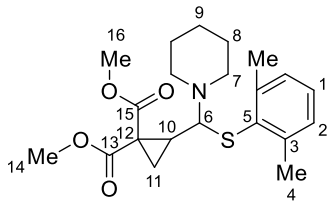

In a vial, piperidine (10 µL, 0.1 mmol), aldehyde **298** (15 µL, 0.1 mmol), DMTP (13 µL, 0.11mol) and CD_2Cl_2 (1 mL) were combined. **^{1}H NMR** (500 MHz, CD_2Cl_2): δ 7.09-7.06 (3H, s, H_{1+2}), 3.93 (1H, d, *J* = 8.7 Hz, H_6), 3.69 (3H, s, H_{14}), 3.67 (3H, s, H_{16}), 2.88-2.79 (2H, m, H_{7A}), 2.58 (7H, s, H_{4+10}), 2.46-2.38 (2H, m, H_{7B}), 1.50-1.37 (6H, s, H_{8+9}), 1.35 (1H, dd, *J* = 7.6, 4.9 Hz, H_{11A}), 1.19 (1H, dd, *J* = 9.2, 4.9 Hz, H_{11B}). **^{13}C NMR** (126 MHz, CD_2Cl_2): δ 170.1 (C_{13}), 168.6 (C_{15}), 143.1 (C_3), 134.2 (C_5), 128.4 (C_2), 128.0 (C_1), 78.0 (C_6), 52.9 (C_{14}), 52.6 (C_{16}), 49.6 (C_7), 33.1 (C_{12}), 32.4 (C_{10}), 26.3 (C_8), 24.7 (C_9), 22.6 (C_4), 22.2 (C_{11}).

Dimethyl 2-(3-oxopropyl)malonate (338)

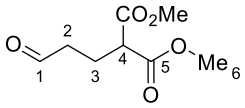

To a 4 mL clear glass screw cap vial was added 4-phenylpiperidine (32.2 mg, 0.2 mmol) and a stirrer bar (10 mm, cylindrical). The vial was sealed with a PTFE/Silicone-lined septa cap, a needle was inserted through the septa and the vial was evacuated/backfilled with N_2. Anhydrous degassed CH_2Cl_2 was added, followed by the liquid reagents using a microsyringe, in the order dimethyl 2-formylcyclopropane-1,1-dicarboxylate (31.5 µL, 0.2 mmol), DMTP (53.3 µL, 0.4 mmol). The N_2 needle was removed, and the vial was sealed with parafilm and placed on an upturned crystallization dish on a stirrer plate. A 40 W Kessil A160WE Tuna Blue lamp was placed 3 cm from the face of the vial with a desk-top fan positioned above for cooling. The stirrer plate was set to 1000 rpm and the vial was irradiated for 18 hours with the lamp set to max frequency and max intensity. Upon acid work-up, a single aldehydic product was observable by crude ^{1}H NMR. Purification by flash column chromatography (7:3 PE/Et_2O) gave the above alicyclic aldehyde as a colorless oil (24.6 mg, 65%). **^{1}H NMR** (600 MHz, $CDCl_3$): δ 9.75 (1H, t, *J* = 1.1 Hz, H_1), 3.74 (6H, s, H_6), 3.45 (1H, t, *J* = 7.3 Hz, H_4), 2.57 (2H, t, *J* = 6.8 Hz, H_2), 2.22 (2H, q, *J* = 7.3 Hz, H_3). **^{13}C NMR** (151 MHz, $CDCl_3$): δ = 200.6 (C_1), 169.5 (C_5), 52.8 (C_6), 50.4 (C_4), 41.1 (C_2), 21.2 (C_3). Data consistent with literature.[314]

Dimethyl 4-((4-cyanopiperidin-1-yl)methyl)spiro[4.4]nonane-2,2-dicarboxylate (379)

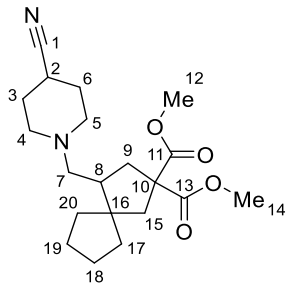

Following **GP A**, piperidine-4-carbonitrile (22.5 µL, 0.2 mmol), dimethyl 2-formylcyclopropane-1,1-dicarboxylate (44.7 mg, 0.24 mmol), methylenecyclopentane (42.1 µL, 0.4 mmol) and DMTP (53.3 µL, 0.4 mmol) were reacted over 24 hours and purified by flash column chromatography (PE/Et_2O 1:1 to 1:4) to give the title compound as a colorless oil (58.2 mg, 80%). **^{1}H NMR** (400 MHz, $CDCl_3$): δ 3.69 (3H, s, H_{12}), 3.68 (3H, s, H_{14}), 2.72-2.62 (1H, m, H_{4A}), 2.62-2.45 (3H, m, $H_{2+5A+9A}$), 2.38 (1H, d, *J* = 13.8 Hz, H_{15A}), 2.35-2.11 (4H, m, $H_{5B+7+4B}$), 2.07-1.91 (3H, m, $H_{15B+8+9B}$), 1.94-1.74 (4H, m, H_{3+6}), 1.63-1.48 (5H, m, $H_{17A+18+19}$), 1.46-1.30 (2H, m, $H_{17B+20A}$), 1.28-1.19 (1H, m, H_{20B}). **^{13}C NMR** (100 MHz, $CDCl_3$): δ 173.6 (C_{11}), 173.3 (C_{13}), 121.9 (C_1), 59.1 (C_7), 57.8 (C_{10}), 52.8 (C_{12+16}), 52.8 (C_{14}), 52.0 (C_5), 51.8 (C_4), 47.5 (C_{15}), 43.8 (C_8), 39.4 (C_9), 37.9 (C_{17}), 31.8 (C_{20}), 29.0 (C_{3+6}), 26.3 (C_2), 24.6 (C_{18}), 24.2 (C_{19}). **IR** (CH_2Cl_2, cm^{-1}): 2951, 2866, 1729, 1434, 1384, 1253, 1197, 1170, 1138, 1103, 1047. **HRMS** (FTMS +p NSI) calculated for $C_{20}H_{30}N_2O_4H$ $[M+H]^+$ 363.2278, found 363.2280.

Dimethyl 4-(morpholinomethyl)spiro[4.4]nonane-2,2-dicarboxylate (380)

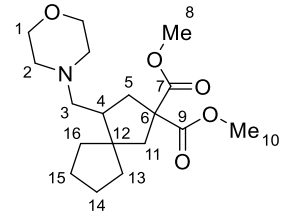

Following **GP A**, morpholine (17.5 µL, 0.2 mmol), dimethyl 2-formylcyclopropane-1,1-dicarboxylate (44.7 mg, 0.24 mmol), methylenecyclopentane (42.1 µL, 0.4 mmol) and DMTP (53.3 µL, 0.4 mmol) were reacted over 24 hours and purified by flash column chromatography (PE/Et_2O 7:3 to 1:1) to give the title compound as a colorless oil (57.3 mg, 84%). **^{1}H NMR** (400 MHz, $CDCl_3$) δ 3.79-3.61 (10H, m, H_{1+8+10}), 2.58-2.49 (1H, m, H_{5A}), 2.49-2.16 (7H, m, $H_{2A+11A+2B+3}$), 2.11-1.91 (3H, m, $H_{4+11B+5B}$), 1.66-1.46 (5H, m, $H_{13A+14+15}$), 1.46-1.33 (2H, m, $H_{13B+16A}$), 1.27-1.19 (1H, m, H_{16B}). **^{13}C NMR** (101 MHz, $CDCl_3$) δ 173.7 (C_7), 173.4 (C_9), 67.1 (C_1), 59.5 (C_3), 57.8 (C_6), 54.2 (C_2), 52.8 (C_8), 52.8 (C_{12}), 52.8 (C_{10}), 47.5 (C_{11}), 43.4 (C_4), 39.5 (C_5), 37.9 (C_{13}), 31.8 (C_{16}), 24.7 (C_{14}), 24.2 (C_{15}). **IR** (CH_2Cl_2, cm^{-1}): 2952, 2863, 2809, 1731, 1435, 1257, 1198, 1173, 1117, 1070, 1034, 1009. **HRMS** (FTMS +p NSI) calculated for $C_{18}H_{29}NO_5H$ $[M+H]^+$: 340.2118, found 340.2120.

Dimethyl 4-((4-(*tert*-butoxycarbonyl)piperazin-1-yl)methyl)spiro[4.4]nonane-2,2-dicarboxylate (381)

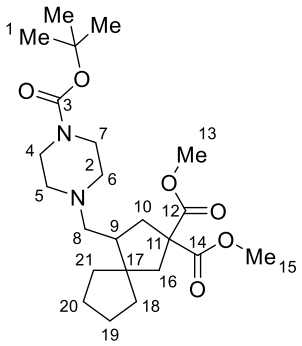

Following **GP A**, 1-Boc-piperazine (37.3 mg, 0.2 mmol), dimethyl 2-formylcyclopropane-1,1-dicarboxylate (44.7 mg, 0.24 mmol), methylenecyclopentane (42.1 µL, 0.4 mmol) and DMTP (53.3 µL, 0.4 mmol) were reacted over 24 hours and purified by flash column chromatography (PE/Et_2O 7:3 to 1:1) to give the title compound as a colorless oil (67.6 mg, 77%). **^{1}H NMR** (400 MHz, $CDCl_3$) δ 3.68 (3H, s, H_{13}), 3.67 (3H, s, H_{15}), 3.42-3.31 (2H, m, H_7), 2.93-2.83 (2H, m, H_4), 2.53 (1H, dd, *J* = 12.4, 5.5 Hz, H_{10A}), 2.42-2.33 (2H, m, H_{16A+6A}), 2.30-2.18 (3H, m, H_{6B+5}), 2.10-2.92 (3H, m, $H_{9+16B+10B}$), 1.66-1.47 (5H, m, $H_{18A+19+20}$), 1.47-1.31 (11H, m, $H_{1+18B+21A}$), 1.28-1.18 (1H, m, H_{21B}). **^{13}C NMR** (101 MHz, $CDCl_3$) δ 173.7 (C_{12}), 173.4 (C_{14}), 154.9 (C_3), 79.6 (C_2), 59.1 (C_5), 57.9 (C_{11}), 53.5 (C_6), 52.8 (C_{13}), 52.7 (C_{15+17}), 47.5 (C_{16}), 45.9 (C_4), 43.7 (C_9), 43.5 (C_7), 39.5 (C_{10}), 37.9 (C_{18}), 31.8 (C_{21}), 28.5 (C_1), 24.7 (C_{19}), 24.2 (C_{20}). **IR** (CH_2Cl_2, cm^{-1}) 2952, 2869, 2808, 1733, 1697, 1422, 1365, 1247, 1172, 1123, 1004. **HRMS** (FTMS +p NSI) calculated for $C_{23}H_{38}N_2O_6H$ $[M+H]^+$: 439.2803, found 439.2796.

Dimethyl 4-((1,4-dioxa-8-azaspiro[4.5]decan-8-yl)methyl)spiro[4.4]nonane-2,2-dicarboxylate (382)

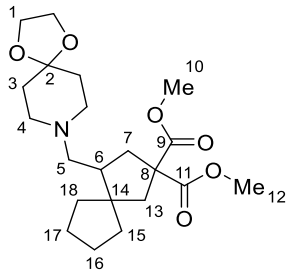

Following **GP A**, 1,4-dioxa-8-azaspiro[4.5]decane (25.6 µL, 0.2 mmol), dimethyl 2-formylcyclopropane-1,1-dicarboxylate (44.7 mg, 0.24 mmol), methylenecyclopentane (42.1 µL, 0.4 mmol) and DMTP (53.3 µL, 0.4 mmol) were reacted over 24 hours and purified by flash column chromatography (4:1 PE/EtOAc to EtOAc) to give the title compound as a colorless oil (61.5 mg, 78%). **^{1}H NMR** (400 MHz, $CDCl_3$) δ 3.91 (4H, s, H_4), 3.68 (3H, s, H_{10}), 3.68 (3H, s, H_{12}), 2.58-2.46 (2H, m, H_{7A+1A}), 2.46-2.34 (3H, m, H_{1+13A}), 2.34-2.19 (2H, m, H_5), 2.08-1.94 (3H, m, $H_{6+13B+7B}$), 1.69 (4H, t, *J* = 5.8 Hz, H_3), 1.63-1.48 (5H, m, $H_{15A+16+17}$), 1.46-1.32 (2H, m, $H_{15B+18A}$), 1.27-1.18 (1H, m, H_{18B}). **^{13}C NMR** (101 MHz, $CDCl_3$) δ 173.7 (C_9), 173.4 (C_{11}), 107.5 (C_2), 64.3 (C_4), 58.6 (C_5), 57.9 (C_8), 52.9 (C_{14}), 52.8 (C_{10}), 52.7 (C_{12}), 51.8 (C_1), 47.6 (C_{13}), 44.1 (C_6), 39.6 (C_7), 37.9 (C_{15}), 34.9 (C_3), 31.7 (C_{18}), 24.7 (C_{16}), 24.2 (C_{17}). **IR** (CH_2Cl_2, cm^{-1}) 2952, 2876, 2812, 1732, 1435, 1364, 1253,

1198, 1166, 1144, 1088, 1040. **HRMS** (FTMS +c ESI) calculated for $C_{21}H_{33}NO_6H$ $[M+H]^+$ 396.2386, found 396.2365.

Dimethyl 4-((4-hydroxypiperidin-1-yl)methyl)spiro[4.4]nonane-2,2-dicarboxylate (383)

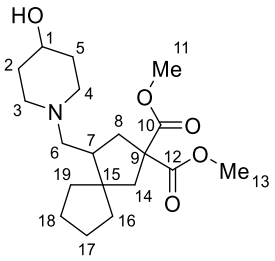

Following **GP A**, 4-hydroxypiperidine (20.2 mg, 0.2 mmol), dimethyl 2-formylcyclopropane-1,1-dicarboxylate (44.7 mg, 0.24 mmol), methylenecyclopentane (42.1 µL, 0.4 mmol) and DMTP (53.3 µL, 0.4 mmol) were reacted over 24 hours and purified by flash column chromatography (CH_2Cl_2 to CH_2Cl_2/MeOH 19:1) to give the title compound as a colorless oil (62.4 mg, 88%). **^{1}H NMR** (400 MHz, $CDCl_3$) δ 3.73-3.65 (6H, m, H_{11+13}), 3.66-3.58 (1H, m, H_1), 2.83-2.72 (1H, m, H_{3A}), 2.71-2.62 (1H, m, H_{4A}), 2.53 (1H, dd, J = 12.5, 5.7 Hz, H_{8A}), 2.38 (1H, d, J = 13.8 Hz, H_{14A}), 2.31-2.19 (2H, m, H_6), 2.17-2.08 (1H, m, H_{4B}), 2.07-1.91 (4H, m, $H_{7+3B+14B+8B}$), 1.89-1.78 (2H, m, H_2), 1.63-1.46 (7H, m, $H_{16A+5+17+18}$), 1.45-1.31 (2H, m, $H_{16B+19A}$), 1.25-1.20 (1H, m, H_{19B}). **^{13}C NMR** (101 MHz, $CDCl_3$) δ 173.7 (C_{10}), 173.4 (C_{12}), 68.1 (C_1), 58.9 (C_6), 57.9 (C_9), 52.9 (C_{15}), 52.8 (C_{11}), 52.8 (C_{13}), 52.0 (C_4), 51.2 (C_3), 47.5 (C_{14}), 44.0 (C_7), 39.7 (C_8), 37.8 (C_{16}), 34.6 (C_{2+5}), 31.7 (C_{19}), 24.7 (C_{17}), 24.2 (C_{18}). **IR** (CH_2Cl_2, cm^{-1}) 2947, 2871, 1730, 1435, 1367, 1254, 1198, 1172, 1107, 1066, 1018. **HRMS** (FTMS +p NSI) calculated for $C_{19}H_{31}NO_5H$ $[M+H]^+$ 354.2275, found 354.2278.

Dimethyl 4-(thiazolidin-3-ylmethyl)spiro[4.4]nonane-2,2-dicarboxylate (384)

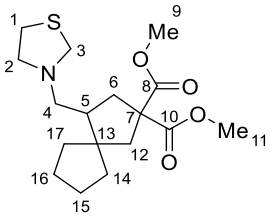

Following **GP A**, thiazolidine (15.8 µL, 0.2 mmol), dimethyl 2-formylcyclopropane-1,1-dicarboxylate (41.0 mg, 0.22 mmol), methylenecyclopentane (42.1 µL, 0.4 mmol) and DMTP (53.3 µL, 0.4 mmol) were reacted over 24 hours and purified by flash column chromatography (9:1 to 3:2 PE/Et_2O) to give the title compound as a colorless oil (49.2 mg, 72%). **^{1}H NMR** (400 MHz, $CDCl_3$): δ 4.08-3.99 (2H, m, H_3), 3.71 (3H, s, H_9), 3.71 (3H, s, H_{11}), 3.11-2.97 (2H, m, H_2), 2.89-2.80 (2H, m, H_1), 2.63 (1H, dd, J = 13.5, 6.6 Hz, H_{6A}), 2.46 (1H, dd, J = 12.3, 4.4 Hz, H_{4A}), 2.35 (1H, d, J = 13.8 Hz, H_{12A}), 2.20-2.05 (3H, m, $H_{4B+12B+6B}$), 2.01-1.90 (1H, m, H_5), 1.62-1.52 (5H, m, $H_{15+16+14A}$), 1.50-1.44 (1H, m, H_{14B}), 1.39-1.30 (1H, m, H_{17A}), 1.29-1.21 (1H, m, H_{17B}). **^{13}C NMR** (101 MHz, $CDCl_3$): δ 173.6 (C_9), 173.4 (C_{11}), 61.2 (C_3), 58.4 (C_2), 57.9 (C_7), 53.6 (C_4), 52.9 (C_{10}), 52.8 (C_{12}), 52.7 (C_{13}), 47.5 (C_{12}), 46.4 (C_5), 39.5 (C_6), 38.0 (C_{14}), 32.1 (C_{17}), 29.7 (C_1), 24.7 (C_{15}), 24.1 (C_{16}). **IR**

(CH_2Cl_2, cm^{-1}) 2950, 2870, 1731, 1435, 1253, 1223, 1199, 1168, 1107, 1052. **HRMS** (ASAP SOLID) calculated for $C_{17}H_{27}NO_4SH$ $[M+H]^+$ 342.1739, found 342.1741.

Dimethyl 4-((benzyl(methyl)amino)methyl)spiro[4.4]nonane-2,2-dicarboxylate (385)

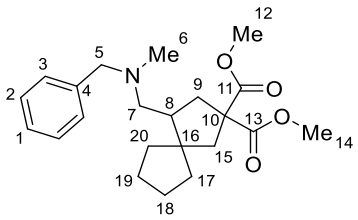

Following **GP A**, *N*-benzylmethylaniline (25.8 µL, 0.2 mmol), dimethyl 2-formylcyclopropane-1,1-dicarboxylate (44.7 mg, 0.24 mmol), methylenecyclopentane (63.1 µL, 0.6 mmol) and DMTP (53.3 µL, 0.4 mmol) were reacted over 24 hours and purified by flash column chromatography (PE to 7:3 PE/EtOAc) to give the title compound as a colorless oil (60.8 mg, 81%). **^{1}H NMR** (400 MHz, $CDCl_3$) δ = 7.34-7.27 (4H, m, H_{2+3}), 7.25-7.19 (1H, m, H_1), 3.72 (3H, s, H_{12}), 3.70 (3H, s, H_{14}), 3.54 (1H, d, *J* = 13.2 Hz, H_{5A}), 3.39 (1H, d, *J* = 13.1 Hz, H_{5B}), 2.65 (1H, dd, *J* = 13.0, 6.1 Hz, H_{9A}), 2.40 (1H, d, *J* = 13.8 Hz, H_{15A}), 2.37-2.30 (2H, m, H_7), 2.14 (3H, s, H_6), 2.13-1.99 (3H, m, $H_{8+15B+9B}$), 1.68-1.52 (5H, m, $H_{17A+18+19}$), 1.50-1.43 (1H, m, H_{17B}), 1.40-1.31 (1H, m, H_{20A}), 1.25-1.19 (1H, m, H_{20B}). **^{13}C NMR** (100 MHz, $CDCl_3$) δ = 173.7 (C_{11}), 173.5 (C_{13}), 139.4 (C_4), 129.0, 128.3, 127.0 (C_1), 62.8 (C_5), 58.4 (C_7), 57.9 (C_{10}), 52.8 (C_{12}), 52.8 (C_{16}), 52.8 (C_{14}), 47.6 (C_{15}), 44.5 (C_8), 42.5 (C_6), 39.5 (C_9), 37.9 (C_{17}), 31.8 (C_{20}), 24.7 (C_{18}), 24.2 (C_{19}). **IR** (CH_2Cl_2, cm^{-1}) 2950, 2866, 2775, 1732, 1434, 1256, 1199, 1172, 1024. **HRMS** (FTMS +p NSI) calculated for $C_{22}H_{31}NO_4H$ $[M+H]^+$ 374.2326, found 374.2326.

Dimethyl 4-((dibenzylamino)methyl)spiro[4.4]nonane-2,2-dicarboxylate (386)

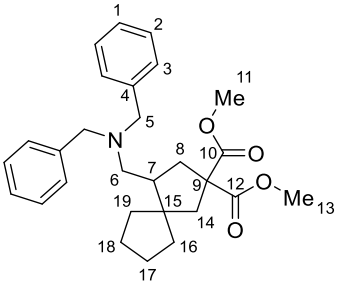

Following **GP A** with activated 4Å molecular sieves (50 mg), dibenzylamine (38.5 µL, 0.2 mmol), dimethyl 2-formylcyclopropane-1,1-dicarboxylate (44.7 mg, 0.24 mmol), methylenecyclopentane (42.1 µL, 0.4 mmol) and DMTP (53.3 µL, 0.4 mmol) were reacted over 24 hours and purified by flash column chromatography (19:1 to 4:1 PE/Et_2O) to give the title compound as a colorless oil (49.9 mg, 55%). **^{1}H NMR** (400 MHz, $CDCl_3$): δ = 7.38-7.27 (8H, m, H_{2+3}), 7.26-7.19 (2H, m, H_1), 3.73 (3H, s, H_{11}), 3.70-3.63 (5H, m, H_{5A+13}), 3.41 (2H, d, *J* = 13.6 Hz, H_{5B}), 2.72 (1H, dd, *J* = 13.5, 6.6 Hz, H_{8A}), 2.46-2.30 (3H, m, H_{6+14A}), 2.22-2.12 (1H, m, H_7), 2.02 (1H, d, *J* = 13.7 Hz, H_{14B}), 1.85 (1H, dd, *J* = 13.8, 11.3 Hz, H_{8B}), 1.68-1.37 (6H, m, $H_{16A+17+18+16B}$),

1.16-1.08 (2H, m, H_{19}). **^{13}C NMR** (101 MHz, $CDCl_3$): δ = 173.8 (C_{10}), 173.4 (C_{12}), 139.7 (C_4), 129.0 (C_3), 128.2 (C_2), 126.9 (C_1), 58.9 (C_5), 57.8 (C_9), 54.4 (C_6), 52.8 (C_{11}), 52.8 (C_{13}), 52.6 (C_{15}), 47.9 (C_{14}), 44.5 (C_7), 40.0 (C_8), 37.7 (C_{16}), 31.5 (C_{19}), 24.5 (C_{17}), 24.2 (C_{18}). **IR** (CH_2Cl_2, cm^{-1}) 2952, 2872, 2802, 1733, 1494, 1452, 1435, 1366, 1251, 1196, 1172, 1121, 1060, 1028. **HRMS** (FTMS +p NSI) calculated for $C_{28}H_{35}NO_4H$ $[M+H]^+$ 450.2639, found 450.2634.

Dimethyl 4-((methyl(phenyl)amino)methyl)spiro[4.4]nonane-2,2-dicarboxylate (387)

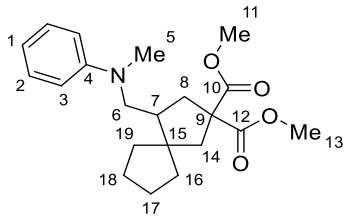

Following **GP A**, *N*-methylaniline (21.7 µL, 0.2 mmol), dimethyl 2-formylcyclopropane-1,1-dicarboxylate (44.7 mg, 0.24 mmol), methylenecyclopentane (42.1 µL, 0.4 mmol) and 2,6-dimethylbenzenethiol (53.3 µL, 0.4 mmol) were reacted over 24 hours and purified by flash column chromatography (100% PE to PE/Et_2O 4:1) to give the title compound as a colorless oil (47.7 mg, 66%). **^{1}H NMR** (400 MHz, $CDCl_3$) δ = 7.29-7.19 (2H, m, H_3), 6.74-6.65 (3H, m, H_{2+1}), 3.72 (3H, s, H_{11}), 3.69 (3H, s, H_{13}), 3.48 (1H, dd, *J* = 14.5, 3.4 Hz, H_{6A}), 3.13 (1H, dd, *J* = 14.5, 10.1 Hz, H_{6B}), 2.94 (3H, s, H_5), 2.53 (1H, dd, *J* = 12.9, 6.2 Hz, H_{8A}), 2.38 (1H, d, *J* = 13.8 Hz, H_{14A}), 2.30-2.21 (1H, m, H_7), 2.20-2.11 (2H, m, H_{8B+14B}), 1.75-1.54 (6H, m, $H_{16A+17+18+16B}$), 1.53-1.44 (1H, m, H_{19A}), 1.40-1.32 (1H, m, H_{19B}). **^{13}C NMR** (101 MHz, $CDCl_3$) δ = 173.5 (C_{10}), 173.3 (C_{12}), 149.7 (C_4), 129.2 (C_3), 116.2 (C_1), 112.3 (C_2), 58.0 (C_9), 53.6 (C_6), 52.9 (C_{11}), 52.9 (C_{13}), 52.8 (C_{15}), 47.3 (C_{14}), 45.2 (C_7), 39.3 (C_{16}), 39.1 (C_5), 37.6 (C_8), 31.7 (C_{19}), 24.7 (C_{17}), 24.2 (C_{18}). **IR** (CH_2Cl_2, cm^{-1}) 2949, 2870, 1732, 1599, 1507, 1434, 1364, 1260, 1196, 1171, 1111. **HRMS** (FTMS +p NSI) calculated for $C_{21}H_{29}NO_4H$ $[M+H]^+$: 360.2169, found 360.2173.

Dimethyl 4-((4-(8-chloro-5,6-dihydro-11*H*-benzo[5,6]cyclohepta[1,2-*b*]pyridin-11-ylidene) piperidin-1-yl)methyl)spiro[4.4]nonane-2,2-dicarboxylate (388)

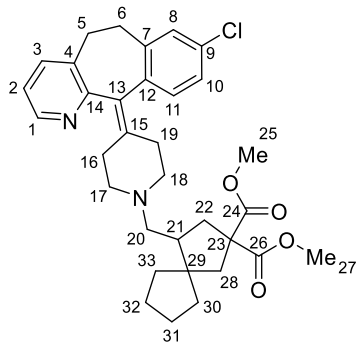

Following **GP A**, Desloratadine (62.2 mg, 0.2 mmol), dimethyl 2-formylcyclopropane-1,1-dicarboxylate (41.0 mg, 0.22 mmol), methylenecyclopentane (42.1 µL, 0.4 mmol) and 2,6-dimethylbenzenethiol (53.3 µL, 0.4

mmol) were reacted over 24 hours and purified by flash column chromatography (PE/EtOAc 7:3 to 100% EtOAc) to give the title compound as a light brown foam (69.5 mg, 62%, 1:1 dr).

^{1}H NMR (400 MHz, $CDCl_3$) δ 8.40-8.34 (2H, m, H_1), 7.40 (2H, d, J = 7.7 Hz, H_2), 7.16-7.08 (3H, m, $H_{8+10+11}$), 7.08-7.02 (1H, m, H_3), 3.68 (6H, s, H_{25+27}), 3.44-3.27 (2H, m, H_{17}), 2.86-2.63 (4H, m, $H_{18+16A+19A}$), 2.67-1.86 (13H, m, $H_{22+28+21+20+5+6+16B+19B}$), 1.65-1.46 (5H, m, $H_{30+33+31A}$), 1.46-1.30 (2H, m, $H_{31B+32A}$), 1.28-1.17 (1H, m, H_{32B}). **^{13}C NMR** (100 MHz, $CDCl_3$) δ 173.7 ($C_{25+25'}$), 173.4 (C_{27}), 173.4 ($C_{27'}$), 157.7 ($C_{14+14'}$), 146.7 ($C_{1+1'}$), 139.6 ($C_{Q1+Q1'}$), 138.0 (C_{Q2}), 137.9 ($C_{Q2'}$), 137.3 (C_1), 137.3 ($C_{1'}$), 133.5 ($C_{Q3+Q3'}$), 132.7 ($C_{Q4+Q4'}$), 132.5 ($C_{Q5+Q5'}$), 130.9, 129.0, 129.0, 126.0 ($C_{8+10+11+8'+10'+11'}$), 122.1 ($C_{3+3'}$), 58.8 (C_{20}), 58.8 ($C_{20'}$), 57.9 ($C_{23+23'}$), 55.7(C_{16}), 55.6 ($C_{16'}$), 55.0 (C_{19}), 54.9 ($C_{19'}$), 52.9 (C_{29}), 52.9 ($C_{29'}$), 52.8 ($C_{25+25'}$), 52.7 ($C_{27+27'}$), 47.6 (C_{28}), 47.5 ($C_{28'}$), 43.9 (C_{21}), 43.8 ($C_{21'}$), 39.7 (C_{22}), 39.7 ($C_{22'}$), 37.9 (C_{30}), 37.8 ($C_{30'}$), 31.9 ($C_{6+6'}$), 31.7 (C_{17}), 31.7 ($C_{17'}$), 31.5 (C_5), 31.5 ($C_{5'}$), 31.0 ($C_{C33+C33'}$), 30.8($C_{C18+C18'}$), 24.7 ($C_{31+31'}$), 24.2 ($C_{32+32'}$). **IR** (CH_2Cl_2, cm^{-1}): 2949, 1731, 1436, 1255, 1197, 1171, 1115. **HRMS** (FTMS +p NSI) calculated for $C_{33}H_{39}ClN_2O_4H$ $[M+H]^+$ 563.2671, found 563.2661.

Dimethyl 4-((methyl(3-phenyl-3-(4-(trifluoromethyl)phenoxy)propyl)amino)methyl)spiro[4.4] nonane-2,2-dicarboxylate (389)

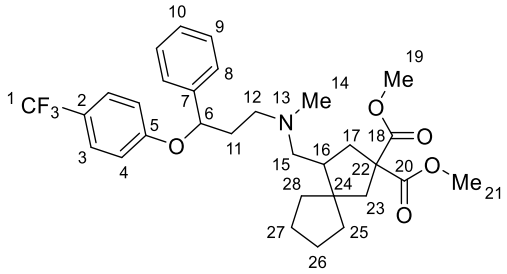

Following **GP A**, Fluoxetine hydrochloride (69.2 mg, 0.2 mmol), dimethyl 2-formylcyclopropane-1,1-dicarboxylate (41.0 mg, 0.22 mmol), methylenecyclopentane (63.1 µL, 0.6 mmol) and DMTP (53.3 µL, 0.4 mmol) were reacted over 24 hours and purified by flash column chromatography (PE/EtOAc 9:1 to 7:3) to give the title compound as a yellow oil (82.1 mg, 73%, 1:1 dr).

^{1}H NMR (400 MHz, $CDCl_3$): δ 7.38-7.14 (11H, $H_{3+8+9+10+3'+8'+9'+10'}$), 6.88-6.79 (4H, $H_{4+4'}$), 5.23 (2H, dd, J = 8.4, 4.7 Hz, $H_{6+6'}$), 3.66 (3H, s, H_{19}), 3.62 (3H, s, $H_{19'}$), 3.61 (3H, s, H_{21}), 3.57 (3H, s, $H_{21'}$), 2.58-1.79 (22H, m, $H_{11+12+15+16+17+23+11'+12'+15'+16'+17'+23'}$), 2.12 (3H, s, H_{14}), 2.12 (3H, s, $H_{14'}$), 1.57-1.39 (10H, m, $H_{26+27+25A}$), 1.37-1.19 (4H, m, $H_{25B+28A}$), 1.18-1.10 (2H, m, H_{28B}). **^{13}C NMR** (101 MHz, $CDCl_3$): δ 173.7 (C_{18}), 173.6 ($C_{18'}$), 173.5 (C_{20}), 173.4 ($C_{20'}$), 169.4 (C_5), 160.8 ($C_{5'}$), 141.5 (C_7), 141.4 ($C_{7'}$), 128.8, 128.8, 127.9, 127.8, 126.8, 126.8, 126.0, 125.9 ($C_{3/3'/8/8'/9/9'/10/10'}$), 122.8 (t, J = 33.1 Hz, $C_{2+2'}$), 121.3 (d, J = 171.8 Hz, $C_{1+1'}$), 115.9 (C_4), 115.9 ($C_{4'}$), 78.4 (C_6), 78.4 ($C_{6'}$), 58.7 (C_{15}), 58.6 ($C_{15'}$), 57.9 (C_{22}), 57.8 ($C_{22'}$), 54.6 (C_{12}), 54.4 ($C_{12'}$), 52.8 (C_{19}), 52.8 ($C_{19'}$), 52.8 (C_{21}), 52.7 ($C_{21'}$), 47.6 (C_{23}), 47.4 ($C_{23'}$), 44.6 (C_{16}), 44.5 ($C_{16'}$), 42.6 (C_{14}), 42.5 ($C_{14'}$), 39.8 (C_{11}), 39.5 ($C_{11'}$), 37.8 (C_{17}), 37.7 ($C_{17'}$), 36.8 (C_{25}), 36.6 ($C_{25'}$), 31.8 (C_{28}), 31.7 ($C_{28'}$), 24.6 (C_{26}), 24.5 ($C_{26'}$), 24.2 (C_{27}), 24.1 ($C_{27'}$). **^{19}F NMR** (376 MHz, $CDCl_3$): -61.5 (F_1). **IR** (CH_2Cl_2, cm^{-1}): 2951, 1731, 1614,

1517, 1453, 1435, 1324, 1248, 1199, 1159, 1109, 1067, 1009. **HRMS** (FTMS +p ESI) calculated for $C_{31}H_{38}O_5N_1F_3H$ $[M+H]^+$: 562.2775, found 562.2767.

Dimethyl 4-((4-cyanopiperidin-1-yl)methyl)spiro[4.5]decane-2,2-dicarboxylate (399)

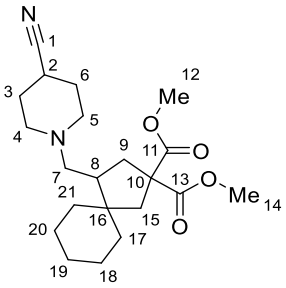

Following **GP A**, piperidine-4-carbonitrile (22.5 µL, 0.2 mmol), dimethyl 2-formylcyclopropane-1,1-dicarboxylate (41.0 mg, 0.22 mmol), methylenecyclohexane (120 µL, 1.0 mmol) and 2,6-dimethylbenzenethiol (53.3 µL, 0.4 mmol) were reacted over 24 hours and purified by flash column chromatography (PE/EtOAc 9:1 to 1:1) to give the title compound as a colorless oil (67.2 mg, 79%). **^{1}H NMR** (400 MHz, $CDCl_3$): δ = 3.69 (3H, s, H_{12}), 3.68 (3H, s, H_{14}), 2.72-2.44 (5H, m, $H_{4A+2+15A+4B+9A}$), 2.41-2.26 (2H, m, H_{5A+7A}), 2.26-2.11 (2H, m, H_{7B+2B}), 1.03-1.74 (7H, m, $H_{9B+15B+3+6+8}$), 1.66-1.45 (4H, m, $H_{18A+20A+19A+17A}$), 1.42-1.18 (4H, m, $H_{19B+20B+21A+17B}$), 1.16-1.02 (2H, m, $H_{18B+21B}$). **^{13}C NMR** (100 MHz, $CDCl_3$): δ = 173.7 (C_{11}), 173.4 (C_{13}), 121.9 (C_1), 58.7 (C_7), 57.7 (C_{10}), 52.9 (C_{12}), 52.8 (C_{14}), 51.8 (C_{4+5}), 46.1 (C_8), 44.8 (C_{16}), 43.5 (C_{15}), 38.3 (C_9), 38.0 (C_{17}), 29.7 (C_{21}), 28.9 (C_{3+6}), 26.4 (C_{18}), 26.3 (C_2), 24.0 (C_{20}), 22.4 (C_{19}). **IR** (CH_2Cl_2, cm^{-1}): 2927, 2854, 1730, 1434, 1252, 1199, 1137, 1109, 1058. **HRMS** (FTMS +p NSI) calculated for $C_{21}H_{32}N_2O_4H$ $[M+H]^+$: 377.2435, found 377.2434.

Dimethyl 8-((4-cyanopiperidin-1-yl)methyl)spiro[3.4]octane-6,6-dicarboxylate (400)

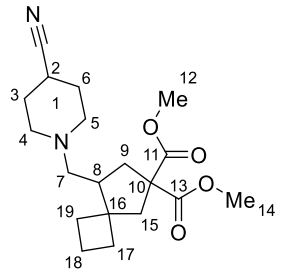

Following **GP A**, piperidine-4-carbonitrile (22.5 µL, 0.2 mmol), dimethyl 2-formylcyclopropane-1,1-dicarboxylate (41.0 mg, 0.22 mmol), methylenecyclobutane (92.6 µL, 1.0 mmol) and 2,6-dimethylbenzenethiol (53.3 µL, 0.4 mmol) were reacted over 24 hours and purified by flash column chromatography (PE/EtOAc 9:1 to 1:1) to give the title compound as a colorless oil (53.2 mg, 76%). **^{1}H NMR** (400 MHz, $CDCl_3$): δ = 3.69 (3H, s, H_{12}), 3.69 (3H, s, H_{14}), 2.79-2.52 (4H, $H_{H4A,2,5A,15A}$), 2.49-2.30 (3H, m, $H_{7A,9A,5B}$), 2.29-2.14 (3H, m, $H_{4B,15B,5B,7B}$), 2.04-1.76 (10H, m, $H_{17A,19A,8,9B,3,6,18A,19B}$), 1.76-1.67 (1H, m, H_{18B}), 1.66-1.57 (1H, m, H_{17B}). **^{13}C NMR** (100 MHz, $CDCl_3$): δ = 173.39 (C_{11}), 173.22 (C_{13}), 121.98 (C_1), 59.46 (C_7),

57.64 (C_{10}), 52.80 (C_{12}), 52.77 (C_{14}), 51.98 (C_4), 51.87 (C_5), 48.64 (C_{16}), 47.21 (C_{15}), 43.97 (C_8), 38.04 (C_9), 31.82 (C_{19}), 29.01 (C_{3+6}), 27.75 (C_{17}), 26.38 (C_2), 16.19 (C_{18}). **IR** (CH_2Cl_2, cm^{-1}): 2952, 2811, 1731, 1435, 1258, 1198, 1108. **HRMS** (FTMS +p NSI) calculated for $C_{19}H_{28}N_2O_4H$ $[M+H]^+$ 349.2122, found 349.2125.

8-Benzyl 2,2-dimethyl 4-((4-cyanopiperidin-1-yl)methyl)-8-azaspiro[4.5]decane-2,2,8-tricarboxylate (401)

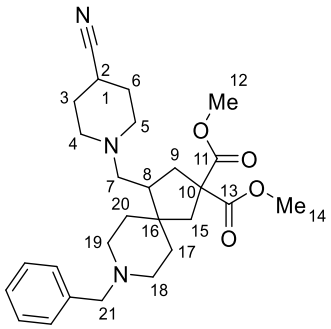

Following **GP A**, piperidine-4-carbonitrile (22.5 µL, 0.2 mmol), dimethyl 2-formylcyclopropane-1,1-dicarboxylate (41.0 mg, 0.22 mmol), benzyl 4-methylenepiperidine-1-carboxylate (231 mg, 1.0 mmol) and 2,6-dimethylbenzenethiol (53.3 µL, 0.4 mmol) were reacted over 24 hours and purified by flash column chromatography (PE/EtOAc 8:2 to 100% EtOAc) to give the title compound as a colorless oil (79.0 mg, 78%). **^{1}H NMR** (400 MHz, $CDCl_3$): δ = 7.38-7.27 (5H, m, H_{X+X+X}), 5.11 (3H, s, H_{23}), 4.02 (2H, bs, $H_{18A+19A}$), 3.71 (3H, s, H_{12}), 3.69 (3H, s, H_{14}), 3.07-2.76 (2H, m, $H_{19B+19B}$), 2.68-2.46 (5H, m, $H_{4A+15A+2+5A+9A}$), 2.37-2.10 (4H, m, $H_{7A+5B+4B+7B}$), 2.06-1.70 (8H, m, $H_{15B+9B+8+3+6+17A}$), 1.37 (1H, bs, H_{20A}), 1.29-1.16 (2H, m, $H_{20B+17B}$). **^{13}C NMR** (101 MHz, $CDCl_3$): δ = 173.2 (C_{11}), 173.0 (C_{13}), 155.3 (C_{21}), 136.9 (C_{23}), 128.5 (C_{25}), 128.0 (C_{26}), 127.9 (C_{24}), 121.7 (C_1), 67.0 (C_{22}), 58.4 (C_7), 57.6 (C_{10}), 53.0 (C_{12}), 52.9 (C_{14}), 51.9 (C_4), 51.6 (C_5), 45.5 (C_8), 43.2 (C_{16}), 42.3 (C_{15}), 41.9 (C_{19}), 40.6 (C_{18}), 38.0 (C_9), 36.7 (C_{17}), 29.3 (C_{20}), 28.8 (C_{3+6}), 26.2 (C_2). **IR** (CH_2Cl_2, cm^{-1}): 2949, 2784, 1729, 1694, 1497, 1432, 1384, 1357, 1234, 1202, 1156, 1138, 1091. **HRMS** (FTMS +p ESI) calculated for $C_{27}H_{37}N_3O_4H$ $[M+H]^+$ 468.2854, found 468.2857.

Dimethyl 4-((4-cyanopiperidin-1-yl)methyl)-3,3-diethylcyclopentane-1,1-dicarboxylate (402)

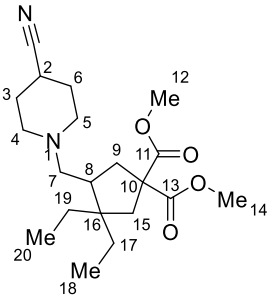

Following **GP A**, piperidine-4-carbonitrile (22.5 µL, 0.2 mmol), dimethyl 2-formylcyclopropane-1,1-dicarboxylate (41.0 mg, 0.22 mmol), 2-ethyl-1-butene (122 µL, 1.0 mmol) and 2,6-dimethylbenzenethiol (53.3 µL, 0.4 mmol) were reacted over 24 hours and purified by flash column chromatography (PE/EtOAc 9:1 to

1:1) to give the title compound as a colorless oil (48.4 mg, 66%). **^{1}H NMR** (400 MHz, $CDCl_3$): δ = 3.70 (3H, s, H_{12}), 3.69 (3H, s, H_{14}), 2.77-2.64 (1H, m, H_{4A}), 2.64-2.55 (1H, m, H_2), 2.55-2.43 (2H, m, H_{5A+9A}), 2.43-2.11 (5H, m, $H_{5B+15A+7+4B}$), 2.11-1.97 (3H, m, $H_{9B+15B+8}$), 1.97-1.74 (4H, m, H_{3+6}), 1.47-1.35 (1H, m, H_{17A}), 1.35-1.25 (1H, m, H_{17B}), 1.25-1.16 (2H, m, H_{19}), 0.87-0.72 (6H, m, H_{18+20}). **^{13}C NMR** (101 MHz, $CDCl_3$): δ = 173.8 (C_{11}), 173.4 (C_{13}), 122.0 (C_1), 58.8 (C_7), 57.7 (C_{10}), 52.8 (C_{12}), 52.8 (C_{14}), 51.8 (C_{4+5}), 46.9 (C_{16}), 43.1 (C_8), 42.5 (C_{15}), 38.6 (C_9), 29.0 (C_3), 29.0 (C_6), 28.9 (C_{17}), 26.4 (C_2), 25.2 (C_{19}), 8.7 (C_{18}), 8.6 (C_{20}). **IR** (CH_2Cl_2, cm^{-1}): 2955, 2784, 1730, 1435, 1381, 1254, 1199, 1163, 1076, 1006. **HRMS** (FTMS +p ESI) calculated for $C_{20}H_{32}N_2O_4H$ $[M+H]^+$ 365.2435, found 365.2437.

Dimethyl 3-butyl-4-((4-cyanopiperidin-1-yl)methyl)cyclopentane-1,1-dicarboxylate (403)

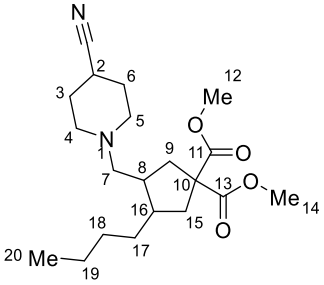

Following **GP A**, piperidine-4-carbonitrile (22.5 µL, 0.2 mmol), dimethyl 2-formylcyclopropane-1,1-dicarboxylate (41.0 mg, 0.22 mmol), 1-hexene (124 µL, 1.0 mmol) and 2,6-dimethylbenzenethiol (53.3 µL, 0.4 mmol) were reacted over 24 hours and purified by flash column chromatography (PE/EtOAc 9:1 to 1:1) to give the title compound as a colorless oil (42.7 mg, 59%, 9:1 dr). **^{1}H NMR** (400 MHz, $CDCl_3$): δ = 3.71 (3H, s, H_{12}), 3.70 (3H, s, H_{14}), 2.73-2.63 (1H, m, H_{4A}), 2.63-2.51 (2H, m, H_{2+5A}), 2.41-2.09 (8H, m, $H_{9A+5B+15A+7A+16+9B+4B+7B}$), 2.08-1.96 (2H, m, H_{15B+8}), 1.96-1.76 (4H, m, H_{3+6}), 1.39-1.08 (6H, m, $H_{17A+19+18A+18B+17B}$), 0.88 (3H, t, *J* = 7.0 Hz, H_{20}). **^{13}C NMR** (100 MHz, $CDCl_3$): δ = 173.6 (C_{11}), 173.5 (C_{13}), 122.0 (C_1), 58.8 (C_{10}), 57.9 (C_7), 52.9 (C_{12}), 52.8 (C_{14}), 51.7 (C_{4+5}), 41.6 (C_8), 38.9 (C_{15}), 38.7 (C_{16}), 37.9 (C_9), 30.7 (C_{18}), 29.0 (C_{3+6}), 28.7 (C_{17}), 26.4 (C_2), 23.0 (C_{19}), 14.2 (C_{20}). **IR** (CH_2Cl_2, cm^{-1}): 2952, 1731, 1435, 1257, 1198, 1167. **HRMS** (FTMS +p NSI) calculated for $C_{20}H_{32}N_2O_4H$ $[M+H]^+$ 365.2435, found 365.2437.

Dimethyl 3-((4-cyanopiperidin-1-yl)methyl)-4-phenylcyclopentane-1,1-dicarboxylate (404)

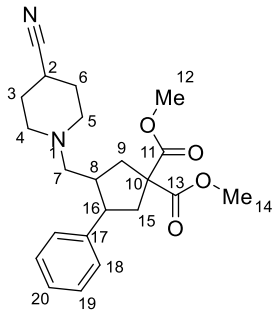

Following **GP A**, piperidine-4-carbonitrile (22.5 µL, 0.2 mmol), dimethyl 2-formylcyclopropane-1,1-dicarboxylate (44.7 mg, 0.24 mmol), styrene (46.0 µL, 0.4 mmol) and 2,6-dimethylbenzenethiol (53.3 µL, 0.4

mmol) were reacted over 24 hours and purified by flash column chromatography (PE/Et_2O 1:1 to 3:7) to give the title compound as a colorless oil (61.2 mg, 80%, 8:1 dr). **^{1}H NMR** (400 MHz, $CDCl_3$): δ = 7.30-7.23 (2H, m, H_{19}), 7.22-7.13 (3H, m, H_{20+18}), 3.76 (3H, s, H_{12}), 3.76 (3H, s, H_{14}), 3.42 (1H, dt, *J* = 9.8, 7.6 Hz, H_{16}), 2.71 (1H, dd, *J* = 13.9, 7.5 Hz, H_{15A}), 2.62-2.37 (6H, m, $H_{15B+8+9A+2+4A+5A}$), 2.33-2.23 (1H, m, H_{9B}), 2.18-1.93 (2H, m, H_{4B+5B}), 1.91-1.65 (6H, m, $H_{7A+7B+3+6}$). **^{13}C NMR** (101 MHz, $CDCl_3$): δ = 173.2 (C_{11}), 173.0 (C_{13}), 140.9 (C_{17}), 128.4 (C_{18}), 128.2 (C_{19}), 126.4 (C_{20}), 122.0 (C_1), 59.1 (C_{10}), 58.8 (C_7), 53.0 (C_{12}), 52.9 (C_{14}), 51.4 (C_{4+5}), 46.3 (C_{16}), 40.2 (C_8), 38.2 (C_{15}), 38.1 (C_9), 29.0 (C_3), 28.9 (C_6), 26.3 (C_2). **IR** (CH_2Cl_2, cm^{-1}): 2952, 2785, 1728, 1496, 1434, 1383, 1254, 1198, 1169, 1104, 1079, 1062, 1008. **HRMS** (FTMS +p NSI) calculated for $C_{22}H_{28}N_2O_4H$ $[M+H]^+$: 385.2122, found 385.2123.

Dimethyl 3-(4-bromophenyl)-4-((dimethylamino)methyl)cyclopentane-1,1-dicarboxylate (405)

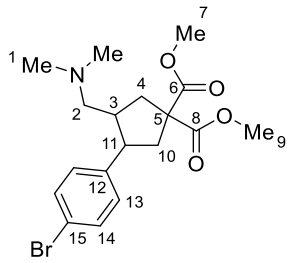

Following **GP A**, piperidine-4-carbonitrile (22.5 µL, 0.2 mmol), dimethyl 2-formylcyclopropane-1,1-dicarboxylate (44.7 mg, 0.24 mmol), 4-vinylanisole (53.2 µL, 0.4 mmol) and 2,6-dimethylbenzenethiol (53.3 µL, 0.4 mmol) were reacted over 24 hours and purified by flash column chromatography (PE/Et_2O 9:1 to 1:9) to give the title compound as a colorless oil (48.9 mg, 59%, 9:1 dr). **^{1}H NMR** (400 MHz, $CDCl_3$): δ = 7.40 (2H, d, *J* = 8.0 Hz, H_{14}), 7.05 (2H, d, *J* = 8.1 Hz, H_{13}), 3.75 (6H, s, H_{7+9}), 3.37 (1H, q, *J* = 8.4 Hz, H_{11}), 2.67 (1H, dd, *J* = 13.9, 7.4 Hz, H_{10A}), 2.61-2.41 (3H, m, $H_{10B+4A+3}$), 2.25 (1H, dd, *J* = 13.5, 6.8 Hz, H_{4B}), 2.06 (6H, s, H_1), 1.84 (1H, t, *J* = 11.3 Hz, H_{2A}), 1.57 (1H, dd, *J* = 12.1, 4.9 Hz, H_{2B}). **^{13}C NMR** (101 MHz, $CDCl_3$) δ = 173.2 (C_6), 172.9 (C_8), 140.1 (C_{12}), 131.3 (C_{14}), 130.1 (C_{13}), 120.2 (C_{15}), 60.4 (C_2), 59.1 (C_5), 53.0 (C_7), 52.9 (C_9), 45.8 (C_{11}), 45.8 (C_1), 40.7 (C_3), 38.2 (C_{10}), 38.0 (C_4). **IR** (CH_2Cl_2, cm^{-1}): 2951, 2817, 1731, 1489, 1434, 1267, 1199, 1162, 1099, 1071, 1010. **HRMS** (FTMS +p ESI) calculated for $C_{18}H_{24}BrNO_4H$ $[M+H]^+$: 398.0961, found 398.0960.

Dimethyl 3-((4-cyanopiperidin-1-yl)methyl)-4-(4-methoxyphenyl)cyclopentane-1,1-dicarboxylate (406)

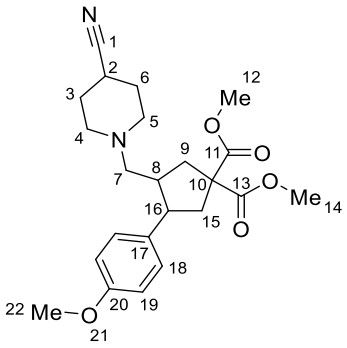

Following **GP A**, piperidine-4-carbonitrile (22.5 µL, 0.2 mmol), dimethyl 2-formylcyclopropane-1,1-dicarboxylate (44.7 mg, 0.24 mmol), 4-vinylanisole (53.2 µL, 0.4 mmol) and 2,6-dimethylbenzenethiol (53.3 µL, 0.4 mmol) were reacted over 24 hours and purified by flash column chromatography (PE/Et_2O 9:1 to 1:9) to give the title compound as a colorless oil (48.9 mg, 59%, 9:1 dr). **^{1}H NMR** (400 MHz, $CDCl_3$): δ = 7.07 (2H, d, *J* = 8.6 Hz, H_{18}), 6.81 (2H, d, *J* = 8.6 Hz, H_{19}), 3.78 (3H, s, H_{22}), 3.76 (3H, s, H_{12}), 3.75 (3H, s, H_{14}), 3.42-3.31 (1H, m, H_{16}), 2.69 (1H, dd, *J* = 13.9, 7.6 Hz, H_{15A}), 2.58-2.37 (6H, m, $H_{15B+2+8+9A+4A+5A}$), 2.30-2.22 (1H, m, H_{9B}), 2.18-2.07 (1H, bs, H_{4B}), 2.07-1.95 (1H, bs, H_{5B}), 1.91-1.67 (6H, m, $H_{7A+7B+3+6}$). **^{13}C NMR** (100 MHz, $CDCl_3$): δ = 173.3 (C_{11}), 173.1 (C_{13}), 158.1 (C_{20}), 133.0 (C_{17}), 129.3 (C_{18}), 122.0 (C_1), 113.6 (C_{19}), 59.1 (C_{10}), 58.9 (C_7), 55.3 (C_{22}), 53.0 (C_{12}), 52.9 (C_{14}), 51.8 (C_4), 51.5 (C_5), 45.5 (C_{16}), 40.2 (C_8), 38.5 (C_{15}), 38.1 (C_9), 29.0 (C_3), 29.0 (C_6), 26.3 (C_2). **IR** (CH_2Cl_2, cm^{-1}): 2952, 2837, 1728, 1611, 1513, 1434, 1247, 1197, 1180, 1100, 1065, 1035, 1008. **HRMS** (FTMS +p ESI) calculated for $C_{23}H_{30}N_2O_5H$ $[M+H]^+$: 415.2227, found 415.2224.

Dimethyl 3-((4-cyanopiperidin-1-yl)methyl)-4-(pyridin-4-yl)cyclopentane-1,1-dicarboxylate (407)

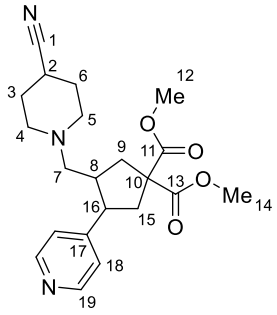

Following **GP A**, piperidine-4-carbonitrile (22.5 µL, 0.2 mmol), dimethyl 2-formylcyclopropane-1,1-dicarboxylate (41.0 mg, 0.22 mmol), 4-vinylpyridine (43.1 µL, 0.4 mmol) and 2,6-dimethylbenzenethiol (53.3 µL, 0.4 mmol) were reacted over 24 hours and purified by flash column chromatography (EtOAc to EtOAc/MeOH 9:1) to give the title compound as a colorless oil (46.5 mg, 60%, 9:1 dr). **^{1}H NMR** (400 MHz, $CDCl_3$): δ = 8.48 (2H, d, *J* = 6.0 Hz, H_{19}), 7.10(2H, d, *J* = 6.1 Hz, H_{18}), 3.76 (3H, s, H_{12}), 3.76 (3H, s, H_{14}), 3.38 (1H, q, *J* = 8.3 Hz, H_{16}), 2.72 (1H, dd, *J* = 14.1, 7.6 Hz, H_{15A}), 2.62-2.40 (5H, m, $H_{8+15B+2+9A+4A}$), 2.39-2.32 (1H, m, H_{5A}), 2.23 (1H, dd, *J* = 13.7, 7.6 Hz, H_{9B}), 2.10-1.97 (2H, m, H_{4B+5B}), 1.88 (1H, dd, *J* = 12.6, 8.7 Hz, H_{7A}), 1.83-1.64 (5H, m, H_{7B+3+6}). **^{13}C NMR** (100 MHz, $CDCl_3$): δ = 173.0 (C_{12}), 172.7 (C_{14}), 150.4 (C_{17}),

149.6 (C_{19}), 124.0 (C_{18}), 121.8 (C_1), 59.0 (C_{10}), 58.5 (C_7), 53.1 (C_{12}), 53.1 (C_{14}), 51.7 (C_4), 51.4 (C_5), 45.8 (C_{16}), 40.2 (C_8), 38.0 (C_9), 37.8 (C_{15}), 28.9 (C_3), 28.9 (C_6), 26.3 (C_2). **IR** (CH_2Cl_2, cm^{-1}): 2952, 2779, 1728, 1598, 1434, 1415, 1384, 1255, 1198, 1169, 1111, 1065. **HRMS** (FTMS +p ESI) calculated for $C_{21}H_{27}N_3O_4H$ $[M+H]^+$: 386.2074, found 386.2070.

3-Butyl 1,1-dimethyl 4-((4-cyanopiperidin-1-yl)methyl)cyclopentane-1,1,3-tricarboxylate (408)

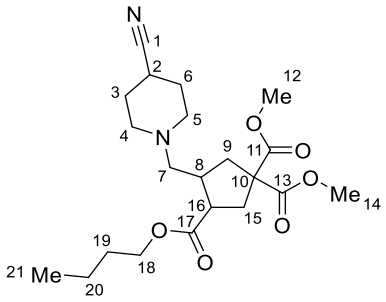

Following **GP A**, piperidine-4-carbonitrile (22.5 µL, 0.2 mmol), dimethyl 2-formylcyclopropane-1,1-dicarboxylate (41.0 mg, 0.22 mmol), butyl acrylate (57.3 µL, 0.4 mmol) and 2,6-dimethylbenzenethiol (53.3 µL, 0.4 mmol) were reacted over 24 hours and purified by flash column chromatography (9:1 PE/EtOAc to 100% EtOAc) to give the title compound as a colorless oil (23.9 mg, 29%, 1:1 dr). **^{1}H NMR** (400 MHz, $CDCl_3$): δ 4.12-3.94 (4H, m, H_{18}), 3.80-3.67 (14H, m, $H_{12+12'+14+14'+4}$), 2.99-2.85 (1H, m, H_{16}), 2.71-2.11 (24H, m, $H_{2+2'+8+8'+16+16'+4'+5+5'+7+7'+9+9'+15+15'}$), 1.94-1.64 (8H, m, $H_{3+3'+6+6'}$), 1.64-1.53 (4H, m, $H_{19+19'}$), 1.38 (4H, h, *J* = 7.4 Hz , $H_{20+20'}$), 1.44-1.32 (6H, t, *J* = 7.4 Hz, $H_{21+21'}$). **^{13}C NMR** (100 MHz, $CDCl_3$): δ 174.4 (C_{17}), 173.8 ($C_{17'}$), 173.0 (C_{11}), 172.6 ($C_{11'}$), 172.1 (C_{13}), 172.1 ($C_{13'}$), 121.9 (C_1), 121.9 ($C_{1'}$), 64.7 (C_{18}), 64.5 ($C_{18'}$), 62.7 ($C_{7+7'}$), 59.2 (C_{10}), 59.2 ($C_{10'}$), 59.1 ($C_{4/5}$), 53.1 (C_{12}), 53.0 ($C_{12'}$), 53.0 (C_{14}), 52.9 ($C_{14'}$), 51.8 ($C_{4'}$), 51.8 ($C_{5'}$), 49.0 (C_{16}), 45.7 ($C_{16'}$), 40.8 (C_8), 39.3 ($C_{8'}$), 38.4 (C_9), 38.1 ($C_{9'/15/15'}$), 38.0 ($C_{9'/15/15'}$), 36.4 ($C_{9'/15/15'}$), 30.8 (C_{19}), 30.8 ($C_{19'}$), 29.0 (C_3), 29.0 ($C_{3'}$), 29.0 (C_6), 29.0 ($C_{6'}$), 26.3 (C_2), 26.3 ($C_{2'}$), 19.4 (C_{20}), 19.3 ($C_{20'}$), 13.9 ($C_{21+21'}$). **IR** (CH_2Cl_2, cm^{-1}): 2956, 2815, 1730, 1435, 1257, 1198, 1171, 1066. **HRMS** (TOF MS ASAP+) calculated for $C_{21}H_{32}N_2O_6H$ $[M+H]^+$: 409.2339, found 409.2342.

Dimethyl 6-((4-cyanopiperidin-1-yl)methyl)hexahydro-4*H*-cyclopenta[*b*]furan-4,4-dicarboxylate (409)

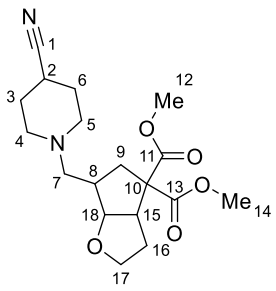

Following **GP A**, piperidine-4-carbonitrile (22.5 µL, 0.2 mmol), dimethyl 2-formylcyclopropane-1,1-dicarboxylate (41.0 mg, 0.22 mmol), styrene (30.2 µL, 0.4 mmol) and 2,6-dimethylbenzenethiol (53.3 µL, 0.4 mmol) were reacted over 24 hours and purified by flash column chromatography (PE/EtOAc 7:3 to 3:7) to

give the title compound as a colorless oil (26.2 mg, 37%, >20:1 dr). **^{1}H NMR** (400 MHz, $CDCl_3$): δ = 4.32 (1H, t, *J* = 6.1 Hz, H_{18}), 3.87-3.80 (1H, m, H_{17A}), 3.73 (3H, s, H_{12}), 3.71 (3H, s, H_{14}), 3.54-3.43 (2H, H_{17B+15}), 2.70-2.54 (3H, $H_{4A+5A+2}$), 2.37-2.22 (2H, H_{5B+4B}), 2.11-2.05 (2H, m, H_9), 1.04-1.79 (6H, m, $H_{16A+8+3+6}$), 1.39-1.28 (1H, m, H_{16B}). **^{13}C NMR** (100 MHz, $CDCl_3$) δ = 172.5 (C_{11}), 170.5 (C_{13}), 122.0 (C_1), 83.9 (C_{18}), 68.5 (C_{17}), 63.1 (C_{10}), 57.2 (C_5), 53.1 (C_{12}), 52.6 (C_{14}), 51.9 (C_4), 48.3 (C_{15}), 39.6 (C_8), 35.9 (C_9), 30.5 (C_{16}), 28.9 (C_{3+6}), 26.3 (C_2). **IR** (CH_2Cl_2, cm^{-1}): 2953, 1730, 1435, 1275, 1249, 1232, 1195, 1161, 1074, 1035. **HRMS** (FTMS +p NSI) calculated for $C_{18}H_{26}N_2O_5H$ $[M+H]^+$: 351.1914, found 351.1917.

1-(Cyclopropylmethyl)-4-phenylpiperidine (417)

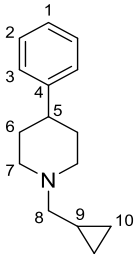

^{1}H NMR (400 MHz, $CDCl_3$): δ = 7.33-7.27 (2H, m, H_2), 7.27-7.22 (2H, m, H_3), 7.22-7.16 (1H, m, H_1), 3.28 (2H, d, *J* = 11.9 Hz, H_{7A}), 2.52 (1H, tt, *J* = 11.7, 4.2 Hz, H_5), 2.38 (2H, d, *J* = 6.6 Hz, H_8), 2.17 (2H, td, *J* = 11.7, 3.0 Hz, H_{7B}), 2.02-1.82 (4H, m, H_6), 1.04-0.91 (1H, m, H_9), 0.63-0.50 (2H, m, H_{10A}), 0.23-0.10 (2H, m, H_{10B}). **^{13}C NMR** (100 MHz, $CDCl_3$): δ = 146.1 (C_4), 128.6 (C_2), 127.0 (C_3), 126.3 (C_1), 64.0 (C_8), 54.3 (C_7), 42.6 (C_5), 33.1 (C_6), 8.2 (C_9), 4.3 (C_{10}). **IR** (CH_2Cl_2, cm^{-1}): 3402, 2931, 2767, 2740, 1494, 1453, 1377, 1329, 1125, 1100, 1017. **HRMS** (FTMS +p ESI) calculated for $C_{15}H_{21}NH$ $[M+H]^+$: 216.1747, found 216.1742.

5.2.2. Radical Reductive Amination

***N*,*N*-Dibenzylbutan-1-amine (446)**

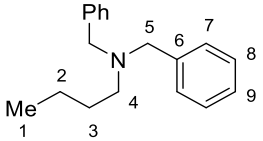

Following **GP B**, dibenzylamine (38.4 µL, 0.20 mmol), butyraldehyde (21.6 µL, 0.24 mmol), DMTP (53.3 µL, 0.40 mmol) and potassium *tert*-butoxide (11.2 mg, 0.10 mmol) were reacted over 24 hours and purified by flash column chromatography (PE to 1:19 Et_2O/PE) to give the title compound as a colorless oil (49.5 mg, 98%). **^{1}H NMR** (400 MHz, $CDCl_3$) δ = 7.42 (4H, d, *J* = 7.4 Hz, H_7), 7.36 (4H, t, *J* = 7.5 Hz, H_8), 7.27 (2H, t, *J* = 7.3 Hz, H_9), 3.60 (4H, s, H_5), 2.47 (2H, t, *J* = 7.2 Hz, H_4), 1.55 (2H, m, H_3), 1.35 (2H, m, H_2), 0.89 (3H, t, *J* = 7.3 Hz, H_1). **^{13}C NMR** (101 MHz, $CDCl_3$) δ = 140.2 (C_6), 128.9 (C_9), 128.2 (C_8), 126.8 (C_7), 58.4 (C_5), 53.3 (C_4), 29.4 (C_3), 20.6 (C_2), 14.2 (C_1). Data consistent with literature.[315]

Gram-scale reaction (454):

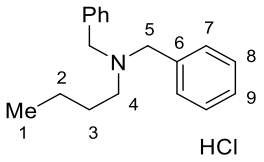

To a 25 mL clear glass microwave vial was added 4 Å molecular sieve (2.50 g). The vial was sealed with a PTFE/Silicone-lined septa cap, set under vacuum, and heated to re-activate the molecular sieve. The vial was charged with potassium *tert*-butoxide (561 mg, 5.0 mmol), sealed and a needle was inserted through the septa and the contents evacuated/backfilled with N_2. Anhydrous dimethylformamide (10 mL) was added, followed by dibenzylamine (1.9 mL, 10 mmol), thiophenol (2.0 mL, 20 mmol) and butyraldehyde (1.1 mL, 12 mmol). The vial was sealed with parafilm and placed of a stirrer/hotplate. Four 40 W Kessil A160WE Tuna Blue lamps were placed around the vial with a desk-fan positioned above for cooling. The stirrer plate was set to 1000 rpm and the vial was irradiated for 48 hours with the lamp set to max frequency and max intensity. After 24 hours additional thiophenol (2.0 mL, 20 mmol) was added to complete the reaction. Upon completion, the reaction mixture was filtered, and the solvent was removed *in vacuo*. The residue was purified by flash column chromatography (99:1 PE/EtOAc), followed by acidification of the product using HCl (2.6 M in MeOH, 30.0 mL). The solvent was removed in vacuo, CH2Cl2 (4.0 mL) was added to solvate the product, followed by hexane (20 mL). The CH_2Cl_2 portion of the solvent was removed in in vacuo and the remaining solvent was removed using a syringe. This procedure was repeated five times to give the title product as brown solid (1.99 g, 69%).

1-Benzylpiperidine (447)

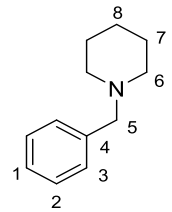

Following **GP B**, piperidine (19.8µL, 0.20 mmol), benzaldehyde (24.3 µL, 0.24 mmol), 2,6-dimethylbenzenethiol (53.3 µL, 0.40 mmol) and potassium *tert*-butoxide (11.2 mg, 0.10 mmol) were reacted over 24 hours and purified by flash column chromatography (EtOAc/PE 1:9) to give the title compound as a yellow oil (32.7 mg, 93%). **^{1}H NMR** (400 MHz, $CDCl_3$): δ = 7.39 – 7.23 (5H, m, $H_{1,2,3}$), 3.51 (2H, s, H_5), 2.41 (4H, t, *J* = 5.2 Hz, H_6), 1.60 (4H, p , *J* = 5.2 Hz, H_7), 1.46 (2H, d, *J* = 5.1 Hz, H_8). **^{13}C NMR** (100 MHz, $CDCl_3$): δ = 129.5 (C_3), 128.7 (C_4), 128.3 (C_2), 127.1 (C_1), 63.9 (C_5), 54.5 (C_6), 25.9 (C_7), 24.4 (C_8). Data consistent with literature.[316]

_N_-Benzyl-_N_-methyl-1-phenylmethanamine (448)

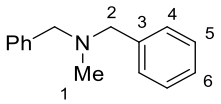

Following **GP B**, dibenzylamine (38.4 µL, 0.20 mmol), formaldehyde solution (37%, 17.9 µL, 0.24 mmol), DMTP (53.3 µL, 0.40 mmol) and potassium *tert*-butoxide (11.2 mg, 0.10 mmol) were reacted over 24 hours and purified by flash column chromatography (1:19 to 1:9 EtOAc/PE) to give the title compound as a colorless oil (39.1 mg, 93%). **^{1}H NMR** (400 MHz, $CDCl_3$): δ = 7.41 (4H, d, *J* = 7.0 Hz, H_4), 7.36 (4H, t, *J* = 7.1 Hz, H_5), 7.29 (2H, t, *J* = 7.1 Hz, H_6), 3.57 (4H, s, H_2), 2.23 (3H, s, H_1). **^{13}C NMR** (100 MHz, $CDCl_3$): δ = 139.4 (C_3), 129.1 (C_6), 128.4 (C_5), 127.1 (C_4), 6 (C_2), 42.4 (C_1). Data consistent with literature.[317]

_N_-Cyclohexyl-_N_-methylcyclohexanamine (449)

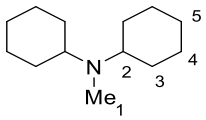

Following **GP B**, dicyclohexylamine (39.9 µL, 0.20 mmol), 37% aqueous formaldehyde solution (17.9 µL, 0.24 mmol), DMTP (53.3 µL, 0.40 mmol) and potassium *tert*-butoxide (11.2 mg, 0.10 mmol) were reacted over 24 hours and purified by flash column chromatography (EtOAc to 1:9 2.6 M NH_3 in MeOH/EtOAc) to give the title compound as a colorless solid (31.2 mg, 78%). **^{1}H NMR** (400 MHz, $CDCl_3$): δ = 2.56 (2H, m, H_2), 2.29 (3H, s, H_1), 1.80 (8H, m, $H_{3A/3B/4A/4B}$), 1.63 (2H, d, *J* = 12.6 Hz, $H_{5A/5B}$), 1.27 (8H, m, $H_{3A/3B/4A/4B}$), 1.20 (2H, m, $H_{5A/5B}$). **^{13}C NMR** (101 MHz, $CDCl_3$): δ = 59.7 (C_2), 33.0 (C_1) 30.5 (C_3), 26.4 (C_4), 26.3 (C_5). Data consistent with literature.[318]

1-Benzyl-4-(pyrrolidin-1-yl)piperidine (460)

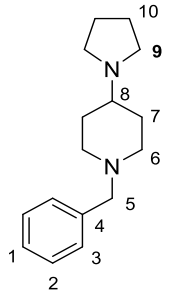

Following **GP B**, 1-benzyl-4-(pyrrolidin-1-yl)-1,2,3,6-tetrahydropyridine (48.4 mg, 0.20 mmol), DMTP (53.3 µL, 0.40 mmol) and potassium *tert*-butoxide (11.2 mg, 0.10 mmol) were reacted over 24 hours and purified by flash column chromatography (EtOAc to 1:9 2.6 M NH_3 in MeOH/EtOAc) to give the title compound as a colorless solid (31.2 mg, 78%). **^{1}H NMR** (400 MHz, $CDCl_3$): δ 7.33 (4H, m, H_{2+3}), 7.25 (1H, m, H_1), 3.52 (2H, s, H_5), 2.90 (2H, d, *J* = 12.0 Hz, $H_{6A/6B}$), 2.58 (4H, m, H_9), 2.06 (3H, m, $H_{6A/6B+8}$), 1.87 (2H, m, $H_{7A/7B}$), 1.80 (4H, m, H_{10}), 1.60 (2H, qd, *J* = 12.0, 3.8 Hz, $H_{7A/7B}$). **^{13}C NMR** (101 MHz, $CDCl_3$): δ 138.9 (C_4), 129.1 (C_3), 128.3 (C_2), 127.0 (C_1), 63.0 (C_5), 62.23 (C_8), 52.7 (C_6), 51.5 (C_9), 31.4 (C_7), 23.4 (C_{10}). Data consistent with literature.[319]

4-((2-Amino-3,5-dibromobenzyl)(methyl)amino)cyclohexan-1-ol (452)

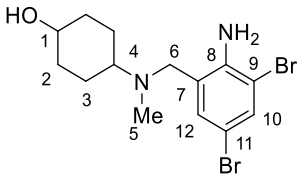

Following **GP B**, ambroxol hydrochloride (82.9 mg, 0.20 mmol), formaldehyde solution (37%, 29.8 µL, 0.40 mmol), DMTP (53.3 µL, 0.40 mmol) and potassium *tert*-butoxide (44.9 mg, 0.40 mmol) were reacted over 24 hours and purified by flash column chromatography (CH_2Cl_2 to 1:9 2.6 M NH_3 in MeOH/EtOAc) to give the title compound as a pale yellow solid (46.6 mg, 61%). **^{1}H NMR** (400 MHz, $CDCl_3$): δ 7.47 (1H, d, *J* = 2.2 Hz, H_{10}), 7.04 (1H, d, *J* = 2.2 Hz, H_{12}), 5.42 (2H, s, NH_2), 3.58 (3H, m, H_{1+6}), 2.45 (1H, m, H_4), 2.12 (3H, s, H_5), 2.05 (2H, dd, *J* = 11.8, 3.8 Hz, $H_{2A/2B}$), 1.86 (2H, m, $H_{3A/3B}$), 1.44 (2H, m, $H_{3A/3B}$), 1.30 (2H, m, $H_{2A/2B}$). **^{13}C NMR** (101 MHz, $CDCl_3$): δ 144.1 (C_8), 133.2 (C_{10}), 131.8 (C_{12}), 125.9 (C_7), 110.2 (C_9), 108.3 (C_{11}), 70.7 (C_1), 61.0 (C_4), 58.2 (C_6), 36.6 (C_5), 34.8 (C_2), 25.8 (C_3). **IR** (CH_2Cl_2, cm^{-1}): 3435, 2930, 2856, 1666, 1605, 1550, 1459, 1384, 1259, 1232, 1195, 1096, 1063, 1029. **HRMS** (FTMS +p NSI) calculated for $C_{18}H_{19}FN_3O_3H$ $[M+H]^+$ 392.9995, found 392.9995.

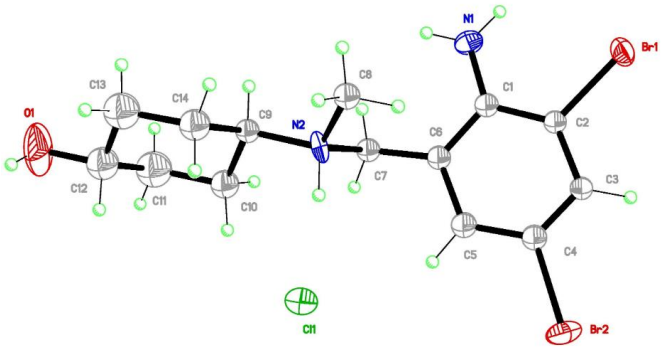

1-Cyclopropyl-6-fluoro-7-(4-methylpiperazin-1-yl)-4-oxo-1,4-dihydroquinoline-3-carboxylic acid (453)

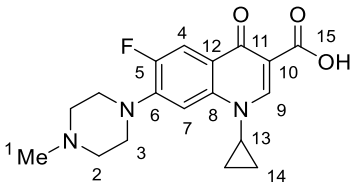

Following **GP B**, ciprofloxacin (66.2 mg, 0.20 mmol), formaldehyde solution (37%, 22.4 µL, 0.30 mmol), 2,6-DMTP (53.3 µL, 0.40 mmol) and cesium carbonate (97.7 mg, 0.30 mmol) were solved in DMF (10.0 mL) and reacted over 48 hours. The reaction mixture was acidified using 1.0 HCl-solution (0.5 mL), filtered over Celite and the solvent was removed *in vacuo*. After washing the residue with water (2 x 10 mL), CH_2Cl_2 (2 x 2 mL) and petroleum ether (2 x 10 mL) to obtain the product as white solid (55.3 mg, 80%). **^{1}H NMR** (400 MHz, CD_3OD): δ 8.84 (1H, s, H_9), 8.03 (1H, d, *J* = 12.9 Hz, H_4), 7.69 (1H, d, *J* = 7.3 Hz, H_7), 3.99 (2H, m, $H_{3A/3B}$),

3.79 (1H, m, H_{13}), 3.69 (2H, m, $H_{2A/2B}$), 3.42 (4H, m, $H_{2A/2B/3A/3B}$), 3.03 (3H, s, H_1), 1.42 (2H, d, J = 6.2 Hz, H_{14A}), 1.24 (2H, s, H_{14B}). **^{13}C NMR** (126 MHz, CD_3OD): δ 178.5 (C_{11}), 169.6 (C_{15}), 156.0 (C_5), 154.1 (C_5), 149.8 (C_9), 145.3 (C_6), 140.7 (C_{12}), 122.1 (C_8), 113.01 (C_4), 112.8 (C_{10}), 108.4 (C_7), 54.5 (C_2), 48.2 (C_3), 43.7 (C_1), 37.0 (C_{13}), 8.6 (C_{14}). **^{19}F NMR** (376 MHz, $CDCl_3$): δ -119.8 (C_5). **IR** (CH_2Cl_2, cm^{-1}): 3077, 3005, 2397, 1729, 1672, 1632, 1506, 1476, 1436, 1390, 1335, 1270, 1219, 1189, 1170, 1106, 1058, 1028. **HRMS** (FTMS +p NSI) calculated for $C_{18}H_{19}FN_3O_3H$ $[M+H]^+$ 346.1561, found 346.1562.

***tert*-Butyl (1-butylpiperidin-4-yl)carbamate (473)**

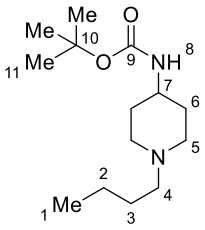

Following **GP B**, 4-aminopiperidine (21.2 µL, 0.20 mmol), butyraldehyde (18.0 µL, 0.24 mmol), 2,6-dimethylbenzenethiol (53.3 µL, 0.40 mmol) and potassium *tert*-butoxide (4.5 mg, 0.04 mmol) were reacted over 24 hours. Triethylamine (55.8 µL, 0.40 mmol) and di-*tert*-butyl dicarbonate (87.3 mg, 0.40 mmol) were added, the reaction mixture was stirred for additional 3 hours and purified by flash column chromatography (EtOAc to NH_3 (10% in MeOH)/EtOAc 1:9) to give the title compound as a colorless solid (30.6 mg, 60%). **^{1}H NMR** (400 MHz, $CDCl_3$): δ = 4.44 (1H, bs, H_8), 3.44 (1H, bs, H_7), 2.83 (2H, d, H_{5A}), 2.33-2.25 (2H, m, H_4), 2.09-1.96 (2H, m, H_{5B}), 1.91(2H, d, H_{6A}), 1.52-1.35 (13H, m, $H_{3+11+6B}$) 1.35-1.23 (2H, m, H_2), 0.90 (3H, t, H_1). **^{13}C NMR** (101 MHz, $CDCl_3$): δ = 155.3 (C_9), 79.3 (C_{10}), 58.7 (C_4), 52.6 (C_5), 48.0 (C_7), 32.8 (C_6), 29.5 (C_3), 28.6 (C_{11}), 21.0 (C_2), 14.2 (C_1). HMBC between H_4 and C_5, H_{5B} and C_4. Crystal structure below.

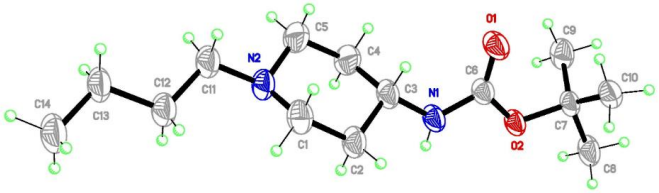

***tert*-Butyl ((1-butylpiperidin-4-yl)methyl)carbamate (524)**

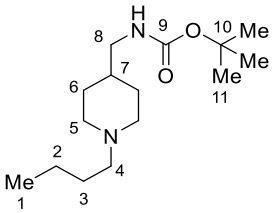

Following **GP B**, 4-(aminomethyl)piperidine (24.0 µL, 0.20 mmol), butyraldehyde (18.0 µL, 0.24 mmol), 2,6-dimethylbenzenethiol (53.3 µL, 0.40 mmol) and potassium *tert*-butoxide (4.5 mg, 0.10 mmol) were reacted over 48 hours. After 24 hours additional 2,6-dimethylbenzenethiol (53.3 µL, 0.40 mmol) was added to complete the reaction. Triethylamine (111.6 µL, 0.80 mmol) and. di-*tert*-butyl dicarbonate (174.6 mg,

0.80 mmol) were added, the reaction mixture was stirred for additional 3 hours and purified by flash column chromatography (EtOAc to 2.6 M NH_3 in MeOH/EtOAc 1:9)/EtOAc 1:9) to give the title compound as a colorless solid (24.8 mg, 46%). **^{1}H NMR** (400 MHz, Chloroform-*d*) δ = 4.59 (1H, s, N*H*), 3.01 (2H, m, H_8), 2.92 (2H, dt, J = 12.0, 3.1 Hz, H_{5a} or H_{5b}), 2.30 (2H, m, H_4), 1.88 (2H, td, J = 11.9, 3.0 Hz, H_{5a} or H_{5b}), 1.66 (2H, m, H_{6a} or H_{6b}), 1.51 – 1.39 (12H, m, H_3, H_7, H_{11}), 1.35 – 1.23 (4H, m, H_2, H_{4a} or H_{4b}), 0.90 (3H, t, J = 7.3 Hz, H_1). **^{13}C NMR** (101 MHz, $CDCl_3$): δ = 156.2 (C_9), 79.2 ($_{C10}$) 59.0 (C_3), 53.7 (C_5), 46.2 (C_8), 36.6 (C_7), 30.0 (C_6), 29.4 (C_3), 28.6 (C_{11}), 21.06 (C_2), 14.2 (C_1). **IR** (CH_2Cl_2, cm^{-1}): 2931, 2764, 1687, 1523, 1452, 1395, 1325, 1305, 1276, 1237, 1173, 1101, 1045. **HRMS** (FTMS +p NSI) calculated for $C_{18}H_{19}FN_3O_3H$ $[M+H]^+$ 271.2380, found 271.2379.

***N*-((1-Butylpiperidin-4-yl)methyl)benzamide (476)**

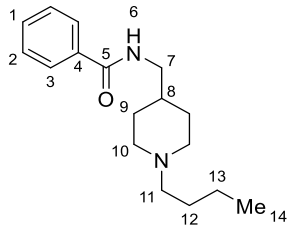

^{1}H NMR (400 MHz, $CDCl_3$) δ = 7.37 (5H, bs, $H_{1\text{-}5}$), 4.71 (1H, bs, H_{10A}), 3.74 (1H, bs, $H_{10'A}$), 2.96 (1H, bs, $H_{10'B}$), 2.75 (1H, bs, H_{10B}), 2.58 (2H, t, *J* = 7.1 Hz, H_{11}), 2.55-2.46 (2H, m, H_7), 1.94-1.61 (3H, m, $H_{9A+9'A+8}$), 1.50-1.40 (2H, m, H_{12}), 1.39-1.04 (4H, m, $H_{13+9B+9'B}$), 0.90 (3H, t, *J* = 7.23 Hz, H). **^{13}C NMR** (100 MHz, $CDCl_3$) δ = 170.4 (C_5), 136.5 (C_4), 129.5 (C_1), 128.5 ($C_{2/3}$), 126.9 ($C_{2/3}$), 55.8 (C_7), 50.1 (C_{11}), 48.0 ($C_{10'}$), 42.4 (C_{10}), 31.2 ($C_{9'}$), 30.4 (C_9), 36.9 (C_8), 32.4 (C_{12}), 20.6 (C_{13}), 14.1 (C_{14}).). **IR** (CH_2Cl_2, cm^{-1}): 2925, 2858, 1627, 1577, 1433, 1273, 1126. **HRMS** (FTMS +p NSI) calculated for $C_{18}H_{19}FN_3O_3H$ $[M+H]^+$ 271.2380, found 271.2379.

***N*2-Butyl-*N*6-propyl-4,5,6,7-tetrahydrobenzo[*d*]thiazole-2,6-diamine (505)**

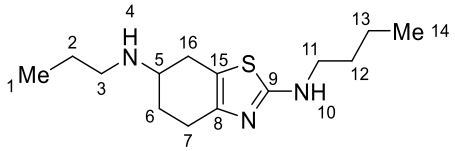

Following **GP B**, Pramipexole (43.2 mg, 0.20 mmol), butyraldehyde (18.0 µL, 0.24 mmol), DMTP (53.3 µL, 0.40 mmol) and cesium carbonate (13.2 mg, 0.04 mmol) were reacted over 24 hours and purified by flash column chromatography (EtOAc to 1:19 2.6 M NH_3 in MeOH/EtOAc) to give the title compound as a yellow solid (44.3 mg, 83%). **^{1}H NMR** (400 MHz, $CDCl_3$): δ 5.18 (1H, s, H_{10}), 3.18 (2H, t, *J* = 7.1 Hz, H_{11}), 2.96 (1H, m, H_4), 2.90-2.80 (1H, m, H_{16A}), 2.69-2.54 (4H, m, H_{3+7}), 2.44-2.34 (1H, m, H_{16B}), 2.02-1.95 (1H, m, H_{6A}), 1.74-1.64 (1H, m, H_{6B}), 1.63-1.55 (2H, m, H_{12}), 1.54-1.46 (2H, m, H_2), 1.43-1.34 (2H, m, H_{13}), 0.95-0.88 (6H, m, H_{1+14}). **^{13}C NMR** (101 MHz, $CDCl_3$): δ = 168.2 (C_9), 145.3 (C_8), 113.9 (C_{15}), 54.2 (C_5), 49.4 (C_3), 45.8 (C_4), 31.6 (C_5), 30.3 (C_8), 29.7 (C_{10}), 25.3 (C_{11}), 23.6 (C_2), 20.2 (C_6), 13.9 (C_7), 12.0 (C_1). **IR** (CH_2Cl_2, cm^{-1}):

3208, 3095, 2955, 2955, 2925, 2870, 1539, 1455, 1365, 1292, 1265, 1199, 1125, 1091. **HRMS** (FTMS +p NSI) calculated for $C_{11}H_{19}N_3SH$ $[M+H]^+$ 268.1842, found 268.1840. Crystal structure below.

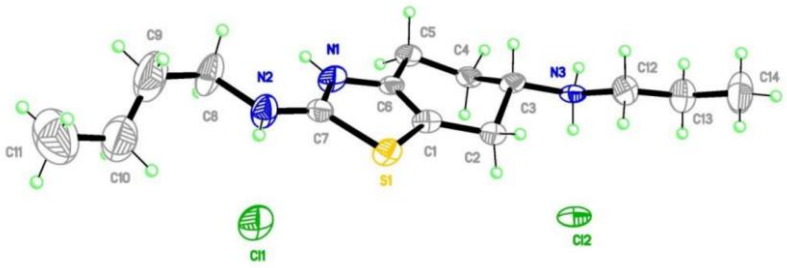

(*S*)-N^2,N^6-Dipropyl-4,5,6,7-tetrahydrobenzo[*d*]thiazole-2,6-diamine (507)

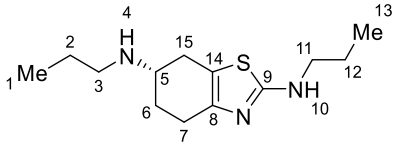

Following **GP B**, Pramipexole (42.3 mg, 0.2 mmol), propionaldehyde (17.3 µL, 0.24 mmol), cesium carbonate (13.0 mg, 0.04 mmol) and DMTP (53.3 µL, 0.4 mmol) were reacted over 24 hours and purified by flash column chromatography (EA to 1:19 2.3 M NH_3 in MeOH/EA) to give the title compound as a light yellow oil (49.5 mg, 95%). **^{1}H NMR** (400 MHz, $CDCl_3$): δ 3.20-3.10 (1H, m, H_5), 3.01-.291 (1H, m), 2.84 (1H, dd, *J* = 15.3, 4.9 Hz), 2.70-2.48 (4H, m), 2.43-2.32 (1H, m), 2.04-1.93 (1H, m), 1.74-1.41 (6H, m), 0.99-0.85 (6H, m). **^{13}C NMR** (100 MHz, $CDCl_3$): δ 168.5 (C_9), 145.5 (C_8), 114.0 (C_{14}), 54.4 (C_5), 49.6 (C_3), 48.0 (C_{11}), 30.5 (C_{15}), 29.9 (C_6), 25.5 (C_7), 23.9 (C_2), 23.1 (C_{12}), 12.2 (C_1), 11.8 (C_{13}). **IR** (CH_2Cl_2, cm^{-1}): 3208, 3095, 2955, 2955, 2925, 2870, 1539, 1455, 1365, 1292, 1265, 1199, 1125, 1091.

(*S*)-N^6,N^6-dipropyl-4,5,6,7-tetrahydrobenzo[*d*]thiazole-2,6-diamine (508)

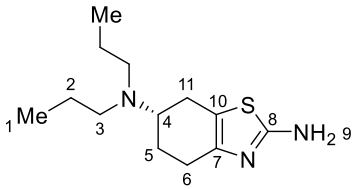

To a round bottomed flask was added pramipexole (42.3 mg, 0.2 mmol), a magnetic stirrer bar, CH_2Cl_2 (2 mL), propionaldehyde (15 µL, 0.21 mmol) and acetic acid (11.4 µL, 0.2 mmol). Sodium triacetoxyborohydride (55.1 mg, 0.26 mmol) was added portionwise, then the mixture was stirred for 20 hours. The reaction was quenched with 1% aqueous NaOH solution, the organic layer separated, and the aqueous layer extracted twice with CH_2Cl_2. The combined organic layers were washed with brine, concentrated *in vacuo*, then the crude residue was purified by flash column chromatography (EtOAc to 1:9 2.6 M NH_3 in MeOH/EtOAc), to give the title compound as a colorless oil (33.9 mg, 67%). **^{1}H NMR** (400 MHz, $CDCl_3$): δ 4.93 (2H, br. s, H_9), 3.05-2.95 (1H, m, H_4), 2.73-2.59 (2H, m, H_{6A+11A}), 2.59-2.49 (2H, m, H_{6B+11B}), 2.48-2.35 (4H, m, H_3), 2.01-1.92 (1H, m,

H_{5A}), 1.75-1.61 (1H, m, H_{5B}), 1.43 (4H, h, *J* = 7.4 Hz, H_2), 0.86 (6H, t, *J* = 7.3 Hz, H_1). **^{13}C NMR** (101 MHz, $CDCl_3$): δ 165.6 (C_8), 145.2 (C_7), 117.6 (C_{10}), 57.6 (C_4), 52.9 (C_3), 26.7 ($C_{6/11}$), 25.9 (C_5), 25.1 ($C_{6/11}$), 22.4 (C_2), 11.9 (C_1). **IR** (CH_2Cl_2, cm^{-1}): 3208, 3095, 2955, 2955, 2925, 2870, 1539, 1455, 1365, 1292, 1265, 1199, 1125, 1091.

6. References

(1) Douglas, J. J.; Sevrin, M. J.; Stephenson, C. R. J. Visible Light Photocatalysis: Applications and New Disconnections in the Synthesis of Pharmaceutical Agents. *Org. Process Res. Dev.* **2016**, *20* (7), 1134–1147. https://doi.org/10.1021/acs.oprd.6b00125.

(2) Kärkäs, M. D.; Porco, J. A.; Stephenson, C. R. J. Photochemical Approaches to Complex Chemotypes: Applications in Natural Product Synthesis. *Chem. Rev.* **2016**, *116* (17), 9683–9747. https://doi.org/10.1021/acs.chemrev.5b00760.

(3) Politano, F.; Oksdath-Mansilla, G. Light on the Horizon: Current Research and Future Perspectives in Flow Photochemistry. *Org. Process Res. Dev.* **2018**, *22* (9), 1045–1062. https://doi.org/10.1021/acs.oprd.8b00213.

(4) Crisenza, G. E. M.; Melchiorre, P. Chemistry Glows Green with Photoredox Catalysis. *Nat. Commun.* **2020**, *11* (1), 1–4. https://doi.org/10.1038/s41467-019-13887-8.

(5) Vollmer, J. J.; Servis, K. L. Woodward-Hoffmann Rules: Cycloaddition Reactions. *J. Chem. Educ.* **1970**, *47* (7), 491. https://doi.org/10.1021/ed047p491.

(6) Schultz, D.; Campeau, L.-C. Harder, Better, Faster. *Nat. Chem.* **2020**, *12* (8), 661–664. https://doi.org/10.1038/s41557-020-0510-8.

(7) DiRocco, D. A.; Dykstra, K.; Krska, S.; Vachal, P.; Conway, D. V.; Tudge, M. Late-Stage Functionalization of Biologically Active Heterocycles Through Photoredox Catalysis. *Angew. Chem. Int. Ed.* **2014**, *53* (19), 4802–4806. https://doi.org/10.1002/anie.201402023.

(8) Noël, T. A Personal Perspective on the Future of Flow Photochemistry. *J. Flow Chem.* **2017**, *7* (3), 87–93. https://doi.org/10.1556/1846.2017.00022.

(9) Kln, P.; Wirz, J. *Photochemistry of Organic Compounds*; John Wiley & Sons, Ltd: Chichester, UK, 2009. https://doi.org/10.1002/9781444300017.

(10) Khazova, M.; O'Hagan, J. B. Optical Radiation Emissions from Compact Fluorescent Lamps. *Radiat. Prot. Dosimetry* **2008**, *131* (4), 521–525. https://doi.org/10.1093/rpd/ncn234.

(11) Kessil LED Lights https://www.kessil.com/photoreaction/PR160L.php (accessed Apr 27, 2020).

(12) Le, C. "Chip"; Wismer, M. K.; Shi, Z.-C.; Zhang, R.; Conway, D. V.; Li, G.; Vachal, P.; Davies, I. W.; MacMillan, D. W. C. A General Small-Scale Reactor To Enable Standardization and Acceleration of Photocatalytic Reactions. *ACS Cent. Sci.* **2017**, *3* (6), 647–653. https://doi.org/10.1021/acscentsci.7b00159.

(13) Kessil LED Lights https://www.kessil.com/photoreaction/index.php (accessed Apr 5, 2020).

(14) Pitzer, K. S.; Hildebrand, J. H. Color and Bond Character. *J. Am. Chem. Soc.* **1941**, *63* (9), 2472–2475. https://doi.org/10.1021/ja01854a044.

(15) Benesi, H. A.; Hildebrand, J. H. A Spectrophotometric Investigation of the Interaction of Iodine with Aromatic Hydrocarbons. *J. Am. Chem. Soc.* **1949**, *71* (8), 2703–2707. https://doi.org/10.1021/ja01176a030.

(16) Mulliken, R. S. Structures of Complexes Formed by Halogen Molecules with Aromatic and with Oxygenated Solvents1. *J. Am. Chem. Soc.* **1950**, *72* (1), 600–608. https://doi.org/10.1021/ja01157a151.

(17) Mulliken, R. S. Molecular Compounds and Their Spectra. II. *J. Am. Chem. Soc.* **1952**, *74* (3), 811–824. https://doi.org/10.1021/ja01123a067.

(18) Haga, N.; Nakajima, H.; Takayanagi, H.; Tokumaru, K. Photoinduced Electron Transfer between Acenaphthylene and Tetracyanoethylene: Effect of Irradiation Mode on Reactivity of the Charge-Transfer Complex and the Resulted Radical Ion Pair in Solution and Crystalline State. *J. Org. Chem.* **1998**, *63* (16), 5372–5384. https://doi.org/10.1021/jo9801824.

(19) Hilinski, E. F.; Masnovi, J. M.; Amatore, C.; Kochi, J. K.; Rentzepis, P. M. Charge-Transfer Excitation of Electron Donor-Acceptor Complexes. Direct Observation of Ion Pairs by Time-Resolved (Picosecond) Spectroscopy. *J. Am. Chem. Soc.* **1983**, *105* (19), 6167–6168. https://doi.org/10.1021/ja00357a042.

(20) Rosokha, S. V.; Kochi, J. K. Fresh Look at Electron-Transfer Mechanisms via the Donor/Acceptor Bindings in the Critical Encounter Complex. *Acc. Chem. Res.* **2008**, *41* (5), 641–653. https://doi.org/10.1021/ar700256a.

(21) Zou, C.; Miers, J. B.; Ballew, R. M.; Dlott, D. D.; Schuster, G. B. Electron Transfer and Back Electron Transfer in Photoexcited Ion Pairs: Forward and Back Directions Have Different Maximum Rates. *J. Am. Chem. Soc.* **1991**, *113* (20), 7823–7825. https://doi.org/10.1021/ja00020a088.
(22) Narra, S.; Nishimura, Y.; Witek, H. A.; Shigeto, S. Mechanism of Back Electron Transfer in an Intermolecular Photoinduced Electron Transfer Reaction: Solvent as a Charge Mediator. *ChemPhysChem* **2014**, *15* (14), 2945–2950. https://doi.org/10.1002/cphc.201402411.
(23) Cantacuzène, D.; Dorme, R. Cetones α perfluorees. *Tetrahedron Lett.* **1975**, *16* (25), 2031–2034. https://doi.org/10.1016/S0040-4039(00)75286-5.
(24) Cantacuzène, D.; Wakselman, C.; Dorme, R. Condensation of Perfluoroalkyl Iodides with Unsaturated Nitrogen Compounds. *J. Chem. Soc. Perkin 1* **1977**, No. 12, 1365–1371. https://doi.org/10.1039/P19770001365.
(25) Haszeldine, R. N. 534. Studies in Spectroscopy. Part V. Molecular Compound Formation with Polyhalogeno-Iodo-Compounds. *J. Chem. Soc. Resumed* **1953**, No. 0, 2622–2626. https://doi.org/10.1039/JR9530002622.
(26) Russell, G. A.; Wang, K. Electron Transfer Processes. 53. Homolytic Alkylation of Enamines by Electrophilic Radicals. *J. Org. Chem.* **1991**, *56* (11), 3475–3479. https://doi.org/10.1021/jo00011a007.
(27) Wade, P. A.; Morrison, H. A.; Kornblum, N. Substitution Reactions Which Proceed via Radical Anion Intermediates. Part 30. Effect of Light on Electron Transfer Substitution at a Saturated Carbon Atom. *J. Org. Chem.* **1987**, *52* (14), 3102–3107. https://doi.org/10.1021/jo00390a026.
(28) Rossi, R. A.; Pierini, A. B.; Peñéñory, A. B. Nucleophilic Substitution Reactions by Electron Transfer. *Chem. Rev.* **2003**, *103* (1), 71–168. https://doi.org/10.1021/cr960134o.
(29) Hoz, S.; Bunnett, J. F. A Quantitative Study of the Photostimulated Reaction of Iodobenzene with Diethyl Phosphite Ion. *J. Am. Chem. Soc.* **1977**, *99* (14), 4690–4699. https://doi.org/10.1021/ja00456a027.
(30) Bunnett, J. F. Aromatic Substitution by the SRN1 Mechanism. *Acc. Chem. Res.* **1978**, *11* (11), 413–420. https://doi.org/10.1021/ar50131a003.
(31) Fox, M. A.; Younathan, J.; Fryxell, G. E. Photoinitiation of the SRN1 Reaction by Excitation of Charge-Transfer Complexes. *J. Org. Chem.* **1983**, *48* (18), 3109–3112. https://doi.org/10.1021/jo00166a038.
(32) Gardner, H. C.; Kochi, J. K. Charge Transfer Spectra and the Alkylation of Tetracyanoethylene with the Organometallic Derivatives of Lead, Tin, and Mercury. *J. Am. Chem. Soc.* **1976**, *98* (9), 2460–2469. https://doi.org/10.1021/ja00425a013.
(33) Fukuzumi, S.; Mochida, K.; Kochi, J. K. A Unified Mechanism for Thermal and Photochemical Activation of Charge-Transfer Processes with Organometals. Steric Effects in the Insertion of Tetracyanoethylene. *J. Am. Chem. Soc.* **1979**, *101* (20), 5961–5972. https://doi.org/10.1021/ja00514a016.
(34) Dohi, T.; Ito, M.; Yamaoka, N.; Morimoto, K.; Fujioka, H.; Kita, Y. Unusual Ipso Substitution of Diaryliodonium Bromides Initiated by a Single-Electron-Transfer Oxidizing Process. *Angew. Chem. Int. Ed.* **2010**, *49* (19), 3334–3337. https://doi.org/10.1002/anie.200907281.
(35) Cheng, Y.; Yuan, X.; Ma, J.; Yu, S. Direct Aromatic C□H Trifluoromethylation via an Electron-Donor–Acceptor Complex. *Chem. – Eur. J.* **2015**, *21* (23), 8355–8359. https://doi.org/10.1002/chem.201500896.
(36) Siu, J. C.; Sauer, G. S.; Saha, A.; Macey, R. L.; Fu, N.; Chauviré, T.; Lancaster, K. M.; Lin, S. Electrochemical Azidooxygenation of Alkenes Mediated by a TEMPO–N3 Charge-Transfer Complex. *J. Am. Chem. Soc.* **2018**, *140* (39), 12511–12520. https://doi.org/10.1021/jacs.8b06744.
(37) Rosokha, S. V.; Newton, M. D.; Jalilov, A. S.; Kochi, J. K. The Spectral Elucidation versus the X-Ray Structure of the Critical Precursor Complex in Bimolecular Electron Transfers: Application of Experimental/Theoretical Solvent Probes to Ion-Radical (Redox) Dyads. *J. Am. Chem. Soc.* **2008**, *130* (6), 1944–1952. https://doi.org/10.1021/ja076591b.
(38) Berionni, G.; Bertelle, P.-A.; Marrot, J.; Goumont, R. X-Ray Structure of a CT Complex Relevant to Diels−Alder Reactivity of Anthracenes. *J. Am. Chem. Soc.* **2009**, *131* (51), 18224–18225. https://doi.org/10.1021/ja908747j.
(39) Kochi, J. K. Electron Transfer and Charge Transfer: Twin Themes in Unifying the Mechanisms of Organic and Organometallic Reactions. *Angew. Chem. Int. Ed. Engl.* **1988**, *27* (10), 1227–1266. https://doi.org/10.1002/anie.198812273.
(40) Kisch, H. Charge-Transfer in Ion Pairs: Design of Photoreactivity in Solution and Electrical Dark- and Photoconductivity in the Solid. *Coord. Chem. Rev.* **1993**, *125* (1), 155–171. https://doi.org/10.1016/0010-8545(93)85015-V.

(41) Billing, R. Optical and Photoinduced Electron Transfer in Ion Pairs of Coordination Compounds. *Coord. Chem. Rev.* **1997**, *159*, 257–270. https://doi.org/10.1016/S0010-8545(96)01288-X.
(42) Rathore, R.; Kochi, J. K. Donor/Acceptor Organizations and the Electron-Transfer Paradigm for Organic Reactivity. In *Advances in Physical Organic Chemistry*; Academic Press, 2000; Vol. 35, pp 193–318. https://doi.org/10.1016/S0065-3160(00)35014-6.
(43) Kosower, E. M. Additions to Pyridinium Rings. I. 1-Methylpyridinium Iodide. *J. Am. Chem. Soc.* **1955**, *77* (14), 3883–3885. https://doi.org/10.1021/ja01619a060.
(44) Kosower, E. M.; Klinedinst, P. E. Additions to Pyridinium Rings. II. Charge-Transfer Complexes as Intermediates. *J. Am. Chem. Soc.* **1956**, *78* (14), 3493–3497. https://doi.org/10.1021/ja01595a061.
(45) Kosower, E. M. THE EFFECT OF SOLVENT ON CHARGE-TRANSFER COMPLEX SPECTRA. *J. Am. Chem. Soc.* **1956**, *78* (21), 5700–5701. https://doi.org/10.1021/ja01602a070.
(46) Kosower, E. M. The Effect of Solvent on Spectra. I. A New Empirical Measure of Solvent Polarity: Z-Values. *J. Am. Chem. Soc.* **1958**, *80* (13), 3253–3260. https://doi.org/10.1021/ja01546a020.
(47) Bockman, T. M.; Kochi, J. K. Photoinduced Electron Transfer in Contact Ion Pairs. *J. Am. Chem. Soc.* **1988**, *110* (4), 1294–1295. https://doi.org/10.1021/ja00212a049.
(48) Kochi, J. K.; Michael Bockman, T. Organometallic Ions and Ion Pairs. In *Advances in Organometallic Chemistry*; Stone, F. G. A., West, R., Eds.; Academic Press, 1991; Vol. 33, pp 51–124. https://doi.org/10.1016/S0065-3055(08)60694-2.
(49) Bockman, T. M.; Kochi, J. K. Charge-Transfer Ion Pairs. Structure and Photoinduced Electron Transfer of Carbonylmetalate Salts. *J. Am. Chem. Soc.* **1989**, *111* (13), 4669–4683. https://doi.org/10.1021/ja00195a022.
(50) Fehlner, T. P.; Ulman, J.; Nugent, W. A.; Kochi, J. K. Effect of Alkyl Substituents on the First Ionization Potential and on 5d10 Ionization in Dialkylmercury Compounds. *Inorg. Chem.* **1976**, *15* (10), 2544–2547. https://doi.org/10.1021/ic50164a045.
(51) Zhu, D.; Kochi, J. K. Alkylation of Pyridinium Acceptors via Thermal and Photoinduced Electron Transfer in Charge-Transfer Salts with Organoborates. *Organometallics* **1999**, *18* (2), 161–172. https://doi.org/10.1021/om9808054.
(52) Bockman, T. M.; Hubig, S. M.; Kochi, J. K. Direct Observation of Carbon−Carbon Bond Cleavage in Ultrafast Decarboxylations. *J. Am. Chem. Soc.* **1996**, *118* (18), 4502–4503. https://doi.org/10.1021/ja960112j.
(53) Bockman, T. M.; Hubig, S. M.; Kochi, J. K. Direct Observation of Ultrafast Decarboxylation of Acyloxy Radicals via Photoinduced Electron Transfer in Carboxylate Ion Pairs. *J. Org. Chem.* **1997**, *62* (7), 2210–2221. https://doi.org/10.1021/jo9617833.
(54) Saielli, G. Ion-Pairing of Octyl Viologen Diiodide in Low-Polar Solvents: An Experimental and Computational Study. *J. Phys. Chem. A* **2008**, *112* (35), 7987–7995. https://doi.org/10.1021/jp802747h.
(55) Orimoto, Y.; Ishimoto, K.; Aoki, Y. Role of Pyridinium Groups and Iodide Ions in Photoelectrochromism in Viologen-Based Ion-Pair Charge-Transfer Complexes: Molecular Orbital Analysis. *J. Phys. Chem. C* **2018**, *122* (8), 4546–4556. https://doi.org/10.1021/acs.jpcc.7b10281.
(56) Huang, Y.-D.; Huo, P.; Shao, M.-Y.; Yin, J.-X.; Shen, W.-C.; Zhu, Q.-Y.; Dai, J. A New Type of Charge-Transfer Salts Based on Tetrathiafulvalene–Tetracarboxylate Coordination Polymers and Methyl Viologen. *Inorg. Chem.* **2014**, *53* (7), 3480–3487. https://doi.org/10.1021/ic402926n.
(57) Tuerk, T.; Resch, U.; Fox, M. A.; Vogler, A. Cadmium Benzenethiolate Clusters of Various Size: Molecular Models for Metal Chalcogenide Semiconductors. *J. Phys. Chem.* **1992**, *96* (9), 3818–3822. https://doi.org/10.1021/j100188a046.
(58) Tuerk, T.; Resch, U.; Fox, M. A.; Vogler, A. Spectroscopic Studies of Zinc Benzenethiolate Complexes: Electron Transfer to Methyl Viologen. *Inorg. Chem.* **1992**, *31* (10), 1854–1857. https://doi.org/10.1021/ic00036a024.
(59) Lu, Z.; Yoon, T. P. Visible Light Photocatalysis of [2+2] Styrene Cycloadditions by Energy Transfer. *Angew. Chem. Int. Ed.* **2012**, *51* (41), 10329–10332. https://doi.org/10.1002/anie.201204835.
(60) Farney, E. P.; Yoon, T. P. Visible-Light Sensitization of Vinyl Azides by Transition-Metal Photocatalysis. *Angew. Chem. Int. Ed.* **2014**, *53* (3), 793–797. https://doi.org/10.1002/anie.201308820.
(61) Alonso, R.; Bach, T. A Chiral Thioxanthone as an Organocatalyst for Enantioselective [2+2] Photocycloaddition Reactions Induced by Visible Light. *Angew. Chem. Int. Ed.* **2014**, *53* (17), 4368–4371. https://doi.org/10.1002/anie.201310997.

(62) Hedstrand, D. M.; Kruizinga, W. H.; Kellogg, R. M. Light Induced and Dye Accelerated Reductions of Phenacyl Onium Salts by 1,4-Dihydropyridines. *Tetrahedron Lett.* **1978**, *19* (14), 1255–1258. https://doi.org/10.1016/S0040-4039(01)94515-0.
(63) Cano-Yelo, H.; Deronzier, A. Photo-Oxidation of Some Carbinols by the Ru(II) Polypyridyl Complex-Aryl Diazonium Salt System. *Tetrahedron Lett.* **1984**, *25* (48), 5517–5520. https://doi.org/10.1016/S0040-4039(01)81614-2.
(64) Okada, K.; Okamoto, K.; Morita, N.; Okubo, K.; Oda, M. Photosensitized Decarboxylative Michael Addition through N-(Acyloxy)Phthalimides via an Electron-Transfer Mechanism. *J. Am. Chem. Soc.* **1991**, *113* (24), 9401–9402. https://doi.org/10.1021/ja00024a074.
(65) Prier, C. K.; Rankic, D. A.; MacMillan, D. W. C. Visible Light Photoredox Catalysis with Transition Metal Complexes: Applications in Organic Synthesis. *Chem. Rev.* **2013**, *113* (7), 5322–5363. https://doi.org/10.1021/cr300503r.
(66) Arias-Rotondo, D. M.; McCusker, J. K. The Photophysics of Photoredox Catalysis: A Roadmap for Catalyst Design. *Chem. Soc. Rev.* **2016**, *45* (21), 5803–5820. https://doi.org/10.1039/C6CS00526H.
(67) Ochola, J. R.; Wolf, M. O. The Effect of Photocatalyst Excited State Lifetime on the Rate of Photoredox Catalysis. *Org. Biomol. Chem.* **2016**, *14* (38), 9088–9092. https://doi.org/10.1039/C6OB01717G.
(68) Shaw, M. H.; Twilton, J.; MacMillan, D. W. C. Photoredox Catalysis in Organic Chemistry. *J. Org. Chem.* **2016**, *81* (16), 6898–6926. https://doi.org/10.1021/acs.joc.6b01449.
(69) Romero, N. A.; Nicewicz, D. A. Organic Photoredox Catalysis. *Chem. Rev.* **2016**, *116* (17), 10075–10166. https://doi.org/10.1021/acs.chemrev.6b00057.
(70) McAtee, R. C.; McClain, E. J.; Stephenson, C. R. J. Illuminating Photoredox Catalysis. *Trends Chem.* **2019**, *1* (1), 111–125. https://doi.org/10.1016/j.trechm.2019.01.008.
(71) Lima, C. G. S.; de M. Lima, T.; Duarte, M.; Jurberg, I. D.; Paixão, M. W. Organic Synthesis Enabled by Light-Irradiation of EDA Complexes: Theoretical Background and Synthetic Applications. *ACS Catal.* **2016**, *6* (3), 1389–1407. https://doi.org/10.1021/acscatal.5b02386.
(72) Yuan, Y.; Majumder, S.; Yang, M.; Guo, S. Recent Advances in Catalyst-Free Photochemical Reactions via Electron-Donor-Acceptor (EDA) Complex Process. *Tetrahedron Lett.* **2020**, *61* (8), 151506. https://doi.org/10.1016/j.tetlet.2019.151506.
(73) Crisenza, G. E. M.; Mazzarella, D.; Melchiorre, P. Synthetic Methods Driven by the Photoactivity of Electron Donor–Acceptor Complexes. *J. Am. Chem. Soc.* **2020**, *142* (12), 5461–5476. https://doi.org/10.1021/jacs.0c01416.
(74) Pham, P. V.; Nagib, D. A.; MacMillan, D. W. C. Photoredox Catalysis: A Mild, Operationally Simple Approach to the Synthesis of α-Trifluoromethyl Carbonyl Compounds. *Angew. Chem. Int. Ed.* **2011**, *50* (27), 6119–6122. https://doi.org/10.1002/anie.201101861.
(75) Cho, D. W.; Lee, H.-Y.; Oh, S. W.; Choi, J. H.; Park, H. J.; Mariano, P. S.; Yoon, U. C. Photoaddition Reactions of 1,2-Diketones with Silyl Ketene Acetals. Formation of β-Hydroxy-γ-Ketoesters. *J. Org. Chem.* **2008**, *73* (12), 4539–4547. https://doi.org/10.1021/jo800473x.
(76) Fukuzumi, S.; Fujita, M.; Otera, J. Addition of Ketene Silyl Acetals to 10-Methylacridone via Photoinduced Electron Transfer. *J. Org. Chem.* **1993**, *58* (20), 5405–5410. https://doi.org/10.1021/jo00072a023.
(77) Tobisu, M.; Furukawa, T.; Chatani, N. Visible Light-Mediated Direct Arylation of Arenes and Heteroarenes Using Diaryliodonium Salts in the Presence and Absence of a Photocatalyst. *Chem. Lett.* **2013**, *42* (10), 1203–1205. https://doi.org/10.1246/cl.130547.
(78) Hennig, H.; Brede, O.; Billing, R.; Schönewerk, J. Photoinduced Chain Reactions of Alcohols in the Presence of Diphenyliodonium Ion Pairs with Cyanometallates—Steady State UV/Visible Spectroscopic and Pulse Radiolysis Studies. *Chem. – Eur. J.* **2001**, *7* (10), 2114–2121. https://doi.org/10.1002/1521-3765(20010518)7:10<2114::AID-CHEM2114>3.0.CO;2-D.
(79) Silvi, M.; Melchiorre, P. Enhancing the Potential of Enantioselective Organocatalysis with Light. *Nature* **2018**, *554* (7690), 41–49. https://doi.org/10.1038/nature25175.
(80) Arceo, E.; Jurberg, I. D.; Álvarez-Fernández, A.; Melchiorre, P. Photochemical Activity of a Key Donor–Acceptor Complex Can Drive Stereoselective Catalytic α-Alkylation of Aldehydes. *Nat. Chem.* **2013**, *5* (9), 750–756. https://doi.org/10.1038/nchem.1727.
(81) Arceo, E.; Bahamonde, A.; Bergonzini, G.; Melchiorre, P. Enantioselective Direct α-Alkylation of Cyclic Ketones by Means of Photo-Organocatalysis. *Chem. Sci.* **2014**, *5* (6), 2438. https://doi.org/10.1039/c4sc00315b.

(82) Kornblum, N. Substitution Reactions Which Proceed via Radical Anion Intermediates. *Angew. Chem. Int. Ed. Engl.* **1975**, *14* (11), 734–745. https://doi.org/10.1002/anie.197507341.
(83) Rossi, R. A.; Pierini, A. B.; Peñéñory, A. B. Nucleophilic Substitution Reactions by Electron Transfer. *Chem. Rev.* **2003**, *103* (1), 71–168. https://doi.org/10.1021/cr960134o.
(84) Kandukuri, S. R.; Bahamonde, A.; Chatterjee, I.; Jurberg, I. D.; Escudero-Adán, E. C.; Melchiorre, P. X-Ray Characterization of an Electron Donor–Acceptor Complex That Drives the Photochemical Alkylation of Indoles. *Angew. Chem. Int. Ed.* **2015**, *54* (5), 1485–1489. https://doi.org/10.1002/anie.201409529.
(85) Cismesia, M. A.; Yoon, T. P. Characterizing Chain Processes in Visible Light Photoredox Catalysis. *Chem. Sci.* **2015**, *6* (10), 5426–5434. https://doi.org/10.1039/C5SC02185E.
(86) Nappi, M.; Bergonzini, G.; Melchiorre, P. Metal-Free Photochemical Aromatic Perfluoroalkylation of α-Cyano Arylacetates. *Angew. Chem. Int. Ed.* **2014**, *53* (19), 4921–4925. https://doi.org/10.1002/anie.201402008.
(87) Fernández-Alvarez, V. M.; Nappi, M.; Melchiorre, P.; Maseras, F. Computational Study with DFT and Kinetic Models on the Mechanism of Photoinitiated Aromatic Perfluoroalkylations. *Org. Lett.* **2015**, *17* (11), 2676–2679. https://doi.org/10.1021/acs.orglett.5b01069.
(88) Guo, Q.; Wang, M.; Liu, H.; Wang, R.; Xu, Z. Visible-Light-Promoted Dearomative Fluoroalkylation of β-Naphthols through Intermolecular Charge Transfer. *Angew. Chem. Int. Ed.* **2018**, *57* (17), 4747–4751. https://doi.org/10.1002/anie.201800767.
(89) Xie, J.; Li, J.; Wurm, T.; Weingand, V.; Sung, H.-L.; Rominger, F.; Rudolph, M.; Hashmi, A. S. K. A General Photoinduced Electron Transfer-Directed Chemoselective Perfluoroalkylation of N,N-Dialkylhydrazones. *Org. Chem. Front.* **2016**, *3* (7), 841–845. https://doi.org/10.1039/C6QO00158K.
(90) Liang, K.; Li, N.; Zhang, Y.; Li, T.; Xia, C. Transition-Metal-Free α-Arylation of Oxindoles via Visible-Light-Promoted Electron Transfer. *Chem. Sci.* **2019**, *10* (10), 3049–3053. https://doi.org/10.1039/C8SC05170D.
(91) Woźniak, Ł.; Murphy, J. J.; Melchiorre, P. Photo-Organocatalytic Enantioselective Perfluoroalkylation of β-Ketoesters. *J. Am. Chem. Soc.* **2015**, *137* (17), 5678–5681. https://doi.org/10.1021/jacs.5b03243.
(92) Spell, M. L.; Deveaux, K.; Bresnahan, C. G.; Bernard, B. L.; Sheffield, W.; Kumar, R.; Ragains, J. R. A Visible-Light-Promoted O-Glycosylation with a Thioglycoside Donor. *Angew. Chem. Int. Ed.* **2016**, *55* (22), 6515–6519. https://doi.org/10.1002/anie.201601566.
(93) Liu, B.; Lim, C.-H.; Miyake, G. M. Visible-Light-Promoted C–S Cross-Coupling via Intermolecular Charge Transfer. *J. Am. Chem. Soc.* **2017**, *139* (39), 13616–13619. https://doi.org/10.1021/jacs.7b07390.
(94) Liu, B.; Lim, C.-H.; Miyake, G. M. Light-Driven Intermolecular Charge Transfer Induced Reactivity of Ethynylbenziodoxol(on)e and Phenols. *J. Am. Chem. Soc.* **2018**, *140* (40), 12829–12835. https://doi.org/10.1021/jacs.8b05870.
(95) Marzo, L.; Wang, S.; König, B. Visible-Light-Mediated Radical Arylation of Anilines with Acceptor-Substituted (Hetero)Aryl Halides. *Org. Lett.* **2017**, *19* (21), 5976–5979. https://doi.org/10.1021/acs.orglett.7b03001.
(96) Hsu, C.-W.; Sundén, H. α-Aminoalkyl Radical Addition to Maleimides via Electron Donor–Acceptor Complexes. *Org. Lett.* **2018**, *20* (7), 2051–2054. https://doi.org/10.1021/acs.orglett.8b00597.
(97) Li, Y.; Miao, T.; Li, P.; Wang, L. Photo-Driven Synthesis of C6-Polyfunctionalized Phenanthridines from Three-Component Reactions of Isocyanides, Alkynes, and Sulfinic Acids by Electron Donor–Acceptor Complex. *Org. Lett.* **2018**, *20* (7), 1735–1739. https://doi.org/10.1021/acs.orglett.8b00171.
(98) Cao, Z.-Y.; Ghosh, T.; Melchiorre, P. Enantioselective Radical Conjugate Additions Driven by a Photoactive Intramolecular Iminium-Ion-Based EDA Complex. *Nat. Commun.* **2018**, *9* (1), 1–10. https://doi.org/10.1038/s41467-018-05375-2.
(99) Ho, H. E.; Pagano, A.; Rossi-Ashton, J. A.; Donald, J. R.; Epton, R. G.; Churchill, J. C.; James, M. J.; O'Brien, P.; Taylor, R. J. K.; Unsworth, W. P. Visible-Light-Induced Intramolecular Charge Transfer in the Radical Spirocyclisation of Indole-Tethered Ynones. *Chem. Sci.* **2020**, *11* (5), 1353–1360. https://doi.org/10.1039/C9SC05311E.
(100) Morack, T.; Mück-Lichtenfeld, C.; Gilmour, R. Bioinspired Radical Stetter Reaction: Radical Umpolung Enabled by Ion-Pair Photocatalysis. *Angew. Chem. Int. Ed.* **2019**, *58* (4), 1208–1212. https://doi.org/10.1002/anie.201809601.

(101) Zhang, H.-H.; Yu, S. Visible-Light-Induced Radical Acylation of Imines with α-Ketoacids Enabled by Electron-Donor–Acceptor Complexes. *Org. Lett.* **2019**, *21* (10), 3711–3715. https://doi.org/10.1021/acs.orglett.9b01169.
(102) Xie, S.; Li, D.; Huang, H.; Zhang, F.; Chen, Y. Intermolecular Radical Addition to Ketoacids Enabled by Boron Activation. *J. Am. Chem. Soc.* **2019**, *141* (41), 16237–16242. https://doi.org/10.1021/jacs.9b09099.
(103) Jiang, H.; Bak, J. R.; López-Delgado, F. J.; Jørgensen, K. A. Practical Metal- and Additive-Free Methods for Radical-Mediated Reduction and Cyclization Reactions. *Green Chem.* **2013**, *15* (12), 3355–3359. https://doi.org/10.1039/C3GC41520A.
(104) Silva, G. P. da; Ali, A.; Silva, R. C. da; Jiang, H.; Paixão, M. W. Tris(Trimethylsilyl)Silane and Visible-Light Irradiation: A New Metal- and Additive-Free Photochemical Process for the Synthesis of Indoles and Oxindoles. *Chem. Commun.* **2015**, *51* (82), 15110–15113. https://doi.org/10.1039/C5CC06329A.
(105) Davies, J.; Booth, S. G.; Essafi, S.; Dryfe, R. A. W.; Leonori, D. Visible-Light-Mediated Generation of Nitrogen-Centered Radicals: Metal-Free Hydroimination and Iminohydroxylation Cyclization Reactions. *Angew. Chem. Int. Ed. 54* (47), 14017–14021. https://doi.org/10.1002/anie.201507641.
(106) Mao, R.; Yuan, Z.; Li, Y.; Wu, J. N-Radical-Initiated Cyclization through Insertion of Sulfur Dioxide under Photoinduced Catalyst-Free Conditions. *Chem. – Eur. J.* **2017**, *23* (34), 8176–8179. https://doi.org/10.1002/chem.201702040.
(107) Fawcett, A.; Pradeilles, J.; Wang, Y.; Mutsuga, T.; Myers, E. L.; Aggarwal, V. K. Photoinduced Decarboxylative Borylation of Carboxylic Acids. *Science* **2017**, *357* (6348), 283–286. https://doi.org/10.1126/science.aan3679.
(108) Candish, L.; Teders, M.; Glorius, F. Transition-Metal-Free, Visible-Light-Enabled Decarboxylative Borylation of Aryl N-Hydroxyphthalimide Esters. *J. Am. Chem. Soc.* **2017**, *139* (22), 7440–7443. https://doi.org/10.1021/jacs.7b03127.
(109) Zhang, J.; Li, Y.; Xu, R.; Chen, Y. Donor–Acceptor Complex Enables Alkoxyl Radical Generation for Metal-Free C(Sp3)–C(Sp3) Cleavage and Allylation/Alkenylation. *Angew. Chem. Int. Ed.* **2017**, *56* (41), 12619–12623. https://doi.org/10.1002/anie.201707171.
(110) Wu, J.; Bär, R. M.; Guo, L.; Noble, A.; Aggarwal, V. K. Photoinduced Deoxygenative Borylations of Aliphatic Alcohols. *Angew. Chem. Int. Ed.* **2019**, *58* (52), 18830–18834. https://doi.org/10.1002/anie.201910051.
(111) Wu, J.; He, L.; Noble, A.; Aggarwal, V. K. Photoinduced Deaminative Borylation of Alkylamines. *J. Am. Chem. Soc.* **2018**, *140* (34), 10700–10704. https://doi.org/10.1021/jacs.8b07103.
(112) Wu, J.; Grant, P. S.; Li, X.; Noble, A.; Aggarwal, V. K. Catalyst-Free Deaminative Functionalizations of Primary Amines by Photoinduced Single-Electron Transfer. *Angew. Chem. Int. Ed.* **2019**, *58* (17), 5697–5701. https://doi.org/10.1002/anie.201814452.
(113) Yang, M.; Cao, T.; Xu, T.; Liao, S. Visible-Light-Induced Deaminative Thioesterification of Amino Acid Derived Katritzky Salts via Electron Donor–Acceptor Complex Formation. *Org. Lett.* **2019**, *21* (21), 8673–8678. https://doi.org/10.1021/acs.orglett.9b03284.
(114) Fu, M.-C.; Shang, R.; Zhao, B.; Wang, B.; Fu, Y. Photocatalytic Decarboxylative Alkylations Mediated by Triphenylphosphine and Sodium Iodide. *Science* **2019**, *363* (6434), 1429–1434. https://doi.org/10.1126/science.aav3200.
(115) Bosque, I.; Bach, T. 3-Acetoxyquinuclidine as Catalyst in Electron Donor–Acceptor Complex-Mediated Reactions Triggered by Visible Light. *ACS Catal.* **2019**, *9* (10), 9103–9109. https://doi.org/10.1021/acscatal.9b01039.
(116) Emmanuel, M. A.; Greenberg, N. R.; Oblinsky, D. G.; Hyster, T. K. Accessing Non-Natural Reactivity by Irradiating Nicotinamide-Dependent Enzymes with Light. *Nature* **2016**, *540* (7633), 414–417. https://doi.org/10.1038/nature20569.
(117) Biegasiewicz, K. F.; Cooper, S. J.; Gao, X.; Oblinsky, D. G.; Kim, J. H.; Garfinkle, S. E.; Joyce, L. A.; Sandoval, B. A.; Scholes, G. D.; Hyster, T. K. Photoexcitation of Flavoenzymes Enables a Stereoselective Radical Cyclization. *Science* **2019**, *364* (6446), 1166–1169. https://doi.org/10.1126/science.aaw1143.
(118) Barton, D. H. R.; George, M. V.; Tomoeda, M. 369. Photochemical Transformations. Part XIII. A New Method for the Production of Acyl Radicals. *J. Chem. Soc. Resumed* **1962**, No. 0, 1967–1974. https://doi.org/10.1039/JR9620001967.

(119) Zard, S. Z. On the Trail of Xanthates: Some New Chemistry from an Old Functional Group. *Angew. Chem. Int. Ed. Engl.* **1997**, *36* (7), 672–685. https://doi.org/10.1002/anie.199706721.
(120) Z. Zard, S.; Mestre, F.; Tailham, C. Xanthates as a Source of Stabilised Carbon Centered Radicals Using Visible Light. *HETEROCYCLES* **1989**, *28* (1), 171. https://doi.org/10.3987/COM-88-S77.
(121) Zard, S. Z. Xanthates and Related Derivatives as Radical Precursors. **2012**, 23.
(122) Schweitzer-Chaput, B.; Horwitz, M. A.; de Pedro Beato, E.; Melchiorre, P. Photochemical Generation of Radicals from Alkyl Electrophiles Using a Nucleophilic Organic Catalyst. *Nat. Chem.* **2019**, *11* (2), 129–135. https://doi.org/10.1038/s41557-018-0173-x.
(123) Silvi, M.; Arceo, E.; Jurberg, I. D.; Cassani, C.; Melchiorre, P. Enantioselective Organocatalytic Alkylation of Aldehydes and Enals Driven by the Direct Photoexcitation of Enamines. *J. Am. Chem. Soc.* **2015**, *137* (19), 6120–6123. https://doi.org/10.1021/jacs.5b01662.
(124) Bahamonde, A.; Melchiorre, P. Mechanism of the Stereoselective α-Alkylation of Aldehydes Driven by the Photochemical Activity of Enamines. *J. Am. Chem. Soc.* **2016**, *138* (25), 8019–8030. https://doi.org/10.1021/jacs.6b04871.
(125) Filippini, G.; Nappi, M.; Melchiorre, P. Photochemical Direct Perfluoroalkylation of Phenols. *Tetrahedron* **2015**, *71* (26), 4535–4542. https://doi.org/10.1016/j.tet.2015.02.034.
(126) Silvi, M.; Verrier, C.; Rey, Y. P.; Buzzetti, L.; Melchiorre, P. Visible-Light Excitation of Iminium Ions Enables the Enantioselective Catalytic β-Alkylation of Enals. *Nat. Chem.* **2017**, *9* (9), 868–873. https://doi.org/10.1038/nchem.2748.
(127) Trowbridge, A.; Walton, S. M.; Gaunt, M. J. New Strategies for the Transition-Metal Catalyzed Synthesis of Aliphatic Amines. *Chem. Rev.* **2020**, *120* (5), 2613–2692. https://doi.org/10.1021/acs.chemrev.9b00462.
(128) Roughley, S. D.; Jordan, A. M. The Medicinal Chemist's Toolbox: An Analysis of Reactions Used in the Pursuit of Drug Candidates. *J. Med. Chem.* **2011**, *54* (10), 3451–3479. https://doi.org/10.1021/jm200187y.
(129) Hofmann, A. W. V.; Clark, J. V. Researches Regarding the Molecular Constitution of the Volatile Organic Bases. *Philos. Trans. R. Soc. Lond.* **1850**, *140*, 93–131. https://doi.org/10.1098/rstl.1850.0006.
(130) texte, D. chemische G. A. du. Berichte der Deutschen chemischen Gesellschaft zu Berlin https://gallica.bnf.fr/ark:/12148/bpt6k90711d (accessed May 6, 2020).
(131) Howk, B. W.; Little, E. L.; Scott, S. L.; Whitman, G. M. Alkali Metal-Catalyzed Amination of Olefins. *J. Am. Chem. Soc.* **1954**, *76* (7), 1899–1902. https://doi.org/10.1021/ja01636a048.
(132) Coulson, D. R. Catalytic Addition of Secondary Amines to Ethylene (Contribution No. 1720). *Tetrahedron Lett.* **1971**, *12* (5), 429–430. https://doi.org/10.1016/S0040-4039(01)96459-7.
(133) Müller, T. E.; Hultzsch, K. C.; Yus, M.; Foubelo, F.; Tada, M. Hydroamination: Direct Addition of Amines to Alkenes and Alkynes. *Chem. Rev.* **2008**, *108* (9), 3795–3892. https://doi.org/10.1021/cr0306788.
(134) Huang, L.; Arndt, M.; Gooßen, K.; Heydt, H.; Gooßen, L. J. Late Transition Metal-Catalyzed Hydroamination and Hydroamidation. *Chem. Rev.* **2015**, *115* (7), 2596–2697. https://doi.org/10.1021/cr300389u.
(135) Musacchio, A. J.; Lainhart, B. C.; Zhang, X.; Naguib, S. G.; Sherwood, T. C.; Knowles, R. R. Catalytic Intermolecular Hydroaminations of Unactivated Olefins with Secondary Alkyl Amines. *Science* **2017**, *355* (6326), 727–730. https://doi.org/10.1126/science.aal3010.
(136) Eschweiler, W. Ersatz von an Stickstoff Gebundenen Wasserstoffatomen Durch Die Methylgruppe Mit Hülfe von Formaldehyd. **1905**. https://doi.org/10.1002/cber.190503801154.
(137) Borch, R. F.; Durst, H. D. Lithium Cyanohydridoborate, a Versatile New Reagent. *J. Am. Chem. Soc.* **1969**, *91* (14), 3996–3997. https://doi.org/10.1021/ja01042a078.
(138) Abdel-Magid, A. F.; Mehrman, S. J. A Review on the Use of Sodium Triacetoxyborohydride in the Reductive Amination of Ketones and Aldehydes. *Org. Process Res. Dev.* **2006**, *10* (5), 971–1031. https://doi.org/10.1021/op0601013.
(139) Li, M.-L.; Yu, J.-H.; Li, Y.-H.; Zhu, S.-F.; Zhou, Q.-L. Highly Enantioselective Carbene Insertion into N–H Bonds of Aliphatic Amines. *Science* **2019**, *366* (6468), 990–994. https://doi.org/10.1126/science.aaw9939.
(140) Trost, B. M.; Van Vranken, D. L. Asymmetric Transition Metal-Catalyzed Allylic Alkylations. *Chem. Rev.* **1996**, *96* (1), 395–422. https://doi.org/10.1021/cr9409804.

(141) Johannsen, M.; Jørgensen, K. A. Allylic Amination. *Chem. Rev.* **1998**, *98* (4), 1689–1708. https://doi.org/10.1021/cr970343o.
(142) Ohmura, T.; Hartwig, J. F. Regio- and Enantioselective Allylic Amination of Achiral Allylic Esters Catalyzed by an Iridium−Phosphoramidite Complex. *J. Am. Chem. Soc.* **2002**, *124* (51), 15164–15165. https://doi.org/10.1021/ja028614m.
(143) Nystrom, R. F.; Brown, W. G. Reduction of Organic Compounds by Lithium Aluminum Hydride. III. Halides, Quinones, Miscellaneous Nitrogen Compounds1. *J. Am. Chem. Soc.* **1948**, *70* (11), 3738–3740. https://doi.org/10.1021/ja01191a057.
(144) Nugent, T. C.; El-Shazly, M. Chiral Amine Synthesis – Recent Developments and Trends for Enamide Reduction, Reductive Amination, and Imine Reduction. *Adv. Synth. Catal.* **2010**, *352* (5), 753–819. https://doi.org/10.1002/adsc.200900719.
(145) Staudinger, H.; Meyer, J. Über Neue Organische Phosphorverbindungen III. Phosphinmethylenderivate Und Phosphinimine. *Helv. Chim. Acta* **1919**, *2* (1), 635–646. https://doi.org/10.1002/hlca.19190020164.
(146) McNally, A.; Haffemayer, B.; Collins, B. S. L.; Gaunt, M. J. Palladium-Catalysed C–H Activation of Aliphatic Amines to Give Strained Nitrogen Heterocycles. *Nature* **2014**, *510* (7503), 129–133. https://doi.org/10.1038/nature13389.
(147) Calleja, J.; Pla, D.; Gorman, T. W.; Domingo, V.; Haffemayer, B.; Gaunt, M. J. A Steric Tethering Approach Enables Palladium-Catalysed C–H Activation of Primary Amino Alcohols. *Nat. Chem.* **2015**, *7* (12), 1009–1016. https://doi.org/10.1038/nchem.2367.
(148) He, C.; Whitehurst, W. G.; Gaunt, M. J. Palladium-Catalyzed C(Sp3)–H Bond Functionalization of Aliphatic Amines. *Chem* **2019**, *5* (5), 1031–1058. https://doi.org/10.1016/j.chempr.2018.12.017.
(149) Majetich, G.; Wheless, K. Remote Intramolecular Free Radical Functionalizations: An Update. *Tetrahedron* **1995**, *51* (26), 7095–7129. https://doi.org/10.1016/0040-4020(95)00406-X.
(150) Davies, H. M. L.; Manning, J. R. Catalytic C–H Functionalization by Metal Carbenoid and Nitrenoid Insertion. *Nature* **2008**, *451* (7177), 417–424. https://doi.org/10.1038/nature06485.
(151) Blicke, F. F. The Mannich Reaction. In *Organic Reactions*; American Cancer Society, 2011; pp 303–341. https://doi.org/10.1002/0471264180.or001.10.
(152) Kouznetsov, V. V.; Galvis, C. E. P. Strecker Reaction and α-Amino Nitriles: Recent Advances in Their Chemistry, Synthesis, and Biological Properties. *Tetrahedron* **2018**, *74* (8), 773–810. https://doi.org/10.1016/j.tet.2018.01.005.
(153) Candeias, N. R.; Montalbano, F.; Cal, P. M. S. D.; Gois, P. M. P. Boronic Acids and Esters in the Petasis-Borono Mannich Multicomponent Reaction. *Chem. Rev.* **2010**, *110* (10), 6169–6193. https://doi.org/10.1021/cr100108k.
(154) Kumar, R.; Flodén, N. J.; Whitehurst, W. G.; Gaunt, M. J. A General Carbonyl Alkylative Amination for Tertiary Amine Synthesis. *Nature* **2020**, 1–6. https://doi.org/10.1038/s41586-020-2213-0.
(155) Hu, J.; Wang, J.; Nguyen, T. H.; Zheng, N. The Chemistry of Amine Radical Cations Produced by Visible Light Photoredox Catalysis. *Beilstein J. Org. Chem.* **2013**, *9* (1), 1977–2001. https://doi.org/10.3762/bjoc.9.234.
(156) Griller, D.; Lossing, F. P. Thermochemistry of .Alpha.-Aminoalkyl Radicals. *J. Am. Chem. Soc.* **1981**, *103* (6), 1586–1587. https://doi.org/10.1021/ja00396a061.
(157) Cohen, S. G.; Parola, A.; Parsons, G. H. Photoreduction by Amines. *Chem. Rev.* **1973**, *73* (2), 141–161. https://doi.org/10.1021/cr60282a004.
(158) Renaud, P.; Giraud, L. 1-Amino- and 1-Amidoalkyl Radicals: Generation and Stereoselective Reactions. *Synthesis* **1996**, *1996* (8), 913–926. https://doi.org/10.1055/s-1996-4332.
(159) Aurrecoechea, J. M.; Suero, R. Recent Developments in Cyclization Reactions of α-Aminoalkyl Radicals. *Arkivoc* **2004**, *2004* (14), 10. https://doi.org/10.3998/ark.5550190.0005.e02.
(160) Beatty, J. W.; Stephenson, C. R. J. Amine Functionalization via Oxidative Photoredox Catalysis: Methodology Development and Complex Molecule Synthesis. *Acc. Chem. Res.* **2015**, *48* (5), 1474–1484. https://doi.org/10.1021/acs.accounts.5b00068.
(161) Nakajima, K.; Miyake, Y.; Nishibayashi, Y. Synthetic Utilization of α-Aminoalkyl Radicals and Related Species in Visible Light Photoredox Catalysis. *Acc. Chem. Res.* **2016**, *49* (9), 1946–1956. https://doi.org/10.1021/acs.accounts.6b00251.

(162) Urry, W. H.; Juveland, O. O.; Stacey, F. W. THE PEROXIDE AND LIGHT INDUCED REACTIONS OF AMINES WITH OLEFINS: A ONE-STEP SYNTHESIS OF d,l-CONIINE. *J. Am. Chem. Soc.* **1952**, *74* (23), 6155–6155. https://doi.org/10.1021/ja01143a546.

(163) Shaw, M. H.; Shurtleff, V. W.; Terrett, J. A.; Cuthbertson, J. D.; MacMillan, D. W. C. Native Functionality in Triple Catalytic Cross-Coupling: Sp3 C–H Bonds as Latent Nucleophiles. *Science* **2016**, *352* (6291), 1304–1308. https://doi.org/10.1126/science.aaf6635.

(164) Bachi, M. D.; Hoornaert, C. Free-Radical Annelation in the Synthesis of Bicyclic β-Lactams. 1. Synthesis of 8-Oxo-5-Oxa-1-Azabicyclo[4.2.0]Octane and 9-Oxo-6-Oxa-1-Azabicyclo[5.2.0]Nonane Derivatives. *Tetrahedron Lett.* **1981**, *22* (28), 2689–2692. https://doi.org/10.1016/S0040-4039(01)92971-5.

(165) Bachi, M. D.; Hoornaert, C. Free-Radical Annelation in the Synthesis of Bicyclic β-Lactams. 2. Alternative Use of Chloro-, Phenylseleno-, and Phenylthio-Functionalities as Free-Radical Precursors. *Tetrahedron Lett.* **1981**, *22* (28), 2693–2694. https://doi.org/10.1016/S0040-4039(01)92972-7.

(166) Hart, D. J.; Tsai, Y.-M. New Methods for Alkaloid Synthesis: .Alpha.-Acylamino Radical Cyclizations. *J. Am. Chem. Soc.* **1982**, *104* (5), 1430–1432. https://doi.org/10.1021/ja00369a050.

(167) Keck, G. E.; Enholm, E. J. Synthetic Studies on Pyrrolizidine Alkaloids. II. Intramolecular Additions of Radicals and Electrophiles to Allylstannanes as Methods for Ring Closure. *Tetrahedron Lett.* **1985**, *26* (28), 3311–3314. https://doi.org/10.1016/S0040-4039(00)98285-6.

(168) Nicolaou, K. C.; Magolda, R. L.; Sipio, W. J.; Barnette, W. E.; Lysenko, Z.; Joullie, M. M. Phenylselenoetherification. A Highly Efficient Cyclization Process for the Synthesis of Oxygen- and Sulfur-Heterocycles. *J. Am. Chem. Soc.* **1980**, *102* (11), 3784–3793. https://doi.org/10.1021/ja00531a020.

(169) McIntosh, J. M.; Schram, C. K. Reductive Desulfurization Using Tributyltin Hydride. *Can. J. Chem.* **1977**, *55* (21), 3755–3757. https://doi.org/10.1139/v77-529.

(170) Padwa, A.; Nimmesgern, H.; Wong, G. S. K. Synthesis of the Pyrrolidine Ring System by Radical Cyclization. *J. Org. Chem.* **1985**, *50* (26), 5620–5627. https://doi.org/10.1021/jo00350a038.

(171) Arya, P.; Wayner, D. D. M. Thiazolidine Derivatives: A New Source of α-Aminoalkyl Radicals for Carbon-Carbon Bond Formation in Synthesis. *Tetrahedron Lett.* **1991**, *32* (44), 6265–6268. https://doi.org/10.1016/0040-4039(91)80143-T.

(172) Curran, D. P.; Sun, S. Cram's Rule for Radicals: Stereoselective Hydrogen Abstraction Reactions of N□H Substituted Radicals. *Tetrahedron Lett.* **1993**, *34* (39), 6181–6184. https://doi.org/10.1016/S0040-4039(00)73704-X.

(173) Lewis, F. D.; Ho, T.-I. Selectivity of Tertiary Amine Oxidations. *J. Am. Chem. Soc.* **1980**, *102* (5), 1751–1752. https://doi.org/10.1021/ja00525a061.

(174) Smith, P. A. S.; Loeppky, R. N. Nitrosative Cleavage of Tertiary Amines. *J. Am. Chem. Soc.* **1967**, *89* (5), 1147–1157. https://doi.org/10.1021/ja00981a021.

(175) Smith, P. J.; Mann, C. K. Electrochemical Dealkylation of Aliphatic Amines. *J. Org. Chem.* **1969**, *34* (6), 1821–1826. https://doi.org/10.1021/jo01258a063.

(176) Yoon, U. C.; Mariano, P. S. Mechanistic and Synthetic Aspects of Amine-Enone Single Electron Transfer Photochemistry. *Acc. Chem. Res.* **1992**, *25* (5), 233–240. https://doi.org/10.1021/ar00017a005.

(177) Su, Z.; Mariano, P. S.; Falvey, D. E.; Yoon, U. C.; Oh, S. W. Dynamics of Anilinium Radical α-Heterolytic Fragmentation Processes. Electrofugal Group, Substituent, and Medium Effects on Desilylation, Decarboxylation, and Retro-Aldol Cleavage Pathways. *J. Am. Chem. Soc.* **1998**, *120* (41), 10676–10686. https://doi.org/10.1021/ja981541f.

(178) S. Davidson, R.; P. Orton, S. Photo-Induced Electron-Transfer Reactions: Fragmentation of 2-Aminoethanols. *J. Chem. Soc. Chem. Commun.* **1974**, *0* (6), 209–210. https://doi.org/10.1039/C39740000209.

(179) Condie, A. G.; González-Gómez, J. C.; Stephenson, C. R. J. Visible-Light Photoredox Catalysis: Aza-Henry Reactions via C−H Functionalization. *J. Am. Chem. Soc.* **2010**, *132* (5), 1464–1465. https://doi.org/10.1021/ja909145y.

(180) McNally, A.; Prier, C. K.; MacMillan, D. W. C. Discovery of an α-Amino C–H Arylation Reaction Using the Strategy of Accelerated Serendipity. *Science* **2011**, *334* (6059), 1114–1117. https://doi.org/10.1126/science.1213920.

(181) Miyake, Y.; Nakajima, K.; Nishibayashi, Y. Visible-Light-Mediated Utilization of α-Aminoalkyl Radicals: Addition to Electron-Deficient Alkenes Using Photoredox Catalysts. *J. Am. Chem. Soc.* **2012**, *134* (7), 3338–3341. https://doi.org/10.1021/ja211770y.

(182) Thullen, S. M.; Rovis, T. A Mild Hydroaminoalkylation of Conjugated Dienes Using a Unified Cobalt and Photoredox Catalytic System. *J. Am. Chem. Soc.* **2017**, *139* (43), 15504–15508. https://doi.org/10.1021/jacs.7b09252.

(183) McManus, J. B.; Onuska, N. P. R.; Nicewicz, D. A. Generation and Alkylation of α-Carbamyl Radicals via Organic Photoredox Catalysis. *J. Am. Chem. Soc.* **2018**, *140* (29), 9056–9060. https://doi.org/10.1021/jacs.8b04890.

(184) Nakajima, K.; Miyake, Y.; Nishibayashi, Y. Synthetic Utilization of α-Aminoalkyl Radicals and Related Species in Visible Light Photoredox Catalysis. *Acc. Chem. Res.* **2016**, *49* (9), 1946–1956. https://doi.org/10.1021/acs.accounts.6b00251.

(185) Kunai, A.; Harada, J.; Nishihara, M.; Yanagi, Y.; Sasaki, K. The Electrolytic Behavior of Tetrasubstituted Iminium Salt in Acetonitrile. *Bull. Chem. Soc. Jpn.* **1983**, *56* (8), 2442–2446. https://doi.org/10.1246/bcsj.56.2442.

(186) Martin, S. F.; Yang, C.-P.; Laswell, W. L.; Rüeger, H. Application of Reductive, Single Electron Transfer Processes to the Generation and Cyclization of ω-Unsaturated α-Amino Radicals. *Tetrahedron Lett.* **1988**, *29* (51), 6685–6687. https://doi.org/10.1016/S0040-4039(00)82428-4.

(187) Enholm, E. J.; Forbes, D. C.; Holub, D. P. A Route to Vicinal Diamines from the Samarium(II) Iodide-Mediated Coupling of Aldimines. *Synth. Commun.* **1990**, *20* (7), 981–987. https://doi.org/10.1080/00397919008052801.

(188) Imamoto, T.; Nishimura, S. Samarium Diiodide-Promoted Reductive Coupling of Imines. *Chem. Lett.* **1990**, *19* (7), 1141–1142. https://doi.org/10.1246/cl.1990.1141.

(189) Aurrecoechea, J. M.; Fernández-Acebes, A. Synthesis of Vicinal Diamines by SmI2-Promoted Reduction of N-(N′,N′-Dialkylaminoalkyl)Benzotriazoles. *Tetrahedron Lett.* **1992**, *33* (33), 4763–4766. https://doi.org/10.1016/S0040-4039(00)61280-7.

(190) Mariano, P. S. The Photochemistry of Iminium Salts and Related Heteroaromatic Systems. *Tetrahedron* **1983**, *39* (23), 3845–3879. https://doi.org/10.1016/S0040-4020(01)90889-0.

(191) Mariano, P. S. Electron-Transfer Mechanisms in Photochemical Transformations of Iminium Salts. *Acc. Chem. Res.* **1983**, *16* (4), 130–137. https://doi.org/10.1021/ar00088a003.

(192) Mariano, P. S.; Stavinoha, J. L.; Pepe, G.; Meyer, E. F. Novel Photochemical Addition Reactions of Iminium Salts. Electron Transfer Initiated Additions of Olefins to 2-Phenyl-1-Pyrrolinium Perchlorate. *J. Am. Chem. Soc.* **1978**, *100* (22), 7114–7116. https://doi.org/10.1021/ja00490a078.

(193) Stavinoha, J. L.; Mariano, P. S. Electron-Transfer Photochemistry of Iminium Salts. Olefin Photoadditions to 2-Phenyl-1-Pyrrolinium Perchlorate. *J. Am. Chem. Soc.* **1981**, *103* (11), 3136–3148. https://doi.org/10.1021/ja00401a036.

(194) Hager, D.; MacMillan, D. W. C. Activation of C–H Bonds via the Merger of Photoredox and Organocatalysis: A Coupling of Benzylic Ethers with Schiff Bases. *J. Am. Chem. Soc.* **2014**, *136* (49), 16986–16989. https://doi.org/10.1021/ja5102695.

(195) Nakajima, M.; Fava, E.; Loescher, S.; Jiang, Z.; Rueping, M. Photoredox-Catalyzed Reductive Coupling of Aldehydes, Ketones, and Imines with Visible Light. *Angew. Chem. Int. Ed.* **2015**, *54* (30), 8828–8832. https://doi.org/10.1002/anie.201501556.

(196) Uraguchi, D.; Kinoshita, N.; Kizu, T.; Ooi, T. Synergistic Catalysis of Ionic Brønsted Acid and Photosensitizer for a Redox Neutral Asymmetric α-Coupling of N-Arylaminomethanes with Aldimines. *J. Am. Chem. Soc.* **2015**, *137* (43), 13768–13771. https://doi.org/10.1021/jacs.5b09329.

(197) Qi, L.; Chen, Y. Polarity-Reversed Allylations of Aldehydes, Ketones, and Imines Enabled by Hantzsch Ester in Photoredox Catalysis. *Angew. Chem. Int. Ed.* **2016**, *55* (42), 13312–13315. https://doi.org/10.1002/anie.201607813.

(198) Lee, K. N.; Lei, Z.; Ngai, M.-Y. β-Selective Reductive Coupling of Alkenylpyridines with Aldehydes and Imines via Synergistic Lewis Acid/Photoredox Catalysis. *J. Am. Chem. Soc.* **2017**, *139* (14), 5003–5006. https://doi.org/10.1021/jacs.7b01373.

(199) Leitch, J. A.; Rossolini, T.; Rogova, T.; Maitland, J. A. P.; Dixon, D. J. α-Amino Radicals via Photocatalytic Single-Electron Reduction of Imine Derivatives. *ACS Catal.* **2020**, *10* (3), 2009–2025. https://doi.org/10.1021/acscatal.9b05011.

(200) Guo, X.; Wenger, O. S. Reductive Amination by Photoredox Catalysis and Polarity-Matched Hydrogen Atom Transfer. *Angew. Chem. Int. Ed.* **2018**, *57* (9), 2469–2473. https://doi.org/10.1002/anie.201711467.
(201) Trowbridge, A.; Reich, D.; Gaunt, M. J. Multicomponent Synthesis of Tertiary Alkylamines by Photocatalytic Olefin-Hydroaminoalkylation. *Nature* **2018**, *561* (7724), 522–527. https://doi.org/10.1038/s41586-018-0537-9.
(202) Zhang, H.-H.; Yu, S. Visible-Light-Induced Radical Acylation of Imines with α-Ketoacids Enabled by Electron-Donor–Acceptor Complexes. *Org. Lett.* **2019**, *21* (10), 3711–3715. https://doi.org/10.1021/acs.orglett.9b01169.
(203) Chen, W.; Liu, Z.; Tian, J.; Li, J.; Ma, J.; Cheng, X.; Li, G. Building Congested Ketone: Substituted Hantzsch Ester and Nitrile as Alkylation Reagents in Photoredox Catalysis. *J. Am. Chem. Soc.* **2016**, *138* (38), 12312–12315. https://doi.org/10.1021/jacs.6b06379.
(204) Flamigni, L.; Barbieri, A.; Sabatini, C.; Ventura, B.; Barigelletti, F. Photochemistry and Photophysics of Coordination Compounds: Iridium. In *Photochemistry and Photophysics of Coordination Compounds II*; Balzani, V., Campagna, S., Eds.; Topics in Current Chemistry; Springer: Berlin, Heidelberg, 2007; pp 143–203. https://doi.org/10.1007/128_2007_131.
(205) Buzzetti, L.; Crisenza, G. E. M.; Melchiorre, P. Mechanistic Studies in Photocatalysis. *Angew. Chem. Int. Ed.* **2019**, *58* (12), 3730–3747. https://doi.org/10.1002/anie.201809984.
(206) Lovering, F.; Bikker, J.; Humblet, C. Escape from Flatland: Increasing Saturation as an Approach to Improving Clinical Success. *J. Med. Chem.* **2009**, *52* (21), 6752–6756. https://doi.org/10.1021/jm901241e.
(207) Taylor, R. D.; MacCoss, M.; Lawson, A. D. G. Rings in Drugs. *J. Med. Chem.* **2014**, *57* (14), 5845–5859. https://doi.org/10.1021/jm4017625.
(208) Batey, R. A.; Motherwell, W. B. Samarium(II) Iodide Promoted Radical Ring Opening Reactions of Cyclopropyl Ketones. *Tetrahedron Lett.* **1991**, *32* (43), 6211–6214. https://doi.org/10.1016/0040-4039(91)80791-4.
(209) Ferguson, L. N. Ring Strain and Reactivity of Alicycles. *J. Chem. Educ.* **1970**, *47* (1), 46. https://doi.org/10.1021/ed047p46.
(210) Hao, W.; Wu, X.; Sun, J. Z.; Siu, J. C.; MacMillan, S. N.; Lin, S. Radical Redox-Relay Catalysis: Formal [3+2] Cycloaddition of N-Acylaziridines and Alkenes. *J. Am. Chem. Soc.* **2017**, *139* (35), 12141–12144. https://doi.org/10.1021/jacs.7b06723.
(211) Hashimoto, T.; Kawamata, Y.; Maruoka, K. An Organic Thiyl Radical Catalyst for Enantioselective Cyclization. *Nat. Chem.* **2014**, *6* (8), 702–705. https://doi.org/10.1038/nchem.1998.
(212) Feldman, K. S.; Romanelli, A. L.; Ruckle, R. E.; Miller, R. F. Cyclopentane Synthesis via Free Radical Mediated Addition of Functionalized Alkenes to Substituted Vinyl Cyclopropanes. *J. Am. Chem. Soc.* **1988**, *110* (10), 3300–3302. https://doi.org/10.1021/ja00218a050.
(213) Hao, W.; Harenberg, J. H.; Wu, X.; MacMillan, S. N.; Lin, S. Diastereo- and Enantioselective Formal [3 + 2] Cycloaddition of Cyclopropyl Ketones and Alkenes via Ti-Catalyzed Radical Redox Relay. *J. Am. Chem. Soc.* **2018**, *140* (10), 3514–3517. https://doi.org/10.1021/jacs.7b13710.
(214) Huang, X.; Lin, J.; Shen, T.; Harms, K.; Marchini, M.; Ceroni, P.; Meggers, E. Asymmetric [3+2] Photocycloadditions of Cyclopropanes with Alkenes or Alkynes through Visible-Light Excitation of Catalyst-Bound Substrates. *Angew. Chem. Int. Ed.* **2018**, *57* (19), 5454–5458. https://doi.org/10.1002/anie.201802316.
(215) Maity, S.; Zhu, M.; Shinabery, R. S.; Zheng, N. Intermolecular [3+2] Cycloaddition of Cyclopropylamines with Olefins by Visible-Light Photocatalysis. *Angew. Chem. Int. Ed.* **2012**, *51* (1), 222–226. https://doi.org/10.1002/anie.201106162.
(216) Amador, A. G.; Sherbrook, E. M.; Yoon, T. P. Enantioselective Photocatalytic [3 + 2] Cycloadditions of Aryl Cyclopropyl Ketones. *J. Am. Chem. Soc.* **2016**, *138* (14), 4722–4725. https://doi.org/10.1021/jacs.6b01728.
(217) Burchak, O. N.; Masson, G.; Py, S. SmI2-Mediated Reductive Cross-Coupling Reactions of α-Cyclopropyl Nitrones. *Synlett* **2010**, *2010* (11), 1623–1626. https://doi.org/10.1055/s-0030-1258084.
(218) Guo, X.; Wenger, O. S. Reductive Amination by Photoredox Catalysis and Polarity-Matched Hydrogen Atom Transfer. *Angew. Chem. Int. Ed.* **2018**, *57* (9), 2469–2473. https://doi.org/10.1002/anie.201711467.

(219) Newcomb, M. Radical Kinetics and Clocks. In *Encyclopedia of Radicals in Chemistry, Biology and Materials*; American Cancer Society, 2012. https://doi.org/10.1002/9781119953678.rad007.
(220) Fischer, H.; Radom, L. Factors Controlling the Addition of Carbon-Centered Radicals to Alkenes—An Experimental and Theoretical Perspective. *Angew. Chem. Int. Ed.* **2001**, *40* (8), 1340–1371. https://doi.org/10.1002/1521-3773(20010417)40:8<1340::AID-ANIE1340>3.0.CO;2-#.
(221) Roberts, B. P. Polarity-Reversal Catalysis of Hydrogen-Atom Abstraction Reactions: Concepts and Applications in Organic Chemistry. *Chem. Soc. Rev.* **1999**, *28* (1), 25–35. https://doi.org/10.1039/A804291H.
(222) Margrey, K. A.; Nicewicz, D. A. A General Approach to Catalytic Alkene Anti-Markovnikov Hydrofunctionalization Reactions via Acridinium Photoredox Catalysis. *Acc. Chem. Res.* **2016**, *49* (9), 1997–2006. https://doi.org/10.1021/acs.accounts.6b00304.
(223) Tripp, J. C.; Schiesser, C. H.; Curran, D. P. Stereochemistry of Hexenyl Radical Cyclizations with Tert-Butyl and Related Large Groups: Substituent and Temperature Effects. *J. Am. Chem. Soc.* **2005**, *127* (15), 5518–5527. https://doi.org/10.1021/ja042595u.
(224) Singh, A.; Teegardin, K.; Kelly, M.; Prasad, K. S.; Krishnan, S.; Weaver, J. D. Facile Synthesis and Complete Characterization of Homoleptic and Heteroleptic Cyclometalated Iridium(III) Complexes for Photocatalysis. *J. Organomet. Chem.* **2015**, *776*, 51–59. https://doi.org/10.1016/j.jorganchem.2014.10.037.
(225) Zhu, D.-L.; Wu, Q.; Li, H.-Y.; Li, H.-X.; Lang, J.-P. Hantzsch Ester as a Visible-Light Photoredox Catalyst for Transition-Metal-Free Coupling of Arylhalides and Arylsulfinates. *Chem. – Eur. J.* **2020**, *26* (16), 3484–3488. https://doi.org/10.1002/chem.201905281.
(226) Wu, J.; Grant, P. S.; Li, X.; Noble, A.; Aggarwal, V. K. Catalyst-Free Deaminative Functionalizations of Primary Amines by Photoinduced Single-Electron Transfer. *Angew. Chem. Int. Ed.* **2019**, *58* (17), 5697–5701. https://doi.org/10.1002/anie.201814452.
(227) Zhang, J.; Li, Y.; Xu, R.; Chen, Y. Donor–Acceptor Complex Enables Alkoxyl Radical Generation for Metal-Free C(Sp3)–C(Sp3) Cleavage and Allylation/Alkenylation. *Angew. Chem. Int. Ed.* **2017**, *56* (41), 12619–12623. https://doi.org/10.1002/anie.201707171.
(228) Wayner, D. D. M.; Clark, K. B.; Rauk, A.; Yu, D.; Armstrong, D. A. C−H Bond Dissociation Energies of Alkyl Amines: Radical Structures and Stabilization Energies. *J. Am. Chem. Soc.* **1997**, *119* (38), 8925–8932. https://doi.org/10.1021/ja971365v.
(229) Luo, Y.-R. *Handbook of Bond Dissociation Energies in Organic Compounds*; CRC Press: Boca Raton, Fla, 2003.
(230) Dénès, F.; Pichowicz, M.; Povie, G.; Renaud, P. Thiyl Radicals in Organic Synthesis. *Chem. Rev.* **2014**, *114* (5), 2587–2693. https://doi.org/10.1021/cr400441m.
(231) Feray, L.; Bertrand, M. P.; Soderquist, J. A. Triisopropylsilanethiol. In *Encyclopedia of Reagents for Organic Synthesis*; American Cancer Society, 2010. https://doi.org/10.1002/047084289X.rn00636.pub2.
(232) Kano, T.; Maruoka, K. Unique Properties of Chiral Biaryl-Based Secondary Amine Catalysts for Asymmetric Enamine Catalysis. *Chem. Sci.* **2013**, *4* (3), 907–915. https://doi.org/10.1039/C2SC21612D.
(233) 9009083 - LED Strip, 1 m, 60 LEDs, Blue, 24 VDC, 14.4 W, IP20 https://uk.farnell.com/ledxon-modular/9009083/led-single-5050-14-4w-blue/dp/2214013 (accessed Apr 5, 2020).
(234) Optics - Imaging - Photonics - Optomechanics - Lasers | Edmund Optics https://www.edmundoptics.com/ (accessed Apr 7, 2020).
(235) Escoubet, S.; Gastaldi, S.; Vanthuyne, N.; Gil, G.; Siri, D.; Bertrand, M. P. Thiyl Radical Mediated Racemization of Nonactivated Aliphatic Amines. *J. Org. Chem.* **2006**, *71* (19), 7288–7292. https://doi.org/10.1021/jo061033l.
(236) Janousek, B. K.; Reed, K. J.; Brauman, J. I. Electron Photodetachment from Mercaptyl Anions (RS-). Electron Affinities of Mercaptyl Radicals and the Sulfur-Hydrogen Bond Strength in Mercaptans. *J. Am. Chem. Soc.* **1980**, *102* (9), 3125–3129. https://doi.org/10.1021/ja00529a040.
(237) Zhou, R.; Goh, Y. Y.; Liu, H.; Tao, H.; Li, L.; Wu, J. Visible-Light-Mediated Metal-Free Hydrosilylation of Alkenes through Selective Hydrogen Atom Transfer for Si−H Activation. *Angew. Chem. Int. Ed.* **2017**, *56* (52), 16621–16625. https://doi.org/10.1002/anie.201711250.
(238) Bordwell, F. G.; Zhang, X.-M.; Satish, A. V.; Cheng, J.-P. Assessment of the Importance of Changes in Ground-State Energies on the Bond Dissociation Enthalpies of the O-H Bonds in Phenols and the S-H Bonds in Thiophenols. *J. Am. Chem. Soc.* **1994**, *116* (15), 6605–6610. https://doi.org/10.1021/ja00094a015.

(239) Fu, Y.; Lin, B.-L.; Song, K.-S.; Liu, L.; Guo, Q.-X. Substituent Effects on the S–H Bond Dissociation Energies of Thiophenols. *J. Chem. Soc. Perkin Trans. 2* **2002**, No. 7, 1223–1230. https://doi.org/10.1039/B201003H.
(240) Mao, R.-Z.; Guo, F.; Xiong, D.-C.; Li, Q.; Duan, J.; Ye, X.-S. Photoinduced C–S Bond Cleavage of Thioglycosides and Glycosylation. *Org. Lett.* **2015**, *17* (22), 5606–5609. https://doi.org/10.1021/acs.orglett.5b02823.
(241) Fava, A.; Calvin, M. Absorption Spectra of Aromatic Disulfides. **1956**.
(242) Dénès, F.; Pichowicz, M.; Povie, G.; Renaud, P. Thiyl Radicals in Organic Synthesis. *Chem. Rev.* **2014**, *114* (5), 2587–2693. https://doi.org/10.1021/cr400441m.
(243) Dénès, F.; Schiesser, C. H.; Renaud, P. Thiols, Thioethers, and Related Compounds as Sources of C-Centred Radicals. *Chem. Soc. Rev.* **2013**, *42* (19), 7900–7942. https://doi.org/10.1039/C3CS60143A.
(244) W. M. Haynes. *CRC Handbook of Chemistry and Physics, 95th Edition*; CRC Press/Taylor & Francis: Boca Raton, Fla, 2014.
(245) Dénès, F.; Pichowicz, M.; Povie, G.; Renaud, P. Thiyl Radicals in Organic Synthesis. *Chem. Rev.* **2014**, *114* (5), 2587–2693. https://doi.org/10.1021/cr400441m.
(246) Bonifacic, M.; Asmus, K. D. Adduct Formation and Absolute Rate Constants in the Displacement Reaction of Thiyl Radicals with Disulfides. *J. Phys. Chem.* **1984**, *88* (25), 6286–6290. https://doi.org/10.1021/j150669a046.
(247) Mardirossian, N.; Head-Gordon, M. Thirty Years of Density Functional Theory in Computational Chemistry: An Overview and Extensive Assessment of 200 Density Functionals. *Mol. Phys.* **2017**, *115* (19), 2315–2372. https://doi.org/10.1080/00268976.2017.1333644.
(248) Runge, E.; Gross, E. K. U. Density-Functional Theory for Time-Dependent Systems. *Phys. Rev. Lett.* **1984**, *52* (12), 997–1000. https://doi.org/10.1103/PhysRevLett.52.997.
(249) Marques, M. A. L.; Gross, E. K. U. Time-Dependent Density Functional Theory. *Annu. Rev. Phys. Chem.* **2004**, *55* (1), 427–455. https://doi.org/10.1146/annurev.physchem.55.091602.094449.
(250) Elliott, P.; Burke, K.; Furche, F. Excited States from Time-Dependent Density Functional Theory. *ArXivcond-Mat0703590* **2007**.
(251) Adamo, C.; Jacquemin, D. The Calculations of Excited-State Properties with Time-Dependent Density Functional Theory. *Chem. Soc. Rev.* **2013**, *42* (3), 845–856. https://doi.org/10.1039/C2CS35394F.
(252) Gaussian 16 | Gaussian.com https://gaussian.com/gaussian16/ (accessed Apr 14, 2020).
(253) Lee, C.; Yang, W.; Parr, R. G. Development of the Colle-Salvetti Correlation-Energy Formula into a Functional of the Electron Density. *Phys. Rev. B* **1988**, *37* (2), 785–789. https://doi.org/10.1103/PhysRevB.37.785.
(254) Sherrill, C. D. Basis Sets in Quantum Chemistry http://vergil.chemistry.gatech.edu/courses/chem6485/pdf/basis-sets.pdf.
(255) Cossi, M.; Rega, N.; Scalmani, G.; Barone, V. Energies, Structures, and Electronic Properties of Molecules in Solution with the C-PCM Solvation Model. *J. Comput. Chem.* **2003**, *24* (6), 669–681. https://doi.org/10.1002/jcc.10189.
(256) Barone, V.; Cossi, M. Quantum Calculation of Molecular Energies and Energy Gradients in Solution by a Conductor Solvent Model. *J. Phys. Chem. A* **1998**, *102* (11), 1995–2001. https://doi.org/10.1021/jp9716997.
(257) Grimme, S.; Ehrlich, S.; Goerigk, L. Effect of the Damping Function in Dispersion Corrected Density Functional Theory. *J. Comput. Chem.* **2011**, *32* (7), 1456–1465. https://doi.org/10.1002/jcc.21759.
(258) Yanai, T.; Tew, D. P.; Handy, N. C. A New Hybrid Exchange–Correlation Functional Using the Coulomb-Attenuating Method (CAM-B3LYP). *Chem. Phys. Lett.* **2004**, *393* (1), 51–57. https://doi.org/10.1016/j.cplett.2004.06.011.
(259) Chai, J.-D.; Head-Gordon, M. Long-Range Corrected Hybrid Density Functionals with Damped Atom–Atom Dispersion Corrections. *Phys. Chem. Chem. Phys.* **2008**, *10* (44), 6615–6620. https://doi.org/10.1039/B810189B.
(260) O'Boyle, N. M.; Tenderholt, A. L.; Langner, K. M. Cclib: A Library for Package-Independent Computational Chemistry Algorithms. *J. Comput. Chem.* **2008**, *29* (5), 839–845. https://doi.org/10.1002/jcc.20823.
(261) Alvarez, S. A Cartography of the van Der Waals Territories. *Dalton Trans.* **2013**, *42* (24), 8617–8636. https://doi.org/10.1039/C3DT50599E.

(262) Iwasaki, F.; Saito, Y. The Crystal Structure of the 1:1 Complex of s-Trinitrobenzene and s-Triaminobenzene. *Acta Crystallogr. B* **1970**, *26* (3), 251–260. https://doi.org/10.1107/S0567740870002224.
(263) Legault, C. Y. CYLview, 1.0b http://www.cylview.org/ (accessed Apr 14, 2020).
(264) Avogadro - Free cross-platform molecular editor https://avogadro.cc/ (accessed Apr 20, 2020).
(265) Mori, T.; Inoue, Y. Charge-Transfer Excitation: Unconventional yet Practical Means for Controlling Stereoselectivity in Asymmetric Photoreactions. *Chem. Soc. Rev.* **2013**, *42* (20), 8122–8133. https://doi.org/10.1039/C3CS60117J.
(266) Yang, M.; Cao, T.; Xu, T.; Liao, S. Visible-Light-Induced Deaminative Thioesterification of Amino Acid Derived Katritzky Salts via Electron Donor–Acceptor Complex Formation. *Org. Lett.* **2019**, *21* (21), 8673–8678. https://doi.org/10.1021/acs.orglett.9b03284.
(267) Piwinski, J. J.; Wong, J. K.; Chan, T. M.; Green, M. J.; Ganguly, A. K. Hydroxylated Metabolites of Loratadine: An Example of Conformational Diastereomers Due to Atropisomerism. *J. Org. Chem.* **1990**, *55* (10), 3341–3350. https://doi.org/10.1021/jo00297a065.
(268) Stone, E. A.; Cutrona, K. J.; Miller, S. J. Asymmetric Catalysis upon Helically Chiral Loratadine Analogues Unveils Enantiomer-Dependent Antihistamine Activity. *J. Am. Chem. Soc.* **2020**, *142* (29), 12690–12698. https://doi.org/10.1021/jacs.0c03904.
(269) Capacci, A. G.; Malinowski, J. T.; McAlpine, N. J.; Kuhne, J.; MacMillan, D. W. C. Direct, Enantioselective α-Alkylation of Aldehydes Using Simple Olefins. *Nat. Chem.* **2017**, *9* (11), 1073–1077. https://doi.org/10.1038/nchem.2797.
(270) Tedder, J. M.; Walton, J. C. The Importance of Polarity and Steric Effects in Determining the Rate and Orientation of Free Radical Addition to Olefins: Rules for Determining the Rate and Preferred Orientation. *Tetrahedron* **1980**, *36* (6), 701–707. https://doi.org/10.1016/S0040-4020(01)93680-4.
(271) Podyacheva, E.; Afanasyev, O. I.; Tsygankov, A. A.; Makarova, M.; Chusov, D. Hitchhiker's Guide to Reductive Amination. *Synthesis* **2019**, *51* (13), 2667–2677. https://doi.org/10.1055/s-0037-1611788.
(272) Brown, D. G.; Boström, J. Analysis of Past and Present Synthetic Methodologies on Medicinal Chemistry: Where Have All the New Reactions Gone? *J. Med. Chem.* **2016**, *59* (10), 4443–4458. https://doi.org/10.1021/acs.jmedchem.5b01409.
(273) Emerson, W. S.; Uraneck, C. A. Secondary and Tertiary Amines from Nitro Compounds. *J. Am. Chem. Soc.* **1941**, *63* (3), 749–751. https://doi.org/10.1021/ja01848a029.
(274) Gomez, S.; Peters, J. A.; Maschmeyer, T. The Reductive Amination of Aldehydes and Ketones and the Hydrogenation of Nitriles: Mechanistic Aspects and Selectivity Control. *Adv. Synth. Catal.* **2002**, *344* (10), 1037–1057. https://doi.org/10.1002/1615-4169(200212)344:10<1037::AID-ADSC1037>3.0.CO;2-3.
(275) BILLMAN, J. H.; TAI, K. M. Reduction of Schiff Bases. II. Benzhydrylamines and Structurally Related Compounds1a,b. *J. Org. Chem.* **1958**, *23* (4), 535–539. https://doi.org/10.1021/jo01098a009.
(276) Schellenberg, K. A. The Synthesis of Secondary and Tertiary Amines by Borohydride Reduction1. *J. Org. Chem.* **1963**, *28* (11), 3259–3261. https://doi.org/10.1021/jo01046a537.
(277) Borch, R. F.; Bernstein, M. D.; Durst, H. D. Cyanohydridoborate Anion as a Selective Reducing Agent. *J. Am. Chem. Soc.* **1971**, *93* (12), 2897–2904. https://doi.org/10.1021/ja00741a013.
(278) Mattson, R. J.; Pham, K. M.; Leuck, D. J.; Cowen, K. A. An Improved Method for Reductive Alkylation of Amines Using Titanium(IV) Isopropoxide and Sodium Cyanoborohydride. *J. Org. Chem.* **1990**, *55* (8), 2552–2554. https://doi.org/10.1021/jo00295a060.
(279) Yoon, N. M.; Kim, E. G.; Son, H. S.; Choi, J. Borohydride Exchange Resin, a New Reducing Agent for Reductive Amination. *Synth. Commun.* **1993**, *23* (11), 1595–1599. https://doi.org/10.1080/00397919308011255.
(280) Mićović, I. V.; Ivanović, M. D.; Piatak, D. M.; Bojić, V. D. A Simple Method for Preparation of Secondary Aromatic Amines. *Synthesis* **1991**, *1991* (11), 1043–1045. https://doi.org/10.1055/s-1991-26642.
(281) Bhattacharyya, S.; Chatterjee, A.; Duttachowdhury, S. K. Use of Zinc Borohydride in Reductive Amination: An Efficient and Mild Method for N-Methylation of Amines. *J. Chem. Soc. Perkin 1* **1994**, No. 1, 1–2. https://doi.org/10.1039/P19940000001.
(282) Pienemann, T.; Schäfer, H.-J. Reductive Amination of Ketones and Aldehydes at the Mercury-Cathode. *Synthesis* **1987**, *1987* (11), 1005–1007. https://doi.org/10.1055/s-1987-28148.

(283) Abdel-Magid, A. F.; Carson, K. G.; Harris, B. D.; Maryanoff, C. A.; Shah, R. D. Reductive Amination of Aldehydes and Ketones with Sodium Triacetoxyborohydride. Studies on Direct and Indirect Reductive Amination Procedures1. *J. Org. Chem.* **1996**, *61* (11), 3849–3862. https://doi.org/10.1021/jo960057x.
(284) Abdel-Magid, A. F.; Mehrman, S. J. A Review on the Use of Sodium Triacetoxyborohydride in the Reductive Amination of Ketones and Aldehydes. *Org. Process Res. Dev.* **2006**, *10* (5), 971–1031. https://doi.org/10.1021/op0601013.
(285) Guo, X.; Okamoto, Y.; Schreier, M. R.; Ward, T. R.; Wenger, O. S. Reductive Amination and Enantioselective Amine Synthesis by Photoredox Catalysis: Reductive Amination and Enantioselective Amine Synthesis by Photoredox Catalysis. *Eur. J. Org. Chem.* **2020**, *2020* (10), 1288–1293. https://doi.org/10.1002/ejoc.201900777.
(286) Guo, X.; Wenger, O. S. Reductive Amination by Photoredox Catalysis and Polarity-Matched Hydrogen Atom Transfer. *Angew. Chem. Int. Ed.* **2018**, *57* (9), 2469–2473. https://doi.org/10.1002/anie.201711467.
(287) van As, D. J.; Connell, T. U.; Brzozowski, M.; Scully, A. D.; Polyzos, A. Photocatalytic and Chemoselective Transfer Hydrogenation of Diarylimines in Batch and Continuous Flow. *Org. Lett.* **2018**, *20* (4), 905–908. https://doi.org/10.1021/acs.orglett.7b03565.
(288) Wang, R.; Ma, M.; Gong, X.; Panetti, G. B.; Fan, X.; Walsh, P. J. Visible-Light-Mediated Umpolung Reactivity of Imines: Ketimine Reductions with Cy2NMe and Water. *Org. Lett.* **2018**, *20* (8), 2433–2436. https://doi.org/10.1021/acs.orglett.8b00778.
(289) Xi, Z.-W.; Yang, L.; Wang, D.-Y.; Pu, C.-D.; Shen, Y.-M.; Wu, C.-D.; Peng, X.-G. Visible-Light Photocatalytic Synthesis of Amines from Imines via Transfer Hydrogenation Using Quantum Dots as Catalysts. *J. Org. Chem.* **2018**, *83* (19), 11886–11895. https://doi.org/10.1021/acs.joc.8b01651.
(290) Rong, J.; Seeberger, P. H.; Gilmore, K. Chemoselective Photoredox Synthesis of Unprotected Primary Amines Using Ammonia. *Org. Lett.* **2018**, *20* (13), 4081–4085. https://doi.org/10.1021/acs.orglett.8b01637.
(291) Guo, X.; Okamoto, Y.; Schreier, M. R.; Ward, T. R.; Wenger, O. S. Enantioselective Synthesis of Amines by Combining Photoredox and Enzymatic Catalysis in a Cyclic Reaction Network. *Chem. Sci.* **2018**, *9* (22), 5052–5056. https://doi.org/10.1039/C8SC01561A.
(292) 2,6-<WBR>Dimethylbenzenethiol 306940 https://www.sigmaaldrich.com/catalog/product/aldrich/306940 (accessed Jul 20, 2020).
(293) Morse, P. D.; Nicewicz, D. A. Divergent Regioselectivity in Photoredox-Catalyzed Hydrofunctionalization Reactions of Unsaturated Amides and Thioamides. *Chem. Sci.* **2014**, *6* (1), 270–274. https://doi.org/10.1039/C4SC02331E.
(294) Huang, W.; Chen, W.; Wang, G.; Li, J.; Cheng, X.; Li, G. Thiyl-Radical-Catalyzed Photoreductive Hydrodifluoroacetamidation of Alkenes with Hantzsch Ester as a Multifunctional Reagent. *ACS Catal.* **2016**, *6* (11), 7471–7474. https://doi.org/10.1021/acscatal.6b02420.
(295) 1,4-Cyclohexadiene 125415 https://www.sigmaaldrich.com/catalog/product/aldrich/125415 (accessed Jul 20, 2020).
(296) Middleton, D. S.; MacKenzie, A. R.; Newman, S. D.; Corless, M.; Warren, A.; Marchington, A. P.; Jones, B. Structure–Activity Relationships of 1-Alkyl-5-(3,4-Dichlorophenyl)-5-{2-[3-(Substituted)-1-Azetidinyl]-Ethyl}-2-Piperidones. Part 2: Improving Oral Absorption. *Bioorg. Med. Chem. Lett.* **2005**, *15* (17), 3957–3961. https://doi.org/10.1016/j.bmcl.2005.05.134.
(297) Tran, J. A.; Chen, C. W.; Jiang, W.; Tucci, F. C.; Fleck, B. A.; Marinkovic, D.; Arellano, M.; Chen, C. Pyrrolidines as Potent Functional Agonists of the Human Melanocortin-4 Receptor. *Bioorg. Med. Chem. Lett.* **2007**, *17* (18), 5165–5170. https://doi.org/10.1016/j.bmcl.2007.06.088.
(298) Zhang, X.; Hufnagel, H.; Hou, C.; Opas, E.; McKenney, S.; Crysler, C.; O'Neill, J.; Johnson, D.; Sui, Z. Design, Synthesis and SAR of Indazole and Benzoisoxazole Containing 4-Azetidinyl-1-Aryl-Cyclohexanes as CCR2 Antagonists. *Bioorg. Med. Chem. Lett.* **2011**, *21* (20), 6042–6048. https://doi.org/10.1016/j.bmcl.2011.08.074.
(299) Choi, J.-S.; Hwang, H.; Kim, S.-W.; Lee, B. I.; Lee, J.; Song, H.-J.; Koh, J. S.; Kim, J.-H.; Lee, P. H. Highly Potent and Selective Pyrazolylpyrimidines as Syk Kinase Inhibitors. *Bioorg. Med. Chem. Lett.* **2015**, *25* (20), 4441–4446. https://doi.org/10.1016/j.bmcl.2015.09.011.
(300) Sim, Y. E.; Nwajiobi, O.; Mahesh, S.; Cohen, R. D.; Reibarkh, M. Y.; Raj, M. Secondary Amine Selective Petasis (SASP) Bioconjugation. *Chem. Sci.* **2019**, *11* (1), 53–61. https://doi.org/10.1039/C9SC04697F.

(301) Liu, J.; Fitzgerald, A. E.; Mani, N. S. Reductive Amination by Continuous-Flow Hydrogenation: Direct and Scalable Synthesis of a Benzylpiperazine. *Synthesis* **2012**, *44* (15), 2469–2473. https://doi.org/10.1055/s-0032-1316550.
(302) Loh, Y. Y.; Nagao, K.; Hoover, A. J.; Hesk, D.; Rivera, N. R.; Colletti, S. L.; Davies, I. W.; MacMillan, D. W. C. Photoredox-Catalyzed Deuteration and Tritiation of Pharmaceutical Compounds. *Science* **2017**, *358* (6367), 1182–1187. https://doi.org/10.1126/science.aap9674.
(303) Koszelewski, D.; Lavandera, I.; Clay, D.; Guebitz, G. M.; Rozzell, D.; Kroutil, W. Formal Asymmetric Biocatalytic Reductive Amination. *Angew. Chem. Int. Ed.* **2008**, *47* (48), 9337–9340. https://doi.org/10.1002/anie.200803763.
(304) Huang, H.; Liu, X.; Zhou, L.; Chang, M.; Zhang, X. Direct Asymmetric Reductive Amination for the Synthesis of Chiral β-Arylamines. *Angew. Chem. Int. Ed.* **2016**, *55* (17), 5309–5312. https://doi.org/10.1002/anie.201601025.
(305) Haque, M. B.; Roberts, B. P. Enantioselective Radical-Chain Hydrosilylation of Prochiral Alkenes Using Optically Active Thiol Catalysts. *Tetrahedron Lett.* **1996**, *37* (50), 9123–9126. https://doi.org/10.1016/S0040-4039(96)90165-3.
(306) Hashimoto, T.; Kawamata, Y.; Maruoka, K. An Organic Thiyl Radical Catalyst for Enantioselective Cyclization. *Nat. Chem.* **2014**, *6* (8), 702–705. https://doi.org/10.1038/nchem.1998.
(307) Davies, J.; Booth, S. G.; Essafi, S.; Dryfe, R. A. W.; Leonori, D. Visible-Light-Mediated Generation of Nitrogen-Centered Radicals: Metal-Free Hydroimination and Iminohydroxylation Cyclization Reactions. *Angew. Chem. Int. Ed.* **2015**, *54* (47), 14017–14021. https://doi.org/10.1002/anie.201507641.
(308) Fulmer, G. R.; Miller, A. J. M.; Sherden, N. H.; Gottlieb, H. E.; Nudelman, A.; Stoltz, B. M.; Bercaw, J. E.; Goldberg, K. I. NMR Chemical Shifts of Trace Impurities: Common Laboratory Solvents, Organics, and Gases in Deuterated Solvents Relevant to the Organometallic Chemist. *Organometallics* **2010**, *29* (9), 2176–2179. https://doi.org/10.1021/om100106e.
(309) Skvorcova, M.; Jirgensons, A. Amide-Group-Directed Protonolysis of Cyclopropane: An Approach to 2,2-Disubstituted Pyrrolidines. *Org. Lett.* **2017**, *19* (10), 2478–2481. https://doi.org/10.1021/acs.orglett.7b00584.
(310) Dias, D. A.; Kerr, M. A. Domino Synthesis of Bridged Bicyclic Tetrahydro-1,2-Oxazines: Access to Stereodefined 4-Aminocyclohexanols. *Org. Lett.* **2009**, *11* (16), 3694–3697. https://doi.org/10.1021/ol901454y.
(311) Prieto, L.; Sánchez-Díez, E.; Uria, U.; Reyes, E.; Carrillo, L.; Vicario, J. L. Catalytic Generation of Donor-Acceptor Cyclopropanes under N-Heterocyclic Carbene Activation and Their Stereoselective Reaction with Alkylideneoxindoles. *Adv. Synth. Catal.* **2017**, *359* (10), 1678–1683. https://doi.org/10.1002/adsc.201700198.
(312) Sherry, B. D.; Fürstner, A. Iron-Catalyzed Addition of Grignard Reagents to Activated Vinyl Cyclopropanes. *Chem. Commun.* **2009**, No. 46, 7116–7118. https://doi.org/10.1039/B918818E.
(313) Trowbridge, A.; Reich, D.; Gaunt, M. J. Multicomponent Synthesis of Tertiary Alkylamines by Photocatalytic Olefin-Hydroaminoalkylation. *Nature* **2018**, *561* (7724), 522–527. https://doi.org/10.1038/s41586-018-0537-9.
(314) Wang, L.; Prabhudas, B.; Clive, D. L. J. Formation of Carbocycles by Intramolecular Conjugate Displacement: Scope and Mechanistic Insights. *J. Am. Chem. Soc.* **2009**, *131* (16), 6003–6012. https://doi.org/10.1021/ja900857h.
(315) Mizuta, T.; Sakaguchi, S.; Ishii, Y. Catalytic Reductive Alkylation of Secondary Amine with Aldehyde and Silane by an Iridium Compound. *J. Org. Chem.* **2005**, *70* (6), 2195–2199. https://doi.org/10.1021/jo0481708.
(316) Chen, W.-X.; Zhang, C.-Y.; Lu, J.-M. Highly Efficient Amination in Neat Water of Benzyl Chlorides with Dialkylformamides Catalysed by N-Heterocyclic Carbene-Palladium(II)-1-Methylimidazole Complex. *J. Chem. Res.* **2013**, *37* (10), 611–614. https://doi.org/10.3184/174751913X13787959859344.
(317) Zishiri, V. K.; Hunter, R.; Smith, P. J.; Taylor, D.; Summers, R.; Kirk, K.; Martin, R. E.; Egan, T. J. A Series of Structurally Simple Chloroquine Chemosensitizing Dibemethin Derivatives That Inhibit Chloroquine Transport by PfCRT. *Eur. J. Med. Chem.* **2011**, *46* (5), 1729–1742. https://doi.org/10.1016/j.ejmech.2011.02.026.
(318) Gupta, S.; Sureshbabu, P.; Singh, A. K.; Sabiah, S.; Kandasamy, J. Deoxygenation of Tertiary Amine N-Oxides under Metal Free Condition Using Phenylboronic Acid. *Tetrahedron Lett.* **2017**, *58* (10), 909–913. https://doi.org/10.1016/j.tetlet.2017.01.051.

(319) Ting, P. C.; Lee, J. F.; Anthes, J. C.; Shih, N.-Y.; Piwinski, J. J. Synthesis of Substituted 4(Z)-(Methoxyimino)Pentyl-1-Piperidines as Dual NK1/NK2 Inhibitors. *Bioorg. Med. Chem. Lett.* **2001**, *11* (4), 491–494. https://doi.org/10.1016/S0960-894X(00)00702-2.

(320) Lee, C.; Yang, W.; Parr, R. G. Development of the Colle-Salvetti Correlation-Energy Formula into a Functional of the Electron Density. *Phys. Rev. B* **1988**, *37* (2), 785–789. https://doi.org/10.1103/PhysRevB.37.785.

(321) Becke, A. D. Density-functional Thermochemistry. III. The Role of Exact Exchange. *J. Chem. Phys.* **1993**, *98* (7), 5648–5652. https://doi.org/10.1063/1.464913.

(322) Barone, V.; Cossi, M. Quantum Calculation of Molecular Energies and Energy Gradients in Solution by a Conductor Solvent Model. *J. Phys. Chem. A* **1998**, *102* (11), 1995–2001. https://doi.org/10.1021/jp9716997.

(323) Cossi, M.; Rega, N.; Scalmani, G.; Barone, V. Energies, Structures, and Electronic Properties of Molecules in Solution with the C-PCM Solvation Model. *J. Comput. Chem.* **2003**, *24* (6), 669–681. https://doi.org/10.1002/jcc.10189.

(324) Grimme, S.; Ehrlich, S.; Goerigk, L. Effect of the Damping Function in Dispersion Corrected Density Functional Theory. *J. Comput. Chem.* **2011**, *32* (7), 1456–1465. https://doi.org/10.1002/jcc.21759.

(325) CYLview Visualization Software / (accessed Jul 22, 2020).

(326) Yanai, T.; Tew, D. P.; Handy, N. C. A New Hybrid Exchange–Correlation Functional Using the Coulomb-Attenuating Method (CAM-B3LYP). *Chem. Phys. Lett.* **2004**, *393* (1), 51–57. https://doi.org/10.1016/j.cplett.2004.06.011.

(327) Avogadro - Free cross-platform molecular editor https://avogadro.cc/ (accessed Jul 22, 2020).

(328) O'Boyle, N. M.; Tenderholt, A. L.; Langner, K. M. Cclib: A Library for Package-Independent Computational Chemistry Algorithms. *J. Comput. Chem.* **2008**, *29* (5), 839–845. https://doi.org/10.1002/jcc.20823.

(329) Chai, J.-D.; Head-Gordon, M. Long-Range Corrected Hybrid Density Functionals with Damped Atom–Atom Dispersion Corrections. *Phys. Chem. Chem. Phys.* **2008**, *10* (44), 6615–6620. https://doi.org/10.1039/B810189B.

Appendices

A.1. ^{1}H and ^{13}C NMR Spectra

A.1.1. Charge-Transfer Cyclization

2-(3-Cyano-1-(dibenzylamino)propyl)cyclopentane-1-carbonitrile (281)

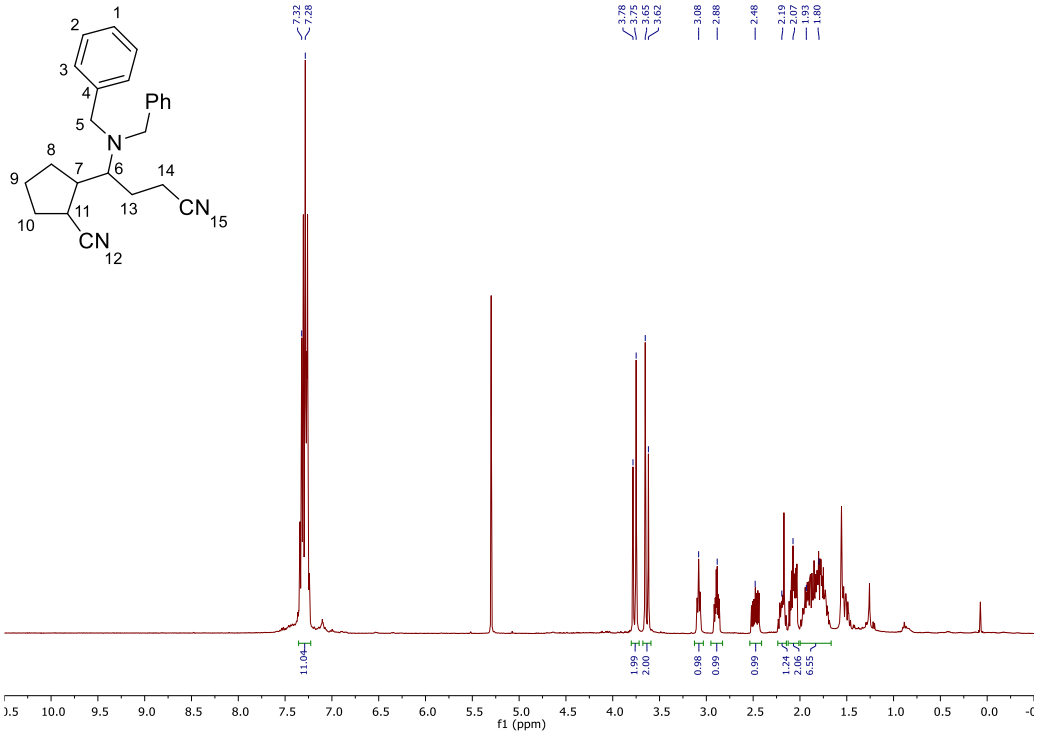

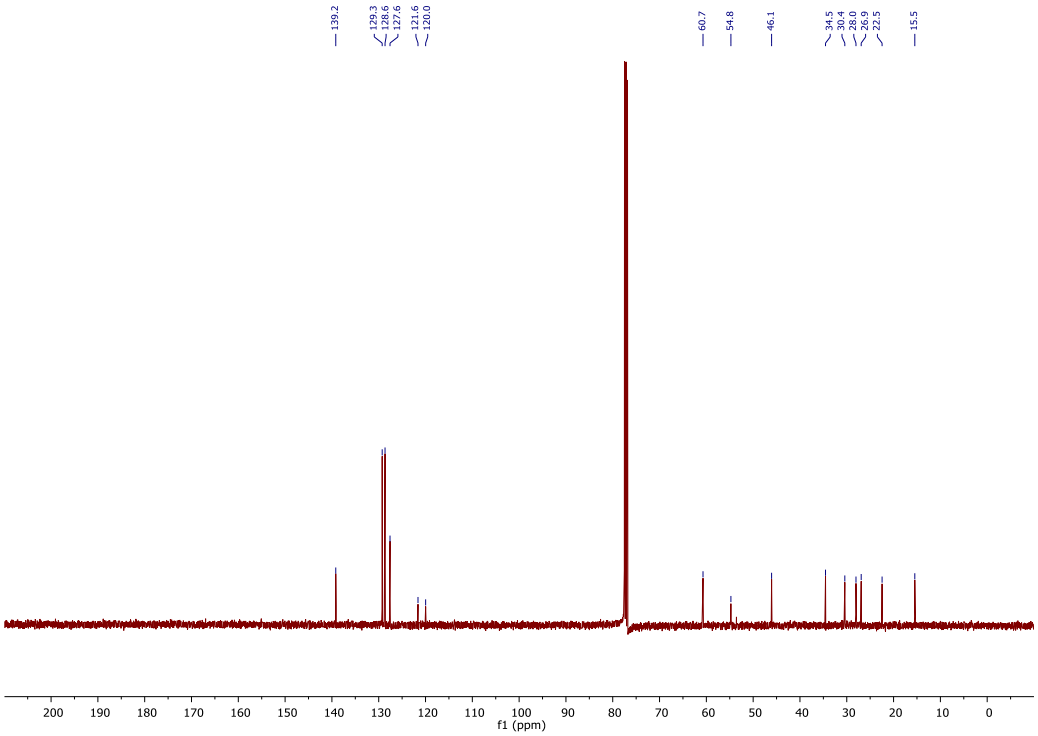

4-Cyclopropyl-4-(dibenzylamino)butanenitrile (280)

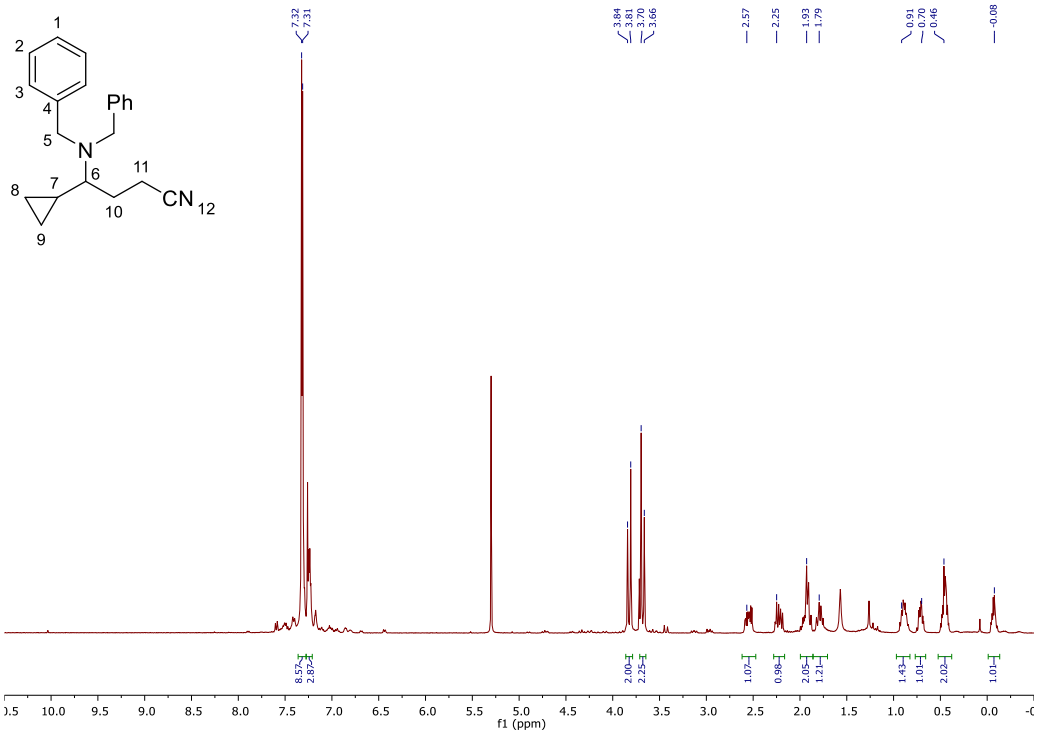

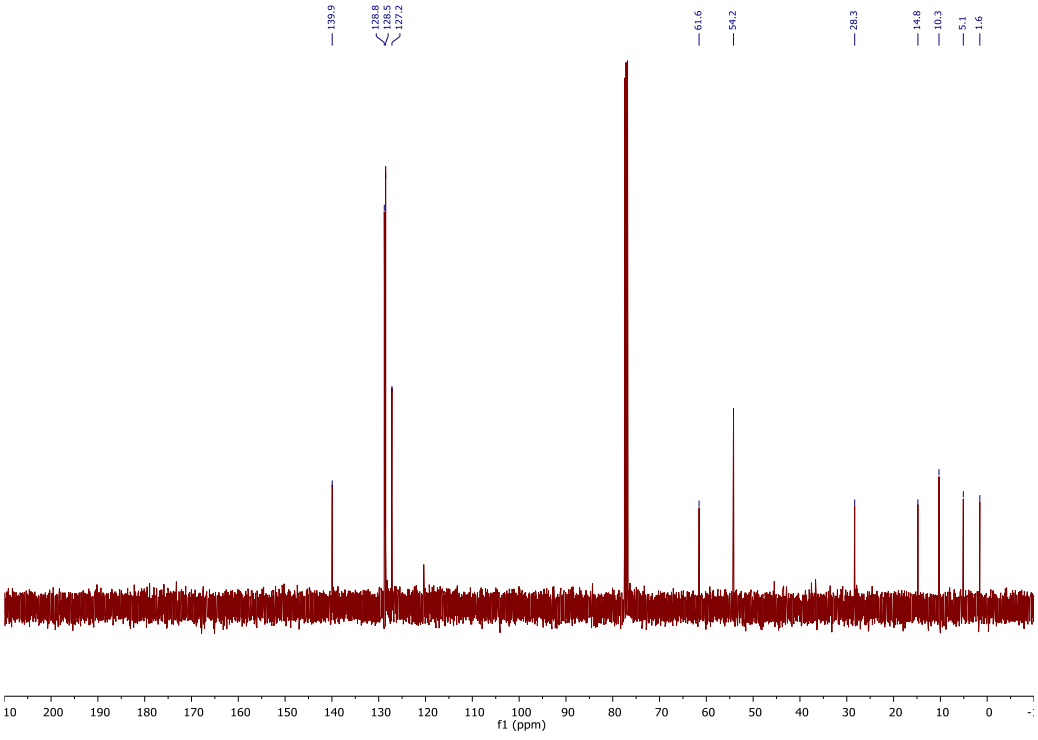

(2,2-Dimethylcyclopropyl)methanol (293)

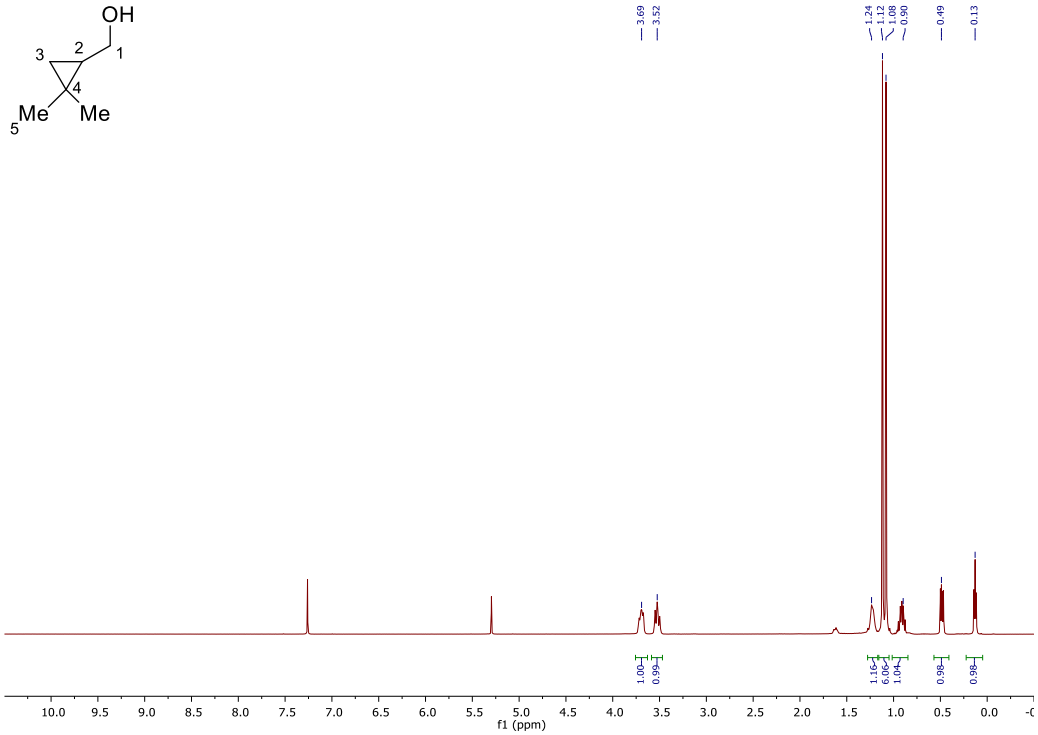

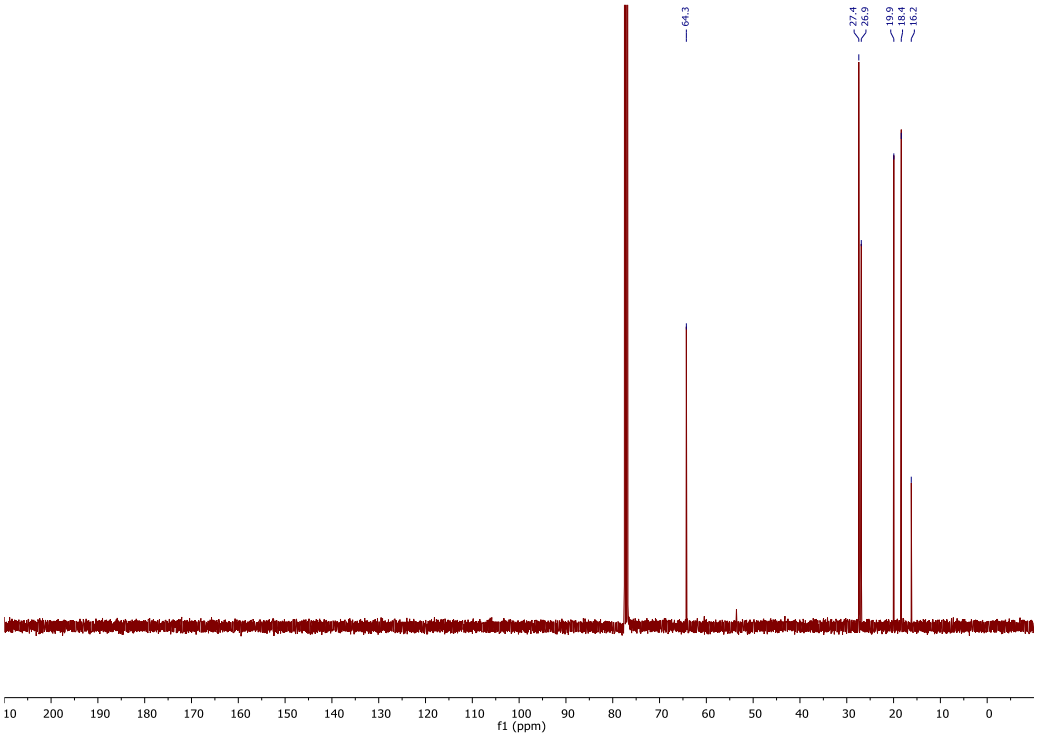

2,2-Dimethylcyclopropane-1-carbaldehyde (294)

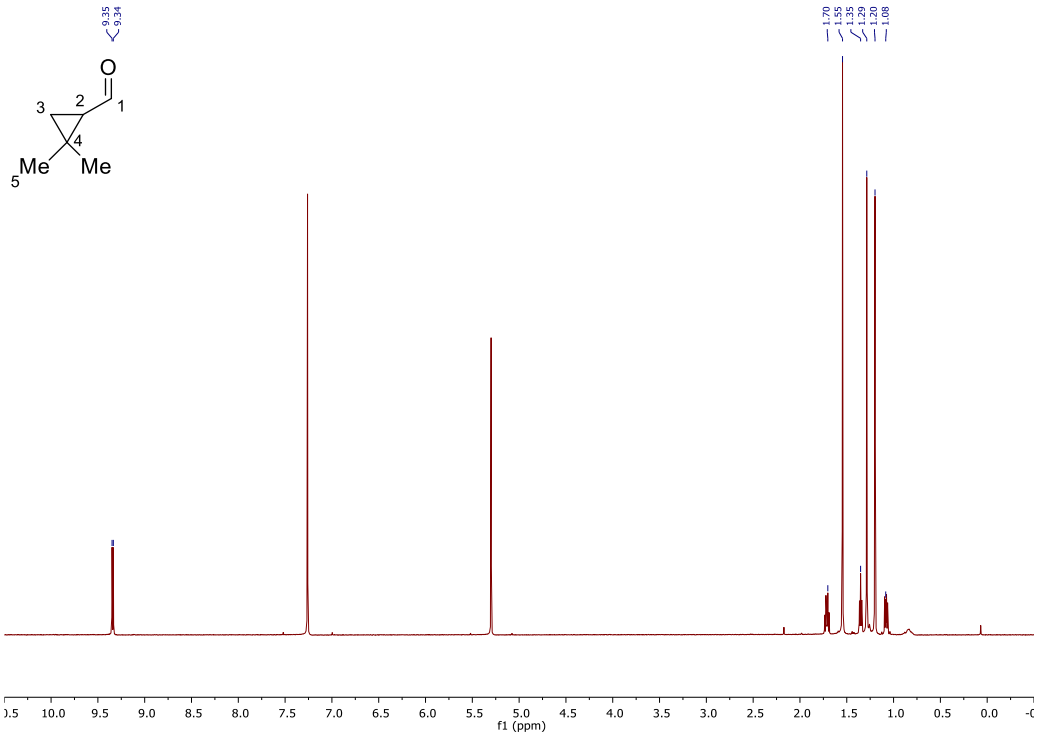

Dimethyl 2-formylcyclopropane-1,1-dicarboxylate (298)

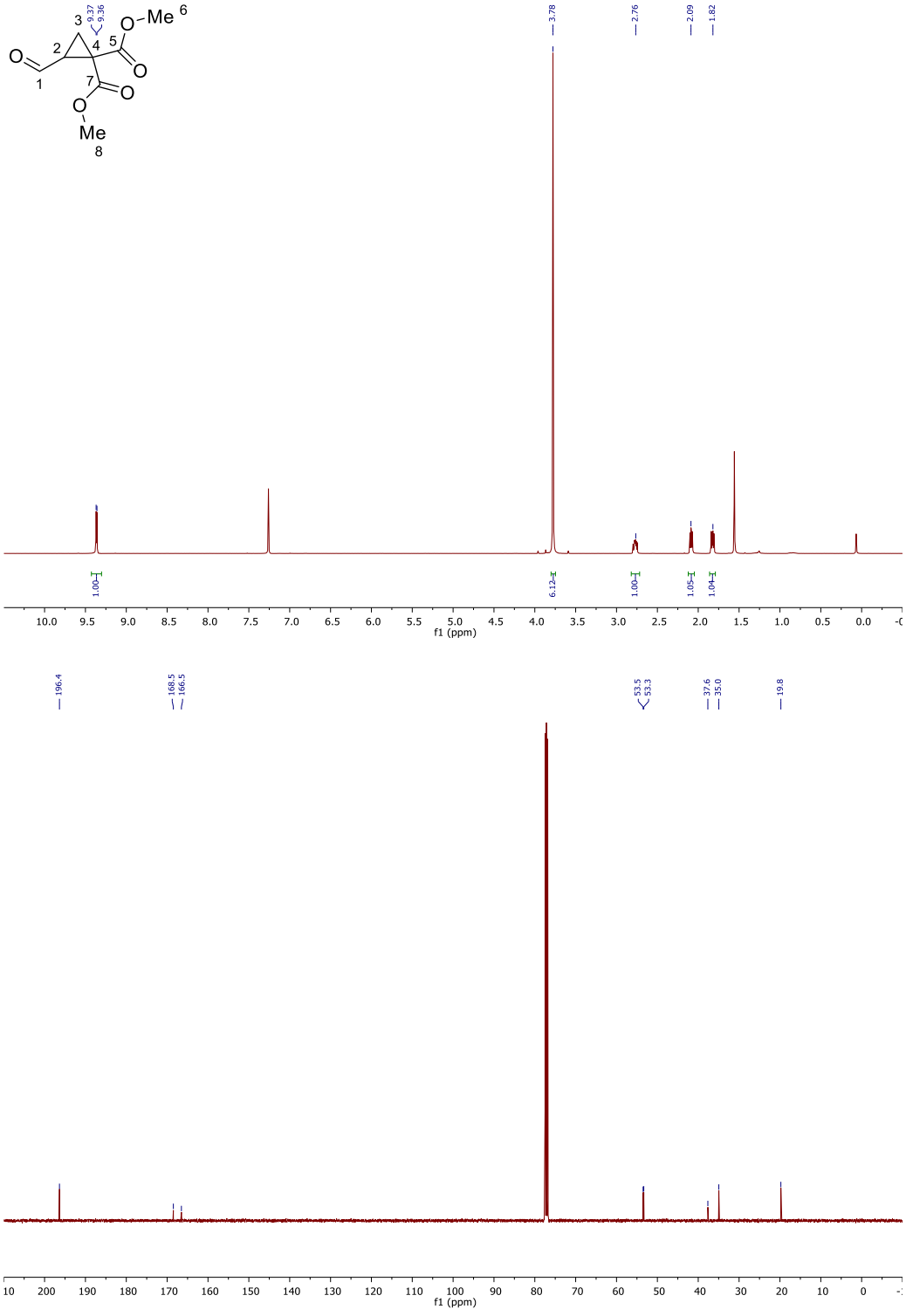

Bis(2-methoxyethyl) 2,6-dimethyl-1,4-dihydropyridine-3,5-dicarboxylate (314)

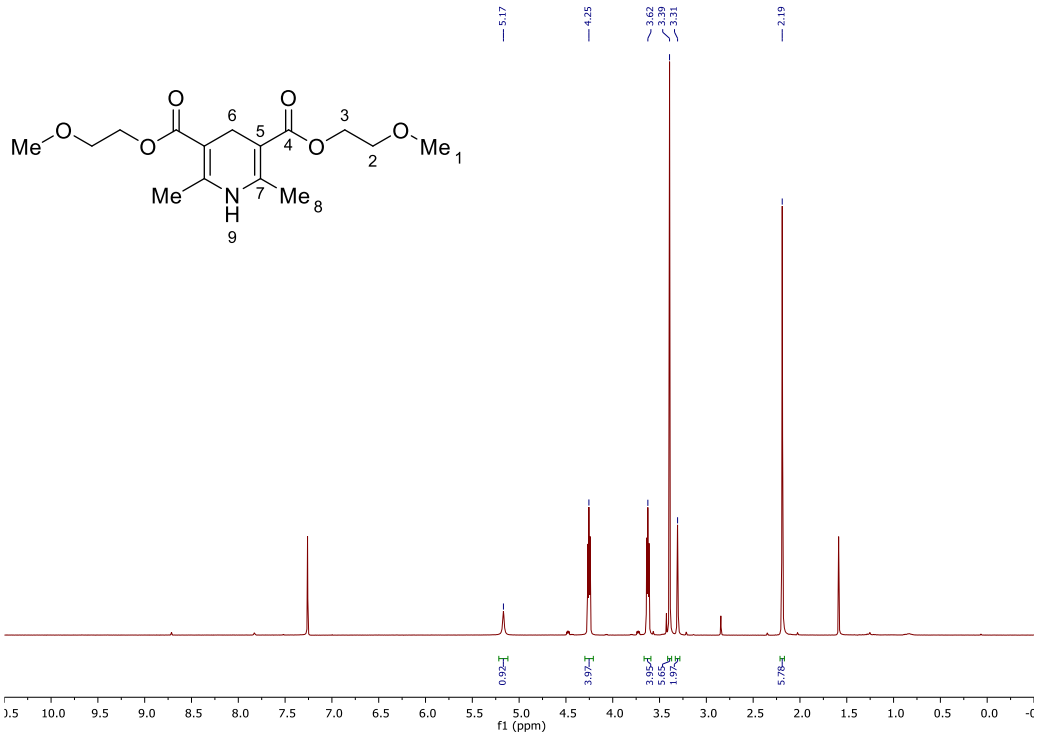

Dimethyl 4-((4-phenylpiperidin-1-yl)methyl)spiro[4.4]nonane-2,2-dicarboxylate (301)

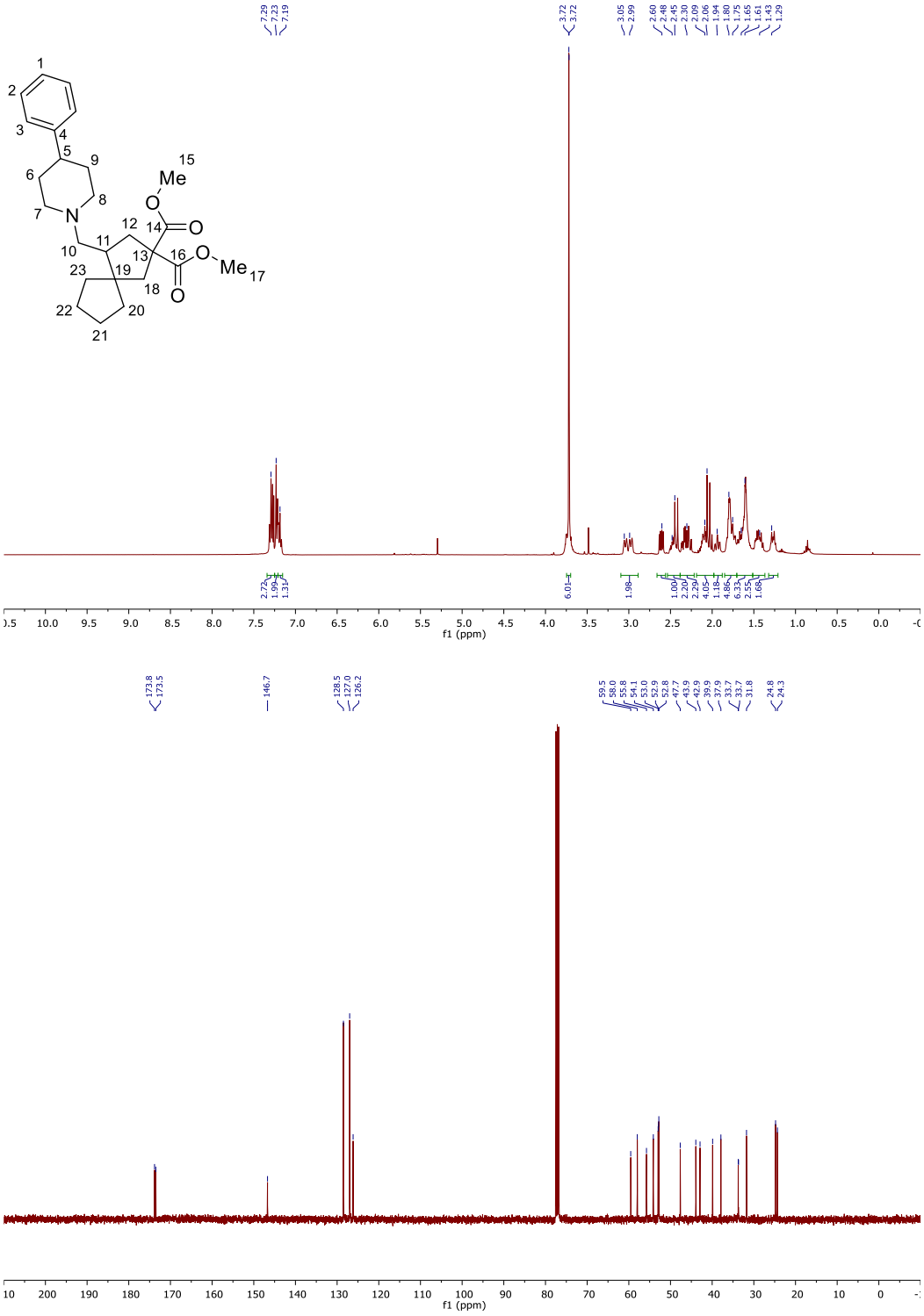

Dimethyl 2-(3-(4-phenylpiperidin-1-yl)propyl)malonate (302)

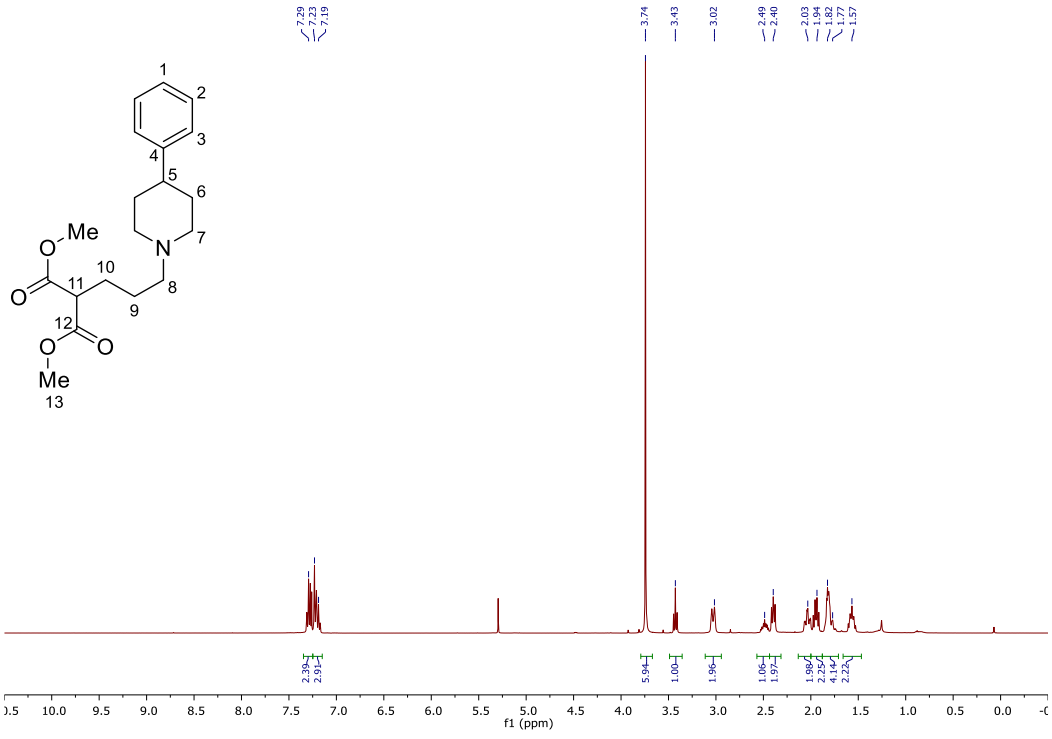

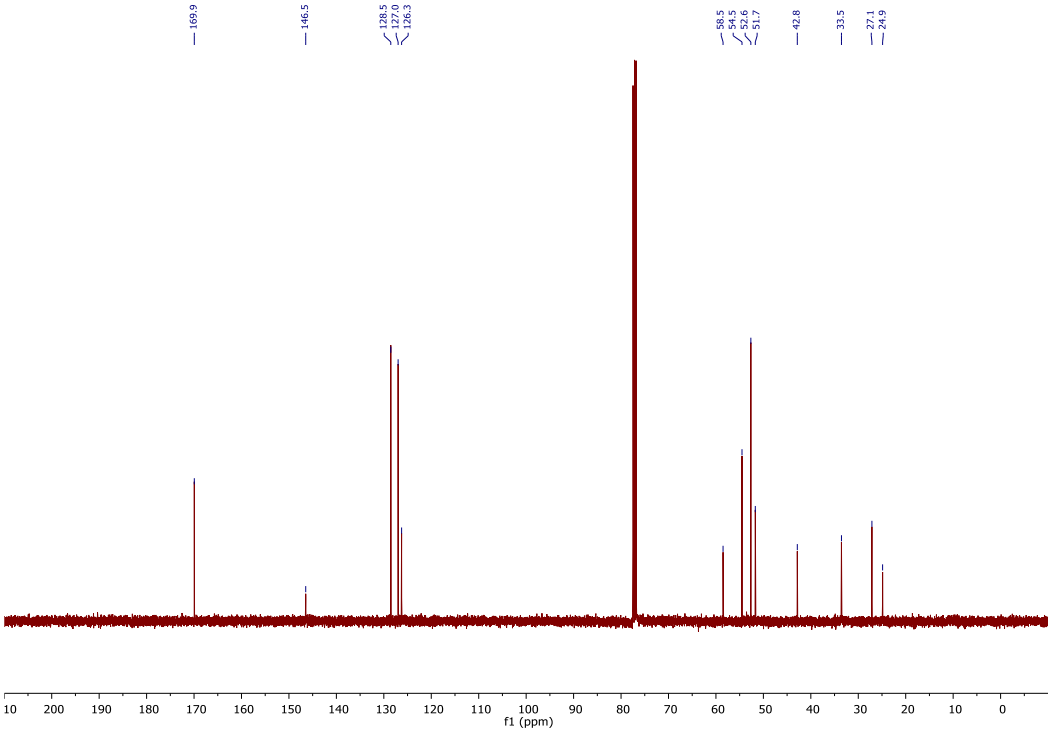

Dimethyl 3-(4-bromophenyl)-4-((dimethylamino)methyl)cyclopentane-1,1-dicarboxylate (315)

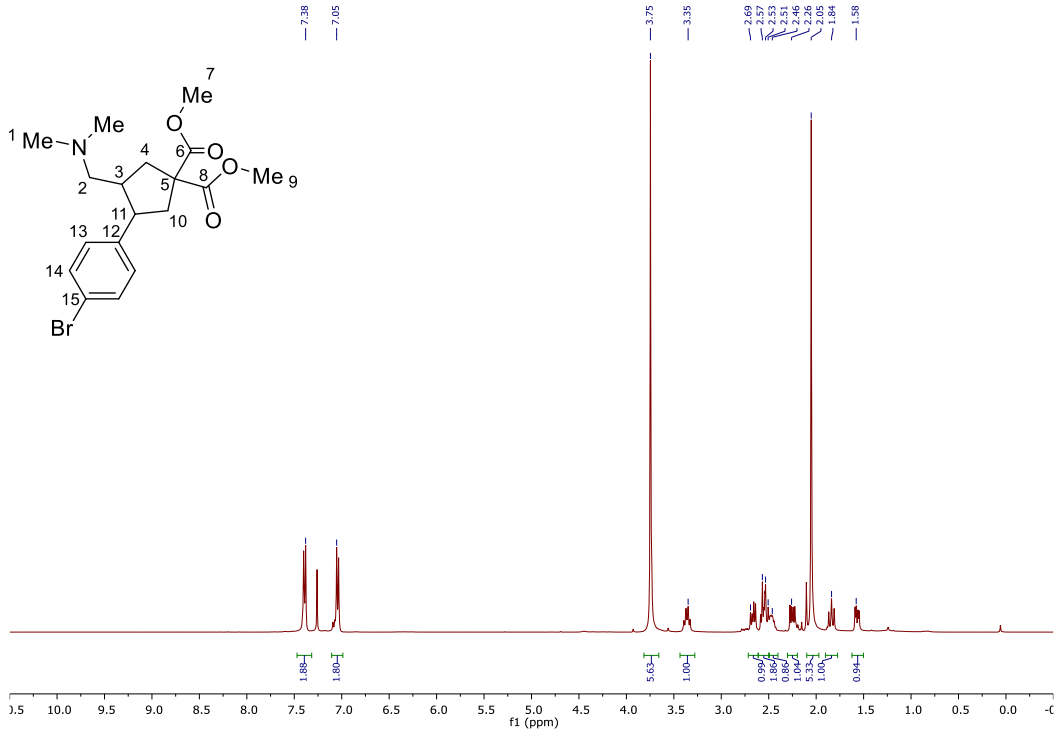

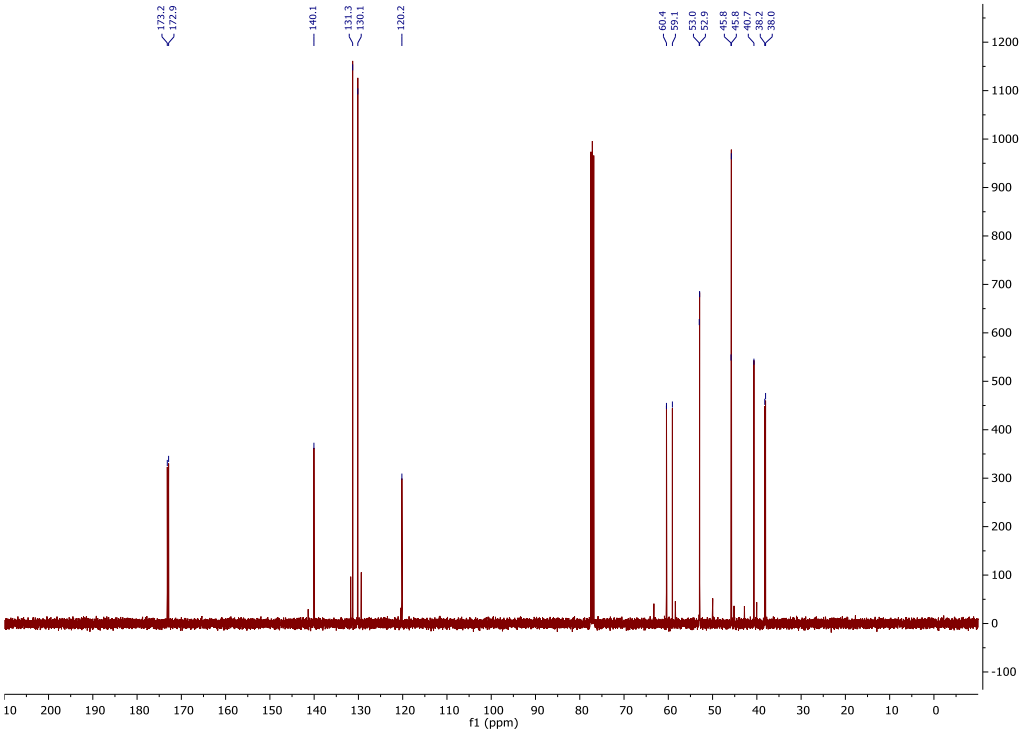

NOESY

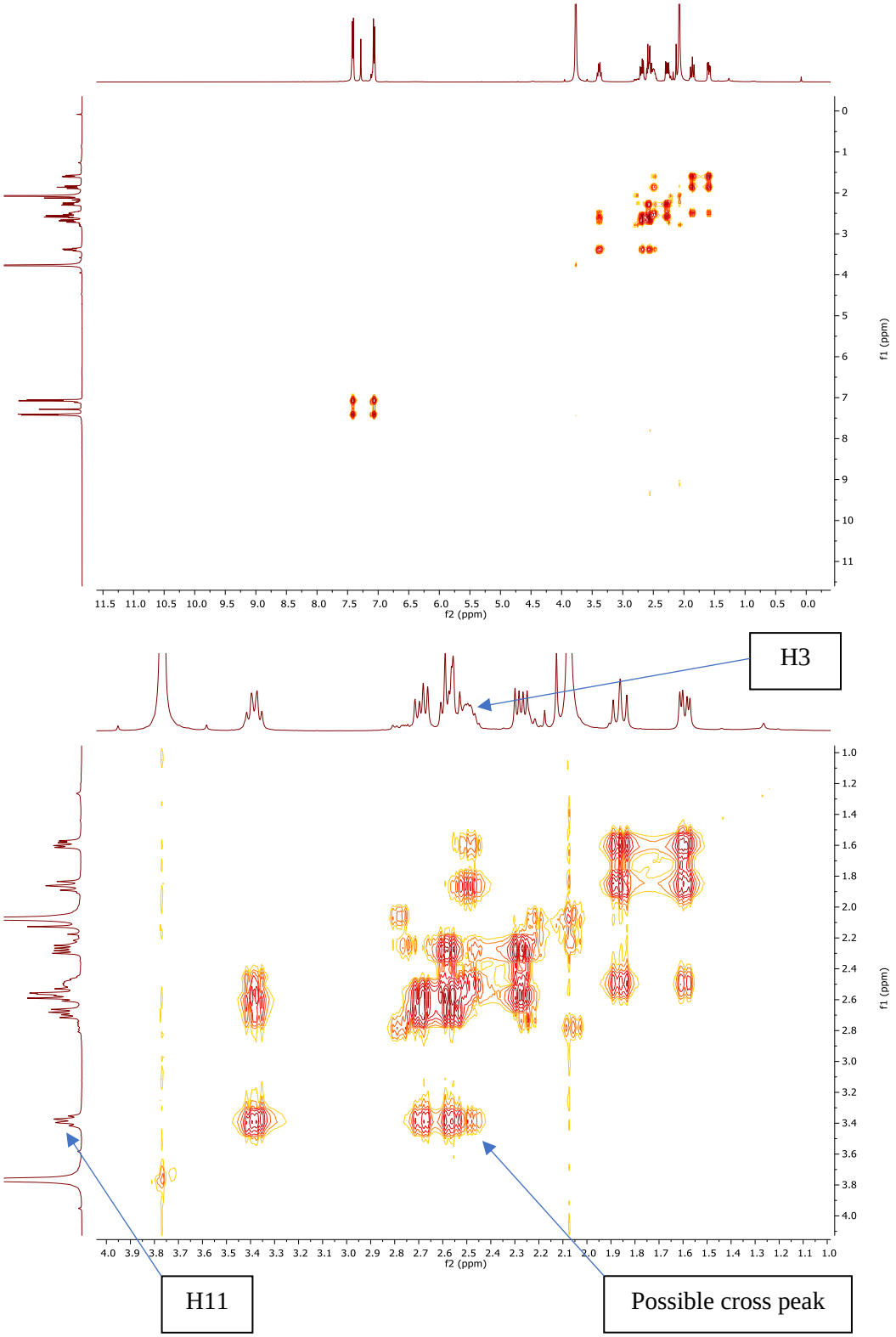

Dimethyl 3-formyl-4-phenylcyclopentane-1,1-dicarboxylate (331)

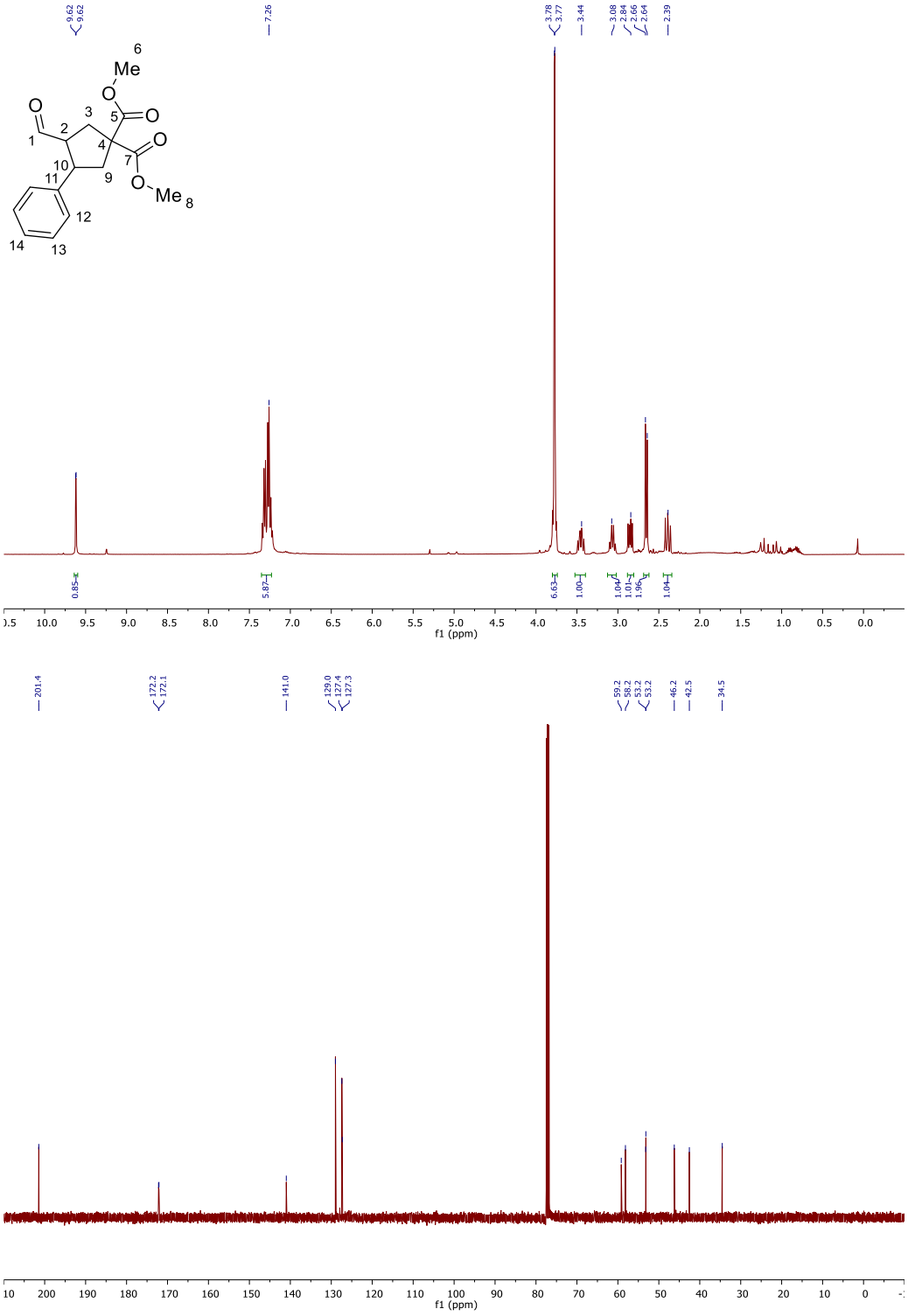

Dimethyl 2-(((2,6-dimethylphenyl)thio)(piperidin-1-yl)methyl)cyclopropane-1,1-dicarboxylate (342)

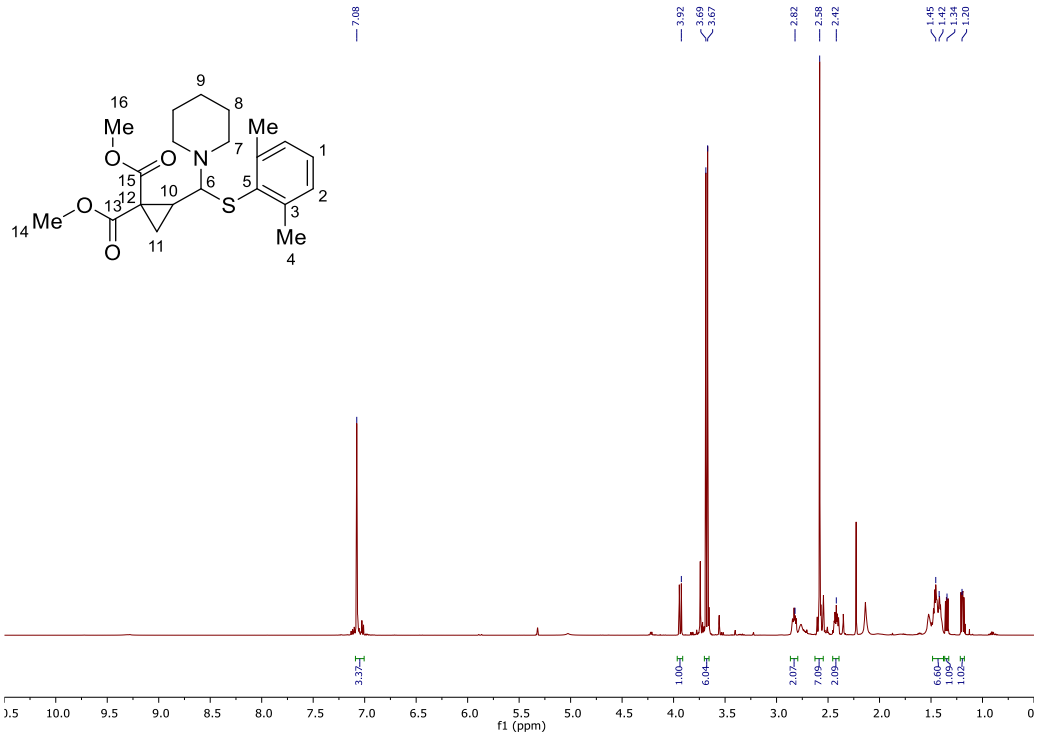

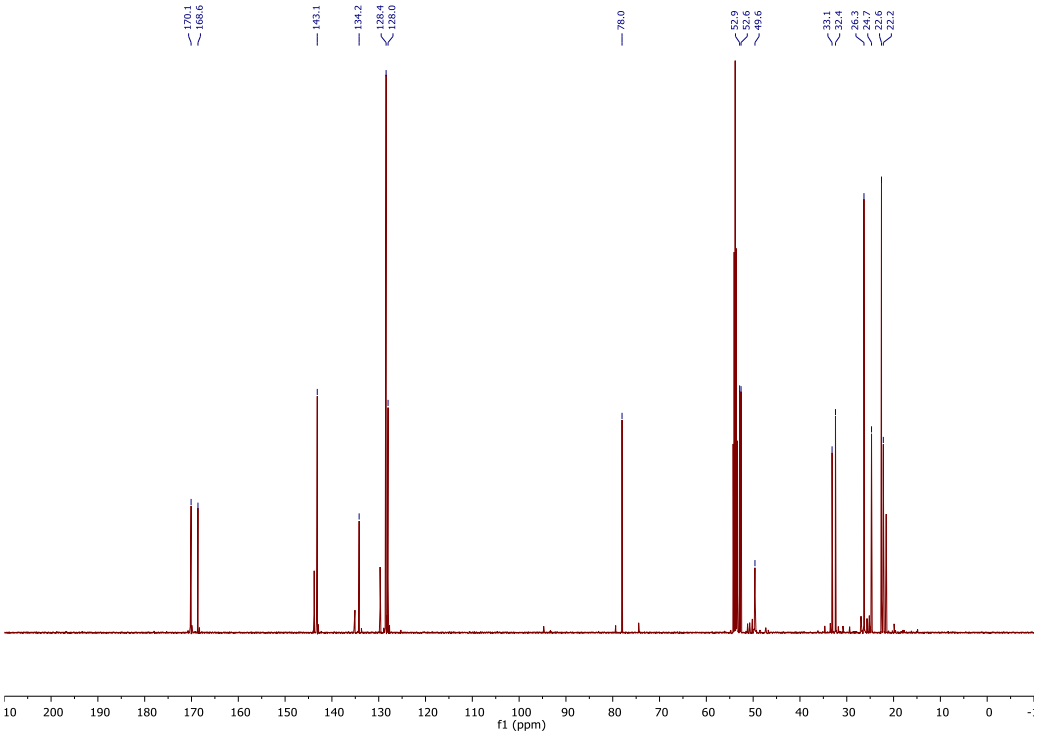

Dimethyl 2-(3-oxopropyl)malonate (338)

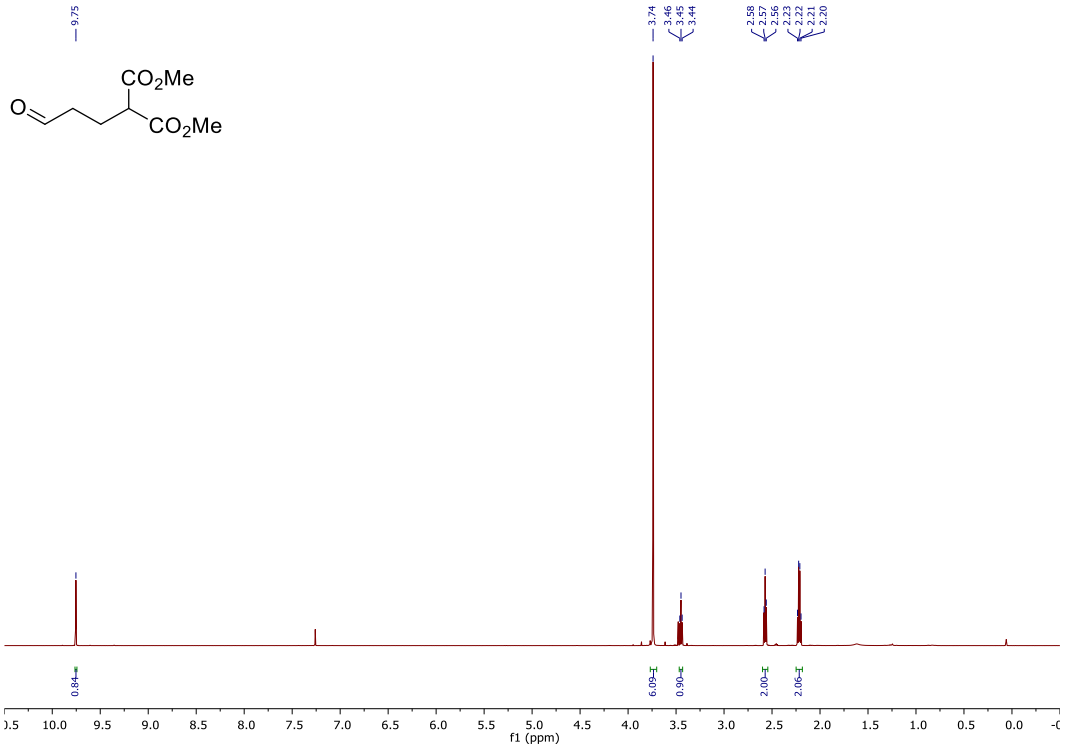

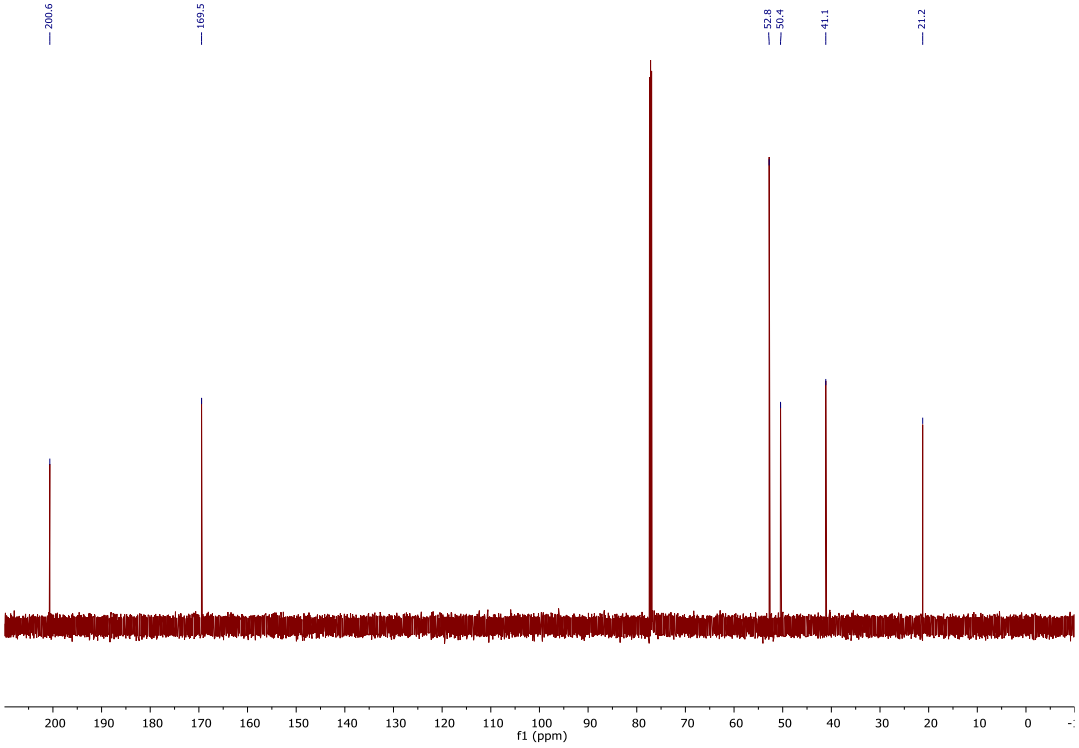

2,6-Dimethylbenzenethiol (340)

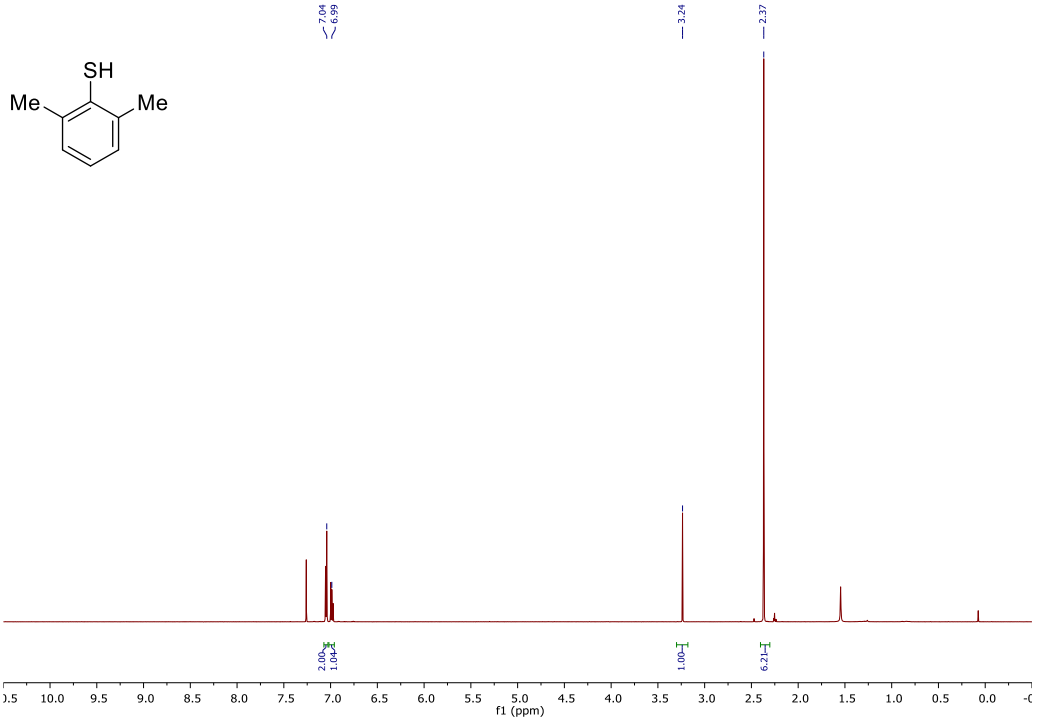

1-(2,6-Dimethylcyclohexa-1,3-dien-1-yl)-2-(2,6-dimethylphenyl)disulfane (345)

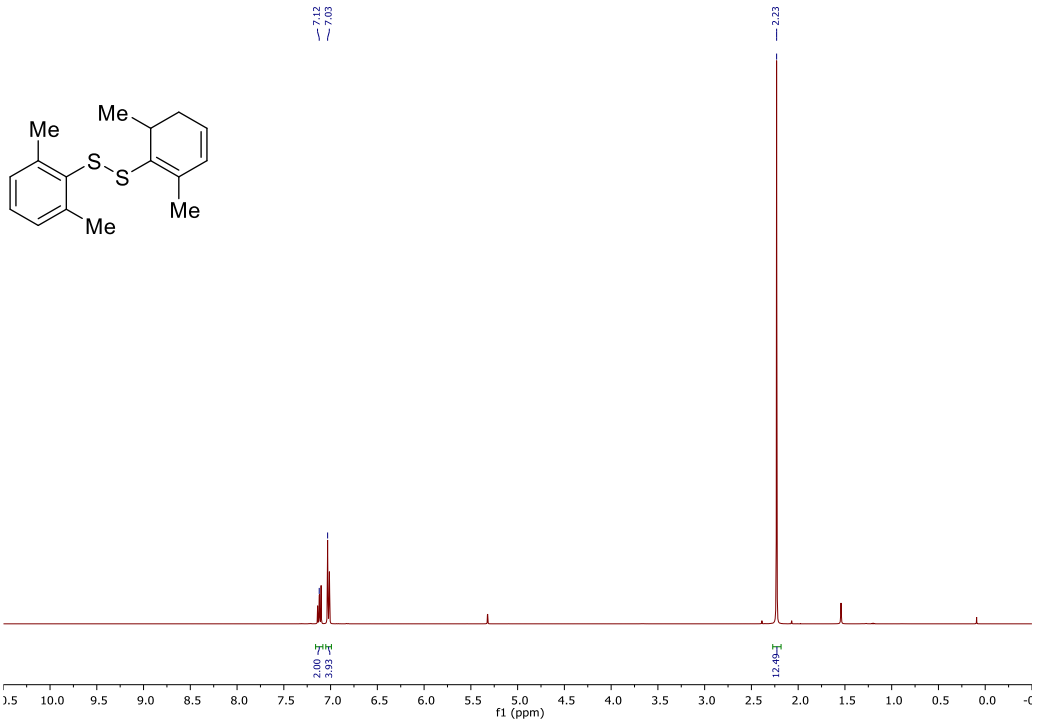

Dimethyl 4-((4-cyanopiperidin-1-yl)methyl)spiro[4.4]nonane-2,2-dicarboxylate (379)

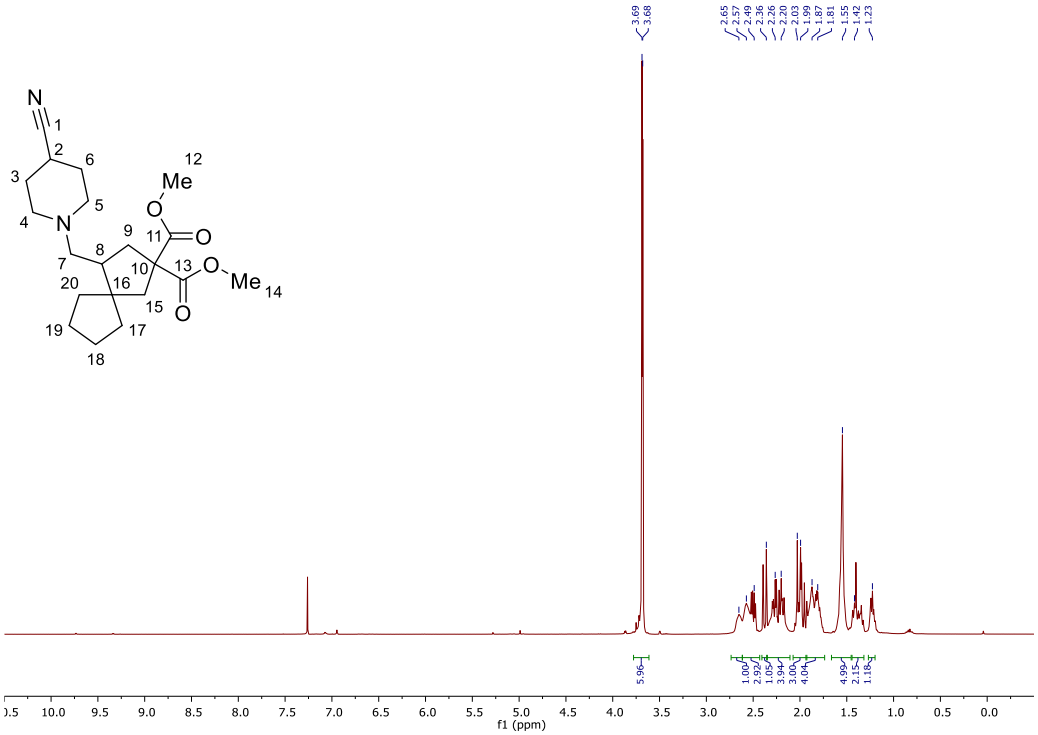

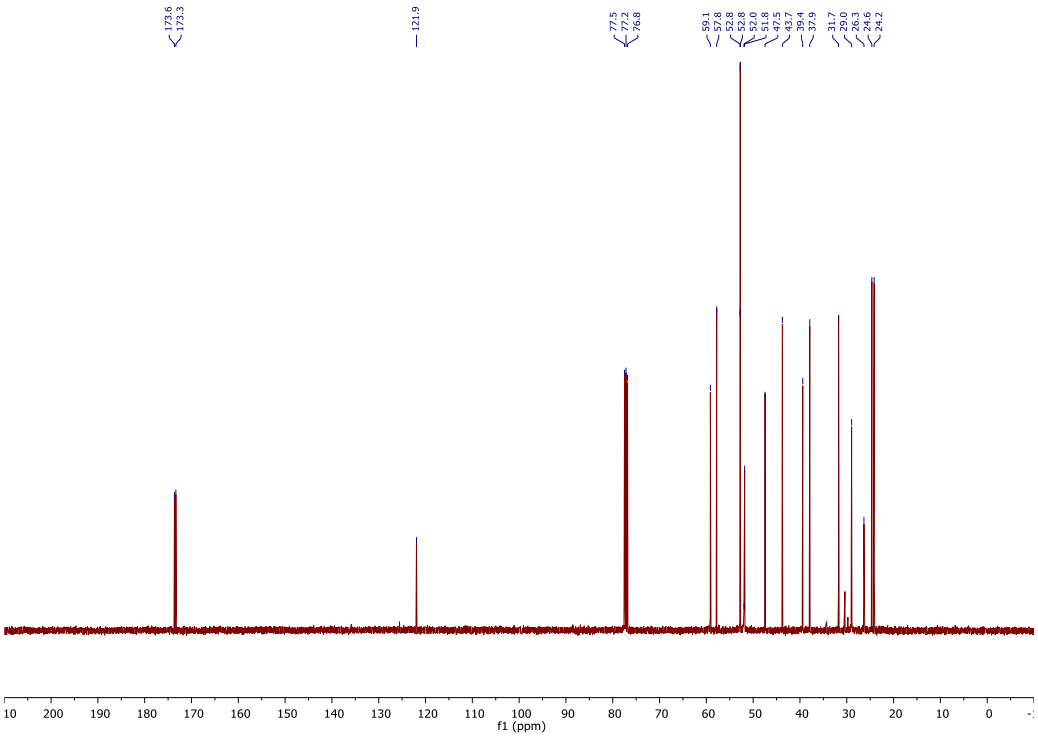

Dimethyl 4-(morpholinomethyl)spiro[4.4]nonane-2,2-dicarboxylate (380)

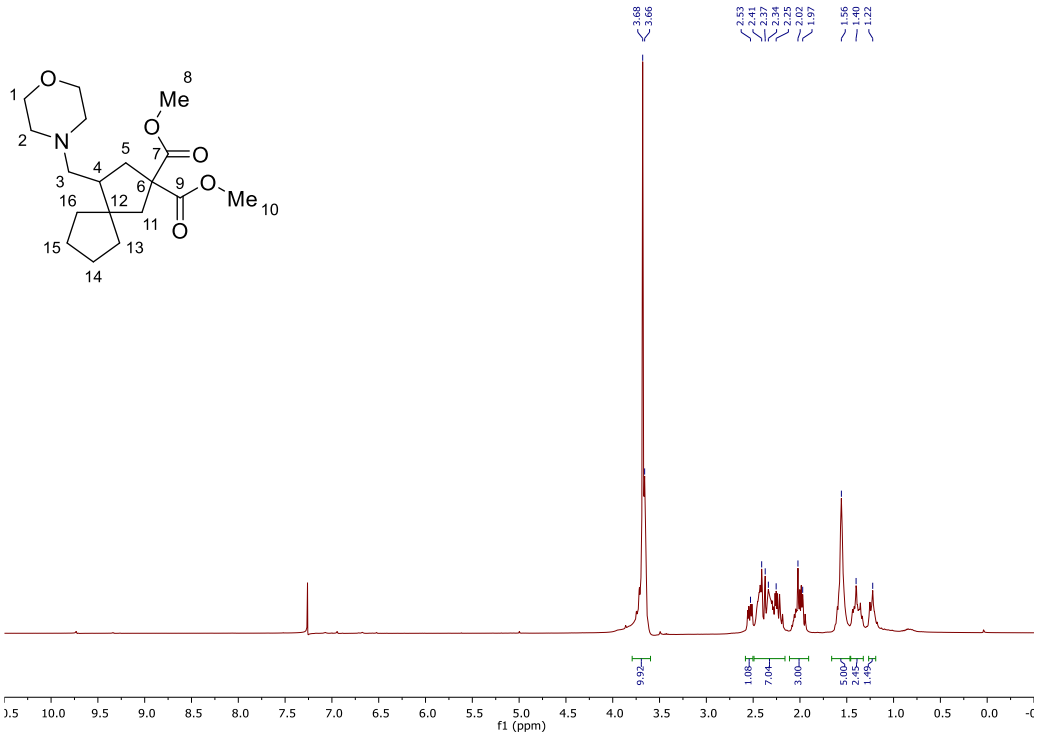

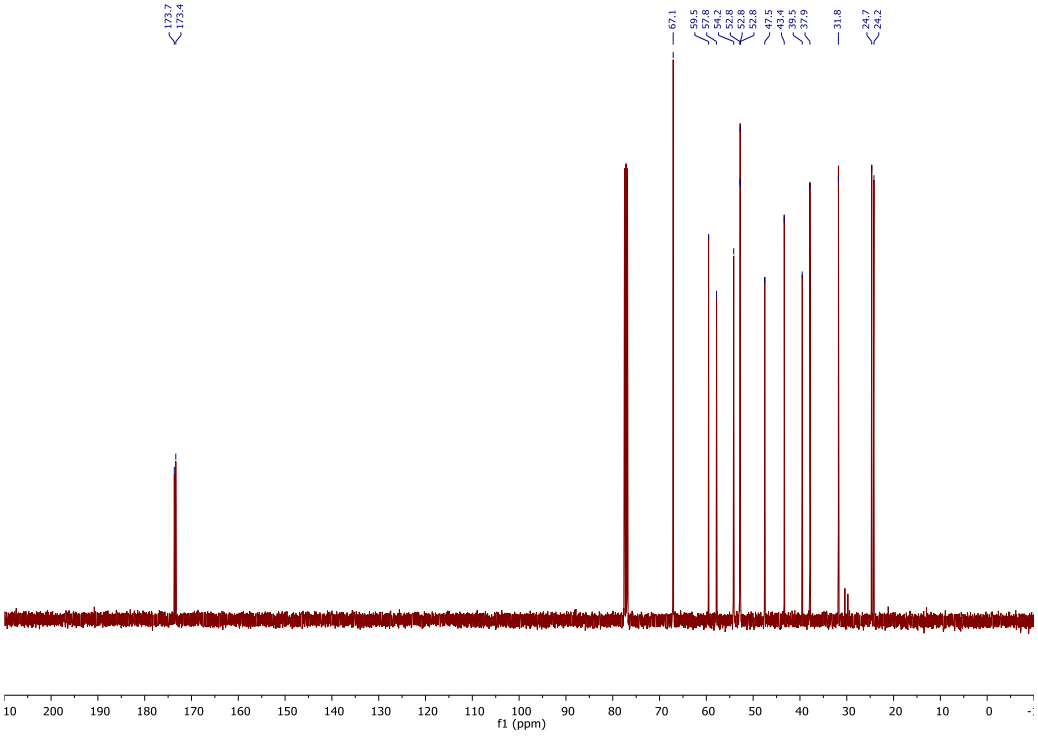

Dimethyl 4-((4-(*tert*-butoxycarbonyl)piperazin-1-yl)methyl)spiro[4.4]nonane-2,2-dicarboxylate (381)

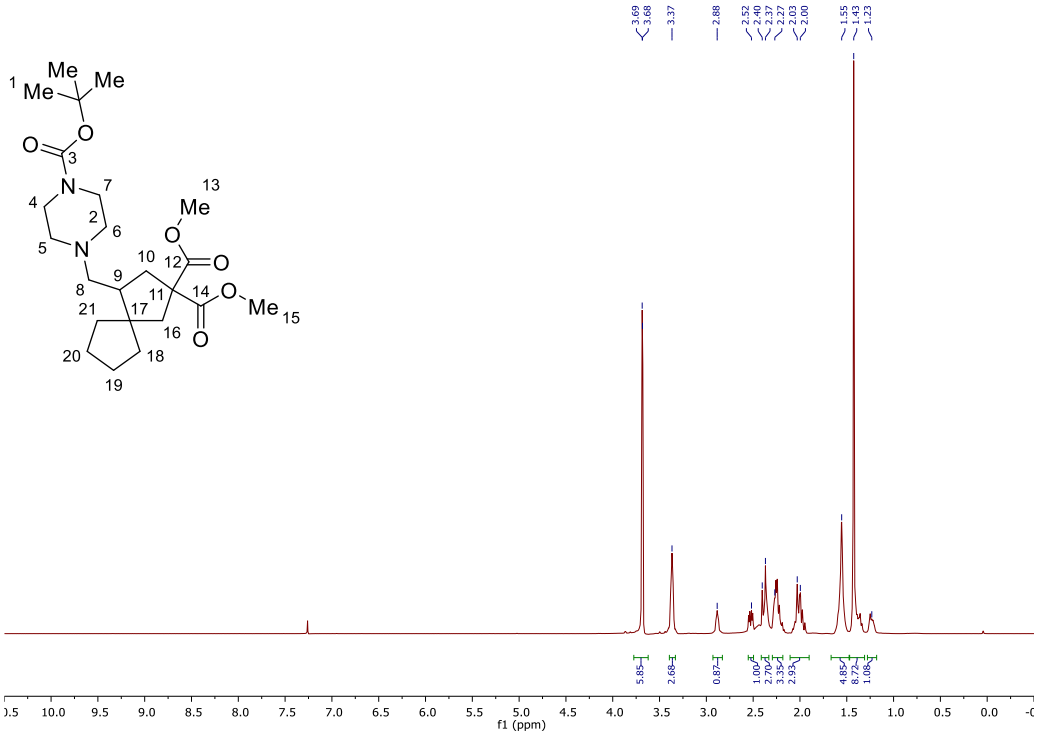

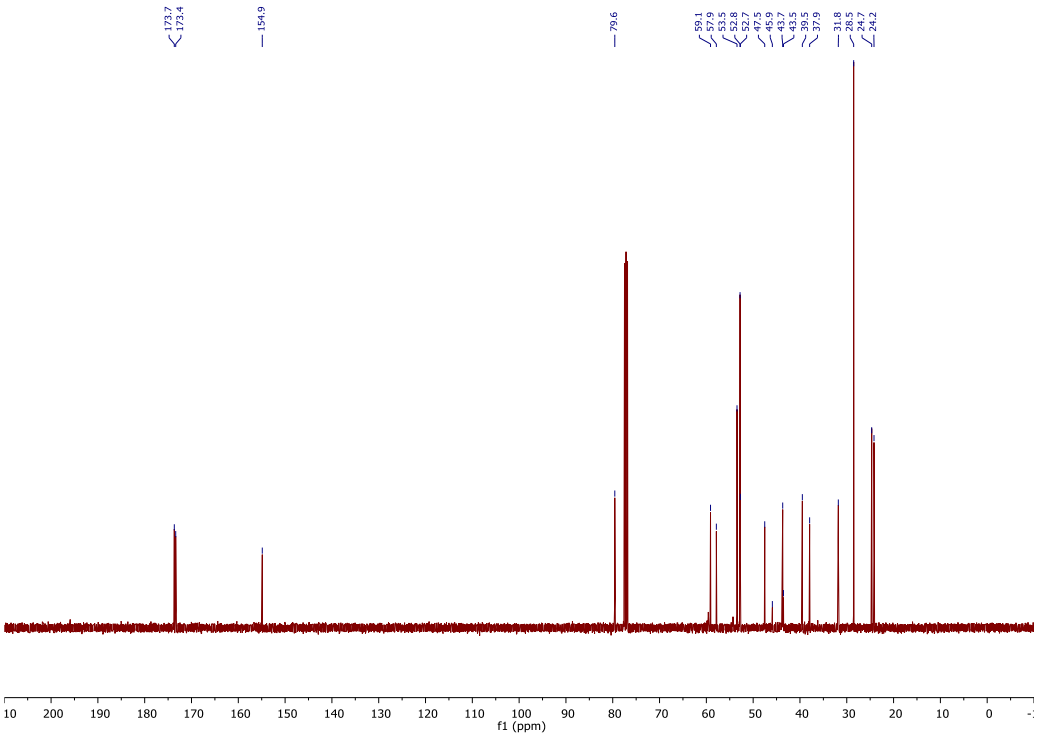

Dimethyl 4-((1,4-dioxa-8-azaspiro[4.5]decan-8-yl)methyl)spiro[4.4]nonane-2,2-dicarboxylate (382)

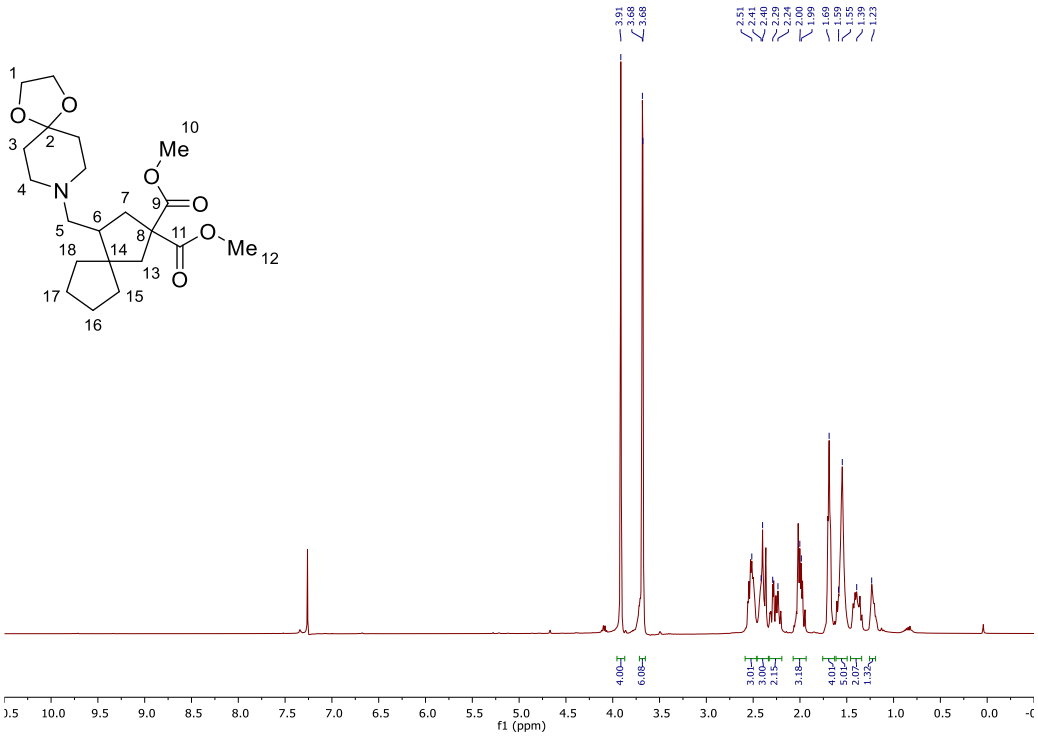

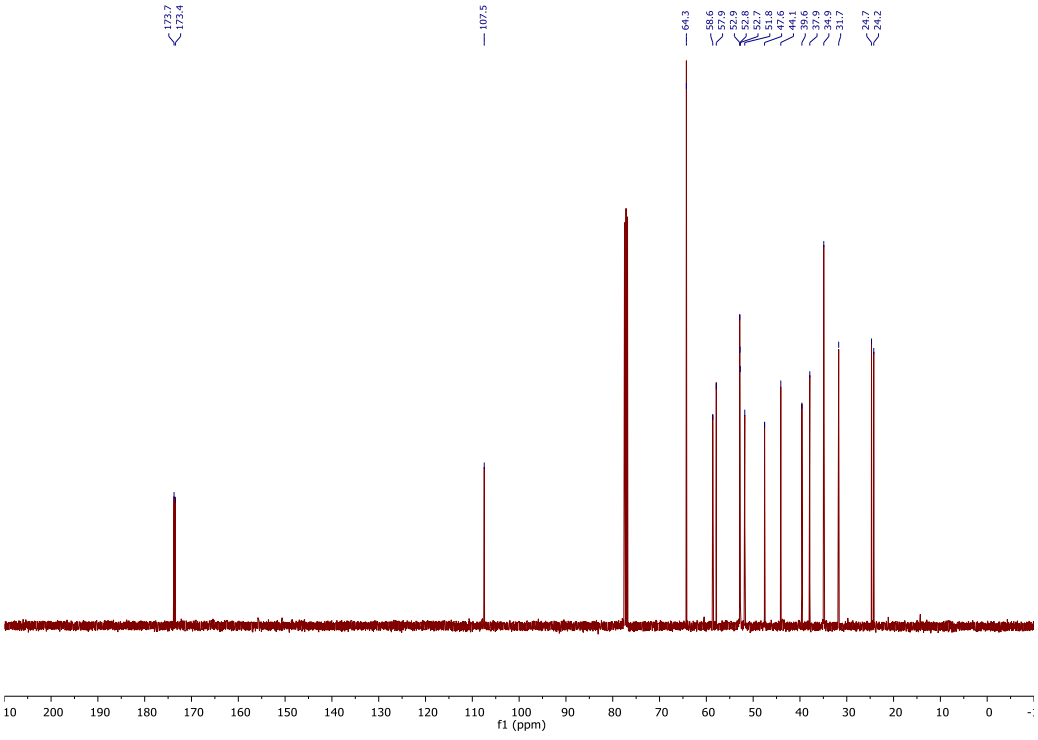

Dimethyl 4-((4-hydroxypiperidin-1-yl)methyl)spiro[4.4]nonane-2,2-dicarboxylate (383)

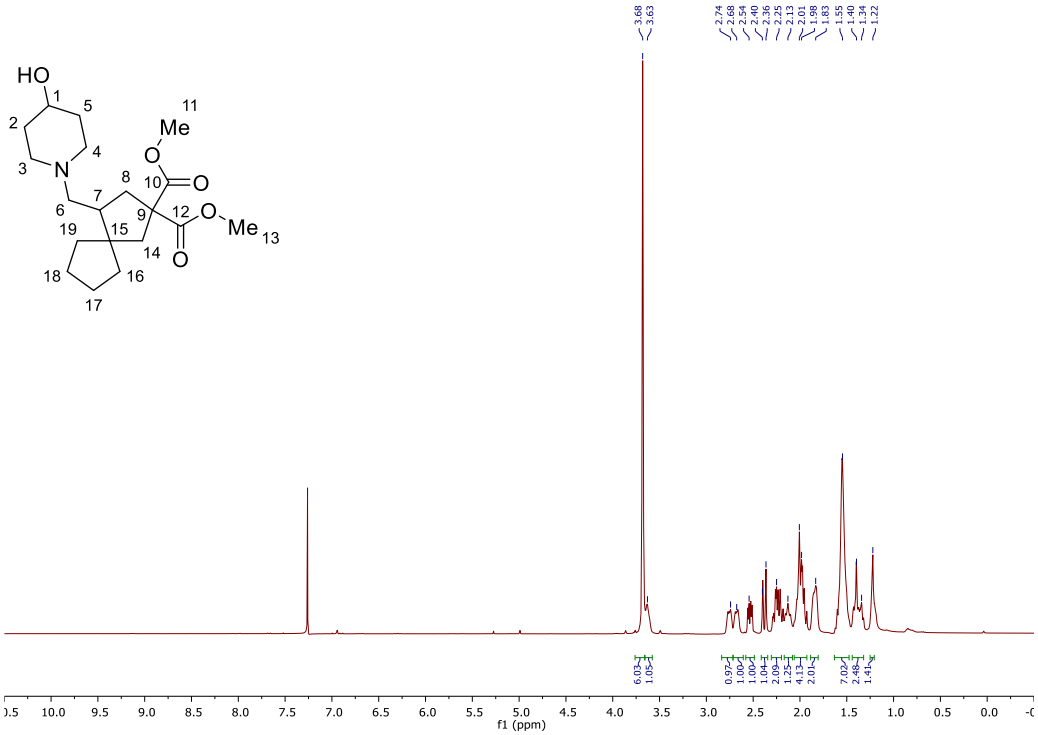

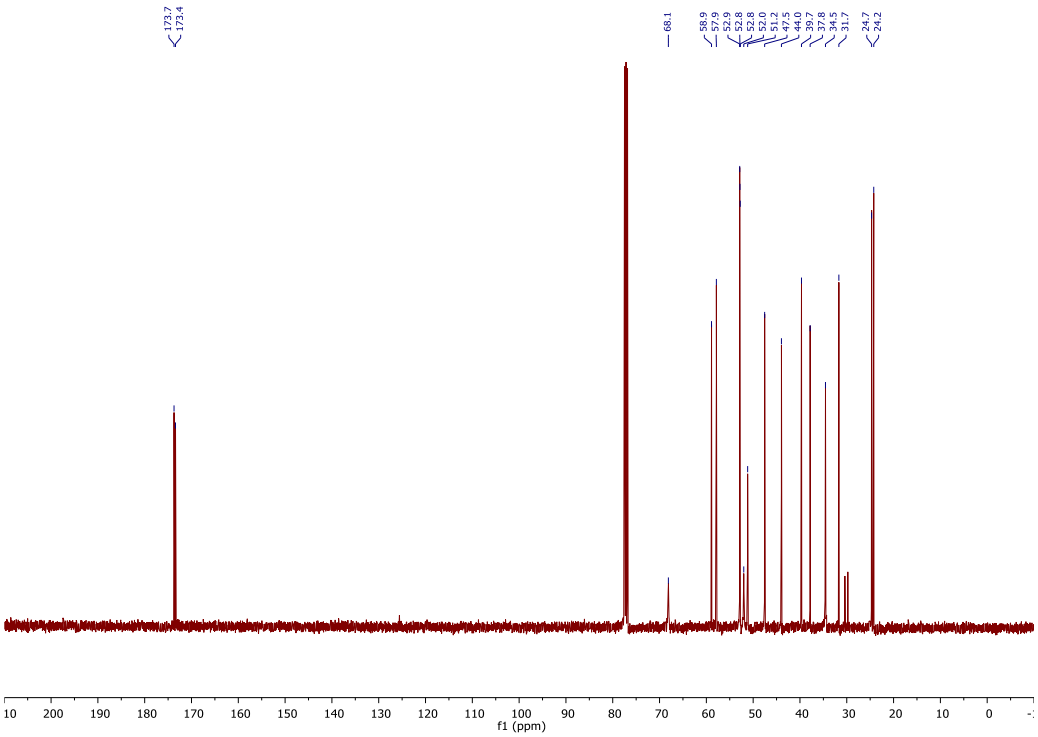

Dimethyl 4-(thiazolidin-3-ylmethyl)spiro[4.4]nonane-2,2-dicarboxylate (384)

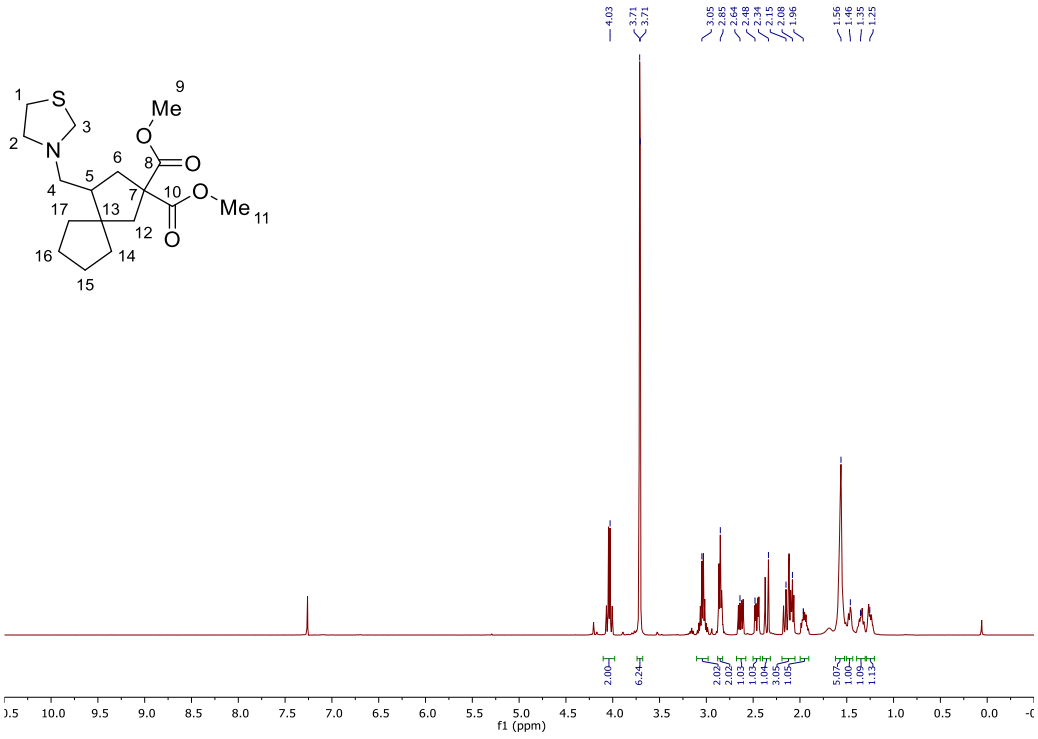

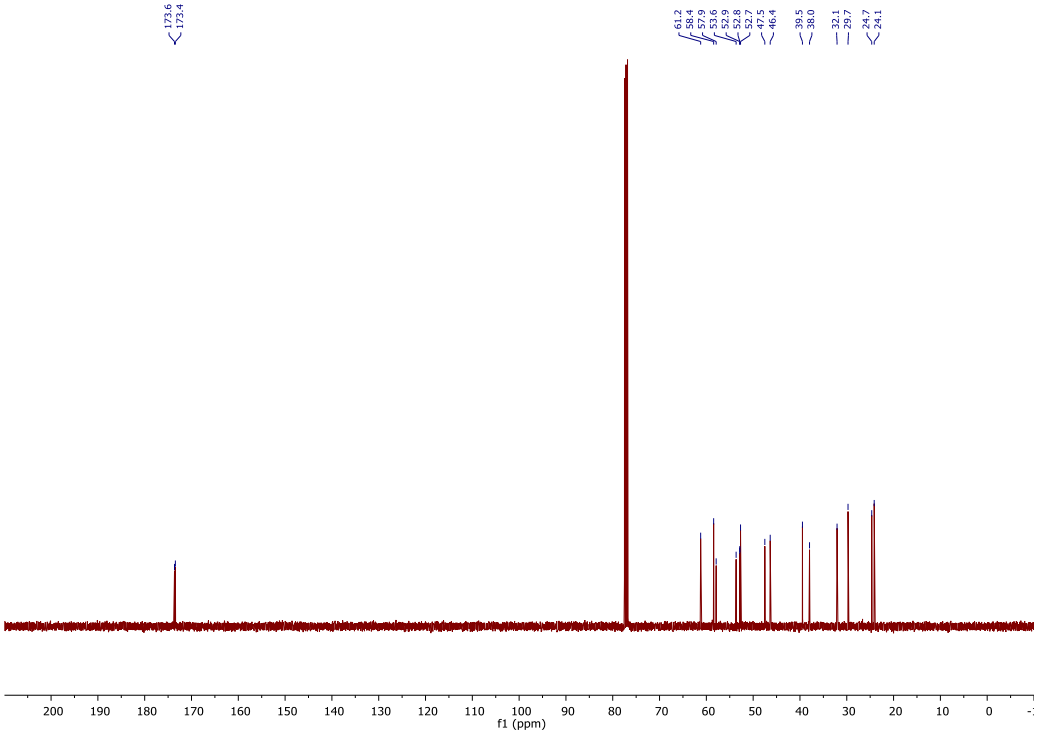

Dimethyl 4-((benzyl(methyl)amino)methyl)spiro[4.4]nonane-2,2-dicarboxylate (385)

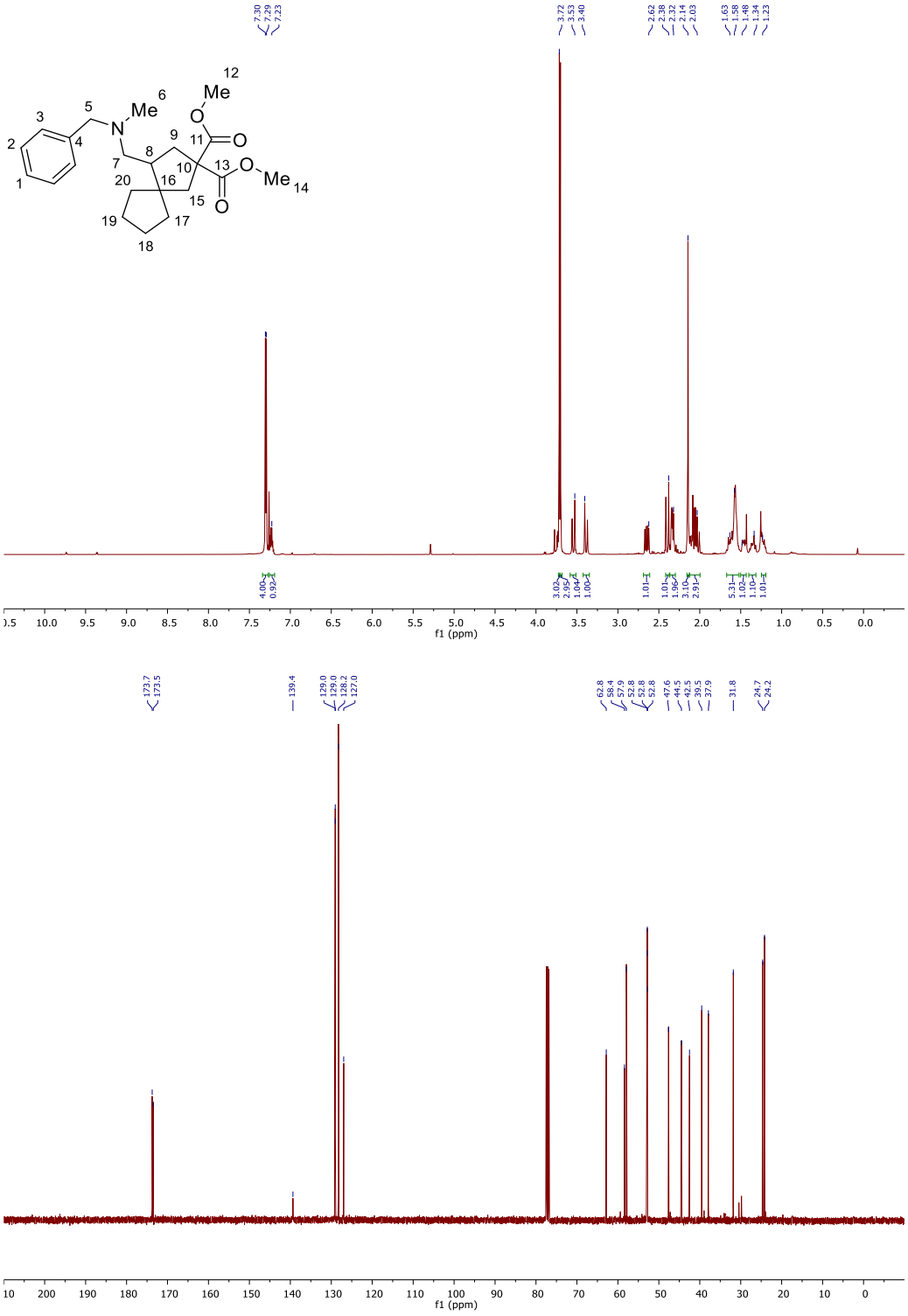

Dimethyl 4-((dibenzylamino)methyl)spiro[4.4]nonane-2,2-dicarboxylate (386)

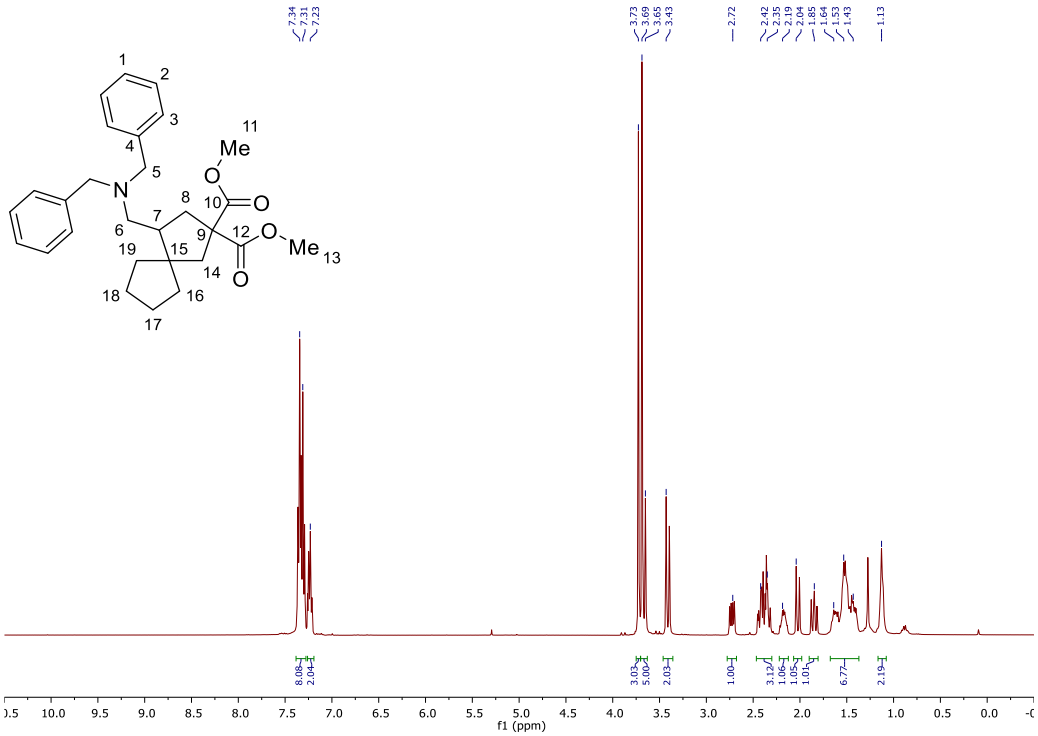

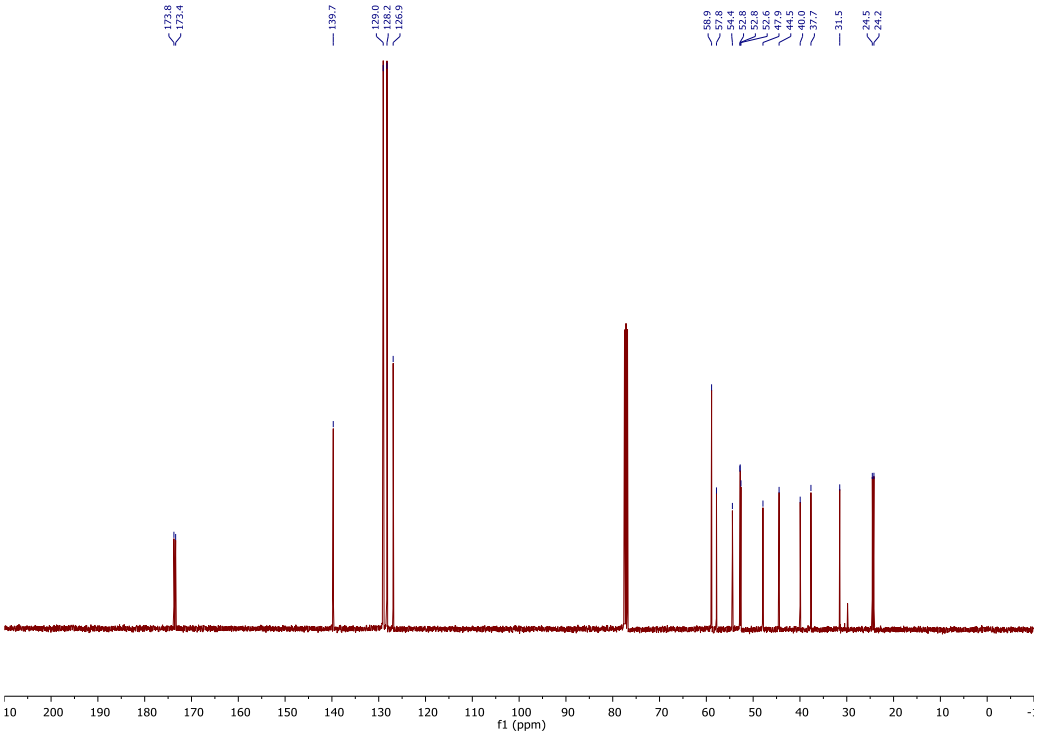

Dimethyl 4-((methyl(phenyl)amino)methyl)spiro[4.4]nonane-2,2-dicarboxylate (387)

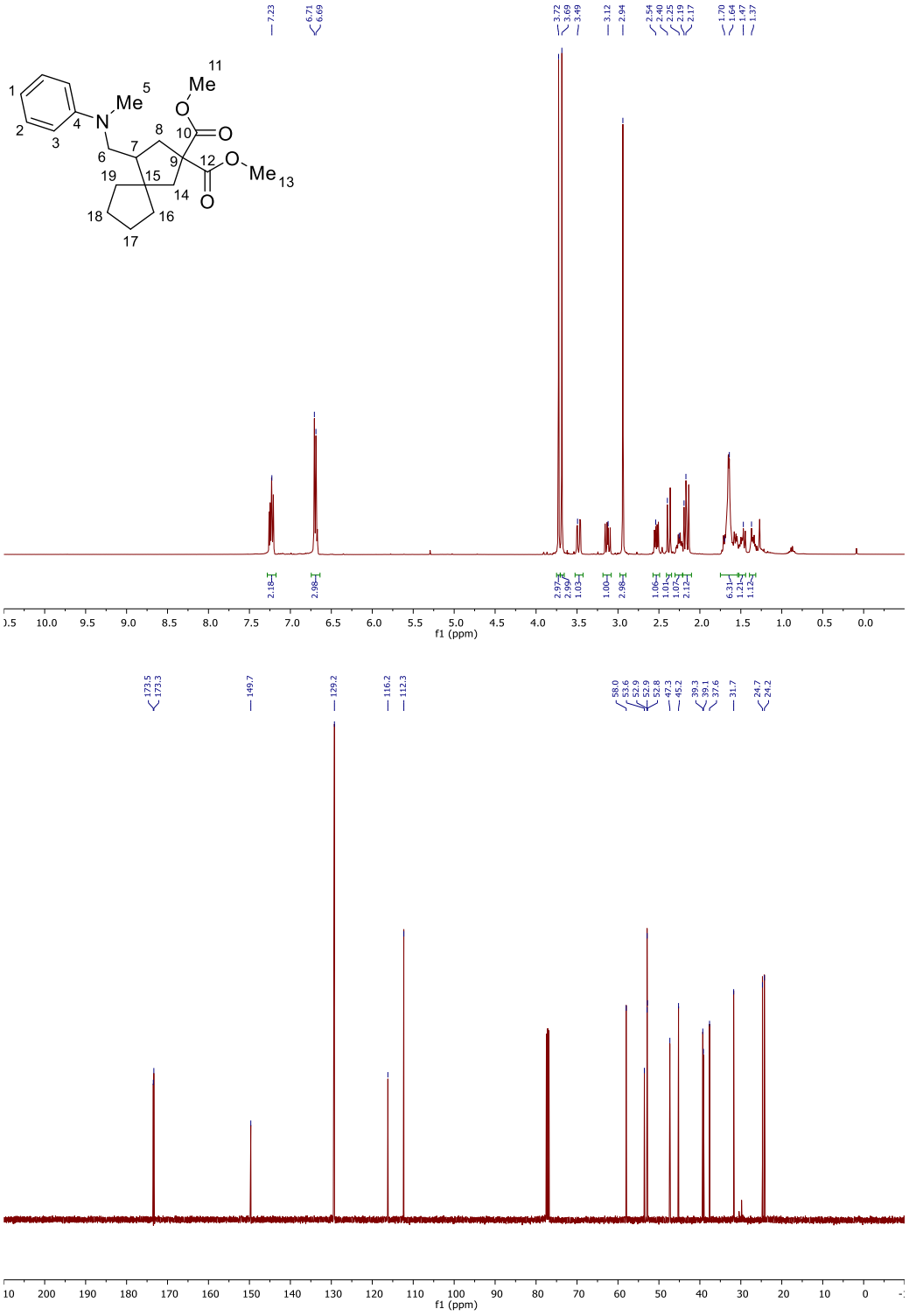

Dimethyl 4-((4-(8-chloro-5,6-dihydro-11*H*-benzo[5,6]cyclohepta[1,2-*b*]pyridin-11-ylidene) piperidin-1-yl)methyl)spiro[4.4]nonane-2,2-dicarboxylate (388)

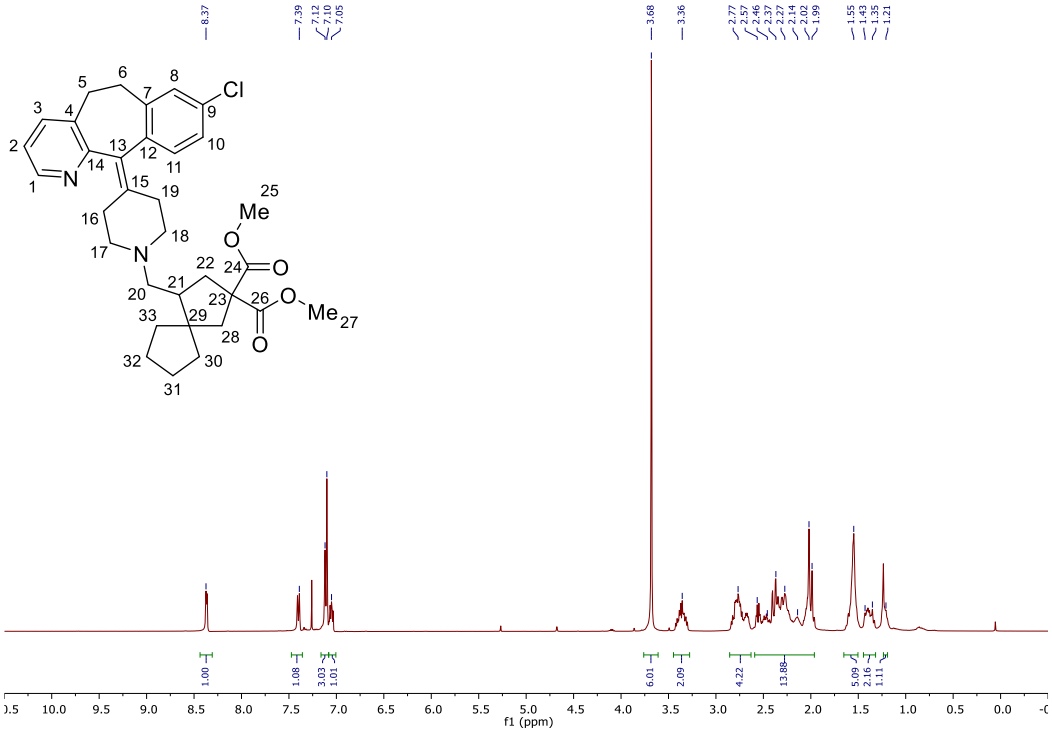

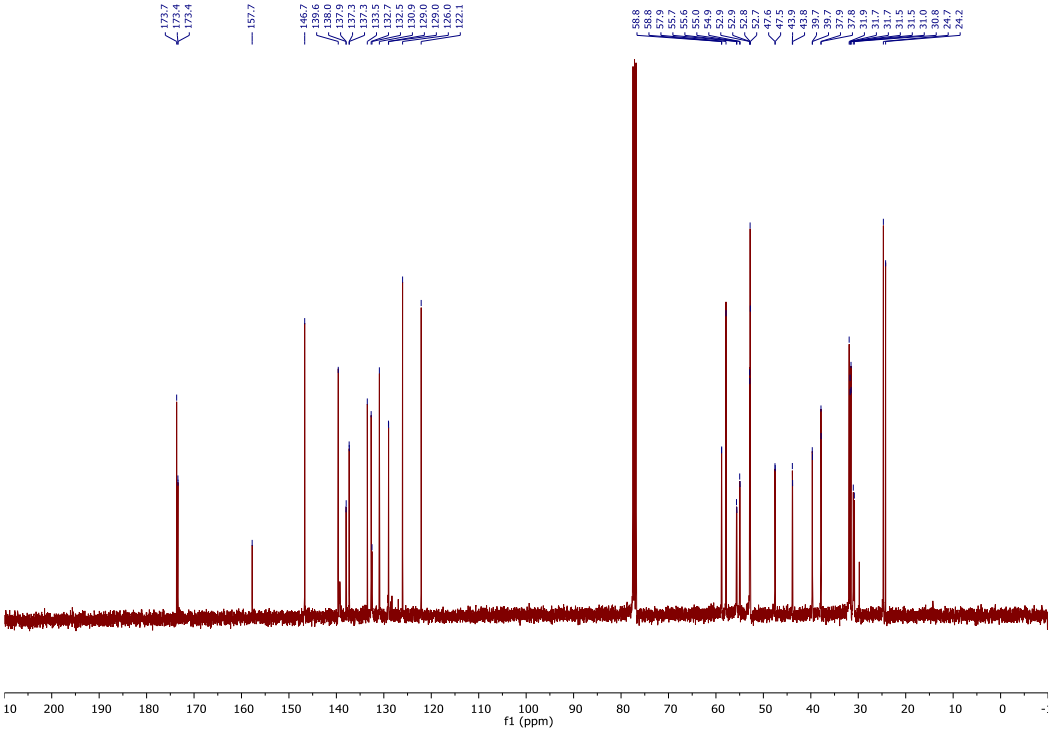

Dimethyl 4-((methyl(3-phenyl-3-(4-(trifluoromethyl)phenoxy)propyl)amino)methyl)spiro[4.4] nonane-2,2-dicarboxylate (389)

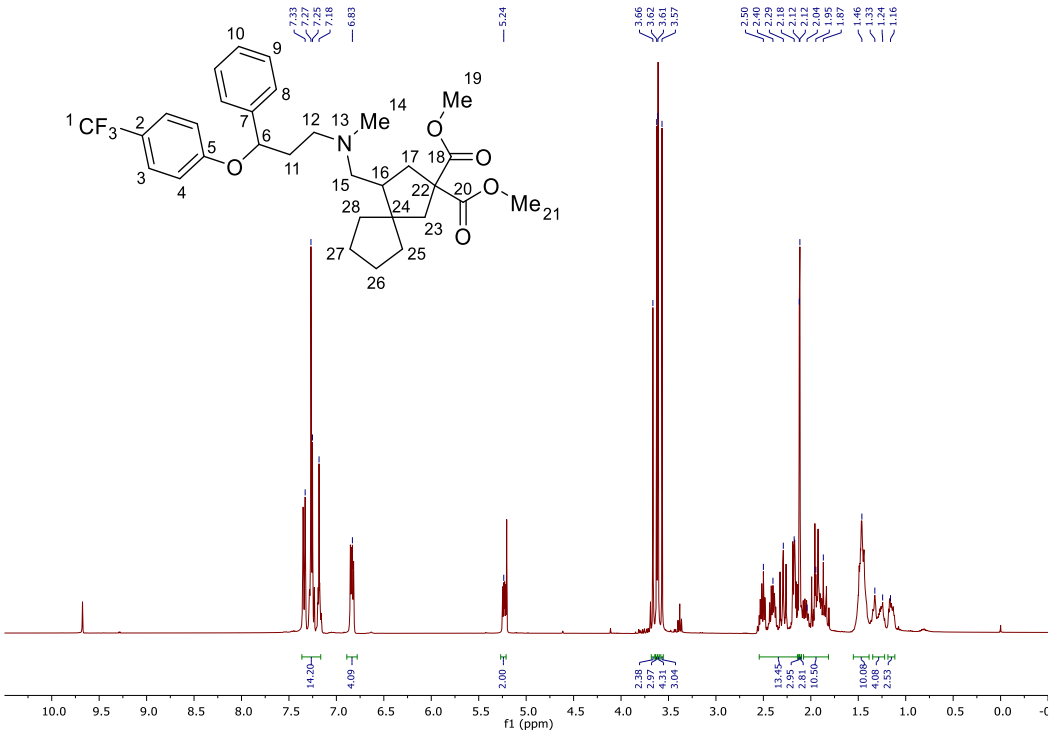

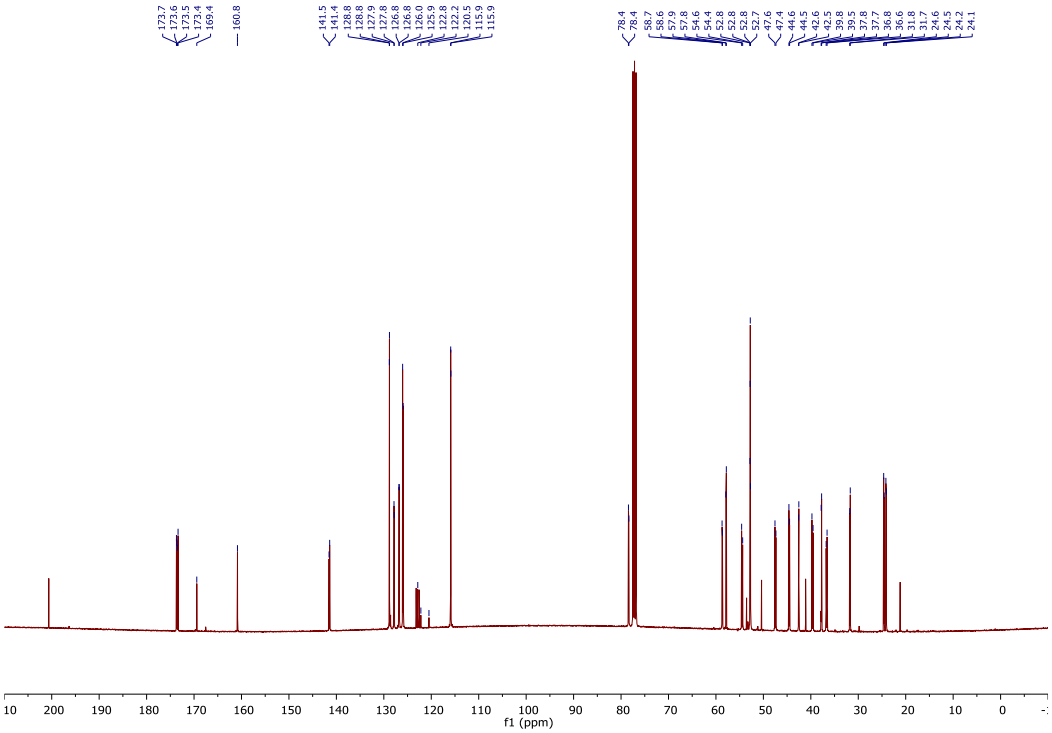

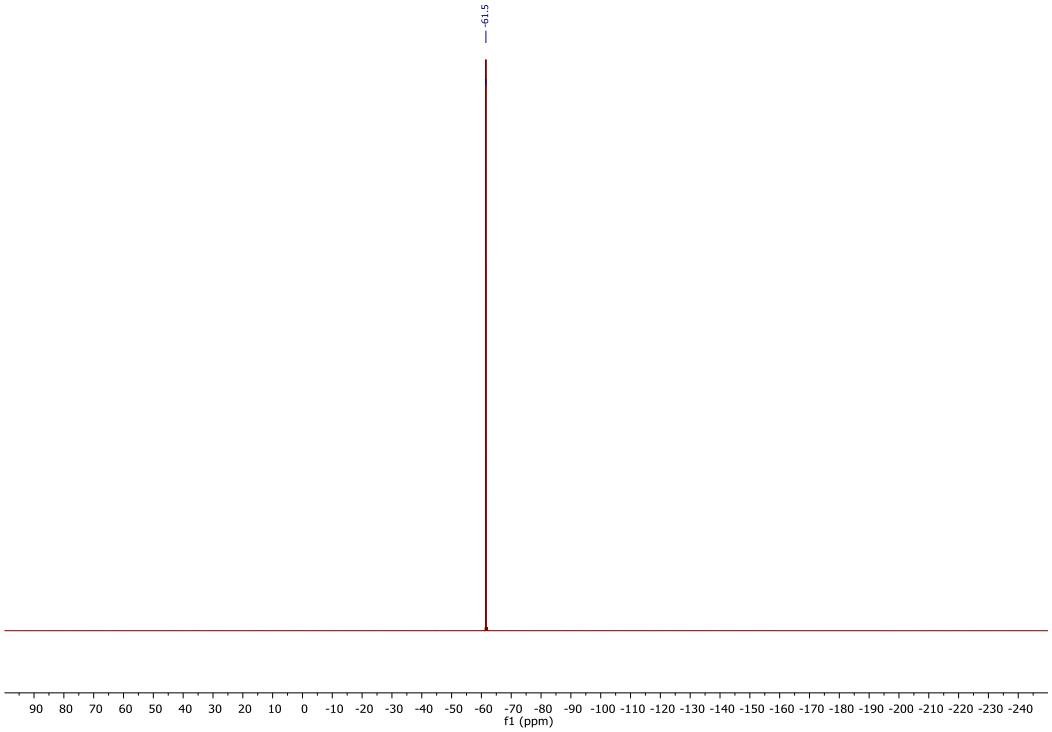
-61.5
90 80 70 60 50 40 30 20 10 0 -10 -20 -30 -40 -50 -60 -70 -80 -90 -100 -110 -120 -130 -140 -150 -160 -170 -180 -190 -200 -210 -220 -230 -240
f1 (ppm)

Dimethyl 4-((4-cyanopiperidin-1-yl)methyl)spiro[4.5]decane-2,2-dicarboxylate (399)

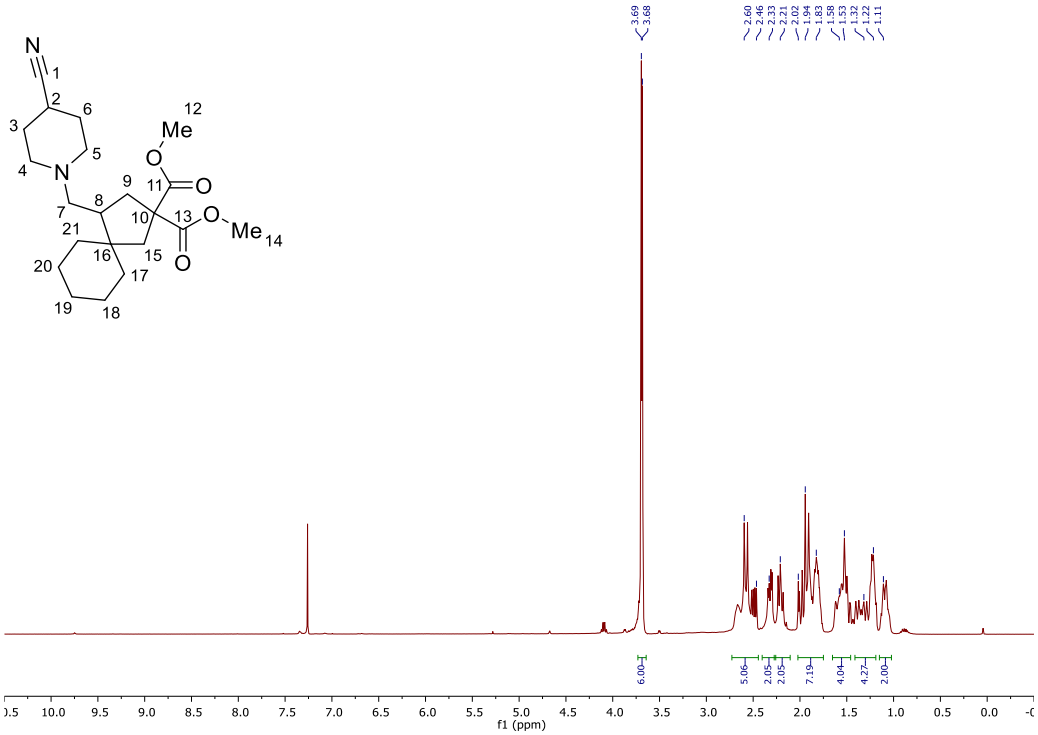

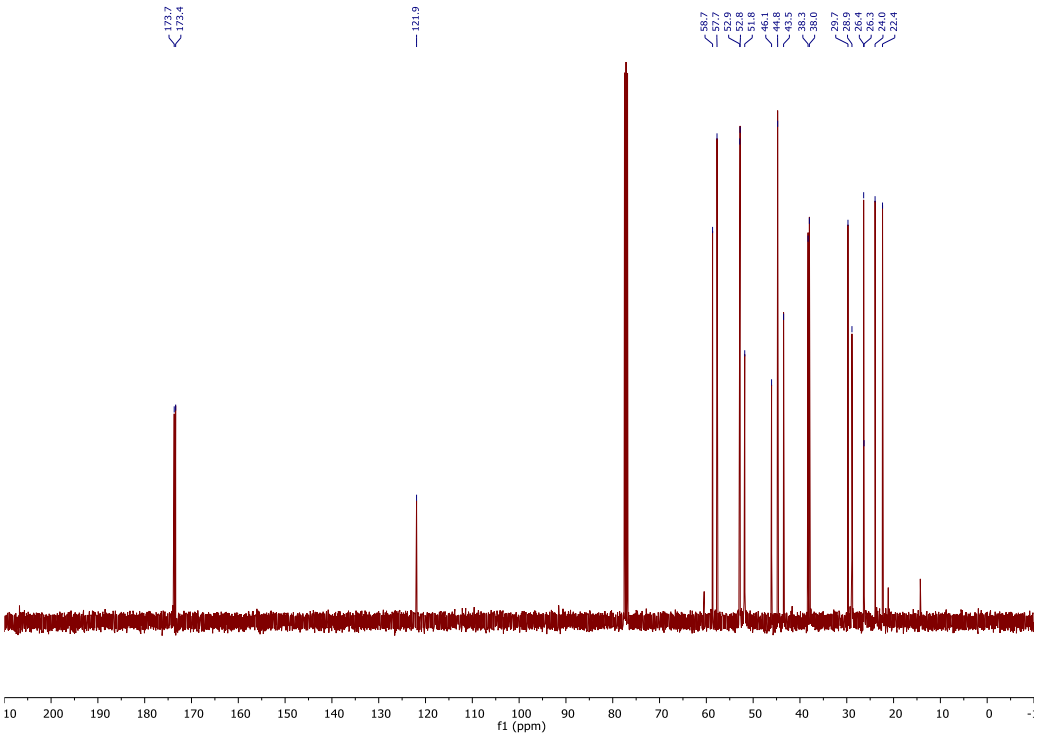

Dimethyl 8-((4-cyanopiperidin-1-yl)methyl)spiro[3.4]octane-6,6-dicarboxylate (400)

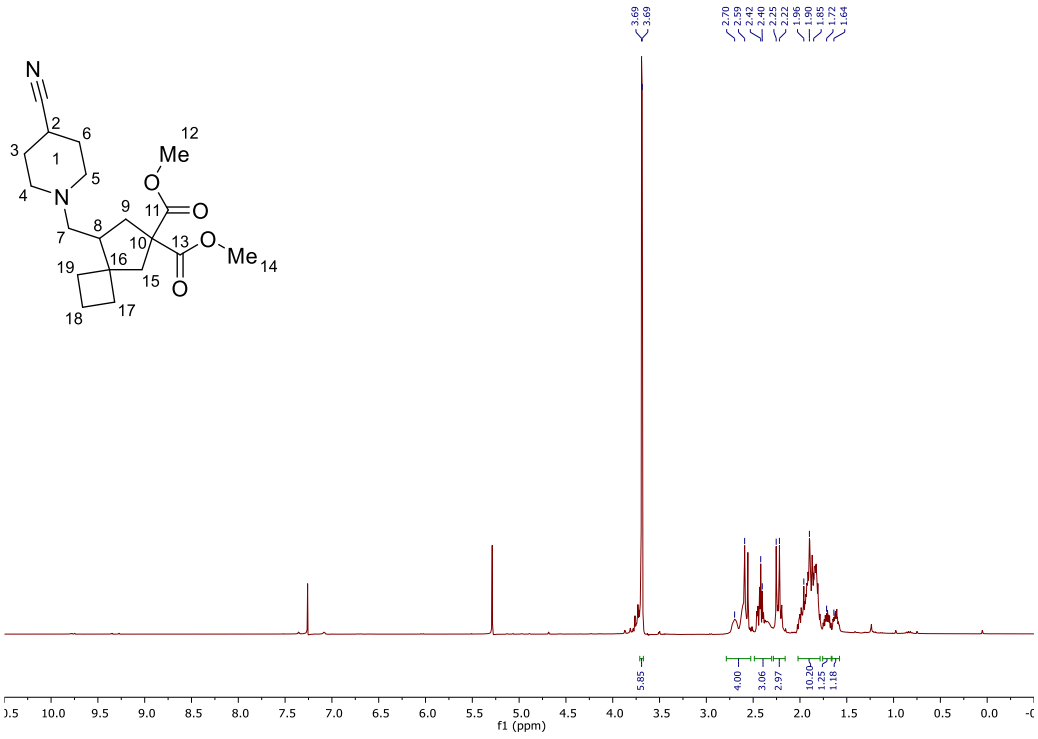

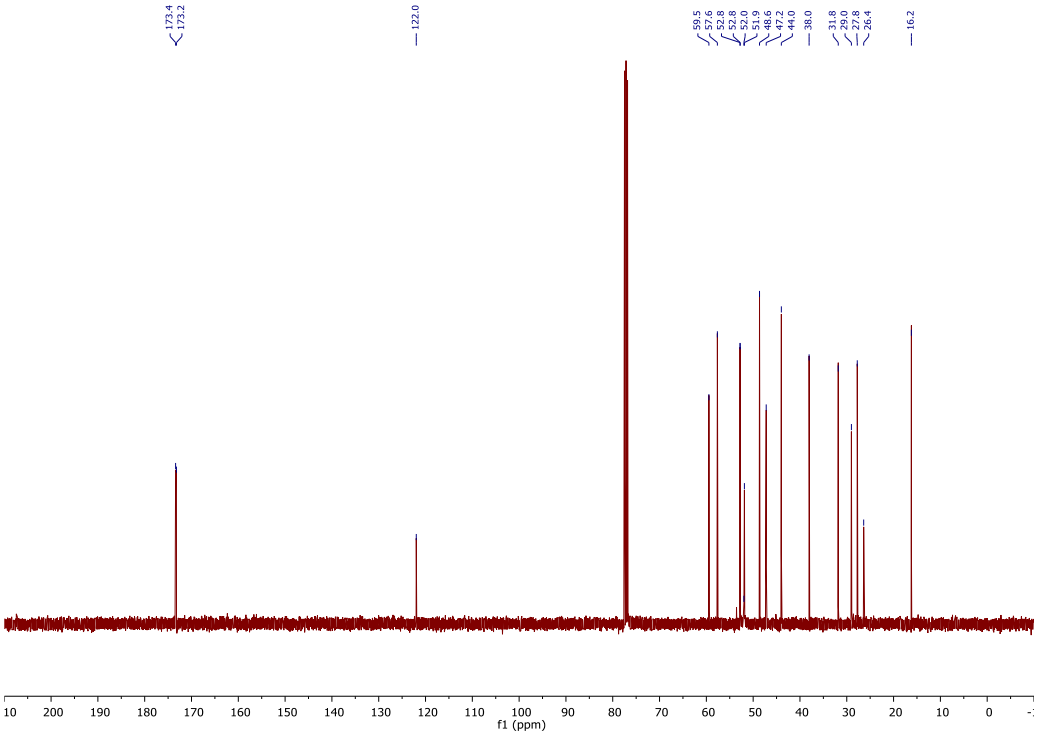

8-Benzyl 2,2-dimethyl 4-((4-cyanopiperidin-1-yl)methyl)-8-azaspiro[4.5]decane-2,2,8-tricarboxylate (401)

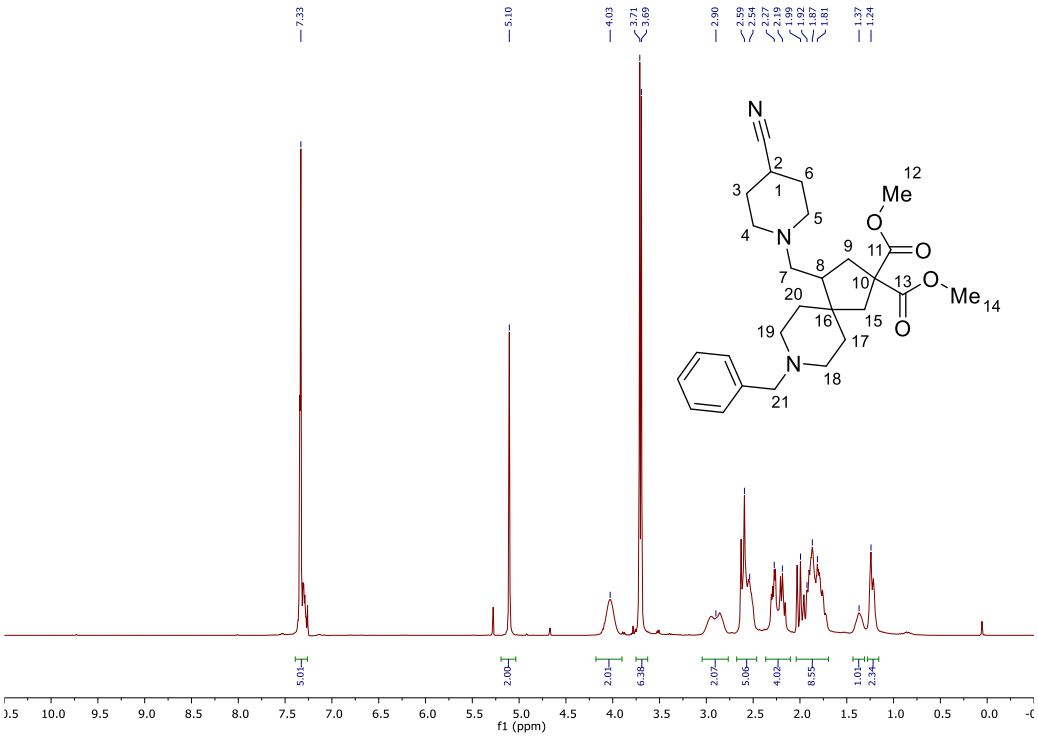

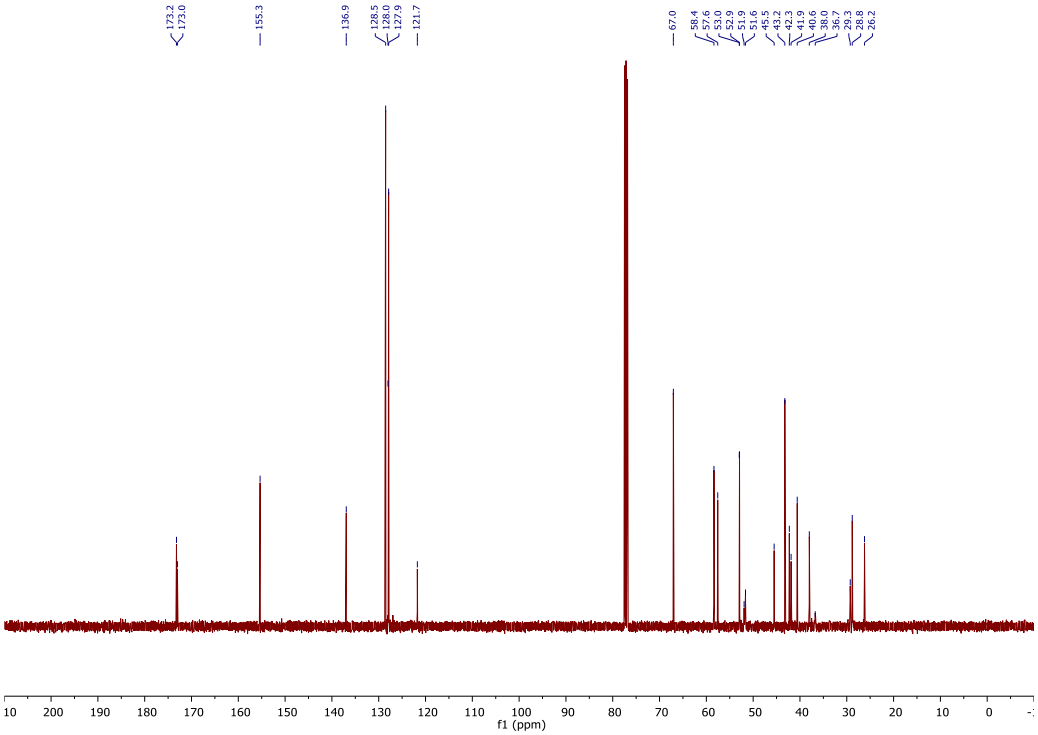

Dimethyl 4-((4-cyanopiperidin-1-yl)methyl)-3,3-diethylcyclopentane-1,1-dicarboxylate (402)

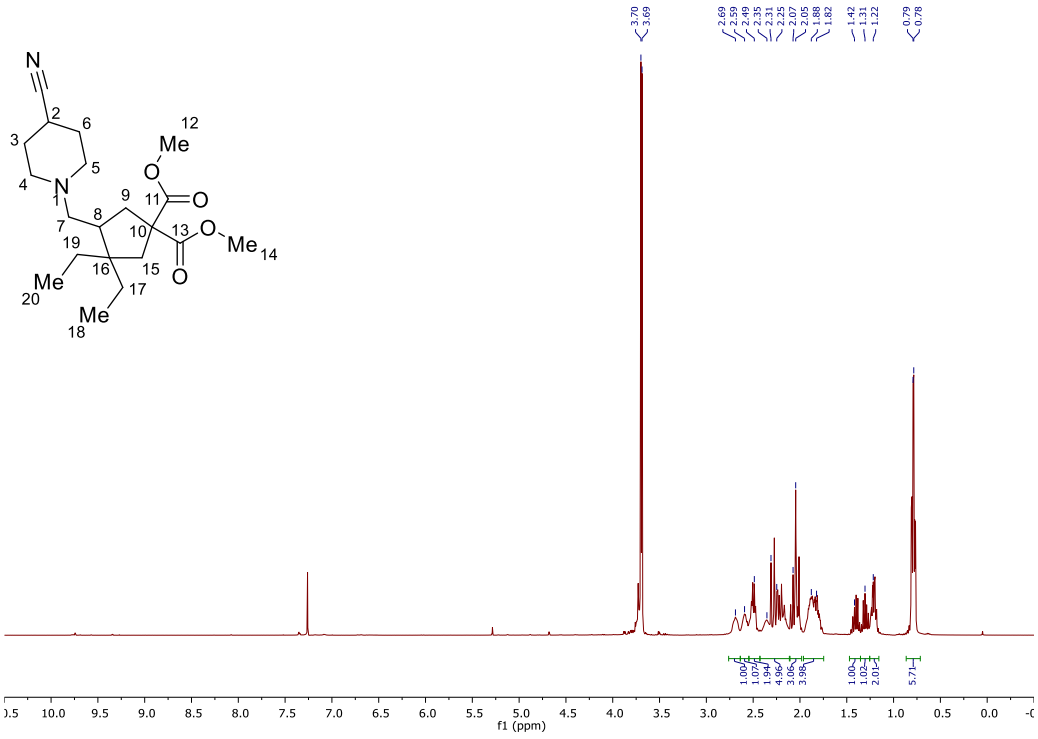

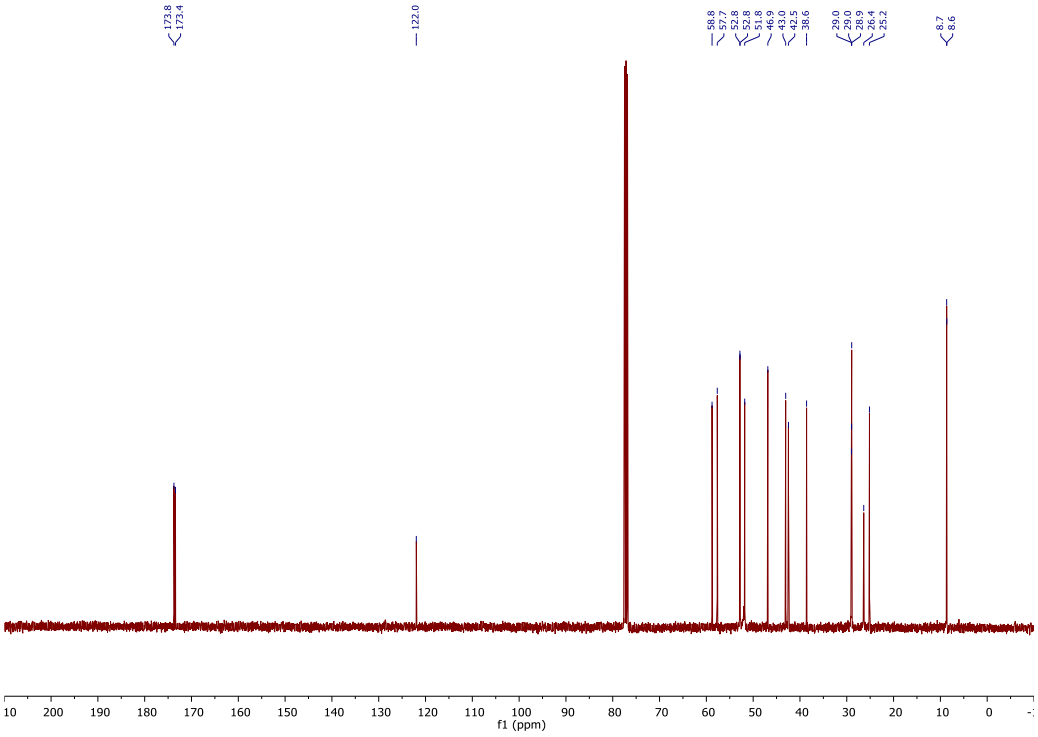

Dimethyl 3-butyl-4-((4-cyanopiperidin-1-yl)methyl)cyclopentane-1,1-dicarboxylate (403)

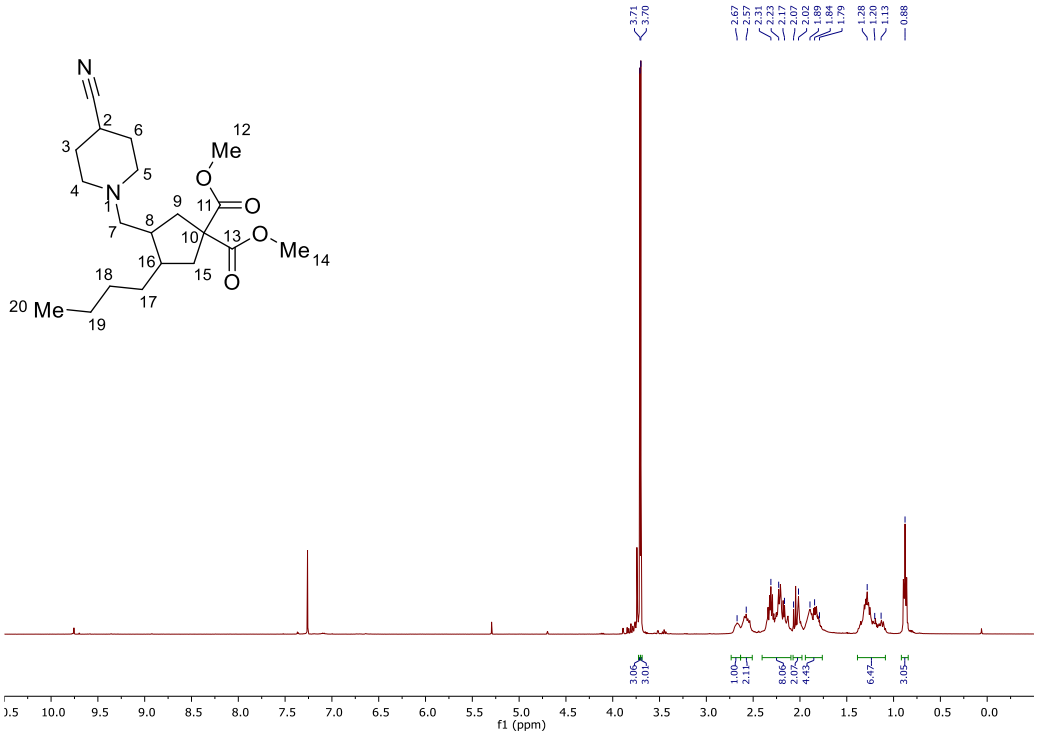

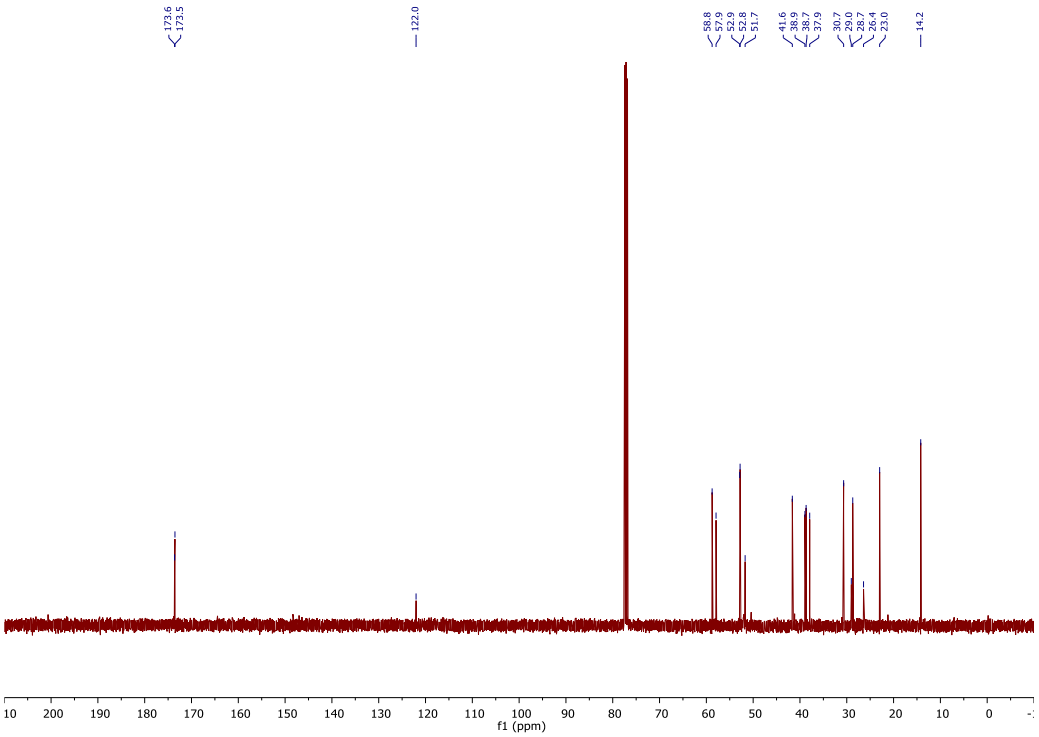

Dimethyl 3-((4-cyanopiperidin-1-yl)methyl)-4-phenylcyclopentane-1,1-dicarboxylate (404)

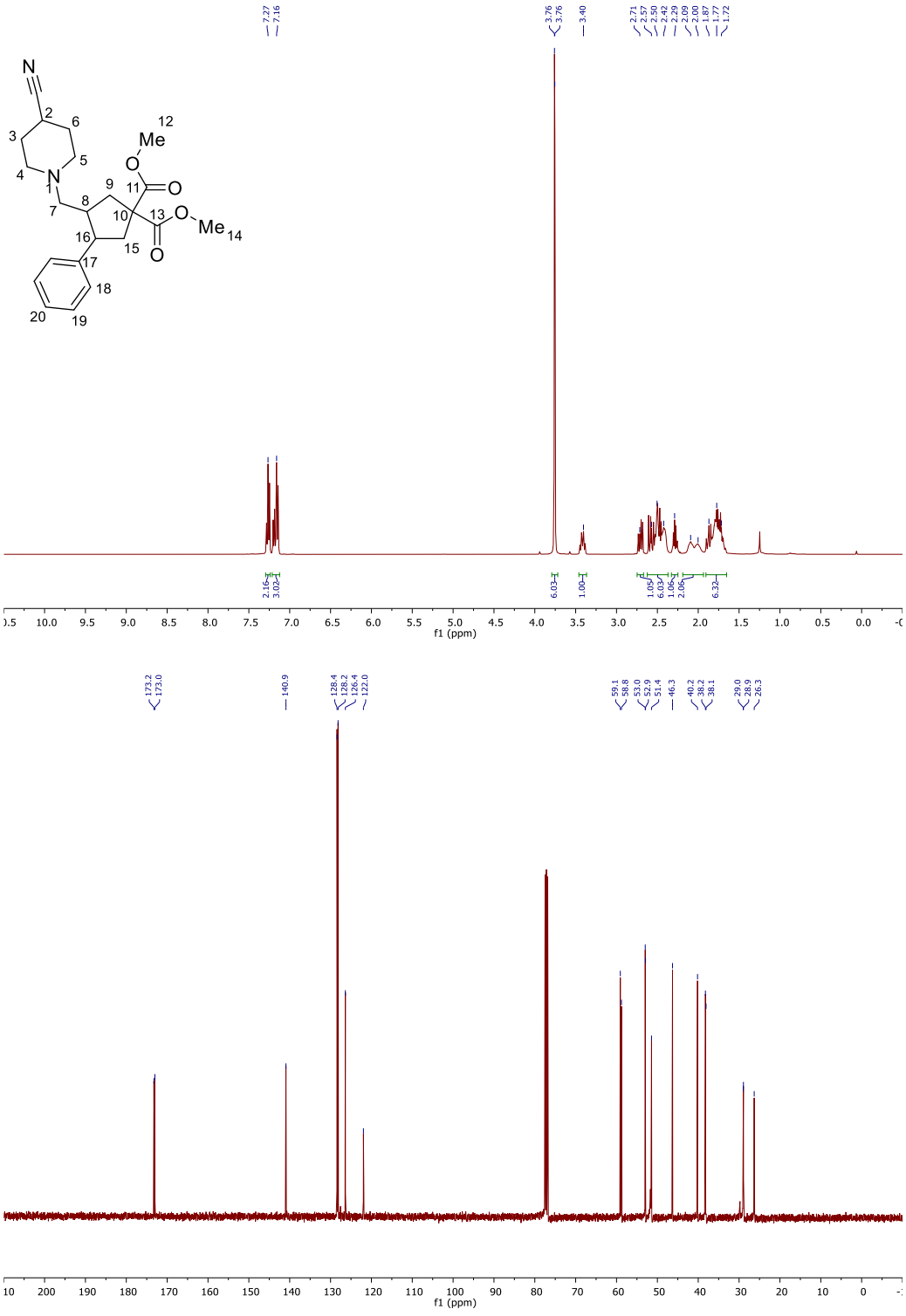

Dimethyl 3-(4-bromophenyl)-4-((dimethylamino)methyl)cyclopentane-1,1-dicarboxylate (405)

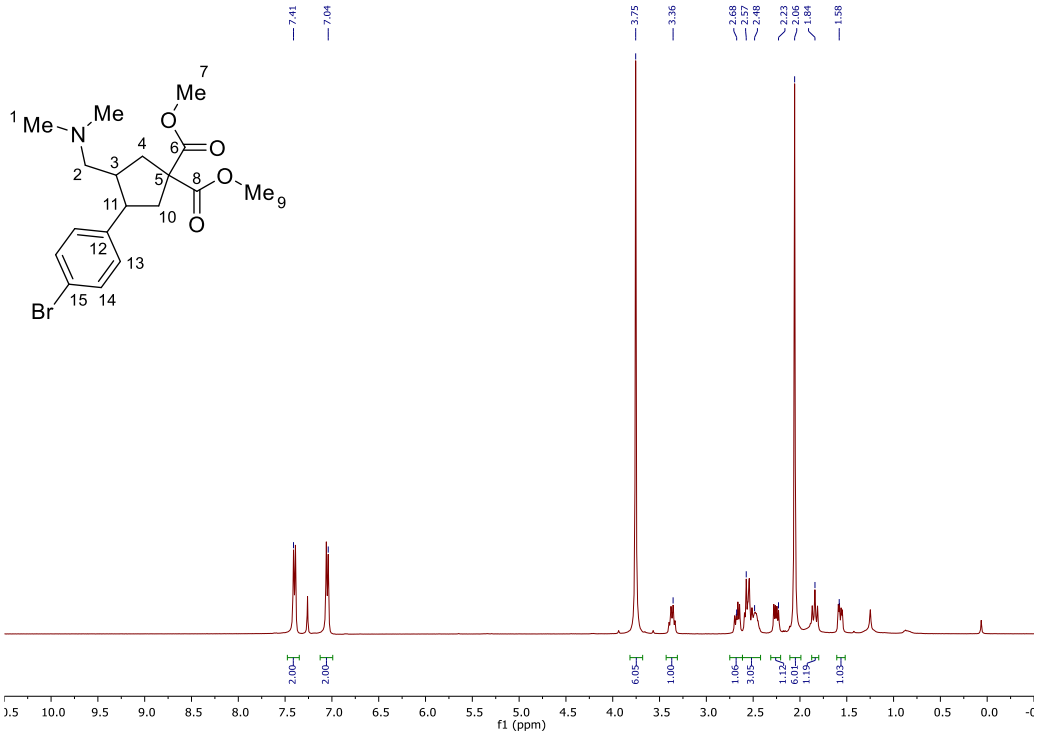

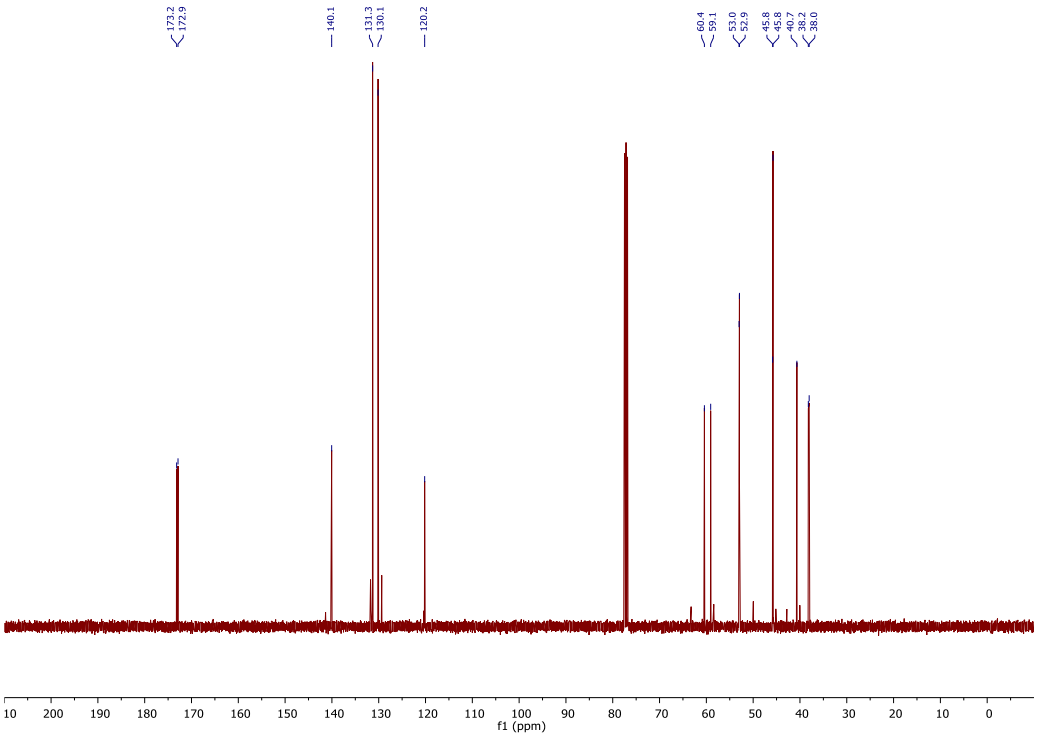

Dimethyl 3-((4-cyanopiperidin-1-yl)methyl)-4-(4-methoxyphenyl)cyclopentane-1,1-dicarboxylate (406)

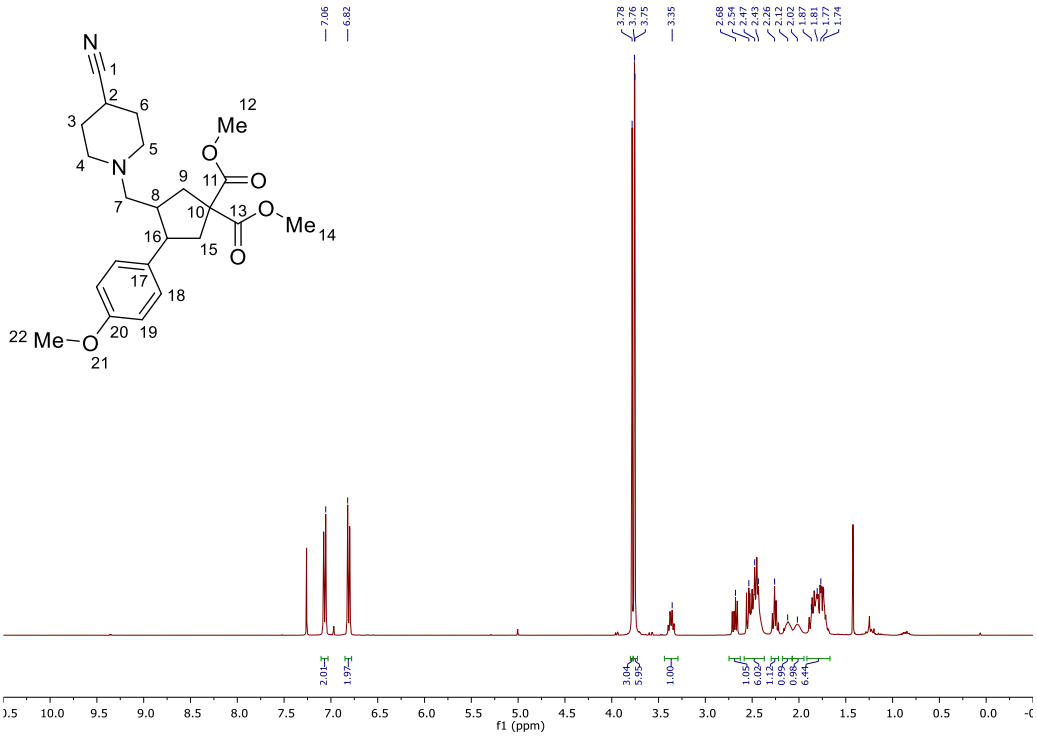

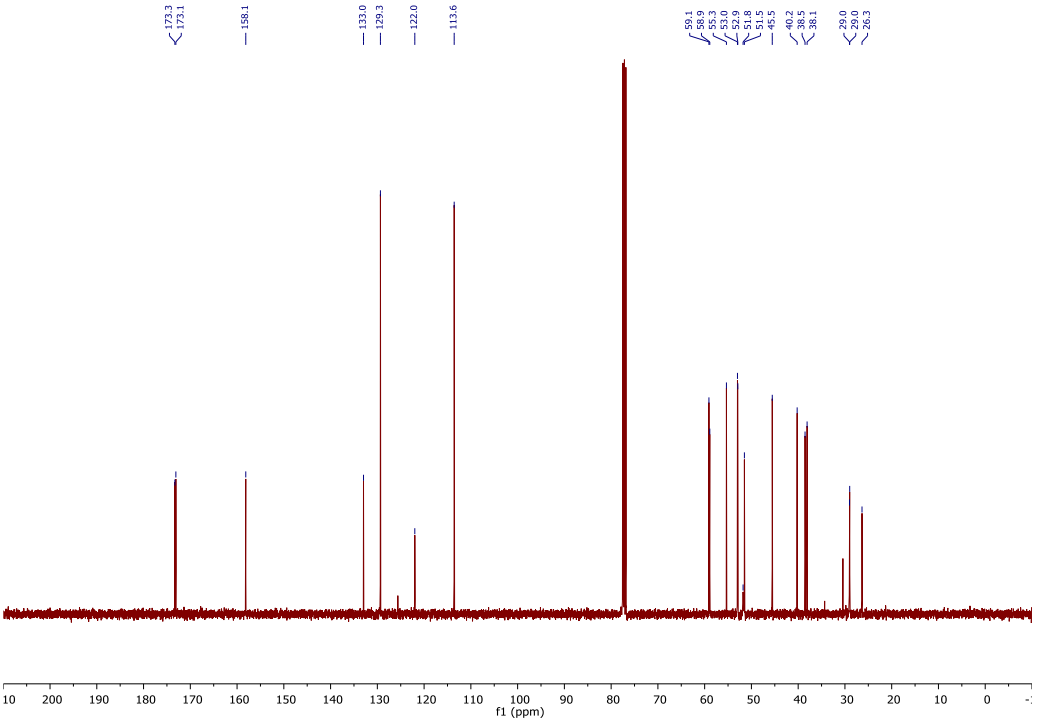

Dimethyl 3-((4-cyanopiperidin-1-yl)methyl)-4-(pyridin-4-yl)cyclopentane-1,1-dicarboxylate (407)

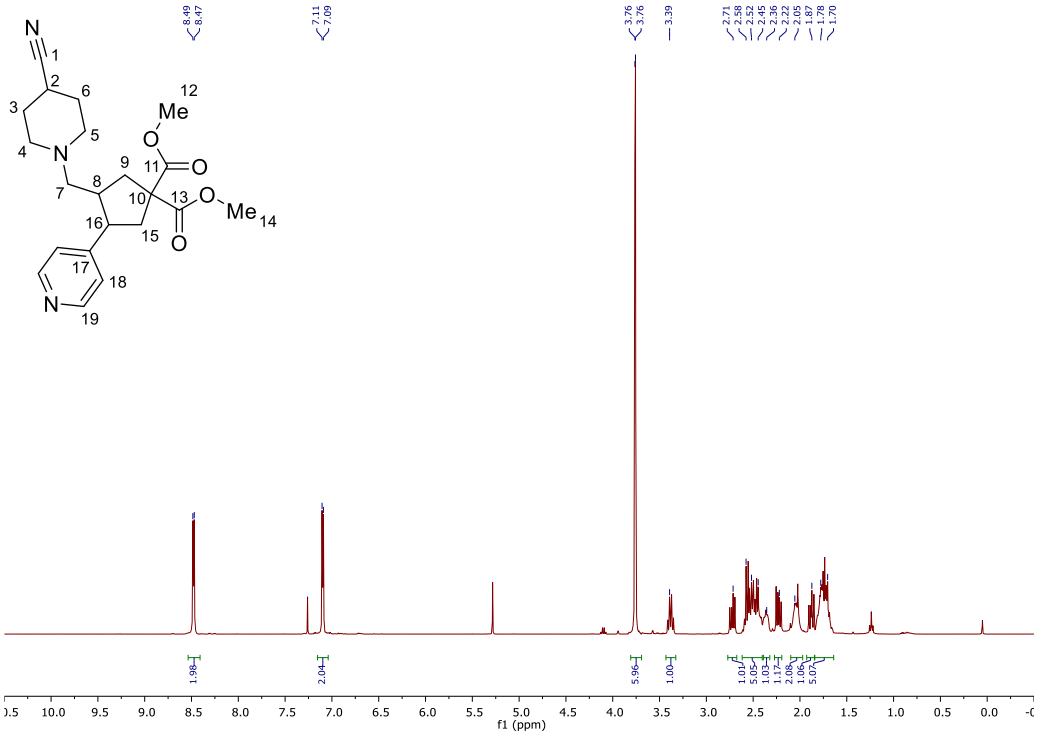

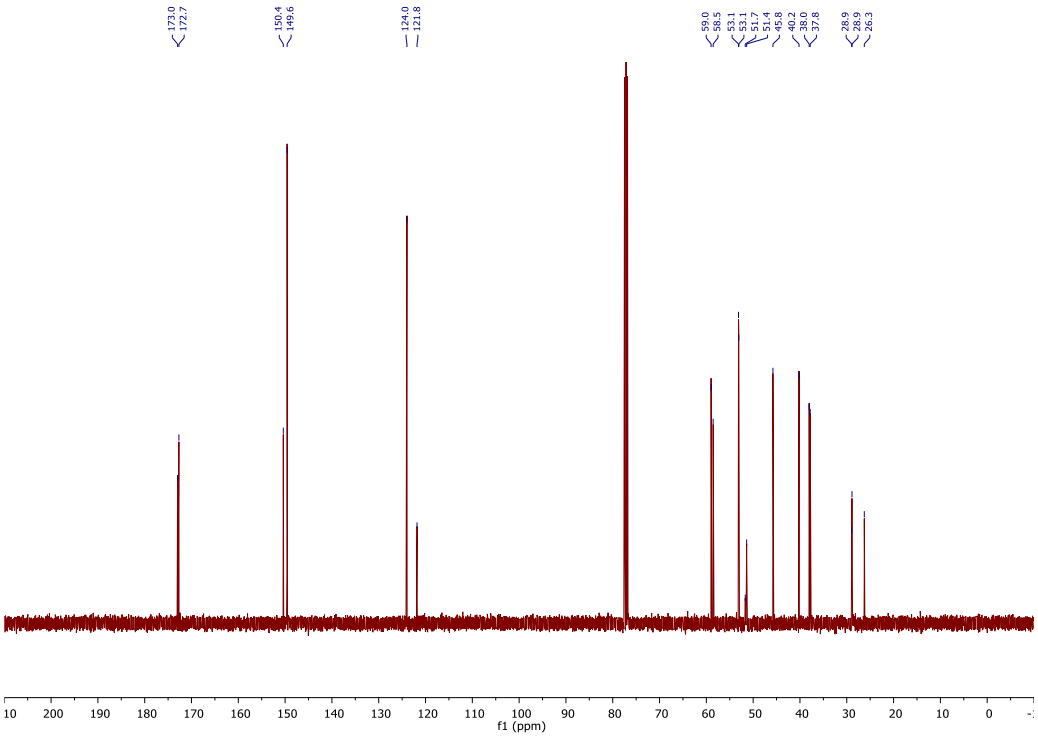

3-Butyl 1,1-dimethyl 4-((4-cyanopiperidin-1-yl)methyl)cyclopentane-1,1,3-tricarboxylate (408)

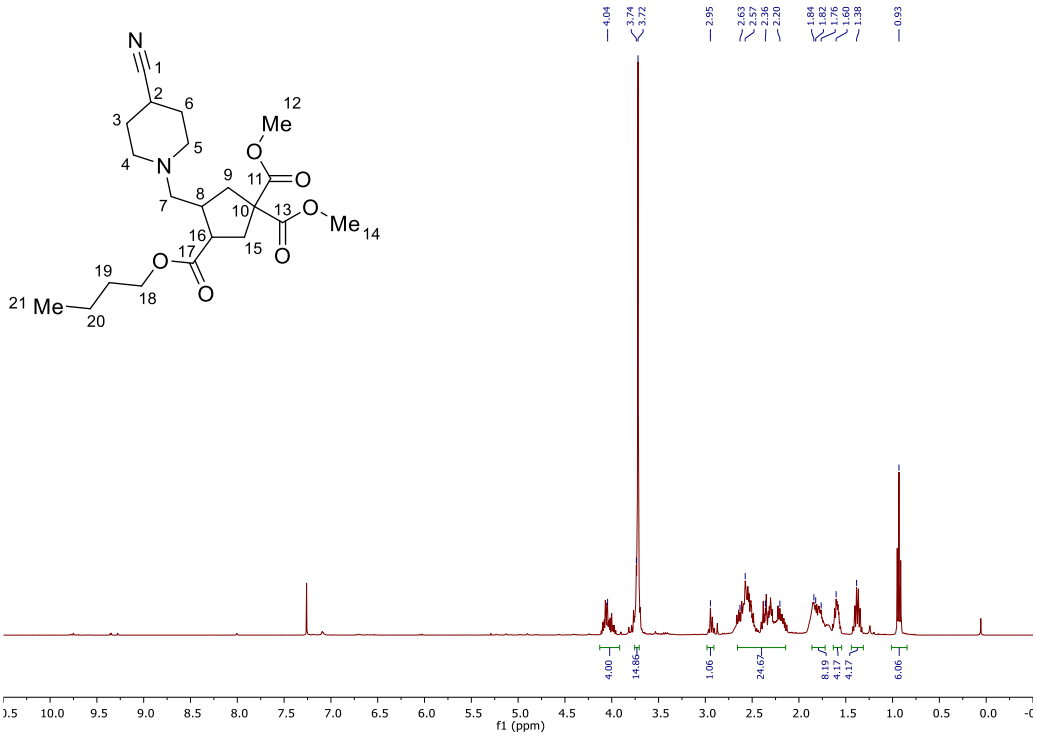

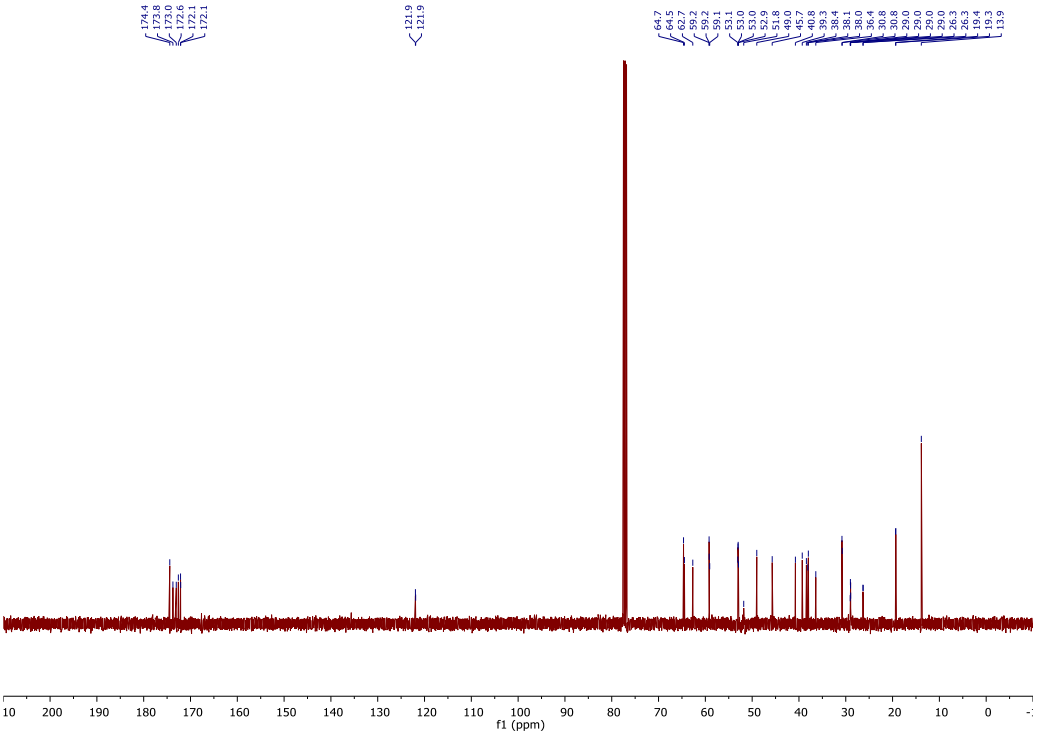

Dimethyl 6-((4-cyanopiperidin-1-yl)methyl)hexahydro-4*H*-cyclopenta[*b*]furan-4,4-dicarboxylate (409)

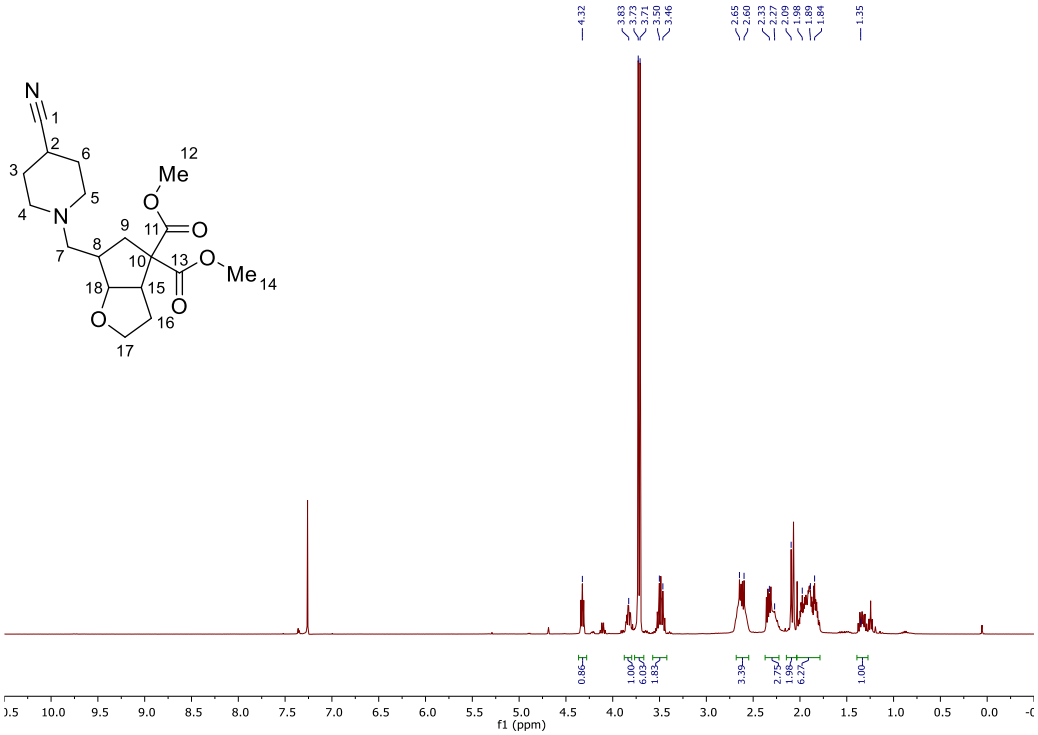

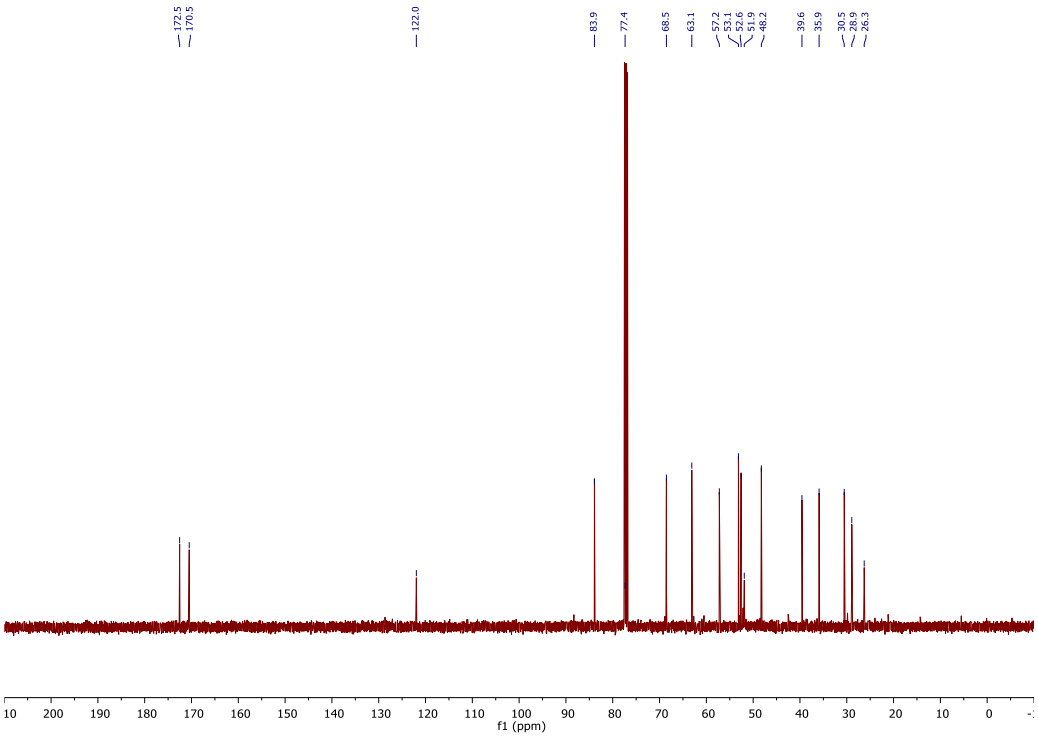

1-(Cyclopropylmethyl)-4-phenylpiperidine (417)

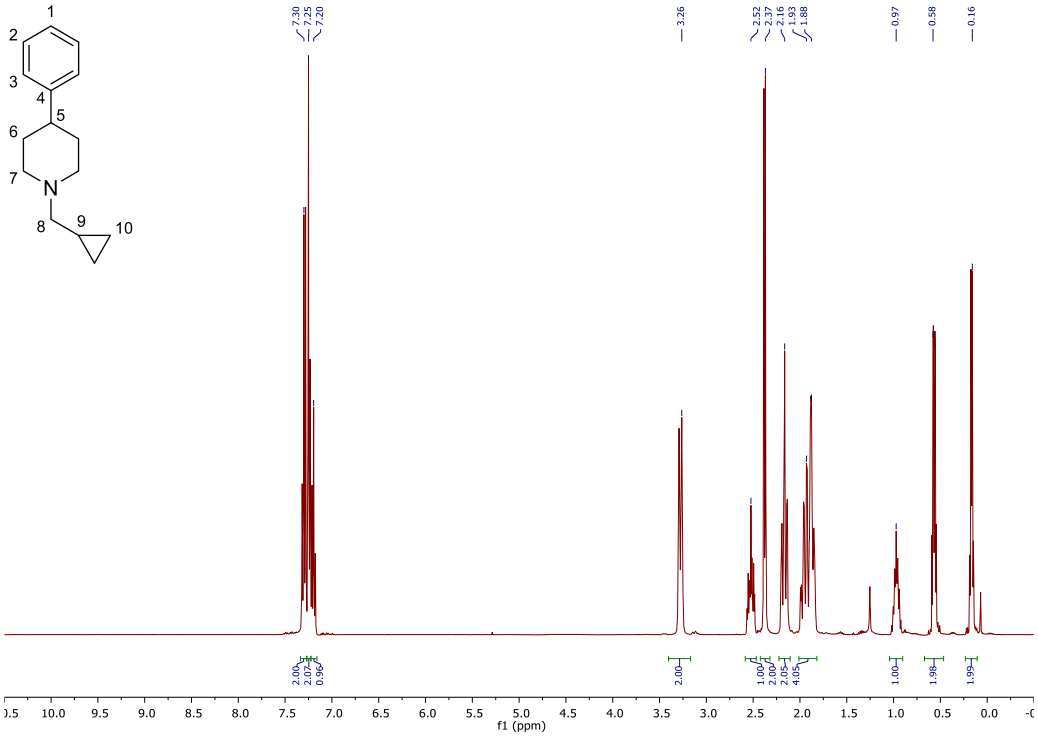

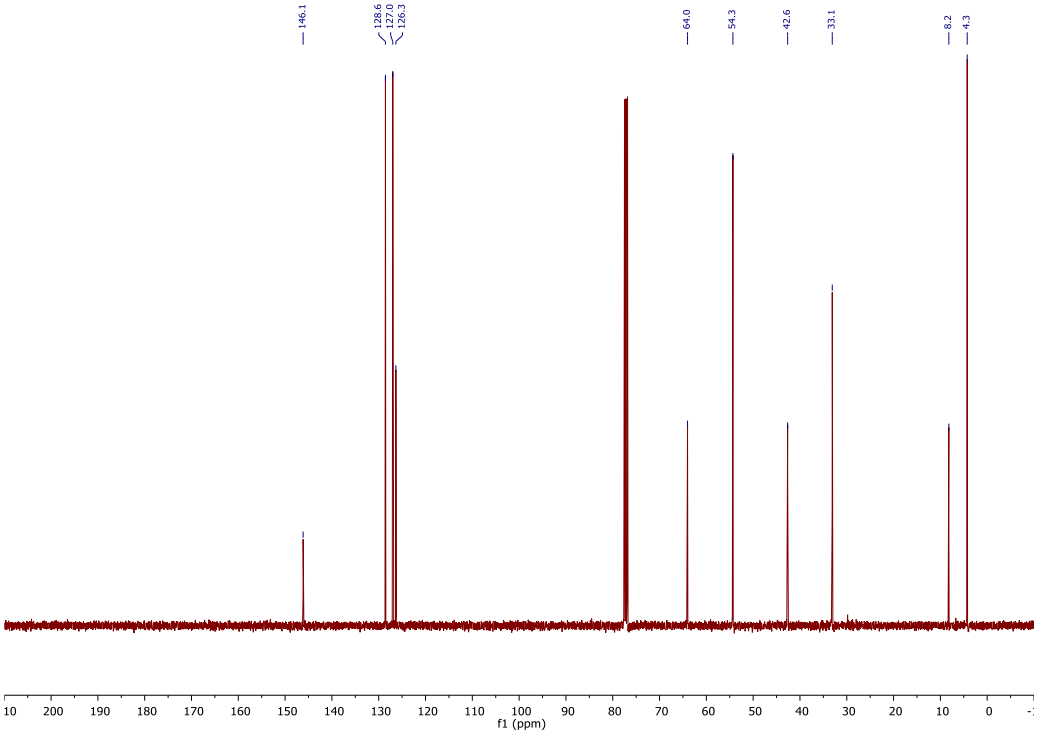

A.1.2. Radical Reductive Amination

N,N-Dibenzylbutan-1-amine (446)

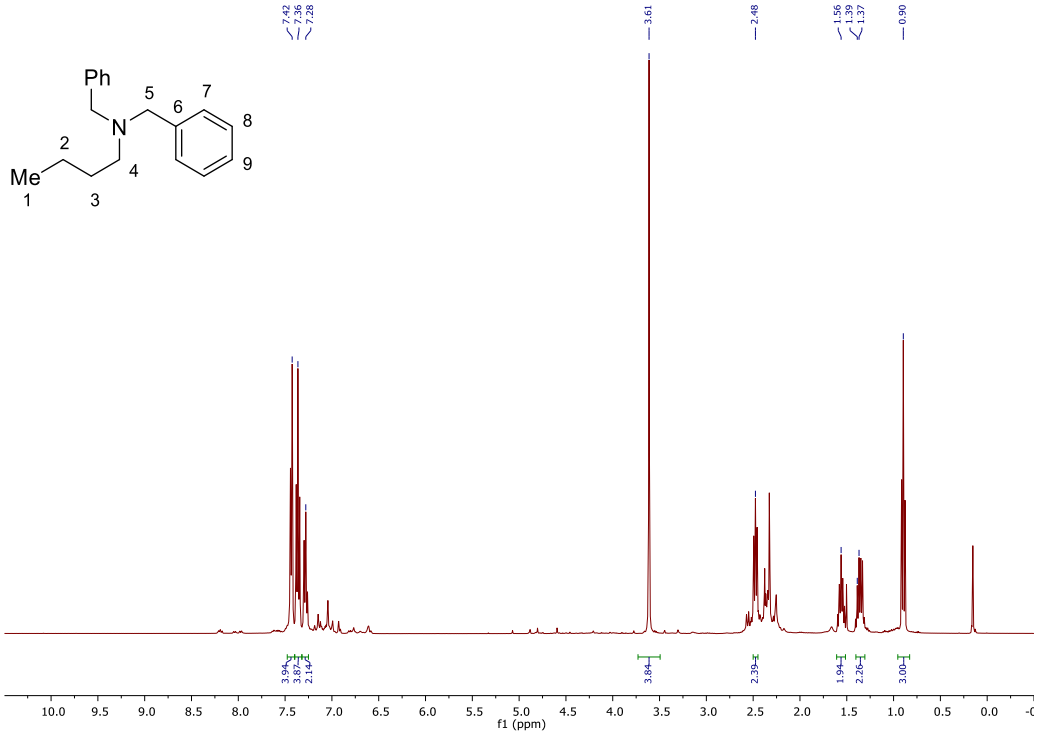

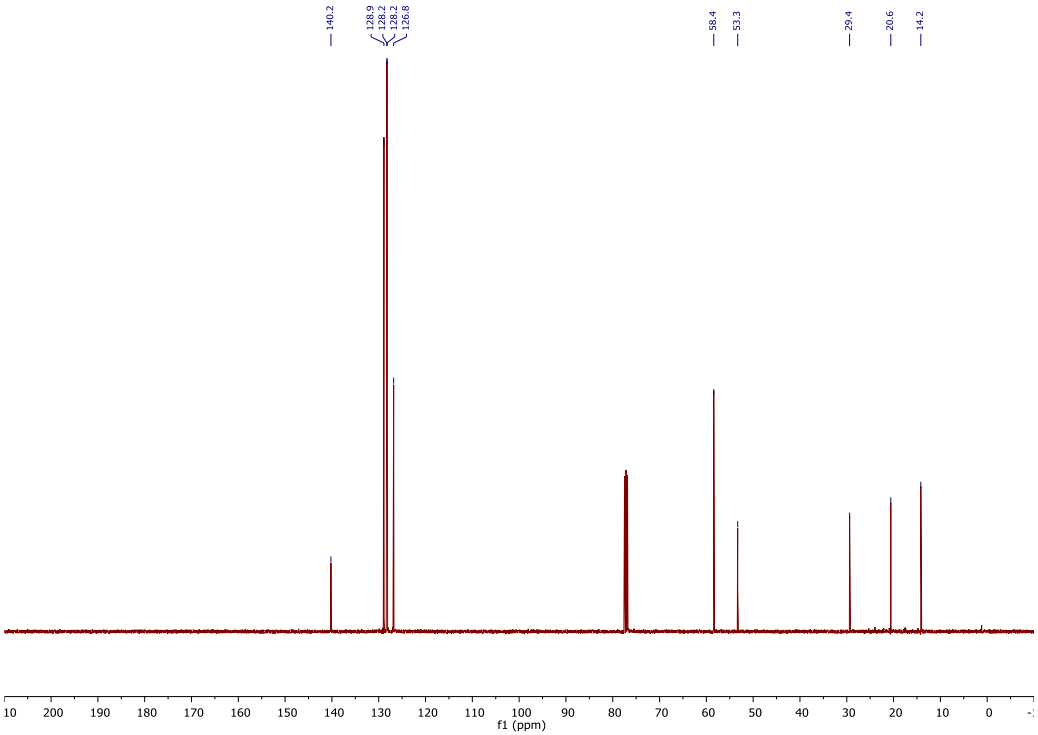

1-Benzylpiperidine (447)

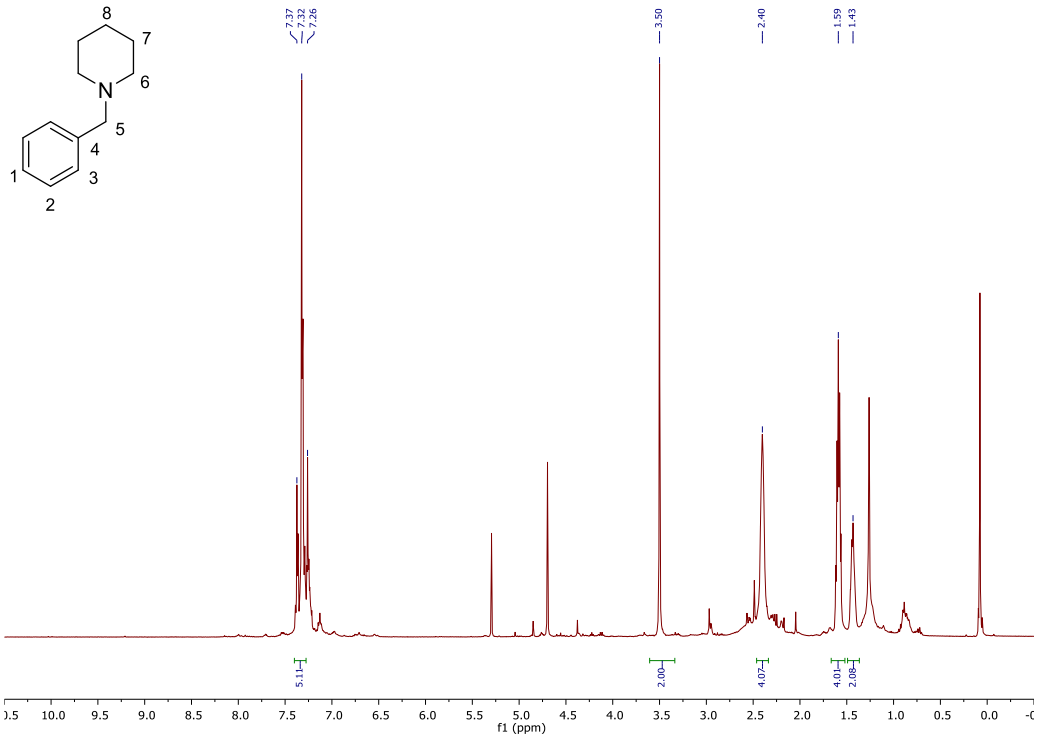

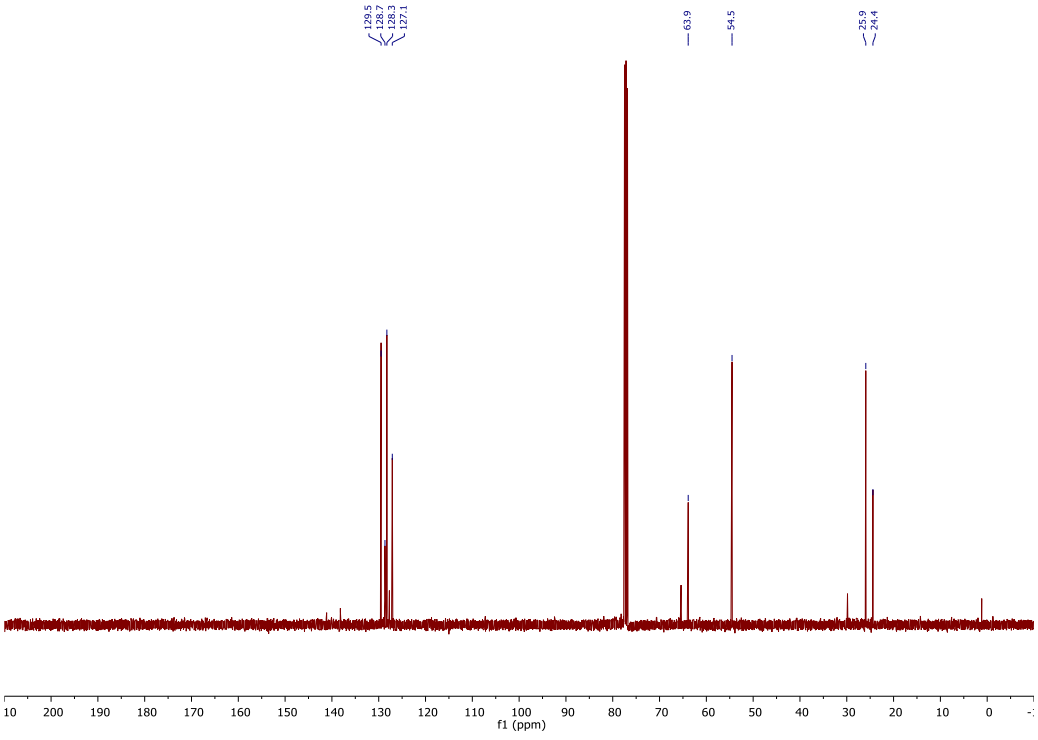

***N*-Benzyl-*N*-methyl-1-phenylmethanamine (448)**

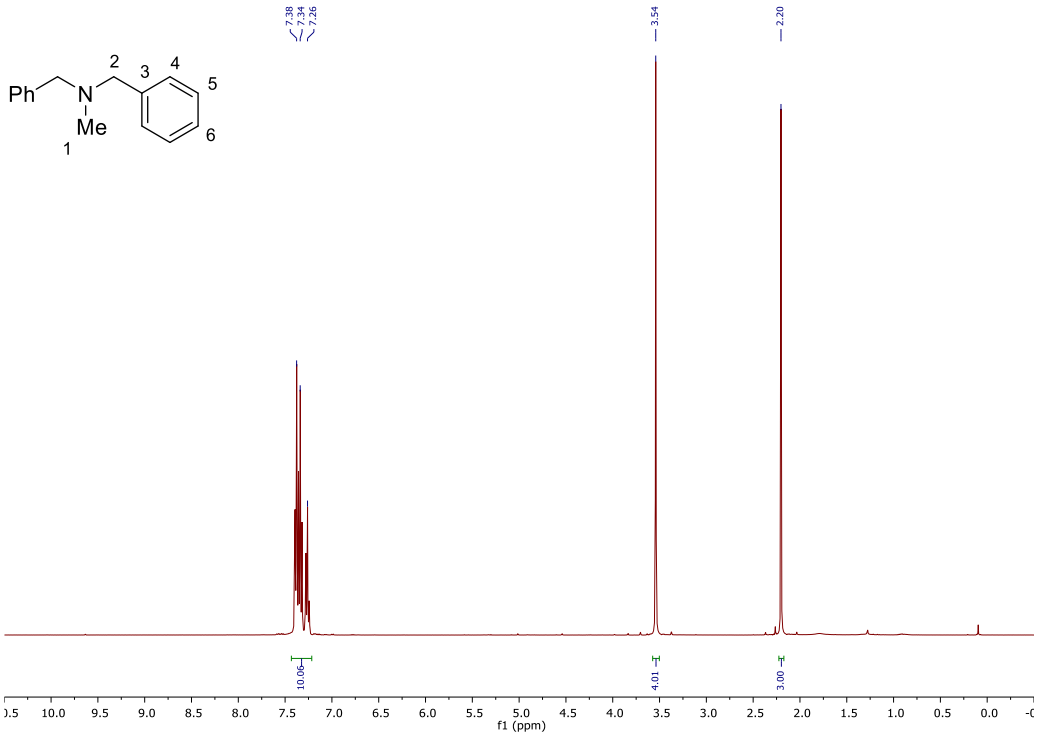

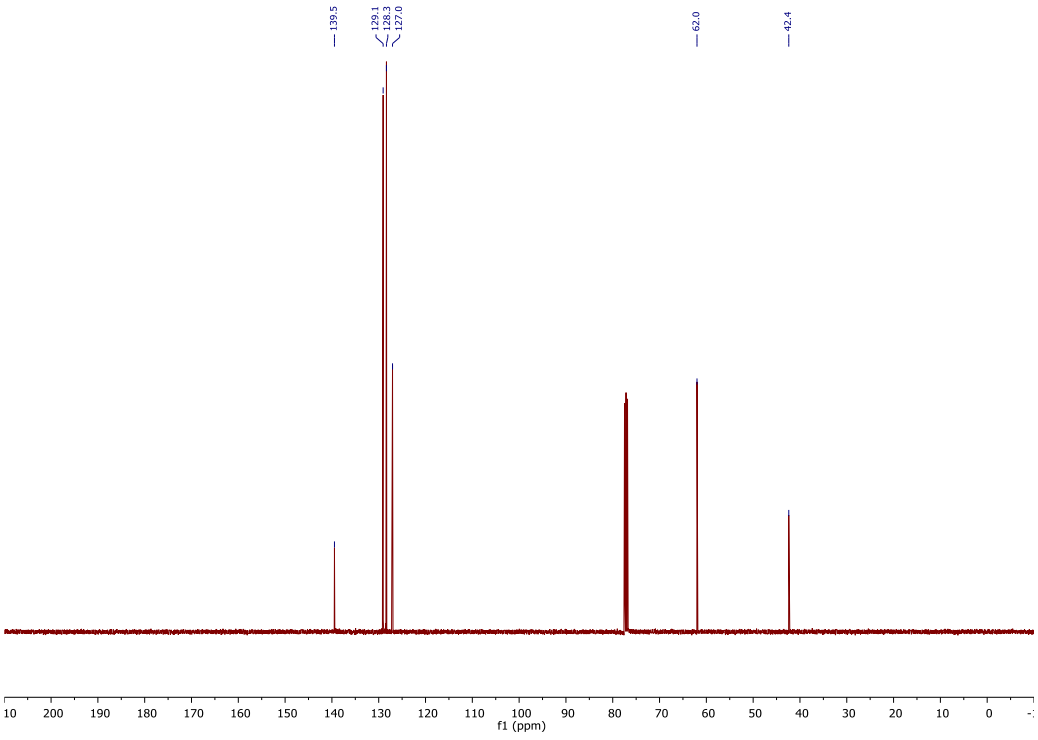

N-Cyclohexyl-*N*-methylcyclohexanamine (449)

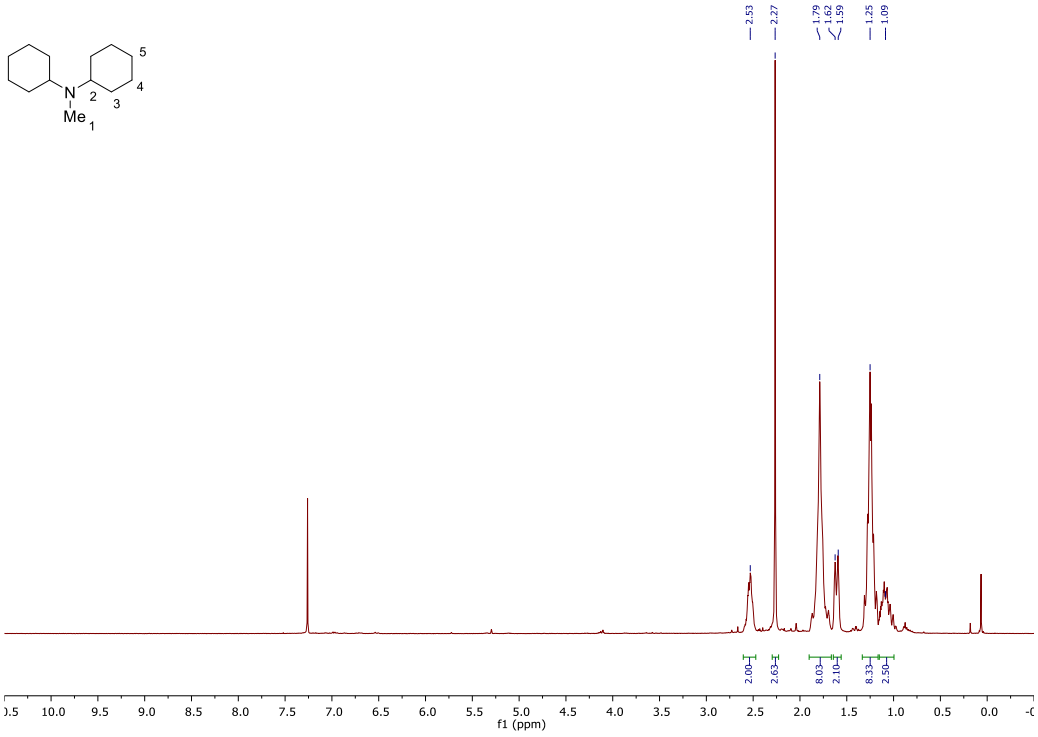

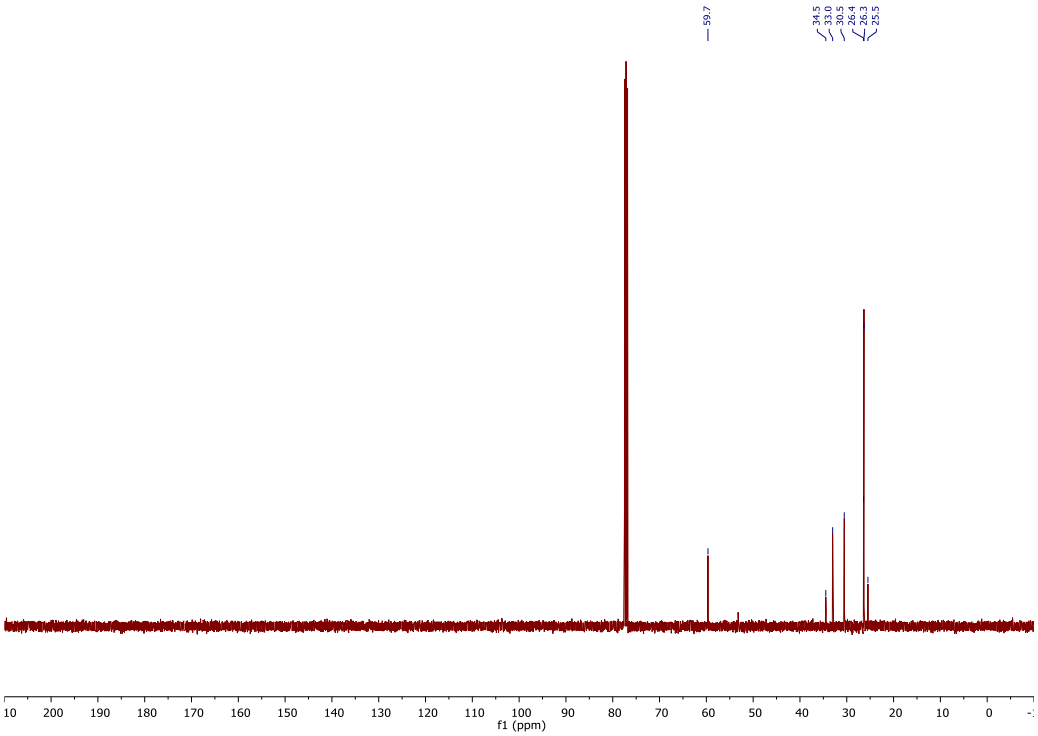

1-Benzyl-4-(pyrrolidin-1-yl)piperidine (460)

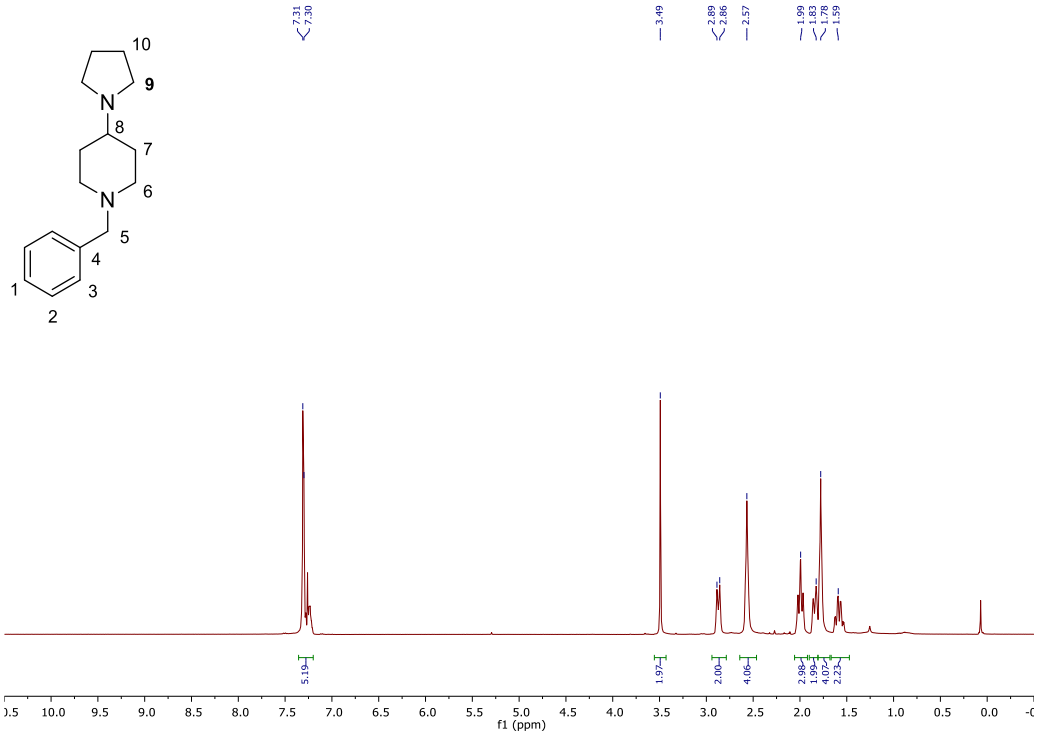

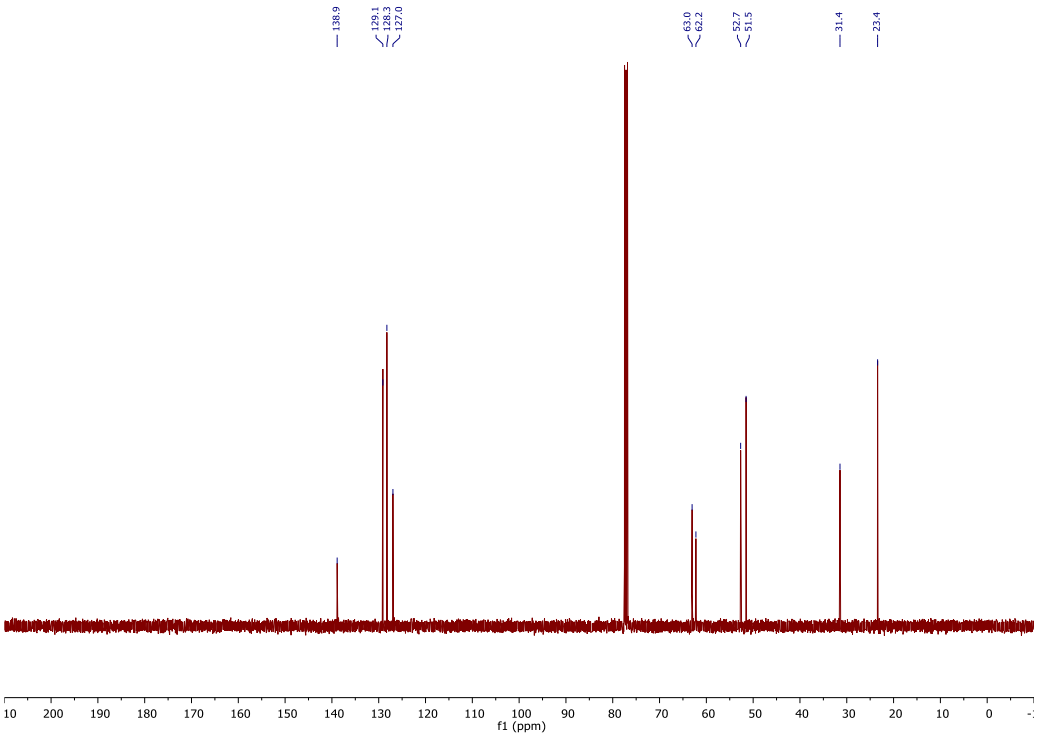

4-((2-Amino-3,5-dibromobenzyl)(methyl)amino)cyclohexan-1-ol (452)

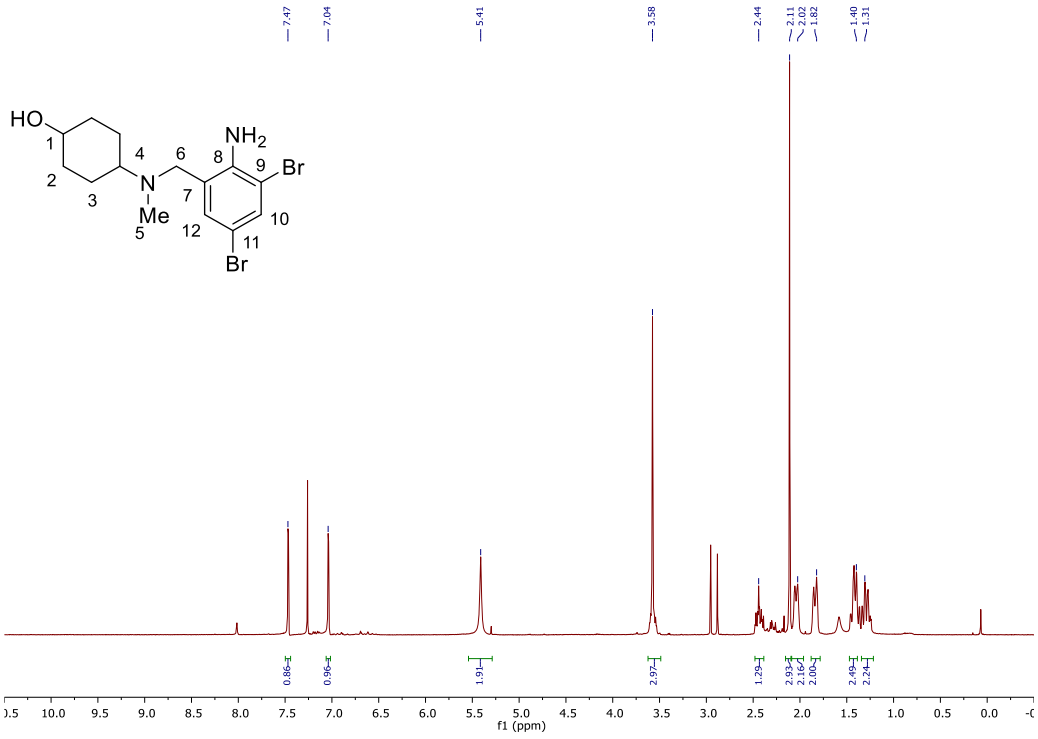

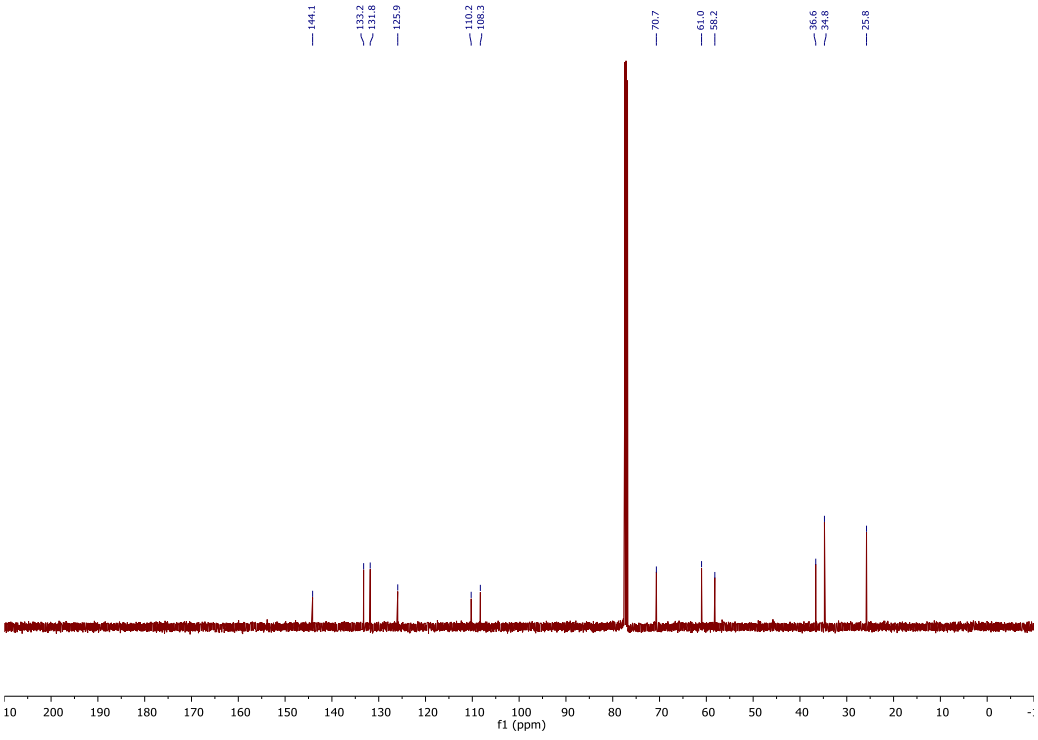

1-Cyclopropyl-6-fluoro-7-(4-methylpiperazin-1-yl)-4-oxo-1,4-dihydroquinoline-3-carboxylic acid (453)

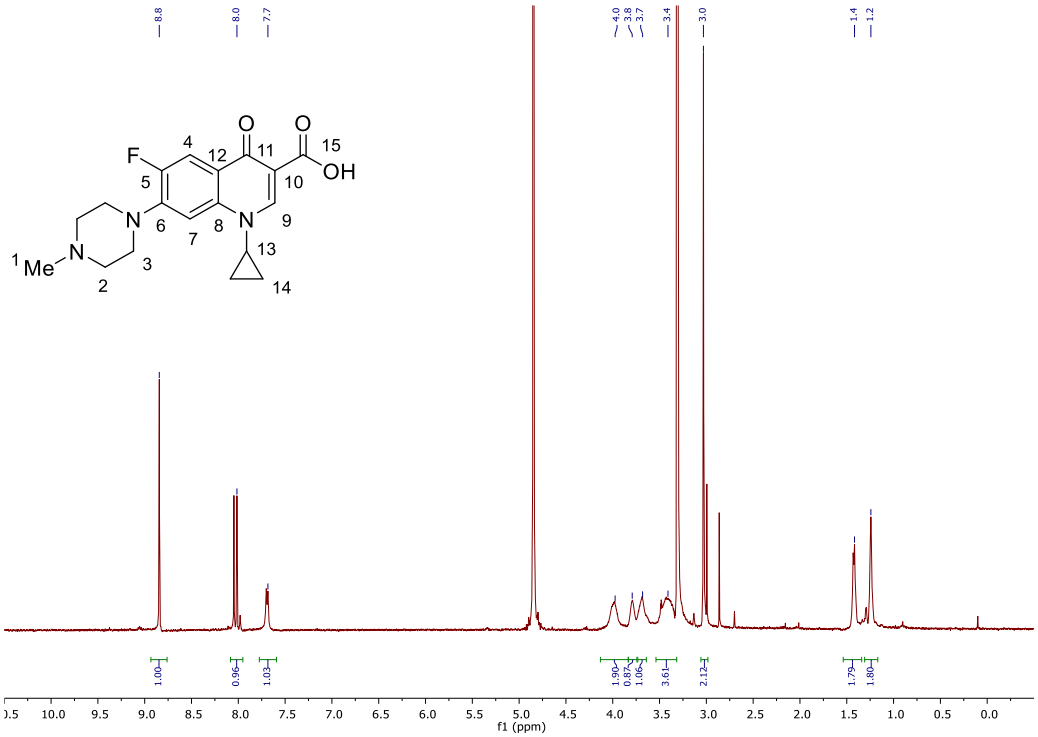

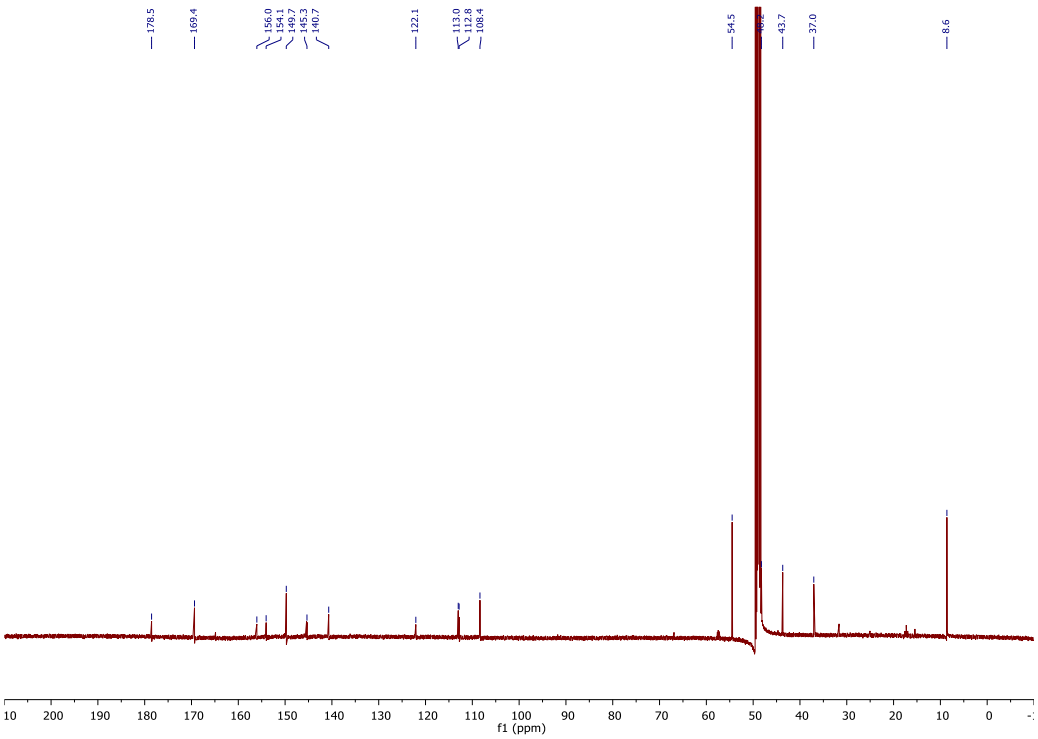

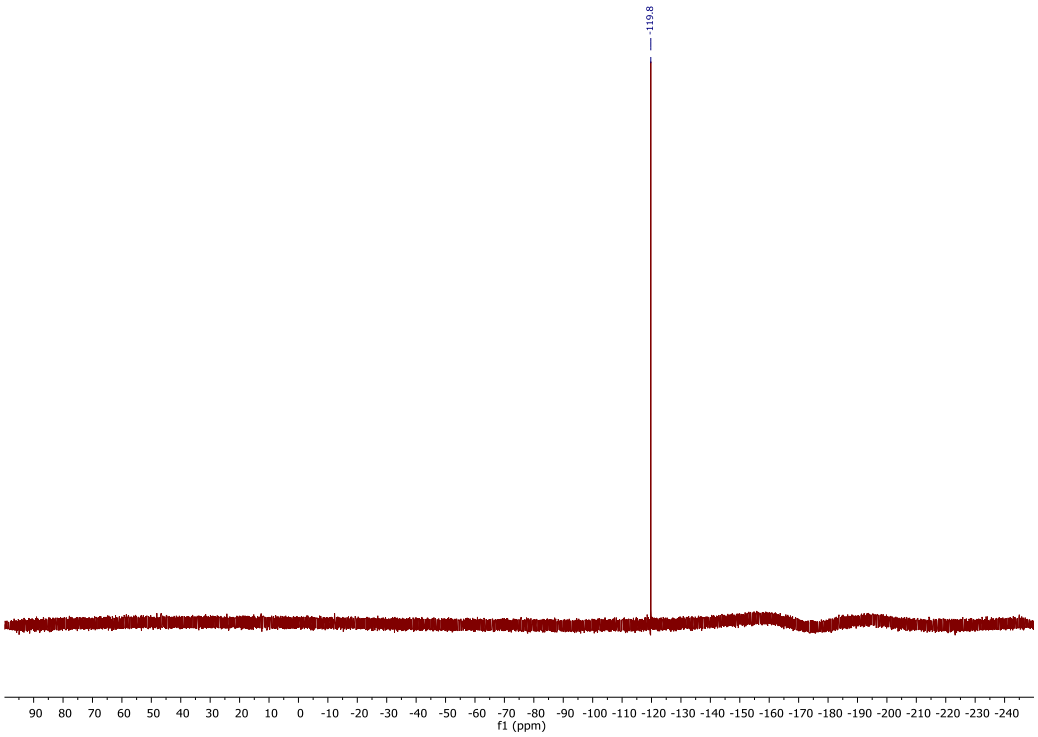
-119.8
90 80 70 60 50 40 30 20 10 0 -10 -20 -30 -40 -50 -60 -70 -80 -90 -100 -110 -120 -130 -140 -150 -160 -170 -180 -190 -200 -210 -220 -230 -240
f1 (ppm)

tert-Butyl (1-butylpiperidin-4-yl)carbamate (473)

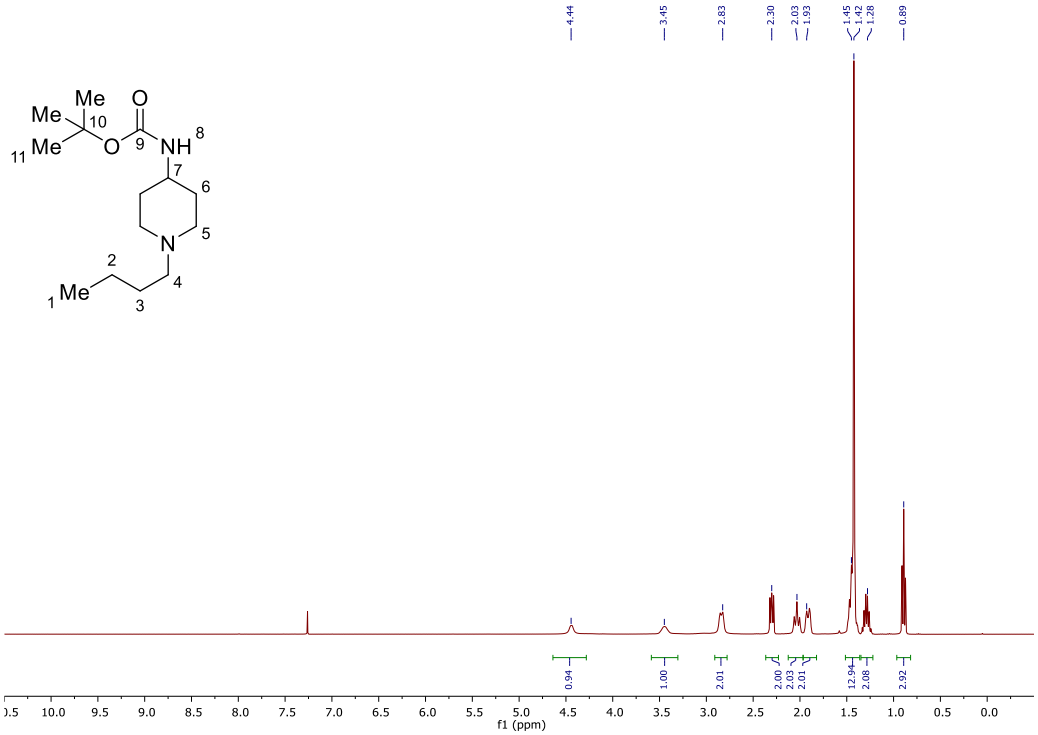

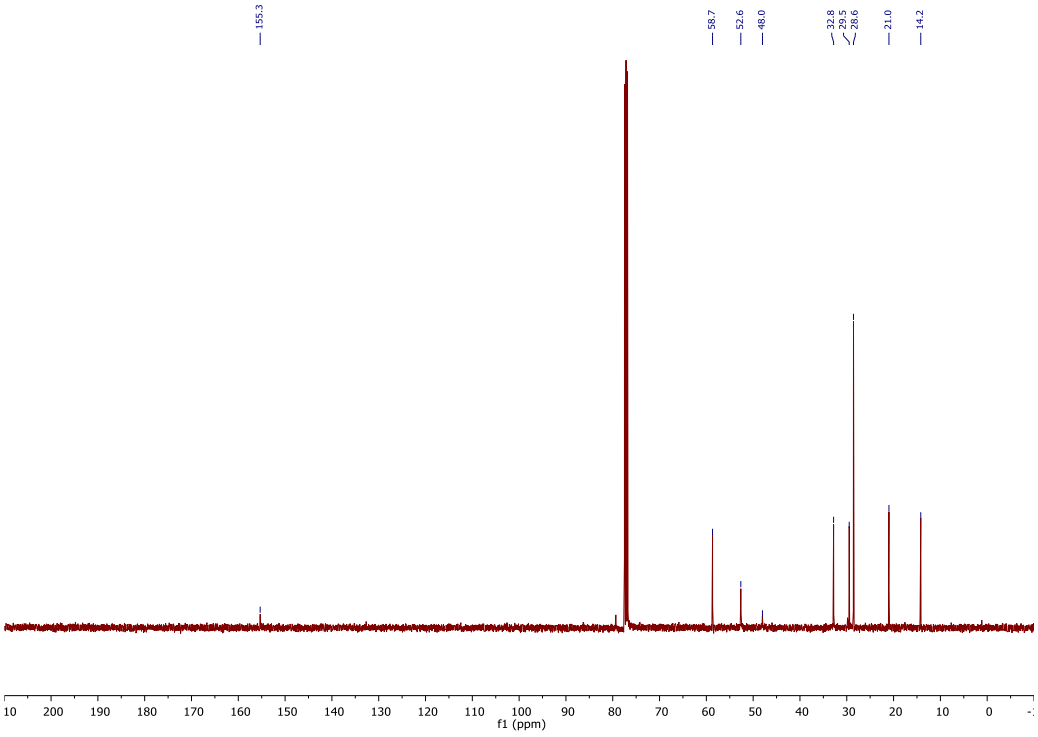

tert-Butyl ((1-butylpiperidin-4-yl)methyl)carbamate (525)

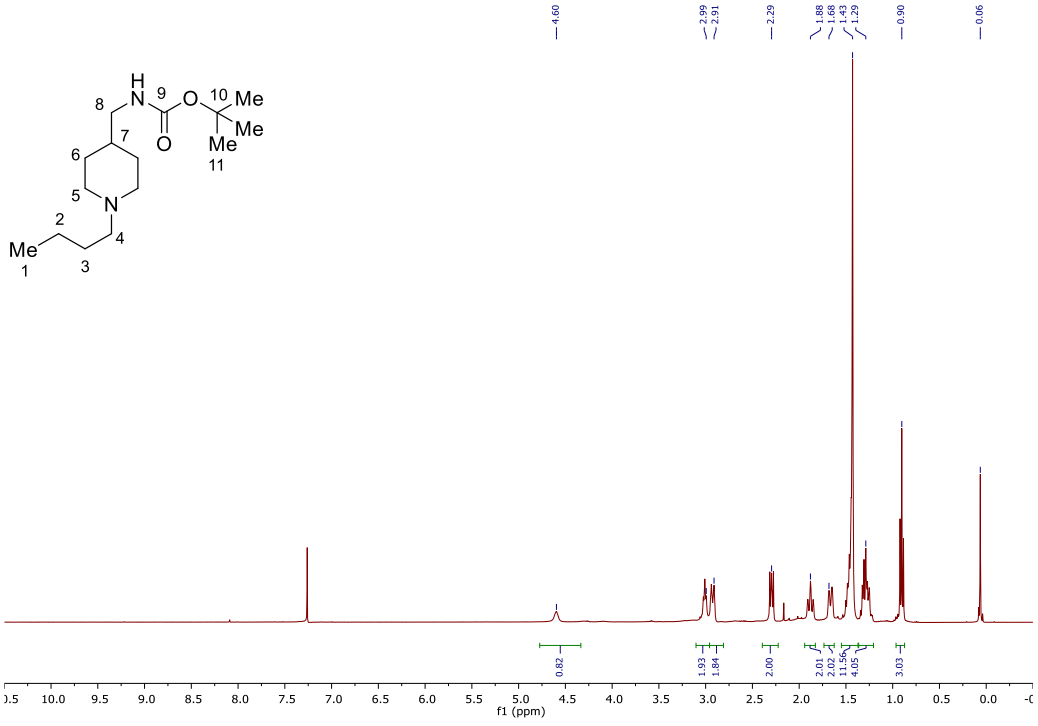

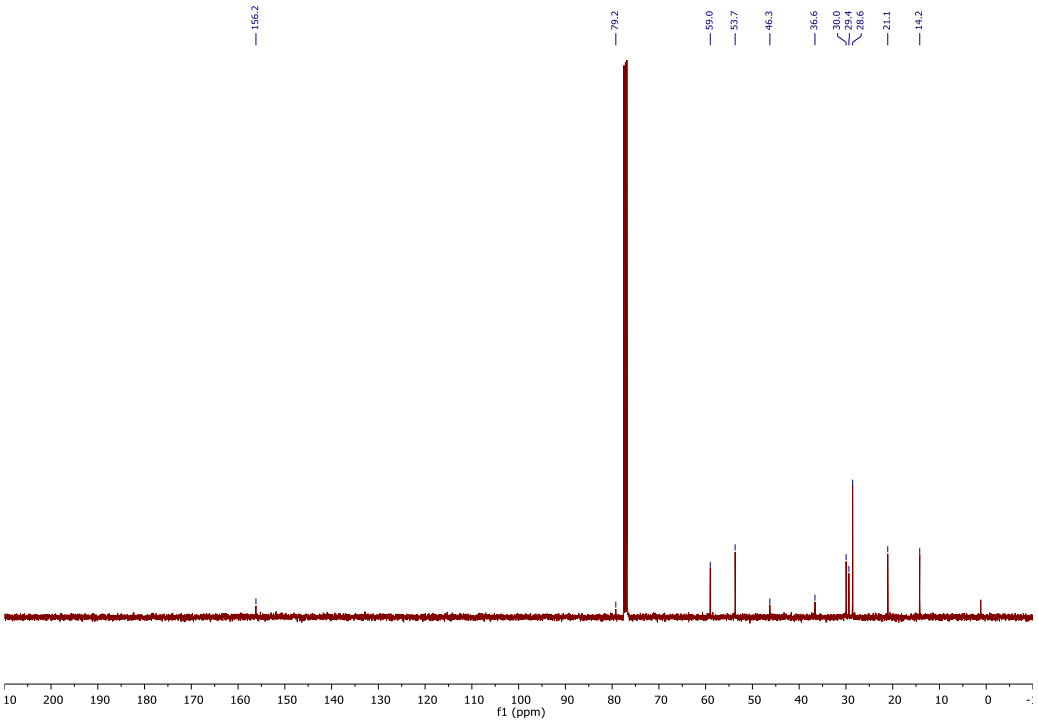

(*S*)-N^6-butyl-N^6-propyl-4,5,6,7-tetrahydrobenzo[*d*]thiazole-2,6-diamine (505)

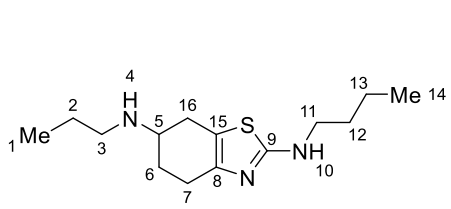

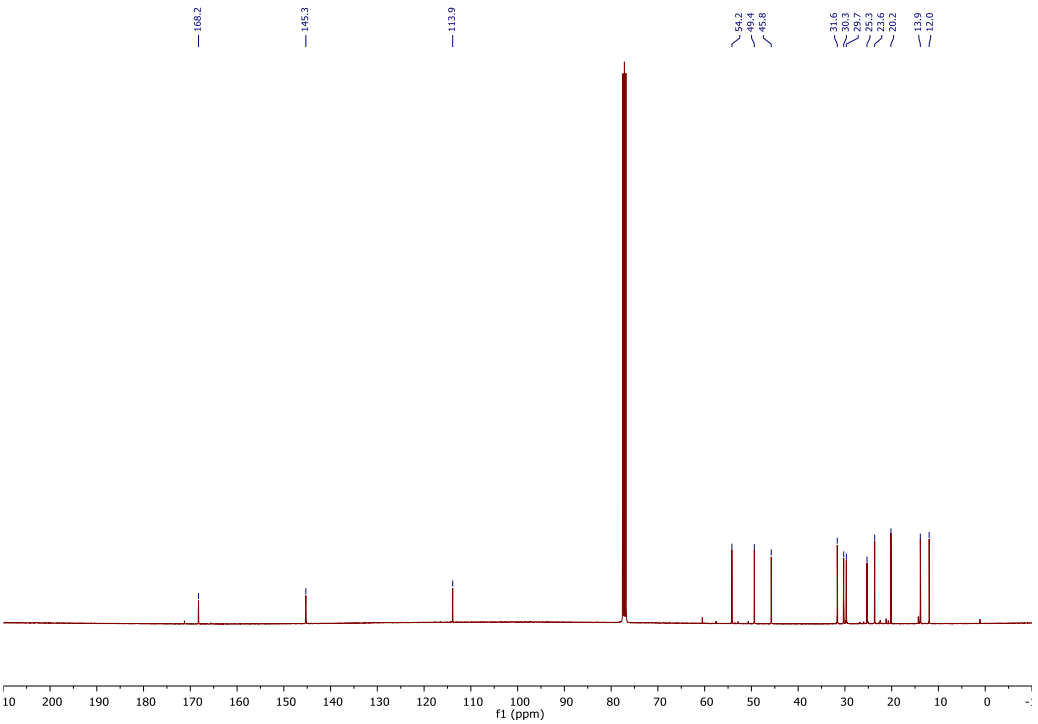

(*S*)-N^2,N^6-Dipropyl-4,5,6,7-tetrahydrobenzo[*d*]thiazole-2,6-diamine (507)

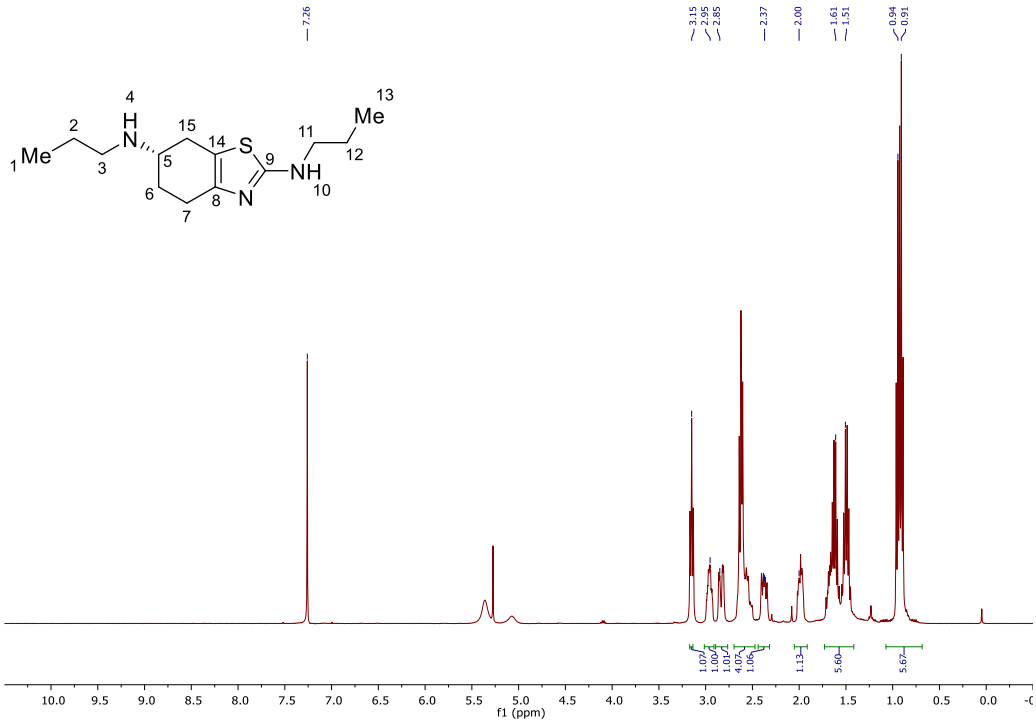

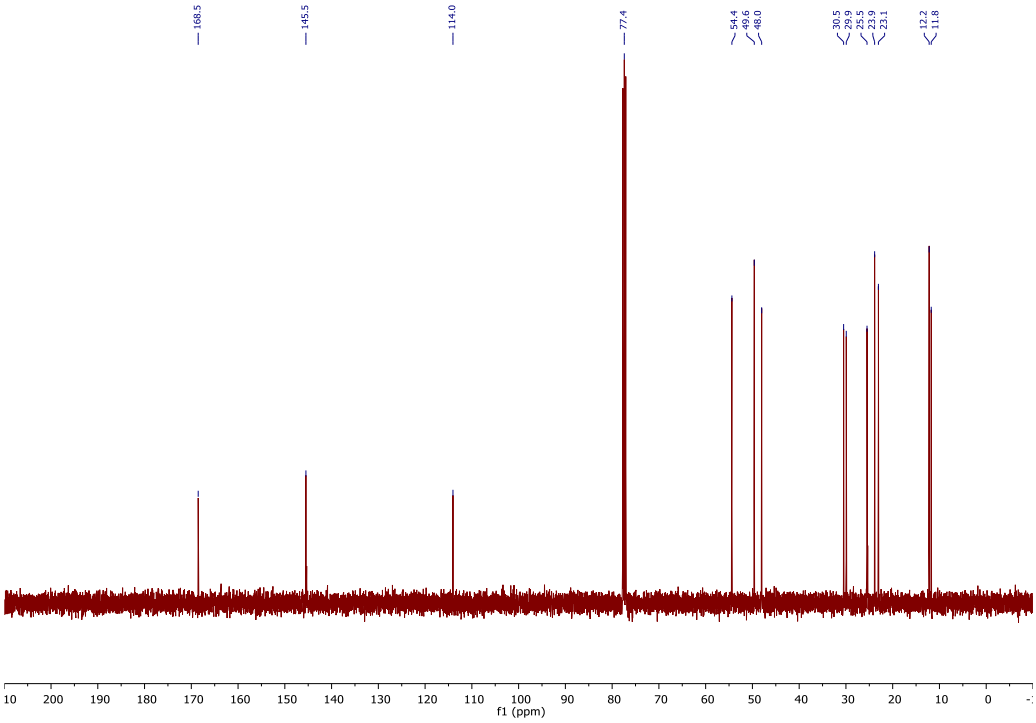

(*S*)-*N*6,*N*6-dipropyl-4,5,6,7-tetrahydrobenzo[*d*]thiazole-2,6-diamine (508)

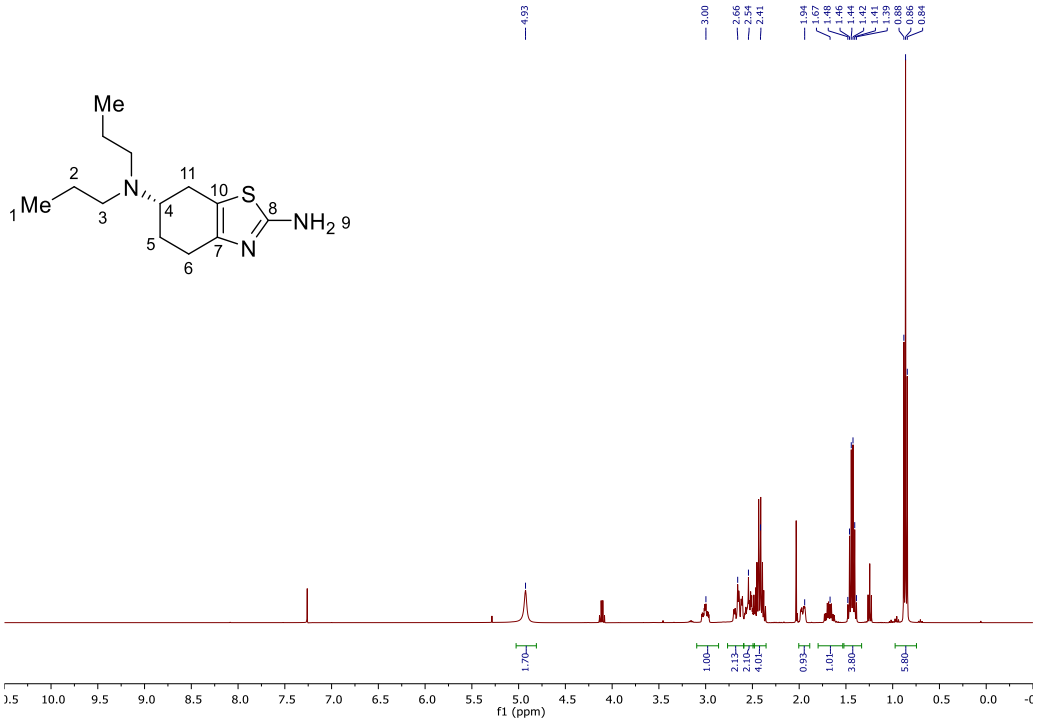

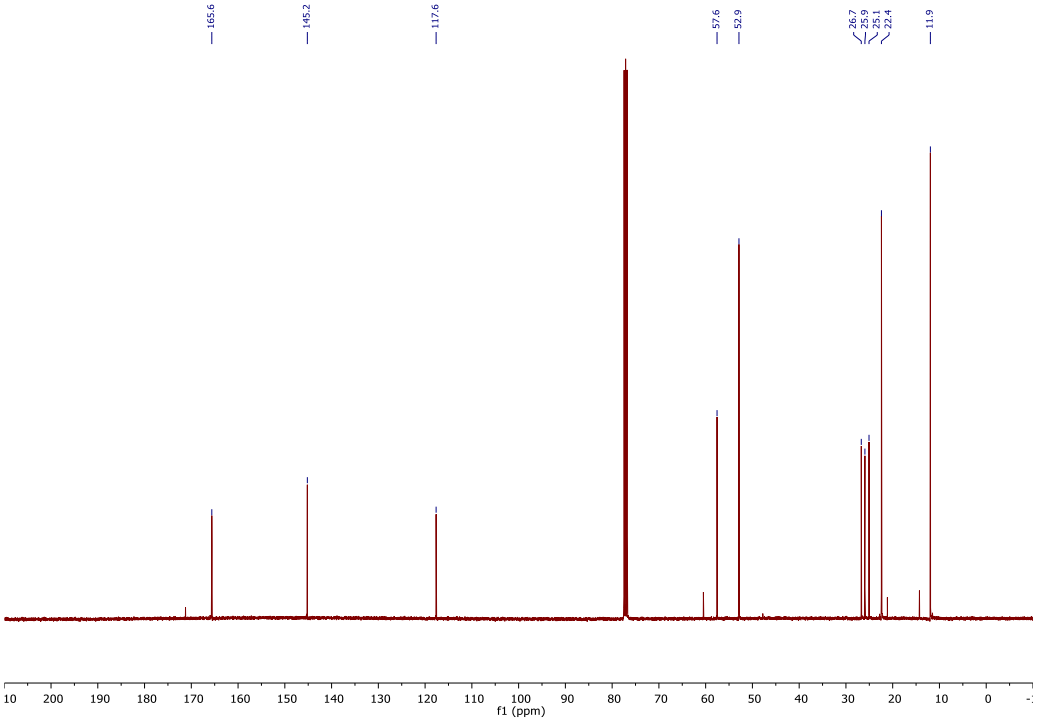

A.2. Computational Data

Density functional theory (DFT) calculations were performed with the Gaussian 16 package, Revision A.03, on the Darwin Supercomputer of the University of Cambridge High Performance Computing Service (http://www.hpc.cam.ac.uk), provided by Dell, using Strategic Research Infrastructure Funding from the Higher Education Funding Council for England.

Geometry optimizations were performed with the B3LYP functional and 6-311+G(d,p) basis set.[320,321] Normal vibrational mode analysis at the same level of theory confirmed that the optimized structures are minima (zero imaginary frequencies). Optimizations were performed in dichloromethane solvent using the conductor-like polarizable continuum model (CPCM) of solvation to account for charged species.[322,323] Dispersion correction was accounted for using the D3 version of Grimme's dispersion with Becke-Johnson damping.[324] Single-point energies were evaluated using the 6-311+G(2d,p) basis set. DFT-optimized structures were illustrated using CYLView.[325]

With the optimized geometries, single point time-dependent DFT (TD-DFT) calculations were conducting for the first 3 excited singlet states using the CAM-B3LYP functional[326] and 6-311+G(d,p) basis set. The CPCM solvation model for dichloromethane was used. Molecular orbitals were illustrated using Avogadro.[327] Calculation of electronic excitations was carried out using GaussSum.[328]

A.2.1. Geometry Optimization

Energy profile

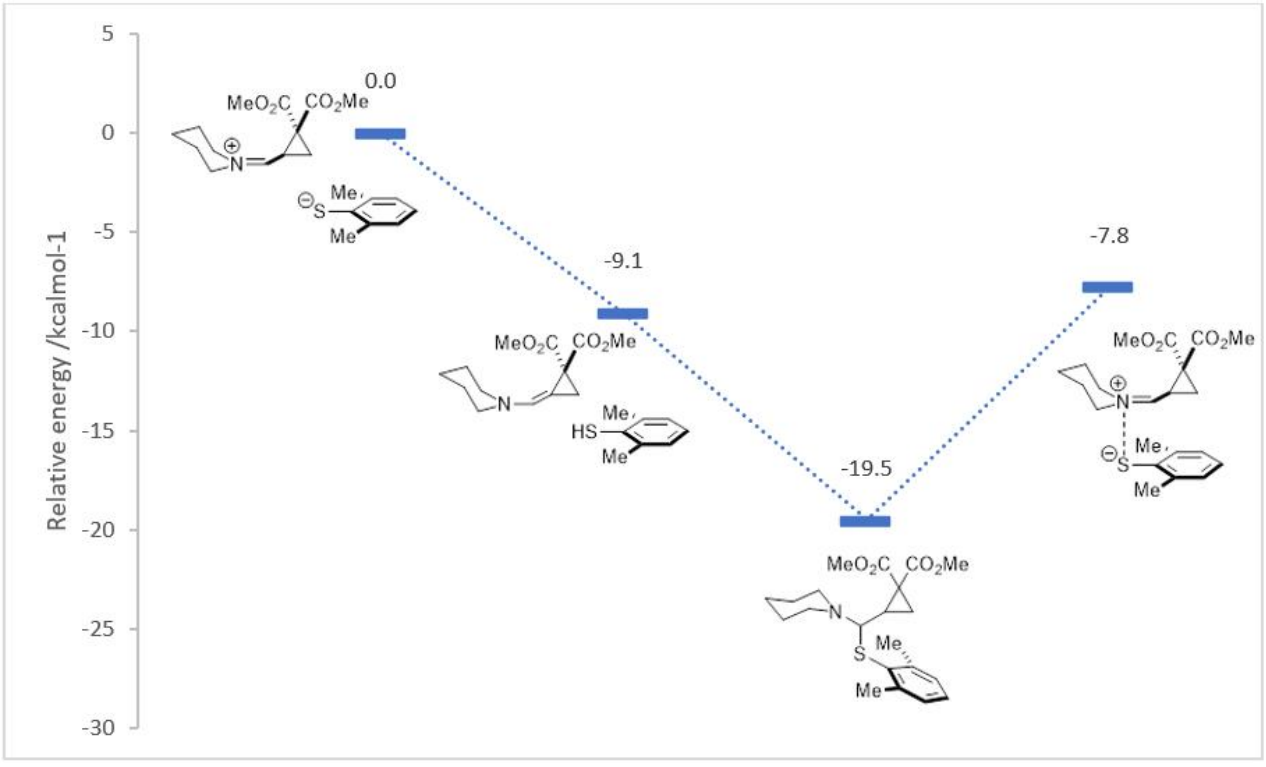

Optimized structures

1-((2,2-Bis(methoxycarbonyl)cyclopropyl)methylene)piperidin-1-ium (526)

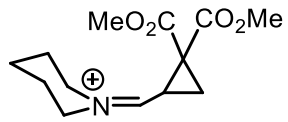

B3LYP/6-311+G(d,p)/scrf(CPCM,solvent=dichloromethane)/EmpiricalDispersion=GD3BJ

Single point energy with 6-311+G(2d,p)

C	0.54605	0.18374	1.64383	H	-4.76469	0.24901	-0.40344
C	1.53438	0.56776	0.52220	H	-3.19423	0.79966	-0.97958
C	1.56995	1.25221	1.86535	H	-3.74658	-0.64535	1.66671
C	1.08900	1.35658	-0.67200	H	-3.30737	1.06172	1.47828
C	2.57745	-0.48371	0.22244	C	-0.88189	0.50948	1.52157
H	1.22958	2.27894	1.89205	H	0.74733	-0.78535	2.08486
H	2.40857	1.01179	2.50405	H	-1.23039	1.48729	1.83123
N	-1.77457	-0.31416	1.10436	O	1.71242	1.41565	-1.70378
C	-1.47697	-1.65688	0.55137	O	3.66789	-0.53116	0.73727
C	-1.95240	-1.72700	-0.90324	O	2.10118	-1.37001	-0.65128
H	-2.01187	-2.37659	1.17463	O	-0.05445	2.01029	-0.43517
H	-0.41097	-1.84638	0.62518	C	-0.56267	2.85478	-1.49756
C	-3.43147	-1.35481	-1.02911	C	2.99907	-2.43433	-1.05074
H	-1.76949	-2.74239	-1.26052	H	0.16152	3.63472	-1.72760
H	-1.33910	-1.05479	-1.51045	H	-1.48070	3.28298	-1.10596
C	-3.69766	0.01694	-0.40412	H	-0.76162	2.25192	-2.38231
H	-4.04432	-2.11192	-0.52778	H	3.28342	-3.02598	-0.18135
H	-3.72595	-1.34968	-2.08049	H	3.88549	-2.01206	-1.52248
C	-3.20569	0.06978	1.04276	H	2.43425	-3.03382	-1.75852

2,6-Dimethylbenzenethiolate (527)

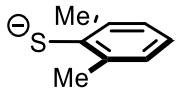

B3LYP/6-311+G(d,p)/scrf(CPCM,solvent=dichloromethane)/EmpiricalDispersion=GD3BJ

Single point energy with 6-311+G(2d,p)

C	-0.43147	0.00098	0.00000	S	-2.20294	0.00470	0.00000
C	0.29738	-1.22121	0.00001	C	-0.41506	-2.54738	0.00002
C	1.69444	-1.20244	0.00001	C	-0.40359	2.54939	-0.00002
C	2.40719	-0.00532	0.00000	H	-1.05487	2.65250	-0.87340
C	1.69976	1.19496	-0.00001	H	0.31732	3.37090	-0.00027
C	0.30279	1.21996	-0.00002	H	-1.05448	2.65272	0.87362
H	2.23977	2.13733	-0.00003	H	0.30204	-3.37221	0.00022
H	3.49163	-0.00773	0.00001	H	-1.06648	-2.64767	-0.87360
H	2.23025	-2.14720	0.00003	H	-1.06680	-2.64749	0.87341

Dimethyl 2-(((2,6-dimethylphenyl)thio)(piperidin-1-yl)methyl)cyclopropane-1,1-dicarboxylate (342)

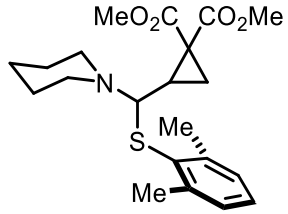

B3LYP/6-311+G(d,p)/CPCM(CH2CL2)/EmpiricalDispersion=GD3BJ

Single point energy with 6-311+G(2d,p)

C	2.76406	-0.56232	-0.56427	H	-3.84788	-1.42348	-2.73260
C	3.39602	0.62594	-0.98857	H	-3.93779	-1.03719	-1.01348
C	4.44416	1.13743	-0.21952	C	-2.65219	-3.35967	-0.11364
C	4.86454	0.49445	0.94057	H	-2.96148	-3.67393	-2.22587
C	4.24951	-0.68734	1.33562	H	-4.45447	-3.44168	-1.32296
C	3.20084	-1.24045	0.59296	C	-1.23418	-2.79923	-0.20015
H	4.58857	-1.20091	2.22865	H	-2.60164	-4.43141	0.09879
H	5.67620	0.90822	1.52801	H	-3.17330	-2.88352	0.72410
H	4.93151	2.05282	-0.53630	H	-0.65822	-3.36145	-0.95332
S	1.37765	-1.20117	-1.51047	H	-0.71652	-2.91665	0.75435
C	2.97452	1.36033	-2.23577	C	-0.03884	-0.69114	-0.29485
C	2.58292	-2.53356	1.06227	H	-0.24979	1.23523	-1.34289
H	1.67632	-2.35667	1.64971	H	0.34034	-0.99841	0.67364
H	3.28027	-3.07575	1.70292	H	3.61471	2.22892	-2.39809
H	2.30170	-3.16899	0.22232	H	1.94030	1.70396	-2.16547
C	-0.14993	0.81295	-0.35455	H	3.03353	0.71889	-3.11802
C	-0.98459	1.55872	0.70562	O	-2.88640	0.65686	1.85300
C	0.54596	1.64751	0.65404	O	-2.44066	3.43597	1.04602
C	-1.68462	0.73130	1.73865	O	-1.41155	3.19476	-0.93798
C	-1.71302	2.80640	0.31173	O	-0.82472	0.04040	2.50576
H	1.07343	1.14917	1.45481	C	-1.40982	-0.90912	3.42149
H	0.95797	2.59743	0.34124	C	-1.96601	4.45608	-1.36877
N	-1.26141	-1.37222	-0.52989	H	-2.02675	-0.39328	4.15663
C	-1.94041	-1.09163	-1.79794	H	-0.56848	-1.39997	3.90329
C	-3.37816	-1.60782	-1.76224	H	-2.01510	-1.63135	2.87370
H	-1.39909	-1.56071	-2.63737	H	-1.62484	5.25922	-0.71567
H	-1.93652	-0.01506	-1.96835	H	-3.05464	4.41036	-1.35937
C	-3.42022	-3.09793	-1.41255	H	-1.59725	4.60120	-2.38056

Cyclopropyl carboximinium thiolate complex (352)

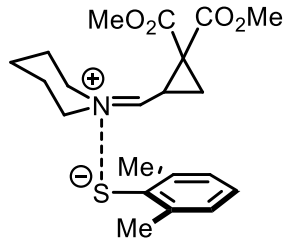

B3LYP/6-311+G(d,p)/CPCM(CH_2Cl_2)/EmpiricalDispersion=GD3BJ

Single point energy with 6-311+G(2d,p)

C	-3.11192	-0.75587	-0.52281	H	1.77011	2.84310	-2.34787
C	-2.33290	-1.94080	-0.36790	H	2.01617	2.45469	-0.65020
C	-2.12754	-2.48464	0.90458	C	-0.47956	3.42253	0.23547
C	-2.65123	-1.88401	2.04442	H	-0.32875	4.03871	-1.82864
C	-3.43282	-0.73691	1.89891	H	0.94681	4.68054	-0.80022
C	-3.68706	-0.17663	0.64602	C	-1.26120	2.12705	0.01697
H	-3.86754	-0.27066	2.77770	H	-1.19715	4.21000	0.47663
H	-2.46818	-2.30612	3.02572	H	0.17690	3.30543	1.10341
H	-1.53384	-3.38833	0.99682	H	-1.99161	2.22142	-0.78790
S	-3.34222	-0.02688	-2.10833	H	-1.77734	1.80056	0.91598
C	-1.75747	-2.64622	-1.56560	C	-0.19343	-0.00984	0.32688
C	-4.60288	1.01472	0.55157	H	0.69590	-1.45408	-1.00901
H	-4.13830	1.84788	0.02073	H	-0.79758	-0.08736	1.22192
H	-4.90395	1.35097	1.54640	H	-1.12654	-3.48356	-1.25886
H	-5.50373	0.76446	-0.01807	H	-1.17503	-1.96609	-2.19302
C	0.76656	-1.08014	0.00474	H	-2.55385	-3.02890	-2.21182
C	2.21538	-1.00755	0.52900	O	3.79969	0.44346	1.57631
C	1.23597	-2.04460	1.03641	O	3.76185	-2.53544	-0.51247
C	2.65232	0.08186	1.45679	O	3.55159	-0.43294	-1.29880
C	3.27061	-1.43350	-0.46154	O	1.62585	0.58028	2.15611
H	0.87928	-1.91270	2.04866	C	1.93007	1.61514	3.12097
H	1.41254	-3.06453	0.72403	C	4.56496	-0.68976	-2.29955
N	-0.33708	1.04631	-0.39127	H	2.59536	1.22161	3.88834
C	0.44264	1.34182	-1.61296	H	0.97192	1.89617	3.54840
C	1.24968	2.62670	-1.41235	H	2.39597	2.46281	2.62034
H	-0.28737	1.45334	-2.41658	H	4.25206	-1.51083	-2.94367
H	1.09017	0.50104	-1.83961	H	5.51005	-0.93395	-1.81564
C	0.34510	3.79127	-1.00100	H	4.64904	0.23371	-2.86510

Cyclopropyl carboximinium thiolate complex, alternative geometry (528)

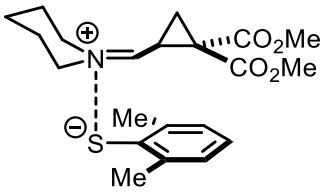

B3LYP/6-311+G(d,p)/CPCM(CH_2Cl_2)/EmpiricalDispersion= GD3BJ

C	-1.65780	-2.09756	-0.50084	C	-3.27097	-2.54879	1.42317
C	-0.31073	-2.02858	-0.96330	H	-3.90521	-1.68392	1.21677
C	0.74913	-2.19775	-0.06684	H	-3.24628	-2.71958	2.50189
C	0.52424	-2.42561	1.28754	H	-3.76622	-3.40067	0.94631
C	-0.79045	-2.51461	1.74429	C	0.78885	1.07708	-0.62788
C	-1.87815	-2.37153	0.87970	C	1.52714	2.36611	-0.41813
H	-0.97998	-2.71159	2.79493	C	2.16304	1.05668	0.02936
H	1.35519	-2.54954	1.97087	H	1.19990	3.01796	0.38029
H	1.76498	-2.13979	-0.44264	H	1.94421	2.84630	-1.29295
S	-3.00542	-1.84090	-1.60698	C	2.17344	0.81665	1.51126
C	-0.00854	-1.80807	-2.42021	C	3.36032	0.59649	-0.75912

O	1.42019	1.38792	2.27258	C	-3.72342	3.15683	0.08989
O	3.04017	-0.12068	1.87394	H	-2.75033	4.00445	-1.66431
C	3.08216	-0.44770	3.28330	H	-1.74062	3.97305	-0.22110
H	2.10253	-0.78994	3.61422	C	-3.37145	2.22134	1.24956
H	3.38597	0.42664	3.85763	H	-4.51573	2.70552	-0.51737
H	3.81906	-1.24081	3.36908	H	-4.11210	4.10264	0.47385
O	4.50041	0.82063	-0.42732	C	-2.74831	0.92093	0.74532
O	3.01267	-0.03176	-1.88520	H	-4.26075	1.96253	1.82865
C	4.09256	-0.44169	-2.75608	H	-2.67125	2.71524	1.93127
H	4.67137	0.42740	-3.06682	H	-3.43767	0.34614	0.12362
H	3.60941	-0.90950	-3.60910	H	-2.40530	0.28723	1.55889
H	4.73590	-1.15251	-2.23889	C	-0.41549	0.75819	0.16444
N	-1.57945	1.22190	-0.11365	H	0.77283	0.69390	-1.63987
C	-1.87620	2.09770	-1.26818	H	-0.34290	0.12257	1.03817
C	-2.49270	3.41137	-0.78412	H	1.06667	-1.72502	-2.58523
H	-2.57639	1.53794	-1.89206	H	-0.50176	-0.90911	-2.80160
H	-0.96267	2.26199	-1.83136	H	-0.39762	-2.63212	-3.02660

Cyclopropyl carboximinium thiolate complex, nitro substituted (357)

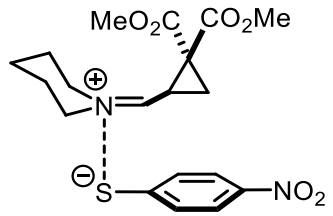

B3LYP/6-311+G(d,p)/CPCM(CH_2Cl_2)/EmpiricalDispersion=GD3BJ

C	-2.68581	1.30108	-1.33622	C	1.60770	3.74593	1.47653
C	-2.38367	0.04020	-1.92696	H	3.02270	3.36799	-0.13473
C	-2.71369	-1.15013	-1.31603	H	2.82313	2.02049	0.97955
C	-3.36665	-1.13468	-0.07451	C	0.49101	3.00233	2.21348
C	-3.72091	0.08575	0.52363	H	1.18775	4.61385	0.95648
C	-3.39331	1.27005	-0.09960	H	2.34233	4.12373	2.19098
H	-4.23988	0.08247	1.47206	C	-0.50531	2.38596	1.23164
N	-3.66096	-2.36754	0.58907	H	-0.06200	3.67587	2.87181
H	-2.46265	-2.09661	-1.77361	H	0.91430	2.21035	2.83933
S	-2.17919	2.78455	-2.05905	H	-1.01173	3.14917	0.63649
H	-1.86788	0.02714	-2.87898	H	-1.25524	1.77987	1.73345
H	-3.66330	2.21004	0.36482	C	-0.05571	0.26747	0.17548
C	0.61937	-0.64901	-0.75607	H	0.73125	-0.26423	-1.76203
C	1.82183	-1.49169	-0.27824	H	-0.83210	-0.11578	0.82521
C	0.49363	-2.12879	-0.61364	O	3.36299	-1.82475	1.51805
C	2.26659	-1.47414	1.15192	O	3.04557	-2.47877	-2.10406
C	2.94312	-1.59954	-1.28280	O	3.77173	-0.56137	-1.16652
H	-0.08207	-2.50997	0.21905	O	1.29058	-1.06103	1.96863
H	0.45887	-2.71467	-1.52159	C	1.58066	-1.04432	3.38701
N	0.20839	1.52003	0.26557	C	4.90606	-0.53401	-2.06532
C	1.27095	2.20848	-0.50198	H	1.80942	-2.05239	3.72972
C	2.28834	2.82332	0.46255	H	0.67538	-0.67236	3.85792
H	0.76495	2.97341	-1.09374	H	2.42132	-0.38023	3.58293
H	1.74368	1.49874	-1.17301	H	4.56128	-0.50088	-3.09827

H	5.52611	-1.41564	-1.90652	O	-3.31258	-3.43264	0.05494
H	5.45052	0.37071	-1.81098	O	-4.24659	-2.33481	1.68282

Alkyliminium thiolate complex (464)

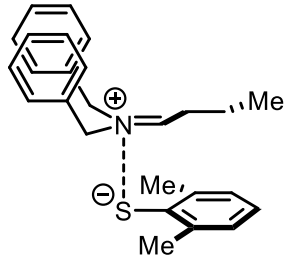

B3LYP/6-311+G(d,p)/CPCM(CH_2Cl_2)/EmpiricalDispersion=GD3BJ

C	-2.95733	-1.14493	0.70834	H	-0.46263	2.21718	-0.29348
C	-3.35286	-0.02625	1.49579	H	-2.06864	1.51052	-0.25365
C	-4.11878	0.99328	0.92528	C	-1.56139	2.38072	-2.16433
C	-4.50716	0.95478	-0.41400	H	-0.67976	2.49306	-2.80343
C	-4.11381	-0.12792	-1.19373	C	-2.15836	3.75193	-1.85230
C	-3.34981	-1.17179	-0.66235	H	-2.28573	1.77681	-2.71863
H	-4.40583	-0.17316	-2.23829	H	-1.44329	4.37863	-1.31133
H	-5.09575	1.75840	-0.84069	H	-3.05442	3.65300	-1.23393
H	-4.41204	1.83572	1.54400	H	-2.43571	4.27477	-2.77034
S	-2.02073	-2.46240	1.41146	C	3.01177	-2.02849	0.19266
C	-2.97865	0.06705	2.95048	C	2.82180	-1.13523	-2.03878
C	-3.01423	-2.34722	-1.54161	C	4.39759	-1.90383	0.12497
H	-1.95539	-2.60508	-1.48979	H	2.54799	-2.42463	1.08883
H	-3.28438	-2.14461	-2.58054	C	4.99593	-1.39156	-1.02472
H	-3.55082	-3.24355	-1.21277	H	5.00769	-2.20391	0.96855
C	-1.17564	1.63430	-0.88103	C	4.20610	-1.01422	-2.11099
N	0.13914	-0.38476	-0.37513	H	6.07367	-1.29143	-1.07699
C	0.47996	0.09407	0.97863	H	2.20884	-0.83183	-2.88076
C	1.74503	0.92434	1.06087	H	4.66833	-0.62351	-3.00976
H	0.55647	-0.79310	1.60299	C	2.36900	1.02603	2.30771
H	-0.37833	0.65433	1.34787	C	3.51737	1.79644	2.46324
C	2.21515	-1.63427	-0.88340	H	1.95879	0.49112	3.15739
C	0.71262	-1.69928	-0.78710	C	4.06074	2.47056	1.36949
H	0.36761	-2.41971	-0.04698	H	3.99280	1.86219	3.43484
H	0.26734	-1.95074	-1.74761	C	3.44385	2.36985	0.12512
C	-0.63430	0.28486	-1.15773	H	4.96011	3.06349	1.48607
H	-0.86491	-0.18134	-2.11005	C	2.28896	1.60395	-0.02740
H	-3.31963	1.01245	3.37848	H	3.86204	2.88215	-0.73325
H	-1.89783	-0.01728	3.09262	H	1.83861	1.52454	-1.0081
H	-3.41883	-0.75574	3.52261				

A.2.2. Time-Dependent DFT

Dimethyl 2-(((2,6-dimethylphenyl)thio)(piperidin-1-yl)methyl)cyclopropane-1,1-dicarboxylate (342)

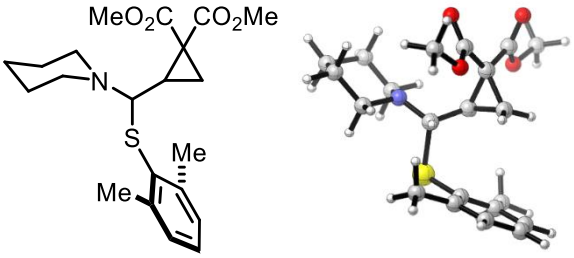

CAM-B3LYP/6-311+G(d,p)/CPCM(CH_2Cl_2)

Excited state	Identity	Energy /eV	Wavelength /nm	Oscillator strength (f)	Spin contamination <S**2>	Initial MO no.	Initial MO identity	Final MO no.	Final MO identity	Contribution coefficient	Percentage contribution
1	Singlet-A	4.8382	256.26	0.0570	0.000	104	HOMO-1	106	LUMO	0.59780	71%
						105	HOMO	106	LUMO	0.26044	14%
2	Singlet-A	5.1075	242.75	0.0062	0.000	102	HOMO-3	108	LUMO+2	-0.19065	7%
						102	HOMO-3	110	LUMO+4	0.11691	3%
						103	HOMO-2	106	LUMO	0.51523	53%
						104	HOMO-1	108	LUMO+2	0.12515	3%
						105	HOMO	108	LUMO+2	0.29498	17%
						105	HOMO	110	LUMO+4	-0.16233	5%
3	Singlet-A	5.2446	236.40	0.4006	0.000	102	HOMO-3	106	LUMO	-0.16972	6%
						104	HOMO-1	106	LUMO	-0.21921	10%
						105	HOMO	106	LUMO	0.61224	75%

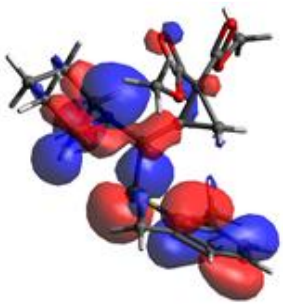

HOMO

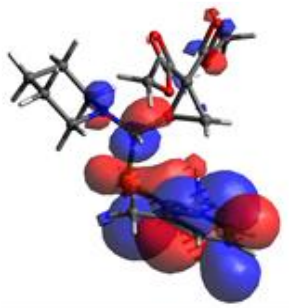

LUMO

Cyclopropyl carboximinium thiolate complex (352)

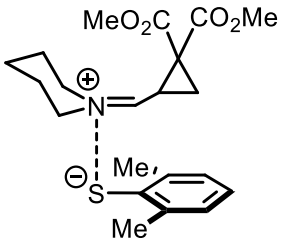

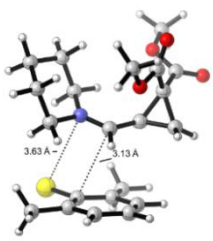

CAM-B3LYP/6-311+G(d,p)/CPCM(CH_2Cl_2)

Excited state	Identity	Energy /eV	Wavelength /nm	Oscillator strength (f)	Spin contamination <S**2>	Initial MO no.	Initial MO identity	Final MO no.	Final MO identity	Contribution coefficient	Percentage contribution
1	Singlet-A	2.7379	452.84	0.0421	0.000	105	HOMO	106	LUMO	0.69950	98%
2	Singlet-A	3.2456	382.01	0.0013	0.000	104	HOMO-1	106	LUMO	0.69726	97%
3	Singlet-A	4.3887	282.51	0.0631	0.000	103	HOMO-2	106	LUMO	0.63247	80%
						105	HOMO	111	LUMO+5	-0.11165	2%
						105	HOMO	113	LUMO+7	-0.24417	12%

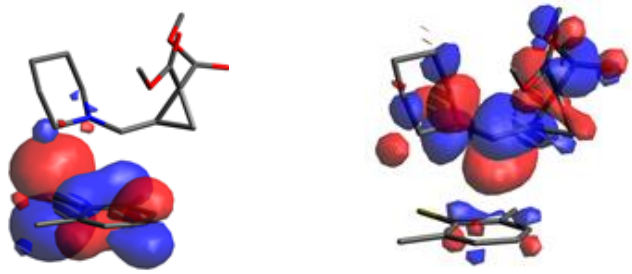

HOMO LUMO

ωB97X-D/6-311+G(d,p)/CPCM(CH_2Cl_2)[329]

Excited state	Identity	Energy /eV	Wavelength /nm	Oscillator strength (f)	Spin contamination <S**2>	Initial MO no.	Initial MO identity	Final MO no.	Final MO identity	Contribution coefficient	Percentage contribution
1	Singlet-A	2.7791	446.13	0.0428	0.000	105	HOMO	106	LUMO	0.69673	97%
2	Singlet-A	3.2965	376.10	0.0014	0.000	104	HOMO-1	106	LUMO	0.69486	97%
3	Singlet-A	4.3948	282.12	0.0546	0.000	103	HOMO-2	106	LUMO	0.66740	89%
						105	HOMO	111	LUMO+5	0.16635	6%

Cyclopropyl carboximinium thiolate complex, alternative geometry (528)

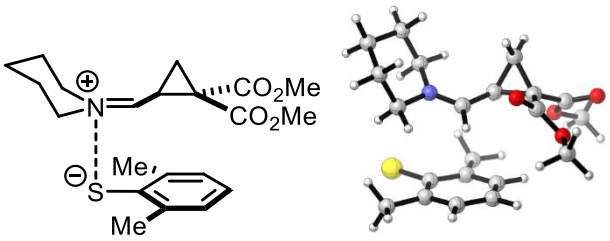

CAM-B3LYP/6-311+G(d,p)/CPCM(CH_2Cl_2)

Excited state	Identity	Energy /eV	Wavelength /nm	Oscillator strength (f)	Spin contamination <S**2>	Initial MO no.	Initial MO identity	Final MO no.	Final MO identity	Contribution coefficient	Percentage contribution
1	Singlet-A	2.8187	439.87	0.0192	0.000	105	HOMO	106	LUMO	0.70350	99%
2	Singlet-A	3.3621	368.77	0.0015	0.000	104	HOMO-1	106	LUMO	0.70108	98%
3	Singlet-A	4.4043	281.51	0.0770	0.000	103	HOMO-2	106	LUMO	-0.12426	3%
						103	HOMO-2	113	LUMO+7	-0.12841	3%
						105	HOMO	107	LUMO+1	0.34235	23%
						105	HOMO	110	LUMO+4	-0.24495	12%
						105	HOMO	112	LUMO+6	-0.17420	6%
						105	HOMO	114	LUMO+8	0.42585	36%
						105	HOMO	115	LUMO+9	-0.12349	3%
						105	HOMO	118	LUMO+12	0.10575	2%

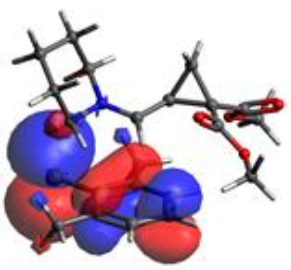

HOMO

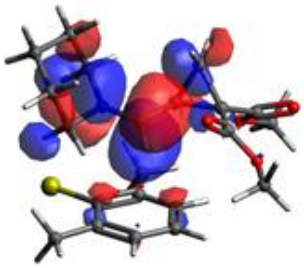

LUMO

Cyclopropyl carboximinium thiolate complex, nitro substituted (357)

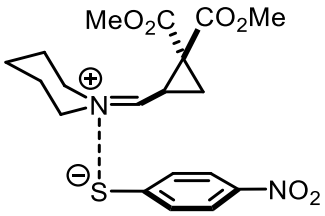

CAM-B3LYP/6-311+G(d,p)/CPCM(CH_2Cl_2)

Excited state	Identity	Energy /eV	Wavelength /nm	Oscillator strength (f)	Spin contamination <S**2>	Initial MO no.	Initial MO identity	Final MO no.	Final MO identity	Contribution coefficient	Percentage contribution
1	Singlet-A	3.0267	409.63	0.5966	0.000	108	HOMO	109	LUMO	0.68845	95%
2	Singlet-A	3.0884	401.46	0.0046	0.000	107	HOMO-1	109	LUMO	0.65824	87%
						107	HOMO-1	110	LUMO+1	0.10869	2%
						107	HOMO-1	118	LUMO+9	-0.15566	5%
3	Singlet-A	3.1603	392.31	0.0234	0.000	108	HOMO	110	LUMO+1	0.70020	98%

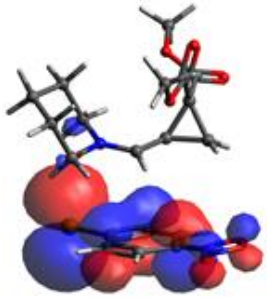

HOMO

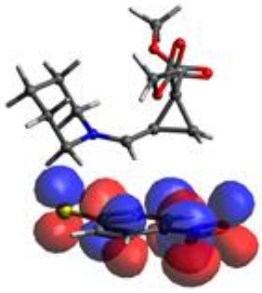

LUMO

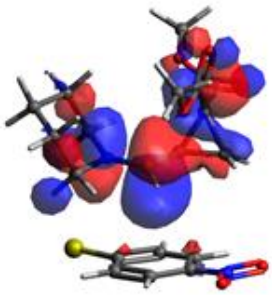

LUMO+1

Analogous calculations were carried out for 4-nitrothiophenol. The 1st excited singlet state was found at λ=411.85nm with f=0.6051, significantly exceeding the other excited states' oscillator strengths. This transition was calculated to be between MO 108 (HOMO) and MO 109 (LUMO). MO visualization showed that the HOMO was found to be largely located on the thiolate, while the LUMO was also located solely on the thiolate. This indicates that visible light absorption promotes a local excitation involving thiolate π-orbitals only. The 3rd excited singlet state was found at λ=394.57nm with 25x lower oscillator strength than the 1st excited state. The transition between HOMO (thiolate) and LUMO+1 (iminium) displayed intermolecular

charge-transfer characteristics. The low predicted probability of charge-transfer is corroborated by experimental evidence which showed 0% yield when 4-nitrothiphenol was used.

Alkyliminium thiolate complex (464)

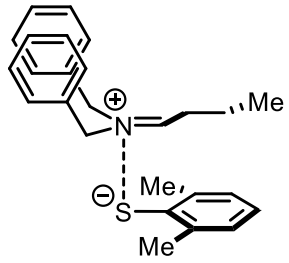

CAM-B3LYP/6-311+G(d,p)/CPCM(CH_2Cl_2)

Excited state	Identity	Energy /eV	Wavelength /nm	Oscillator strength (f)	Spin contamination <S**2>	Initial MO no.	Initial MO identity	Final MO no.	Final MO identity	Contribution coefficient	Percentage contribution
1	Singlet-A	2.8145	440.52	0.0346	0.000	105	HOMO	106	LUMO	0.70061	98%
2	Singlet-A	3.2908	376.76	0.0003	0.000	104	HOMO-1	106	LUMO	0.69831	98%
3	Singlet-A	4.4143	280.87	0.0386	0.000	103	HOMO-2	115	LUMO+9	0.15740	5%
						105	HOMO	107	LUMO+1	-0.16420	5%
						105	HOMO	112	LUMO+6	0.25189	13%
						105	HOMO	113	LUMO+7	0.24796	12%
						105	HOMO	115	LUMO+9	-0.15734	5%
						105	HOMO	116	LUMO+10	0.48834	48%
						105	HOMO	120	LUMO+14	0.10456	2%

A.3. UV-Vis Absorption Spectra

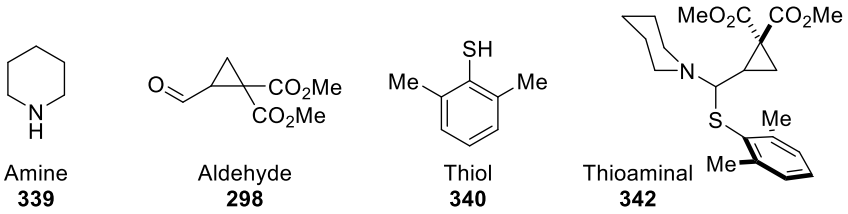

Amine **339** | Aldehyde **298** | Thiol **340** | Thioaminal **342**

Concentration = 0.33 mM

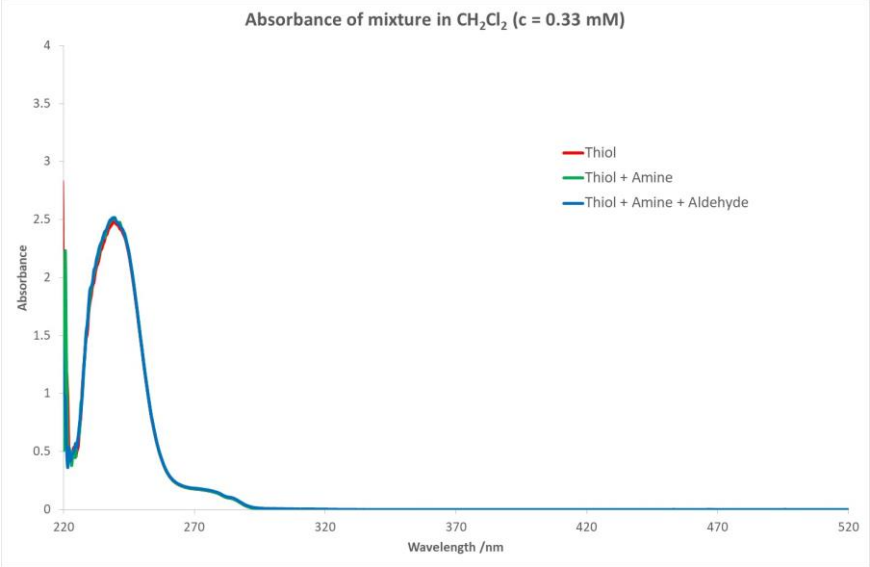

Concentration = 1.7 mM

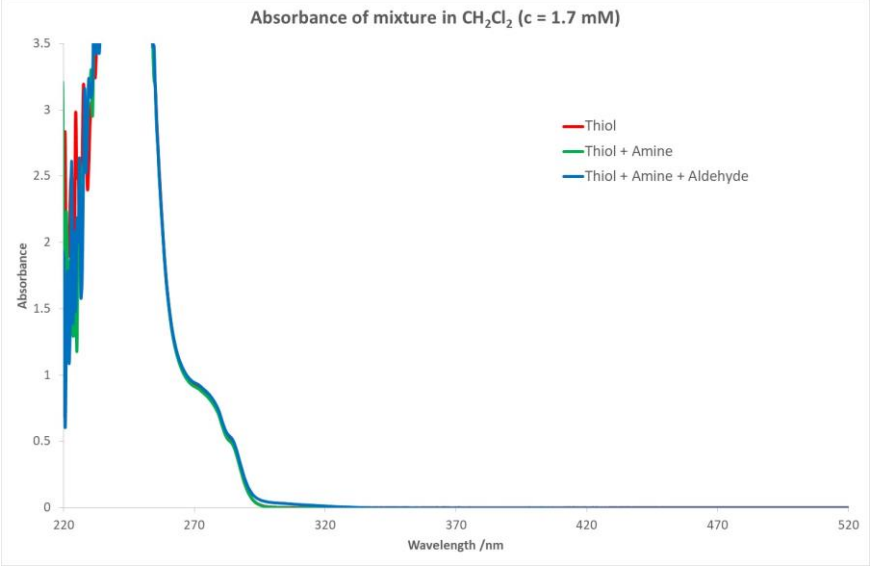

Concentration = 3.3 mM

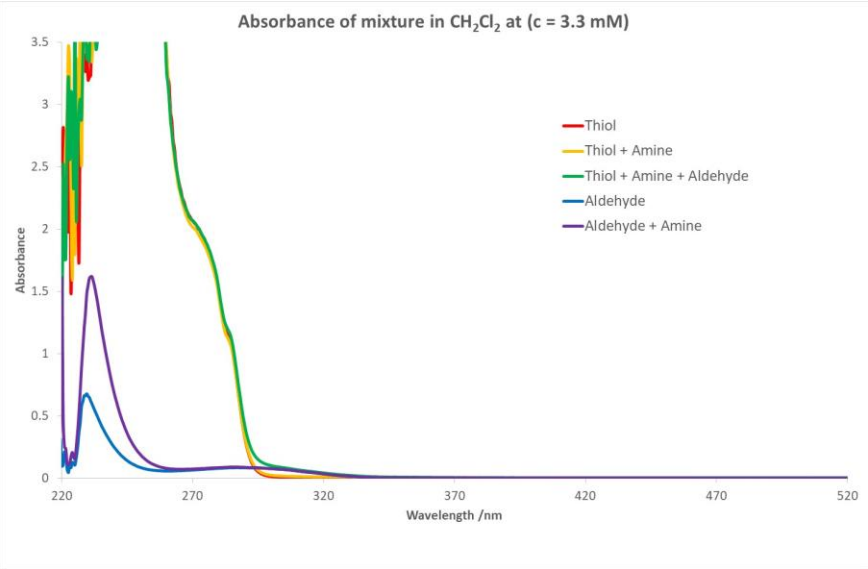

Concentration = 33 mM

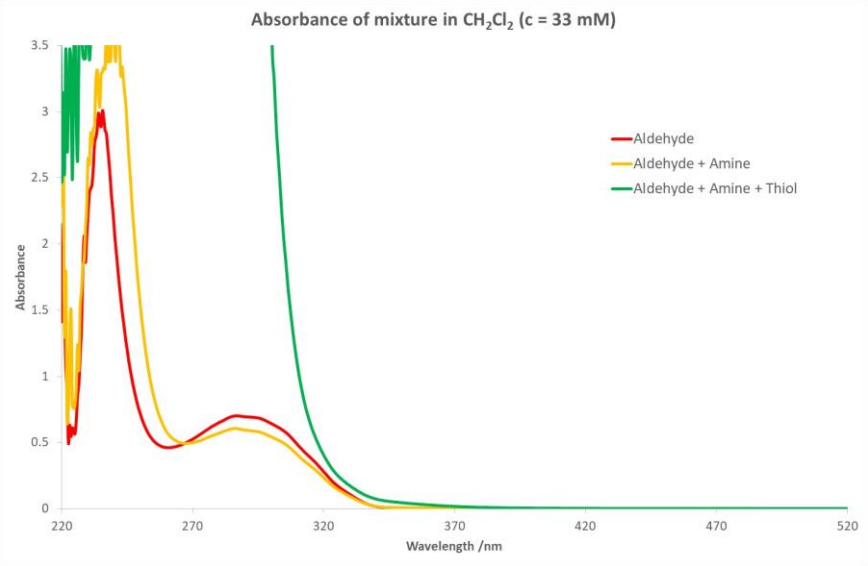

Final thioaminal at different concentrations

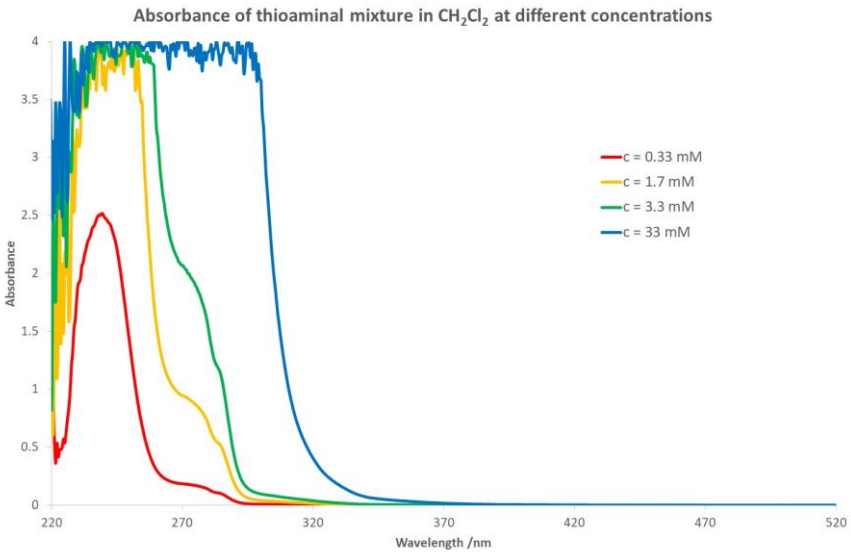

Absorbance of possible sulfur by-products

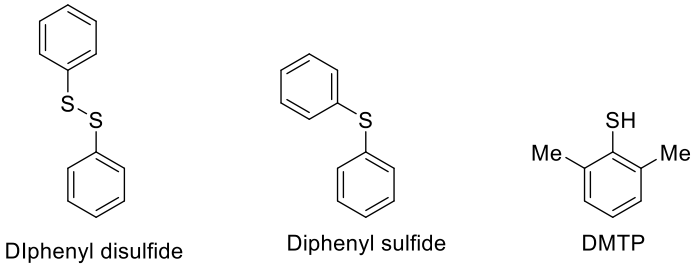

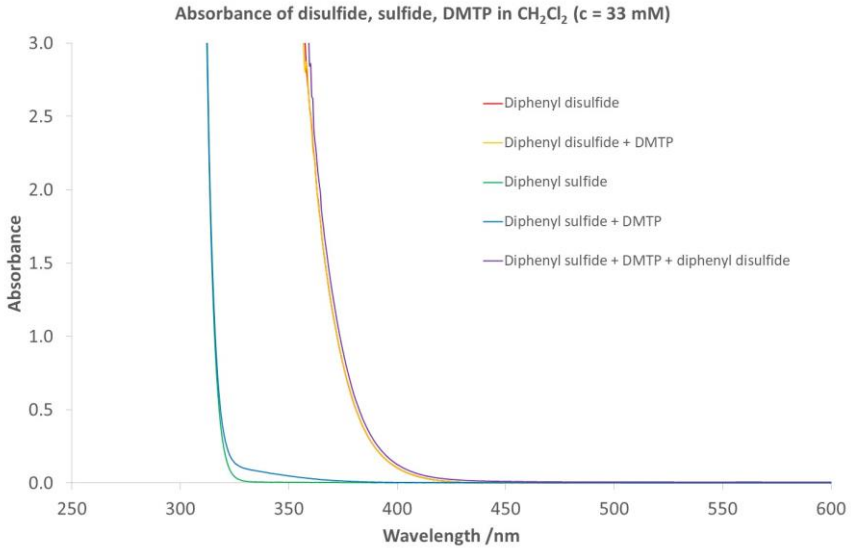

Absorption of thiolate and thiol

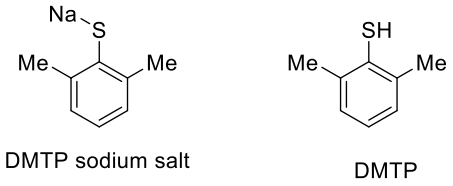

DMTP sodium salt DMTP

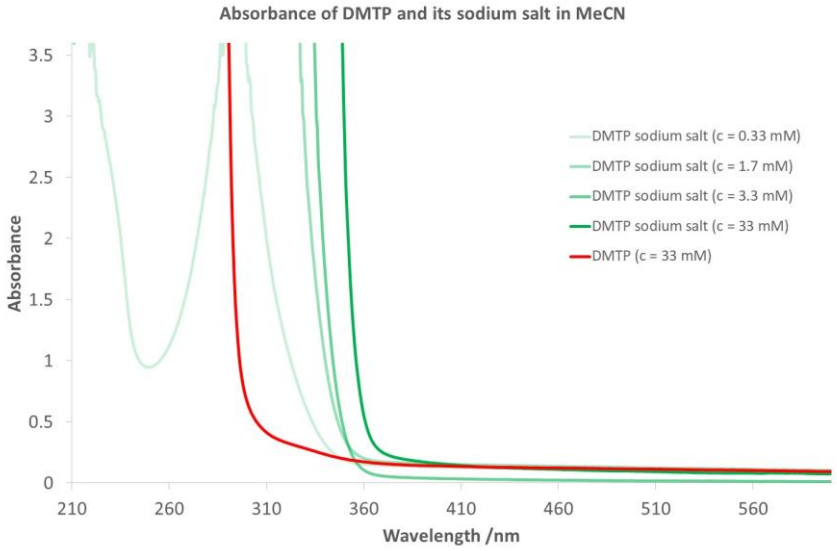

Emission spectrum of LED

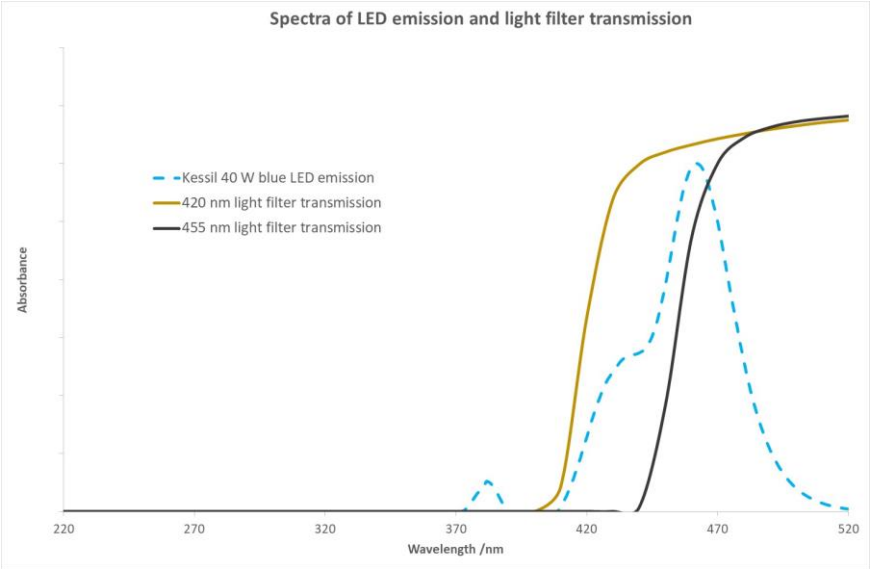

A.4. X-Ray Crystallographic Data

1-((1*S*,2*R*)-2-(4-bromophenyl)-4,4-bis(methoxycarbonyl)cyclopentyl)-*N*,*N*-dimethylmethanaminium perchlorate (317)

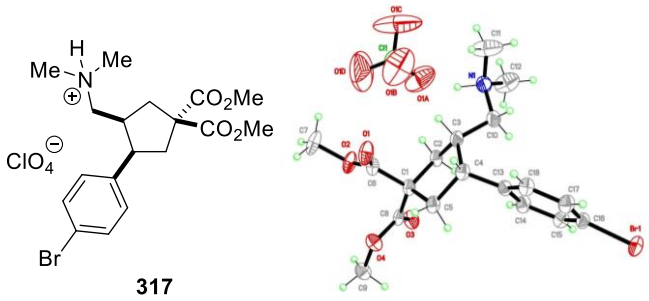

317

_chemical_formula_moiety 'C18 H25 Br N O4 +, Cl O4 -'
_chemical_formula_sum 'C18 H25 Br Cl N O8'
_chemical_formula_weight 498.75

_space_group_crystal_system monoclinic
_space_group_IT_number 14
_space_group_name_H-M_alt 'P 21/n'
_space_group_name_Hall '-P 2yn'

_cell_length_a 6.5320(4)
_cell_length_b 13.6779(8)
_cell_length_c 23.8964(14)
_cell_angle_alpha 90
_cell_angle_beta 94.809(2)
_cell_angle_gamma 90
_cell_volume 2127.5(2)
_cell_formula_units_Z 4
_cell_measurement_temperature 180(2)
_cell_measurement_reflns_used 9723
_cell_measurement_theta_min 3.71
_cell_measurement_theta_max 66.95

_exptl_crystal_description block
_exptl_crystal_colour colourless
_exptl_crystal_density_meas ?
_exptl_crystal_density_method ?
_exptl_crystal_density_diffrn 1.557
_exptl_crystal_F_000 1024
_exptl_transmission_factor_min ?
_exptl_transmission_factor_max ?
_exptl_crystal_size_max 0.220
_exptl_crystal_size_mid 0.220
_exptl_crystal_size_min 0.220
_exptl_absorpt_coefficient_mu 4.189
_shelx_estimated_absorpt_T_min 0.459
_shelx_estimated_absorpt_T_max 0.459
_exptl_absorpt_correction_type multi-scan
_exptl_absorpt_correction_T_min 0.4996
_exptl_absorpt_correction_T_max 0.7528
_exptl_absorpt_process_details 'SADABS (Bruker, 2014)'

_diffrn_ambient_temperature 180(2)
_diffrn_radiation_wavelength 1.54178
_diffrn_radiation_type CuK\a
_diffrn_source 'Incoatec I\mS Cu microsource'
_diffrn_measurement_device_type 'Bruker D8-QUEST PHOTON-100'
_diffrn_measurement_method '\w and \f-scans'
_diffrn_detector_area_resol_mean ?
_diffrn_reflns_number 26810
_diffrn_reflns_av_unetI/netI 0.0318
_diffrn_reflns_av_R_equivalents 0.0540
_diffrn_reflns_limit_h_min -7
_diffrn_reflns_limit_h_max 7
_diffrn_reflns_limit_k_min -16
_diffrn_reflns_limit_k_max 16
_diffrn_reflns_limit_l_min -27
_diffrn_reflns_limit_l_max 28
_diffrn_reflns_theta_min 3.712
_diffrn_reflns_theta_max 67.028
_diffrn_reflns_theta_full 67.028
_diffrn_measured_fraction_theta_max 0.996
_diffrn_measured_fraction_theta_full 0.996
_diffrn_reflns_Laue_measured_fraction_max 0.996
_diffrn_reflns_Laue_measured_fraction_full 0.996
_diffrn_reflns_point_group_measured_fraction_max 0.996
_diffrn_reflns_point_group_measured_fraction_full 0.996
_reflns_number_total 3784
_reflns_number_gt 3646

_reflns_threshold_expression 'I > 2\s(I)'
_reflns_Friedel_coverage 0.000
_reflns_Friedel_fraction_max .
_reflns_Friedel_fraction_full

Dimethyl 6-((4-cyanopiperidin-1-yl)methyl)hexahydro-4H-cyclopenta[b]furan-4,4-dicarboxylate (409)

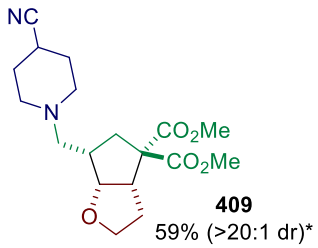

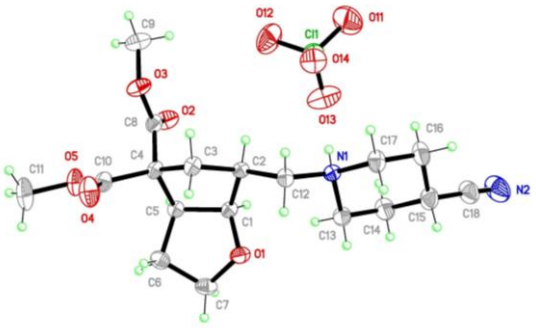

_chemical_formula_moiety 'C18 H27 N2 O5 +, Cl O4 -'
_chemical_formula_sum 'C18 H27 Cl N2 O9'
_chemical_formula_weight 450.86

_space_group_crystal_system triclinic
_space_group_IT_number 2
_space_group_name_H-M_alt 'P -1'
_space_group_name_Hall '-P 1'

_cell_length_a 8.2705(3)
_cell_length_b 11.2103(3)
_cell_length_c 12.7123(4)
_cell_angle_alpha 71.816(2)
_cell_angle_beta 80.032(2)
_cell_angle_gamma 72.745(2)
_cell_volume 1065.14(6)
_cell_formula_units_Z 2
_cell_measurement_temperature 180(2)
_cell_measurement_reflns_used 4980
_cell_measurement_theta_min 3.67
_cell_measurement_theta_max 66.79

_exptl_crystal_description plate
_exptl_crystal_colour colourless
_exptl_crystal_density_meas ?
_exptl_crystal_density_method ?
_exptl_crystal_density_diffrn 1.406
_exptl_crystal_F_000 476
_exptl_transmission_factor_min ?
_exptl_transmission_factor_max ?
_exptl_crystal_size_max 0.180
_exptl_crystal_size_mid 0.100
_exptl_crystal_size_min 0.020
_exptl_absorpt_coefficient_mu 2.058
_shelx_estimated_absorpt_T_min 0.708
_shelx_estimated_absorpt_T_max 0.960
_exptl_absorpt_correction_type multi-scan
_exptl_absorpt_correction_T_min 0.6077
_exptl_absorpt_correction_T_max 0.7528
_exptl_absorpt_process_details 'SADABS (Bruker, 2014)'

_diffrn_ambient_temperature 180(2)
_diffrn_radiation_wavelength 1.54178
_diffrn_radiation_type CuK\a
_diffrn_source 'Incoatec I\mS Cu microsource'
_diffrn_measurement_device_type 'Bruker D8-QUEST PHOTON-100'
_diffrn_measurement_method '\w and \f-scans'
_diffrn_detector_area_resol_mean ?
_diffrn_reflns_number 10125
_diffrn_reflns_av_unetI/netI 0.0460
_diffrn_reflns_av_R_equivalents 0.0466
_diffrn_reflns_limit_h_min -9
_diffrn_reflns_limit_h_max 9
_diffrn_reflns_limit_k_min -13
_diffrn_reflns_limit_k_max 11
_diffrn_reflns_limit_l_min -14
_diffrn_reflns_limit_l_max 15
_diffrn_reflns_theta_min 3.674
_diffrn_reflns_theta_max 66.802
_diffrn_reflns_theta_full 66.802
_diffrn_measured_fraction_theta_max 0.993
_diffrn_measured_fraction_theta_full 0.993
_diffrn_reflns_Laue_measured_fraction_max 0.993
_diffrn_reflns_Laue_measured_fraction_full 0.993
_diffrn_reflns_point_group_measured_fraction_max 0.993
_diffrn_reflns_point_group_measured_fraction_full 0.993
_reflns_number_total 3743
_reflns_number_gt 2967

_reflns_threshold_expression 'I > 2\s(I)'
_reflns_Friedel_coverage 0.000
_reflns_Friedel_fraction_max .
_reflns_Friedel_fraction_full .

4-((2-Amino-3,5-dibromobenzyl)(methyl)amino)cyclohexan-1-ol (452)

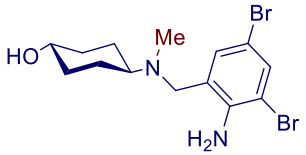

452, 61%
from Ambroxol

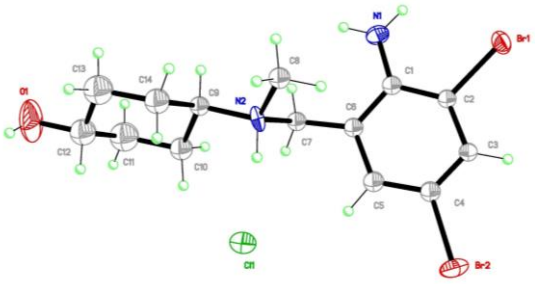

_chemical_formula_moiety 'C14 H21 Br2 N2 O +, Cl -'
_chemical_formula_sum 'C14 H21 Br2 Cl N2 O'
_chemical_formula_weight 428.60

_space_group_crystal_system monoclinic
_space_group_IT_number 9
_space_group_name_H-M_alt 'C c'
_space_group_name_Hall 'C -2yc'

_cell_length_a 52.925(4)
_cell_length_b 6.0878(4)
_cell_length_c 10.8414(7)
_cell_angle_alpha 90
_cell_angle_beta 95.819(5)
_cell_angle_gamma 90
_cell_volume 3475.1(4)
_cell_formula_units_Z 8
_cell_measurement_temperature 180(2)
_cell_measurement_reflns_used 5984
_cell_measurement_theta_min 3.36
_cell_measurement_theta_max 66.72

_exptl_crystal_description plate
_exptl_crystal_colour colourless
_exptl_crystal_density_meas ?
_exptl_crystal_density_method ?
_exptl_crystal_density_diffrn 1.638
_exptl_crystal_F_000 1712
_exptl_transmission_factor_min ?
_exptl_transmission_factor_max ?
_exptl_crystal_size_max 0.120
_exptl_crystal_size_mid 0.100
_exptl_crystal_size_min 0.020
_exptl_absorpt_coefficient_mu 7.312
_shelx_estimated_absorpt_T_min 0.474
_shelx_estimated_absorpt_T_max 0.868

_exptl_absorpt_correction_type multi-scan
_exptl_absorpt_correction_T_min 0.4272
_exptl_absorpt_correction_T_max 0.7528
_exptl_absorpt_process_details 'SADABS (Bruker, 2014)'

_diffrn_ambient_temperature 180(2)
_diffrn_radiation_wavelength 1.54178
_diffrn_radiation_type CuK\a
_diffrn_source 'Incoatec I\mS Cu microsource'
_diffrn_measurement_device_type 'Bruker D8-QUEST PHOTON-100'
_diffrn_measurement_method '\w and \f-scans'
_diffrn_detector_area_resol_mean ?
_diffrn_reflns_number 14593
_diffrn_reflns_av_unetI/netI 0.1303
_diffrn_reflns_av_R_equivalents 0.1151
_diffrn_reflns_limit_h_min -62
_diffrn_reflns_limit_h_max 61
_diffrn_reflns_limit_k_min -7
_diffrn_reflns_limit_k_max 7
_diffrn_reflns_limit_l_min -12
_diffrn_reflns_limit_l_max 12
_diffrn_reflns_theta_min 3.357
_diffrn_reflns_theta_max 66.748
_diffrn_reflns_theta_full 66.748
_diffrn_measured_fraction_theta_max 0.998
_diffrn_measured_fraction_theta_full 0.998
_diffrn_reflns_Laue_measured_fraction_max 0.998
_diffrn_reflns_Laue_measured_fraction_full 0.998
_diffrn_reflns_point_group_measured_fraction_max 0.879
_diffrn_reflns_point_group_measured_fraction_full 0.879

_reflns_number_total 5435
_reflns_number_gt 4312
_reflns_threshold_expression 'I > 2\s(I)'
_reflns_Friedel_coverage 0.760
_reflns_Friedel_fraction_max 0.759
_reflns_Friedel_fraction_full 0.759

tert-Butyl (1-butylpiperidin-4-yl)carbamate (473)

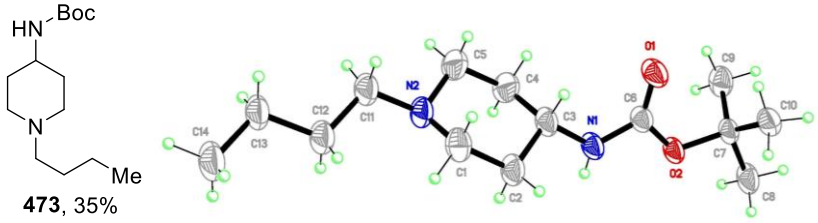

_chemical_formula_moiety 'C14 H28 N2 O2'
_chemical_formula_sum 'C14 H28 N2 O2'
_chemical_formula_weight 256.38

_space_group_crystal_system monoclinic
_space_group_IT_number 14
_space_group_name_H-M_alt 'P 21/c'
_space_group_name_Hall '-P 2ybc'

_cell_length_a 16.4938(11)
_cell_length_b 9.4001(7)
_cell_length_c 10.3091(8)
_cell_angle_alpha 90
_cell_angle_beta 103.424(4)
_cell_angle_gamma 90
_cell_volume 1554.7(2)
_cell_formula_units_Z 4
_cell_measurement_temperature 180(2)
_cell_measurement_reflns_used 5810
_cell_measurement_theta_min 2.75
_cell_measurement_theta_max 66.59

_exptl_crystal_description block
_exptl_crystal_colour colourless
_exptl_crystal_density_meas ?
_exptl_crystal_density_method ?
_exptl_crystal_density_diffrn 1.095
_exptl_crystal_F_000 568
_exptl_transmission_factor_min ?
_exptl_transmission_factor_max ?
_exptl_crystal_size_max 0.220
_exptl_crystal_size_mid 0.120
_exptl_crystal_size_min 0.030
_exptl_absorpt_coefficient_mu 0.574
_shelx_estimated_absorpt_T_min 0.884
_shelx_estimated_absorpt_T_max 0.983
_exptl_absorpt_correction_type multi-scan
_exptl_absorpt_correction_T_min 0.5693
_exptl_absorpt_correction_T_max 0.7528
_exptl_absorpt_process_details 'SADABS (Bruker, 2014)'

_diffrn_ambient_temperature 180(2)
_diffrn_radiation_wavelength 1.54178
_diffrn_radiation_type CuK\a
_diffrn_source 'Incoatec I\mS Cu microsource'
_diffrn_measurement_device_type 'Bruker D8-QUEST PHOTON-100'
_diffrn_measurement_method '\w and \f-scans'
_diffrn_detector_area_resol_mean ?
_diffrn_reflns_number 18605
_diffrn_reflns_av_unetI/netI 0.0521
_diffrn_reflns_av_R_equivalents 0.0817
_diffrn_reflns_limit_h_min -19
_diffrn_reflns_limit_h_max 19
_diffrn_reflns_limit_k_min -11
_diffrn_reflns_limit_k_max 11
_diffrn_reflns_limit_l_min -12
_diffrn_reflns_limit_l_max 11
_diffrn_reflns_theta_min 2.754
_diffrn_reflns_theta_max 66.947
_diffrn_reflns_theta_full 66.947
_diffrn_measured_fraction_theta_max 0.995
_diffrn_measured_fraction_theta_full 0.995
_diffrn_reflns_Laue_measured_fraction_max 0.995
_diffrn_reflns_Laue_measured_fraction_full 0.995
_diffrn_reflns_point_group_measured_fraction_max 0.995
_diffrn_reflns_point_group_measured_fraction_full 0.995
_reflns_number_total 2758
_reflns_number_gt 2042
_reflns_threshold_expression 'I > 2\s(I)'
_reflns_Friedel_coverage 0.000
_reflns_Friedel_fraction_max .
_reflns_Friedel_fraction_full .

(*S*)-N^2-butyl-N^6-propyl-4,5,6,7-tetrahydrobenzo[*d*]thiazole-2,6-diamine (505)

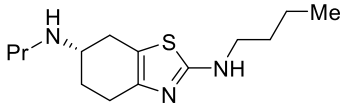

505, 83%

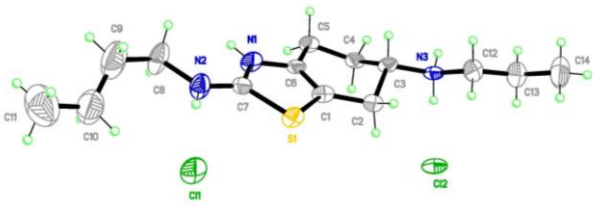

_chemical_formula_moiety 'C14 H27 N3 S 2+, 2(Cl -)'
_chemical_formula_sum 'C14 H27 Cl2 N3 S'
_chemical_formula_weight 340.34

_space_group_crystal_system monoclinic
_space_group_IT_number 4
_space_group_name_H-M_alt 'P 21'
_space_group_name_Hall 'P 2yb'

_cell_length_a 5.2296(4)
_cell_length_b 5.3817(5)
_cell_length_c 32.304(2)
_cell_angle_alpha 90
_cell_angle_beta 92.055(5)
_cell_angle_gamma 90
_cell_volume 908.57(13)
_cell_formula_units_Z 2
_cell_measurement_temperature 220(2)
_cell_measurement_reflns_used 3287
_cell_measurement_theta_min 2.74
_cell_measurement_theta_max 66.58

_exptl_crystal_description plate
_exptl_crystal_colour colourless
_exptl_crystal_density_meas ?
_exptl_crystal_density_method ?
_exptl_crystal_density_diffrn 1.244
_exptl_crystal_F_000 364
_exptl_transmission_factor_min ?
_exptl_transmission_factor_max ?
_exptl_crystal_size_max 0.120
_exptl_crystal_size_mid 0.120
_exptl_crystal_size_min 0.020
_exptl_absorpt_coefficient_mu 4.236
_shelx_estimated_absorpt_T_min 0.630
_shelx_estimated_absorpt_T_max 0.920
_exptl_absorpt_correction_type multi-scan
_exptl_absorpt_correction_T_min 0.513
_exptl_absorpt_correction_T_max 0.753
_exptl_absorpt_process_details 'TWINABS (Bruker, 2014)'

_diffrn_ambient_temperature 220(2)
_diffrn_radiation_wavelength 1.54178
_diffrn_radiation_type CuK\a
_diffrn_source 'Incoatec I\mS Cu microsource'
_diffrn_measurement_device_type 'Bruker D8-QUEST PHOTON-100'
_diffrn_measurement_method '\w and \f-scans'
_diffrn_detector_area_resol_mean ?
_diffrn_reflns_number 7845
_diffrn_reflns_av_unetI/netI 0.1656
_diffrn_reflns_av_R_equivalents ?
_diffrn_reflns_limit_h_min -6
_diffrn_reflns_limit_h_max 6
_diffrn_reflns_limit_k_min -5
_diffrn_reflns_limit_k_max 5
_diffrn_reflns_limit_l_min -38
_diffrn_reflns_limit_l_max 37
_diffrn_reflns_theta_min 2.737
_diffrn_reflns_theta_max 66.788
_diffrn_reflns_theta_full 66.788
_diffrn_measured_fraction_theta_max 0.937
_diffrn_measured_fraction_theta_full 0.938
_diffrn_reflns_Laue_measured_fraction_max 0.937
_diffrn_reflns_Laue_measured_fraction_full 0.938
_diffrn_reflns_point_group_measured_fraction_max 0.856
_diffrn_reflns_point_group_measured_fraction_full 0.856
_reflns_number_total 7845
_reflns_number_gt 5284
_reflns_threshold_expression 'I > 2\s(I)'
_reflns_Friedel_coverage 0.633
_reflns_Friedel_fraction_max 0.752
_reflns_Friedel_fraction_full 0.753